

2017

Analysis and modeling of structure formation in granular and fluid-solid flows

Eric James Murphy
Iowa State University

Follow this and additional works at: <https://lib.dr.iastate.edu/etd>

 Part of the [Chemical Engineering Commons](#), [Mechanical Engineering Commons](#), and the [Oil, Gas, and Energy Commons](#)

Recommended Citation

Murphy, Eric James, "Analysis and modeling of structure formation in granular and fluid-solid flows" (2017). *Graduate Theses and Dissertations*. 16181.
<https://lib.dr.iastate.edu/etd/16181>

This Dissertation is brought to you for free and open access by the Iowa State University Capstones, Theses and Dissertations at Iowa State University Digital Repository. It has been accepted for inclusion in Graduate Theses and Dissertations by an authorized administrator of Iowa State University Digital Repository. For more information, please contact digirep@iastate.edu.

Analysis and modeling of structure formation in granular and fluid-solid flows

by

Eric Murphy

A dissertation submitted to the graduate faculty
in partial fulfillment of the requirements for the degree of
DOCTOR OF PHILOSOPHY

Major: Mechanical Engineering

Program of Study Committee:
Shankar Subramaniam, Major Professor
Alberto Passalacqua
Pranav Shrotriya
Rodney O. Fox
James W. Evans

The student author, whose presentation of the scholarship herein was approved by the program of study committee, is solely responsible for the content of this dissertation. The Graduate College will ensure this dissertation is globally accessible and will not permit alterations after a degree is conferred.

Iowa State University

Ames, Iowa

2017

Copyright © Eric Murphy, 2017. All rights reserved.

TABLE OF CONTENTS

LIST OF TABLES	iii
LIST OF FIGURES	iv
ACKNOWLEDGEMENTS	v
ABSTRACT	vii
CHAPTER 1. INTRODUCTION	1
1.1 Background	1
1.2 Challenges	7
1.3 Research Objectives	10
1.4 Accomplishments and Future Work	16
CHAPTER 2. BINARY COLLISION OUTCOMES FOR INELASTIC SOFT- SPHERE MODELS WITH COHESION	22
2.1 Introduction	23
2.2 Methods	27
2.2.1 Inelastic Sphere Models	28
2.2.2 Short-Ranged Cohesive Potential	30
2.2.3 Inelastic Sphere Models with Cohesion	32
2.2.4 The Cohesive Time-Scale	34
2.2.5 Discrete Element Method	37
2.3 Results and Discussion	37
2.3.1 Conservation of Kinetic Energy	37
2.3.2 Consequences of Cohesive Models on Contact Dynamics	39

2.3.3	Consequences for Macroscopic Systems: Simple Homogeneous Shear . . .	48
2.3.4	Computational Speed-up	55
2.4	Conclusion	57
2.5	Bibliography	59
CHAPTER 3. FREELY COOLING GRANULAR GASES WITH SHORT-		
RANGED ATTRACTIVE POTENTIALS		
3.1	Introduction	82
3.2	Analytic Methods	85
3.2.1	The Binary System with Short-Ranged Attraction	85
3.2.2	Solving the Cohesive Problem	88
3.3	Soft Sphere Discrete Element Method	92
3.4	Results and Discussion	93
3.4.1	Dilute Nearly Elastic Systems	93
3.4.2	Higher Solids Fraction and Inelasticity	95
3.4.3	Accuracy of Mean-Field Closures	98
3.5	Conclusion	102
3.6	Bibliography	103
CHAPTER 4. RHEOLOGICAL REGIME TRANSITIONS IN MODER-		
ATELY DENSE ASSEMBLIES OF DRY COHESIVE GRANULES		
4.1	Introduction	126
4.2	Methods	129
4.3	Results	132
4.3.1	Energetic Collapse of Stress	133
4.3.2	A signature of transition in rheology	137
4.3.3	Contact Anisotropy	143
4.3.4	Implications for Constitutive Modeling	147
4.4	Conclusions	148
4.5	Bibliography	149

CHAPTER 5. SIMPLE SHEAR OF A SLURRY WITH COHESIVE MICRO-	
PARTICLES	172
5.1 Background	172
5.2 Methods	176
5.2.1 Parameters	176
5.2.2 Time-scale for clustering	179
5.2.3 Simulation method	181
5.3 Results	183
5.3.1 Homogeneous Shearing	183
5.3.2 Rough Wall Shearing	186
5.4 Conclusions	189
5.5 Bibliography	189
CHAPTER 6. DEVELOPMENT OF A SOLID-SOLID DRAG LAW AT	
ARBITRARY MACH NUMBER	213
6.1 Background	213
6.2 Analytic Methods	218
6.2.1 Macroscopic Equations	218
6.2.2 The Pseudo-Liouville Operators	219
6.2.3 The Kinetic Integrals	221
6.2.4 Momentum Transfer	225
6.2.5 Energy Balance	228
6.3 Future Work	229
6.4 Bibliography	230
CHAPTER 7. CLUSTERING IN GAS-SOLID FLOWS	254
7.1 Background	254
7.2 Theory	258
7.2.1 Statistics	259
7.2.2 The PDF transport equation	260

7.2.3	Averaging	262
7.2.4	Moment Transport	263
7.2.5	Isotropic case	266
7.3	Modeling	268
7.3.1	Ornstein-Uhlenbeck	270
7.3.2	Multiplicative Noise	272
7.4	Future Work	273
7.5	Bibliography	274
CHAPTER 8. THE HOMOGENEOUSLY COOLING GAS-SOLID FLOW		297
8.1	Introduction	297
8.2	Methods	297
8.2.1	Computational Set-up	299
8.2.2	Analytical Methods	300
8.3	Results and Discussion	302
8.3.1	Moments	302
8.3.2	Evolution Equations	306
8.4	Conclusions	315
CHAPTER 9. SUMMARY AND FUTURE WORK		318
9.1	Summary	318
9.2	Future Work	319
9.3	The homogeneously sedimenting gas-solid flow	320
BIBLIOGRAPHY		327
APPENDIX A. THE APPROACH TIME SCALE		350
APPENDIX B. CONVERGENCE CRITERIA TO RESOLVE PARTICLE		
CROSSING OF THE POTENTIAL WELL		351
APPENDIX C. SOLUTION OF CONTACT DYNAMICS		354

APPENDIX D. THE GEOMETRIC INTERPRETATION OF COLLISION LAWS	356
APPENDIX E. CONSTRUCTING THE EFFECTIVE COEFFICIENT OF RESTITUTION	358
APPENDIX F. THE PSEUDO-LIOUVILLE OPERATOR APPROACH FOR SYSTEMS WITHOUT SHORT-RANGED ATTRACTION	360
APPENDIX G. THE EXTENDED PSEUDO-LIOUVILLE OPERATOR FOR SYSTEMS WITH SHORT-RANGE ATTRACTION	363
APPENDIX H. TEMPERATURE SCALING IN HOMOGENEOUS SHEAR OF COHESIVE GRANULAR PARTICLES	366
APPENDIX I. SCALING OF THE CLUSTER LENGTH-SCALE IN HOMOGENEOUS SHEAR OF MODERATELY DENSE COHESIVE SYSTEMS	368
APPENDIX J. MEASURES FOR DETECTING CLUSTERS IN A DISPERSED SOLID PHASE	371
J.0.1 Natural fluctuations in a sub-sample and the roll of domain size	371
J.0.2 Cluster Characterization	373
J.0.3 The Excess Two-Body Entropy	374
J.0.4 The Configurational Entropy of a Point Process	374
J.0.5 Results and Comparison for Clustering Measures	376
J.0.6 Excess Entropy Results	378
J.0.7 Configurational Entropy of a Point Process Results	380
J.0.8 Evaluation	381

LIST OF TABLES

Table 1.1	The accomplishments corresponding to the research objectives.	17
Table 2.1	Parameters in solution of contact dynamics	41
Table 2.2	Numerical fits to parameters for collapse of ε_{eff}	47
Table 3.1	Parameters used in soft sphere DEM Simulation	92
Table 4.1	Parameters used in simple shear simulations of cohesive granules.	133
Table 5.1	Typical system parameters for lab-scale shear simulations of cementitious materials (Wang et al., 2013).	178
Table 5.2	Important non-dimensional groups for sheared cementitious slurries and their typical values.	178
Table 8.1	Parameters for the preliminary studies on the HCGSF using the PR-DNS code PReIBM.	299
Table C.1	Parameters in solution of contact dynamics	354

LIST OF FIGURES

Figure 1.1	The schematic shows examples of closures that need to be developed under the common multifluid paradigm for multiphase - specifically granular and gas-solid - flows. This paradigm is used in several state-of-the-art research codes in the multiphase flow community including OpenFOAM (Weller et al., 1998) and MFIX from the National Energy Technology Laboratory (Syamlal et al., 1993).	4
Figure 2.1	The functional form of the potential vs. separation is shown for various combinations of models for cohesion and a linear spring. The first model is used in the present work, using an offset d_0 , $V_{total, MS}$. The second uses an inner cut-off at which the force saturates $V_{total, saturated}$ Aarons and Sundaresan (2006); Gu et al. (2014); Abbasfard et al. (2016), and the last does not use a short ranged attractive well $V_{total, no well}$ Kobayashi et al. (2013); Berger et al. (2016). All 3 models have the same value of equilibrium overlap, given by Bo^* , but very different values of potential energy at contact and thus Ha_0	33
Figure 2.2	The boundaries between limiting time steps Δt_c (non-cohesive) and Δt_a (cohesive) for varying particle sizes. For a given d_0/l_{ref} , systems that lie in the region below the boundary corresponding to smaller Bo^* are contact time limited.	36
Figure 2.3	Behavior of the effective coefficient of restitution with non-dimensional well-strength Ha_0 for varying values of contact inelasticity Murphy and Subramaniam (2015).	38

- Figure 2.4 Position response for the LSD system ($\varepsilon_{LSD} = 0.9$), alongside the respective exponentially decaying envelopes. We see that beyond a critical value of Π , particles no longer reconstitute. 42
- Figure 2.5 The contact time t_c for the (a) LSD and (b) KK models are plotted for different levels of dissipation. Similar behavior is found for both models. In particular, we find that for higher values of the Π parameter, the contact time increases until a critical value is reached. At the critical value the contact time becomes infinite, and particles become stuck together due to the inhomogeneous term in the contact force law. 43
- Figure 2.6 The scaled difference in ε_c has been plotted for the (a) LSD and (b) KK models for different levels of dissipation. This plot shows us for which non-dimensional parameters the contact coefficient of restitution is not sensitive to the cohesive contact force. For small levels of Π there is practically no difference between cohesive and non-cohesive systems, in terms of contact dynamics. Regions of physical model validity and non-validity, as well as, model sensitivity to particle stiffness are shown in (b). Beyond a critical value of Π , sticking is observed for both the linear and nonlinear models. 44
- Figure 2.7 A collapse of all data is obtained for (a) the LSD and (b) KK models. The collapse given in Eq. 2.10 captures the behavior of ε_c within 1% over the parameters studied. 45

- Figure 2.8 The complete behavior of the effective coefficient of restitution has been plotted for (a) the LSD model and (b) KK model. The surface is colored by the value of Π to demonstrate that at large enough values of Bo^* , the effects of the inhomogeneous term in the contact force law become important, because contact sticking is a function of Π alone, see Fig. 2.6(a) and 2.6(b). Note that the value of Π_{crit} for the LSD case is 3.86, which coincides with sticking boundary for high, corresponding to $Bo^* < 10^{-4}$. Ordinary non-cohesive behavior is observed not far beyond the critical capture region for both LSD and KK models. 49
- Figure 2.9 The shear stress response for the macroscopic homogeneous simple shear test has been plotted for varying values of particle stiffness for the case of (a) $\varepsilon = 0.9$ and (b) $\varepsilon = 0.6$. We find that for both cases, substantial differences between the stress is found when particle stiffness is too small, indicated by large Bo^* 52
- Figure 2.10 The apparent friction coefficient for (a) $\varepsilon = 0.9$ and (b) $\varepsilon = 0.6$ have been plotted. We find a signature very similar to that observed in the shear stress. Namely, an asymptotic scaling of μ is observed as spring stiffness is increased. 54
- Figure 2.11 The parameter Bo_S for (a) $\varepsilon = 0.9$ and (b) $\varepsilon = 0.6$ have been plotted. The Bond number appears to be sensitive to the transition in the shear stress scaling. This scaling reaching a plateau for $Ha_\gamma > 1$ 56

Figure 3.1 (a) The evolution of temperature for several systems with different values for Ha_0 , obtained from numerical integration of eqn. (3.6). In every case, cooling appears to initially follow Haff's law until some finite time. Thereafter, the apparent dissipation increases, and completely inelastic type cooling is observed. The location of this transition depends on the initial ratio of well-energy at contact to particle temperature, Ha_0 . (b) The ratio of cooling rates between eqns. 3.6 and 3.7 are plotted. These comparisons are made for *instantaneous* cooling rates. Large differences in behavior are expected at high values of Ha and as well as slightly inelastic and extremely inelastic ranges. 90

Figure 3.2 (a)-(c) The cooling response for the dilute nearly elastic DEM systems with (a) $Ha_0 = -0.049$ and (c) $Ha_0 = -0.398$ are plotted alongside different cooling models. Approximately (a) 182 collisions and (c) 74 collisions per particle are acquired over the duration of the respective simulations. (b)-(d) The quality factor, $Q = T_g/T_{g,Haff}$, is plotted for the cases of (b) $Ha_0 = -0.049$ and (d) $Ha_0 = -0.398$. From this we clearly see that at early times, the predictions made by the present theory are valid. This short-time is characterized by the predicted time it takes the system to acquire nearly 1 sticking collision partner per particle. . . 94

Figure 3.3 (a) A single snapshot from a realization of the case $Ha_0 = -0.24$ at end of the simulation is plotted. Particles are colored by the number of particles in the cluster. By the end of the simulation the maximum aggregate has 95 member particles. Note there are still an abundance of dimers, trimers, etc. present. (b) The evolution of the temperature for the two cases without cohesion are plotted for reference from a single realization alongside their respective Haff’s Laws. The case of larger ϵ does a better job of predicting the temperature evolution. (c) The evolution of temperature for the cohesive cases is plotted. One can compare the evolution of DEM data for a single realization alongside Haff’s law, Müller’s theory, and our own theory. The plots show quantitative agreement with our cooling theory for short times, despite growing number of aggregates. (d) The evolution of the coordination number is plotted alongside theoretical predictions. We find that the lower value of Ha_0 has a better prediction of contact formation to longer times. Both predictions for $\langle Z \rangle$ appear to break down shortly after each particle on average has at least one contact. 96

Figure 3.4 Pdf of normal relative velocities plotted for 2 different systems. The red line is obtained from i.i.d. Laplacian statistics. The black line is the pdf constructed from the initial condition and is approximately Maxwellian. The case with $\epsilon = 0$ retains a Maxwell core but appears to pick up exponential tails at early times. The pdf of the strongly cohesive case appears to be converging to the case of an i.i.d. Laplacian pdf even at short times. Both cases are taken at $t/\tau_{Haff} (\epsilon = 0.7) = 1.07$ 98

Figure 3.5 (a)-(b) The pair correlation function $g(r)$ is plotted alongside the transverse and longitudinal velocity correlations for the (a) initial condition and (b) end of the simulation for the completely inelastic case. (c)-(f) The pair correlation function and velocity correlations are plotted for systems with cohesion at their final time in simulation. (c)-(d) The correlations are taken from the moderately cohesive case $Ha_0 = -0.24$. (e)-(f) The correlations are taken from the more strongly cohesive case, $Ha_0 = -2.4$. All correlations are calculated from a single realization. 100

Figure 4.1 The appearance of clusters in a snapshot when $Ha_{\dot{\gamma}} = 0.72$, $Bo^* = 4.2 \times 10^{-10}$ and $D/d_0 = 10^4$ 132

Figure 4.2 (a) The collapse of shear stress for smooth spheres with squared inverse shear rate, i.e. $Ha_{\dot{\gamma}} \sim \dot{\gamma}^{-2}$. The collapse is also energetic depending only on the coefficient of restitution. (b) The same collapse is given for spheres with varying strengths of friction and same coefficient of restitution. The collapse remains energetic. 135

Figure 4.3 An improved collapse of shear stress, with the characteristic velocity scale being temperature rather than shear-rate. 137

Figure 4.4 (a) The behavior of the apparent friction is compared among smooth assemblies with differing coefficients of restitution. (b) The apparent friction for cases with varying friction and $\varepsilon = 0.9$ 138

Figure 4.5 (a) The scaling of the average cluster length-scale in the shear direction is given for smooth spheres, which scales as Ha_T^2 . Percolation is observed for $Ha_T > 1$. (b) The cluster length-scale is given for varying coefficient of friction. Percolation does not correlate with the transition for all cases when friction is present. 141

Figure 4.6 (a) The scaled average local cohesive potential is given for smooth cases. A jump in the potential is shown for all cases at $Ha_T = 1$. (b) The scaled average local cohesive potential for frictional cases shows a marked increase that correlates well with the stress transition. 142

Figure 4.7 A depiction of the spherical harmonic mode u_2^1 . The sphere has been stretched according to the magnitude u_2^1 at that location. A peak occurs at $(\phi = 0, \theta = \pi/4)$ and a valley occurs at $(\phi = 0, \theta = 3\pi/4)$ 144

Figure 4.8 (a) The first anisotropic mode for the smooth cases show a clearly the effects of temperature, shear rate, and cohesion on the contact anisotropy as represented by u_2^1 . (b) The frictional cases show that friction tends to enhance anisotropy in the presence of cohesion. 146

Figure 5.1 The stress comparison between experiment and FLD-DEM are shown for a Portland cement slurry at 3 different volume fractions and shear rates. 185

Figure 5.2 The stress comparison between experiment and FLD-DEM are shown for a fly ash slurry at 3 different volume fractions and shear rates. 186

Figure 5.3 The stress comparison between experiment and FLD-DEM are shown for both Portland cement and fly ash at different volume fractions and shear rates. 187

Figure 5.4 The stress comparison between experiment and FLD-DEM, with and without walls, are shown for fly ash at varying volume fractions and shear rates. 188

Figure 6.1 The evolution of the Mach number in gas-solid flow for a DNS case (Mehrabadi et al., 2016b) with two phases of different sized spheres $a_\alpha/a_\beta = 1/3$, Reynolds number $Re = 50$, solid phase volume fraction $\phi_s = 0.3$, $\rho_s/\rho_f = 1000$, and ratio of volume fractions of $\phi_{s,\alpha}/\phi_{s,\beta} = 3$. The Mach number assumes values as large as 1.6 and levels off between 0.3 and 0.4. These Mach numbers are too large to be accurately described by a diffusion velocity. 216

Figure 6.2 Time evolution for the skewness and excess kurtosis for a DNS case (Mehrabadi et al., 2016b) with two phases of different sized spheres $a_\alpha/a_\beta = 1/3$, Reynolds number $Re = 50$, solid phase volume fraction $\phi_s = 0.3$, solid to fluid phase density of $\rho_s/\rho_f = 1000$, and ratio of volume fractions of $\phi_{s,\alpha}/\phi_{s,\beta} = 3$. These moments of the smaller phase closely mirror that of a equidistributed Maxwellian distribution. There are too few samples in the large particle phase to produce accurate time-resolved statistics. 217

Figure 6.3 A graphical illustration of the domain in phase space over which integration will occur. For a given angle θ only some combinations of θ_u and ϕ_u allow collisions to occur. This leads to complicated expressions in the limits of integration. Note that the physical sphere that we are integrating over has a radius of $a_\alpha + a_\beta$, which is where contact takes place. 227

Figure 7.1 A scatter plot is given for fluctuations in acceleration and velocity. These plot helped to model SDEs governing the evolution of single point velocity using the Ornstein-Uhlenbeck process. Figure reprinted from Tenneti et al. (2016). 271

Figure 8.1 The temperature evolution is compared between two HCGSF cases, one inelastic and one elastic. The inelastic cools noticeably faster than the elastic case, which cools only through interaction with the fluid. Eventually, large discrepancies grow between the analytic prediction and DNS for the inelastic case, presumably due to structure formation. 298

Figure 8.2 The evolution of the radial distribution function $g(r)$ is plot for (a) $\varepsilon = 0.8$ and (b) $\varepsilon = 1$. In the case of inelastic particles, there is clear evidence that clustering is occurring in the domain. 304

Figure 8.3 The evolution of the normalized normal relative velocity $\langle w_{\parallel} \rangle / \sqrt{2T}$ is plot for (a) $\varepsilon = 0.8$ and (b) $\varepsilon = 1$. The elastic case is the only case to show the emergence of significant structure. 305

Figure 8.4 The evolution of the normalized second-order longitudinal structure function $\langle w_{\parallel}^2 \rangle / 2T$ is plot for (a) $\varepsilon = 0.8$ and (b) $\varepsilon = 1$. Both cases show some structure formation with the inelastic case being far more significant. 307

Figure 8.5 The evolution of the normalized second-order longitudinal structure function $\langle w_{\perp}^2 \rangle / 4T$ is plot for (a) $\varepsilon = 0.8$ and (b) $\varepsilon = 1$. Both cases show some structure formation with the inelastic case being far more significant. 308

Figure 8.6 The evolution of the net change in the number density of pairs at a given separation as calculated from $\int_0^t \frac{1}{r^2} \frac{\partial r^2 n^{(2)} \langle w_{\parallel} \rangle}{\partial r} d\tau$ 309

Figure 8.7 (a) The relative acceleration between particles due to hydrodynamics for the inelastic case is shown and is found to have a repulsive character. (b) The normalized pressure like term is shown and has the tendency to lead to clustering particles. 310

Figure 8.8 The evolution of the net change in the normalized longitudinal structure function due to transport given by $-\frac{1}{2T} \int_0^t \frac{1}{r^2 n^{(2)}} \frac{\partial r^2 n^{(2)} \langle w_{\parallel}^3 \rangle}{\partial r} - \frac{2 \langle w_{\parallel} w_{\perp}^2 \rangle}{r} d\tau$ 311

Figure 8.9 (a) The sink of energy from the longitudinal structure function due to hydrodynamic interactions $2 \langle A_{\parallel} w_{\parallel} \rangle m_r / 3\pi D \rho_f \nu 2T$. (b) The sink of energy from the transverse structure function due to hydrodynamic interactions $2 \langle A_{\perp} w_{\perp} \rangle m_r / 3\pi D \rho_f \nu 2T$. Both are for the case of $\varepsilon = 0.8$. 312

Figure 8.10 (a) The sink of energy from the longitudinal structure function due to hydrodynamic interactions $2 \langle A_{\parallel} w_{\parallel} \rangle m_r / 3\pi D \rho_f \nu 2T$. (b) The sink of energy from the transverse structure function due to hydrodynamic interactions $2 \langle A_{\perp} w_{\perp} \rangle m_r / 3\pi D \rho_f \nu 2T$. Both are for the case of $\varepsilon = 1$. . 314

Figure 8.11 The time integrated longitudinal acceleration-velocity statistics due to collisions $-\frac{1}{2T} \int_0^t 2 \langle A_{\parallel, coll} w_{\parallel} \rangle d\tau$ 315

Figure 8.12 The mean acceleration in the flow direction $\langle A_x \rangle$ for a pressure driven gas-solid flow. 316

Figure 9.1 The initial distribution of particles in a pressure driven gas-solid flow is shown. Particles are initially homogeneously distributed with no axial velocity. 321

Figure 9.2 The final configuration of particles in a pressure driven gas-solid flow has less uniformity. Particles are colored by their axial velocity and normalized by their granular temperature, i.e. v_x/T_g . Positively traveling particles are in denser regions than particles moving in the negative direction. 321

Figure 9.3 The three dimensional pair correlation function $g(r_i^{(jk)})$ is shown. Here X is the stream-wise direction. We see strong evidence for clustering in this direction in a plane wave-like structure. 323

Figure 9.4 The mean relative velocity normalized by its spatial average in the stream-wise direction $\langle w_x | r_i^{(jk)} \rangle / \langle |w_x| \rangle$ is given. We see that particles that are positively separated have negative relative velocities on average, and vice-versa for particles with negative separations in the stream-wise direction. This indicates particles are moving towards one another on average. 324

Figure 9.5 The fluctuating relative velocity normalized by its spatial average in the stream-wise direction $\langle w'_x w'_x | r_i^{(jk)} \rangle / T_g$ is given. Similar structure to that of the HCGSF is seen. The velocities of particles closer to one another are less random. 325

Figure 9.6 The scaled mean relative acceleration normalized by its spatial average in the stream-wise direction $\langle A_x | r_i^{(jk)} \rangle / \langle A_x \rangle$ is given. It shows significantly more structure than that of the HCGSF, and like the mean relative velocity shows evidence for clustering. 325

Figure 9.7 The scaled source component of the acceleration-velocity covariance in the stream-wise direction $\langle A'_x w'_x | r_i^{(jk)+} \rangle / \langle A'_x w'_x \rangle$ is given. Significant structure shows that the source of fluctuations is stronger for particles that are well separated. Some wake structure is also seen. 326

Figure 9.8 The scaled sink component of the acceleration-velocity covariance in the stream-wise direction $\langle A'_x w'_x | r_i^{(jk)-} \rangle / \langle A'_x w'_x \rangle$ is given. Some structure is seen in this statistic, with the strongest sink being between particles that are well separated. 326

Figure B.1 Error in energy conservation for the binary particle system for different time steps is shown. Symbols are colored by the non-dimensional well-strength Ha_0 352

Figure B.2	This is the error in the full collision dynamics for the LSD system. If the limiting time-step is used, the total error in the effective coefficient of restitution is as high as 3% when the correct minimum time step is used.	353
Figure D.1	(a)-(c) The geometric interpretation of inelastic hard sphere collisions is shown for varying values of ϵ , from elastic, $\epsilon = 1$ to completely inelastic $\epsilon = 0$. The main difference comes from the changing angle of separation of post-collided particles. Note that for all cases, the system is plotted in particle j 's frame of reference. (d) The collision outcome for a particle pair with sub-critical velocity impact velocity. Post-collision, a rotating particle doublet is formed.	357
Figure H.1	The scaling of temperature by the squared shear rate for frictionless particles in simple shear.	367
Figure I.1	(a) The regions where the first order expansions of eq. I.1 are the leading order terms. (b) The scalings of the steady state dimer population are compared showing that the population scales as $v_{crit,a}^4/T_g^2$ in the area near the stress transition.	369
Figure J.1	A snapshot of the homogeneously cooling granular gas at some later time. Particles have begun to collect into clusters due to energy loss coupled with cohesion.	376
Figure J.2	The evolution of the rdf $g(r)$ is plot for (a) the case where particles are cohesive (b) $\epsilon = 0$. Note that the 2nd order structure functions are shown alongside the rdf for the non-cohesive case.	377

- Figure J.3 (a) The radial distribution function is compared to the indefinite integral form of $S_{excess}^{(2)}$ for the cohesive HCG gas. Both evidence of structure at different distances. (b) The $S_{excess}^{(2)}$ metric is compared for the cohesive HCG case and the completely inelastic case. It is clear that the cohesive case is forming far more structure due to a large number of particles in contact. 379
- Figure J.4 (a) The convergence of S_N to the expected results is shown. Slow convergence is expected due to the need to converge the entire distribution. (b) The normalized ΔS_N is shown for both the cohesive and completely inelastic case. Here, we use the radius r_m of a measurement volume which is a ball rather than V_m . The normalization is by the particle radius r_p . More order is observed in the cohesive clustering case. . . . 381
- Figure J.5 A comparison of the two entropic measures at different length scales. Both show similar sensitivity to structure at different scales. 382

ACKNOWLEDGEMENTS

I would like to thank the many mentors that have provided me with guidance and support over the course of my doctoral program. Firstly, I thank Dr. Shankar Subramaniam for the support, guidance, encouragement, and enthusiasm that he has provided. He has offered me the opportunity to work on some very challenging problems, on which we have made some progress. I would like to thank Dr. Sriram Sundararajan for teaching me a small bit about experimental approaches, and without his guidance I would not have been able to understand surface science. I thank my committee members Drs. Pranav Shrotriya, Rodney Fox, Alberto Passalacqua, and James Evans. Dr. Shrotriya has always been willing to discuss microscale problems of interest and has provided me with a great deal of opportunities outside of the research realm. Dr. Fox has provided me with fantastic feedback and advice, while I have been working on many problems presented in this manuscript. I thank Dr. Evans for introducing me to several methods of modeling, not the least of which being stochastic approaches, and for teaching complicated materials with a degree of clarity that I have seldom seen. Thanks to Dr. Passalacqua for providing me with many conversations over the last several years and stepping up to join my committee. I thank my collaborators that I have worked with over the years, including in no particular order Dr. Ravi Kolakaluri, Dr. Gilson Lomboy, Dr. Kejin Wang, Dr. Mohammad Mehrabadi, and Dr. Alope Kumar. Without their discussions and enthusiasm, I would not have been able to complete these works. I would also like to thank my many lab mates, past and present, for many fruitful discussions that provided me with a broader understanding of transport phenomena in general, and also some good times. I would like to thank my friends and family, including my parents and siblings, without whom attending graduate school would not be possible. Lastly, I thank my wife Ida Murphy, who is surely ready to embrace a marriage to a former graduate student.

These works were supported by the National Science Foundation (NSF) awards CMMI 0927660 and CBET 1134500.

ABSTRACT

Granular and multiphase flows are encountered in a number of industrial processes with particular emphasis in this manuscript given to the particular applications in cement pumping, pneumatic conveying, fluid catalytic cracking, CO₂ capture, and fast pyrolysis of bio-materials. These processes are often modeled using averaged equations that may be simulated using computational fluid dynamics. Closure models are then required that describe the average forces that arise from both interparticle interactions, e.g. shear stress, and interphase interactions, such as mean drag. One of the biggest hurdles to this approach is the emergence of non-trivial spatio-temporal structures in the particulate phase, which can significantly modify the qualitative behavior of these forces and the resultant flow phenomenology. For example, the formation of large clusters in cohesive granular flows is responsible for a transition from solid-like to fluid-like rheology. Another example is found in gas-solid systems, where clustering at small scales is observed to significantly lower in the observed drag. Moreover, there remains the possibility that structure formation may occur at all scales, leading to a lack of scale separation required for traditional averaging approaches. In this context, several modeling problems are treated 1) first-principles based modeling of the rheology of cement slurries, 2) modeling the mean solid-solid drag experienced by polydisperse particles undergoing segregation, and 3) modeling clustering in homogeneous gas-solid flows. The first and third components are described in greater detail.

In the study on the rheology of cements, several sub-problems are introduced, which systematically increase in the number and complexity of interparticle interactions. These interparticle interactions include inelasticity, friction, cohesion, and fluid interactions. In the first study, the interactions between cohesive inelastic particles was fully characterized for the first time. Next, kinetic theory was used to predict the cooling of a gas of such particles. DEM was then used to validate this approach. A study on the rheology of dry cohesive granules with and

without friction was then carried out, where the physics of different flow phenomenology was exhaustively explored. Lastly, homogeneous cement slurry simulations were carried out, and compared with vane-rheometer experiments. Qualitative agreement between simulation and experiment were observed.

Lastly, the physics of clustering in homogeneous gas-solid flows is explored in the hopes of gaining a mechanistic explanation of how particle-fluid interactions lead to clustering. Exact equations are derived, detailing the evolution of the two particle density, which may be closed using high-fidelity particle-resolved direct numerical simulation. Two canonical gas-solid flows are then addressed, the homogeneously cooling gas-solid flow (HCGSF) and sedimenting gas-solid flow (SGSF). A mechanism responsible for clustering in the HCGSF is identified. Clustering of plane-wave like structures is observed in the SGSF, and the exact terms are quantified. A method for modeling the dynamics of clustering in these systems is proposed, which may aid in the prediction of clustering and other correlation length-scales useful for less expensive computations.

CHAPTER 1. INTRODUCTION

1.1 Background

Granular systems are composed of discrete interacting particles and occur naturally over a large range of size scales, from microns to meters. Examples of such granular particles present themselves in a variety of industrial and natural settings on earth, as well as in extraterrestrial environments. In industry, one finds examples of granular materials in biomass reactors (Nacheinius et al., 2015; Marmur and Heindel, 2016), wet granulation of pharmaceuticals (Iveson et al., 2001), powder mixing (Nienow et al., 1992), filtration (Tien and Ramarao, 2007; Kolakaluri et al., 2015), carbon dioxide capture technologies (Sjostrom and Krutka, 2009), food production (Mounfield and Edwards, 1994), construction materials (Lomboy et al., 2011, 2012, 2013), oil recovery/transport (Pettersen, 2007), and nuclear pebble bed reactors (Rycroft et al., 2006), to name a few. In natural settings the granular nature of materials is key to understanding phenomena such as erosion, earthquakes, landslides, and avalanches. Finally, on the extraterrestrial side, understanding granular materials is key to understanding contamination due to Lunar and Martian regolith (Colwell et al., 2007), asteroid mining (Miyamoto et al., 2008), and the formation of the early solar system (Blum et al., 2000; Kothe et al., 2013).

While types of granular particles may vary greatly, exhibiting infinite combinations of sizes, shapes, and material compositions, there are several properties that differentiate granules from more classical particles such as atoms and suspended colloids. Firstly, granular particles interact due to material deformations, and hence, they are governed by the laws of continuum solid mechanics. Granular particles exhibit inelasticity, that is their interactions do not preserve energy in the macroscopic degrees of freedom. Friction and large surface asperities enable individual particles to interact through their angular movements and momentum. These properties

ensure that even a simple system such as a gas of granular particles behaves very differently from its molecular counterpart (Goldhirsch and Zanetti, 1993; van Noije et al., 1997, 1998a). Such granular gases continuously cool through collisional dissipation and have been observed to form gigantic structures known as clusters in the flow.

The properties of granular materials also give rise to unique transport phenomena in driven non-equilibrium systems, which are absent from traditional continuum flows. Phenomena such as the Brazil nut effect (Alam et al., 2006; Sun et al., 2006) and stratification in bi-disperse granular heaps and chute flows (Schlick et al., 2016) demonstrate the unusual nature of granular materials. However, it is the phenomena of jamming that has probably created the most interest in granular materials, due to an analogy with glassy materials (Majmudar et al., 2007; Song et al., 2008). During jamming the rearrangement of grains arrests as a critical value of volume fraction, strain, or stress is achieved, preventing further flow of the material. Note that these jamming points are not unique and exhibit hysteresis (Luding, 2016). Jamming is also accompanied by the emergence of large coherent and fragile force structures known as force chains (Cates et al., 1998b,a) and preceded by the appearance of large transient clusters and vortical structures (Saitoh and Mizuno, 2016) in shear flows at lower volume fractions. The behavior near jamming elucidates a tight connection between the emergence of correlations and phase transition behavior in granular media.

The emergence of structure in granular materials during jamming and in the long-time behavior of the cooling granular gas presents challenges for continuum modelers. The emergence of structure and its influence on transport and mixing is equally important from a more applied perspective. For example, in a screw mixer where heat carrying granules are mixed with biomass to achieve pyrolysis, the dispersion of granular materials is critical to achieving efficient production of bio-fuels (Marmur and Heindel, 2016).

In practice, coarse-grained modeling of industrial scale granular problems must be used. Due to the large computational cost of both number of particles and temporal resolution, interactions between individual particles cannot be simulated. For example, in a dilute system of 100 micron particles with solid volume fraction ϕ_s of 10%, one cubic foot contains 5.2 billion particles. Further, numerical constraints on the time-resolution set by the particle stiffness ensure that

particles can only move a tiny fraction of their diameter in a single time-step, making simulation of large time-scales infeasible. In continuum modeling efforts, one must obtain closures for the evolution of volume fraction, velocity, and temperature (fluctuation energy) fields as is shown on the left side of Fig. 1.1. The nature of these closures depends on the regimes of flow, which are differentiated by observed rheological scaling (Vidyapati and Subramaniam, 2013). The kinetic theory of granular flows is the traditional method of coarse-graining in relatively dilute rapid granular flows (Brilliantov and Pöschel, 2004). The fine-grained description here referring to granular particles interacting through collision laws. Under these circumstances, the method of moments may be applied on the granular version of the Boltzmann-Enskog equation, yielding coupled sets of moment equations. These moment equations govern the transfer of mass, momentum, and heat, and produce terms such as granular cooling that are absent from molecular theories. The accuracy of the closures produced from the kinetic theory, i.e. Boltzmann-Enskog equation, relies on the accuracy of the molecular chaos assumption, scale separation in single point statistics characterized by low Knudsen numbers, and more importantly, it relies on the absence of non-trivial non-scale separated correlated structures in the flow characterized by two-point statistics.

In slower denser flows of granular materials, with solid phase volume fractions of $\phi_s > 0.4$, kinetic theory is inapplicable for extracting continuum closures. Rather, simulations using the discrete element method (DEM) and experiments of canonical flow set-ups are often used to obtain closures. Here the form of constitutive relations and transport equations is presumed, and closures are obtained by measurements of observable quantities, e.g., stress in terms of strain. This approach has the advantage that correlations, e.g., in correlated motion of neighbor particles, may emerge in DEM and experimental set-ups. Hence, correlations need not be explicitly included or modeled as in the case of kinetic theory, where uncorrelated neighbors are assumed in the molecular chaos ansatz. However, challenges remain from assuming the form of closures in transport equations. There is a growing body of work, which indicates that in general quantities that appear in the virial theorem such as microstructure (Sun and Sundaresan, 2011) and fluctuations (Irani et al., 2014; Berzi and Jenkins, 2015a,b; Irani et al., 2016) are not fast and local variables that can be slaved to the slow local macroscopic kinematics, i.e.

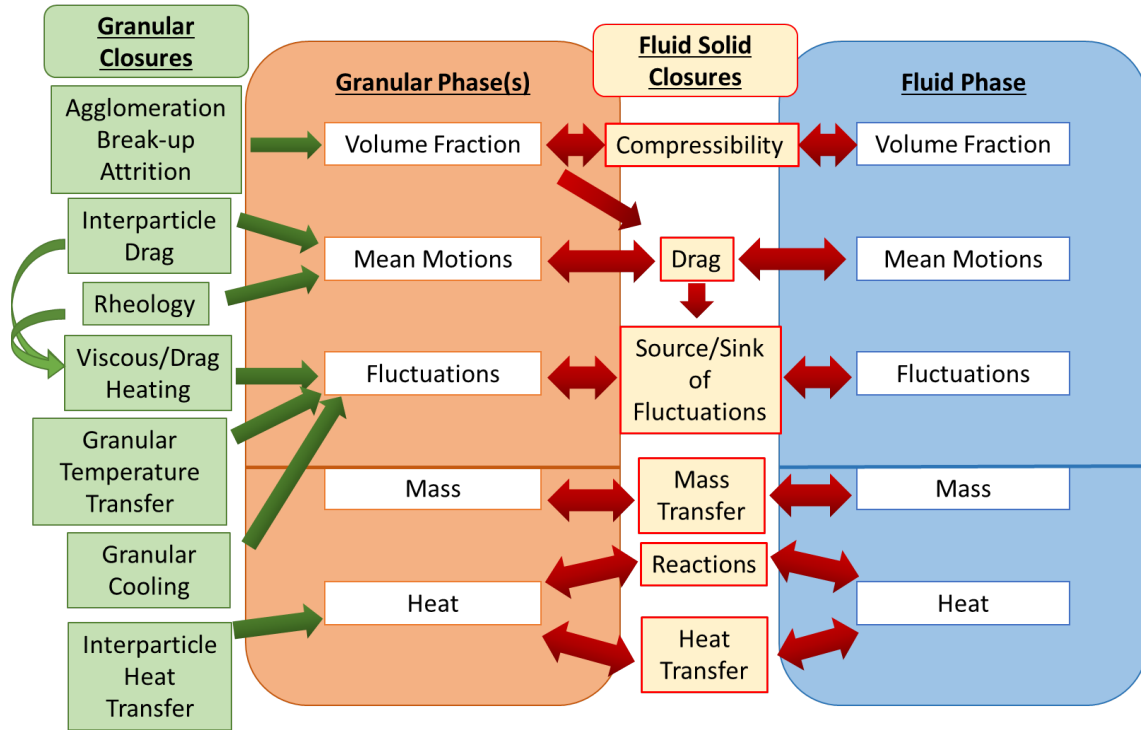


Figure 1.1 The schematic shows examples of closures that need to be developed under the common multifluid paradigm for multiphase - specifically granular and gas-solid - flows. This paradigm is used in several state-of-the-art research codes in the multiphase flow community including OpenFOAM (Weller et al., 1998) and MFIX from the National Energy Technology Laboratory (Syamlal et al., 1993).

the shear rate. In other words, models that only quantify shear stress in terms of strain rate and confining pressure are incomplete, such as the $\mu(I)$ rheology (MiDi, 2004) for hard-sphere granular flows. How to include the effect of slow evolving structure on closures produced by DEM and experiments is highly non-trivial and remains unresolved. Specific challenges on the subject of granular flows will be discussed further in Section 1.2.

Many multiphase systems are far more complicated than those modeled in purely granular settings, where particles may only interact through compliant contacts. There are several commonly encountered interactions leading to attraction and repulsion of particles, e.g. van der Waals, electrostatic forces, and liquid bridging (Israelachvili, 2011). In addition, in terrestrial environments granular particles are also always immersed in fluid. These additional interactions qualitatively alter the nature of the interactions, such as the range of interaction and mecha-

nisms of energy dissipation. Emergent behavior such as clustering should also be affected. For example, interparticle forces such as van der Waals and longer-ranged attractive forces have been shown to hasten and qualitatively change the formation of structure in dilute granular gases (Müller and Luding, 2011; Gonzalez et al., 2014; Murphy and Subramaniam, 2015). In the case of the van der Waals force, sintered-like clumps develop rather than the looser deforming clusters of ordinary granular gases. In more applied scenarios such as lab-scale fluidized beds, particle structures form at a variety of scales, from a few to several hundred particles (Cocco et al., 2010; Chew et al., 2011). The structure formation in such flows may be due to interparticle forces, hydrodynamic interactions or both. Additionally, in computational studies of homogeneous sedimentation in a gas-solid flow, particles were shown to develop clusters and vortical structures even in the absence of characteristic granular interactions, e.g. inelasticity (Yin et al., 2013; Fullmer and Hrenya, 2016) and collisions (Fox, 2016). That is to say that the structure formation can occur due to momentum transfer between the fluid and solid phases alone. The clusters in such flows also drive turbulence in the gaseous phase, which may also eventually break up clusters (Capecelatro et al., 2015). Such instabilities may significantly and adversely affect mixing, heat and mass transfer and subsequent yield of products in chemical reactors.

The way in which the interactions between gas and solid phases in multiphase reactors are described in a coarse-grained *two/multi-fluid* description in modern state-of-the-art codes is depicted in Fig. 1.1. The *averaged* multifluid model treats solid and fluid phases as interpenetrating continua. While this coupling diagram describes the modeling paradigm for many gas-solid flow applications, the main applications under consideration here are fluidized and circulating fluidized bed reactors. These beds operate by attempting to uniformly suspend particles in a flow to sustain a reaction or transport phenomena at the particle fluid interface. The reactors operate under a number of different conditions, which manifest different phenomena depending intimately on the size and density of the particles (Geldart, 1973). Clustering and flow patterns, i.e. instabilities, develop in these devices that can span the scale of pilot scale devices (Chew et al., 2011). Moreover, instabilities also occur in fully resolved PR-DNS simulations without any macroscale inhomogeneity to trigger them (Yin et al., 2013; Murphy

et al., 2015). Modeling closure terms in the presence of these instabilities is non-trivial.

Within the multifluid framework, interactions between phases (cf. 1.1), such as average drag (global drag in experiments) and source and sinks of fluctuations, need to be closed. Furthermore, some of these terms are subject to physical constraints, e.g. the interphase turbulent kinetic energy transfer principle, which couples the source to fluctuating motions to the mean momentum equation through the mean interphase drag (Xu and Subramaniam, 2007; Mehrabadi, 2016). An analogous behavior occurs in pure granular materials, where sources to granular temperature arise from viscous heating and the mean drag between particle species (Jenkins and Mancini, 1987, 1989; Alam et al., 2006; Marchisio and Fox, 2013; Murphy and Subramaniam, 2014). Note that the work considered in this thesis, we restrict ourselves to isothermal systems without mass transfer or reactions, though work in this area is on going. One of the key challenges in modeling the closures and coupled terms in these applications is a lack of scale separation, where there is significant structure at scales both smaller and larger than some coarse-graining scale L_g .

Structure that arises in flows influences all of these closures. For example, it is well known that clustering changes the amount of mean drag and hence also the generation of fluctuations in the fluid (Mehrabadi et al., 2016a). Similarly, in extended kinetic theory treatments of granular flows, correlations in neighboring particle motion connected to slower cooling rates have been found to influence the rheology of granular flows (Berzi and Jenkins, 2015a). There have been several attempts to incorporate the effects of these instabilities on closures in gas-solid flows. For example, the energy minimization multi-scale (EMMS) model (Li et al., 1999) attempts to partition momentum exchange, or drag, interactions into clustered and isolated particle phases, both with unique values for the drag. The portion of particles in these two phases is then slaved to the coarse-grained variables. Similar approaches have been followed, producing data from clustered Particle-Resolved Direct Numerical Simulations (Mehrabadi et al., 2016a), although no such partitioning of drag into clustered and dispersed phases is made. In practice, both of these models require clusters to be smaller than L_g and clustering to be a "fast" process, e.g. lifetime of a cluster is smaller than the time-scale it takes a cluster to traverse a distance L_g . More sophisticated mesoscopic models (Fox, 2014; Capecelatro et al., 2016) also require a

priori knowledge of emergent cluster statistics to be fully closed and slaving of fluctuations at small scales.

The common thread among the disparate applications in granular and multiphase flow applications is the close connection between the emergence of structure on different scales, and its tight connection to coarse-grained modeling. In order to understand how the various interactions on the scale of the particle are coupled to the formation of structure at larger scales, particle scale simulations will be carried out in both granular and multiphase contexts. How these various interactions lead to the formation of interesting structures and their affect on transport phenomena will be explored.

1.2 Challenges

There are several challenges associated with the simulation and modeling of granular and fluid-solid flows. Key challenges are listed as below:

- **Simulation of cohesive granular materials:**

Cohesive granular materials arise in many industrial and natural contexts. DEM may be used to model cohesive granular materials in much the same way as non-cohesive particles. The numerical constraints on particle stiffness and time-steps for the accurate simulation of non-cohesive granular materials are well known (Cleary and Sawley, 2002; Campbell, 2002). These constraints ensure that not only are microscale phenomena, such as particle collisions, well represented, but that collective behavior such as flow patterns are also accurately predicted. Such information on constraints is incomplete for cohesive granular materials. For example, information on how a particular cohesion model changes the restitution behavior of particles during a collision is incomplete, especially in a quantitative sense (Moreno-Atanasio et al., 2007; Gu et al., 2015; Liu et al., 2016; Wilson et al., 2016). Since we are addressing problems from a microscopic approach, it is essential that numerical constraints and changes in microscopic behavior in the presence of cohesion are understood. Furthermore, addressing this knowledge gap provides invaluable insight for analyzing the behavior of macroscopic cohesive granular systems.

- **Aggregation, break-up, and rheology in flows of cohesive granules:**

Flows of cohesive granular materials exhibit transitions in rheological behavior that do not occur in non-cohesive granular materials (Aarons and Sundaresan, 2006; Rognon et al., 2008; Irani et al., 2014; Gu et al., 2014; Singh et al., 2014; Saitoh et al., 2015; Berger et al., 2016). The rheology of these flows is influenced by many factors. In non-cohesive flows, the rheology of non-cohesive granular flows has been shown to depend greatly on the formation of large transient clusters at solid volume fractions close to jamming (Mills et al., 2008). In cohesive systems, granular aggregates form, which may change the rheology. If aggregates grow to the size of the system, force chains may span the transient clusters and alter the nature of momentum transfer, from collisional to elasto-plastic, as is seen in dense granular flows. Hence, the understanding of how cohesive granular materials aggregate and break-up under flow is essential to understanding the rheology of such systems. The connection between particle properties and models to aggregation/rheology is unclear. In addition, emergent unstable behavior such as shear banding remains poorly understood.

- **Rheology of slurries of cementitious particles:**

Cementitious slurries are composed of particles undergoing surface hydration reactions while immersed in water. They share some similarities with the dry cohesive counterparts. However, the principal difference is that collisions in a slurry of micron-sized particles are not allowed to rebound as in foams and emulsions. The particles that compose cements are extremely polydisperse, with a size range from sub-micron to millimeters (Bentz et al., 1999). The particles themselves are also multicomponent, in the sense that they are composed of many different and heterogeneously organized chemical species (Stutzman, 2004). Particle-scale simulation of these systems requires a detailed knowledge and characterization of surface topography and different interparticle forces arising from van der Waals forces, electrical double layers, and friction. Such information is attainable from atomic force microscopy (Lomboy et al., 2011, 2013), but challenges remain in how to account for the large degree of uncertainty in the surface details for ground

cementitious particles. Further, it remains unclear how such inputs for the simplest case of homogeneous monodisperse particles will affect the overall macroscopic behavior. How the aforementioned interparticle forces affect the microstructure and rheology of cement pastes is of great interest to designers of cements and construction engineers.

- **Instabilities in gas-solid flows:**

In gas-solid flows, clusters have been observed to form in experimental (Cocco et al., 2010; Chew et al., 2011; McMillan et al., 2013) and computational studies (Yin et al., 2013; Capecelatro et al., 2014), and even predicted in theoretical studies (Koch, 1990; Koch and Sangani, 1999). Each of these approaches comes with its own strengths and weaknesses. For example, experimental studies are able to produce clustering in practical settings, but the resulting clustering may be difficult to study due to intrusive measurements and may be difficult to quantify. Additionally, it is difficult to deconvolute the effects of walls and confining geometries and gas-particles interactions on particle dispersion, making it difficult to generalize the phenomena.

Theoretical studies reminiscent of mean-field kinetic theory have also been carried out, but are only valid at low Reynolds numbers, i.e. Stokes flow, and high ratios of solid to fluid density (Koch, 1990). The resulting mean-field theories rely on inhomogeneous mechanical perturbations as a source of fluctuations. However, in statistically homogeneous systems natural fluctuations exist and are the source of any instability. That is to say that there is a spectrum of fluctuations with amplitudes characteristic of the system as is the case of equilibrium gases and homogeneous isotropic turbulence (Pope, 2000). Furthermore, information on natural fluctuations that lead instabilities, e.g. velocity fluctuations at all scales, are missing from mean field kinetic theory descriptions (Ortiz de Zarate and Sengers, 2006; van Noije et al., 1997).

Additional studies, both numerical and theoretical, also exist on particle dispersion in one-way coupled isotropic turbulence (Zaichik and Alipchenkov, 2003; Rani et al., 2014; Gustavsson and Mehlig, 2014a; Bragg et al., 2015). However, in multiphase flows velocity fluctuations in the fluid phase are driven by the particle phase. The phases are two way

coupled. Hence, analysis of particle migration in studies on isotropic turbulence are of limited value.

Computations of high physical fidelity are becoming increasingly useful in the study of instabilities. Still, PR-DNS studies that resolve boundary layers near particles are severely limited due to high computation demands. Only small domain sizes and relatively short simulation durations are accessible due to resolution requirements and larger Reynolds numbers. Although, small domains $L/D = 20$ do exhibit clustering (Uhlmann and Doychev, 2014; Murphy et al., 2015), coarse-grained studies are often used, employing large-eddy simulation (LES) (Capecelatro et al., 2014) or Reynolds averaged Navier-Stokes simulations (RANS) (Fullmer and Hrenya, 2016). However, questions about physical accuracy remain in the absence of more resolved simulation data. How to meaningfully compare the results of different simulation techniques is also an open question.

Formation of exact theories for the evolution of two-point particle statistics that require closures is useful. Closure statistics may be extracted from both PR-DNS and coarse-grained treatments, i.e. RANS and coupled DEM and LES. Understanding how a coarse-grained model differs from the predictions of PR-DNS is essential for a quantitative physical understanding of clustering in gas-solid flows. Models, informed by the two-point framework, may also be used to improve coarse-grained models and reduce the hefty computational cost of simulating large gas-solid flows.

1.3 Research Objectives

The primary objectives of this work broadly falls under the use microscale simulations, both DEM and PR-DNS, to obtain information on the emergence of structure and its affect on closures in granular and multiphase flow problems noted in the preceding sections. However, the specific objectives fall into two categories:

- Explore and characterize the microstructure, rheology, and transport of cohesive slurries, specifically cementitious slurries, from a first principles approach.

- Characterize and model the transport, clustering, and separation of solid phases in gas-solid flow environments as applicable to fluidized beds.

The first objective is broken up into four sub-objectives, which aim to approach the complicated nature of cementitious slurries by first treating simpler sub problems. Rigor is brought to each individual sub-task, to ensure a high degree of confidence when treating the full problem of shear flow of submerged cohesive granules. Likewise, the clustering and transport of the solid-phase in gas-solid flows is also broken up into several individual sub-tasks. The first tasks focus on casting and modeling exact equations of particle transport in fluidized bed environments. Several different canonical flow scenarios are then considered. Lastly, stochastic modeling of the exact equations to produce clustering using PR-DNS data is then considered.

The specific research objectives in this study are as follows:

1. Determine the changes in the dynamics of head-on collisions between spheres brought on by the introduction of cohesion.
2. Examine the simplest system of cohesive spheres, the homogeneous cohesive cooling granular gas.
3. Examine regime transition behavior in simple shear flows of cohesive granules, with and without friction.
4. Compare the rheology of cementitious slurries between DEM simulations using detailed information about interparticle interactions obtained from Atomic Force Microscopy and vane rheometer experiments.
5. Develop a solid-solid drag law that accounts for the granular temperature evolution and is applicable for all particle phase Mach numbers.
6. Develop an exact equation framework for analyzing clustering in statistically homogeneous gas-solid flow using data from both specifically PR-DNS simulations and other Euler-Lagrange simulation methodologies. Determine methods for modeling such flows.

7. Examine the unstable clustering and vorticity formation behavior in a homogeneously cooling gas-solid flow.
8. Examine the unstable behavior in a pressure gradient driven gas-solid flow.

These objectives are discussed in more detail below.

Determine head-on collision behavior for cohesive granules

The restitution behavior for inelastic hard spheres with van der Waals interactions has been known in the scientific literature for some time. However, when a soft-sphere model is used the restitution behavior has not been clearly understood, primarily in regard to the particle stiffness and the interaction between dissipation and cohesion (Moreno-Atanasio et al., 2007; Gu et al., 2015; Liu et al., 2016; Wilson et al., 2016). Moreover, the guidelines for selection of numerical parameters with the additional short-ranged attractive well, such as time step, have not been addressed in satisfactory detail. In the current study we present a model for determining the restitution behavior for two commonly used soft-sphere models with cohesion added. The connection between stiffness requirements for accurate solutions and physical applicability of the cohesion model is also addressed. Time-scale restrictions are also established and related to the analytic time-scale produced by the amount of time taken to cross the attractive potential well. Finally, it is shown that if proper care is not taken in regard to selection of particle stiffness, a rheological regime transition for simple shear is not predicted correctly. This result is consistent with several studies on fluidization Moreno-Atanasio et al. (2007); Kobayashi et al. (2013); Liu et al. (2016); Gu et al. (2015, 2016); Wilson et al. (2016). The source of error is attributed to two distinct mechanisms that allow particles to aggregate, kinematic and contact sticking. Particles with insufficient stiffness exhibit contact sticking, while physically reasonable stiffness leads to almost exclusively kinematic sticking. Opportunities for computational acceleration are also discussed.

The homogeneously cooling cohesive granular gas

The homogeneously cooling cohesive granular gas is an analog of a hard-sphere gas, used to model simple molecular gases (Haff, 1983). In this case, particles lose energy due to inelastic collisions and also have an additional short-ranged attractive well, which may serve to aggregate particles. The Pseudo-Liouville theory (Ernst et al., 1969; van Noije et al., 1998a) is employed to study this system. The theory is used to predict cooling rates for such 'sticky' gases, in terms of solid volume fraction ϕ_s , inelasticity $1 - \epsilon^2$, and the ratio of the well potential at contact to the granular kinetic energy Ha . The theory is valid in the dilute limit and where only binary particle collisions are expected. In addition to the cooling law, a coordination number evolution equation and a set of population balance equations for long-time evolution are also derived. It is shown that the former can be used to predict the breakdown of the theory. The results are compared with both DEM and the theory of Müller and Luding (2011). The two theories differ in their treatment of what occurs in a collision, with the theory presented herein explicitly treating aggregation. It is found that the theory developed in this study correctly predicts both the cooling rate and the time where the temperature should diverge from predicted behavior. The theory also performs better than the theory of Müller and Luding (2011) in the regime of interest, indicating that explicit treatment of aggregation is necessary for treating inelastic hard-sphere gases with short-ranged attraction.

Regime transition in homogeneous simple shear of cohesive granules

The transition in rheological behavior of cohesive granules below the jamming volume fraction of non-cohesive granules is studied in more detail (Aarons and Sundaresan, 2006; Rognon et al., 2008; Gu et al., 2014). Frictionless systems are treated first. The transition is found to occur at a value of $Ha_T = 1$, an energy scaling which is the ratio of interparticle cohesive energy to kinetic energy. This energy scaling uses the granular temperature T and diameter D to define an energy scale. Frictional cases are also addressed and found to exhibit a different rheological transition but also follows an energetic scaling. Frictionless systems are found to be thermodynamically unstable but mechanically stable at sufficiently large cohesion. However,

if enough friction is present ($\mu_f \geq 0.1$) then the pressure remains positive. The emergence of structure is then explored using several different measures. Scaling behavior is extracted, and the regime transition is found to be due to percolation of the simulation domain by emerging clusters. Cohesion is seen to decrease fabric isotropy, while friction promotes anisotropy consistent with other studies (Singh et al., 2014; Berger et al., 2016). The anisotropy is shown to be at the heart of why friction retains positive pressures with increasing cohesion. A connection to non-local stress closures is also discussed (Kamrin and Koval, 2012; Berzi and Jenkins, 2015a).

Cement rheology

Simulation of cement pastes is carried out using a combination of fast lubrication dynamics (FLD) (Kumar and Higdon, 2010; Kumar, 2010), an approximation to Stokesian dynamics (Brady and Bossis, 1988) for creeping, i.e. low Reynolds number, particle laden flows, and DEM. A non-dimensional and time-scale analysis is performed and it is predicted that such flows form physical gels under shear, i.e. a deforming network of particle contacts. Simple shear flow calculations are performed with interaction forces obtained from AFM. Vane-rheometer experiments on slurries of fly ash and Portland cement at different solid volume fractions $\phi_s = 0.35 - 0.55$ were used for comparison. The correct trends are predicted with volume fraction, friction coefficient, and Hamaker constant. The correct rheological scaling with shear rate is also made, and shown to behave approximately as a Bingham fluid. The effect of confining walls is also considered. However, quantitative agreement between stresses in simulation and experiment remains elusive, consistent with dry, non-cohesive studies (Vidyapati et al., 2012).

Solid-Solid Drag Law

The description of the frictional force felt as two gases of granular particles move through one another is known as a solid-solid drag law. This force is present even in the absence of number density or thermal gradients, which are responsible for segregation in hydrodynamic, i.e. low Knudsen number, inhomogeneous flows (Garzo et al., 2007a,b). While several theories for the solid-solid drag flow exist, they can be valid at different Mach numbers, i.e. the ratio of interphase slip to thermal speed of the granules. For example, hydrodynamic theories produce

drag laws valid for infinitesimal Mach numbers (Jenkins and Mancini, 1987, 1989; Alam et al., 2006). An infinite Mach number theory is the standard (Syamlal, 1987) in the software MFIx. Note that other more advanced theories exist that account for more moments, but do not produce explicit drag laws (Marchisio and Fox, 2013). The theory developed herein utilizes the Pseudo-Liouville theory to rigorously derive the solid-solid drag force and thermal coupling between homogeneous counter-flowing solid-phases. Comparison with both DEM and PR-DNS (Mehrabadi et al., 2016b) cases will then sought.

Exact framework for clustering in homogenous gas-solid flows

An exact equation set is derived for the transport of the two-point density in statistically homogeneous gas-solid flows. These equations are similar to those used to analyze the transport of inertial particles in one-way coupled isotropic turbulence (Reeks, 1980; Zaichik and Alipchenkov, 2003; Rani et al., 2014; Bragg and Collins, 2014b). This equation set is used to produce coupled hierarchical transport equations for Eulerian moments, which evolve in separation space. These equations benefit from being able to be modeled by generic Euler-Lagrange methods for gas-solid flows, e.g. RANS, large eddy simulations, PR-DNS, etc. The moments describe the evolution of the radial distribution function, often used to indicate clustering, and velocity correlations or structure functions (Pope, 2000). Spherically symmetric equations are also produced for modeling isotropic cases. The equations appear remarkably similar to those produced in the Reynolds stress transport theory of isotropic turbulence (Pope, 2000). The structure of the equations is then discussed, and two possible mechanisms of clustering are identified connected to vorticity and cluster formation.

Fokker-Planck equations (FPE) are proposed for modeling the unclosed terms in the moment transport equations, by identifying corresponding source and sink terms in the FPE and exact equation set. The equations must be simulated using stochastic differential equations, which implicitly model transport terms in the FPE. The effect of modeling under different stochastic systems is discussed. An optimization procedure must be carried out, in order to match the transport terms arising in the equations.

The homogeneous cooling gas-solid flow

The first system to be explored using the exact equation set is the homogeneously cooling gas-solid flow (HCGSF). Yin et al. (2013) first treated this system using lattice Boltzmann simulations and observed the appearance of both vorticity and later clustering. However, a mechanistic explanation for the emergence of structure was never obtained. In these simulations, particles are prepared initially as a randomly arranged assortment of spheres with randomly initialized velocities in a quiescent gas. The particles are then allowed to evolve. The gas of particles cools through interaction with the fluid, which eventually dissipates the fluctuating energy through viscosity. Inelasticity also dissipates energy when present. This system is purely dissipative and spherically symmetric in separation space, allowing for better converged statistics compared to systems without spherical symmetry. Structure in relative velocity statistics is found to develop. Clustering indicated by structure in the density correlations also develops, if inelasticity is present. The mechanism of clustering is also discussed.

The pressure gradient driven gas-solid flow

In all terrestrial applications, gravity plays a significant role due to the large differences in density between in gas and solid in industrial gas-solid flows. A system similar to the HCGSF is studied in this work, where a mean pressure-gradient rather than gravity is used to drive the flow. The product of the mean slip between the gas and solid phase and mean drag force provide a power, which is required to sustain the flow. This power also feeds the fluctuations in both the solid and fluid phases, and also has a spectrum or two-point structure. We are interested in how spatial signatures in the source and sink statistics relate to and result in clustering.

A coarse grid PR-DNS $D/\Delta x = 10$ of the pressure-driven system is carried out at ratios of particles to fluid density of 100 and 1000. Here D is the particle diameter and Δx is the grid spacing. The systems are elastic and prepared at a volume fraction of $\phi_s = 0.2$. We find from DNS that statistics in the two-point theory do show evidence of clustering. The clustering manifests itself in the development of 'plane-wave' like structures and voids within a realization.

Several statistics are quantified. The need for larger scale simulations is discussed.

1.4 Accomplishments and Future Work

Completed tasks, which were involved in the research objectives, are given in Table 1.4.

Table 1.1 The accomplishments corresponding to the research objectives.

Objectives	Results	Conclusions
Determine the effect of cohesion on the collision dynamics between two spheres	<ol style="list-style-type: none"> 1. Numerical constraints for performing accurate macro-scale simulations are established. 2. The region in the problem's parameter space where the model is physically applicable is established. 3. The restitution and sticking behavior is completely characterized. 4. Two different mechanisms for aggregation/sticking are identified, kinematic and contact sticking. 5. The effect of the two sticking mechanisms on the rheology of macro-scale shear is observed. 6. Possible methods of computational speed-up are identified. 	<ol style="list-style-type: none"> 1. Accurate and physically applicable macro-scale simulations require numerically stiff particles. 2. Physically reasonable particles almost exclusively stick or aggregate due to a kinematic sticking mechanism. 3. The two different mechanisms for sticking lead to quantitatively different rheological scalings. 4. Computational speed-up can be achieved in absence of friction by assuring that a few non-dimensional parameters are not altered.

Table 1.1 (Continued)

Objectives	Results	Conclusions
Study the homogeneously cooling cohesive granular gas by means of kinetic theory and DEM simulations.	<ol style="list-style-type: none"> 1. The cooling behavior for a gas of cohesive granules is solved using kinetic theory, namely the pseudo-Liouville theory. 2. The cooling law is validated using DEM simulations. 3. A time scale for the breakdown of the cooling law is predicted and validated. 4. Two-point structure of the density and velocity field are characterized. 5. The granular temperature evolution is compared to existing cooling laws. 	<ol style="list-style-type: none"> 1. The kinetic theory is capable of predicting the evolution of granular temperature and aggregation rate at time scales, where binary collisions dominate. 2. The present theory performs better at predicting the evolution of granular temperature than competing theories. 3. The two-point structure indicates that grazing collisions are suppressed by cohesion, retaining the accuracy of the molecular chaos assumption. 4. Instabilities in granular gases with cohesion are qualitatively different from non-cohesive granular gases.
Study the rheology of dry cohesive granular assemblies.	<ol style="list-style-type: none"> 1. DEM simulations of dry cohesive granules in shear are carried out with and without friction. 2. A rheological transition is determined to be the result of percolation of particle contacts. 3. The scaling of the rheology is characterized in the region in shear rate near a rheological transition. 4. The structure of the shear flows is analyzed, including emerging length scales and anisotropy. 	<ol style="list-style-type: none"> 1. The correct scaling of structure, e.g. coordination number and cluster length-scale, with variation in granular temperature and cohesion are correctly predicted in the region of the transition. 2. The scaling of the transition in both non-frictional and frictional cases is energetic. 3. Frictional cases exhibit greater anisotropy. 4. Smooth sphere cases are metastable under the percolation threshold and have an isotropic microstructure. 5. Local rheology models are likely inadequate for device scale flows.

Table 1.1 (Continued)

Objectives	Results	Conclusions
Compare the rheological predictions from simulation of cementitious slurries with vane rheometer experiments.	<ol style="list-style-type: none"> 1. Coupled fast lubrication dynamics simulations of cementitious slurries, Portland cement and fly ash, are carried out using interparticle force data obtained from atomic force microscopy. 2. The rheological scaling is compared with macroscopic vane rheometer experiments and found to be in qualitative agreement. 3. The structure in these flows is predicted and analyzed. 	<ol style="list-style-type: none"> 1. The slurries are correctly predicted to percolate. 2. Numerical and experimental results predict the same qualitative rheological trends, i.e. that of a Bingham fluid. 3. Stress measurement results disagree quantitatively by about an order of magnitude. 4. Fly ash, which is more spherical than Portland cement, shows better agreement between simulation and experiment. 5. The inclusion of walls yields better agreement between simulation and experiment.
Produce a solid-solid drag law for polydispersed particles using kinetic theory.	<ol style="list-style-type: none"> 1. Kinetic theory is used to obtain evolution equations for slip and granular kinetic energy for polydispersed particle flows with arbitrary Mach number. 2. Homogeneous PR-DNS simulations with bidispersed particles have near Maxwellian statistics with appreciable Mach numbers. 	<ol style="list-style-type: none"> 1. The kinetic theory produces distinct terms unique to polydispersed flows, including drag, interphase energy transfer, drag heating, and an energy partitioning term. 2. The terms produced will differ from those obtained in previous kinetic theories.

Table 1.1 (Continued)

Objectives	Results	Conclusions
Produce an exact modeling framework for studying clustering in homogeneous gas-solid flows.	<ol style="list-style-type: none"> 1. Exact equations are cast for modeling clustering using data from Euler-Lagrange simulations, specifically PR-DNS. 2. Specialized isotropic versions of the exact equations are also produced. 3. Transport terms in the exact moment transport equations are nearly identical to those in the Reynolds stress transport theory of isotropic turbulence. 4. Two distinct mechanisms for clustering are identified due to relative accelerations or higher order moments, which exhibit different time scale signatures. 5. A stochastic modeling framework is produced, where Fokker-Planck equations are used for modeling and stochastic differential equations are used for dynamic simulation. 	<ol style="list-style-type: none"> 1. A mechanism known as the separation dependent sink should be the dominant mechanism of clustering in isotropic flows. 2. Sources and sinks in the exact moment equations can be identified with sources and sinks in the moment equations produced from the Fokker-Planck equations. 3. A state-dependent inertial Fokker-Planck equation is required to model clustering, whereas a non-state dependent model is overdetermined.

Table 1.1 (Continued)

Objectives	Results	Conclusions
Study clustering using exact equations in a homogeneously cooling gas-solid flow.	<ol style="list-style-type: none"> 1. PR-DNS studies of clustering in homogeneously cooling gas-solid flows are performed. 2. Evidence of vorticity formation and clustering are obtained. 3. Vorticity forms due to acceleration-velocity correlations arising from inelastic collisions. 	<ol style="list-style-type: none"> 1. The spectrum of heating is responsible for clustering and vorticity formation in these flows. 2. Homogeneous flows will cluster and form vortices due to inelasticity in particle collision and viscous interactions with the fluid. 3. Vorticity formation precedes cluster formation. 4. The exact method produces dynamic information about clustering, which has been missing from prior approaches.
Study cluster formation in sedimenting or pressure driven gas-solid flows.	<ol style="list-style-type: none"> 1. PR-DNS of pressure driven DNS is carried out. 2. The exact equations show that the system is clustering. 	<ol style="list-style-type: none"> 1. These flows form 'plane-wave' like instabilities. 2. Clustering is identified by statistics in the exact equations. 3. The simulations performed are currently inadequate for producing converged statistics necessary for modeling.

CHAPTER 2. BINARY COLLISION OUTCOMES FOR INELASTIC SOFT-SPHERE MODELS WITH COHESION

This chapter contains a previous draft of the manuscript titled “Binary Collision Outcomes for Inelastic Soft-sphere Models with Cohesion,” which has been published in *Powder Technology* authored by E. Murphy and S. Subramaniam Murphy and Subramaniam (2017).

Abstract

We present an in-depth study on the restitution coefficient and sticking behavior of two models commonly used in the Discrete Element Method (DEM) community for simulating fine cohesive powders. The cohesion in this study is the result of the van der Waals force which is added to commonly used contact force models. We obtain a collapse of the restitution behavior depending on four independent non-dimensional variables governing the dynamics of the system, and a quantitative model for the restitution behavior is presented. Additionally, the physical validity of the DEM models under consideration is shown to be governed by the Tabor parameter, commonly used in the surface science community. If the Tabor parameter is too large such models are not applicable, in a physical sense, and a theory for compliant contacts is needed. We show that the Tabor parameter can be cast in terms of non-dimensional quantities used by the DEM community, and depends on particle stiffness. While softer particles are often used to reduce temporal resolution requirements, we find particle restitution and sticking become sensitive to spring stiffness. This is particularly evident at stiffness values near the limit of physical validity set by the Tabor parameter. Generally, we find that particle stiffness appears to decrease the dissipation of energy in the presence of cohesion. Large differences in restitution and sticking behavior are discussed in the presence or absence of a short-ranged

attractive well. Lastly, the effect of restitution on rheological regime transitions in sheared cohesive assemblies is addressed, where a transition from inertial to quasistatic stress scaling occurs. The occurrence of the transition correlates excellently with the transition from restituting to sticking behavior. This study demonstrates, echoing fluidization studies by several authors, that understanding the microscopic restituting and sticking behavior is important when performing macro-scale simulations involving multiple physical interactions. Possible approaches for obtaining computational speed-up are also discussed.

2.1 Introduction

Transport, aggregation, and dispersion of micron sized particles is a topic central to many industrial and academic problems alike. From an industrial perspective, the aggregation and transport properties control the fluidization of Geldart class A and C powders Geldart (1973); Kim and Arastoopour (2002); Moreno-Atanasio et al. (2007); Kobayashi et al. (2013); Liu et al. (2016), the filtration efficiencies in granular filters Tien and Ramarao (2007), materials processing Castellanos et al. (1999), powder mixing Nienow et al. (1992), and powder rheology Aarons and Sundaresan (2006); Brewster et al. (2005); Rognon et al. (2008); Gu et al. (2014); Saitoh et al. (2015). Aggregation behavior is also important to extra-terrestrial problems such as contamination by lunar and Martian regolith Colwell et al. (2007) and aggregation of early planetesimals in the early solar system Bridges et al. (1996); Blum et al. (2000); Colwell et al. (2007). On the more academic side, some progress has been made in kinetic theoretic approaches for cohesive particle systems Kim and Arastoopour (2002); Liu (2011); Gonzalez et al. (2014); Murphy and Subramaniam (2015); Takada et al. (2015a). In treating this myriad of problems it has become clear that the Discrete Element Method is an indispensable tool for exploring the role of cohesion and inelasticity in the macroscale behavior of micron-scale particulate systems. We restrict ourselves in this paper to treatment of cohesion arising from the van der Waals potential, although electrostatics and liquid bridging are two other commonly encountered sources of cohesion.

Interest in simulating cohesive powders using the DEM is relatively recent, when considering that the Bradley model Bradley (1932) for van der Waals cohesion was developed in

1932, and is still used for rigid spheres. This mature body of research on cohesion from van der Waals interactions Israelachvili (2011) has produced a number of models accounting for varying degrees of surface deformations Johnson et al. (1971); Derjaguin et al. (1975); Maugis (1992); Grierson et al. (2005), contact geometries and roughness Morrow et al. (2003); Waters et al. (2009); Prokopovich and Starov (2011); Persson and Scaraggi (2014); Afferrante et al. (2015); Perni and Prokopovich (2015). Additionally, methodologies for choosing between models Tabor (1977); Johnson and Greenwood (1997); Yao et al. (2007) as well as methods for extraction of parameters in force models Rumpf (1958); Binnig et al. (1986) have been developed. These descriptions all treat quasistatic contact mechanics problems, and hence, little has been developed within the surface science community to help understand how cohesion and energy dissipation mechanisms interact. We note that there have been several attempts to incorporate the combined effects of cohesion and visco-elasticity Brilliantov and Pöschel (2004); Brilliantov et al. (2007) or plastic deformation Thornton and Ning (1998); Tomas (2000); Walton (2004); Luding (2008); Pasha et al. (2014). The models most commonly used in the DEM community are superpositions of repulsive/dissipative force models and a cohesion model Moreno-Atanasio et al. (2007); Kobayashi et al. (2013); Aarons and Sundaresan (2006); Rognon et al. (2008); Galvin and Benyahia (2014), which vary subtly in form e.g. whether particle separations less than the interatomic distance d_0 are considered Aarons and Sundaresan (2006); Gu et al. (2014) and whether a short-ranged attractive well is present Kobayashi et al. (2013); Rognon et al. (2008). The consequences of these small differences between these models are in general not well-documented in the literature, which severely complicates comparison of different simulation data.

The two contact force models considered in this paper are the Kuwabara-Kono (KK) Kuwabara and Kono (1987); Brilliantov et al. (1996) model and its linearized variant the linear spring-dashpot (LSD) model Cundall and Strack (1979a); Walton (1984). The combination of the contact force models and cohesion models produces a list of four independent non-dimensional parameters: (i) the ratio of short-ranged interparticle potential to kinetic energy Murphy and Subramaniam (2015) Ha_0 , (ii) the ratio of the cohesive force at contact to the characteristic spring force or modified Bond number Aarons and Sundaresan (2006); Rognon

et al. (2008) Bo^* , (iii) the ratio of characteristic spring potential energy to the interparticle kinetic energy k^* , and (iv) the coefficient of restitution for the equivalent system without cohesion ε . We stress that the modified Bond number differs from the Bond number used in other powder studies in the presence of gravity Nase et al. (2001); Singh et al. (2014); Berger et al. (2016). An additional important non-dimensional parameter is the particle length scale normalized by the intermolecular separation distance l_{ref}/d_0 , but it is not independent of the four noted above.

We touch on the importance of regimes of physical validity of the models established by the surface science community, and its relation to the model sensitivity. These points are connected by the particle stiffness, and have been largely ignored by the DEM community. The models addressed are additive, much like the model of Derjaguin, MÅ $\frac{1}{4}$ ller, and Toporov (DMT) Derjaguin et al. (1975), which is valid only for very stiff particles. By additive we mean that the total interaction is the sum of individual interactions, e.g. elastic, dissipative, and cohesive. We stress that from a surface science perspective this is very odd, considering a heated debate Grierson et al. (2005) over the applicability of nearly rigid DMT vs the model of Johnson, Kendall, and Roberts (JKR) Johnson et al. (1971) for compliant surfaces that was eventually settled by Tabor’s analysis Tabor (1977). We show that the Tabor parameter μ_T , which sets limits on model validity, can be cast in terms of non-dimensional quantities used in the DEM community, namely Bo^* and l_{ref}/d_0 . The Tabor parameter sets strict limits on the range of validity of additive, i.e. nearly rigid, models in the parameter space.

In DEM simulations of non-cohesive particles the sensitivity of particle kinematics and stress on changes in particle stiffness is generally regarded to be small when the system is correctly scaled Tsuji et al. (1993); Silbert et al. (2001). As a result, smaller stiffnesses are used, which drastically reduces computational demands. Nevertheless, several instances exist, where the effect of particle stiffness has been identified and addressed, and has not always been found to be insignificant Makse et al. (2000); Campbell (2002); Silbert et al. (2007); Otsuki et al. (2010); Singh et al. (2015). Also, in several fluidization studies Moreno-Atanasio et al. (2007); Kobayashi et al. (2013); Liu et al. (2016); Gu et al. (2015, 2016); Wilson et al. (2016) particle stiffness has been observed to have a dramatic affect on particle transport and clustering.

Kobayashi et al. Kobayashi et al. (2013) gave an analysis of the restitution behavior for the LSD model without the presence of the short-ranged attractive potential and showed that the sensitivity to stiffness is due to its influence on the coefficient of restitution. Our model for the coefficient of restitution, described in section 3.3, both *quantifies* and explains why sensitivity to spring stiffness is a feature of both the LSD and KK models, with and without a short-ranged potential. It also allows us to relate this feature back to the limits of physical model validity. Additionally, we note that the inclusion of the short-ranged potential completely alters the scaling of the sticking behavior.

With these arguments in mind, this paper is structured to answer three basic questions concerning the use of additive cohesive models in the DEM community, by treating binary collisions from both kinematic and dynamic approaches:

1. What are the new numerical constraints for simulating short-ranged cohesive models in the short-ranged potential well and how do they compare to constraints without cohesion?
2. How does the incorporation of cohesion change the energy dissipation and particle trapping behavior, and what are the constraints on numerical parameters such as stiffness, in order to ensure realistic physics?
3. Do the above constraints affect the macroscopic behavior of a particulate system?

Several authors have addressed some of the above questions, primarily in the context of fluidization. It is thus important to distinguish the results of this work from previous studies. On the issue of time-step, several authors have explored how the choice of time-step affects the results Kobayashi et al. (2013); Liu et al. (2016); Gu et al. (2015); Wilson et al. (2016). What distinguishes this work from the others is that a physically relevant reference time-scale, the time to cross the potential well, is identified, against which convergence criteria can be judged. This is then related to requirements for non-cohesive systems. Several works Kobayashi et al. (2013); Liu et al. (2016); Gu et al. (2015); Wilson et al. (2016) also focus on particle dissipation, trapping behavior and effect of particle stiffness. Trapping behavior and dissipation have been primarily explored through numerical simulations, without providing a general form for the coefficient of restitution. Although, Kobayashi et al. Kobayashi et al. (2013) does give a

transcendental form for both the contact time and coefficient of restitution in the absence of a potential well. Additionally, Abbasfard et al. Abbasfard et al. (2016) gave an asymptotic solution for the contact time for the cohesive LSD model based on small dissipation. In this manuscript, we provide a full characterization of the rebound and sticking behavior for both the cohesive LSD and KK models for all dissipation levels, with and without a potential well. We have also identified the appropriate method for scaling of the dissipation and sticking for more generic contact laws. Likewise, several authors Kobayashi et al. (2013); Liu et al. (2016); Gu et al. (2015); Wilson et al. (2016) have numerically explored the effect of particle stiffness, and Wilson et al. Wilson et al. (2016) identify the values of stiffness for which such models are physically valid. We explicitly identify through the *quantified* sticking behavior, what values of numerical stiffness are allowed for ensuring realistic physics and how they compare to physical stiffness. Lastly, we explore the effects of stiffness on a system of cohesive granules subjected to simple homogeneous shear.

Implications for capturing the correct physics for some cohesive particulate systems are obvious. For example, the filtration rate for particle laden gas-solid flows traveling through a filter depends intimately on particle capture physics. Fluidization of Geldart C particles and consequently the reaction efficiency in fluidized beds, depends on energy dissipation and particle trapping Moreno-Atanasio et al. (2007); Kobayashi et al. (2013); Liu et al. (2016). The behavior is also at the heart of rheological transitions in dense cohesive flows Aarons and Sundaresan (2006); Brewster et al. (2005); Rognon et al. (2008); Gu et al. (2014). It is our hope to demonstrate to the reader that the careful fundamental treatment of the binary particle system has implications for problems of interest to the DEM community.

2.2 Methods

Contact force laws for cohesive systems have traditionally been developed by the surface science community as a means to extract surface energies via force microscopy techniques. We stress that the needs, in terms of fidelity and accuracy, of the DEM and surface science communities are different. In this paper we seek to give a thorough treatment to a subset of popular DEM models, which are for nearly rigid cohesive particles. Hence, hereafter we concern

ourselves with systems that have Tabor parameters Tabor (1977) μ_T , which is a ratio between the critical depth of penetration on contact d_c and interatomic length-scale d_0 , much less than unity. Such particles have small radius of curvature at the point of contact Afferrante et al. (2015), high Youngs modulus, small strength of cohesion indicated by the Hamaker constant, or a combination thereof. Note that the interatomic length-scale, the distance between atomic nuclei, is often considered to be anywhere between 0.167 nm Israelachvili (2011) and 0.4 nm Aarons and Sundaresan (2006); Kobayashi et al. (2013). Situations that fall under this criterion are often described by the DMT model Derjaguin et al. (1975) in the surface science context.

Many other models exist for describing contacts with higher cohesion energies or softer particles and the development of such models remains an active area of research. For $\mu_T > 5$ the JKR theory Johnson et al. (1971) is often employed, with several additional theories to solve problems in the transition regime Johnson et al. (1971); Derjaguin et al. (1975); Maugis (1992); Grierson et al. (2005). One current trend in the surface science community has been in the direction of forming precise coarse-grained cohesion energy potentials Morrow et al. (2003); Waters et al. (2009); Prokopovich and Starov (2011); Persson and Scaraggi (2014); Afferrante et al. (2015); Perni and Prokopovich (2015), for surfaces with multiple asperities and surface features at multiple length-scales. On the other hand, from an applications perspective there is interest in extending cohesion models to incorporate dissipation for use in DEM simulation, e.g. introducing the dissipative effects of visco-elasticity and plasticity.

The models that we consider are simple and widely used in the DEM community. They are a superposition of different contact force laws, e.g. KK and LSD models, and cohesion models. Although simple, such models retain many essential features of cohesive granular collisions and interactions, as discussed in sections 2.2.1 and 2.2.3. To further motivate looking at such models in detail, we emphasize to the reader that the interactions, i.e. contact force laws between granular particles, are always coarse-grained. That is to say that surface features much smaller than the diameter of the particle are not resolved, and in general, there is no guarantee of separation of scales of roughness and particle geometry. While a complete microscopic description of surfaces is relatively easy to obtain via microscopy techniques to aid in calculating surface energies from Atomic Force Microscopy, such exact descriptions do not necessarily benefit the

DEM community. Sources of uncertainty arise from fluctuations in material composition and surface topography. These fluctuations may even evolve due to surface reaction, wear, plastic deformation, and attrition. In the light of these difficulties, we do not expect that device-scale problems can be addressed inexpensively from a first principles coarse-graining approach, where a complete characterization of the micro-scale is sought.

A valuable alternative is a top-down approach, in which an understanding of the the correspondence between microscopic and macroscopic behaviors and phenomenology is sought. A thorough understanding of the phenomenology of these widely used models is particularly necessary to build intuition for use in large and complex simulations of industrial processes such as fluidized beds. It is in this spirit that we treat the KK and LSD models with an additional short-ranged attractive force, and extract behavior of energy dissipation and particle aggregation in head-on collisions. Later, we explore the effects of model selection on the behavior of regime transition in a shear flow, which is typically robust Vidyapati et al. (2012); Chialvo et al. (2012).

2.2.1 Inelastic Sphere Models

Contact force models for granular particles have several essential features that distinguish them from hard-sphere and other conservative force models. Chief among these features are the presence of a non-vanishing contact time t_c and inelasticity, which dissipates particle energy and is parameterized by a coefficient of restitution ε . Often the behavior of t_c and ε is experimentally observed by varying impact velocity $v_c = v_i^{(jk)} \hat{r}_i^{(jk)}$ between a pair of granules, indexed j and k . Note that here $v_i^{(jk)}$ and $r_i^{(jk)}$ are the relative velocity and separation vectors, and a subscript denotes the vector component. Unit vectors are marked by a caret. In the absence of more fine-grained and robust data, the behavior of these two parameters may be considered sufficient to discriminate between possible contact force law models for different collision scenarios Brilliantov et al. (1996); Di Renzo and Di Maio (2004); Stevens and Hrenya (2005); Thornton et al. (2013), in a top-down approach.

In this work, we seek to elaborate on the relationship between t_c and ε for some commonly used cohesive contact models. The non-cohesive contact force model that we consider is given

by the equation of motion, Eq. 2.1, which is a generalization of many commonly used granular force models Luding et al. (1994); Luding (1998): including the linear spring-dashpot (LSD) model, Hertzian contact model, and the Kuwabara-Kono (KK) model as special cases. The non-dimensional equation of motion for particles in contact, i.e. having a non-dimensional overlap $\delta^* = r_i^{(jk)*} \hat{r}_i^{(jk)} - 1 \leq 0$, is given by

$$\frac{d^2\delta^*}{dt^{*2}} + k^* \left(b^* \delta^{*p} \frac{d\delta^*}{dt^*} + \delta^{*q} \right) = 0 \quad (2.1)$$

where the reference quantities used in the non-dimensionalization of spatial and temporal quantities, e.g. $t^* = t/t_{ref}$, are given as the sum of particle radii $l_{ref} = a^{(j)} + a^{(k)}$ and $t_{ref} = l_{ref}/|v_c|$, where v_c is the pair relative normal velocity at contact. The non-dimensional group b^* is a ratio of characteristic damping and spring forces, given as $b^* = b|v_c|/(kl_{ref})$ for the LSD and KK models, respectively. The last non-dimensional group k^* is the ratio of a characteristic spring energy to the kinetic energy in the normal pair relative velocity. In a conservative system this ratio defines the maximum overlap during a collision, and the exact form depends on the choice of model: $k^* = kl_{ref}^{5/2} a_r^{1/2}/(m_r v_c^2)$ for the KK model and $k^* = kl_{ref}^2/(m_r v_c^2)$ for the LSD model (note the k in the LSD model has dimensions of force per unit length whereas it is force per length squared in the KK model). Different values of the exponents p and q correspond to different models. For linear elastic and visco-elastic materials the Hertz ($q = 3/2, b^* = 0$) and KK ($q = 3/2, p = 1/2$) models are the appropriate descriptions. The LSD contact model is obtained by setting the exponents p and q as $p = 0$ and $q = 1$. The parameters m_r and a_r are the reduced mass $m_r = m^{(j)}m^{(k)}/(m^{(j)} + m^{(k)})$ and effective radius of the particle pair, $a_r = a^{(j)}a^{(k)}/(a^{(j)} + a^{(k)})$, respectively.

While the Hertzian and KK models are often used because they may be obtained by solving the deformation problem for colliding smooth spheres in an inelastic half-space using appropriate constitutive models Brilliantov et al. (1996), the LSD model is often employed due to simplicity and computationally inexpensive linear terms. The LSD model can be derived as a linearization of the KK model using either a characteristic collision velocity or by matching ε_{KK} and ε_{LSD} . This is an example where model parameters may be obtained from either a top-down or first-principles approach using material parameters. The simplicity of the LSD

model offers a clean treatment of the parameters ε and t_c in terms of contact force model parameters, e.g. k^* and b^* . In Appendix C it is shown that in terms of non-dimensional parameters the contact time is given as $t_c^* = \pi/\sqrt{k^* - b^{*2}k^{*2}/4}$ and the coefficient of restitution as $\varepsilon = \varepsilon_{LSD} = \exp(-b^*k^*t_c^*/2)$. Note that an approximate solution for ε_{KK} also exists Brilliantov and Pöschel (2004) but for brevity we do not present it here.

Lastly, it is worth mentioning that simulating ordinary granular materials using realistic parameter values is very expensive. The resolution constraint for properly capturing collisions scales with the contact time, which in the absence of dissipation scales as, $t_c^* \propto k^{*-1/2}$. Realistic values of k^* are often $O(10^{13})$, e.g. 100 micron fused silica beads Oliver and Pharr (1992) sheared at $\dot{\gamma} = 10\text{s}^{-1}$ with $v_c \approx l_{ref}\dot{\gamma}$. The spring constant for equal sized particles is calculated as $k = 2E/3(1 - \nu^2)$ Brilliantov and Pöschel (2004), where E and ν are the Young's modulus and Poisson ratio. Fortunately, for many systems the high values of k^* imply a scale separation between macroscopic time-scales, such as the inverse shear rate $\dot{\gamma}^{-1}$, and microscopic scales, such as collisional and also contact deformation time-scales, which is also a requirement for the inertial number rheology MiDi (2004). Large k^* also implies that particles in the system do not deform much relative to their size, i.e. $\delta/l_{ref} \ll 1$. Many computed statistical quantities in non-cohesive granular systems have been found to be insensitive to changes in particle stiffness, and so k^* may be relaxed to speed up computations Tsuji et al. (1993); Silbert et al. (2001). Particles are typically allowed to deform less than 1% of their diameter Cleary and Sawley (2002). Larger deformations can lead to rheology that depends on particle stiffness Makse et al. (2000); Campbell (2002); Silbert et al. (2007); Otsuki et al. (2010); Singh et al. (2015). Conversely, in sections 2.3.2 and 2.3.3 we show that when cohesion is added to these models, the system dynamics is sensitive to particle stiffness, especially when stiffnesses are softer than those required for physical validity of the models by the Tabor parameter constraint.

2.2.2 Short-Ranged Cohesive Potential

Now that we have introduced the equations for inelastic soft-spheres, we shift our focus to short-ranged attractive potentials. In treating cohesive systems, we separate the collision process into three stages: (i) the approach through an attractive well extending a short distance

beyond the particle surface, (ii) contact, and (iii) separation through the well. Such a sequence of stages is appropriate in the DMT limit Derjaguin et al. (1975). The attractive potential that we consider is known as the van der Waals potential, see Eq. 2.2. This potential is active during the first and third phases and appropriate for particles with an effective radius of curvature at contact a_r much larger than the inter-atomic distance d_0 Israelachvili (2011)

$$\frac{d^2x}{dt^2} = -\frac{Aa_r}{6m_r(x+d_0)^2}, \quad \forall x \in (0, \infty). \quad (2.2)$$

Here A is the Hamaker constant of the material configuration, and the separation distance is given as $x = r_i^{(jk)} \hat{r}_i^{(jk)} - 1$. Note that this force does not diverge at contact, but rather reaches a maximum force defined by the inter-atomic distance. Since the model in Eq. 2.2 is conservative, we may use the Hamiltonian formalism to express the dynamics. We remind the reader that the Hamiltonian $\mathcal{H}\{x, v\}$ is the sum of the kinetic energy T and potential energy V and is conserved throughout stages (i) and (iii) of the collision. The dynamics obey,

$$\frac{m_r}{2}v^2 - \frac{Aa_r}{6(x+d_0)} = \frac{m_r}{2}v_c^2 - \frac{Aa_r}{6d_0}, \quad (2.3)$$

where v_c is again the impact velocity. Since the range over which particles feel one another is very small compared to length-scales such as the mean-free path for collisional flows, realistic unbound particulate systems of interest will only spend a small portion of their time in strongly attractive regions of the well. The potential of 2 particles separated by 9 interatomic separations is 10% of particles in contact, i.e. $V(x = 9d_0) = V(x = 0)/10$. It thus makes sense to non-dimensionalize the energy in this system according to the relative kinetic energy of a free binary particle system, since that energy is more accessible. In this free particle limit, i.e. $\lim_{x \rightarrow \infty} V(x) = 0$, one obtains a relationship between collisional and free particle relative velocities, v_c and v_f given by the non-dimensional Hamiltonian as

$$\lim_{x \rightarrow \infty} \mathcal{H}^* = 1 = \left(\frac{v_c}{v_f}\right)^2 - Ha_0, \quad (2.4)$$

with one parameter $Ha_0 = V(0)/T(v_f) = Aa_r/(3m_r v_f^2 d_0)$ that completely determines the dynamics.

There has not been a consistent treatment of the van der Waals potential near contact within the DEM community. Rather than using the off-set d_0 here, several authors Aarons and Sundaresan (2006); Gu et al. (2014); Abbasfard et al. (2016) interpret the length scale d_0 as an inner cut-off. A length scale at which the force saturates rather than diverging at contact. This results in a potential at contact and also Ha_0 that is twice as large (see Fig. 2.1). There are two reasons for not interpreting d_0 as a resolved length scale: (i) d_0 is the length at which atoms feel strong repulsions due to electron shells, and so the behavior at this scale is repulsive and the particles are technically in contact, and (ii) in DEM contact force models, particles feel one another through the laws of continuum mechanics. Atomistic information leading to the laws of contact mechanics has been coarse-grained. Other authors have chosen to not to resolve the well at all Kobayashi et al. (2013); Rognon et al. (2008); Berger et al. (2016) see Fig. 2.1, which gives $Ha_0 = 0$. We will show in Sections 2.3.1, 2.3.2, and 2.3.3 that Ha_0 is an important parameter in determining the micro- and macroscale dynamics. Lastly, we note that the approach here is general, relying only on the potential at contact, and hence Ha_0 can be used to classify short-range potentials of arbitrary shape.

2.2.3 Inelastic Sphere Models with Cohesion

For the second stage of the collision process we consider an additive constant attractive force to the two models considered in Section 2.2.1. In the absence of dissipation, this additive model combined with the short-ranged attractive well is exactly the DMT model. We note that authors have begun using the force models that we present here without the short-ranged well Kobayashi et al. (2013); Rognon et al. (2008), beyond contact. We show in section 2.3.2 that the dissipative behavior depends on the combination of models for the short-ranged attractive potential and contact force. The general contact force model with cohesion, again applicable when $\delta^* < 0$, is given by

$$\frac{d^2\delta^*}{dt^{*2}} + k^* \left(b^* \delta^{*p} \frac{d\delta^*}{dt^*} + \delta^{*q} + Bo^* \right) = 0. \quad (2.5)$$

A single new parameter enters in Eq. 2.5 when compared with Eq. 2.1: the modified Bond number Bo^* , which has been introduced elsewhere Aarons and Sundaresan (2006); Rognon

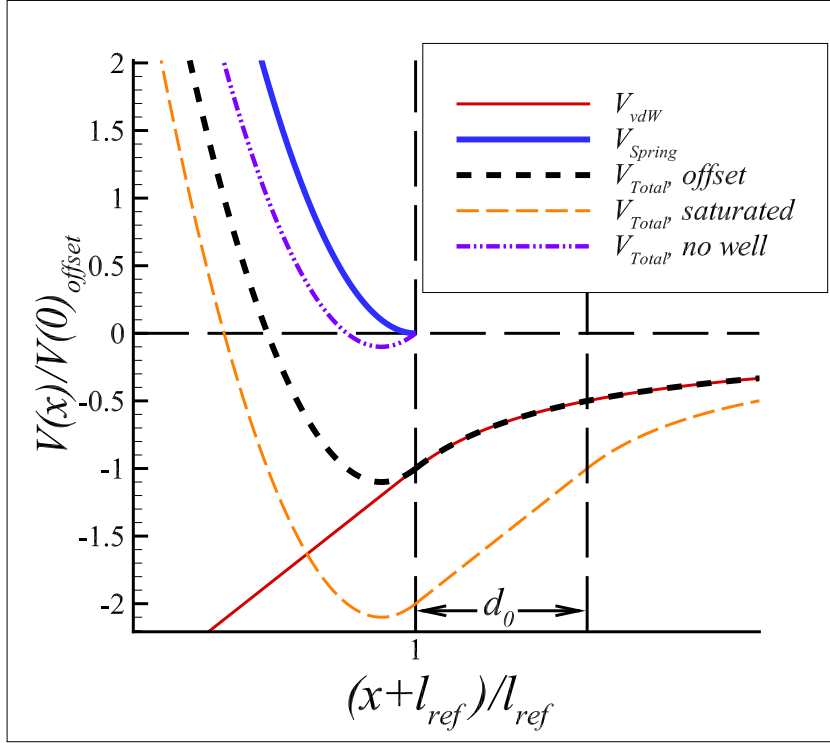


Figure 2.1 The functional form of the potential vs. separation is shown for various combinations of models for cohesion and a linear spring. The first model is used in the present work, using an offset d_0 , V_{total} , MS . The second uses an inner cut-off at which the force saturates V_{total} , *saturated* Aarons and Sundaresan (2006); Gu et al. (2014); Abbasfard et al. (2016), and the last does not use a short ranged attractive well V_{total} , *no well* Kobayashi et al. (2013); Berger et al. (2016). All 3 models have the same value of equilibrium overlap, given by Bo^* , but very different values of potential energy at contact and thus Ha_0 .

et al. (2008). This term introduces inhomogeneity into the formerly homogeneous ODE for the contact force law. The modified Bond number is a ratio of the cohesive contact forces to a characteristic spring force given by $Aa_r^{1/2}/(6kl_{ref}^{3/2}d_0^2)$ for the KK type model and by $Aa_r/(6kl_{ref}d_0^2)$ for the LSD type model. Note that in Section 2.2.1 the collisional and free particle velocities were identical, $v_c = v_f$, whereas this is not the case with cohesion. Due to the presence of the short-ranged well, we must also correct the parameters k^* , b^* , and t^* , which all depend on v_c . We use the relationship in Eq. 2.4 to redefine these quantities; k^* in the LSD case becomes $k^* = kl_{ref}^2/(mv_f^2(1 + Ha_0))$. These new definitions incorporate the effect of initial particle separations beyond the strongly attractive region of the potential well. In Appendix C we solve the LSD version of Eq. 2.5 from which we can obtain the behavior of the coefficient of restitution at contact, ε_c .

Finally, we note that the parameter μ_T used by surface scientists, which for the DMT model is given as $\mu_T = (a_r\Delta\lambda^2/E^{*2}d_0^3)^{1/3}$, where $\Delta\lambda$ and E^{*2} are the surface energy and effective elastic modulus, respectively. The Tabor parameter can be cast in terms of DEM parameters for the KK model, $\mu_T = (2Bo^*/(3\pi))^{2/3}l_{ref}/d_0$. This relation is invaluable in determining realistic particle parameters for use in systems with particles modeled by Eq. 2.5. We remind the reader that the term Bo^* defining μ_T is directly related to particle stiffness and hence it influences numerical time step requirements. This relationship is also useful in determining whether stringent requirements, namely $\mu_T \ll 1$, must be used in simulation. In Section 2.3.2, we show how $m\mu_T$ can be related to the coefficient of restitution.

2.2.4 The Cohesive Time-Scale

Having introduced our models, we now explore some of the consequences of the introduction of cohesion. We observe that the addition of a short-ranged attractive force introduces a new time scale into the problem, the time to traverse the potential well. Understanding this time scale is important from two stand-points. Firstly, it allows us to form convergence criteria for conserved quantities in the approach stage of the dynamics, e.g. the system Hamiltonian \mathcal{H}^* . Secondly, analyzing the convergence allows us to judge the computational requirements of simulating these cohesive systems compared to their non-cohesive counterparts.

A naïve approach would be to form the natural time scale from Eq. 2.3 as $t_a = d_0/v_f$. One could of course improve on this estimate using the solution of the dynamics. This is similar to the way t_c is an improvement over the natural time-scale for the conservative LSD model $t_{LSD} = \sqrt{m_r/k}$. In Appendix A we have solved Eq. 2.3 using finite initial separations corresponding to three different Hamiltonians \mathcal{H}^* : negative, zero, and positive.

Because the solutions to Eq. 2.3 are quite complicated, see Eq. A.1, we seek a numerical fit to the solutions. The initial separation is set to $x = 9d_0$, which is the steepest region of the well and thus most difficult to resolve. To first order this fit is given as

$$\tilde{t}_{a,fit} = \sqrt{\frac{2000}{40 + Ha_0}}. \quad (2.6)$$

This fit depends only on the well energy parameter Ha_0 , and time has been non-dimensionalized as $\tilde{t} = tv_f/d_0$. Note that this fit provides the correct large Ha_0 scaling, which is $\tilde{t}_{a,fit} \propto Ha_0^{-1/2}$ in Eq. A.1. Additionally, it provides a conservative estimate for smaller values.

In Appendix B, a convergence study is presented for particles initially separated by $x = 99d_0$. It is found that obtaining 1% error in energy conservation requires using a time step of $\Delta\tilde{t} = \tilde{t}_{a,fit}/100$.

Now we consider how the new cohesive time-step constraint compares to the time-step constraint used in the LSD model, i.e. $\Delta t_c^* = t_c^*/50$. To find which is limiting, we plot borders in Fig. 2.2 separating regions in parameter space where $\Delta t_c < \Delta t_a$ is satisfied. We find that for a given non-dimensional well-strength Ha_0 , if we decrease the modified Bond number Bo^* , or rather increase the particle stiffness, eventually the contact time step becomes limiting. The border where the transition occurs depends on both the well-strength Ha_0 and inter-atomic distance relative to particle size d_0/l_{ref} .

Realistic values for the Tabor parameter, where this model is valid on physical grounds are $\mu_T \ll 1$. For micron-sized particles the modified Bond numbers must be $Bo^* < O(10^{-6})$, which is usually under the limiting time step border in Fig. 2.2. Hence, for most realistically stiff systems the collision time-step is limiting, e.g. at $Ha_0 < 10^{-4}$ for the case of smooth micron sized particles. This makes sense, because $\mu_T < 1$ means that the characteristic length-scale for the particle contacts is smaller than the inter-atomic distance, or in other words nearly rigid

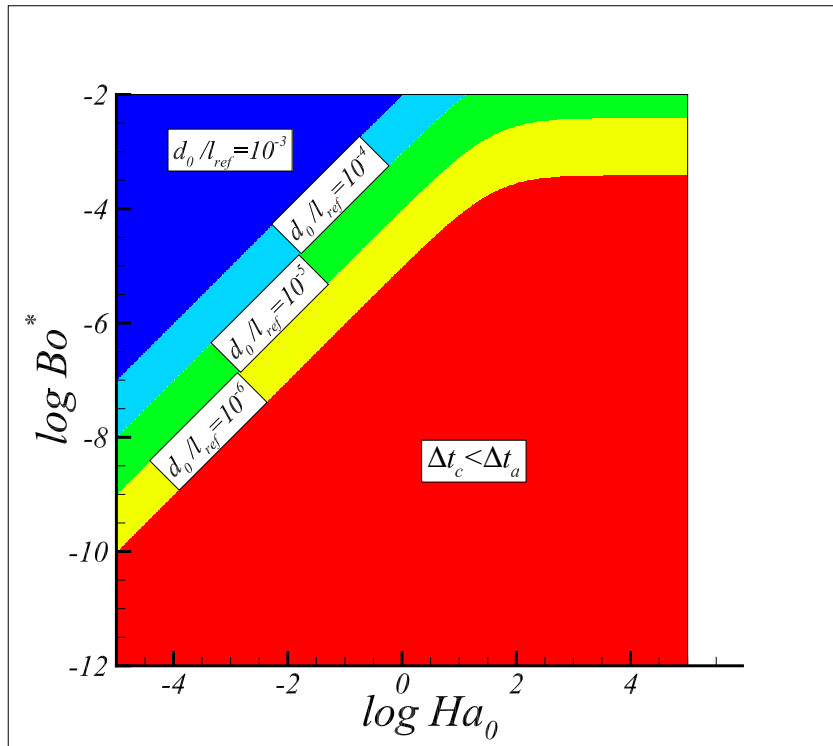


Figure 2.2 The boundaries between limiting time steps Δt_c (non-cohesive) and Δt_a (cohesive) for varying particle sizes. For a given d_0/l_{ref} , systems that lie in the region below the boundary corresponding to smaller Bo^* are contact time limited.

particles which are very stiff. In Section 2.3.2 we explore whether such stiff particles must be used for producing accurate results. In Appendix B, we also show that if the limiting time-scale is adhered to, the error in energy conservation through all three stages of the collision process is within 3%.

2.2.5 Discrete Element Method

In the studies in Section 2.3 and Appendix B we have made use of the LAMMPS Plimpton (1995) molecular dynamics software developed at Sandia National Laboratories. LAMMPS, like many other molecular dynamics codes, uses velocity-Verlet integration, which is a symplectic integrator. All convergence information and error scaling that are presented are for this integrator. Equations 2.2 and 2.5 govern the systems that we treat. The homogeneously sheared simulations presented in Section 2.3.3 employed a deforming triclinic domain, which is equivalent to Lees-Edwards boundary conditions Lees and Edwards (1972).

2.3 Results and Discussion

Both in the prior Sections and in the Appendices, we addressed issues related to the first open question that we posed: What are the simulation constraints introduced by the inclusion of short-ranged attraction? In the remaining sections, we seek to answer the remaining two questions. In the first two subsections, we address the question of what the effect of cohesion on energy dissipation and particle trapping is, and also the question of what range of numerical parameters produce accurate physics in the binary collision case. In the last subsection, we look at the very simple macroscopic problem of homogeneous simple shear, in order to address whether the constraints on parameters implied by these findings actually matter in the context of macro-scale systems.

2.3.1 Conservation of Kinetic Energy

Before addressing model-specific consequences of cohesion, it is worthwhile to explore the effect of cohesion from the short-ranged attractive well given a coefficient of restitution at contact ε_c . This is effectively a hard-sphere assumption, where the dissipation arises from

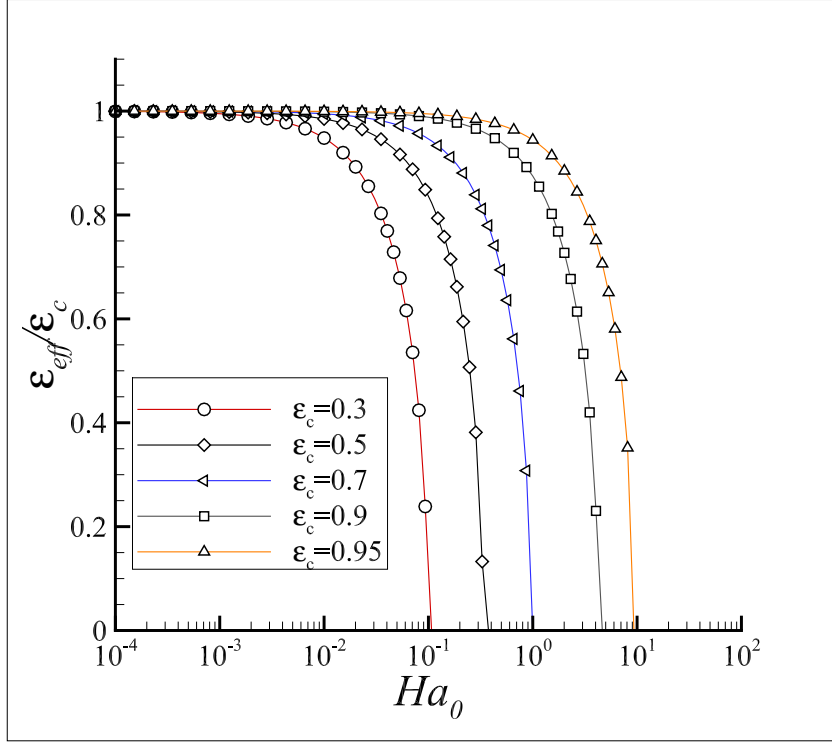


Figure 2.3 Behavior of the effective coefficient of restitution with non-dimensional well-strength Ha_0 for varying values of contact inelasticity Murphy and Subramaniam (2015).

defined kinematic collision laws. We are interested in an effective coefficient of restitution defined as the ratio of the velocity at the edge of a potential well cut-off after a collision to the velocity at the edge before a collision, $\epsilon_{\text{eff}} = \left| v'_f / v_f \right|$. In the case that a particle cannot reach the edge of the potential well, due to energy loss in a collision, the effective coefficient of restitution is zero, i.e. $\epsilon_{\text{eff}} = 0$. This is a purely kinematic problem and can straightforwardly be solved using Eq. 2.3. For simplicity, we will make the infinite initial separation approximation $V(\tilde{t}_0) \approx 0$, as we did in obtaining Eq. 2.4. Considering all three kinematic stages of the collision process (approach, contact, and separation) one obtains the expression

$$\epsilon_{\text{eff}} = \begin{cases} (\epsilon_c^2 - (1 - \epsilon_c^2) Ha_0)^{1/2} & : v_f \in (-\infty, v_{\text{crit}}) \\ 0 & : v_f \in [v_{\text{crit}}, 0] \end{cases}. \quad (2.7)$$

Here of course the initial or free particle normal relative velocity v_f is negative. This relationship has been plotted in Fig. 2.3. Interestingly, we find that there are two different

qualitative behaviors exhibited by Eq. 2.7, separated by a critical velocity, v_{crit} . The critical velocity is given by $v_{crit} = -\sqrt{-2V(x=0)(1-\varepsilon_c^2)/m_r\varepsilon_c^2}$ Dahneke (1975). In the very weak cohesive limit, as $Ha_0 \rightarrow 0$, we see almost no difference between ε_{eff} and ε_c . As the non-dimensional well-strength is increased, the acceleration due to the attractive force increases, which increases the impact velocity. The result is an increase in the net amount of energy dissipated. The effective coefficient of restitution decreases due to an increase in dissipation. At the critical velocity, particles are knocked from an unbounded state, $\mathcal{H} > 0$, into a bounded state, $\mathcal{H} < 0$, and hence, can no longer exit the potential well. In this case, subsequent collisions continually knock the pair Hamiltonian \mathcal{H} to lower and lower values, as discussed by Murphy and Subramaniam Murphy and Subramaniam (2015). If the contact is described by Eq. 2.5 rather than a hard-sphere collision law, particles eventually become stuck in contact.

2.3.2 Consequences of Cohesive Models on Contact Dynamics

The presence of cohesion introduces an inhomogeneous term k^*Bo^* into the contact dynamics. It is possible that the cohesive contact dynamics produce a coefficient of restitution at contact that is different from the non-cohesive system. Quantifying the effect of the inhomogeneous term on ε_c is important for predicting the correct rebound/sticking behavior given by Eq. 2.7. Before analyzing the sticking behavior we look at scaling arguments, to see how the solutions may be collapsed. This exercise is valuable because of the large parameter space, which consists of four independent parameters, Ha_0 , Bo^* , k^* , and b^* . In order to gain some insight into how the system response may be collapsed, we re-express Eq. 2.5, taking conservative terms to the LHS and dissipative terms to the RHS as has been done in the study of the KK model Brilliantov and Pöschel (2004),

$$\frac{d}{d\delta^*} \left[\frac{1}{2} \left(\frac{d\delta^*}{dt^*} \right)^2 + k^* \left(\frac{1}{q+1} \delta^{*q+1} + Bo^* \delta^* \right) \right] = -k^* b^* \delta^{*p} \frac{d\delta^*}{dt^*}. \quad (2.8)$$

When the dissipative RHS is non-zero, the change in the LHS over the duration of a collision depends on the path taken during the collision. Our analysis is made easier by the fact that we already characterize the change in energy on the LHS, without cohesion, by the coefficient of restitution ε_c . Moreover, the non-cohesive value of ε_c is uniquely determined by a single non-

dimensional group for the LSD and KK models. For the LSD case the coefficient of restitution is determined solely by τ^*/ω^* (see Eqs. C.2 and C.3), whereas it is determined by the non-dimensional group $k^{*2/5}b^*$ (in our notation) for the KK model Brilliantov and Pöschel (2004). By fixing ε_c of the corresponding non-cohesive case, we expect that the cohesive dynamics governing the variation of the contact time t_c and coefficient of restitution during contact ε_c will depend only on parameters on the LHS of Eq. 2.8.

The non-dimensional group we denote as Π has shown success in collapsing data presented in this section, and is given as

$$\Pi = 2\delta_{eq}^*Bo^*k^* = Bo^{*1/q}\frac{l_{ref}}{d_0}\frac{Ha_0}{(1+Ha_0)} = \left(\frac{3\pi}{2}\right)^{1/q}\mu_T\frac{Ha_0}{(1+Ha_0)}. \quad (2.9)$$

Here $\delta_{eq}^* = Bo^{*1/q}$ is the resting overlap between two particles due to cohesion. The expression for Π is given in 3 different forms, since each is useful under different circumstances. The first and third forms have valuable physical interpretations. The first is a combination of the equilibrium overlap due to cohesion and the ratio of cohesive force at contact to a characteristic impact force. We note that the first expression can also be used in the absence of the short-range potential well. The third form is technically only valid for the Hertzian spring case, and shows an explicit dependence on the Tabor parameter. This also depends on the energy term $Ha_0/(1+Ha_0)$, which may take values between 0 and 1, for small and large values of Ha_0 , respectively. The second form shows explicit dependence on non-dimensional groups, which appear in the non-dimensional equations of motion for particles in contact and near contact. In addition, we expect this method of scaling to apply to the general contact laws in Eq. 2.5 with arbitrary exponents p and q . Overall, large cohesive forces lead to an increase in Π , whereas large impact velocity and particle stiffness lead to a decrease in Π .

In addition to the kinematic mode of particle capture discussed in Section 2.3.1, there is another mode in which particles may stick during stage (ii) of the collision process. We will refer to the second mode of particle capture as contact sticking. Kobayashi et al. Kobayashi et al. (2013) studied collisions between cohesive particles without short-ranged attraction and found that cohesion generally increases dissipation in a particle collision, and with large enough cohesion contact sticking occurs. This phenomena is demonstrated Fig. 2.4, where two particle

Table 2.1 Parameters in solution of contact dynamics

Parameter	Range	# of Samples	Model
Bo^*	$10^{-10} - 10^{-4}$	100	LSD/KK
$\frac{Ha_0}{1+Ha_0}$	$10^{-5} - 1$	100	LSD/KK
l_{ref}/d_0	$10^{-6} - 10^{-3}$	4	LSD/KK
ε_{LSD}	$0.5 - 0.99$	7	LSD
$k^{*2/5}b^*$	$0.05 - 1$	7	KK

systems with different values of Π collide. One system is unable to rebound to $\delta^* = 0$, indicating contact sticking. The increase in dissipation makes sense because cohesion increases relative velocities during a collision, leading to an increase in both collisional dissipation, contact time, and maximum overlaps.

We are now curious about two questions in particular:

1. Is the increase in dissipation due to contact cohesion significant for realistically stiff systems?
2. How soft can we make the springs without compromising the physics?

In order to answer these two questions, we carry out a parameter study for both the LSD and KK models. For the LSD systems with cohesion the analytic solutions for the position response Eq. C.1 and the velocity C.3 were used to find the contact time t_c and contact coefficient of restitution ε_c . A bisection method was used to find the second zero in the position solution to within machine precision, which yields the contact time t_c , see Fig. 2.5(a). The solution of the velocity equation then gives $\varepsilon_c = f(t_c)$, see Fig. 2.6(a). We solved the KK model with and without cohesion via velocity-Verlet integration. For each case we used a time-step of $k^{*-1/2}/10^4$. Both the contact time and coefficient of restitution were extracted. The parameters used can be found in table 2.3.2.

We plot the solutions for the contact time, t_c , in Fig. 2.5(a)-2.5(b) for the LSD and KK systems, respectively, and corresponding contact coefficient of restitutions, ε_c , in Fig. 2.6(a)-2.6(b). Both the viscoelastic and linearized systems have the same qualitative behavior for both t_c and ε_c . For all cases, an increase in Π results in an increase in the contact time t_c and a corresponding decrease in the contact coefficient of restitution ε_c . This is consistent with

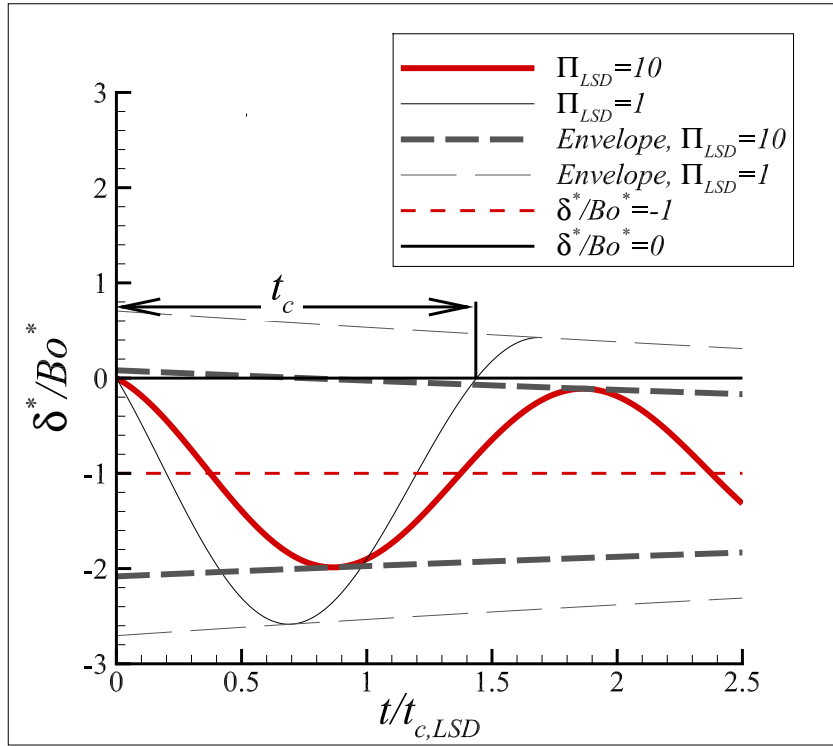
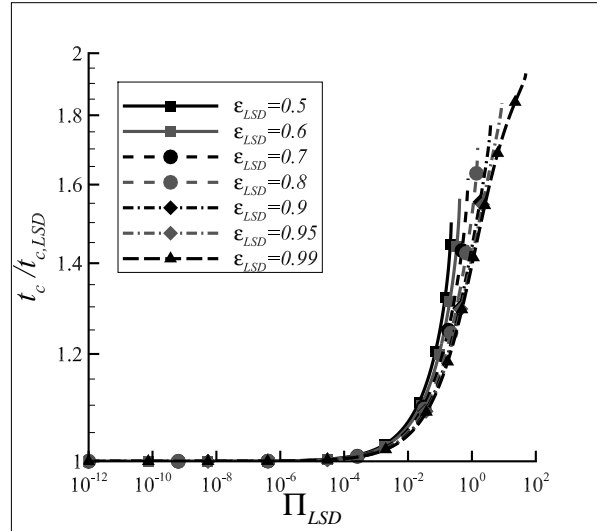
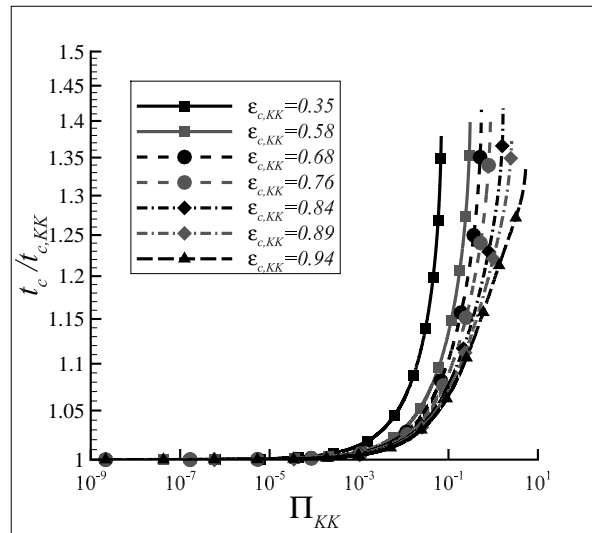


Figure 2.4 Position response for the LSD system ($\varepsilon_{LSD} = 0.9$), alongside the respective exponentially decaying envelopes. We see that beyond a critical value of Π , particles no longer restitute.

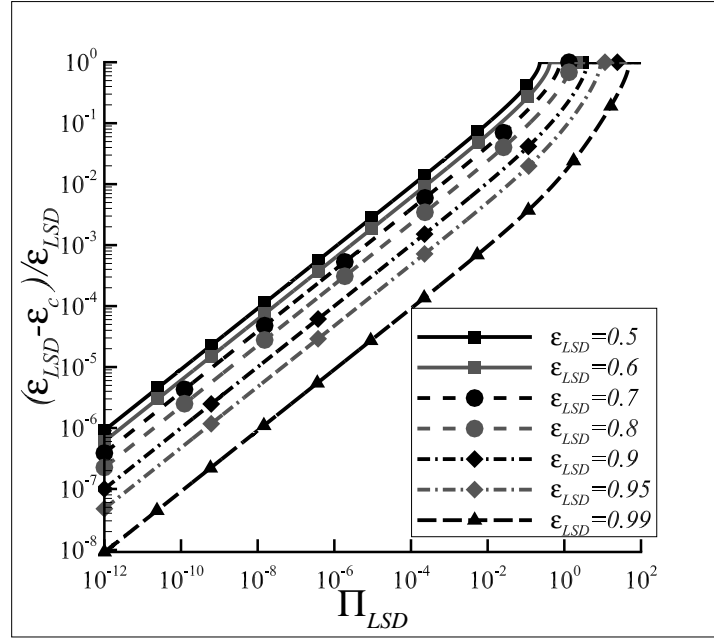


(a)

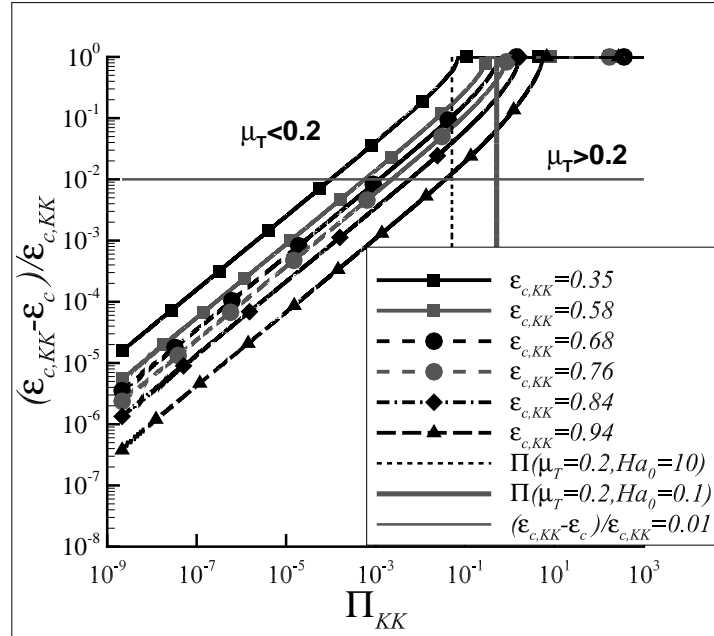


(b)

Figure 2.5 The contact time t_c for the (a) LSD and (b) KK models are plotted for different levels of dissipation. Similar behavior is found for both models. In particular, we find that for higher values of the Π parameter, the contact time increases until a critical value is reached. At the critical value the contact time becomes infinite, and particles become stuck together do to the inhomogeneous term in the contact force law.

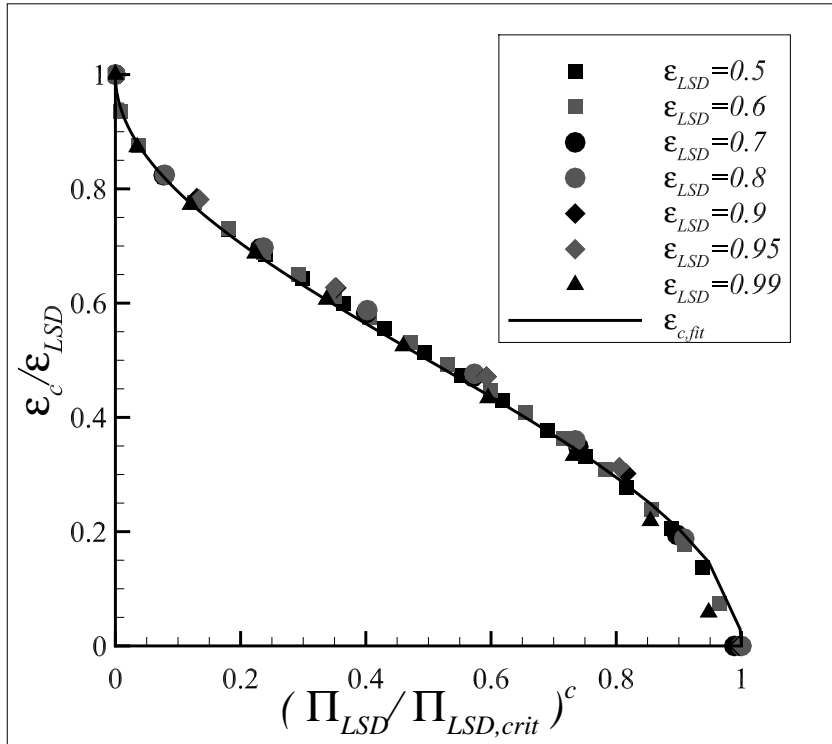


(a)

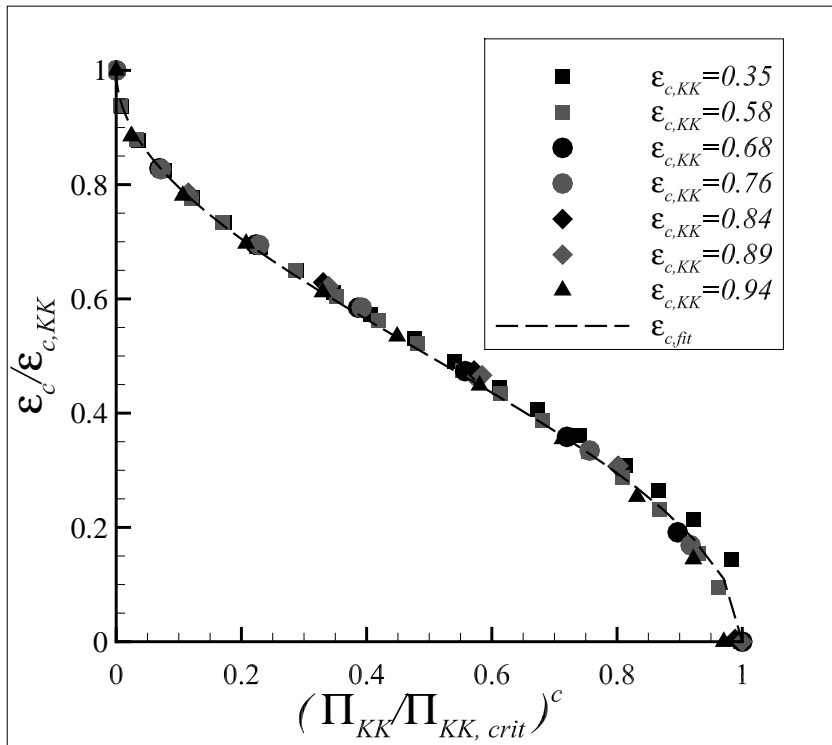


(b)

Figure 2.6 The scaled difference in ϵ_c has been plotted for the (a) LSD and (b) KK models for different levels of dissipation. This plot shows us for which non-dimensional parameters the contact coefficient of restitution is not sensitive to the cohesive contact force. For small levels of Π there is practically no difference between cohesive and non-cohesive systems, in terms of contact dynamics. Regions of physical model validity and non-validity, as well as, model sensitivity to particle stiffness are shown in (b). Beyond a critical value of Π , sticking is observed for both the linear and nonlinear models.



(a)



(b)

Figure 2.7 A collapse of all data is obtained for (a) the LSD and (b) KK models. The collapse given in Eq. 2.10 captures the behavior of ε_c within 1% over the parameters studied.

our intuition given above for how the relative strength of cohesion should affect dissipation. Furthermore, at a particular value of Π , we see that t_c reaches a maximum finite value after which the contact time is infinite, indicating contact sticking. The critical value of Π for which sticking occurs decreases with increasing inelasticity, i.e. particles with higher inelasticity stick better than nearly elastic particles. In the limit of completely elastic collisions, sticking is not possible. However, any finite amount of dissipation allows for sticking given sufficient cohesive forces.

Let us now consider the two questions raised above. In Fig. 2.6(b), we have partitioned the response of the contact coefficient of restitution into quadrants depending on the limiting value of the Tabor parameter and percentage difference between values of ε_c for cohesive and non-cohesive systems. The vertical line divides the plot into regions where the DMT model is applicable (left) and where it is not applicable (right). The horizontal line represents the acceptable percentage difference of 1% between the non-cohesive and cohesive values of ε_c . For smooth 10 micron fused silica glass beads and using an inter-atomic distance of $d_0 = 0.4$ nm, the Tabor parameter is $\mu_T = 0.15$. This corresponds to a value of $Bo^{*2/3}l_{ref}/d_0 = 0.42$. In this region of Fig. 2.6(a) and 2.6(b), it appears that ε_c may be sensitive to variation in Π , since not all points are below the horizontal line. *Particles with realistic stiffness can be sensitive to numerical variation in the stiffness*, and may also stick due to contact sticking. As a result, we must seek to understand the quantitative effects of the inhomogeneity on the coefficient of restitution.

In order to further collapse the simulation data, we seek a functional form for the coefficient of restitution at contact that collapses the cohesive ε_c with variation in Π . All model constants will depend on the non-cohesive coefficient of restitution. The functional form is

$$\begin{aligned} \frac{\varepsilon_c}{\varepsilon_\alpha} &= \frac{a}{\pi} \arccos \left(2 \left(\frac{\Pi}{\Pi_{crit}} \right)^c - 1 \right) \quad \forall \Pi < \Pi_{crit} \\ a &= 1 - (1 - \varepsilon_\alpha)^{d_1} \\ c &= b_1 \varepsilon_\alpha^{d_2} + (1 - \varepsilon_\alpha)^{d_3} \\ \Pi_{crit} &= \exp \left(-b_2 \varepsilon_\alpha^{d_4} + b_3 (1 - \varepsilon_\alpha)^{d_5} \right), \end{aligned} \tag{2.10}$$

Table 2.2 Numerical fits to parameters for collapse of ε_{eff} .

Parameter	α =LSD	α =KK,fit
b_1	0.504	0.306
b_2	122.9	12.62
b_3	122.2	11.92
d_1	0	7.227
d_2	2.155	0.170
d_3	-0.119	-0.224
d_4	-0.017	-0.160
d_5	-0.008	-0.067

with parameters given in table 2.3.2.

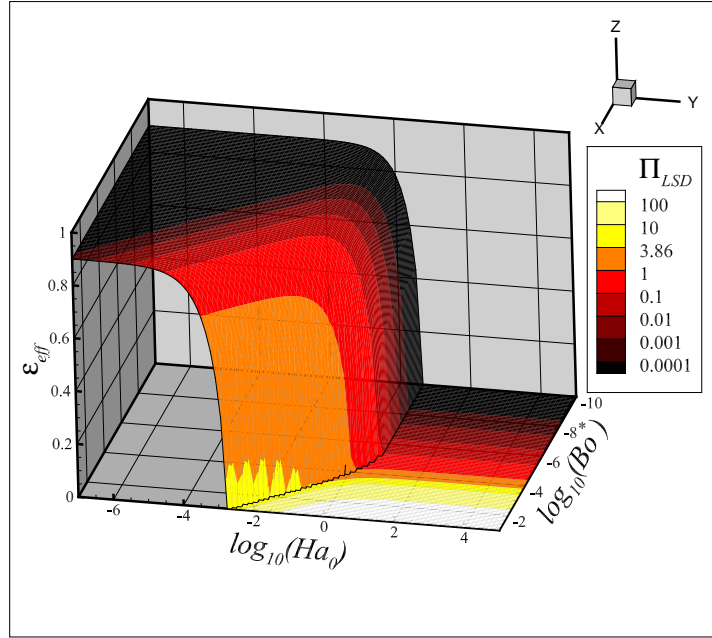
The fit of the parameters have been selected to have certain limiting behaviors. All model parameters are a function of the dissipation only. First, the inverse cosine term ensures that in the limit of small Π , ε_c tends towards non-cohesive behavior, and is zero for $\Pi > \Pi_{crit}$. The critical value of Π , where sticking occurs, tends towards 0 for small ε_α and ∞ for $\varepsilon_\alpha \rightarrow 1$, where α is a placeholder for the LSD or KK models. This results in particles always sticking in the completely inelastic limit, and never sticking in the elastic limit. The exponent c is bounded from below by unity and above by ∞ and increases with ε_α . The last parameter $a = \varepsilon_{KK}/\varepsilon_{KK,Padé}$ arises from an imperfect Padé approximation of the KK model behavior that can be found in Brilliantov and Pöschel (2004), and is only significantly different from unity for large impact velocities. The collapse of the data is given in Fig. 2.7(a) and 2.7(b). We find that the error in the fit for the wide range of parameters studied is under 1%.

The last task for this section is to explore what the effective coefficient of restitution for the entire collision process looks like when all three stages of the collision are considered. Figures 2.8(a) and 2.8(b) contain a surface for ε_c at different values of Bo^* and Ha_0 . The surfaces are colored by values of Π . The LSD case has been plotted for $\varepsilon_{LSD} = 0.9$, while the KK case has been plotted for $b^{*5}k^{*2}Ha_0^{1/2} = 9.9$. Both are for 10 micron particles. Note that $b^{*5}k^{*2}Ha_0^{1/2}$ is not velocity dependent and only depends on material and surface parameters. Changing the cohesive well parameters, e.g. A or d_0 , will change the value of $b^{*5}k^{*2}Ha_0^{1/2}$. Hence, we stress that the variation in Ha_0 shown in Fig. 2.8(b) is from varying the kinetic energy only. In both cases, we see that the behavior for small Bo^* is not affected by the contact force inhomogeneity.

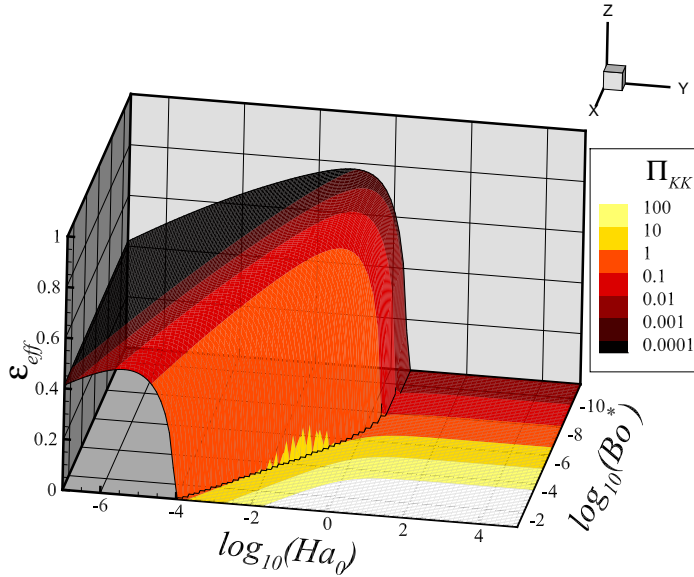
This is indicated by the sticking boundary being only a function of Ha_0 . Departures from the kinematic description given by Eq. 2.7 are governed by the contact sticking behavior. The transition from kinematic to contact sticking behavior is shown by the capture boundary at higher Bo^* coinciding with level-set curves of Π . We see the contact sticking behavior most clearly for the LSD case, where the level curve of $\Pi_{crit} \approx 3.86$ is shown, and coincides with the sticking boundary for large modified Bond numbers, i.e. $Bo^* > 10^{-4}$. We remind the reader that the non-dimensional group Π in Fig. 2.6(a)-2.6(b) governs sticking during stage two of the collision process. Non-cohesive behavior is observed outside of the immediate region where particles stick, i.e. low Ha_0 . Finally, in the absence of the short-ranged attractive well Kobayashi et al. (2013); Berger et al. (2016), the coefficient of restitution depends only on Π and hence behaves *qualitatively* different from systems where attractive wells are present.

2.3.3 Consequences for Macroscopic Systems: Simple Homogeneous Shear

In device scale simulations it is of interest to know how sensitive macroscopic quantities are to variation in microscopic parameters. In practice there is no reason to adhere to the constraints imposed on realistic particle stiffness, if the observables obtained from macro-scale problems are not sensitive to changes in stiffness. For certain situations, such as particle filtration, it is clear from the analysis in Section 2.3.2 that the average particle capture dynamics will be sensitive to the sticking behavior of individual collisions. This sensitivity has also been shown in fluidization studies Moreno-Atanasio et al. (2007); Kobayashi et al. (2013); Liu et al. (2016); Gu et al. (2015, 2016); Wilson et al. (2016). It is not clear that non-equilibrium steady states, such as homogeneous simple shear, will be sensitive to the effect that particle stiffness has on collisional dissipation and capture. Without cohesion, we already know that the stresses in rapidly sheared granular homogeneous assemblies are not especially sensitive to changes in parameters controlling energy dissipation Vidyapati et al. (2012); Chialvo et al. (2012), e.g. ε or friction μ_f . Studies on the shear of cohesive granular materials have shown that a new regime transition between quasi-static $(\sigma_{xy}) \propto \dot{\gamma}^0$ and Bagnold scaling $(\sigma_{xy}) \propto \dot{\gamma}^2$ emerges Aarons and Sundaresan (2006); Gu et al. (2014) at volume fractions much lower than the jamming point $\phi_s \ll \phi_{s,jam}$ Chialvo et al. (2012). Similar transitions have also been



(a)



(b)

Figure 2.8 The complete behavior of the effective coefficient of restitution has been plotted for (a) the LSD model and (b) KK model. The surface is colored by the value of Π to demonstrate that at large enough values of Bo^* , the effects of the inhomogeneous term in the contact force law become important, because contact sticking is a function of Π alone, see Fig. 2.6(a) and 2.6(b). Note that the value of Π_{crit} for the LSD case is 3.86, which coincides with sticking boundary for high, corresponding to $Bo^* < 10^{-4}$. Ordinary non-cohesive behavior is observed not far beyond the critical capture region for both LSD and KK models.

observed in several other works. The phenomena of cohesion causing quasistatic stress scaling to appear at volume fractions lower than expected has also been observed in two-dimensional wall bounded constant pressure flows Berger et al. (2016) of highly frictional and dissipative particles. It is noteworthy to mention that those simulations were performed using particles with a coefficient of restitution of zero, and hence, are expected to always experience contact sticking from a collision. Simulations of cohesive elasto-plastic particles slowly sheared in a split annular shear cells have also indicated a transition which depends on a Bond number, defined by the ratio of maximum adhesive force to expected force between a pair of particles $Bo_S = |F_{i,vdW}(\delta^* = 0)| / \langle |F_i^{(jk)}| \rangle$ Singh et al. (2014). Much like in the homogeneous simple shear cases, small cohesion, corresponding to $Bo_S < 1$, has almost no effect on the stress, while larger values of Bond numbers and cohesion have a pronounced effect on stress and flow profiles for large values of Bo_S .

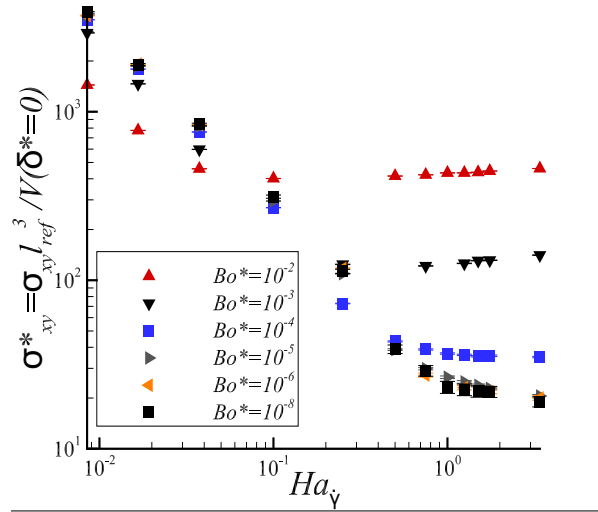
We will explore the region very close to the regime transition brought on by cohesion for the friction less LSD model cases in homogeneous simple shear with $\varepsilon_{LSD} = 0.6, 0.9$ and $\phi_s = 0.55$ using LAMMPS. A cubic periodic domain was used with 3500 particles. Several parameters were varied in the study including A , k , and $\dot{\gamma}$ to produce varying $Ha_{\dot{\gamma}}$, Bo^* , and hence the non-dimensional group Π_{LSD} . Here we make the approximation that $v_f \approx \dot{\gamma}l_{ref}$ so that $Ha_0 \approx Ha_{\dot{\gamma}}$. As a result, $Ha_{\dot{\gamma}}$ is proportional to $\dot{\gamma}^{-2}$. We report here also values of the inertial number $I = \dot{\gamma}l_{ref}\sqrt{\rho/p}$ relevant to the so-called $\mu(I)$ rheology. Here p and ρ are the particle pressure and density, respectively. At the smallest values of $Ha_{\dot{\gamma}}$, the inertial number is approximately 0.2. This value is not uniquely determined by the volume fraction for large values of cohesion Berger et al. (2016) and varies somewhat between 0.05 and 0.25 at higher values of $Ha_{\dot{\gamma}}$. This is due to the effect that cohesion has on the normalizing pressure. Inertial numbers of 0.2 are quite large and also indicate an inertial scaling of the stress for equivalent non-cohesive systems. We note that Singh et al. Singh et al. (2014) only explored very low inertial numbers in their split annular shear cell simulations.

The results of this parameter study are shown in Fig. 2.9(a) and 2.9(b). Here the proper non-dimensionalization of the shear stress is given as $\sigma_{xy}^* = \sigma_{xy}l_{ref}^3/V(0)$, which is a potential energy scaling. Given in raw non-dimensional form this is $6\sigma_{xy}d_0^3l_{ref}^3/Aa_r$. We find that the

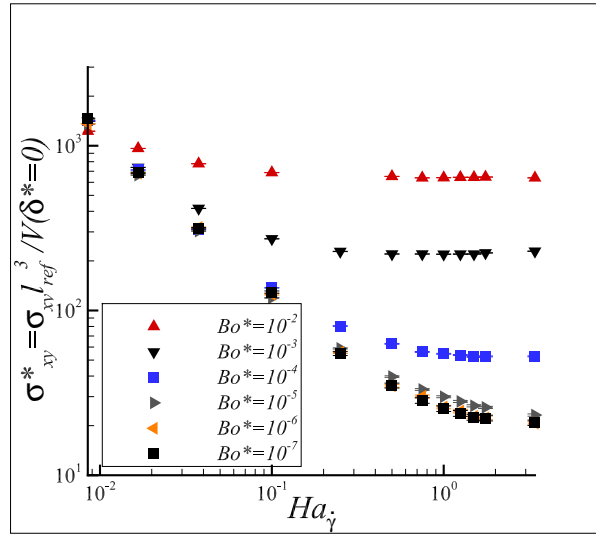
scaled stress shows the Bagnold to quasi-static transition for cases with large contact stiffness, i.e. low Bo^* . Stark differences appear for softer particles, which can be quasistatic for all values of $Ha_{\dot{\gamma}}$. The behavior of ε_{eff} is the primary driver for differences in the observed stress. An asymptotic behavior in the stress is observed as particle stiffness is increased, i.e. Bo^* decreased. This is consistent with the behavior of ε_{eff} in Fig. 2.8(a), where ε_{eff} is not sensitive to changes in Bo^* . The insensitivity of stress and ε_{eff} to changes in particle stiffness occurs at small values of Π , i.e. $\Pi_{LSD} \ll \Pi_{LSD,crit}$. This is the region where the inhomogeneous term does not affect ε_c significantly. Hence, we find that the transition in the asymptotic stress scaling is due to kinetic sticking. Note that for the case of $Bo^* = 10^{-5}$ we reduced the shear rate by two orders of magnitude, while maintaining the same Bo^* , $Ha_{\dot{\gamma}}$, and Π_{LSD} . No differences in stress were observed. We have also confirmed that stress in the equivalent systems without cohesion did not depend on stiffness. Additionally, using nearest neighbor estimates, we find that the mean free-flight time for equivalent non-cohesive particles remains much larger than the collision time for all cases.

The important finding obtained from Fig. 2.9(a) and 2.9(b) is that significant differences in the *qualitative* stress behavior occur if insufficiently hard particles are used corresponding to $Bo^* > 10^{-5}$. This corresponds to larger values of Π , where contact sticking is expected, $\Pi_{LSD} \gg \Pi_{LSD,crit}$. As values of Bo^* are increased further above $Bo^* = 10^{-5}$, the differences in the stress become more extreme. At large values of $Ha_{\dot{\gamma}}$ we find that generally an increase in Bo^* (or decrease in stiffness) leads to an increase in shear stress. We find that this is due to the formation of large particle clusters. The softer and non-confined particle contacts dissipate energy slower, leading in an increase in steady state granular temperature and particle stress. For the case of $\varepsilon = 0.9$ at small values of $Ha_{\dot{\gamma}}$, stress is seen to decrease with increasing Bo^* . This reduction in stress is due to a decrease in the coefficient of restitution for increasing Π , which lowers the particle temperature and decreases stress. As shear rates are decreased, there is a formation of smaller temporary non-percolating (floating) clusters. These contacts, which should not substantially contribute to the stress, may also play a role.

Interestingly, for the case of $\varepsilon = 0.6$ and $Bo^* = 10^{-2}$, we find that the shear stress is nearly quasistatic over the entire range of cases examined. Note that this value of Bo^* means there



(a)



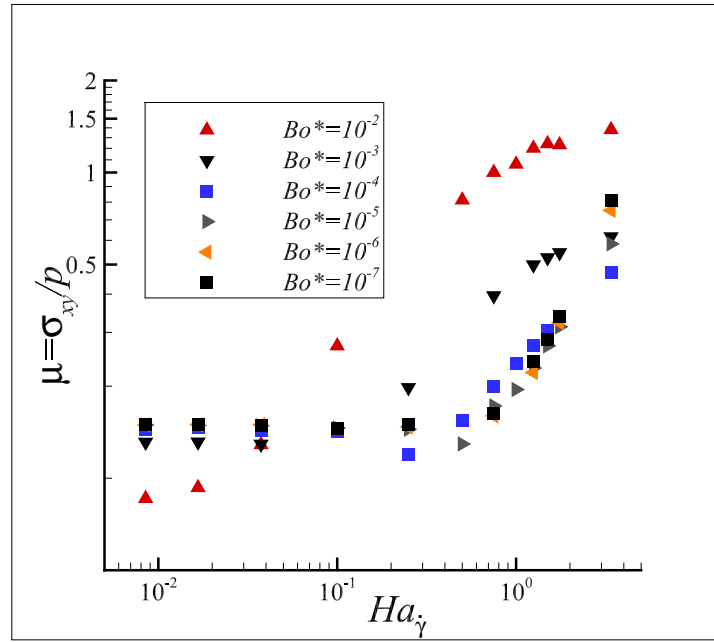
(b)

Figure 2.9 The shear stress response for the macroscopic homogeneous simple shear test has been plotted for varying values of particle stiffness for the case of (a) $\varepsilon = 0.9$ and (b) $\varepsilon = 0.6$. We find that for both cases, substantial differences between the stress is found when particle stiffness is too small, indicated by large Bo^* .

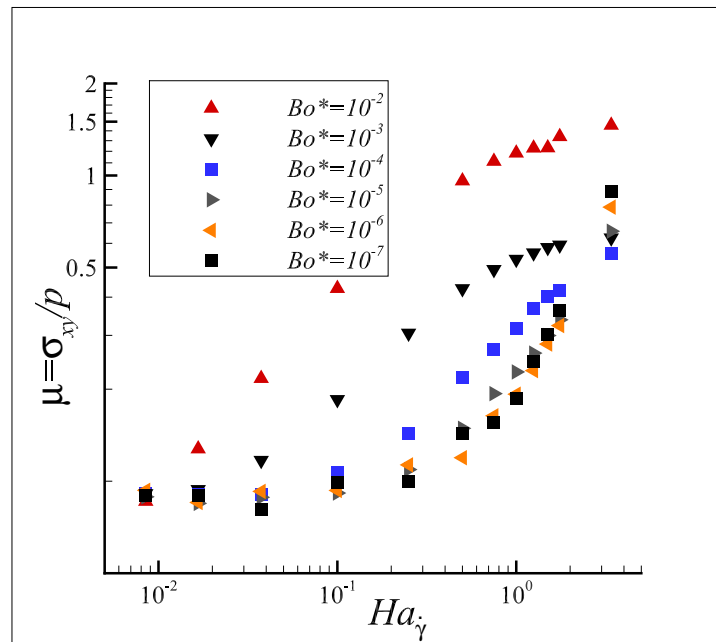
will be a resting overlap of 1% of the particle diameter, an acceptable overlap for non-cohesive systems. Values of Π for these cases are between 9 and 75. These are much higher than the $\Pi_{LSD,crit} = 0.42$, which determines whether contact sticking is occurring. The Π values for the case of $Bo^* = 10^{-5}$ are between 9×10^{-3} and 7.5×10^{-2} . This indicates that the difference in the *quantitative* stress and *qualitative* stress scaling between large and small stiffness is due to contact sticking. It is also clear that the different values of $\Pi_{LSD,crit}$, due to differences in ε_{LSD} , lead to *qualitatively* different responses in stress for the same modified Bond number. Overall, we know that differences in stress scaling between soft and hard particles are due to the presence of contact sticking. More precisely, contact sticking leads to quasistatic stress scaling, where it would not occur if only kinematic sticking is present. Additionally, we now know that the asymptotic stress scaling, which displays a transition near $Ha_\gamma = 1$, is due to kinematic sticking, i.e. as defined in Eq. 2.7.

We now consider the relationship of the stress scalings for cohesive particles with other works. In Fig. 2.10(a) and 2.10(b) we have plot the apparent macroscopic friction coefficient of the cohesive assembly, $\mu = \sigma_{xy}/p$. Note that by looking at plots of μ and the scaled shear stress, one may also infer the parameter $\eta = |F_{i,vdW}(\delta^* = 0)|/l_{ref}^2 p$ used in previous studies Rognon et al. (2008); Berger et al. (2016). For our particular model this parameter is $\eta = \mu l_{ref}/\sigma_{xy}^* d_0$ and is observed to take values from approximately 0.1 to 50. The behavior of μ echoes what was observed in plots of the scaled shear stress. The values of μ reach an asymptotic behavior with decreasing Bo^* , and behave much differently if particles exhibit contact sticking. For the asymptotic scaling, we find that pressure and shear stress are proportional to one another for $Ha_\gamma < 1$. An increase in μ is observed for $Ha_\gamma > 1$, due to the pressure retaining a nearly inertial/Bagnold scaling for the stiffest cases. Interestingly, the values of μ for the contact sticking cases level off at $Ha_\gamma > 1$, and exhibit apparent friction coefficients greater than unity. These large friction coefficients were observed previously in relatively low volume fraction simulations of cohesive granules Rognon et al. (2008). Some additional findings are in agreement with those of Berger et al. Berger et al. (2016), namely that both μ and the coordination number (not shown) increase with increasing η .

Lastly, we consider the behavior of the Bond number Bo_S . Singh et al. Singh et al. (2014)



(a)

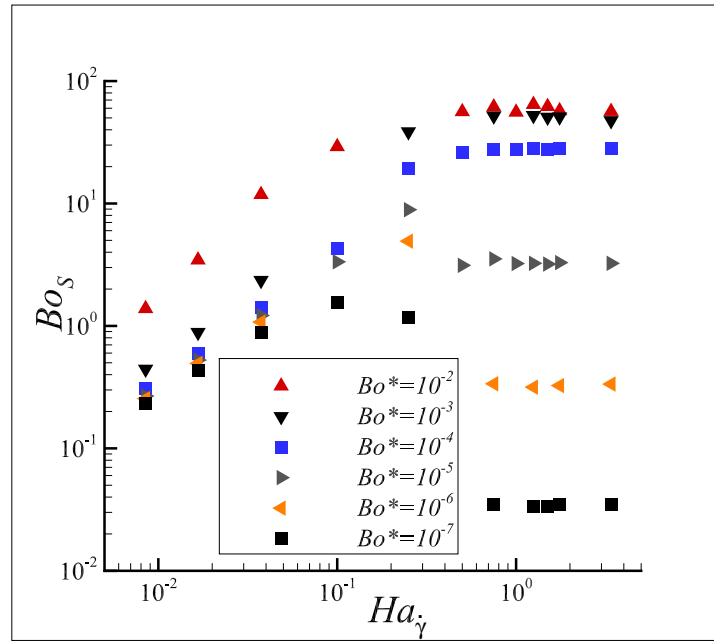


(b)

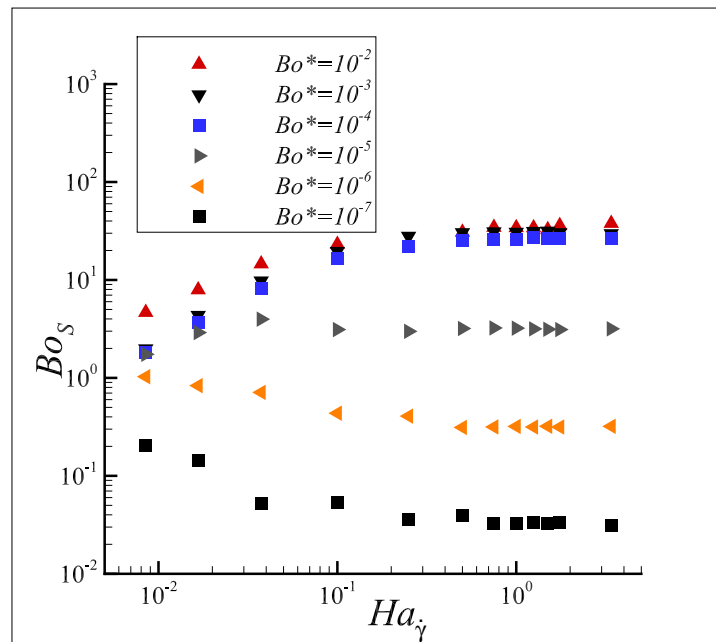
Figure 2.10 The apparent friction coefficient for (a) $\varepsilon = 0.9$ and (b) $\varepsilon = 0.6$ have been plotted. We find a signature very similar to that observed in the shear stress. Namely, an asymptotic scaling of μ is observed as spring stiffness is increased.

showed that this parameter could be considered as a control parameter for slow flows of cohesive elasto-plastic particles. At $Bo_S < 1$ cohesion was found to have almost no effect on the flow, whereas systems with $Bo_S > 1$ were dominated by cohesion. The Bond number has been plotted in Fig. 2.11(a) and 2.11(b). While the parameter Bo_S does appear to be responsive in the vicinity of the transition, i.e. $Ha_\gamma \approx 1$, the value of $Bo_S = 1$ does not appear to be very important for all cases. Nor does it appear to exhibit the same scaling as observed in slow, confined flows. Interestingly, for the case of $\varepsilon_{LSD} = 0.9$ and $Bo^* = 10^{-7}$ the transition in the behavior does appear to happen when $Bo_S \approx 1$. However, above the transition where cohesion dominates, in fact $Bo_S \ll 1$, which is in disagreement with findings from slow flows Singh et al. (2014). Generally, we find that Bo_S increases with Bo^* . Both the trend in Bo_S with increasing Bo^* , and the sudden drop in Bo_S near the transition for $\varepsilon_{LSD} = 0.9$ can be explained by "frustrated" particles. The stress scaling transition coincides with the formation of giant transient clusters in the domain. As particles become harder and harder, rearrangements become more difficult leading to the build-up of stress in the form of large fluctuations. This is echoed by the behavior of the cases with $Bo^* > 10^{-4}$, where Bo_S saturates indicating that particles are soft enough to avoid the build-up of strong forces. Below the transition, i.e. $Ha_\gamma \ll 1$, for systems that do not experience contact sticking, these clusters do not exist, and hence, they do not experience low values of Bo_S . This interpretation is similar to that reached by Singh et al. The discrepancy in the scaling, however, arises for several reasons. Firstly, we note that in the slowly sheared case the maximum adhesive force and normalizing mean force both scale almost identically with the pressure. This leaves Bo_S to depend almost linearly on the strength of the adhesive spring. Our force model on the other hand has a constant adhesive force in contact, and a mean force which should depend on both the pressure and the number of particles between which forces are computed. Note that the particles that feel one another through attractive forces are not necessarily in contact. Secondly, the essence of this particular transition is the sticking of particles, which serves to increase the number of particles in a cluster. This again alters the scaling.

Clearly, the effects of collisional dissipation and particle capture at the microscale do propagate to affect macroscopic observables in simulations in a non-trivial manner. The essence of



(a)



(b)

Figure 2.11 The parameter Bo_S for (a) $\varepsilon = 0.9$ and (b) $\varepsilon = 0.6$ have been plotted. The Bond number appears to be sensitive to the transition in the shear stress scaling. This scaling reaching a plateau for $Ha_\gamma > 1$.

this regime transition is due to the behavior of the coefficient of restitution. Additional work on quantifying the behavior of clusters near the transition in these systems is of interest and will be the subject of future reports.

2.3.4 Computational Speed-up

This paper has thus far focused on numerical constraints of using the model herein. We now focus briefly on potential methods for obtaining computational speed-up, as indicated by the scaling revealed herein. We note that there have already been two methods focusing on speed-up in this area Kobayashi et al. (2013); Gu et al. (2015). There are several ways that are quite easy to identify. The simplest method can be used for cases where $\Pi \ll \Pi_{crit}$. To achieve speed-up in these cases, one should increase Bo^* , as much as possible until the percentage difference in ε_c between the non-cohesive and cohesive systems becomes unacceptable. For cases where there is no potential well and where obtaining the correct contact sticking is the most important element, the coefficient of restitution may be increased or the dissipation parameter b^* may be lowered. This will push the value of Π_{crit} to higher values, allowing for softer springs to be used. This does, however, have the unfortunate side effect of subtly altering the dissipation behavior.

Without accounting for particle friction another approach could be to numerically alter the cohesion laws, as is frequently done with stiffness in non-cohesive settings. For systems without a potential well, this would mean altering A and k such that Bo^* , or more importantly Π is kept constant. This was the approach taken by Kobayashi et al. Kobayashi et al. (2013). We note that Π will change only if Bo^* is changed. For cases with a short-range well, both Bo^* and Ha_0 must be kept constant. Gu et al. Gu et al. (2015) accomplished this by also altering the shape of the potential well, namely the saturation cut-off, to keep Ha_0 constant. Perhaps many more methods of computational speed-up may be found using insight from the quantified behavior presented herein. However, at present the primary deficiency of all of these speed-up methods, is that they are expected to not perform extremely well in denser systems in the presence of friction.

2.4 Conclusion

In this paper we have considered the effect of cohesion and dissipation in two popular models used within the DEM community to simulate fine powders. In doing so we have sought to answer three fundamental questions of interest for simulating systems, where such particles present themselves: (1) What are the new convergence constraints from introducing cohesion? (2) How does cohesion change the dissipation and particle sticking behavior in collisions while varying parameters? (3) Do the constraints obtained from microscopic simulations affect the measurements in macroscopic systems?

In answering these questions we have introduced new time-scale constraints from analytic solution and obtained a quantitative description of the energy dissipation and sticking behavior. We show that realistic values for particle stiffness must be used in cohesive simulations in order to capture the correct sticking behavior. We also show that inclusion of the short-ranged attractive well changes the particle sticking behavior, as compared to previous detailed studies on fluidization. Lastly, we demonstrate that the rheological transition behavior of sheared attractive particles depends intimately on the microscale sticking behavior, which can be sensitive to variation in particle stiffness. This is especially true when using numerical stiffness softer than those required for physical validity of the model. Additionally, we identify possible methods for achieving computational speed-up. It is our hope that these fundamental results will be used both in a practical manner for choosing simulation parameters and to improve intuition in the simulation of complex physical and chemical systems, such as simulation of fluidized beds in chemical processing of Geldart C powders, powder rheology, filtration, material processing, and contamination.

Acknowledgment

We gratefully acknowledge the support provided for this work from NSF grant no. 0927660.

2.5 Bibliography

- Aarons, L. and Sundaresan, S. (2006). Shear flow of assemblies of cohesive and non-cohesive granular materials. *Powder Technology*, 169(1):10–21.
- Abbasfard, H., Evans, G., and Moreno-Atanasio, R. (2016). Effect of van der Waals force cut-off distance on adhesive collision parameters in DEM simulation. *Powder Technology*, 299:9–18.
- Afferrante, L., Ciavarella, M., and Demelio, G. (2015). Adhesive contact of the weierstrass profile. In *Proc. R. Soc. A*, volume 471, page 20150248. The Royal Society.
- Aitcin, P. (2000). Cements of yesterday and today - concrete of tomorrow. *Cement and Concrete Research*, 31(9):1349–1359.
- Alam, M., Trujillo, L., and Herrmann, H. (2006). Hydrodynamic theory for reverse brazil nut segregation and the non-monotonic ascension dynamics. *Journal of Statistical Physics*, 124:587–623.
- Bagnold, R. A. (1954). Experiments on a gravity-free dispersion of large solid spheres in a newtonian fluid under shear. In *Proceedings of the Royal Society of London A: Mathematical, Physical and Engineering Sciences*, volume 225, pages 49–63. The Royal Society.
- Ball, R. and Melrose, J. (1997). A simulation technique for many spheres in quasi-static motion under frame-invariant pair drag and brownian forces. *Physica A*, 247:444–472.
- Baranyai, A. and Evans, D. (1989). Direct entropy calculation from computer-simulation of liquids. *Physical Review A*, 40(7):3817–3822.
- Batrak, O., Patino, G., Simonin, O., Flour, I., Le Guevel, T., and Perez, E. (2005). Unlike particles size collision model in 3d unsteady polydispersed simulation of circulating fluidized bed. *8th Annual Conference on Fluidized Bed Technology*, 315.

- Bec, J., Biferale, L., Cencini, M., Lanotte, A., and Toschi, F. (2010). Intermittency in the velocity distribution of heavy particles in turbulence. *Journal of Fluid Mechanics*, 646:527–536.
- Beetstra, R., van der Hoef, M., and Kuipers, J. (2007). Drag force of intermediate reynolds number flows past mono- and bidisperse arrays of spheres. *AIChE Journal*, 53:489.
- Bentz, D., Ferraris, C., Galler, M., Hansen, A., and Guynn, J. (2012). Influence of particle size distributions on yield stress and viscosity of cement-fly ash pastes. *Cement and Concrete Research*, 42(2):404–409.
- Bentz, D. P., Garboczi, E. J., Haecker, C. J., and Jensen, O. M. (1999). Effects of cement particle size distribution on performance properties of portland cement-based materials. *Cement and Concrete Research*, 29:1663–1671.
- Berger, N., Azéma, E., Douce, J.-F., and Radjai, F. (2016). Scaling behaviour of cohesive granular flows. *EPL (Europhysics Letters)*, 112(6):64004.
- Berzi, D. and Jenkins, J. T. (2015a). Inertial shear bands in granular materials. *Physics of Fluids*, 27:033303.
- Berzi, D. and Jenkins, J. T. (2015b). Steady shearing flows of deformable, inelastic spheres. *Soft matter*, 11(24):4799–4808.
- Binnig, G., Quate, C. F., and Gerber, C. (1986). Atomic force microscope. *Physical review letters*, 56(9):930.
- Blum, J., Wurm, G., Kempf, S., Poppe, T., Klahr, H., Kozasa, T., Rott, M., Henning, T., Dorschner, J., Schrapler, R., Keller, H., Markiewicz, W., Mann, I., Gustafson, B., Giovane, F., Neuhaus, D., Fechtig, H., Grun, E., Feuerbacher, B., Kochan, H., Ratke, L., El Goresy, A., Morfill, G., Weidenschilling, S., Schwehm, G., Metzler, K., and Ip, W. (2000). Growth and form of planetary seedlings: Results from a microgravity aggregation experiment. *Physical Review Letters*, 85(12):2426–2429.

- Bradley, R. S. (1932). Lxxix. the cohesive force between solid surfaces and the surface energy of solids. *The London, Edinburgh, and Dublin Philosophical Magazine and Journal of Science*, 13(86):853–862.
- Brady, J. F. and Bossis, G. (1988). Stokesian dynamics. *Annual Reviews of Fluid Mechanics*, 20:111–157.
- Bragg, A. D. and Collins, L. R. (2014a). New insights from comparing statistical theories for inertial particles in turbulence: I. spatial distribution of particles. *New Journal of Physics*, 16:055013.
- Bragg, A. D. and Collins, L. R. (2014b). New insights from comparing statistical theories for inertial particles in turbulence: II. relative velocities. *New Journal of Physics*, 16:055014.
- Bragg, A. D., Ireland, P. J., and Collins, L. R. (2015). On the relationship between the non-local clustering mechanism and preferential concentration. *Journal of Fluid Mechanics*, 780:327–343.
- Brewster, R., Grest, G. S., Landry, J. W., and Levine, A. J. (2005). Plug flow and the breakdown of bagnold scaling in cohesive granular flows. *Physical Review E*, 72(6):061301.
- Bridges, F. G., Supulver, K. D., Lin, D., Knight, R., and Zafra, M. (1996). Energy loss and sticking mechanisms in particle aggregation in planetesimal formation. *Icarus*, 123(2):422–435.
- Brilliantov, N. V., Albers, N., Spahn, F., and Pöschel, T. (2007). Collision dynamics of granular particles with adhesion. *Physical Review E*, 76(5):051302.
- Brilliantov, N. V. and Pöschel, T. (2004). Collision of adhesive viscoelastic particles. *HINRICHSEN:GRANULAR MEDIA O-BK*, pages 189–209.
- Brilliantov, N. V. and Pöschel, T. (2004). *Kinetic Theory of Granular Gases*. Oxford University Press, New York.
- Brilliantov, N. V., Spahn, F., Hertzsch, J.-M., and Pöschel, T. (1996). Model for collisions in granular gases. *Physical review E*, 53(5):5382.

- Brito, R. and Ernst, M. (1998). Extension of haff's cooling law in granular flows. *Europhysics Letters*, 43(5):497.
- Campbell, C. S. (2002). Granular shear flows at the elastic limit. *Journal of fluid mechanics*, 465:261–291.
- Capecelatro, J., Desjardins, O., and Fox, R. O. (2014). Numerical study of collisional particle dynamics in cluster-induced turbulence. *Journal of Fluid Mechanics*, 747:R2.
- Capecelatro, J., Desjardins, O., and Fox, R. O. (2015). On fluid-particle dynamics in fully developed cluster-induced turbulence. *Journal of Fluid Mechanics*, 780:578–635.
- Capecelatro, J., Desjardins, O., and Fox, R. O. (2016). Strongly coupled fluid-particle flows in vertical channels. ii. turbulence modeling. *Physics of Fluids*, 28:033307.
- Carnahan, N. and Starling, K. (1969). Equation of state for nonattractive rigid spheres. *Journal of Chemical Physics*, 51(2):635–636.
- Castellanos, A., Valverde, J. M., Pérez, A. T., Ramos, A., and Watson, P. K. (1999). Flow regimes in fine cohesive powders. *Physical Review Letters*, 82(6):1156.
- Cates, M., Wittmer, J., Bouchaud, J., and Claudin, P. (1998a). Jamming and static stress transmission in granular materials. *Chaos*, 9(3):511–522.
- Cates, M., Wittmer, J., Bouchaud, J., and Claudin, P. (1998b). Jamming, force chains, and fragile matter. *Physical Review Letters*, 81(9):1841–1844.
- Chew, J. W., Parker, D. M., Cocco, R. A., and Hrenya, C. M. (2011). Cluster characteristics of continuous size distributions and binary mixtures of group b particles in dilute riser flow. *Chemical Engineering Journal*, 178:348–358.
- Chialvo, S., Sun, J., and Sundaresan, S. (2012). Bridging the rheology of granular flows in three regimes. *Physical Review E*, 85(2):021305.
- Chun, J., Koch, D. L., Rani, S. L., Ahluwalia, A., and Collins, L. R. (2005). Clustering of aerosol particles in isotropic turbulence. *Journal of Fluid Mechanics*, 536:219–251.

- Cleary, P. W. and Sawley, M. L. (2002). DEM modelling of industrial granular flows: 3D case studies and the effect of particle shape on hopper discharge. *Applied Mathematical Modelling*, 26(2):89–111.
- Cocco, R., Shaffer, F., Hays, R., Karri, S. R., and Knowlton, T. (2010). Particle clusters in and above fluidized beds. *Powder Technology*, 203:3–11.
- Colwell, J., Batiste, S., Horányi, M., Robertson, S., and Sture, S. (2007). Lunar surface: Dust dynamics and regolith mechanics. *Reviews of Geophysics*, 45(2):RG2006.
- Cundall, P. and Strack, O. (1979a). A discrete numerical model for granular assemblies. *Geotechnique*, 29(1):47–65.
- Cundall, P. A. and Strack, O. D. (1979b). A discrete numerical model for granular assemblies. *Geotechnique*, 29(1):47–65.
- Dahneke, B. (1975). Further measurements of the bouncing of small latex spheres. *Journal of Colloid and Interface Science*, 51(1):58–65.
- Daley, D. and Vere-Jones, D. (1988). *An introduction to the theory of point processes*. Springer-Verlag.
- DeCicco, A. and Hartzell, C. (2016). System-level design considerations for asteroid despin via neutral beam emitting spacecraft. In *IEEE Aerospace Conference Proceedings (Big Sky, MT)*.
- Derjaguin, B., Muller, V., and Toporov, Y. (1975). Effect of contact deformations on the adhesion of particles. *Journal of Colloid and Interface Science*, 53(2):314–326.
- Di Renzo, A. and Di Maio, F. P. (2004). Comparison of contact-force models for the simulation of collisions in dem-based granular flow codes. *Chemical Engineering Science*, 59(3):525–541.
- Eaton, J. and Fessler, J. (1994). Preferential concentration of particles by turbulence. *International Journal of Multiphase Flow*, 20:169–209.

- Ernst, M., Dorfman, J., Hoegy, W., and van Leeuwen, J. (1969). Hard-sphere dynamics and binary-collision operators. *Physica*, 45(1):127–146.
- Esipov, S. and Pöschel, T. (1997). The granular phase diagram. *Journal of Statistical Physics*, 86(5/6):1385–1395.
- Ferraris, C., Obla, K., and Hill, R. (2001). The influence of mineral admixtures on the rheology of cement paste and concrete. *Cement and Concrete Research*, 31(2):245–255.
- Fox, R. (2014). On multiphase turbulence models for collisional fluid-particle flows. *Journal of Fluid Mechanics*, 742:368–424.
- Fox, R. O. (2016). Private communication.
- Fullmer, W. D. and Hrenya, C. M. (2016). Quantitative assessment of fine-grid kinetic-theory-based predictions of mean-slip in unbounded fluidization. *AIChE Journal*, 62(1):11–17.
- Galvin, J. E. and Benyahia, S. (2014). The effect of cohesive forces on the fluidization of aeratable powders. *AIChE Journal*, 60(2):473–484.
- Garzo, V., Dufty, J. W., and Hrenya, C. M. (2007a). Enskog theory for polydisperse granular mixtures. i. navier-stokes order transport. *Physical Review E*, 76(3):031303.
- Garzo, V., Fullmer, W. E., Hrenya, C. M., and Yin, X. (2016). Transport coefficients of solid particles immersed in a viscous gas. *Physical Review E*, 93:012905.
- Garzo, V., Hrenya, C. M., and Dufty, J. W. (2007b). Enskog theory for polydisperse granular mixtures. ii. sonine polynomial approximation. *Physical Review E*, 76(3):031304.
- Garzo, V., Tenneti, S., Subramaniam, S., and Hrenya, C. (2012). Enskog kinetic theory for monodisperse gas-solid flows. *Journal of Fluid Mechanics*, 712:129–168.
- Gaume, J., Chambon, G., and Naaim, M. (2011). Quasistatic to inertial transition in granular materials and the role of fluctuations. *Physical Review E*, 84:051304.
- Geldart, D. (1973). Types of gas fluidization. *Powder technology*, 7(5):285–292.

- Gidaspow, D., Jung, J., and Singh, R. K. (2004). Hydrodynamics of fluidization using kinetic theory: an emerging paradigm 2002 flour-daniel lecture. *Powder Technology*, 148:123–141.
- Goldhirsch, I. and Zanetti, G. (1993). Clustering instability in dissipative gases. *Physical Review Letters*, 70(11):1619–1622.
- Goldshtein, A. and Shapiro, M. (1995). Mechanics of collisional motion of granular materials. part 1. general hydrodynamic equations. *Journal of Fluid Mechanics*, 282:75–114.
- Gollin, D., Berzi, D., and Bowman, E. (2017). Extended kinetic theory applied to inclined granular flows: role of boundaries. *Granular Matter*, 19(3):1564–1583.
- Gonzalez, R. G. and Garzo, V. (2016). Instabilities in granular gas-solid flows. *arXiv:1611.03269*.
- Gonzalez, S., Thornton, A., and Luding, S. (2014). Free cooling phase-diagram of hard-spheres with short-and long-range interactions. *The European Physical Journal Special Topics*, 223(11):2205–2225.
- Gourdel, c., Simonin, O., and Brunier, E. (1998). Modelling and simulation of gas-solid turbulent flows with a binary mixture of particles. *Third International Conference on Multiphase Flows*, 315.
- Gourdel, c., Simonin, O., and Brunier, E. (1999). Two-maxwellian equilibrium distribution function for the modelling of a binary mixture of particles. *6th International Conference on Circulating Fluidized Beds*, 315.
- Grierson, D., Flater, E., and Carpick, R. (2005). Accounting for the jkr–dmt transition in adhesion and friction measurements with atomic force microscopy. *Journal of adhesion science and technology*, 19(3-5):291–311.
- Gu, Y., Chialvo, S., and Sundaresan, S. (2014). Rheology of cohesive granular materials across multiple dense-flow regimes. *Physical Review E*, 90(3):032206.
- Gu, Y., Ozel, A., and Sundaresan, S. (2015). A modified cohesion model for CFD–DEM simulations of fluidization. *Powder Technology*, 296:17–28.

- Gu, Y., Ozel, A., and Sundaresan, S. (2016). Numerical studies of the effects of fines on fluidization. *AIChE Journal*.
- Gustavsson, K. and Mehlig, B. (2014a). Clustering of particles falling in a turbulent flow. *Physical Review Letters*, 112:214501.
- Gustavsson, K. and Mehlig, B. (2014b). Relative velocities of inertial particles in turbulent aerosols. *Journal of Turbulence*, 15(1):34–69.
- Gustavsson, K. and Mehlig, B. (2016). Statistical models for spatial patterns of heavy particles in turbulence. *Advances in Physics*, 65(1):1–57.
- Haecker, C., Garboczi, E., J.W., B., Bohn, R., Sun, Z., Shah, S., and Voigt, T. (2005). Modeling the linear elastic properties of portland cement paste. *Cement and Concrete Research*, 35:1948–1960.
- Haff, P. (1983). Grain flow as a fluid-mechanical phenomenon. *Journal of Fluid Mechanics*, 134:401–430.
- Hatzes, A., Bridges, F., Lin, D., and Sachtjen, S. (1991). Coagulation of particles in saturn’s rings: Measurement of the cohesive force of water frost. *Icarus*, 89:113–121.
- Hill, R. J., Koch, D., and Ladd, A. (2001a). The first effects of fluid inertia on flows in ordered and random arrays of spheres. *Journal of Fluid Mechanics*, 448:213–241.
- Hill, R. J., Koch, D., and Ladd, A. (2001b). Moderate-reynolds-number flows in ordered and random arrays of spheres. *Journal of Fluid Mechanics*, 448:243–278.
- Irani, E., Chaudhuri, P., and Heussinger, C. (2014). Impact of attractive interactions on the rheology of dense athermal particles. *Physical Review Letters*, 112:188303.
- Irani, E., Chaudhuri, P., and Heussinger, C. (2016). Athermal rheology of weakly attractive soft particles. *Physical Review E*, 94:052608.
- Israelachvili, J. N. (2011). *Intermolecular and surface forces: revised third edition*. Academic press.

- Iveson, S., Litster, J., Hapgood, K., and Ennis, B. (2001). Nucleation, growth and breakage phenomena in agitated wet granulation processes: a review. *Powder Technology*, 117(1-2):3–39.
- Jenkins, J. and Mancini, F. (1987). Balance laws and constitutive relations for plane flows of a dense, binary mixture of smooth, nearly elastic, circular disks. *Journal of Applied Mechanics*, 1(54):27–34.
- Jenkins, J. and Mancini, F. (1989). Kinetic theory for binary mixtures of smooth, nearly elastic spheres. *Physics of Fluids, A*, 1(12):2050–2057.
- Johnson, K. and Greenwood, J. (1997). An adhesion map for the contact of elastic spheres. *Journal of colloid and interface science*, 192(2):326–333.
- Johnson, K., Kendall, K., and Roberts, A. (1971). Surface energy and the contact of elastic solids. *Proceedings of the Royal Society London A*, 324:301–313.
- Jop, P., Forterre, Y., and Pouliquen, O. (2006). A constitutive law for dense granular flows. *Nature*, 441(7094):727–730.
- Kamrin, K. and Koval, G. (2012). Nonlocal constitutive relation for steady granular flow. *Physical Review Letters*, 108(17):178301.
- Kim, H. and Arastoopour, H. (2002). Extension of kinetic theory to cohesive particle flow. *Powder Technology*, 122(1):83–94.
- Kim, S. and Karrila, S. (1991). *Microhydrodynamics: principles and selected applications*. Butterworth-Heinemann.
- Kobayashi, T., Tanaka, T., Shimada, N., and Kawaguchi, T. (2013). Dem-cfd analysis of fluidization behavior of geldart group a particles using a dynamic adhesion force model. *Powder Technology*, 248:143–152.
- Koch, D. L. (1990). Kinetic theory for a monodisperse gas-solid suspension. *Physics of Fluids A*, 2(10):1711–1723.

- Koch, D. L. and Sangani, A. S. (1999). Particle pressure and marginal stability limits for a homogeneous monodisperse gas-fluidized bed: kinetic theory and numerical simulations. *Journal of Fluid Mechanics*, 400:229–263.
- Kolakaluri, R., Murphy, E., Subramaniam, S., Brown, R., and Fox, R. (2015). Filtration model for polydisperse aerosols in gas-solid flow using granule-resolved direct numerical simulation. *AIChE Journal*, 61(11):3594–3606.
- Kothe, S., Blum, J., Weidling, R., and GÃ¼ttler, C. (2013). Free collisions in a microgravity many-particle experiment. iii. the collision behavior of sub-millimeter-sized dust aggregates. *Icarus*, 225:75–85.
- Kulchitsky, A., Johnson, J., Reeves, D., and Wilkinson, A. (2014). Discrete element method simulation of a boulder extraction from an asteroid. In *Proceedings of the 14th ASCE Biennial International Conference on Engineering, Science, Construction, and Operations in Challenging Environments (St. Louis, Missouri, USA,)*, pages 485–494.
- Kumar, A. (2010). *Microscale Dynamics in Suspensions of Non-spherical Particles*. PhD thesis, University of Illinois Urbana-Champaign.
- Kumar, A. and Higdon, J. (2010). Origins of the anomalous stress behavior in charged colloidal suspensions under shear. *Physical Review E*, 82:051401.
- Kuwabara, G. and Kono, K. (1987). Restitution coefficient in a collision between two spheres. *Japanese journal of applied physics*, 26(8R):1230.
- Lanotte, A., Bec, J., Biferale, L., Cencini, M., and Toschi, F. (2011). About scaling properties of relative velocity between heavy particles in turbulence. *Journal of Physics Conference series*, 318:052010.
- Launder, B. (1990). Phenomenological modelling: present... and future? in j.l. lumley (ed.). *Whither Turbulence? Turbulence at a Crossroads*, pages 439–485.
- Lees, A. and Edwards, S. (1972). The computer study of transport processes under extreme conditions. *Journal of Physics C: Solid State Physics*, 5(15):1921.

- Leyvraz (2003). Scaling theory and exactly solved models in the kinetics of irreversible aggregation. *Physics Reports*, 383:92–212.
- Li, J., Cheng, C., Zhang, Z., Yuan, J., Nemet, A., and Fett, F. (1999). The emms model - its application, development and updated concepts. *Chemical Engineering Science*, 54(22):5409–5425.
- Liard, M., Martys, N., George, W., Lootens, D., and Hebraud, P. (2014). Scaling laws for the flow of generalized newtonian suspensions. *Journal of Rheology*, 58:1993–2015.
- Liu, A. J. and Nagel, S. R. (2010). The jamming transition and the marginally jammed solid. *Annual Review of Condensed Matter Physics*, 1:347–369.
- Liu, L. (2011). Kinetic theory of aggregation in granular flow. *AIChE Journal*, 57(12):3331–3343.
- Liu, P., Kellogg, K., LaMarche, C., and Hrenya, C. (2017). Dynamics of singlet-doublet collisions of cohesive particles. *Chemical Engineering Journal*, 324:380–391.
- Liu, P., LaMarche, C. Q., Kellogg, K. M., and Hrenya, C. M. (2016). Fine-particle deflu-idization: Interaction between cohesion, Young’s modulus and static bed height. *Chemical Engineering Science*, 145:266–278.
- Lois, G., Blawdziewicz, J., and O’Hern, C. S. (2008). Jamming transition and new perco-lation universality classes in particulate systems with attraction. *Physical Review Letters*, 100:028001.
- Lomboy, G., Sundararajan, S., and Wang, K. (2013). Micro- and macroscale coefficients of friction of cementitious materials. *Cement and Concrete Research*, 54:21–28.
- Lomboy, G., Sundararajan, S., Wang, K., and Subramaniam, S. (2011). A test method for determining adhesion forces and hamaker constants of cementitious materials using atomic force microscopy. *Cement and Concrete Research*, 41(11):1157–1166.

- Lomboy, G. R., Wang, K., and Quanji, Z. (2012). Properties of cementitious materials in their dry state and their influences on viscosity of the cementitious pastes. *Powder Technology*, 229:104–111.
- Luding, S. (1998). Collisions & contacts between two particles. In *Physics of dry granular media*, pages 285–304. Springer.
- Luding, S. (2008). Cohesive, frictional powders: contact models for tension. *Granular matter*, 10(4):235–246.
- Luding, S. (2016). Granular matter: So much for the jamming point. *Nature Physics*, 12:531–532.
- Luding, S. and Alonso-Marroquin, F. (2011). The critical-state yield stress (termination locus) of adhesive powders from a single numerical experiment. *Granular Matter*, 13:109–119.
- Luding, S., Clément, E., Blumen, A., Rajchenbach, J., and Duran, J. (1994). Anomalous energy dissipation in molecular-dynamics simulations of grains: The detachment effect. *Physical Review E*, 50(5):4113.
- Luding, S., Huthmann, M., McNamara, S., and Zippelius, A. (1998). Homogeneous cooling of rough, dissipative particles: Theory and simulation. *Physical Review E*, 58(3):3416–3425.
- Majmudar, T., Sperl, M., Luding, S., and Behringer, R. (2007). Jamming transition in granular systems. *Physical Review Letters*, 98:058001.
- Makse, H. A., Johnson, D. L., and Schwartz, L. M. (2000). Packing of compressible granular materials. *Physical review letters*, 84(18):4160.
- Marchisio, D. L. and Fox, R. O. (2013). *Computational Models for Polydisperse Particulate and Multiphase Systems*. Cambridge University Press.
- Markutsya, S., Fox, R., and Subramaniam, S. (2014). Characterization of sheared colloidal aggregation using langevin dynamics simulation. *Physical Review E*, 89:062312.

- Marmur, B. L. and Heindel, T. J. (2016). Effect of particle size, density, and concentration on granular mixing in a double screw pyrolyzer. *Powder Technology*, 302:222–235.
- Martys, N. and Ferraris, C. (2002). Simulation of sec flow. In *First North American Conference on the Design and Use of Self-Consolidating Concrete. Proceedings. Chicago, IL,*.
- Martys, N., Khalil, M., George, W., and Lootens, D. (2012). Stress propagation in a concentrated colloidal suspension under shear. *European Physical Journal E*, 35(3):1–7.
- Matsunaga, T., Kim, J., Hardcastle, S., and Rohatgi, P. (2002). Crystallinity and selected properties of fly ash particles. *Materials Science and Engineering*, A325:333–343.
- Maugis, D. (1992). Adhesion of spheres: the jkr-dmt transition using a dugdale model. *Journal of colloid and interface science*, 150(1):243–269.
- Maxey, M. (1987). The gravitational settling of aerosol particles in homogeneous turbulence and random flow fields. *Journal of Fluid Mechanics*, 174:441–465.
- Mckay, W. and Mckay, J. (1971). *Building Construction Vol. Ii (Fourth Edition)*. Orient Longman Private Limited.
- McMillan, J., Shaffer, F., Gopalan, B., Chew, J. W., Hrenya, C., Hays, R., Karri, S. R., and Cocco, R. (2013). Particle cluster dynamics during fluidization. *Chemical Engineering Science*, 100:39–51.
- McNamara, S. and Young, W. (1992). Inelastic collapse and clumping in a one-dimensional granular medium. *Physics of Fluids A*, 4(3):496–504.
- Mehrabadi, M. (2016). *Analysis of gas-solid flow using particle-resolved direct numerical simulation: flow physics and modeling*. PhD thesis, Iowa State University.
- Mehrabadi, M., Murphy, E., and Subramaniam, S. (2016a). Development of a gas-solid drag law for clustered particles using particle-resolved direct numerical simulation. *Chemical Engineering Science*, 152:199–212.

- Mehrabadi, M., Tenneti, S., and Subramaniam, S. (2016b). Importance of the fluid-particle drag model in predicting segregation in bidisperse gas-solid flow. *International Journal of Multiphase Flow*, 86:99–114.
- MiDi, G. (2004). On dense granular flows. *The European Physical Journal E*, 14(4):341–365.
- Miller, A. and Gidaspow, D. (1992). Dense, vertical gas-solid flow in a pipe. *AIChE Journal*, 38(11):1801–1815.
- Mills, P., Rognon, P., and Chevier, F. (2008). Rheology and structure of granular materials near the jamming transition. *EPL (Europhysics Letters)*, 81:64005.
- Miyamoto, H., Kargel, J., Fink, W., and Furfaro, R. (2008). Granular processes on itokawa, a small near-earth asteroid: Implications for resource utilization. *Space Exploration Technologies, Proceedings of SPIE*, 6960:69600I.
- Monchaux, R., Bourgoin, M., and Cartellier, A. (2010). Preferential concentration of heavy particles: a voronoi analysis. *Physics of Fluids*, 22(10):103304.
- Moreno-Atanasio, R., Xu, B., and Ghadiri, M. (2007). Computer simulation of the effect of contact stiffness and adhesion on the fluidization behaviour of powders. *Chemical engineering science*, 62(1):184–194.
- Morrow, C., Lovell, M., and Ning, X. (2003). A jkr–dmt transition solution for adhesive rough surface contact. *Journal of Physics D: Applied Physics*, 36(5):534.
- Mounfield, C. and Edwards, S. (1994). A model for the packing of irregularly shaped grains. *Physica A*, 210:301–316.
- Müller, M.-K. and Luding, S. (2011). Homogeneous cooling with repulsive and attractive long-range potentials. *Mathematical Modelling of Natural Phenomena*, 6(4):118–150.
- Murphy, E., Mehrabadi, M., Tenneti, S., and Subramaniam, S. (2015). Modeling two-point particle dynamics of homogeneous gas-solid flows to describe clustering and stability. In *68th annual meeting of the American physical society division of fluid dynamics, At Boston, MA*.

- Murphy, E. and Subramaniam, S. (2014). A model for solid-solid drag in bidisperse gas-solid flows. In *67th Annual Meeting of the APS Division of Fluid Dynamics*, volume 59.
- Murphy, E. and Subramaniam, S. (2015). Freely cooling granular gases with short-ranged attractive potentials. *Physics of Fluids (1994-present)*, 27(4):043301.
- Murphy, E. and Subramaniam, S. (2017). Binary collision outcomes for inelastic soft-sphere models with cohesion. *Powder Technology*, 305:462–476.
- Nachenius, R., van de Wardt, T., Ronsse, F., and Prins, W. (2015). Effect of particle size, density, and concentration on granular mixing in a double screw pyrolyzer. *Fuel Processing Technology*, 130:87–95.
- Narayanan, K. and Ramamurthy, K. (2000). Structure and properties of aerated concrete: a review. *Cement and Concrete Composites*, 22(5):321–329.
- Nase, S. T., Vargas, W. L., Abatan, A. A., and McCarthy, J. (2001). Discrete characterization tools for cohesive granular material. *Powder Technology*, 116(2):214–223.
- Nauman, E. B. (2001). *Chemical Reactor Design, Optimization, and Scaleup*. McGraw-Hill.
- Nienow, A., Edwards, M., and Harnby, N. (1992). *Mixing in the Process Industries: Mixing of Cohesive Powders*. Elsevier, Oxford, 2nd edition.
- of Chemistry, T. R. S. (2008). The concrete conundrum. *Chemistry World*.
- Oliver, W. C. and Pharr, G. M. (1992). An improved technique for determining hardness and elastic modulus using load and displacement sensing indentation experiments. *Journal of materials research*, 7(06):1564–1583.
- Ortiz de Zarate, J. and Sengers, J. (2006). *Hydrodynamic Fluctuations in Fluids and Fluid Mixtures*. Elsevier.
- Oseen, C. (1927). Neuere methoden und ergebnisse in der hydrodynamik. *Akademische Verlagsgesellschaft*.

- Otsuki, M., Hayakawa, H., and Luding, S. (2010). Behavior of pressure and viscosity at high densities for two-dimensional hard and soft granular materials. *Progress of Theoretical Physics Supplement*, 184:110–133.
- Pasha, M., Dogbe, S., Hare, C., Hassanpour, A., and Ghadiri, M. (2014). A linear model of elasto-plastic and adhesive contact deformation. *Granular Matter*, 16(1):151–162.
- Pathak, S., Jabeen, Z., Dibyendu, D., and Rajesh, R. (2014). Energy decay in three-dimensional freely cooling granular gas. *Physical Review Letters*, 112:038001.
- Paul, E. L., Atiemo-Obeng, V. A., and Kresta, S. M. (2004). *Handbook of industrial mixing: science and practice*. John Wiley ”&” Sons.
- Perni, S. and Prokopovich, P. (2015). Multi-asperity elliptical jkr model for adhesion of a surface with non-axially symmetric asperities. *Tribology International*, 88:107–114.
- Persson, B. N. and Scaraggi, M. (2014). Theory of adhesion: Role of surface roughness. *The Journal of chemical physics*, 141(12):124701.
- Pettersen, O. (2007). Sandstone compaction, grain packing and critical state theory. *Petroleum Geoscience*, 13:63–67.
- Plimpton, S. (1995). Fast parallel algorithms for short-range molecular dynamics. *Journal of Computational Physics*, 117:1–19.
- Pope, S. B. (2000). *Turbulent Flows*. Cambridge University Press.
- Prokopovich, P. and Starov, V. (2011). Adhesion models: From single to multiple asperity contacts. *Advances in colloid and interface science*, 168(1):210–222.
- Rahman, M., Wiklund, J., Kotze, R., and Hakansson, U. (2017). Yield stress of cement grouts. *Tunnelling and Underground Space Technology*, 61:50–60.
- Rani, S. L., Dhariwal, R., and Koch, D. L. (2014). A stochastic model for the relative motion of high stokes number particles in isotropic turbulence. *Journal of Fluid Mechanics*, 756:870–902.

- Reeks, M. (1980). Eulerian direct interaction applied to the statistical motion of particles in a turbulent flow. *Journal of Fluid Mechanics*, 97:569–590.
- Rognon, P. G., Roux, J.-N., Naaïm, M., and Chevoir, F. (2008). Dense flows of cohesive granular materials. *Journal of Fluid Mechanics*, 596:21–47.
- Rong, L., Dong, K., and Yu, A. (2014). Lattice-boltzmann simulation of fluid flow through packed beds of spheres: effect of particle size distribution. *Chemical Engineering Science*, 116:508–523.
- Rotne, J. and Prager, S. (1969). Variational treatment of hydrodynamic interaction in polymers. *Journal of Chemical Physics*, 50:4831–4837.
- Roussel, N., Lemaitre, A., Flatt, R., and Coussot, P. (2010). Steady state flow of cement suspensions: A micromechanical state of the art. *Cement and Concrete Research*, 40(1):77–84.
- Roussel, N., Ovarlez, G., Garrault, S., and Brumaud, C. (2012). The origins of thixotropy of fresh cement pastes. *Cement and Concrete Research*, 42(1):148–157.
- Rumpf, H. (1958). Grundlagen und methoden des granulierens. *Chemie Ingenieur Technik*, 30(3):144–158.
- Rycroft, C., Grest, G., Landry, J., and Bazant, M. (2006). Analysis of granular flow in a pebble-bed nuclear reactor. *Physical Review E*, 74:021306.
- Saha, S. and Alam, M. (2016). Normal stress differences, their origin and constitutive relations for a sheared granular fluid. *Journal of Fluid Mechanics*, 795:549–580.
- Saitoh, K. and Mizuno, H. (2016). Enstrophy cascades in two-dimensional dense granular flows. *Physical Review E*, 94:022908.
- Saitoh, K., Takada, S., and Hayakawa, H. (2015). Hydrodynamic instabilities in shear flows of dry cohesive granular particles. *Soft matter*, 11(32):6371–6385.

- Schäfer, J., Dippel, S., and Wolf, D. (1996). Force schemes in simulation of granular material. *J. Phys. I France*, 6:5–20.
- Schlick, C. P., Isner, A. B., Freireich, B. J., Fan, Y., Umbanhowar, P. B., Ottino, J. M., and Lueptow, R. M. (2016). A continuum approach for predicting segregation in flowing polydisperse granular materials. *Journal of Fluid Mechanics*, 797:95–109.
- Shah, S. and Wang, K. (2004). Development of green cement for sustainable concrete using cement kiln dust and fly ash. In *Proceedings of the International Workshop on Sustainable Development and Concrete Technology*.
- Shannon, C. (1948). A mathematical theory of communication. *Bell System Technical Journal*, 27(3):379–423.
- Silbert, L. E., Ertas, D., Grest, G. S., Halsey, T. C., Levine, D., and Plimpton, S. J. (2001). Granular flow down an inclined plane: Bagnold scaling and rheology. *Physical Review E*, 64(5):051302.
- Silbert, L. E., Grest, G. S., Brewster, R., and Levine, A. J. (2007). Rheology and contact lifetimes in dense granular flows. *Physical review letters*, 99(6):068002.
- Singh, A., Magnanimo, V., Saitoh, K., and Luding, S. (2014). Effect of cohesion on shear banding in quasistatic granular materials. *Physical Review E*, 90(2):022202.
- Singh, A., Magnanimo, V., Saitoh, K., and Luding, S. (2015). The role of gravity or pressure and contact stiffness in granular rheology. *New journal of physics*, 17(4):043028.
- Sjostrom, S. and Krutka, H. (2009). Evaluation of solid sorbents as a retrofit technology for co2 capture. *Fuel*, 89(6):1298–1306.
- Song, C., Wang, P., and Makse, H. A. (2008). A phase diagram for jammed matter. *Nature*, 453(7195):629–632.
- Stevens, A. and Hrenya, C. (2005). Comparison of soft-sphere models to measurements of collision properties during normal impacts. *Powder Technology*, 154(2):99–109.

- Stoyan, D., Kendall, W., and Mecke, J. (1995). *Stochastic geometry and its applications*. John Wiley and Sons, New York, 2nd edition.
- Stutzman, P. (2004). Scanning electron microscopy imaging of hydraulic cement microstructure. *Cement and Concrete Composites*, 26:957–966.
- Subramaniam, S. (2000). Statistical representation of a spray as a point process. *Physics of Fluids*, 12(10):2413–2431.
- Subramaniam, S. (2001). Statistical modeling of sprays using the droplet distribution function. *Physics of Fluids*, 13(3):624–642.
- Subramaniam, S. (2012). Stability limits for gas-solid suspensions with finite fluid inertia using particle-resolved direct numerical simulations. *NSF Annual Report 1134500*.
- Subramaniam, S. (2014). Stability limits for gas-solid suspensions with finite fluid inertia using particle-resolved direct numerical simulations. *NSF Annual Report 1134500*.
- Sun, J., Battaglia, F., and Subramaniam, S. (2006). Dynamics and structures of segregation in a dense, vibrating granular bed. *Physical Review E*, 74(6):061307.
- Sun, J. and Sundaresan, S. (2011). A constitutive model with microstructure evolution for flow of rate-independent granular materials. *Journal of Fluid Mechanics*, 682:590–616.
- Sundaram, S. and Collins, L. (1997). Collision statistics in an isotropic, particle-laden turbulent suspension i. direct numerical simulations. *Journal of Fluid Mechanics*, 335:75–109.
- Syamlal, M. (1987). The particle-particle drag term in a multiphase model of fluidization. *Technical Report DOE/MC/21353-2373, NTIS/DE87006500, National Technical Information Service*.
- Syamlal, M. and O’Brien, T. (1987). A generalized drag correlation for multiparticle systems. *Technical Report, Morgantown Energy Technology Center DOE Report*.
- Syamlal, M., Rogers, W., and O’Brien, T. (1993). Mfix documentation: Theory guide. *Morgantown Energy Technology Center Morgantown, WV, USA*, page 54.

- Tabor, D. (1977). Surface forces and surface interactions. *Journal of colloid and interface science*, 58(1):2–13.
- Takada, S., Saitoh, K., and Hayakawa, H. (2014). Simulation of cohesive fine powders under a plane shear. *Physical Review E*, 90(6):062207.
- Takada, S., Saitoh, K., and Hayakawa, H. (2015a). Kinetic theory for dilute cohesive granular gases with a square well potential. *arXiv preprint arXiv:1506.04578*.
- Takada, S., Saitoh, K., and Hisao, H. (2015b). Simulation of cohesive fine powders under a plane shear. *Physical Review E*, 90:062207.
- Tenneti, S., Garg, G., and Subramaniam, S. (2011). Drag law for monodisperse gas-solid systems using particle-resolved direct numerical simulation of flow past fixed assemblies of spheres. *International Journal of Multiphase Flows*, 37(9):1072–1092.
- Tenneti, S., Mehrabadi, M., and Subramaniam, S. (2016). Stochastic lagrangian model for hydrodynamic acceleration of inertial particles in gas-solid suspensions. *Journal of Fluid Mechanics*, 788:695–729.
- Tenneti, S. and Subramaniam, S. (2014). Particle-resolved direct numerical simulation for gas-solid flow model development. *Annual Review of Fluid Mechanics*, 46:199–230.
- Thornton, C., Cummins, S. J., and Cleary, P. W. (2013). An investigation of the comparative behaviour of alternative contact force models during inelastic collisions. *Powder Technology*, 233:30–46.
- Thornton, C. and Ning, Z. (1998). A theoretical model for the stick/bounce behaviour of adhesive, elastic-plastic spheres. *Powder technology*, 99(2):154–162.
- Tien, C. and Ramarao, B. (2007). *Granular Filtration of Aerosols and Hydrosols*. Elsevier, Oxford, 2nd edition.
- Tomas, J. (2000). Particle adhesion fundamentals and bulk powder consolidation. *KONA Powder and Particle Journal*, 18(0):157–169.

- Torquato, S. (1995). Mean nearest-neighbor distance in random packings of hard d-dimensional spheres. *Physical Review Letters*, 74(12):2156–2159.
- Trizac, E. and Hansen, J. (1995). Dynamic scaling behavior of ballistic coalescence. *Physical Review Letters*, 74(21):4114–4117.
- Trizac, E. and Hansen, J. (1996). Dynamics and growth of particles undergoing ballistic coalescence. *Journal of Statistical Physics*, 86(5-6):1345–1370.
- Tsuji, Y., Kawaguchi, T., and Tanaka, T. (1993). Discrete particle simulation of two-dimensional fluidized bed. *Powder technology*, 77(1):79–87.
- Uhlmann, M. and Doychev, T. (2014). Sedimentation of a dilute suspension of rigid spheres at intermediate galileo numbers: the effect of clustering upon the particle motion. *Journal of Fluid Mechanics*, 752:310–348.
- UNEP, U. N. E. P. (2012). Greening cement production has a big role to play in reducing greenhouse gas emissions. *UNEP Report 2012, Environmental Science Alert Thematic Focus: Resource Efficiency, Harmful Substances and Hazardous Waste, and Climate Change*.
- van der Hoef, M., Beestra, R., and Kuipers, J. (2005). Lattice-boltzmann simulations of low-reynolds-number flow past mono- and bidisperse arrays of spheres: results for the permeability and drag force. *Journal of Fluid Mechanics*, 528:233–254.
- van Noije, T., Ernst, M., and Brito, R. (1998a). Ring kinetic theory for an idealized granular gas. *Physica A*, 251:266–283.
- van Noije, T., Ernst, M., and Brito, R. (1998b). Spatial correlations in compressible granular flows. *Physical Review E*, 57(5):R4893.
- van Noije, T., Ernst, M., Brito, R., and Orza, J. (1997). Mesoscopic theory of granular fluids. *Physical Review Letters*, 79(3):411–414.
- Vidyapati and Subramaniam, S. (2013). Granular flow in silo discharge: Discrete element method simulations and model assessment. *Industrial "E" Engineering Chemistry Research*, 52(36):13171–13182.

- Vidyapati, V., Langroudi, M. K., Sun, J., Sundaresan, S., Tardos, G., and Subramaniam, S. (2012). Experimental and computational studies of dense granular flow: Transition from quasi-static to intermediate regime in a couette shear device. *Powder Technology*, 220:7–14.
- von Karman, T. and Howarth, L. (1938). On the statistical theory of isotropic turbulence. *Proceedings of the Royal Society of London. Series A, Mathematical and Physical Sciences*, 164(917):192–215.
- Walton, O. R. (1984). Application of molecular dynamics to macroscopic particles. *International Journal of Engineering Science*, 22(8):1097–1107.
- Walton, O. R. (2004). Potential discrete element simulation applications ranging from airborne fines to pellet beds. *SAE 2004 Transactions J. Aerospace*.
- Wang, K., Subramaniam, S., and Sundararajan, S. (2013). Final report: Understanding rheology of cement-based materials through integrated experiments and computations at multiple scales. *Final Report NSF CBET Grant No. 0927660*.
- Waters, J., Lee, S., and Guduru, P. (2009). Mechanics of axisymmetric wavy surface adhesion: Jkr–dmt transition solution. *International Journal of Solids and Structures*, 46(5):1033–1042.
- Weller, H., Tabor, G., Jasak, H., and Fureby, C. (1998). A tensorial approach to computational continuum mechanics using object-oriented techniques. *Computers in Physics*, 12(6):620–631.
- Wilson, R., Dini, D., and van Wachem, B. (2016). A numerical study exploring the effect of particle properties on the fluidization of adhesive particles. *AIChE Journal*, 62(5):1467–1477.
- Wylie, J. J. and Koch, D. L. (2000). Particle clustering due to hydrodynamic interactions. *Physics of Fluids*, 12(5):964–970.
- Xing, Z., Kenty, B., Li, Z., and Lee, S. (2009). Scale-up analysis for a cho cell culture process in large-scale bioreactors. *Biotechnology and Bioengineering*, 103(4):733–746.
- Xu, Y. and Subramaniam, S. (2007). Consistent modeling of interphase turbulent kinetic energy transfer in particle-laden turbulent flows. *Physics of Fluids*, 19:085101.

- Yao, H., Ciavarella, M., and Gao, H. (2007). Adhesion maps of spheres corrected for strength limit. *Journal of colloid and interface science*, 315(2):786–790.
- Yin, X., Zenk, J. R., Mitrano, P. P., and Hrenya, C. M. (2013). Impact of collisional versus viscous dissipation on flow instabilities in gas-solid systems. *Journal of Fluid Mechanics*, 727:R2.
- Zaichik, L. and Alipchenkov, V. (2003). Pair dispersion and preferential concentration of particles in isotropic turbulence. *Physics of Fluids*, 15:1776–1787.
- Zaichik, L. I. and Alipchenkov, V. M. (2009). Statistical models for predicting pair dispersion and particle clustering in isotropic turbulence and their applications. *New Journal of Physics*, 11:103018.
- Zamankhan, P. (2005). Kinetic theory of multicomponent dense mixtures of slightly inelastic spherical particles. *Physical Review E*, 52(5):4877–4891.
- Zhang, Q. and Kamrin, K. (2017). Microscopic description of the granular fluidity field in nonlocal flow modeling. *Physical Review Letters*, 118:058001.

CHAPTER 3. FREELY COOLING GRANULAR GASES WITH SHORT-RANGED ATTRACTIVE POTENTIALS

This chapter is an article titled “Freely Cooling Granular Gases with Short-Ranged Attractive Potentials” published in *Physics of Fluids* authored by E. Murphy and S. Subramaniam (Murphy and Subramaniam, 2015).

Abstract

We treat the case of an undriven gas of inelastic hard-spheres with short-ranged attractive potentials via an extension of the pseudo-Liouville operator formalism. New evolution equations for the granular temperature and coordination number are obtained. The granular temperature exhibits deviation from both Haff’s law and the case of long-ranged potentials. We verify this departure using soft-sphere discrete element method (DEM) simulations. Excellent agreement is found for the duration of the simulation even beyond where exclusively binary collisions are expected. Simulations show the emergence of strong spatial-velocity correlations on the length-scale of the last peak in the pair-correlation function, but do not show strong correlations beyond this length-scale. We argue that molecular chaos may remain an adequate approximation if the system is modelled as a Smoluchowski type equation with aggregation and break-up processes.

3.1 Introduction

The use of micron-sized particles is ubiquitous in industry, and the properties of particles at this scale are of interest in a host of applications: fluidization of Geldart C powders (Geldart, 1973; Kim and Arastoopour, 2002), filtration (Tien and Ramarao, 2007), materials processing

(Castellanos et al., 1999) , powder mixing (Nienow et al., 1992), rheology (Brewster et al., 2005; Aarons and Sundaresan, 2006; Rognon et al., 2008; Takada et al., 2015b), etc. These particles also present themselves in extra-terrestrial problems, such as aggregation of planetesimals in the early solar system (Blum et al., 2000), and contamination by Martian and Lunar regolith (Colwell et al., 2007). These particles are interesting not only due to their ubiquity, but also due to their unusual behavior. Energy is not conserved in collisions due to many internal degrees of freedom, and yet reversible short-range interactions remain important. The combination of these two interactions leads to particle trapping/sticking in binary collisions. That is, for collisions below a critical impact velocity, $|v_{crit}|$ (absolute value of the normal component of the relative velocity), a pair of particles does not retain adequate kinetic energy after a collision to re-emerge from a short-ranged potential well. They appear to stick after a binary collision, an impermissible result in both classical conservative and granular systems. The presence of this sticking mechanism qualitatively changes the behavior of many-particle systems.

Few kinetic theory approaches have been proposed and adequately developed for handling systems with both dissipation and attractive wells, where sticking behavior may present itself. One approach has been to focus on systems where sticking does not occur (Müller and Luding, 2011) and treat weaker long-range interactions. An alternative approach is to treat the sticking systems with aggregation and break-up processes (Liu, 2011; Kim and Arastoopour, 2002). This approach, though attractive, has two short-comings that arise from approximating the collision integral, which we stress is unknown *a priori*: (1) dissipation from multi-particle collisions has been found to behave quite differently from binary systems (Kothe et al., 2013), and (2) evolution of the scattering cross-section is not known, i.e. aggregates develop unknown intraparticle structure. Often this lacking information is handled by treating systems in the limit where *all* particles stick to one another, producing larger spheres, the so-called ballistic coalescence (Trizac and Hansen, 1995, 1996; Leyvraz, 2003). Recently, such theories have been applied to assessing the long-time cooling behavior of granular gases (Pathak et al., 2014).

We will treat systems where a sticking behavior is present using an extension of the pseudo-Liouville approach (Ernst et al., 1969) and subsequently explore the validity of such a theory. In an effort to understand these systems from a first principles approach, we study the sim-

ple problem of a gas of cohesive particles cooling via inelastic collisions. The problem of a homogeneous gas of inelastic hard-spheres was first considered by Haff (1983). Through a heuristic treatment Haff predicted the evolution of energy in a gas of such particles, known today as Haff's law. More thorough treatments followed, employing the pseudo-Liouville operator theory (Luding et al., 1998) and Sonine polynomial expansions (Goldshtein and Shapiro, 1995). Other studies identified a number of instabilities and interesting behavior (McNamara and Young, 1992; Goldhirsch and Zanetti, 1993), including the growth of vortical structures and two-point density correlations, i.e. clustering. We expect that the nature of such instabilities is qualitatively changed in the presence of short-range attractive potentials, and we show evidence of interesting consequences of sticking by examining two-point correlations.

We solve the mean-field temperature evolution problem with the addition of short-range attractive potentials, building on the long-range results of Müller and Luding (2011) for dilute systems. The main difference between the approach developed in this work and that of Müller and Luding (2011) is the form of the final ODE governing the decay of kinetic energy. The discrepancy in temperature evolution equations arises from differences in treatment of the collision dynamics: single collision event (Müller and Luding, 2011) vs. infinite series of recollision events. (Müller and Luding, 2011) show that long-range attractive potentials accelerate cooling by effectively increasing the range of interaction, and hence the number of particles with which a given particle will collide. The amount of dissipation in a collision is also affected. Empirically fit corrections for higher density are also proposed by the authors (Müller and Luding, 2011).

For particles with short-range potentials, i.e. range of interaction much smaller than the mean free path and with collision durations much shorter than the free flight time, the treatment can be simplified. Collisions are again considered as discrete events, but the effective coefficient of restitution must be modified. A full population balance theory, presented in the appendix, includes unclosed monomer-cluster and cluster-cluster terms in the collision integral. Our approach is thus able to treat the decay due to particle re-collision and aggregation. The theory may be simplified in the short-time limit, where the number of sticking collision events is small. A cooling law is also established in this limit by solving the final differential equation numerically, which we compare with Haff's law and the results of (Müller and Luding, 2011).

Finally, we compare our results with soft-sphere DEM. For short times, where the number of sticking collision events is small, we quantitatively predict departure from both aforementioned cooling laws.

3.2 Analytic Methods

3.2.1 The Binary System with Short-Ranged Attraction

We begin our analytic treatment with a focus on the mechanics of a binary inelastic hard-sphere system. Interactions within the system are completely defined by so-called collision rules. Later these rules will be used to construct collision operators appropriate for cases when cohesion is present. The simplest and most frequently used collision model is found in eqn. 3.1: a collision between two inelastic hard-spheres with constant coefficient of restitution. The most general form of the model relating pre-collisional velocities and post-collisional velocities is often given as

$$\begin{aligned} v_i'^{(j)} &= v_i^{(j)} - \frac{m^{(k)}}{m^{(j)} + m^{(k)}} (1 + \epsilon) \left(v_l^{(kj)} \hat{r}_l^{(jk)} \right) \hat{r}_i^{(jk)} \\ v_i'^{(k)} &= v_i^{(k)} - \frac{m^{(j)}}{m^{(j)} + m^{(k)}} (1 + \epsilon) \left(v_l^{(jk)} \hat{r}_l^{(jk)} \right) \hat{r}_i^{(jk)}, \end{aligned} \quad (3.1)$$

where subscripts denote vector components of velocities v and positions r . Einstein notation is also used, where repeated indicies indicate an inner product. A single superscript indicates a particle index and a quantity associated with that particle in the laboratory frame. Two superscripts indicate a relative vector constructed from the inertial reference frame of the particle with the first superscript, that is $v_l^{(jk)} = v_l^{(k)} - v_l^{(j)}$. Lastly, a unit vector is indicated by a caret. A single parameter determining the outcome of a collision is the coefficient of restitution, given by ϵ . The physical limits that ϵ may take are $\epsilon \in [0, 1]$.

In a similar vein, collision rules may also be constructed for cases with short-ranged attraction so that we may apply the pseudo-Liouville operator theory. Whereas the instantaneous nature of hard-sphere collisions guarantees that we may straightforwardly construct collision rules for use in the pseudo-Liouville theory, particles with attractive wells are afforded no such

luxury. We impose a few restrictions to set a context such that the collision events still remain essentially discrete and binary. The first restriction is that the length-scale of the potential well, l_{well} , must be much smaller than the particle diameter D . This is true for micron sized particles, where interactions such as the van der Waals force remain important, $D/l_{well} = O(100)$. When considering the granular gas, we will also restrict ourselves to cases where the mean-free path λ is sufficiently large ($\lambda > l_{well}$). Lastly, we assume that the time-scale for the duration of a collision, i.e. the time it takes a particle to enter the well, collide, and exit the well, is much smaller than the free-flight time. The two latter assumption restricts our cases to systems of moderate dilution, depending on solids volume fraction, particle properties, and thermal speed of the granules. Together, the three restrictions allow us to treat systems with the additional short-ranged attraction as approximately hard-sphere systems.

The attractive potential we consider is the van der Waals potential for macroscopic spheres,

$$\Phi(x) = \Phi_{vdW}(x) = -\frac{AR_s}{6x}, \quad (3.2)$$

where A and R_s denote the effective Hamaker constant for the materials that comprise the particles, and the effective radius of curvature of the particle surfaces, respectively. The effective radius of curvature takes the value $R_s = D/4$ for smooth spheres. The effective separation distance between two surfaces of identical particles x is defined as $x = \left| r_{\parallel}^{(jk)} \right| - 2a + d_0$, with the potential at contact $x = d_0$ being defined as Φ_c . Details about using this potential to construct collision laws may be found in appendix E.

Three stages of the collision process are identified: approach, collision, and separation (see appendix E for details). If all three stages of a collision between the cohesive particles are considered, one obtains an equation relating the normal relative velocity of a pair of particles before entering the well, $v_{\parallel,1}^{(jk)}$ to the normal relative velocity of a pair exiting the well $v_{\parallel,4}^{(jk)}$.

We refer to the relationship as an effective coefficient of restitution, given by

$$\epsilon_{\text{eff}} = -\frac{v_{\parallel,4}^{(jk)}}{v_{\parallel,1}^{(jk)}} = \begin{cases} (\epsilon^2 + (1 - \epsilon^2) Ha_p)^{1/2} & : v_{\parallel}^{(jk)} \in (-\infty, v_{crit}) \\ 0 & : v_{\parallel}^{(jk)} \in [v_{crit}, 0], \end{cases} \quad (3.3)$$

where $Ha_p = 4\Phi_c / \left(mv_{\parallel}^{(jk)2} \right)$ and the critical velocity is $v_{crit} = -\sqrt{-4\Phi_c(1 - \epsilon^2)/m\epsilon^2}$. The

dimensionless quantity Ha_p is the ratio of potential energy at contact to the kinetic energy present in the normal component of the relative velocity at the edge of the potential well. Note that Ha_p and v_{crit} are negative quantities. This asymptotic expression was previously derived by Dahneke (1975) and experimentally verified for $1.27 \mu m$ latex spheres impacting a fused silica surface. In the dilute granular gas problem, the probability of particles beginning within the active region of the well is small, due to the short-ranged nature of the interaction, so we do not consider collisions between initially separating pairs.

The effective coefficient of restitution has interesting behavior, as shown in fig. 2.3 for different values of ϵ . There exist two qualitatively different solutions, depending on the normal relative velocity at the edge of the well, $v_{\parallel,1}^{(jk)} = v_{i,1}^{(jk)} \hat{r}_i^{(jk)}$. First, if the magnitude of the initial velocity is greater than the critical velocity, particles only experience an attenuation of the effective coefficient of restitution ϵ_{eff} . Particle pairs with more kinetic energy in the normal relative degree of freedom or alternatively weaker potentials, i.e. low $|Ha_p|$, experience almost no difference between ϵ_{eff} and ϵ . As $|Ha_p|$ is increased, the discrepancy between ϵ_{eff} and ϵ also increases, and collisions become more dissipative. The angle of separation for the collision partners also decreases (see figs. D.1(a)-D.1(b) in appendix D). Eventually, the initial kinetic energy is low enough that qualitatively different behavior emerges, where particles no longer have sufficient kinetic energy to exit the well. In this case, particles cannot reach the edge of well and instead fall back into contact, and the pair experiences a rapid succession of recollisions. This quickly dissipates the energy in the $\hat{r}_{\parallel}^{(jk)}$ degree of freedom. The conceptual picture for this collision outcome differs from the completely inelastic case (see figs. D.1(c)-D.1(d) in appendix D). For all practical purposes, these particles have stuck to one another forming a dimer. Additionally, the tangential components of relative velocity are transformed into rotating degrees of freedom for the newly formed dimer (see fig. D.1(d)). This result is fully characterized by $Ha_{crit,p} = -\epsilon^2 / (1 - \epsilon^2)$, which is only a function of ϵ .

We submit that much more complicated models for binary particle systems have been considered and thoroughly treated in the past. As an example, we point to Brilliantov et al. (2007), who considered the addition of the van der Waals force to collisions between smooth visco-elastic particles. They also accounted for the increase in cohesive force at contact due

to a substantial increase in contact area, which is consistent with the JKR theory (Johnson et al., 1971). Although, the model we consider is far less sophisticated, it maintains many of the key features obtained by the sophisticated model (Brilliantov et al., 2007). For example, the relationship between ϵ_{eff} and impact velocity at low impact velocities remains qualitatively similar. Both theories also display dissipation and particle size-dependent critical impact velocities, under which particles adhere to one another, as observed in experiments (Hatzes et al., 1991; Bridges et al., 1996). The advantage of our model is that we can explicitly express ϵ_{eff} as a function of the single parameter Ha_p , which allows for a cleaner analytic treatment in the following sections.

3.2.2 Solving the Cohesive Problem

A thorough treatment using the pseudo-Liouville operator theory on a system of inelastic spheres is contained in appendix F. In order to apply the pseudo-Liouville theory, as mentioned in section 3.2.1, we must be able to approximate dilute systems of dissipative hard-spheres with short-ranged attractive potentials, as hard-sphere systems with an altered hard-core distance, $|r_{i,c}^{(jk)}| = 2a + l_{\text{well}}$. In the treatment that follows we neglect the additional length-scale l_{well} , since $l_{\text{well}} \ll a$. In appendix G we have developed an extension to the pseudo-Liouville operator that is applicable to systems with short-ranged attraction. The complete theory forms a set of population balance equations, which account for the enhanced dissipation from restituting and sticking collisions, as well as the aggregation and break-up of aggregates. However, because we do not know the source and sink terms in the aggregate–monomer and aggregate–aggregate difference operators *a priori*, we must restrict ourselves to a theory for cooling that only accounts for the loss of energy due to monomer–monomer collisions, eqn. G.8. For this theory to be valid, we must restrict ourselves to a time interval, when these monomer–monomer interactions dominate. Note that this restriction leaves open the possibility for the development of aggregation and break-up kernels from simulation data, to extend the applicability of the theory to later times.

The pseudo-Liouville operators that we will use for the cohesive case are given by eqns. G.2 and G.3, for restituting and sticking collisions, respectively. For restituting collisions, the

difference operator is identical to that of eqn. F.2 with ϵ_{eff} replacing ϵ . The sticking collisions use the difference operator eqn. G.8. Following the procedure described in appendix F up to eqn. F.5, one obtains a one-dimensional integral equation for the evolution of the ensemble-averaged kinetic energy per particle in terms of collision frequency $\omega = 16\pi^{1/2}a^2ng_cT_g^{1/2}(t)$ and granular temperature, T_g :

$$\begin{aligned} \left\langle \frac{\partial E_{kin,p}(t)}{\partial t} \right\rangle = & -\frac{m\omega}{4\sqrt{2}T_g} \left(\int_{-\infty}^0 dv_{\parallel} \exp\left(-\frac{v_{\parallel}^2}{2T_g}\right) |\sqrt{2}v_{\parallel}| v_{\parallel}^2 \right. \\ & \left. - \sqrt{2}\epsilon^2 \int_{-\infty}^{v_{crit}/\sqrt{2}} dv_{\parallel} \exp\left(-\frac{v_{\parallel}^2}{2T_g}\right) |v_{\parallel}| \left(v_{\parallel}^2 + \frac{2\Phi_c(1-\epsilon^2)}{m\epsilon^2} \right) \right). \end{aligned} \quad (3.4)$$

The limits for the first term represent the sink for all pre-collisional energy, which is the same for both the restituting and sticking pseudo-Liouville operators (see appendix G). The second integral arises only from the pseudo-Liouville operator for restituting collisions when $v_{\parallel} \leq v_{crit}/\sqrt{2}$. Evaluating the integrals gives the evolution of the ensemble-averaged kinetic energy per particle:

$$\begin{aligned} \left\langle \frac{\partial E_{kin,p}(t)}{\partial t} \right\rangle = & -\frac{m}{4}\omega \left(2T_g - \epsilon^2 \left(2T_g - \frac{v_{crit}^2}{2} \right) \exp\left(-\frac{v_{crit}^2}{4T_g}\right) \right. \\ & \left. - \frac{2\Phi_c(1-\epsilon^2)}{m} \exp\left(-\frac{v_{crit}^2}{4T_g}\right) \right). \end{aligned} \quad (3.5)$$

Further simplifying by substituting for v_{crit} , we obtain the final evolution equation for the ensemble-averaged kinetic energy per particle:

$$\begin{aligned} \left\langle \frac{\partial E_{kin,p}(t)}{\partial t} \right\rangle = & -\frac{m}{2}\omega T_g \left(1 - \epsilon^2 \exp\left(-\frac{v_{crit}^2}{4T_g}\right) \right) \\ = & -\frac{m}{2}\omega T_g \left(1 - \epsilon^2 \exp\left(-\frac{Ha}{4Ha_{crit,p}}\right) \right), \end{aligned} \quad (3.6)$$

where $Ha = 4\Phi_c/mT_g$ is the ratio of cohesive energy to average kinetic energy contained in the normal relative velocity, which is defined in terms of the granular temperature. We remind the reader that $Ha_{crit,p} = Ha_p(v_{\parallel}^{(jk)} = v_{crit}) = -\epsilon^2/(1-\epsilon^2)$. This evolution equation appears strikingly similar to that obtained by Haff for inelastic spheres (see eqn. F.7), with the exception of the exponential factor multiplying ϵ^2 , and the parameter v_{crit} . This exponential factor determines the apparent inelasticity of the system. In the limit of very high granular

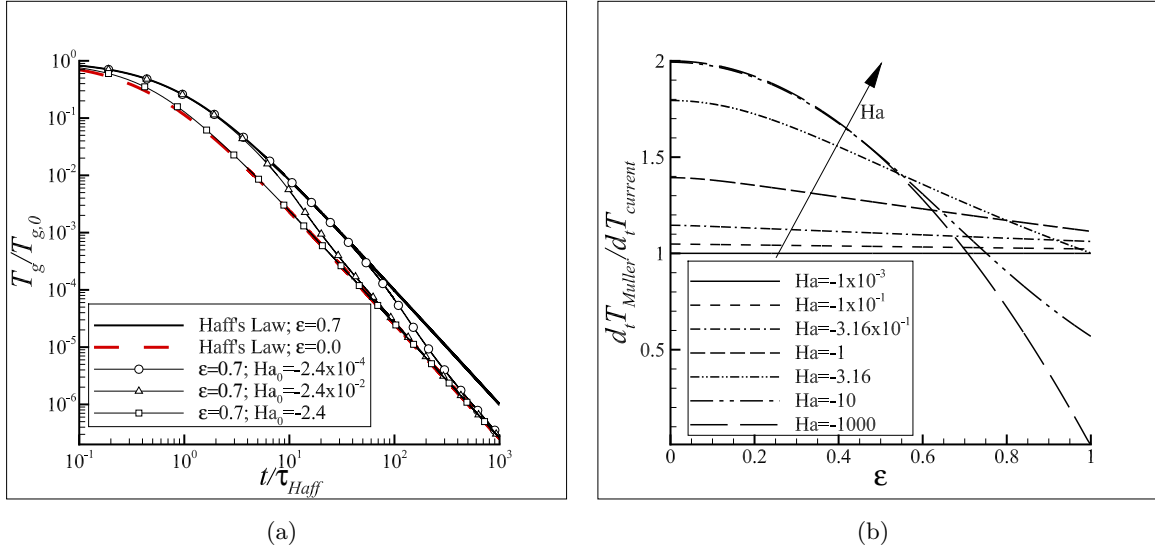


Figure 3.1 (a) The evolution of temperature for several systems with different values for Ha_0 , obtained from numerical integration of eqn. (3.6). In every case, cooling appears to initially follow Haff's law until some finite time. Thereafter, the apparent dissipation increases, and completely inelastic type cooling is observed. The location of this transition depends on the initial ratio of well-energy at contact to particle temperature, Ha_0 . (b) The ratio of cooling rates between eqns. 3.6 and 3.7 are plotted. These comparisons are made for *instantaneous* cooling rates. Large differences in behavior are expected at high values of Ha and as well as slightly inelastic and extremely inelastic ranges.

temperature $T_g \gg v_{crit}^2$ in eqn. 3.6, for example, we obtain cooling behavior that is nearly unchanged from that of a non-cohesive system. As fig. 3.1(a) shows, as cooling progresses the apparent inelasticity increases, until in the limit of $T_g \ll v_{crit}^2$ completely inelastic cooling behavior is expected.

Müller and Luding (2011) obtained a cooling law for a granular gas undergoing weak long-range interactions using the pseudo-Liouville operator formalism that also looks similar to Haff's law:

$$\left\langle \frac{\partial E_{kin,p}(t)}{\partial t} \right\rangle = -\frac{m}{2} \omega T_g (1 - \epsilon^2) \left(2 - \exp\left(\frac{Ha}{2}\right) \right), \quad (3.7)$$

and it is useful to compare and contrast the result in eqn. 3.6 with theirs. Before discussing the quantitative differences between the two theories, we will comment on the differences in the approaches. *The main difference between the short-range and long-range theories is that the former considers the possibility of multiple dissipation events, while the latter considers only*

a single dissipation event. More specifically, the theory developed herein says that attractive potentials increase the apparent inelasticity of particles. At sufficiently high values of Ha_p for a given ϵ , particles have the ability to aggregate, thus dissipating all energy in the normal relative velocity. Müller says that the effect of long-range interactions, in addition to increasing the effective inelasticity, is to permit particles that are separating to be pulled into contact. The effect of the long-range interactions is such that, the higher the cohesion the greater the access to more potential collision partners at higher separating velocities. Their theory does not try to explicitly account for repeated collisions, but does indirectly account for them by capturing particles in regions of phase space with insufficient separating velocities. Indeed, full treatment of recollision events requires higher-order ring-type equations (van Noije et al., 1998a), as noted in Müller and Luding (2011). The potentials we consider, with a short-range of interaction allowing for temporal and spatial scale separation, allow us to account for these repeated collision/aggregation events in the context of the mean-field theory.

With high attractive potentials we find that the rate of cooling is doubled in the Müller theory (eqn. 3.7). This is consistent with the increased access to collision partners at contact. Eventually, access is given to all pairs populating the velocity phase space at contact and is not just restricted to approaching collision partners. Figure 3.1(b) shows a comparison of cooling rates between the two theories. In the non-cohesive limit both theories are identical to Haff's Law, and there is no significant difference between the theories for low values of ($|Ha| \ll 1$). The largest differences we find are in the highly cohesive regime for both low and high values of ϵ . In all but one limiting case, Müller's theory predicts higher cooling rates than our current theory. The greatest difference in the predicted cooling rate between the theories is found for highly attractive and nearly elastic particles, where our current theory predicts the gas will cool much faster. The reason for this is that the majority of particles will still aggregate according to our theory, while the Müller theory has an upper limit of cooling only twice as fast as Haff's law. Finally it is interesting to note that there is never a large discrepancy for moderately inelastic cases, i.e. $\epsilon \sim 0.6 - 0.8$, since $Ha_{\text{crit,p}} \sim -1$.

Table 3.1 Parameters used in soft sphere DEM Simulation

Parameters	Dilute	Moderately Dilute
ϵ	0.97	0.7; 0
$k^* = k/(\rho DT_g)$	$5.0 \times 10^7, 4.0 \times 10^8$	7.7×10^{12}
Ha_0	-0.049; -0.398	-0.24 ; -2.4
D/d_0	10^3	10^4
R_s/D	0.25	0.25
$\nu = N\pi D^3/(6L^3)$	0.01	0.084
L/D	30	50
N	515	20146

3.3 Soft Sphere Discrete Element Method

Previous treatment of granular gases often made use of event-driven codes, marching in collisions rather than time. However, in the attractive case the microscopic sticking mechanism necessarily leads to an ever increasing number of repeated collision events within the well, and hence soft-sphere DEM must be used. Use of DEM does not come without its own disadvantages; introducing such disparate length scales makes these simulations exceedingly expensive. This study concerns several soft-sphere systems with a linear spring dash-pot contact model (Cundall and Strack, 1979a). The parameter k is the spring stiffness in this model. First, dilute cases nearly elastic cases, $\epsilon = 0.97$, are considered with several initial values of Ha . Denser and more inelastic systems are also considered consisting of two systems without cohesion and two with cohesion. The two cohesive systems both have a $\epsilon = 0.7$ but start from different initial Ha values. The non-cohesive systems are simulated with $\epsilon = 0$ and 0.7. Using the molecular dynamics package LAMMPS (Plimpton, 1995), particles are initialized according to a Matérn hard-core process (Stoyan et al., 1995) and with Maxwellian velocities with zero net linear momentum. Particles are then allowed to make approximately 20 collisions before dissipation and/or cohesion are activated. Cohesive forces are calculated using the gradient of eqn. 3.2, with a constant cohesive force while particles are in contact $F_{vdw} = AR_s/6d_0^2$. Table 3.1 contains all system parameters necessary to perform the simulations.

3.4 Results and Discussion

3.4.1 Dilute Nearly Elastic Systems

In the spirit of the analysis done by Müller and Luding (2011) for systems with long-range attractive interactions, we look at the cooling predictions made for systems that are nearly elastic, $\epsilon = 0.97$ and also dilute $\nu = 0.01$. The DEM results for two systems with different levels of initial non-dimensionalized cohesion Ha_0 are plotted alongside the predictions made for the present short-ranged theory, the long-ranged theory (Müller and Luding, 2011), and Haff's Law (Haff, 1983) (see figs. 3.2(a) and 3.2(c)). It is seen that the results obtained from DEM most closely match the evolution of the present theory. However, after some time the DEM abruptly diverges from all theories presented here. We find that this behavior occurs as the system rapidly aggregates into small clusters, eventually forming a single cluster as the simulation proceeds.

The accuracy of the predictions are more easily ascertained by looking at the quality factor obtained by normalizing the temperature by Haff's Law, $Q = T_g/T_{g,Haff}$. It is clear from figs. 3.2(b) and 3.2(d) that the theory presented herein offers the best agreement with results from DEM. The long-range theory over predicts the rate of cooling (note that this was predicted in fig. 3.1(b)) up until the rapid clustering event occurs. The cooling law that we present remains valid for these systems for a finite time interval, the extent of which is useful to ascertain.

We discussed in section 3.2.2 that the cooling law is expected to fail, when the dynamics of the cooling from monomer–monomer interactions no longer dominate the system. We can estimate this time by applying the pseudo-Liouville theory as follows to obtain the rate for number of sticking collision events per partner. To obtain this we simply need to use the sticking piece of the extended pseudo-Liouville operator (see eqn. G.3) and the difference operator in eqn. G.4. This operator gives the loss of monomers per sticking collision, and applying the normal apparatus contained in appendix F we can obtain the evolution equation for the ensemble-averaged number of sticking collisions per particle, i.e. coordination number $\langle Z \rangle$:

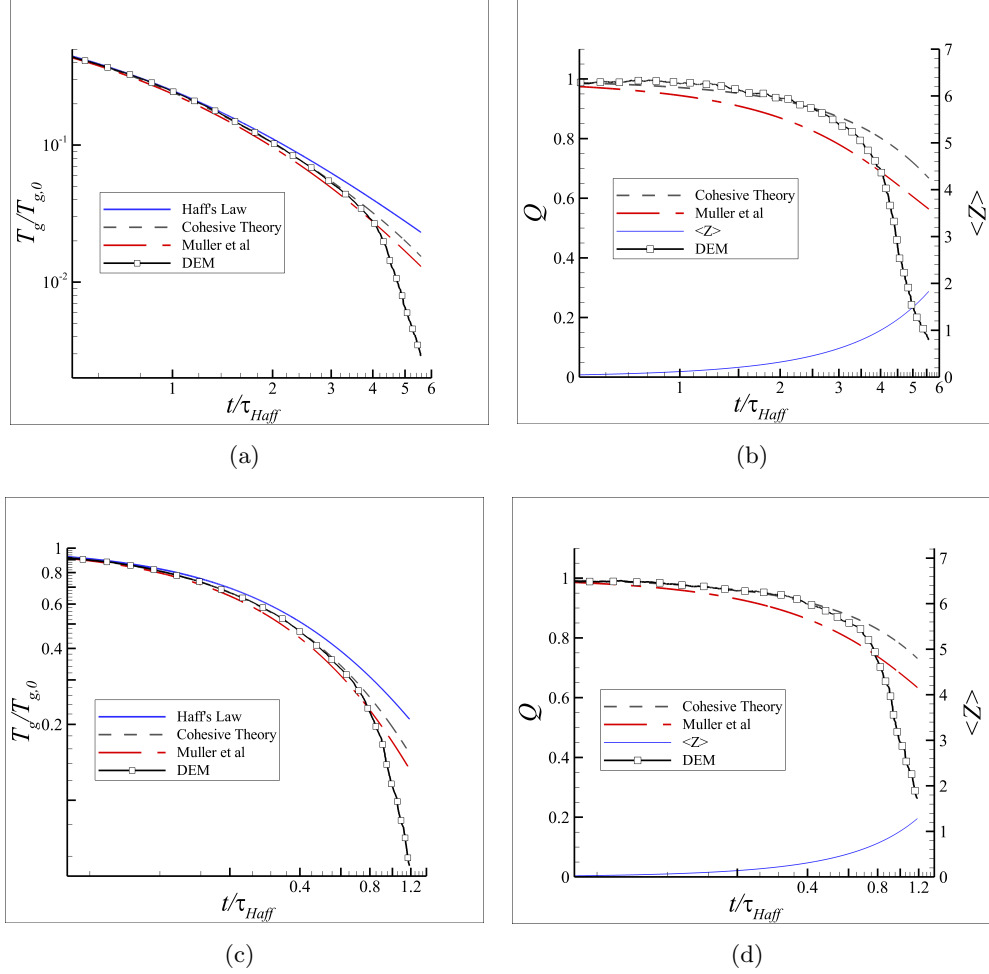


Figure 3.2 (a)-(c) The cooling response for the dilute nearly elastic DEM systems with (a) $Ha_0 = -0.049$ and (c) $Ha_0 = -0.398$ are plotted alongside different cooling models. Approximately (a) 182 collisions and (c) 74 collisions per particle are acquired over the duration of the respective simulations. (b)-(d) The quality factor, $Q = T_g/T_{g,Haff}$, is plotted for the cases of (b) $Ha_0 = -0.049$ and (d) $Ha_0 = -0.398$. From this we clearly see that at early times, the predictions made by the present theory are valid. This short-time is characterized by the predicted time it takes the system to acquire nearly 1 sticking collision partner per particle.

$$\left\langle \frac{\partial Z(t)}{\partial t} \right\rangle = \omega \left(1 - \exp \left(-\frac{v_{crit}^2}{4T_g(t)} \right) \right), \quad (3.8)$$

The coordination number differs from the collision frequency by only the additional exponential term, which determines the number of collisions that may stick. Solving this equation, which is coupled to eqn. 3.6, one can predict when the temperature predictions should fail. We find that the neighborhood where $\langle Z \rangle \rightarrow 1$, in figs. 3.2(b) and 3.2(d), correlates well to time at which the DEM rapidly deviates from the predictions of our theory. This seems to confirm that the reason for departure is that the dynamics are no longer dominated by monomer–monomer collisions.

3.4.2 Higher Solids Fraction and Inelasticity

In order to assess the model’s capability to predict cooling outside of the range of validity, we also consider the accuracy of predictions for higher densities, $\nu = 0.087$, and inelasticity, $\epsilon = 0.97$. As an illustration of what aggregation in these systems looks like, we show in fig. 3.3(a) a visualization of aggregates at the end of a simulation for a case where $Ha_0 = -0.24$. There are several large aggregates present in the system, with as many as 95 particles in the largest aggregate. Smaller particle aggregates, e.g. dimers, trimers, tetramers, etc. also exist in great number throughout the domain.

Figure 3.3(c) shows a comparison of the DEM behavior with all three cooling laws. For reference, we have also included the non-cohesive cases, where $\epsilon = 0$ and 0.7 (see fig. 3.3(b)). Our theory again *quantitatively* predicts the departure in cooling behavior from Haff’s law at short-times. The error in our prediction at the end of the strongly cohesive case ($Ha_0 = -2.4$) remains under 15% after ~ 7 collisions per particle. The moderately cohesive case ($Ha_0 = -0.24$) is under 2% after ~ 12 collisions per particle, which is approximately the same error in the non-cohesive case with $\epsilon = 0.7$. The error in the completely inelastic case $\epsilon = 0$ is also $\sim 15\%$. Similar findings regarding the accuracy of temperature predictions in denser systems were reported for the long-range attraction study with a comparative solid volume fractions (Müller and Luding, 2011).

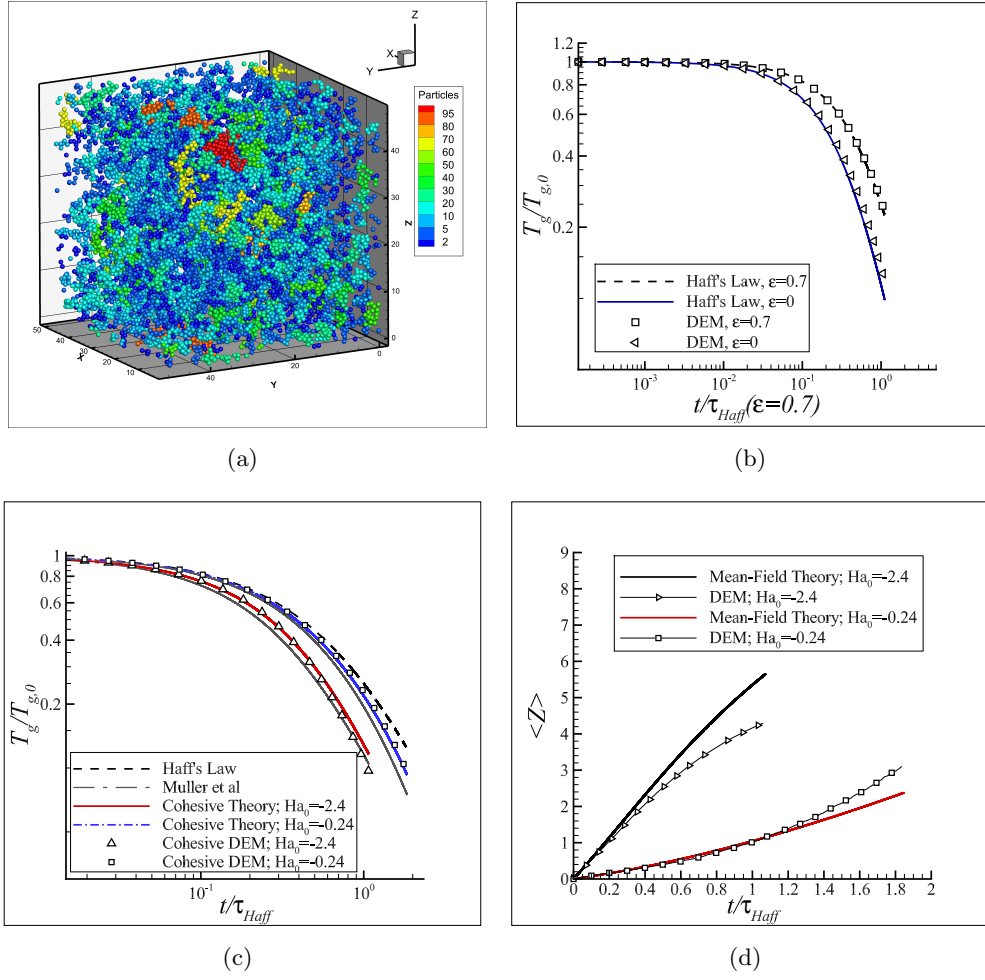


Figure 3.3 (a) A single snapshot from a realization of the case $Ha_0 = -0.24$ at end of the simulation is plotted. Particles are colored by the number of particles in the cluster. By the end of the simulation the maximum aggregate has 95 member particles. Note there are still an abundance of dimers, trimers, etc. present. (b) The evolution of the temperature for the two cases without cohesion are plotted for reference from a single realization alongside their respective Haff's Laws. The case of larger ϵ does a better job of predicting the temperature evolution. (c) The evolution of temperature for the cohesive cases is plotted. One can compare the evolution of DEM data for a single realization alongside Haff's law, Müller's theory, and our own theory. The plots show quantitative agreement with our cooling theory for short times, despite growing number of aggregates. (d) The evolution of the coordination number is plotted alongside theoretical predictions. We find that the lower value of Ha_0 has a better prediction of contact formation to longer times. Both predictions for $\langle Z \rangle$ appear to break down shortly after each particle on average has at least one contact.

The discrepancy between Müller and Luding (2011) theory and ours is most visible in the $Ha_0 = -0.24$ case, where they over predict the cooling behavior. At short times, our theory also agrees better with the case of stronger cohesion. The system, however, is not well predicted by either theory at the final time, which we attribute to the large amount of aggregates in the system. We expect that the theories would show larger disagreement between one another if highly inelastic or slightly inelastic particles were considered as mentioned in section 3.2.2. Ultimately, the better agreement between DEM and our theory in this regime means that accounting for sticking, as discussed in section 3.2.1, is essential for the accurate prediction of temperature evolution in systems with dissipation and short-ranged attractive potentials.

We also look at the number of contacts in the system to determine how far outside the range of expected validity our predictions have been made (see fig. 3.3(d)).

Comparing the average coordination number per particle $\langle Z \rangle$ from DEM to the numerical solution to eqn. 3.8 we find good agreement for both moderate ($Ha_0 = -0.24$) and strong cohesion ($Ha_0 = -2.4$) at early times (see fig. 3.3(d)). Both cases show disagreement shortly after the times where $\langle Z \rangle = 1$: $t/\tau_{Haff} \approx 0.2$ for $Ha_0 = -2.4$ and $t/\tau_{Haff} \approx 1$ for $Ha_0 = -0.24$. In the strongly cohesive case, $Ha_0 = -2.4$, the theory appears to over-predict the number of contacts formed after this time, while the theory under-predicts the formation of contacts for the moderately cohesive case. We do not yet have a firm explanation for this difference. However, note that the current theory does not fully account for aggregation events. Inevitably, any mechanistic explanation relies on information about the packing of monomers as more and more aggregation events occur. Examining packing information is beyond the scope of this study.

In comparing the prediction of temperature and coordination number, we observe quite unexpected behavior. Looking at fig. 3.3(d) and comparing with more dilute systems of section 3.4.1, one would expect that the temperature predictions would be quite poor. Yet, if we look at the moderately cohesive case, where by the end of the simulation $\langle Z \rangle \simeq 3$, we find that the temperature prediction is no worse than the predictions made where Haff's Law holds (see fig. 3.3(b)). It does appear as though sensitivity of the temperature on developing aggregate structure is not very important at these early times for systems that are sufficiently large.

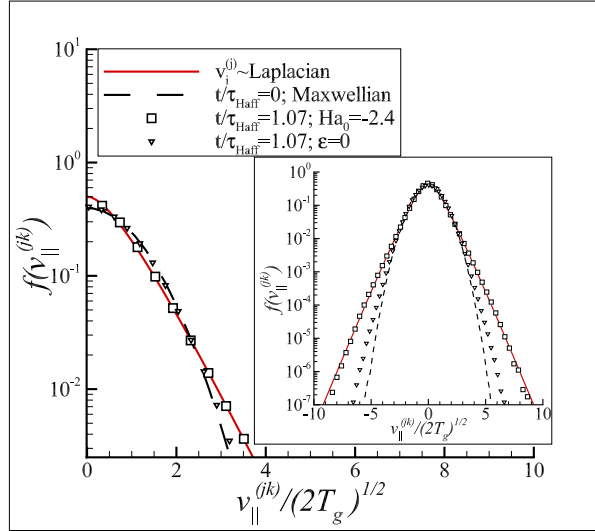


Figure 3.4 Pdf of normal relative velocities plotted for 2 different systems. The red line is obtained from i.i.d. Laplacian statistics. The black line is the pdf constructed from the initial condition and is approximately Maxwellian. The case with $\epsilon = 0$ retains a Maxwell core but appears to pick up exponential tails at early times. The pdf of the strongly cohesive case appears to be converging to the case of an i.i.d. Laplacian pdf even at short times. Both cases are taken at $t/\tau_{Haff} (\epsilon = 0.7) = 1.07$.

We believe that for too small a box size, an initial cluster can grow to dominate the system dynamics more readily.

3.4.3 Accuracy of Mean-Field Closures

The low error in the temperature evolution is promising. However, it is still of interest to explore in some detail the evolution of pair statistics, which provide closure for the mean-field kinetic theory. We first examine the pdf of normal relative velocities, $f(v_{\parallel}^{(jk)})$, plotted in fig. 3.4. The pdfs displayed are instantaneous pair statistics calculated from $N(N-1)$ samples in a single realization. The initial pdf is approximately that of an i.i.d. Maxwellian with variance $2T_g$ consistent with the theory. We have also plotted the result obtained for i.i.d. Laplace distributed particles, i.e. double exponential distribution. Note that the distribution is given by $\text{Laplace}(v_i^{(j)}; T_g) \sim 1/2\sqrt{T_g} \exp(-|v_i^{(j)}|/(\sqrt{T_g}))$. The distribution of normal relative velocities $v_{\parallel}^{(jk)}$ given i.i.d Laplace distributed particle velocities $v_i^{(j)}$ is found to be $f(z) = 1/2(1 + 2|z|) \exp(-2|z|)$, where $z = v_{\parallel}^{(jk)}/\sqrt{2T_g}$. This is the well-known asymptotic similarity

solution (Esipov and Pöschel, 1997) of the Boltzmann equation governing tail statistics in a granular gas obtained via the Lorentz gas model.

The comparison between statistics in the fully inelastic ($\epsilon = 0$) case and the strongly cohesive case ($Ha_0 = -2.4$) is interesting. We find that for the inelastic case, an exponential like tail begins to form even at these relatively short times, see inset of fig. 3.4. At low velocities the pdf remains essentially Maxwellian, in agreement with previous studies. On the other hand, the cohesive case has different and surprising behavior. The entire pdf seems to agree well with the i.i.d. Laplace distribution, even for very low velocities. The mechanism leading to this nice result seems rooted in the selective inelastic behavior and microscopic sticking instability. We note at initial time $v_{crit}^2 / (2T_g) = -1.12$ and at the final time $v_{crit}^2 / (2T_g) = -3.6$. Every collision with a velocity between the critical value and zero sticks, resulting in a growing population of particle pairs where $v_{\parallel}^{(jk)} = 0$. Particles colliding in the tail portions experience relatively little change from the cohesion. Finally, particles that have stuck do not separate to collide again as in the completely inelastic case, but instead remain with the transverse portion of their relative velocities intact in the rotational degrees of freedom.

The more interesting behavior to observe is the emergence of spatial pair correlations, which serve as a measure to determine the adequacy of the molecular chaos assumption and the appropriateness of the Enskog correction factor used, g_c . For example, fig. 3.5(a) displays the pair correlation function $g(r)$ at the initial time. The relative velocity correlations conditional on separation between a pair of particles, $\langle v_{\alpha}^{2(jk)} | r \rangle$, in the longitudinal ($\alpha = \parallel$) and transverse directions ($\alpha = \perp$) are also plotted. Note that these are all from a single snapshot from a single realization. We have plotted the correlations at initial time for reference in fig. 3.5(a). At initialization, the pair correlation function displays typical behavior, with a small peak due to excluded volume effects. The velocity correlations also appear negligible; the velocity near contact appears well-predicted by the molecular chaos result $\langle v_i^{(jk)} v_l^{(jk)} \rangle = 2T_g$.

The completely inelastic case gains a large peak in $g(r)$ near contact, indicating that the Enskog correction factor may not provide an accurate closure. Velocity correlations close to contact likewise appear to be developing with longitudinal correlations extending further than transverse correlations, i.e. developing bias towards grazing collisions. At large distances

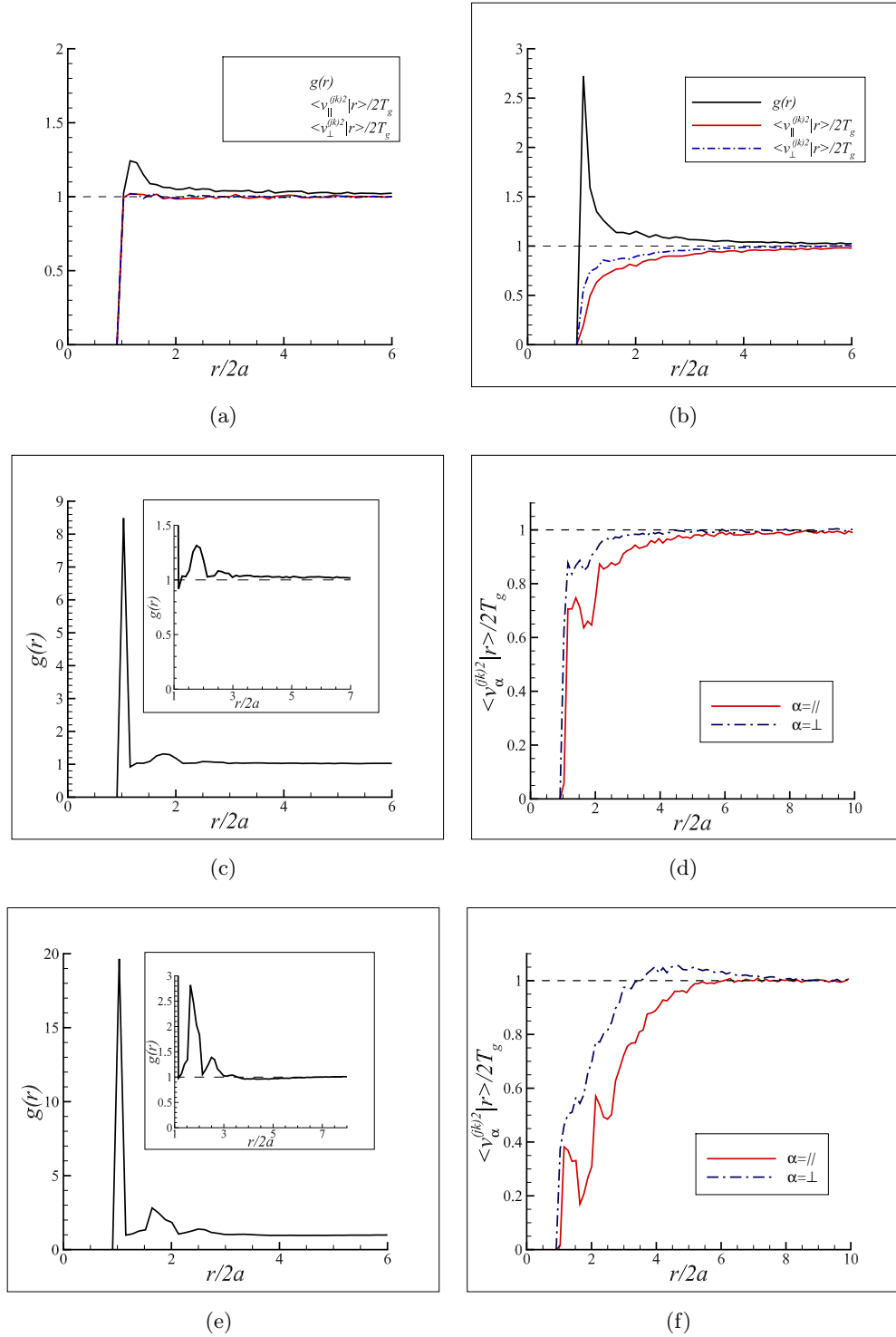


Figure 3.5 (a)-(b) The pair correlation function $g(r)$ is plotted alongside the transverse and longitudinal velocity correlations for the (a) initial condition and (b) end of the simulation for the completely inelastic case. (c)-(f) The pair correlation function and velocity correlations are plotted for systems with cohesion at their final time in simulation. (c)-(d) The correlations are taken from the moderately cohesive case $Ha_0 = -0.24$. (e)-(f) The correlations are taken from the more strongly cohesive case, $Ha_0 = -2.4$. All correlations are calculated from a single realization.

correlations do not appear to be present. This behavior has been observed and explored before and is thus not surprising. However, the correlations in the inelastic limit provide a nice comparison with the cohesive cases. Note that at early times, appreciable correlations do not develop for the non-cohesive case where $\epsilon = 0.7$, and so we have not plotted them.

We first observe that in the cohesive case, fine structure appears in $g(r)$ not just at contact but further out. These fine structures indicate the formation of coordination shells, which give rough detail about the average size of aggregates. The stronger cohesion case, fig. 3.5(e), shows coordination structure out to $\sim 4D$ indicating that aggregate structures of at least $8D$ exists in the simulation box. The coordination peaks are followed by a slight trough extending to $\sim 6D$ indicating the area surrounding aggregates is underpopulated.

The correlations in normal relative velocities also display fine structure in the cohesive cases (see figs. 3.5(d) and 3.5(f)). One finds that troughs develop in the longitudinal component at the same location as the coordination shells. This indicates a high population of particles moving neither away nor towards one another at these locations. The peaks in the longitudinal component occur in between these shells. The transverse component has much smoother structure. We attribute this structure primarily to the rotation of aggregates.

The most important feature of the velocity correlations found in figs. 3.5(c) - 3.5(f) is that the velocity correlations do not seem to extend beyond the aggregate length-scale inferred from $g(r)$. This implies that molecular chaos may still be an adequate model if a mean-field type theory of aggregation and break-up as presented in appendix G is constructed. This result is counter-intuitive; the sticking behavior of inelastic systems with cohesion can serve to preserve molecular chaos. The sticking result does not allow pairs with more highly correlated velocities to separate and undergo further collisions with other particles, i.e. bias towards grazing collisions should be subdued. Local correlation/order is trapped in new larger aggregate structures, which do not diffuse as is the case for the traditional inelastic hard-sphere gas (van Noije et al., 1997) or undergo viscous heating (Goldhirsch and Zanetti, 1993). As a final remark, the addition of short-ranged attraction will have more of an effect on the granular gas than to simply hasten the formation of instabilities, which is also discussed independently in a paper by Gonzalez et al. (2014). For example, it is well-known that at late times the

traditional granular gas shows a strong correlation between regions of high density and low temperature (Goldhirsch and Zanetti, 1993; Brito and Ernst, 1998). Even relatively weak cohesion would change the behavior of these regions, collapsing and arresting them in large aggregate structures with tensile strength. Indeed, there are many questions yet to be addressed and satisfactorily understood where short-ranged interactions are present with far reaching implications, particularly for powder processing and fluidized reactor technologies.

3.5 Conclusion

In this paper we have considered an extension to the freely cooling granular gas in the presence of short-ranged attractive potentials. The theory developed herein makes use of spatial and temporal scale separation to treat collisions as discrete events via an extension to the pseudo-Liouville operator formalism. The predicted cooling behavior is qualitatively different from that predicted for long-range potentials in other work (Müller and Luding, 2011), and agrees well with DEM over a relatively short simulation time, where the dynamics are dominated by monomer–monomer interactions. In addition, new criteria determining the validity of the mean-field theory are given based on the number of contacts formed, though the cooling predictions appear to surpass expectations for the larger boxes studied. We also note some differences in the formation and evolution of clusters and velocity correlations that arise due to sticking.

Lastly, the behavior of pair statistics determining the applicability of the mean-field theory is explored. We find that spatial-velocity correlations extend about as far as density correlations at a given time. Molecular chaos appears to remain an adequate approximation for population balance models including aggregation and break-up processes. We form the foundation of this framework through the extended pseudo-Liouville operator theory. The theory developed here has implications for building transport models of highly sheared cohesive granular systems. Questions about the ultimate trajectory of these systems, aggregate structure, and aggregate collision outcomes remain, and merit further study.

Acknowledgment

We gratefully acknowledge the support provided for this work from NSF grant CMMI 0927660, and partially from NSF grant CBET 1134500.

3.6 Bibliography

- Aarons, L. and Sundaresan, S. (2006). Shear flow of assemblies of cohesive and non-cohesive granular materials. *Powder Technology*, 169(1):10–21.
- Abbasfard, H., Evans, G., and Moreno-Atanasio, R. (2016). Effect of van der Waals force cut-off distance on adhesive collision parameters in DEM simulation. *Powder Technology*, 299:9–18.
- Afferrante, L., Ciavarella, M., and Demelio, G. (2015). Adhesive contact of the weierstrass profile. In *Proc. R. Soc. A*, volume 471, page 20150248. The Royal Society.
- Aitcin, P. (2000). Cements of yesterday and today - concrete of tomorrow. *Cement and Concrete Research*, 31(9):1349–1359.
- Alam, M., Trujillo, L., and Herrmann, H. (2006). Hydrodynamic theory for reverse brazil nut segregation and the non-monotonic ascension dynamics. *Journal of Statistical Physics*, 124:587–623.
- Bagnold, R. A. (1954). Experiments on a gravity-free dispersion of large solid spheres in a newtonian fluid under shear. In *Proceedings of the Royal Society of London A: Mathematical, Physical and Engineering Sciences*, volume 225, pages 49–63. The Royal Society.
- Ball, R. and Melrose, J. (1997). A simulation technique for many spheres in quasi-static motion under frame-invariant pair drag and brownian forces. *Physica A*, 247:444–472.
- Baranyai, A. and Evans, D. (1989). Direct entropy calculation from computer-simulation of liquids. *Physical Review A*, 40(7):3817–3822.

- Batrak, O., Patino, G., Simonin, O., Flour, I., Le Guevel, T., and Perez, E. (2005). Unlike particles size collision model in 3d unsteady polydispersed simulation of circulating fluidized bed. *8th Annual Conference on Fluidized Bed Technology*, 315.
- Bec, J., Biferale, L., Cencini, M., Lanotte, A., and Toschi, F. (2010). Intermittency in the velocity distribution of heavy particles in turbulence. *Journal of Fluid Mechanics*, 646:527–536.
- Beetstra, R., van der Hoef, M., and Kuipers, J. (2007). Drag force of intermediate reynolds number flows past mono- and bidisperse arrays of spheres. *AIChE Journal*, 53:489.
- Bentz, D., Ferraris, C., Galler, M., Hansen, A., and Guynn, J. (2012). Influence of particle size distributions on yield stress and viscosity of cement-fly ash pastes. *Cement and Concrete Research*, 42(2):404–409.
- Bentz, D. P., Garboczi, E. J., Haecker, C. J., and Jensen, O. M. (1999). Effects of cement particle size distribution on performance properties of portland cement-based materials. *Cement and Concrete Research*, 29:1663–1671.
- Berger, N., Azéma, E., Douce, J.-F., and Radjai, F. (2016). Scaling behaviour of cohesive granular flows. *EPL (Europhysics Letters)*, 112(6):64004.
- Berzi, D. and Jenkins, J. T. (2015a). Inertial shear bands in granular materials. *Physics of Fluids*, 27:033303.
- Berzi, D. and Jenkins, J. T. (2015b). Steady shearing flows of deformable, inelastic spheres. *Soft matter*, 11(24):4799–4808.
- Binnig, G., Quate, C. F., and Gerber, C. (1986). Atomic force microscope. *Physical review letters*, 56(9):930.
- Blum, J., Wurm, G., Kempf, S., Poppe, T., Klahr, H., Kozasa, T., Rott, M., Henning, T., Dorschner, J., Schrapler, R., Keller, H., Markiewicz, W., Mann, I., Gustafson, B., Giovane, F., Neuhaus, D., Fechtig, H., Grun, E., Feuerbacher, B., Kochan, H., Ratke, L., El Goresy, A.,

- Morfill, G., Weidenschilling, S., Schwehm, G., Metzler, K., and Ip, W. (2000). Growth and form of planetary seedlings: Results from a microgravity aggregation experiment. *Physical Review Letters*, 85(12):2426–2429.
- Bradley, R. S. (1932). Lxxix. the cohesive force between solid surfaces and the surface energy of solids. *The London, Edinburgh, and Dublin Philosophical Magazine and Journal of Science*, 13(86):853–862.
- Brady, J. F. and Bossis, G. (1988). Stokesian dynamics. *Annual Reviews of Fluid Mechanics*, 20:111–157.
- Bragg, A. D. and Collins, L. R. (2014a). New insights from comparing statistical theories for inertial particles in turbulence: I. spatial distribution of particles. *New Journal of Physics*, 16:055013.
- Bragg, A. D. and Collins, L. R. (2014b). New insights from comparing statistical theories for inertial particles in turbulence: II. relative velocities. *New Journal of Physics*, 16:055014.
- Bragg, A. D., Ireland, P. J., and Collins, L. R. (2015). On the relationship between the non-local clustering mechanism and preferential concentration. *Journal of Fluid Mechanics*, 780:327–343.
- Brewster, R., Grest, G. S., Landry, J. W., and Levine, A. J. (2005). Plug flow and the breakdown of bagnold scaling in cohesive granular flows. *Physical Review E*, 72(6):061301.
- Bridges, F. G., Supulver, K. D., Lin, D., Knight, R., and Zafra, M. (1996). Energy loss and sticking mechanisms in particle aggregation in planetesimal formation. *Icarus*, 123(2):422–435.
- Brilliantov, N. V., Albers, N., Spahn, F., and Pöschel, T. (2007). Collision dynamics of granular particles with adhesion. *Physical Review E*, 76(5):051302.
- Brilliantov, N. V. and Pöschel, T. (2004). Collision of adhesive viscoelastic particles. *HINRICHSEN:GRANULAR MEDIA O-BK*, pages 189–209.

- Brilliantov, N. V. and Pöschel, T. (2004). *Kinetic Theory of Granular Gases*. Oxford University Press, New York.
- Brilliantov, N. V., Spahn, F., Hertzsch, J.-M., and Pöschel, T. (1996). Model for collisions in granular gases. *Physical review E*, 53(5):5382.
- Brito, R. and Ernst, M. (1998). Extension of haff's cooling law in granular flows. *Europhysics Letters*, 43(5):497.
- Campbell, C. S. (2002). Granular shear flows at the elastic limit. *Journal of fluid mechanics*, 465:261–291.
- Capecelatro, J., Desjardins, O., and Fox, R. O. (2014). Numerical study of collisional particle dynamics in cluster-induced turbulence. *Journal of Fluid Mechanics*, 747:R2.
- Capecelatro, J., Desjardins, O., and Fox, R. O. (2015). On fluid-particle dynamics in fully developed cluster-induced turbulence. *Journal of Fluid Mechanics*, 780:578–635.
- Capecelatro, J., Desjardins, O., and Fox, R. O. (2016). Strongly coupled fluid-particle flows in vertical channels. ii. turbulence modeling. *Physics of Fluids*, 28:033307.
- Carnahan, N. and Starling, K. (1969). Equation of state for nonattractive rigid spheres. *Journal of Chemical Physics*, 51(2):635–636.
- Castellanos, A., Valverde, J. M., Pérez, A. T., Ramos, A., and Watson, P. K. (1999). Flow regimes in fine cohesive powders. *Physical Review Letters*, 82(6):1156.
- Cates, M., Wittmer, J., Bouchaud, J., and Claudin, P. (1998a). Jamming and static stress transmission in granular materials. *Chaos*, 9(3):511–522.
- Cates, M., Wittmer, J., Bouchaud, J., and Claudin, P. (1998b). Jamming, force chains, and fragile matter. *Physical Review Letters*, 81(9):1841–1844.
- Chew, J. W., Parker, D. M., Cocco, R. A., and Hrenya, C. M. (2011). Cluster characteristics of continuous size distributions and binary mixtures of group b particles in dilute riser flow. *Chemical Engineering Journal*, 178:348–358.

- Chialvo, S., Sun, J., and Sundaresan, S. (2012). Bridging the rheology of granular flows in three regimes. *Physical Review E*, 85(2):021305.
- Chun, J., Koch, D. L., Rani, S. L., Ahluwalia, A., and Collins, L. R. (2005). Clustering of aerosol particles in isotropic turbulence. *Journal of Fluid Mechanics*, 536:219–251.
- Cleary, P. W. and Sawley, M. L. (2002). DEM modelling of industrial granular flows: 3D case studies and the effect of particle shape on hopper discharge. *Applied Mathematical Modelling*, 26(2):89–111.
- Cocco, R., Shaffer, F., Hays, R., Karri, S. R., and Knowlton, T. (2010). Particle clusters in and above fluidized beds. *Powder Technology*, 203:3–11.
- Colwell, J., Batiste, S., Horányi, M., Robertson, S., and Sture, S. (2007). Lunar surface: Dust dynamics and regolith mechanics. *Reviews of Geophysics*, 45(2):RG2006.
- Cundall, P. and Strack, O. (1979a). A discrete numerical model for granular assemblies. *Geotechnique*, 29(1):47–65.
- Cundall, P. A. and Strack, O. D. (1979b). A discrete numerical model for granular assemblies. *Geotechnique*, 29(1):47–65.
- Dahneke, B. (1975). Further measurements of the bouncing of small latex spheres. *Journal of Colloid and Interface Science*, 51(1):58–65.
- Daley, D. and Vere-Jones, D. (1988). *An introduction to the theory of point processes*. Springer-Verlag.
- DeCicco, A. and Hartzell, C. (2016). System-level design considerations for asteroid despin via neutral beam emitting spacecraft. In *IEEE Aerospace Conference Proceedings (Big Sky, MT)*.
- Derjaguin, B., Muller, V., and Toporov, Y. (1975). Effect of contact deformations on the adhesion of particles. *Journal of Colloid and Interface Science*, 53(2):314–326.

- Di Renzo, A. and Di Maio, F. P. (2004). Comparison of contact-force models for the simulation of collisions in dem-based granular flow codes. *Chemical Engineering Science*, 59(3):525–541.
- Eaton, J. and Fessler, J. (1994). Preferential concentration of particles by turbulence. *International Journal of Multiphase Flow*, 20:169–209.
- Ernst, M., Dorfman, J., Hoegy, W., and van Leeuwen, J. (1969). Hard-sphere dynamics and binary-collision operators. *Physica*, 45(1):127–146.
- Esipov, S. and Pöschel, T. (1997). The granular phase diagram. *Journal of Statistical Physics*, 86(5/6):1385–1395.
- Ferraris, C., Obla, K., and Hill, R. (2001). The influence of mineral admixtures on the theology of cement paste and concrete. *Cement and Concrete Research*, 31(2):245–255.
- Fox, R. (2014). On multiphase turbulence models for collisional fluid-particle flows. *Journal of Fluid Mechanics*, 742:368–424.
- Fox, R. O. (2016). Private communication.
- Fullmer, W. D. and Hrenya, C. M. (2016). Quantitative assessment of fine-grid kinetic-theory-based predictions of mean-slip in unbounded fluidization. *AIChE Journal*, 62(1):11–17.
- Galvin, J. E. and Benyahia, S. (2014). The effect of cohesive forces on the fluidization of aeratable powders. *AIChE Journal*, 60(2):473–484.
- Garzo, V., Dufty, J. W., and Hrenya, C. M. (2007a). Enskog theory for polydisperse granular mixtures. i. navier-stokes order transport. *Physical Review E*, 76(3):031303.
- Garzo, V., Fullmer, W. E., Hrenya, C. M., and Yin, X. (2016). Transport coefficients of solid particles immersed in a viscous gas. *Physical Review E*, 93:012905.
- Garzo, V., Hrenya, C. M., and Dufty, J. W. (2007b). Enskog theory for polydisperse granular mixtures. ii. sonine polynomial approximation. *Physical Review E*, 76(3):031304.
- Garzo, V., Tenneti, S., Subramaniam, S., and Hrenya, C. (2012). Enskog kinetic theory for monodisperse gas-solid flows. *Journal of Fluid Mechanics*, 712:129–168.

- Gaume, J., Chambon, G., and Naaim, M. (2011). Quasistatic to inertial transition in granular materials and the role of fluctuations. *Physical Review E*, 84:051304.
- Geldart, D. (1973). Types of gas fluidization. *Powder technology*, 7(5):285–292.
- Gidaspow, D., Jung, J., and Singh, R. K. (2004). Hydrodynamics of fluidization using kinetic theory: an emerging paradigm 2002 flour-daniel lecture. *Powder Technology*, 148:123–141.
- Goldhirsch, I. and Zanetti, G. (1993). Clustering instability in dissipative gases. *Physical Review Letters*, 70(11):1619–1622.
- Goldshtein, A. and Shapiro, M. (1995). Mechanics of collisional motion of granular materials. part 1. general hydrodynamic equations. *Journal of Fluid Mechanics*, 282:75–114.
- Gollin, D., Berzi, D., and Bowman, E. (2017). Extended kinetic theory applied to inclined granular flows: role of boundaries. *Granular Matter*, 19(3):1564–1583.
- Gonzalez, R. G. and Garzo, V. (2016). Instabilities in granular gas-solid flows. *arXiv:1611.03269*.
- Gonzalez, S., Thornton, A., and Luding, S. (2014). Free cooling phase-diagram of hard-spheres with short-and long-range interactions. *The European Physical Journal Special Topics*, 223(11):2205–2225.
- Gourdel, c., Simonin, O., and Brunier, E. (1998). Modelling and simulation of gas-solid turbulent flows with a binary mixture of particles. *Third International Conference on Multiphase Flows*, 315.
- Gourdel, c., Simonin, O., and Brunier, E. (1999). Two-maxwellian equilibrium distribution function for the modelling of a binary mixture of particles. *6th International Conference on Circulating Fluidized Beds*, 315.
- Grierson, D., Flater, E., and Carpick, R. (2005). Accounting for the jkr–dmt transition in adhesion and friction measurements with atomic force microscopy. *Journal of adhesion science and technology*, 19(3-5):291–311.

- Gu, Y., Chialvo, S., and Sundaresan, S. (2014). Rheology of cohesive granular materials across multiple dense-flow regimes. *Physical Review E*, 90(3):032206.
- Gu, Y., Ozel, A., and Sundaresan, S. (2015). A modified cohesion model for CFD–DEM simulations of fluidization. *Powder Technology*, 296:17–28.
- Gu, Y., Ozel, A., and Sundaresan, S. (2016). Numerical studies of the effects of fines on fluidization. *AIChE Journal*.
- Gustavsson, K. and Mehlig, B. (2014a). Clustering of particles falling in a turbulent flow. *Physical Review Letters*, 112:214501.
- Gustavsson, K. and Mehlig, B. (2014b). Relative velocities of inertial particles in turbulent aerosols. *Journal of Turbulence*, 15(1):34–69.
- Gustavsson, K. and Mehlig, B. (2016). Statistical models for spatial patterns of heavy particles in turbulence. *Advances in Physics*, 65(1):1–57.
- Haecker, C., Garboczi, E., J.W., B., Bohn, R., Sun, Z., Shah, S., and Voigt, T. (2005). Modeling the linear elastic properties of portland cement paste. *Cement and Concrete Research*, 35:1948–1960.
- Haff, P. (1983). Grain flow as a fluid-mechanical phenomenon. *Journal of Fluid Mechanics*, 134:401–430.
- Hatzes, A., Bridges, F., Lin, D., and Sachtjen, S. (1991). Coagulation of particles in saturn’s rings: Measurement of the cohesive force of water frost. *Icarus*, 89:113–121.
- Hill, R. J., Koch, D., and Ladd, A. (2001a). The first effects of fluid inertia on flows in ordered and random arrays of spheres. *Journal of Fluid Mechanics*, 448:213–241.
- Hill, R. J., Koch, D., and Ladd, A. (2001b). Moderate-reynolds-number flows in ordered and random arrays of spheres. *Journal of Fluid Mechanics*, 448:243–278.
- Irani, E., Chaudhuri, P., and Heussinger, C. (2014). Impact of attractive interactions on the rheology of dense athermal particles. *Physical Review Letters*, 112:188303.

- Irani, E., Chaudhuri, P., and Heussinger, C. (2016). Athermal rheology of weakly attractive soft particles. *Physical Review E*, 94:052608.
- Israelachvili, J. N. (2011). *Intermolecular and surface forces: revised third edition*. Academic press.
- Iveson, S., Litster, J., Hapgood, K., and Ennis, B. (2001). Nucleation, growth and breakage phenomena in agitated wet granulation processes: a review. *Powder Technology*, 117(1-2):3–39.
- Jenkins, J. and Mancini, F. (1987). Balance laws and constitutive relations for plane flows of a dense, binary mixture of smooth, nearly elastic, circular disks. *Journal of Applied Mechanics*, 1(54):27–34.
- Jenkins, J. and Mancini, F. (1989). Kinetic theory for binary mixtures of smooth, nearly elastic spheres. *Physics of Fluids, A*, 1(12):2050–2057.
- Johnson, K. and Greenwood, J. (1997). An adhesion map for the contact of elastic spheres. *Journal of colloid and interface science*, 192(2):326–333.
- Johnson, K., Kendall, K., and Roberts, A. (1971). Surface energy and the contact of elastic solids. *Proceedings of the Royal Society London A*, 324:301–313.
- Jop, P., Forterre, Y., and Pouliquen, O. (2006). A constitutive law for dense granular flows. *Nature*, 441(7094):727–730.
- Kamrin, K. and Koval, G. (2012). Nonlocal constitutive relation for steady granular flow. *Physical Review Letters*, 108(17):178301.
- Kim, H. and Arastoopour, H. (2002). Extension of kinetic theory to cohesive particle flow. *Powder Technology*, 122(1):83–94.
- Kim, S. and Karrila, S. (1991). *Microhydrodynamics: principles and selected applications*. Butterworth-Heinemann.

- Kobayashi, T., Tanaka, T., Shimada, N., and Kawaguchi, T. (2013). Dem-cfd analysis of fluidization behavior of geldart group a particles using a dynamic adhesion force model. *Powder Technology*, 248:143–152.
- Koch, D. L. (1990). Kinetic theory for a monodisperse gas-solid suspension. *Physics of Fluids A*, 2(10):1711–1723.
- Koch, D. L. and Sangani, A. S. (1999). Particle pressure and marginal stability limits for a homogeneous monodisperse gas-fluidized bed: kinetic theory and numerical simulations. *Journal of Fluid Mechanics*, 400:229–263.
- Kolakaluri, R., Murphy, E., Subramaniam, S., Brown, R., and Fox, R. (2015). Filtration model for polydisperse aerosols in gas-solid flow using granule-resolved direct numerical simulation. *AIChE Journal*, 61(11):3594–3606.
- Kothe, S., Blum, J., Weidling, R., and GÄ¼ttler, C. (2013). Free collisions in a microgravity many-particle experiment. iii. the collision behavior of sub-millimeter-sized dust aggregates. *Icarus*, 225:75–85.
- Kulchitsky, A., Johnson, J., Reeves, D., and Wilkinson, A. (2014). Discrete element method simulation of a boulder extraction from an asteroid. In *Proceedings of the 14th ASCE Biennial International Conference on Engineering, Science, Construction, and Operations in Challenging Environments (St. Louis, Missouri, USA,)*, pages 485–494.
- Kumar, A. (2010). *Microscale Dynamics in Suspensions of Non-spherical Particles*. PhD thesis, University of Illinois Urbana-Champaign.
- Kumar, A. and Higdon, J. (2010). Origins of the anomalous stress behavior in charged colloidal suspensions under shear. *Physical Review E*, 82:051401.
- Kuwabara, G. and Kono, K. (1987). Restitution coefficient in a collision between two spheres. *Japanese journal of applied physics*, 26(8R):1230.

- Lanotte, A., Bec, J., Biferale, L., Cencini, M., and Toschi, F. (2011). About scaling properties of relative velocity between heavy particles in turbulence. *Journal of Physics Conference series*, 318:052010.
- Launder, B. (1990). Phenomenological modelling: present... and future? in j.l. lumley (ed.). *Whither Turbulence? Turbulence at a Crossroads*, pages 439–485.
- Lees, A. and Edwards, S. (1972). The computer study of transport processes under extreme conditions. *Journal of Physics C: Solid State Physics*, 5(15):1921.
- Leyvraz (2003). Scaling theory and exactly solved models in the kinetics of irreversible aggregation. *Physics Reports*, 383:92–212.
- Li, J., Cheng, C., Zhang, Z., Yuan, J., Nemet, A., and Fett, F. (1999). The emms model - its application, development and updated concepts. *Chemical Engineering Science*, 54(22):5409–5425.
- Liard, M., Martys, N., George, W., Lootens, D., and Hebraud, P. (2014). Scaling laws for the flow of generalized newtonian suspensions. *Journal of Rheology*, 58:1993–2015.
- Liu, A. J. and Nagel, S. R. (2010). The jamming transition and the marginally jammed solid. *Annual Review of Condensed Matter Physics*, 1:347–369.
- Liu, L. (2011). Kinetic theory of aggregation in granular flow. *AIChE Journal*, 57(12):3331–3343.
- Liu, P., Kellogg, K., LaMarche, C., and Hrenya, C. (2017). Dynamics of singlet-doublet collisions of cohesive particles. *Chemical Engineering Journal*, 324:380–391.
- Liu, P., LaMarche, C. Q., Kellogg, K. M., and Hrenya, C. M. (2016). Fine-particle deflu-idization: Interaction between cohesion, Young’s modulus and static bed height. *Chemical Engineering Science*, 145:266–278.
- Lois, G., Blawdziewicz, J., and O’Hern, C. S. (2008). Jamming transition and new perco-lation universality classes in particulate systems with attraction. *Physical Review Letters*, 100:028001.

- Lomboy, G., Sundararajan, S., and Wang, K. (2013). Micro- and macroscale coefficients of friction of cementitious materials. *Cement and Concrete Research*, 54:21–28.
- Lomboy, G., Sundararajan, S., Wang, K., and Subramaniam, S. (2011). A test method for determining adhesion forces and hamaker constants of cementitious materials using atomic force microscopy. *Cement and Concrete Research*, 41(11):1157–1166.
- Lomboy, G. R., Wang, K., and Quanji, Z. (2012). Properties of cementitious materials in their dry state and their influences on viscosity of the cementitious pastes. *Powder Technology*, 229:104–111.
- Luding, S. (1998). Collisions & contacts between two particles. In *Physics of dry granular media*, pages 285–304. Springer.
- Luding, S. (2008). Cohesive, frictional powders: contact models for tension. *Granular matter*, 10(4):235–246.
- Luding, S. (2016). Granular matter: So much for the jamming point. *Nature Physics*, 12:531–532.
- Luding, S. and Alonso-Marroquin, F. (2011). The critical-state yield stress (termination locus) of adhesive powders from a single numerical experiment. *Granular Matter*, 13:109–119.
- Luding, S., Clément, E., Blumen, A., Rajchenbach, J., and Duran, J. (1994). Anomalous energy dissipation in molecular-dynamics simulations of grains: The detachment effect. *Physical Review E*, 50(5):4113.
- Luding, S., Huthmann, M., McNamara, S., and Zippelius, A. (1998). Homogeneous cooling of rough, dissipative particles: Theory and simulation. *Physical Review E*, 58(3):3416–3425.
- Majmudar, T., Sperl, M., Luding, S., and Behringer, R. (2007). Jamming transition in granular systems. *Physical Review Letters*, 98:058001.
- Makse, H. A., Johnson, D. L., and Schwartz, L. M. (2000). Packing of compressible granular materials. *Physical review letters*, 84(18):4160.

- Marchisio, D. L. and Fox, R. O. (2013). *Computational Models for Polydisperse Particulate and Multiphase Systems*. Cambridge University Press.
- Markutsya, S., Fox, R., and Subramaniam, S. (2014). Characterization of sheared colloidal aggregation using langevin dynamics simulation. *Physical Review E*, 89:062312.
- Marmur, B. L. and Heindel, T. J. (2016). Effect of particle size, density, and concentration on granular mixing in a double screw pyrolyzer. *Powder Technology*, 302:222–235.
- Martys, N. and Ferraris, C. (2002). Simulation of scc flow. In *First North American Conference on the Design and Use of Self-Consolidating Concrete. Proceedings. Chicago, IL,*.
- Martys, N., Khalil, M., George, W., and Lootens, D. (2012). Stress propagation in a concentrated colloidal suspension under shear. *European Physical Journal E*, 35(3):1–7.
- Matsunaga, T., Kim, J., Hardcastle, S., and Rohatgi, P. (2002). Crystallinity and selected properties of fly ash particles. *Materials Science and Engineering*, A325:333–343.
- Maugis, D. (1992). Adhesion of spheres: the jkr-dmt transition using a dugdale model. *Journal of colloid and interface science*, 150(1):243–269.
- Maxey, M. (1987). The gravitational settling of aerosol particles in homogeneous turbulence and random flow fields. *Journal of Fluid Mechanics*, 174:441–465.
- Mckay, W. and Mckay, J. (1971). *Building Construction Vol. Ii (Fourth Edition)*. Orient Longman Private Limited.
- McMillan, J., Shaffer, F., Gopalan, B., Chew, J. W., Hrenya, C., Hays, R., Karri, S. R., and Cocco, R. (2013). Particle cluster dynamics during fluidization. *Chemical Engineering Science*, 100:39–51.
- McNamara, S. and Young, W. (1992). Inelastic collapse and clumping in a one-dimensional granular medium. *Physics of Fluids A*, 4(3):496–504.
- Mehrabadi, M. (2016). *Analysis of gas-solid flow using particle-resolved direct numerical simulation: flow physics and modeling*. PhD thesis, Iowa State University.

- Mehrabadi, M., Murphy, E., and Subramaniam, S. (2016a). Development of a gas-solid drag law for clustered particles using particle-resolved direct numerical simulation. *Chemical Engineering Science*, 152:199–212.
- Mehrabadi, M., Tenneti, S., and Subramaniam, S. (2016b). Importance of the fluid-particle drag model in predicting segregation in bidisperse gas-solid flow. *International Journal of Multiphase Flow*, 86:99–114.
- MiDi, G. (2004). On dense granular flows. *The European Physical Journal E*, 14(4):341–365.
- Miller, A. and Gidaspow, D. (1992). Dense, vertical gas-solid flow in a pipe. *AIChE Journal*, 38(11):1801–1815.
- Mills, P., Rognon, P., and Chevier, F. (2008). Rheology and structure of granular materials near the jamming transition. *EPL (Europhysics Letters)*, 81:64005.
- Miyamoto, H., Kargel, J., Fink, W., and Furfaro, R. (2008). Granular processes on itokawa, a small near-earth asteroid: Implications for resource utilization. *Space Exploration Technologies, Proceedings of SPIE*, 6960:69600I.
- Monchaux, R., Bourgoïn, M., and Cartellier, A. (2010). Preferential concentration of heavy particles: a voronoi analysis. *Physics of Fluids*, 22(10):103304.
- Moreno-Atanasio, R., Xu, B., and Ghadiri, M. (2007). Computer simulation of the effect of contact stiffness and adhesion on the fluidization behaviour of powders. *Chemical engineering science*, 62(1):184–194.
- Morrow, C., Lovell, M., and Ning, X. (2003). A jkr-dmt transition solution for adhesive rough surface contact. *Journal of Physics D: Applied Physics*, 36(5):534.
- Mounfield, C. and Edwards, S. (1994). A model for the packing of irregularly shaped grains. *Physica A*, 210:301–316.
- Müller, M.-K. and Luding, S. (2011). Homogeneous cooling with repulsive and attractive long-range potentials. *Mathematical Modelling of Natural Phenomena*, 6(4):118–150.

- Murphy, E., Mehrabadi, M., Tenneti, S., and Subramaniam, S. (2015). Modeling two-point particle dynamics of homogeneous gas-solid flows to describe clustering and stability. In *68th annual meeting of the American physical society division of fluid dynamics, At Boston, MA*.
- Murphy, E. and Subramaniam, S. (2014). A model for solid-solid drag in bidisperse gas-solid flows. In *67th Annual Meeting of the APS Division of Fluid Dynamics*, volume 59.
- Murphy, E. and Subramaniam, S. (2015). Freely cooling granular gases with short-ranged attractive potentials. *Physics of Fluids (1994-present)*, 27(4):043301.
- Murphy, E. and Subramaniam, S. (2017). Binary collision outcomes for inelastic soft-sphere models with cohesion. *Powder Technology*, 305:462–476.
- Nachenius, R., van de Wardt, T., Ronsse, F., and Prins, W. (2015). Effect of particle size, density, and concentration on granular mixing in a double screw pyrolyzer. *Fuel Processing Technology*, 130:87–95.
- Narayanan, K. and Ramamurthy, K. (2000). Structure and properties of aerated concrete: a review. *Cement and Concrete Composites*, 22(5):321–329.
- Nase, S. T., Vargas, W. L., Abatan, A. A., and McCarthy, J. (2001). Discrete characterization tools for cohesive granular material. *Powder Technology*, 116(2):214–223.
- Nauman, E. B. (2001). *Chemical Reactor Design, Optimization, and Scaleup*. McGraw-Hill.
- Nienow, A., Edwards, M., and Harnby, N. (1992). *Mixing in the Process Industries: Mixing of Cohesive Powders*. Elsevier, Oxford, 2nd edition.
- of Chemistry, T. R. S. (2008). The concrete conundrum. *Chemistry World*.
- Oliver, W. C. and Pharr, G. M. (1992). An improved technique for determining hardness and elastic modulus using load and displacement sensing indentation experiments. *Journal of materials research*, 7(06):1564–1583.
- Ortiz de Zarate, J. and Sengers, J. (2006). *Hydrodynamic Fluctuations in Fluids and Fluid Mixtures*. Elsevier.

- Oseen, C. (1927). Neuere methoden und ergebnisse in der hydrodynamik. *Akademische Verlagsgesellschaft*.
- Otsuki, M., Hayakawa, H., and Luding, S. (2010). Behavior of pressure and viscosity at high densities for two-dimensional hard and soft granular materials. *Progress of Theoretical Physics Supplement*, 184:110–133.
- Pasha, M., Dogbe, S., Hare, C., Hassanpour, A., and Ghadiri, M. (2014). A linear model of elasto-plastic and adhesive contact deformation. *Granular Matter*, 16(1):151–162.
- Pathak, S., Jabeen, Z., Dibyendu, D., and Rajesh, R. (2014). Energy decay in three-dimensional freely cooling granular gas. *Physical Review Letters*, 112:038001.
- Paul, E. L., Atiemo-Obeng, V. A., and Kresta, S. M. (2004). *Handbook of industrial mixing: science and practice*. John Wiley ”&” Sons.
- Perni, S. and Prokopovich, P. (2015). Multi-asperity elliptical jkr model for adhesion of a surface with non-axially symmetric asperities. *Tribology International*, 88:107–114.
- Persson, B. N. and Scaraggi, M. (2014). Theory of adhesion: Role of surface roughness. *The Journal of chemical physics*, 141(12):124701.
- Petterson, O. (2007). Sandstone compaction, grain packing and critical state theory. *Petroleum Geoscience*, 13:63–67.
- Plimpton, S. (1995). Fast parallel algorithms for short-range molecular dynamics. *Journal of Computational Physics*, 117:1–19.
- Pope, S. B. (2000). *Turbulent Flows*. Cambridge University Press.
- Prokopovich, P. and Starov, V. (2011). Adhesion models: From single to multiple asperity contacts. *Advances in colloid and interface science*, 168(1):210–222.
- Rahman, M., Wiklund, J., Kotze, R., and Hakansson, U. (2017). Yield stress of cement grouts. *Tunnelling and Underground Space Technology*, 61:50–60.

- Rani, S. L., Dhariwal, R., and Koch, D. L. (2014). A stochastic model for the relative motion of high stokes number particles in isotropic turbulence. *Journal of Fluid Mechanics*, 756:870–902.
- Reeks, M. (1980). Eulerian direct interaction applied to the statistical motion of particles in a turbulent flow. *Journal of Fluid Mechanics*, 97:569–590.
- Rognon, P. G., Roux, J.-N., Naaim, M., and Chevoir, F. (2008). Dense flows of cohesive granular materials. *Journal of Fluid Mechanics*, 596:21–47.
- Rong, L., Dong, K., and Yu, A. (2014). Lattice-boltzmann simulation of fluid flow through packed beds of spheres: effect of particle size distribution. *Chemical Engineering Science*, 116:508–523.
- Rotne, J. and Prager, S. (1969). Variational treatment of hydrodynamic interaction in polymers. *Journal of Chemical Physics*, 50:4831–4837.
- Roussel, N., Lemaitre, A., Flatt, R., and Coussot, P. (2010). Steady state flow of cement suspensions: A micromechanical state of the art. *Cement and Concrete Research*, 40(1):77–84.
- Roussel, N., Ovarlez, G., Garrault, S., and Brumaud, C. (2012). The origins of thixotropy of fresh cement pastes. *Cement and Concrete Research*, 42(1):148–157.
- Rumpf, H. (1958). Grundlagen und methoden des granulierens. *Chemie Ingenieur Technik*, 30(3):144–158.
- Rycroft, C., Grest, G., Landry, J., and Bazant, M. (2006). Analysis of granular flow in a pebble-bed nuclear reactor. *Physical Review E*, 74:021306.
- Saha, S. and Alam, M. (2016). Normal stress differences, their origin and constitutive relations for a sheared granular fluid. *Journal of Fluid Mechanics*, 795:549–580.
- Saitoh, K. and Mizuno, H. (2016). Enstrophy cascades in two-dimensional dense granular flows. *Physical Review E*, 94:022908.

- Saitoh, K., Takada, S., and Hayakawa, H. (2015). Hydrodynamic instabilities in shear flows of dry cohesive granular particles. *Soft matter*, 11(32):6371–6385.
- Schäfer, J., Dippel, S., and Wolf, D. (1996). Force schemes in simulation of granular material. *J. Phys. I France*, 6:5–20.
- Schlick, C. P., Isner, A. B., Freireich, B. J., Fan, Y., Umbanhowar, P. B., Ottino, J. M., and Lueptow, R. M. (2016). A continuum approach for predicting segregation in flowing polydisperse granular materials. *Journal of Fluid Mechanics*, 797:95–109.
- Shah, S. and Wang, K. (2004). Development of green cement for sustainable concrete using cement kiln dust and fly ash. In *Proceedings of the International Workshop on Sustainable Development and Concrete Technology*.
- Shannon, C. (1948). A mathematical theory of communication. *Bell System Technical Journal*, 27(3):379–423.
- Silbert, L. E., Ertas, D., Grest, G. S., Halsey, T. C., Levine, D., and Plimpton, S. J. (2001). Granular flow down an inclined plane: Bagnold scaling and rheology. *Physical Review E*, 64(5):051302.
- Silbert, L. E., Grest, G. S., Brewster, R., and Levine, A. J. (2007). Rheology and contact lifetimes in dense granular flows. *Physical review letters*, 99(6):068002.
- Singh, A., Magnanimo, V., Saitoh, K., and Luding, S. (2014). Effect of cohesion on shear banding in quasistatic granular materials. *Physical Review E*, 90(2):022202.
- Singh, A., Magnanimo, V., Saitoh, K., and Luding, S. (2015). The role of gravity or pressure and contact stiffness in granular rheology. *New journal of physics*, 17(4):043028.
- Sjostrom, S. and Krutka, H. (2009). Evaluation of solid sorbents as a retrofit technology for co2 capture. *Fuel*, 89(6):1298–1306.
- Song, C., Wang, P., and Makse, H. A. (2008). A phase diagram for jammed matter. *Nature*, 453(7195):629–632.

- Stevens, A. and Hrenya, C. (2005). Comparison of soft-sphere models to measurements of collision properties during normal impacts. *Powder Technology*, 154(2):99–109.
- Stoyan, D., Kendall, W., and Mecke, J. (1995). *Stochastic geometry and its applications*. John Wiley and Sons, New York, 2nd edition.
- Stutzman, P. (2004). Scanning electron microscopy imaging of hydraulic cement microstructure. *Cement and Concrete Composites*, 26:957–966.
- Subramaniam, S. (2000). Statistical representation of a spray as a point process. *Physics of Fluids*, 12(10):2413–2431.
- Subramaniam, S. (2001). Statistical modeling of sprays using the droplet distribution function. *Physics of Fluids*, 13(3):624–642.
- Subramaniam, S. (2012). Stability limits for gas-solid suspensions with finite fluid inertia using particle-resolved direct numerical simulations. *NSF Annual Report 1134500*.
- Subramaniam, S. (2014). Stability limits for gas-solid suspensions with finite fluid inertia using particle-resolved direct numerical simulations. *NSF Annual Report 1134500*.
- Sun, J., Battaglia, F., and Subramaniam, S. (2006). Dynamics and structures of segregation in a dense, vibrating granular bed. *Physical Review E*, 74(6):061307.
- Sun, J. and Sundaresan, S. (2011). A constitutive model with microstructure evolution for flow of rate-independent granular materials. *Journal of Fluid Mechanics*, 682:590–616.
- Sundaram, S. and Collins, L. (1997). Collision statistics in an isotropic, particle-laden turbulent suspension i. direct numerical simulations. *Journal of Fluid Mechanics*, 335:75–109.
- Syamlal, M. (1987). The particle-particle drag term in a multiphase model of fluidization. *Technical Report DOE/MC/21353-2373, NTIS/DE87006500, National Technical Information Service*.
- Syamlal, M. and O’Brien, T. (1987). A generalized drag correlation for multiparticle systems. *Technical Report, Morgantown Energy Technology Center DOE Report*.

- Syamlal, M., Rogers, W., and O'Brien, T. (1993). Mfix documentation: Theory guide. *Morgantown Energy Technology Center Morgantown, WV, USA*, page 54.
- Tabor, D. (1977). Surface forces and surface interactions. *Journal of colloid and interface science*, 58(1):2–13.
- Takada, S., Saitoh, K., and Hayakawa, H. (2014). Simulation of cohesive fine powders under a plane shear. *Physical Review E*, 90(6):062207.
- Takada, S., Saitoh, K., and Hayakawa, H. (2015a). Kinetic theory for dilute cohesive granular gases with a square well potential. *arXiv preprint arXiv:1506.04578*.
- Takada, S., Saitoh, K., and Hisao, H. (2015b). Simulation of cohesive fine powders under a plane shear. *Physical Review E*, 90:062207.
- Tenneti, S., Garg, G., and Subramaniam, S. (2011). Drag law for monodisperse gas-solid systems using particle-resolved direct numerical simulation of flow past fixed assemblies of spheres. *International Journal of Multiphase Flows*, 37(9):1072–1092.
- Tenneti, S., Mehrabadi, M., and Subramaniam, S. (2016). Stochastic lagrangian model for hydrodynamic acceleration of inertial particles in gas-solid suspensions. *Journal of Fluid Mechanics*, 788:695–729.
- Tenneti, S. and Subramaniam, S. (2014). Particle-resolved direct numerical simulation for gas-solid flow model development. *Annual Review of Fluid Mechanics*, 46:199–230.
- Thornton, C., Cummins, S. J., and Cleary, P. W. (2013). An investigation of the comparative behaviour of alternative contact force models during inelastic collisions. *Powder Technology*, 233:30–46.
- Thornton, C. and Ning, Z. (1998). A theoretical model for the stick/bounce behaviour of adhesive, elastic-plastic spheres. *Powder technology*, 99(2):154–162.
- Tien, C. and Ramarao, B. (2007). *Granular Filtration of Aerosols and Hydrosols*. Elsevier, Oxford, 2nd edition.

- Tomas, J. (2000). Particle adhesion fundamentals and bulk powder consolidation. *KONA Powder and Particle Journal*, 18(0):157–169.
- Torquato, S. (1995). Mean nearest-neighbor distance in random packings of hard d-dimensional spheres. *Physical Review Letters*, 74(12):2156–2159.
- Trizac, E. and Hansen, J. (1995). Dynamic scaling behavior of ballistic coalescence. *Physical Review Letters*, 74(21):4114–4117.
- Trizac, E. and Hansen, J. (1996). Dynamics and growth of particles undergoing ballistic coalescence. *Journal of Statistical Physics*, 86(5-6):1345–1370.
- Tsuji, Y., Kawaguchi, T., and Tanaka, T. (1993). Discrete particle simulation of two-dimensional fluidized bed. *Powder technology*, 77(1):79–87.
- Uhlmann, M. and Doychev, T. (2014). Sedimentation of a dilute suspension of rigid spheres at intermediate galileo numbers: the effect of clustering upon the particle motion. *Journal of Fluid Mechanics*, 752:310–348.
- UNEP, U. N. E. P. (2012). Greening cement production has a big role to play in reducing greenhouse gas emissions. *UNEP Report 2012, Environmental Science Alert Thematic Focus: Resource Efficiency, Harmful Substances and Hazardous Waste, and Climate Change*.
- van der Hoef, M., Beestra, R., and Kuipers, J. (2005). Lattice-boltzmann simulations of low-reynolds-number flow past mono- and bidisperse arrays of spheres: results for the permeability and drag force. *Journal of Fluid Mechanics*, 528:233–254.
- van Noije, T., Ernst, M., and Brito, R. (1998a). Ring kinetic theory for an idealized granular gas. *Physica A*, 251:266–283.
- van Noije, T., Ernst, M., and Brito, R. (1998b). Spatial correlations in compressible granular flows. *Physical Review E*, 57(5):R4893.
- van Noije, T., Ernst, M., Brito, R., and Orza, J. (1997). Mesoscopic theory of granular fluids. *Physical Review Letters*, 79(3):411–414.

- Vidyapati and Subramaniam, S. (2013). Granular flow in silo discharge: Discrete element method simulations and model assessment. *Industrial "E" Engineering Chemistry Research*, 52(36):13171–13182.
- Vidyapati, V., Langroudi, M. K., Sun, J., Sundaresan, S., Tardos, G., and Subramaniam, S. (2012). Experimental and computational studies of dense granular flow: Transition from quasi-static to intermediate regime in a couette shear device. *Powder Technology*, 220:7–14.
- von Karman, T. and Howarth, L. (1938). On the statistical theory of isotropic turbulence. *Proceedings of the Royal Society of London. Series A, Mathematical and Physical Sciences*, 164(917):192–215.
- Walton, O. R. (1984). Application of molecular dynamics to macroscopic particles. *International Journal of Engineering Science*, 22(8):1097–1107.
- Walton, O. R. (2004). Potential discrete element simulation applications ranging from airborne fines to pellet beds. *SAE 2004 Transactions J. Aerospace*.
- Wang, K., Subramaniam, S., and Sundararajan, S. (2013). Final report: Understanding rheology of cement-based materials through integrated experiments and computations at multiple scales. *Final Report NSF CBET Grant No. 0927660*.
- Waters, J., Lee, S., and Guduru, P. (2009). Mechanics of axisymmetric wavy surface adhesion: Jkr–dmt transition solution. *International Journal of Solids and Structures*, 46(5):1033–1042.
- Weller, H., Tabor, G., Jasak, H., and Fureby, C. (1998). A tensorial approach to computational continuum mechanics using object-oriented techniques. *Computers in Physics*, 12(6):620–631.
- Wilson, R., Dini, D., and van Wachem, B. (2016). A numerical study exploring the effect of particle properties on the fluidization of adhesive particles. *AIChE Journal*, 62(5):1467–1477.
- Wylie, J. J. and Koch, D. L. (2000). Particle clustering due to hydrodynamic interactions. *Physics of Fluids*, 12(5):964–970.
- Xing, Z., Kenty, B., Li, Z., and Lee, S. (2009). Scale-up analysis for a cho cell culture process in large-scale bioreactors. *Biotechnology and Bioengineering*, 103(4):733–746.

- Xu, Y. and Subramaniam, S. (2007). Consistent modeling of interphase turbulent kinetic energy transfer in particle-laden turbulent flows. *Physics of Fluids*, 19:085101.
- Yao, H., Ciavarella, M., and Gao, H. (2007). Adhesion maps of spheres corrected for strength limit. *Journal of colloid and interface science*, 315(2):786–790.
- Yin, X., Zenk, J. R., Mitrano, P. P., and Hrenya, C. M. (2013). Impact of collisional versus viscous dissipation on flow instabilities in gas-solid systems. *Journal of Fluid Mechanics*, 727:R2.
- Zaichik, L. and Alipchenkov, V. (2003). Pair dispersion and preferential concentration of particles in isotropic turbulence. *Physics of Fluids*, 15:1776–1787.
- Zaichik, L. I. and Alipchenkov, V. M. (2009). Statistical models for predicting pair dispersion and particle clustering in isotropic turbulence and their applications. *New Journal of Physics*, 11:103018.
- Zamankhan, P. (2005). Kinetic theory of multicomponent dense mixtures of slightly inelastic spherical particles. *Physical Review E*, 52(5):4877–4891.
- Zhang, Q. and Kamrin, K. (2017). Microscopic description of the granular fluidity field in nonlocal flow modeling. *Physical Review Letters*, 118:058001.

CHAPTER 4. RHEOLOGICAL REGIME TRANSITIONS IN MODERATELY DENSE ASSEMBLIES OF DRY COHESIVE GRANULES

This chapter contains a manuscript entitled "Simple Shear of Moderately Dense Cohesive Granules" that has been submitted to Physical Review E by authors E. Murphy, S. Sundararajan, and S. Subramaniam.

4.1 Introduction

As the size of particles in a granular flow are decreased, reaching the micron size range, a number of phenomena appear that are otherwise unimportant to larger particles, e.g. millimeter sized. Cohesion in the form of van der Waals forces, liquid bridging, and longer-ranged electrostatics become important. Repulsive electrostatics may also be present. The cohesive mechanisms cause a number of interesting differences in the characteristic flow behavior when compared to non-cohesive systems. For example, a marked increase in yield stresses are observed with the introduction of cohesion (Aarons and Sundaresan, 2006; Luding and Alonso-Marroquin, 2011; Gu et al., 2014; Irani et al., 2014, 2016). A quasistatic stress scaling, where shear stress does not depend on shear rate (Campbell, 2002), is observed at volume fractions well below volume fractions characteristic of jamming for non-cohesive systems (Aarons and Sundaresan, 2006; Gu et al., 2014). Both of these effects have been observed to cause plug flows in gravity driven chute flows of granular media, where the size of the plug grows with cohesion strength (Brewster et al., 2005). On the other hand, in split cell rheometers, cohesion is observed to increase the size of the shear band, decreasing the size of the static areas of the flow (Singh et al., 2014). In this manuscript we attempt to explore some of the origins of these behaviors from a physics-based microscopic viewpoint, and elucidate some of the challenges in

constitutive modeling of cohesive materials.

We focus primarily on dry cohesive systems with van der Waals cohesion. Systems where the effect of short-ranged cohesion is important are widespread, though the focus in this study is drawn to rheology of moderately dense systems, $\phi_s = 0.55$. On the industrial side, accurate models for micron-sized powder rheology is vital for the simulation and modeling of Geldart C powders in fluidized bed processes (Geldart, 1973; Kim and Arastoopour, 2002; Moreno-Atanasio et al., 2007; Kobayashi et al., 2013; Liu et al., 2016). In processes that depend intimately on the resultant flow field kinematics, such as in powder mixing (Nienow et al., 1992) and materials processing (Castellanos et al., 1999), rheological models of dry cohesive powders must predict the correct yield stress behavior in order to achieve success. In extra-terrestrial settings, rheology is of importance for understanding the transport of and contamination by Martian and lunar regolith (Colwell et al., 2007) as well as for asteroid mining (Kulchitsky et al., 2014; DeCicco and Hartzell, 2016). The discrete element method will be used to extract rheological scalings that are relevant to constitutive modeling in these many different contexts.

The most unique phenomenon brought on by cohesion is a transition from fluid-like behavior to solid-like behavior, that directly depends on both shear-rate and cohesive strength (Aarons and Sundaresan, 2006; Gu et al., 2014; Murphy and Subramaniam, 2017). This transition is observed to occur both in the presence (Aarons and Sundaresan, 2006; Gu et al., 2014) and absence of friction (Takada et al., 2014; Murphy and Subramaniam, 2017). Several generic characteristic features also accompany this transition, which is observed in different combinations of frictional and smooth systems, two and three dimensions, and at constant volume or constant pressure. An increase in particle contacts is observed as the shear rate is decreased or cohesion is increased near the transition for frictional systems (Gu et al., 2014), reminiscent of the transition with volume fraction in non-cohesive systems. Shear banding (Gu et al., 2014; Singh et al., 2014; Irani et al., 2014, 2016; Berger et al., 2016) and more elaborate instabilities (Takada et al., 2014) have also been observed as cohesion is increased in very large systems. However, as cohesion is increased beyond some critical value shear banding may disappear (Gu et al., 2014). An increase in a correlation length-scale for correlated non-affine particle velocities is also observed (Rognon et al., 2008).

Some noteworthy differences from non-cohesive systems have also been reported in the study of cohesive granular systems. For smooth systems below a certain shear rate or strength of cohesion, homogeneous macroscopic systems become thermodynamically unstable (Takada et al., 2014) and can exhibit negative pressures (Irani et al., 2016). Most puzzling is that the transition in frictionless systems is considered energetic in nature, depending only on collisional energy dissipation, van der Waals potential, and shear-rates. The rheological behavior of frictional systems, on the other hand, has often been collapsed by a dynamic scaling, i.e., using the cohesive force at contact (Aarons and Sundaresan, 2006; Rognon et al., 2008; Gu et al., 2014). Whether both scalings are correct and how the transition between scalings happen for vanishing interparticle friction remain unanswered.

Moreover, a clear microscopic and mechanistic picture of why this transition occurs, and an explanation for the differences between frictional and non-frictional cases, is lacking. It is known from the standpoint of the kinetic theory of smooth cohesive spheres that aggregation of particles is sensitive to granular temperature, which scales with the macroscopic shear rate (Kim and Arastoopour, 2002; Murphy and Subramaniam, 2015, 2017; Liu et al., 2017). How this aggregation mechanism fully connects to the observed rheological transition remains an unanswered question.

In our DEM studies, we find an important connection for both frictional and frictionless systems between the fluid to solid-like transition and the ratio of the cohesion energy to the granular temperature and explore this connection in detail. For smooth systems the scaling is robust for all coefficients of restitution. Microstructural measures are introduced, such as a cluster length-scale, which clearly shows that the mechanism behind the rheological transition in frictionless systems is percolation of the domain by particle contact networks. Additionally, non-trivial trends in the shear stress ratio with varying friction are explored and connected to contact anisotropy.

The results obtained herein hint at some difficulties in the constitutive modeling of cohesive granular flows. It is now understood that in ordinary granular flows, non-local rheological behavior is tied to the granular temperature both through interaction with boundaries (Gaume et al., 2011; Zhang and Kamrin, 2017) and increase in local non-affine velocity correlations

that determine collisional energy dissipation (Berzi and Jenkins, 2015b; Gollin et al., 2017). The temperature in these cases is not slaved to the local shear rate and pressure, as was the case in the so-called $\mu(I)$ rheology (MiDi, 2004). We expect that the sensitive dependence of the rheology on granular temperature will also mean that additional transport models for variables, namely temperature, will need to be considered in addition to flow kinematics. Lastly, the emergence of new diverging cluster length-scales must also be accounted for in any proposed rheological model.

4.2 Methods

In this paper we aim to examine the physical basis for the transition in rheological scaling in simple shear, from inertial to quasistatic scaling, for moderately dense assemblies of cohesive granules. To accomplish this analysis we have performed DEM simulations of simple shear using the molecular dynamics code LAMMPS (Plimpton, 1995). Particles in this methodology interact not only due to the ordinary elastic and dissipative models that are active when particles are in contact, but also due to an attractive potential well, which extends beyond contact (Murphy and Subramaniam, 2015, 2017). A generic form of the normal component of the combined contact force law and cohesive force law are given by

$$\mathbf{F}_n^{(ij)} = \begin{cases} (R_{\text{eff}}|\delta|)^p \left(-b_n \mathbf{v}_n^{(ij)} - k_n \delta \hat{\mathbf{n}}^{(ij)} \right) + \mathbf{F}_{c,vdW} & : \delta \leq 0 \\ \frac{-AR_{\text{eff}}}{6(\delta + d_0)^2} \hat{\mathbf{n}}^{(ij)} & : \delta > 0 \end{cases}, \quad (4.1)$$

where b_n and k_n are the normal damping and spring constants of the force law. These forces depend on $\mathbf{n}^{(ij)}$, the normal separation vector from particle i to particle j , the surface separation or overlap $\delta = |\mathbf{n}^{(ij)}| - (R^{(i)} + R^{(j)})$, and pair normal velocity $\mathbf{v}_n^{(ij)}$. Lastly, a caret indicates a unit vector. The van der Waals force is the source of cohesion in this model and is determined by the Hamaker constant A , effective radius at contact $R_{\text{eff}} = R^{(i)}R^{(j)} / (R^{(i)} + R^{(j)})$, which may differ from the radius of the particle, and the interatomic separation distance d_0 , typically taken to be anywhere from 0.167 – 0.4 nm (Aarons and Sundaresan, 2006; Israelachvili, 2011; Kobayashi et al., 2013; Murphy and Subramaniam, 2017). In this model, the van der Waals

force saturates at contact and hence the cohesive force between a pair of particles in contact is given by $\mathbf{F}_{c,vdW} = -\hat{\mathbf{n}}^{(ij)}AR_{\text{eff}}/(6d_0^2)$. This model is consistent with approaches for nearly rigid particles where the Tabor parameter is sufficiently small $\mu_T < 0.1$ (Tabor, 1977) and radius of contact is sufficiently large $R_{\text{eff}} \gg d_0$ (Israelachvili, 2011). Finally, the exponent p is used to select between contact force models such as the linear spring dash-pot (Cundall and Strack, 1979a), $p = 0$, and the Kuwabara-Kono model $p = 1/2$ (Kuwabara and Kono, 1987; Brilliantov et al., 1996).

The tangential forces are governed by similar models given by

$$F_t^{(ij)} = \begin{cases} (R_{\text{eff}}|\delta|)^p (-b_t \mathbf{v}_t - k_t \mathbf{u}^{(ij)}) & : \delta < 0, |F_t| \leq |\mu_f F_n| \\ -\mu_f |F_n| \hat{\mathbf{u}}^{(ij)} & : \delta < 0, |F_t| \geq |\mu_f F_n| \\ 0 & : \delta > 0 \end{cases} \quad (4.2)$$

where a subscript t is used to indicate the tangential counterpart of the normal definitions. Additionally, \mathbf{u}_t is the elastic surface displacement. The tangential force saturates as well, when a yield criterion is met, see Eq. 4.2. Thereafter, a Coulumb friction law is used, where μ_f is the coefficient of friction. The tangential spring stiffness is taken to be $k_t = 2k_n/7$ (Schäfer et al., 1996), when friction is present. The tangential damping is set to zero and not considered in our treatment.

The parameter space of interest for these systems is best discussed in non-dimensional terms. The normal force law given in Eq. 4.1 produces 4 independent non-dimensional groups (Murphy and Subramaniam, 2017). The groups for the linear spring dash-pot variant that we will choose to use are the ratio of the attractive potential at contact to the kinetic energy in the normal relative direction $Ha_p = 2AR_{\text{eff}}/(6m_{\text{eff}}v_{\text{ref}}^2d_0)$, the modified Bond number (Aarons and Sundaresan, 2006) $Bo^* = AR_{\text{eff}}/(6d_0^2k_tD)$, the coefficient of restitution ε , and the scaled particle stiffness $k^* = k/(\rho Dv_{\text{ref}}^2)$. Note that the coefficient of restitution is given by $\varepsilon = \exp\left(-\pi/\sqrt{\frac{4k_n m_{\text{eff}}}{b^2} - 1}\right)$. The tangential force law also produces the important non-dimensional group already introduced μ_f . Here the effective mass is given by $m_{\text{eff}} = m^{(i)}m^{(j)}/(m^{(i)} + m^{(j)})$ and ρ is the particle density. Since we are considering simple shear

flows of granular particles the reference velocity v_{ref} can be chosen to be one of two macroscopic velocity scales: the granular temperature $v_{ref} = \sqrt{T_g} = \sqrt{\langle v_k^{(i)} v_k^{(i)} \rangle} / 3$ or the velocity scale defined by the shear rate $v_{ref} = \dot{\gamma} D$. Both of these reference velocity scales will be used to define a macroscopic Ha_α parameter, where α is a placeholder for the shear rate $\dot{\gamma}$ or temperature T . Additional macroscopic non-dimensional groups are then $T / (\dot{\gamma} D)^2$, the solid volume fraction ϕ , inertial scaling of pressure related to the so-called inertial number (MiDi, 2004; Jop et al., 2006) by $P / (\rho (\dot{\gamma} D)^2) = I^{(-2)}$, and of course any number of ratios between combinations of entries in the stress tensor, e.g. shear stress ratio $\mu = \sigma_{xy} / P$.

Aarons and Sundaresan (2006) and Gu et al. (2014) investigated a transition in stress behavior in sheared cohesive assemblies that occurs at volume fractions below the jamming transition for non-cohesive particles. In this paper we are interested in the physical underpinnings of the transition of assemblies of cohesive particles with and without friction. Towards this end we have chosen to simulate a solid volume fraction of $\phi = 0.55$, while varying other relevant parameters such as ε , Ha , Bo , and μ_f .

Previous studies on head-on collisions of cohesive particles have revealed that for particles that are sufficiently hard-enough, e.g. with stiffnesses satisfying $Bo^* < 10^{-5}$ for $\varepsilon = 0.9$ and $D/d_0 = 10^4$, the restitution behavior is purely a function of the parameter Ha_p and ε Kobayashi et al. (2013); Murphy and Subramaniam (2017). Here the reference velocity is the initial relative velocity between a pair of particles separated beyond the strong cohesive part of the well, at least $10d_0$. The equation for the effective coefficient of restitution ε_{eff} is then given by

$$\varepsilon_{eff} = \begin{cases} (\varepsilon^2 - (1 - \varepsilon^2) Ha_p)^{1/2} & : v_{ref} \in (-\infty, v_{crit}) \\ 0 & : v_{ref} \in [v_{crit}, 0] \end{cases} . \quad (4.3)$$

where the critical initial velocity is $v_{crit} = -\sqrt{-2AR_{eff}(1 - \varepsilon^2) / (6d_0m_{eff}\varepsilon^2)}$ and the corresponding $Ha_{crit} = \varepsilon^2 / (1 - \varepsilon^2)$. The plot of this restitution behavior can be found in Fig. 2.3. This equation first appeared in a treatment by Dahneke (1975), who was investigating the restitution behavior of micron-sized latex spheres impacting a wall. Fig. 2.3 shows two important behaviors: 1) near the critical velocity an increase in cohesion or decrease in velocity

increases dissipation in a particle collision 2) particles with lower restitution coefficient stick together more easily. We expect this change in restitution and sticking behavior brought on by cohesion to play a significant role in the formation of structure during the regime transitions observed in simple shear, especially for frictionless particles.

DEM simulations of simple shear are carried out using a triclinic deforming domain, equivalent to the Lees-Edwards boundary conditions (Lees and Edwards, 1972) at constant volume. In this set-up energy is added to the kinetic energy of the domain through the usual mechanism of viscous heating $\dot{E}_{kin} = \sigma_{xy}\dot{\gamma}$. This heating generates fluctuations in the particle velocities, which are eventually dissipated by collisional and frictional dissipation mechanisms. We expect that for frictionless systems if the characteristic velocity set by the granular temperature is much greater than the critical velocity, cohesion will play little to no role.

As the temperature approaches the critical velocity, the formation of larger clusters is to be expected (see Fig. 4.1.) Eventually, we expect that clusters must become large enough to span the computational domain. The percolation of clusters changes the mechanism of momentum transfer from collisional to yielding. The shear stress should then become quasi-static in nature, i.e. $\sigma_{xy} \sim \dot{\gamma}^0$, consistent with dense flows near the jamming transition for non-cohesive particles Chialvo et al. (2012); Gu et al. (2014). How exactly this transition occurs and how it affects the formation and break-up of aggregate structure remains a mystery.

In the following results section we first explore the behavior of macroscopic quantities, such as shear stress, temperature, and shear stress ratio, near the inertial to quasi-static transition. The relevant non-dimensional parameters used in the following studies is given in Table 5.2.1. We then look at microscopic and cluster measures as a means to explain the emergence of different scaling behaviors in the macroscopic variables. Finally, we look at the contact anisotropy to explain differences in shear stress ratios with and without friction.

4.3 Results

The results section is broken up into four subsections. The first section explores the behavior of macroscopic observables, such as shear stress, shear stress ratio, and granular temperature, both at shear rates above and below the transition. Differences that arise between frictionless

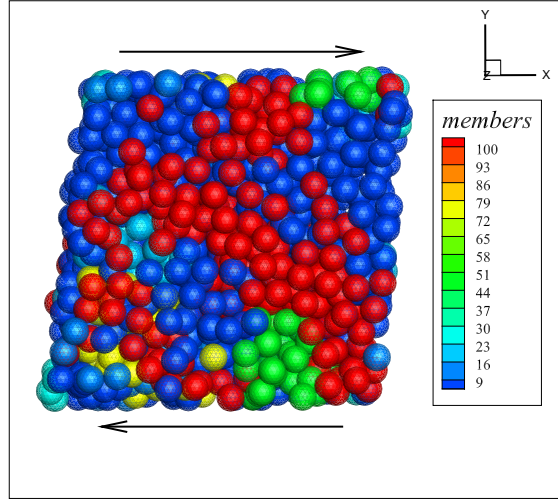


Figure 4.1 The appearance of clusters in a snapshot when $Ha_\gamma = 0.72$, $Bo^* = 4.2 \times 10^{-10}$ and $D/d_0 = 10^4$.

Table 4.1 Parameters used in simple shear simulations of cohesive granules.

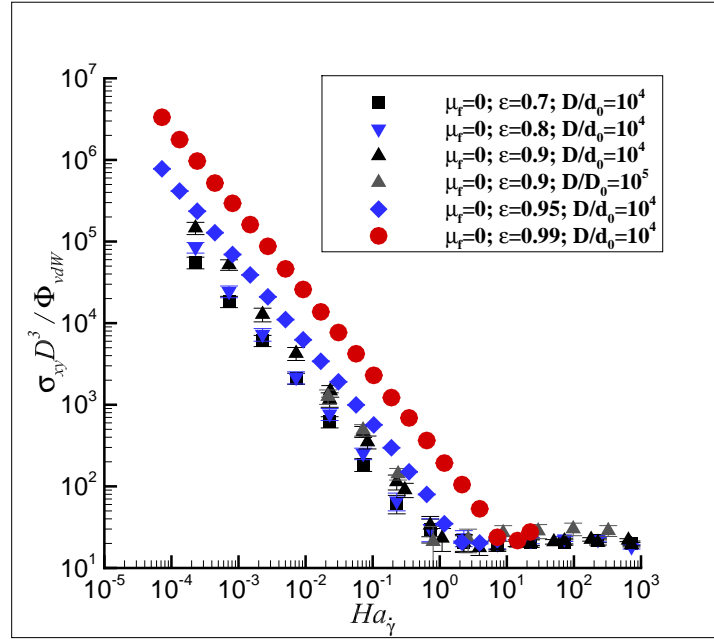
Parameter	Values
ϕ	0.55
ε	0.7; 0.8; 0.9; 0.95; 0.99
Ha_γ	$7.2 \times 10^{-5} - 7.2 \times 10^2$
Bo^*	$4.2 \times 10^{-14} - 4.2 \times 10^{-5}$
k^*	$2 \times 10^8 - 10^{13}$
D/d_0	$10^4 - 10^5$
μ_f	$0; 10^{-5}; 10^{-4}; 10^{-3}; 10^{-2}; 10^{-1}; 5 \times 10^{-1};$

and frictional systems are also discussed. The second section focuses on microscopic quantities such as the average coordination number $\langle Z \rangle$, average cluster length-scales in the directions of principal compression and extension, and the radius of gyration. Scaling of all these quantities is also discussed. In the third section, a connection between contact anisotropy and shear stress ratio behavior is discussed. Finally, challenges in constitutive modeling are discussed.

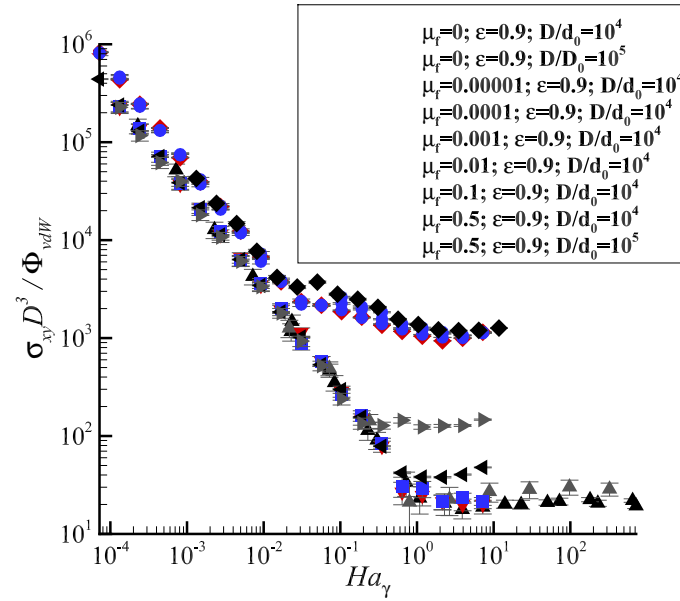
4.3.1 Energetic Collapse of Stress

The shear studies presented here are all performed at a volume fraction, $\nu = 0.55$, below the jamming transition as defined by Chialvo et al. (2012). For non-cohesive particles, momentum transport still occurs primarily due to collisional transport, and Bagnold (Bagnold, 1954) or inertial scaling of the stress is observed. Previous studies in the moderately dense regime at constant volume for cohesive frictional particles have shown an additional transition in the rheology due to the sticking/clumping of particles (Aarons and Sundaresan, 2006; Lois et al., 2008; Gu et al., 2014). This transition was shown to depend on the cohesive force scaled by inertial terms, i.e. the product Bo^*k^* . Recent simulations (Takada et al., 2014) and theory (Saitoh et al., 2015) for sheared systems of cohesive frictionless particles, modeled through a Lennard-Jones potential, also reveal a transition in the behavior. When cohesion is below some threshold value, dispersed particle assemblies were obtained (Takada et al., 2014). However, when the shear rate became small enough or cohesion large enough, particle assemblies became thermodynamically unstable (Saitoh et al., 2015) and formed various patterns. The location of the thermodynamic instability was shown to scale with both the inelasticity $\alpha = 1 - \varepsilon^2$ and a term s analogous to $Ha_{\dot{\gamma}}^{-1}$, in agreement with Eq. 4.3. We now explore how this transition occurs using our force model in Eq. 4.1, and how the introduction of friction changes this transition.

Figure 4.2(a) displays the results of shear simulations for frictionless particles at different values of inelasticity, $Ha_{\dot{\gamma}}$, Bo^* , and D/d_0 , i.e. Hamaker constant, shear rate, and diameter of particle relative to the interatomic distance. There is indeed a transition in the shear stress from inertial to quasi-static scaling for all cases. The location of the transition appears to depend only on the inelasticity of the equivalent non-cohesive model, with more more elastic



(a)



(b)

Figure 4.2 (a) The collapse of shear stress for smooth spheres with squared inverse shear rate, i.e. $Ha_\gamma \sim \dot{\gamma}^{-2}$. The collapse is also energetic depending only on the coefficient of restitution. (b) The same collapse is given for spheres with varying strengths of friction and same coefficient of restitution. The collapse remains energetic.

systems requiring lower shear rates as compared to less elastic granules to achieve an inertial scaling. This is consistent with what is expected from the equation for the critical velocity ε_{eff} Eq. 4.3. We note that the critical value of $Ha_{\dot{\gamma}}$ is not identical to Ha_{crit} . For example, for $\varepsilon = 0.99$ the critical value of $Ha_{\text{crit}} \approx 50$ while $Ha_{\dot{\gamma},\text{crit}} \approx 10$. Further, the scaled shear stress in the quasistatic regime is practically identical for all cases. The most important take-away from this plot is that two values of D/d_0 , as used in the $\varepsilon = 0.9$ cases, yield the same qualitative behavior (location of the transition) and quantitative behavior (magnitude of the shear stress). In the model used, two different values of D/d_0 allows us to differentiate, whether a scaling is truly dynamic or energetic. A dynamic scaling (Aarons and Sundaresan, 2006; Gu et al., 2014) is scaled by a characteristic cohesive force proportional here to d_0^2 , while an energetic scaling (Murphy and Subramaniam, 2015; Saitoh et al., 2015; Murphy and Subramaniam, 2017) utilizes a cohesive potential Φ_{vdW} at contact proportional to d_0 . When two different values of D/d_0 are compared, a collapse of the stress can be only energetic or dynamic, but not both. The collapse here is clearly energetic. We may infer that it may be granular temperature, i.e. velocity fluctuations, that are important in determining transition behavior here, rather than coherent forces acting on the mean velocity.

Cases with varying strengths of friction from quite small $\mu_f = 10^{-5}$ to rather large $\mu_f = 0.5$ are also shown in Fig. 4.2(b), all for a coefficient of restitution of $\varepsilon = 0.9$. A similar story is shown here in regards to the effect of friction. The critical value of $Ha_{\dot{\gamma}}$ decreases with increasing friction, meaning that as friction is increased a higher shear rate is necessary to achieve fluidization. We notice that for small enough friction, e.g. $\mu_f \leq 10^{-4}$, there is practically no difference between stress scaling between smooth and frictional systems. The two most important observations are 1) the location of the transition in stress scaling remains energetic in the presence of friction for $\mu_f = 0.5$ and differing D/d_0 and 2) the scaled stress in all regimes scales energetically. The origin of this transition with and without friction appears to be brought about primarily by energy loss in collisions leading to sticking, which is only affected by the coefficients of restitution and friction.

Finally, we note that the frictional cases saw many instabilities emerge in the quasistatic regime, e.g. shear banding (Gu et al., 2014; Saitoh et al., 2015), so-called flying ice cubes, and

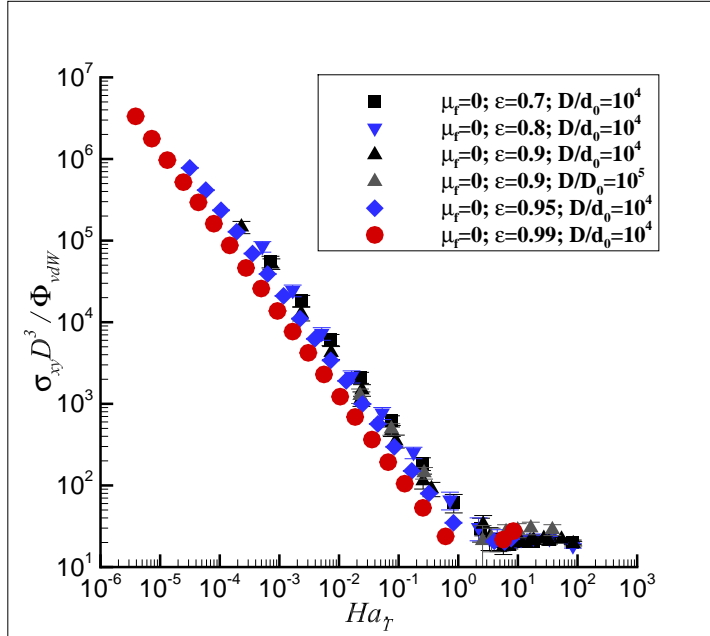


Figure 4.3 An improved collapse of shear stress, with the characteristic velocity scale being temperature rather than shear-rate.

crystallization. Because those instabilities are of little interest in the present study, data points exhibiting the instabilities have been removed from the data presented here. Nonetheless, all data in the inertial regime were stable, and the critical value of Ha_T remained solely determined by ε and μ_f .

Now we explore some details of the transition in more detail, namely a collapse using the granular temperature rather than shear rate as a characteristic velocity scale. Figure 4.3.1 display the shear stress and temperature scaling for smooth systems as a function of Ha_T . The location of the transition in stress for smooth systems occurs at a unique Ha_T for all values of ε , with $Ha_{T,crit} = 1$. Minor differences in stress magnitudes occur in the inertial regime among different ε due to differences in dash-pot strength. Lastly, the frictional cases do not all transition at $Ha_T = 1$. A more detailed characterization of the behavior of the temperature, and an explanation as to why collapse occurs at $Ha_T = 1$ can be found in H.

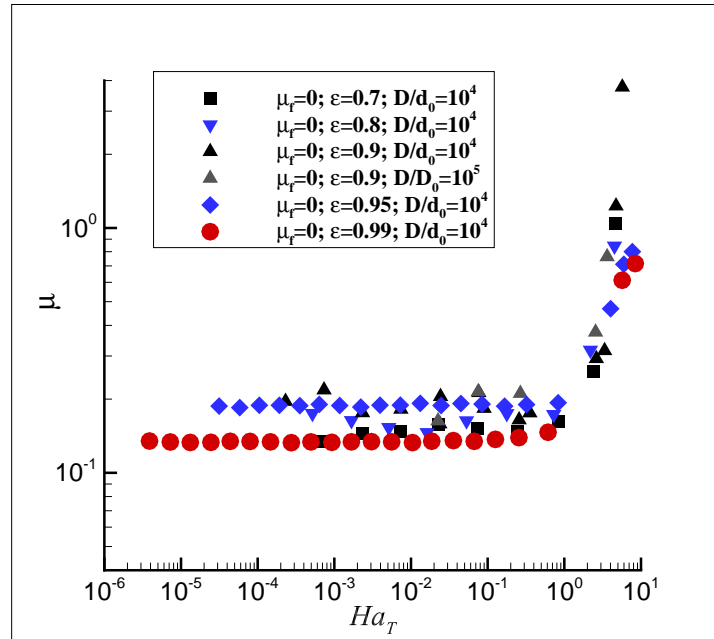
The often used $\mu(I)$ rheology (MiDi, 2004) focuses on the behavior of the shear stress ratio $\mu = \sigma_{xy}/p$ or apparent friction coefficient of the granular assembly. Cohesion is observed to increase the apparent friction, allowing for different values of μ to be observed at the same

volume fraction, as was previously observed (Rognon et al., 2008; Gu et al., 2014; Berger et al., 2016). Here we are interested in how the pressure might scale differently from the shear stress. Figures. 4.4(a) and 4.4(b) display the apparent friction for smooth and frictional systems, respectively. In the absence of friction, we see that all cases more or less scale the same in both the frictional and quasistatic regimes. The cases in the quasistatic regime show much larger values for the apparent friction as compared to the in the inertial regime, i.e., low Ha_T . Small differences are also observed in μ due to the coefficient of restitution as well. Most interestingly here, we observe values of μ that exceed unity, consistent with previous studies in the moderately dense regime (Rognon et al., 2008; Murphy and Subramaniam, 2017). The reason for this is that the smooth systems are observed to be metastable for $Ha_T > 10$, with negative pressures developing. Negative pressures have also been observed in frictionless studies of 2D attractive systems (Irani et al., 2016). As the pressure approaches zero, the apparent friction may become large. In a large enough domain these systems should phase separate into dense and dilute phases, consistent with prior studies (Takada et al., 2014; Irani et al., 2014). This phase separation is beyond the scope of this work.

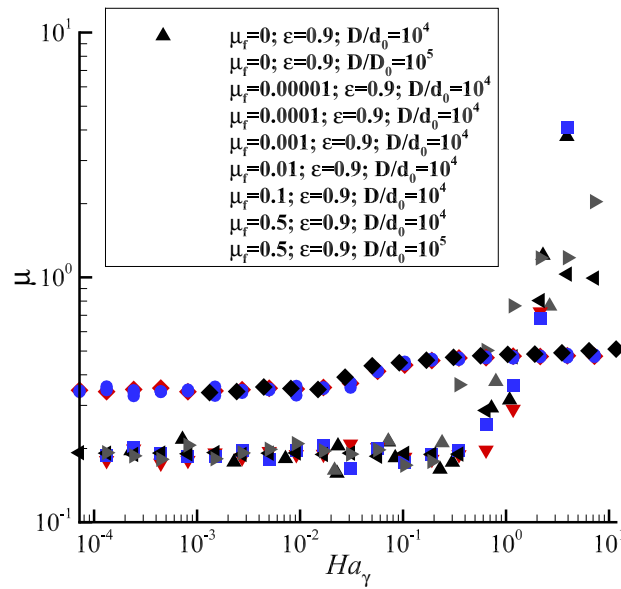
In frictional cases, it is seen that if the friction is small enough, e.g., $\mu_f < 0.1$, similar behavior in the apparent friction is observed. With higher particle friction, the apparent friction begins at $\mu \approx 0.35$ and saturates at a value of $\mu \approx 0.5$ in the quasistatic regime. For very low friction, $\mu_f < 10^{-4}$, some values of μ are still greater than unity. Here again, negative pressures are observed. The microstructural origin for the differing behaviors in μ for large and infinitesimal friction will be explored in Section 4.3.3.

4.3.2 A signature of transition in rheology

The physical underpinnings of the inertial to quasistatic regime transition in granular flows is now explored. A strong correlation has been observed between particle sticking brought on by enhanced collisional dissipation due to cohesion and the location of the regime transition. This leads us to believe that it is the formation of clusters that is ultimately responsible for the regime transition. An average length-scale $\langle \xi_i \rangle$ is now introduced in order to observe this transition



(a)



(b)

Figure 4.4 (a) The behavior of the apparent friction is compared among smooth assemblies with differing coefficients of restitution. (b) The apparent friction for cases with varying friction and $\varepsilon = 0.9$.

$$\xi_i^l = \max \frac{n_i^{jk}}{2} \quad \forall \quad j, k \in \mathcal{C}^l \quad (4.4)$$

$$\langle \xi_i \rangle = \frac{1}{N_p} \sum_{l=1}^{N_c} N_{p,l} \xi_i^l.$$

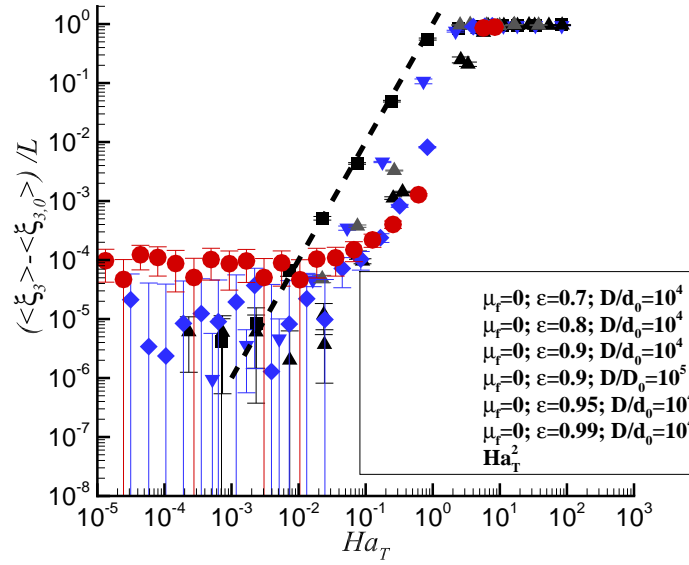
Here \mathcal{C}^l is the set of particle indexes in cluster l , and N_c and $N_{p,l}$ denote the number of clusters and number of particles in cluster, respectively. The coordinate system that ξ_i is based in is aligned with the original box dimensions. Note that this quantity is not a true vector because it does not transform as one. This length scale represents the furthest a disturbance to a particle can travel on average through an aggregate, or half the length of an aggregate in the i -th direction. If this length-scale reaches half the size of the box then the box is percolated in the i -th direction, and a disturbance can reach any location in that dimension. The dimension of interest here is the shear dimension, since the aggregate will be fully connected across the moving boundary (in the direction of shear). There are other measures of the length-scale of particle clusters that do not depend on the coordinate system, such as the radius of gyration tensor. However, this measure is also sensitive to the packing of particles (i.e. dimension of the aggregates). While they behave similarly to the length-scale introduced here, they do not clearly demonstrate the physics of the diverging length-scale. Finally, we note that monomers do not contribute to the length scale ξ_i^l , but they do contribute to the average length scale $\langle \xi_i \rangle$ due to normalization.

We now look to the average cluster length-scales in figs. 4.5(a) and 4.5(b). The reported length scale $\langle \xi_3^* \rangle = 2((\langle \xi_3 \rangle - \langle \xi_{3,0} \rangle) / L)$ scale subtracts off the value observed for an equivalent case without cohesion and is normalized by the height of the cubic domain. Note that the non-constant values $\langle \xi_3^* \rangle$ at low Ha_T and Ha_γ are merely due to very small uncertainty in the average length-scale for non-cohesive systems. Impressively, if we compare the average length-scale for friction-less particles in fig. 4.5(a), we find that the length scale grows exactly as Ha_T^2 , which is predicted from scaling arguments for population balances in I. For the case of $\epsilon = 0.7$ this occurs not only for $Ha_T \ll 1$ but also until the length scale saturates at the size of the box. Percolation of the contact network is the result of the average length-scale reaching the size of the box, and coincides well with the inertial to quasistatic regime transition at $Ha_T = 1$.

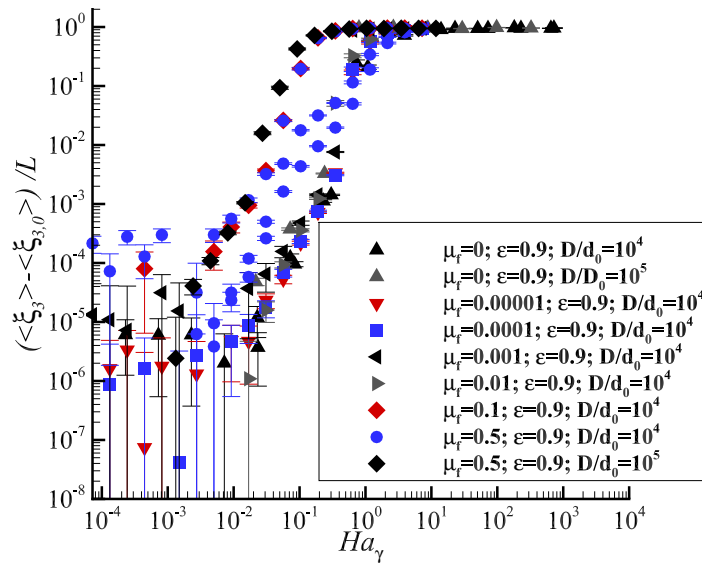
Animations of a few cases with varying $Ha_{\dot{\gamma}}$ are contained in [supplementary materials](#). There we observe that in the case of $Ha_{\dot{\gamma}} = \text{few}$ aggregates are observed and are mostly dimers. As $Ha_{\dot{\gamma}}$ is increased large fluctuations in aggregate size are observed, which is consistent with phase transition phenomenology. At the largest value of $Ha_{\dot{\gamma}} = \text{only}$ a single aggregate is observed with small transient aggregates occasionally forming. The variance in the cluster size distribution peaks during the stress transition, not shown for brevity.

For frictional cases, we observe that percolation does not always coincide with the rheological transition. For cases where $\mu_f = 0.5$ and $D/d_0 = 10^4$ with the same values of $Ha_{\dot{\gamma}}$ but different shear rates, differing values of $\langle \xi_3^* \rangle$ are observed. All three contain an inflection point at the same $Ha_{\dot{\gamma}}$, but percolation is observed at different points. Note that all cases yield shear stresses that are practically identical. The differences in length-scales are likely due to differences in the stiffness compared to shear rate and cohesive force at contact or k^* and $B\sigma^*$.

For frictional cases, a better structural indicator of the stress transition is a jump in the average local cohesive potential, $\langle \Phi_{loc} \rangle / \langle \Phi_{vdw} \rangle$. This is the average total local potential of a particle and all of its neighbors normalized by the potential between two particles in contact, which has been used previously to characterize aggregates in shear flow of nanoscale particles (Markutsya et al., 2014). Due to the extremely short-ranged nature of these potentials, this is a good surrogate for the coordination number in these stiff systems. Figures 4.6(a) and 4.6(b) give the scaled potential for both smooth and frictional cases. For strongly frictional cases $\mu_f \geq 0.1$, the location of the transition coincides with a marked rise in $\langle \Phi_{loc} \rangle / \langle \Phi_{vdw} \rangle$ to $\langle \Phi_{loc} \rangle / \langle \Phi_{vdw} \rangle \approx 2$ in agreement with Gu et al. (2014). For cases with smaller friction, the jump is more extreme, to $\langle \Phi_{loc} \rangle / \langle \Phi_{vdw} \rangle \approx 4$. All cases continue to increase with $Ha_{\dot{\gamma}}$ with larger μ_f generally leading to smaller $\langle \Phi_{loc} \rangle / \langle \Phi_{vdw} \rangle$. This seems to be in agreement with the notion that chains of particles are more stable against buckling as friction is increased, so that fewer redundant contacts are needed. Finally, we note that all cases have $\langle \Phi_{loc} \rangle / \langle \Phi_{vdw} \rangle < 6$, the coordination number for isostatic jamming of smooth spheres (Liu and Nagel, 2010).

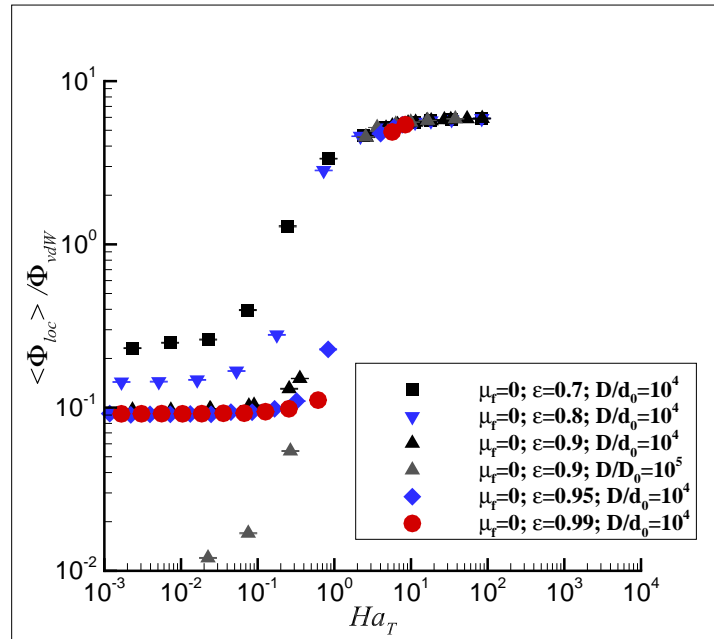


(a)

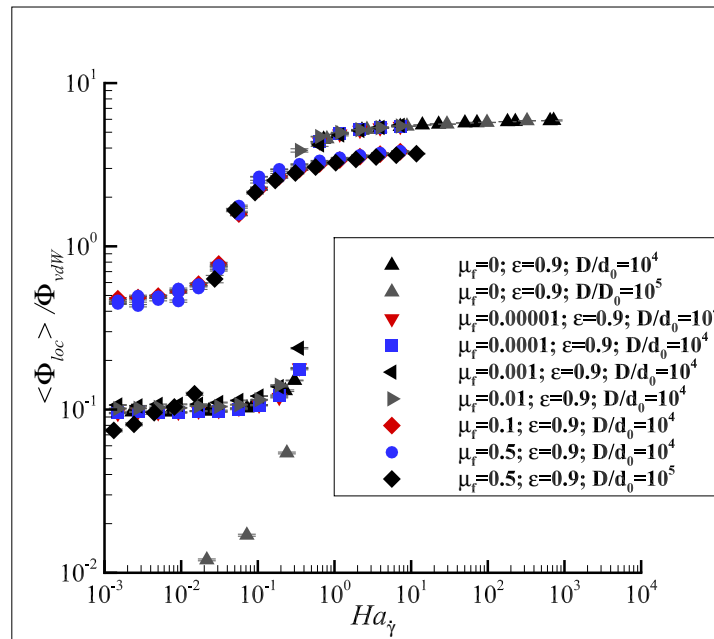


(b)

Figure 4.5 (a) The scaling of the average cluster length-scale in the shear direction is given for smooth spheres, which scales as Ha_T^2 . Percolation is observed for $Ha_T > 1$. (b) The cluster length-scale is given for varying coefficient of friction. Percolation does not correlate with the transition for all cases when friction is present.



(a)



(b)

Figure 4.6 (a) The scaled average local cohesive potential is given for smooth cases. A jump in the potential is shown for all cases at $Ha_T = 1$. (b) The scaled average local cohesive potential for frictional cases shows a marked increase that correlates well with the stress transition.

4.3.3 Contact Anisotropy

Lastly, we examine the microscopic ordering that gives rise to the observation that in the quasistatic regime including friction leads to an increase in shear stress but a decrease in shear stress ratio. Evidence has already been shown in fig. 4.6(b) that lower friction leads to more compact aggregates. The virial equation for stress $\sigma_{ij} = \Sigma_{k \neq l} n_i^{(kl)} F_j^{(kl)} / V$ shows us that the alignment between forces and lines of center for particles in contact is important for determining how the shear stress and shear stress ratio should scale. Here V is the volume of the simulation domain. To that end we extract the radial distribution function at contact in spherical coordinates $g(r = D, \theta, \phi)$ and decompose this function into tesseral spherical harmonics. Here θ is the polar angle at which particles are separated in relation to the axis of shear in the counter-clockwise direction, while $\phi = 0$ is aligned with the negative streaming direction. Spherical harmonics are an extension of Fourier series with spherical periodicity rather than circular periodicity. In this sense, spherical harmonics are a natural extension to the Fourier decomposition used to represent contact anisotropy in 2-dimensions (Berger et al., 2016).

The first spherical harmonic mode is isotropic, and contains information about the isotropic radial distribution function at contact, i.e., $g_c = g(r = D)$. The first spherical harmonic mode to have the reflective symmetry required in $g(r < D, \theta, \phi)$ also aligns with the eigenvectors (compression and extension) of the imposed shear flow. The decomposition in orthonormalized spherical harmonics is as follows

$$g(r < D, \theta, \phi) = u_0^0 Y_0^0 + u_2^1 Y_2^1 + \dots = \frac{1}{2\sqrt{\pi}} \left(u_0^0 + \sqrt{15} u_2^1 \cos \phi \cos(\theta + \theta_{shift}) \sin(\theta + \theta_{shift}) + \dots \right). \quad (4.5)$$

Here the mode coefficients are given by u_l^m , while the mode is given by Y_l^m . The superscript l and the superscript m are indexes for the series terms which go from $(0, \infty)$ and $(0, l)$, respectively. The magnitude of the mode is then found via the orthogonality condition as $u_l^m = \int_0^\pi \int_{\theta_{shift}}^{2\pi + \theta_{shift}} Y_l^m Y_l^m \sin(\theta + \theta_{shift}) d\phi d\theta$. For reference, the anisotropic mode of interest is shown in fig. 4.7 for $\theta_{shift} = 0$, where it is clear that a peak occurs in the direction of maximal compression and a valley in the direction of maximal expansion. In order to reduce

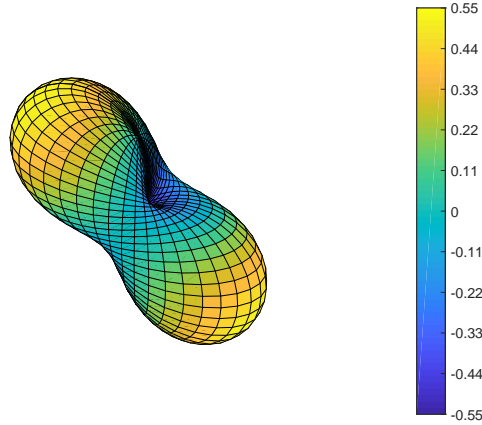


Figure 4.7 A depiction of the spherical harmonic mode u_2^1 . The sphere has been stretched according to the magnitude u_2^1 at that location. A peak occurs at $(\phi = 0, \theta = \pi/4)$ and a valley occurs at $(\phi = 0, \theta = 3\pi/4)$.

the error in integration in the orthogonality condition due to non-uniform bin areas, the sphere is binned in recursively triangulated bins from an initial octahedron with vertices aligned in the x, y, z -directions, rather than evenly distributed bins in ϕ and θ . This method eliminates any sampling bias due to unequal areas, proportional to $\sin \theta$, in the uniform in ϕ and θ sampling. The inclusion of the phase shift in the polar angle θ_{shift} is intended to capture the principal anisotropic mode in the case there is an phase-shift. However, no significant phase-shifting was observed.

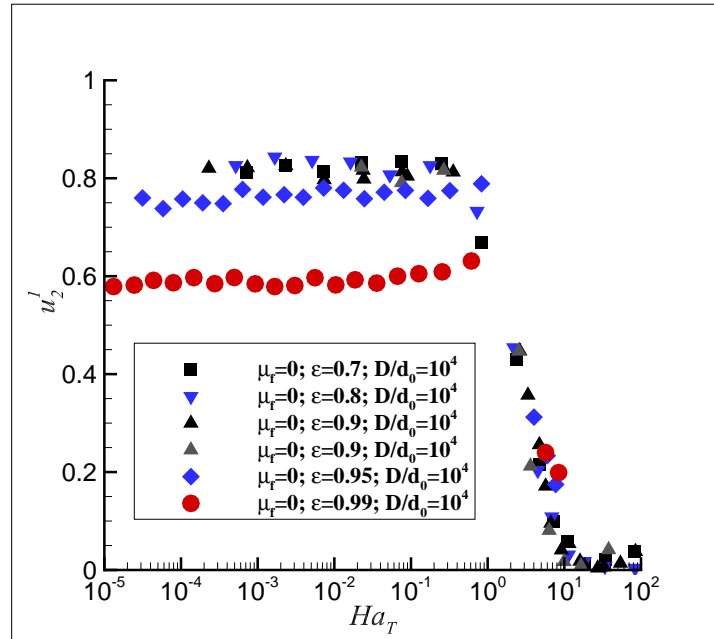
Figures 4.8(a) and 4.8(b) display the interplay of shear, temperature, cohesion and friction on the contact anisotropy through the inertial to quasistatic transition. If we focus on the smooth systems, we see that for all cases, the contact anisotropy collapses above $Ha_T > 1$. For $Ha_T > 1$ the contact anisotropy quickly plummets until above $Ha_T > 10$, where the system can be considered to be essentially isotropic. These contacts do not prefer any directionality. The isotropic behavior in the quasistatic regime is likely due to unstable particle arrangements in the compression direction, which quickly buckle and rearrange. At values of $Ha_T < 1$, there are differences in contact anisotropy u_2^1 due to the coefficient of restitution. Each of these different ϵ have differing scaled temperatures $T/\dot{\gamma}^2$. An increase in scaled temperature, which serves to randomize local velocities, is responsible for the decrease in contact anisotropy brought on by

imposed shear. Overall, in the case of smooth spheres the competition in contact anisotropy appears to be between shear, which enhances anisotropy, and cohesion and temperature, which decrease contact anisotropy.

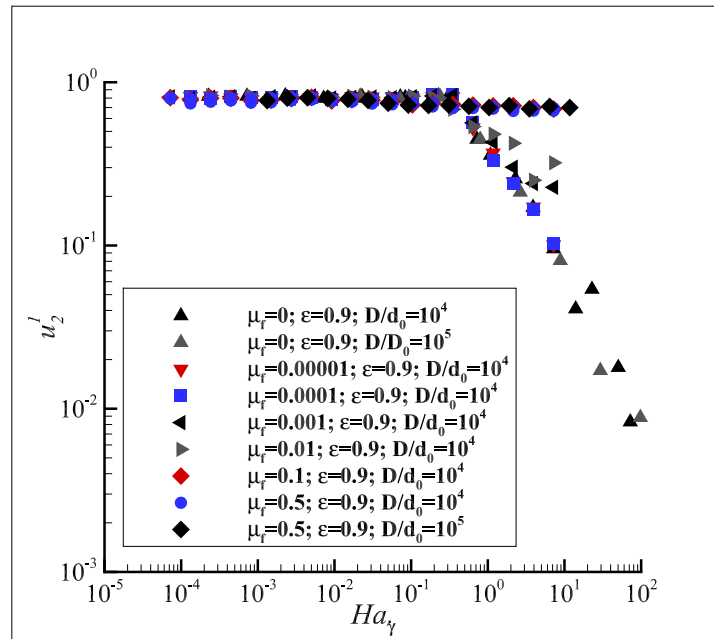
For frictional cases, we see that friction tends to increase the contact anisotropy in the quasistatic regime (c.f. fig. 4.8(b)). Note that these cases are on a log-log plot. For cases where $\mu_f < 0.1$, friction increases the contact anisotropy from what is observed in smooth cases, though not substantially. For $\mu_f \geq 0.1$, we see that although the contact anisotropy is reduced in the quasistatic regime compared to the inertial, consistent with (Berger et al., 2016), the contact anisotropy remains in the same order of magnitude. We attribute the enhancing effect of friction on the contact anisotropy to the increased stability to buckling and rearrangement due to compression. A reduction in the number of sliding contacts was previously observed in two-dimensional studies with cohesion and friction (Rognon et al., 2008).

The origins of the phenomenology observed in the stress and pressure become more obvious when accounting for contact anisotropy. For example, the pressure for smooth cases with $Ha_T > 10$ is negative. The contacts in those cases are isotropic. This means that there will be a larger population of particles aligned in the extension direction of the flow, leading to large cohesive tension forces. These forces eventually become larger in magnitude on average than the compressive forces in the spring-damper components. This reduction in pressure due to isotropization of contacts is also responsible for the greater-than-unity shear stress ratios for cases of $Ha_T \approx 10$, and the meta-stability for $Ha_T > 10$.

For frictional cases, the contact anisotropy is less affected by cohesion in the quasistatic regime. There contacts remain anisotropic, and are primarily aligned in the compression direction. This in turn leads to larger pressures, as can be seen in the definition of the pressure via the virial expression $P = \Sigma_{k \neq l} n_i^{(kl)} F_i^{(kl)} / (d_f V)$. There d_f are the degrees of freedom. The only components of forces that contribute to the pressure are those aligned with the lines of center between the contacting particles. Here a greater population of particles aligned in the compression direction implies a larger pressure. By contributing to the contact anisotropy, friction indirectly contributes to the smaller values of scaled stress μ in the quasistatic regime. Undoubtedly, the above reasoning also lends to arguments about anisotropy in normal stresses.



(a)



(b)

Figure 4.8 (a) The first anisotropic mode for the smooth cases show a clearly the effects of temperature, shear rate, and cohesion on the contact anisotropy as represented by u_2^1 . (b) The frictional cases show that friction tends to enhance anisotropy in the presence of cohesion.

Though such normal stress differences are of interest, they are beyond the scope of the current study.

4.3.4 Implications for Constitutive Modeling

In this work so far the effect of shear and particle properties, such as the coefficients of restitution and friction and strength of cohesion, on rheology in a moderately dense system has been considered. Although the effect of volume fraction is known to have a substantial affect on the rheology of granular systems, even without considering this parameter, rich behavior is observed that must be considered in continuum modeling of granular materials. Firstly, we have observed that the transition from inertial to quasistatic scaling in this regime is energetic in nature. The energetic scaling implies two things a) capturing the temperature dynamics is important for these granular flows b) rheological laws that achieve collapse via a dynamic scaling may be inadequate in this regime.

Moreover, many recent studies have elaborated the need to incorporate temperature evolution in wall bounded flows of non-cohesive granules (Gaume et al., 2011; Zhang and Kamrin, 2017; Gollin et al., 2017). The temperature near the boundaries is not slaved to the shear rate in general, as is assumed in many popular modeling paradigms, the most popular being the $\mu(I)$ rheology (MiDi, 2004). Clearly the effects on temperature are then of concern in simulating wall-bounded cohesive particle systems.

Further, recent work in extended kinetic theory has also shown that accounting for non-affine velocity-velocity correlations in the form of reduced temperature decay from collisions helps to correctly predict many features of wall bounded flows (Berzi and Jenkins, 2015b,a; Gollin et al., 2017). These velocity correlations account for coherent motion of local granules in dense non-cohesive flows. These correlations have been observed to grow in the quasistatic regime for cohesive systems (Rognon et al., 2008), which we have observed as well. In cohesive systems, as local aggregates grow in the inertial regime and eventually percolate the finite-sized system in the quasistatic regime, the motions of particles and their neighbors do become well correlated, with normal relative velocities at contact being small. We expect that dissipation of energy to be very sensitive to aggregation and hence temperature. The combined effects of

friction, cohesion, and granular temperature on normal stress differences, as already mentioned, will need to be explored and accounted for as well, which display non-trivial behavior in non-cohesive systems also (Sun and Sundaresan, 2011; Saha and Alam, 2016). In addition, the diverging cluster length scale poses additional obstacles for local models in the moderately dense regime.

4.4 Conclusions

A regime transition in simple shear simulations of cohesive granules from inertial to quasi-static scaling of the stress is studied. This transition occurs at volume fractions much lower than those where jamming occurs in repulsive systems. The effects of both restitution and friction on the transition are studied. For frictionless systems, the transition occurs at a ratio of cohesive potential energy to fluctuating kinetic energy Ha_T of unity, for any coefficient of restitution less than unity. A unique yield stress is also observed for all frictionless systems. Friction, on the other hand, is observed to increase both energy dissipation and yield stress and yields non-unique locations for the transition and yield stress. Nonetheless, the transition in the stress only collapses with an energetic scaling of the stress and shear rate, rather than a force or dynamic scaling. The scaled shear stress behavior for all systems is also discussed.

The microscopic origin of the transition is further investigated. For systems without friction, percolation is solely responsible for the transition in stress, correlating well with the location of the stress transition $Ha_T = 1$. Frictional systems do not necessarily need to percolate at any time step, but correlate well with a large increase in the local cohesive potential energy. The average cluster length scale is also observed to grow as T^{-2} , near the transition in frictionless systems. The scaling is accounted for by population balance arguments for systems with large granular temperatures.

The microstructural origin of non-trivial shear stress ratio with shear rate and cohesive strength is explored. In the quasistatic regime, friction tends to increase the yield stress but decrease the shear stress ratio over a range of coefficients of friction. Contact anisotropy is responsible for this scaling, where friction may prevent the buckling of contact chains in the direction of maximal compression. Without friction, aggregates are easily compressed and

contacts quickly isotropize, leading to more contacts in tension and thereby decreasing the pressure.

Lastly, some of the repercussions of the sensitivity of the stress to fluctuating kinetic energy are discussed in light of recent works in non-cohesive systems. It is unlikely that the temperature dynamics can be ignored in constitutive modeling and continuum simulation of cohesive systems. Additionally, differences in behavior between different sources of cohesion such as liquid bridging and electrostatics also remain unclear and merit further study.

Acknowledgment

We gratefully acknowledge the support provided for this work from NSF CMMI grant no. 0927660.

4.5 Bibliography

- Aarons, L. and Sundaresan, S. (2006). Shear flow of assemblies of cohesive and non-cohesive granular materials. *Powder Technology*, 169(1):10–21.
- Abbasfard, H., Evans, G., and Moreno-Atanasio, R. (2016). Effect of van der Waals force cut-off distance on adhesive collision parameters in DEM simulation. *Powder Technology*, 299:9–18.
- Afferrante, L., Ciavarella, M., and Demelio, G. (2015). Adhesive contact of the weierstrass profile. In *Proc. R. Soc. A*, volume 471, page 20150248. The Royal Society.
- Aitcin, P. (2000). Cements of yesterday and today - concrete of tomorrow. *Cement and Concrete Research*, 31(9):1349–1359.
- Alam, M., Trujillo, L., and Herrmann, H. (2006). Hydrodynamic theory for reverse brazil nut segregation and the non-monotonic ascension dynamics. *Journal of Statistical Physics*, 124:587–623.

- Bagnold, R. A. (1954). Experiments on a gravity-free dispersion of large solid spheres in a newtonian fluid under shear. In *Proceedings of the Royal Society of London A: Mathematical, Physical and Engineering Sciences*, volume 225, pages 49–63. The Royal Society.
- Ball, R. and Melrose, J. (1997). A simulation technique for many spheres in quasi-static motion under frame-invariant pair drag and brownian forces. *Physica A*, 247:444–472.
- Baranyai, A. and Evans, D. (1989). Direct entropy calculation from computer-simulation of liquids. *Physical Review A*, 40(7):3817–3822.
- Batrak, O., Patino, G., Simonin, O., Flour, I., Le Guevel, T., and Perez, E. (2005). Unlike particles size collision model in 3d unsteady polydispersed simulation of circulating fluidized bed. *8th Annual Conference on Fluidized Bed Technology*, 315.
- Bec, J., Biferale, L., Cencini, M., Lanotte, A., and Toschi, F. (2010). Intermittency in the velocity distribution of heavy particles in turbulence. *Journal of Fluid Mechanics*, 646:527–536.
- Beetstra, R., van der Hoef, M., and Kuipers, J. (2007). Drag force of intermediate reynolds number flows past mono- and bidisperse arrays of spheres. *AIChE Journal*, 53:489.
- Bentz, D., Ferraris, C., Galler, M., Hansen, A., and Guynn, J. (2012). Influence of particle size distributions on yield stress and viscosity of cement-fly ash pastes. *Cement and Concrete Research*, 42(2):404–409.
- Bentz, D. P., Garboczi, E. J., Haecker, C. J., and Jensen, O. M. (1999). Effects of cement particle size distribution on performance properties of portland cement-based materials. *Cement and Concrete Research*, 29:1663–1671.
- Berger, N., Azéma, E., Douce, J.-F., and Radjai, F. (2016). Scaling behaviour of cohesive granular flows. *EPL (Europhysics Letters)*, 112(6):64004.
- Berzi, D. and Jenkins, J. T. (2015a). Inertial shear bands in granular materials. *Physics of Fluids*, 27:033303.

- Berzi, D. and Jenkins, J. T. (2015b). Steady shearing flows of deformable, inelastic spheres. *Soft matter*, 11(24):4799–4808.
- Binnig, G., Quate, C. F., and Gerber, C. (1986). Atomic force microscope. *Physical review letters*, 56(9):930.
- Blum, J., Wurm, G., Kempf, S., Poppe, T., Klahr, H., Kozasa, T., Rott, M., Henning, T., Dorschner, J., Schrapler, R., Keller, H., Markiewicz, W., Mann, I., Gustafson, B., Giovane, F., Neuhaus, D., Fechtig, H., Grun, E., Feuerbacher, B., Kochan, H., Ratke, L., El Goresy, A., Morfill, G., Weidenschilling, S., Schwehm, G., Metzler, K., and Ip, W. (2000). Growth and form of planetary seedlings: Results from a microgravity aggregation experiment. *Physical Review Letters*, 85(12):2426–2429.
- Bradley, R. S. (1932). Lxxix. the cohesive force between solid surfaces and the surface energy of solids. *The London, Edinburgh, and Dublin Philosophical Magazine and Journal of Science*, 13(86):853–862.
- Brady, J. F. and Bossis, G. (1988). Stokesian dynamics. *Annual Reviews of Fluid Mechanics*, 20:111–157.
- Bragg, A. D. and Collins, L. R. (2014a). New insights from comparing statistical theories for inertial particles in turbulence: I. spatial distribution of particles. *New Journal of Physics*, 16:055013.
- Bragg, A. D. and Collins, L. R. (2014b). New insights from comparing statistical theories for inertial particles in turbulence: II. relative velocities. *New Journal of Physics*, 16:055014.
- Bragg, A. D., Ireland, P. J., and Collins, L. R. (2015). On the relationship between the non-local clustering mechanism and preferential concentration. *Journal of Fluid Mechanics*, 780:327–343.
- Brewster, R., Grest, G. S., Landry, J. W., and Levine, A. J. (2005). Plug flow and the breakdown of bagnold scaling in cohesive granular flows. *Physical Review E*, 72(6):061301.

- Bridges, F. G., Supulver, K. D., Lin, D., Knight, R., and Zafra, M. (1996). Energy loss and sticking mechanisms in particle aggregation in planetesimal formation. *Icarus*, 123(2):422–435.
- Brilliantov, N. V., Albers, N., Spahn, F., and Pöschel, T. (2007). Collision dynamics of granular particles with adhesion. *Physical Review E*, 76(5):051302.
- Brilliantov, N. V. and Pöschel, T. (2004). Collision of adhesive viscoelastic particles. *HINRICHSEN:GRANULAR MEDIA O-BK*, pages 189–209.
- Brilliantov, N. V. and Pöschel, T. (2004). *Kinetic Theory of Granular Gases*. Oxford University Press, New York.
- Brilliantov, N. V., Spahn, F., Hertzsch, J.-M., and Pöschel, T. (1996). Model for collisions in granular gases. *Physical review E*, 53(5):5382.
- Brito, R. and Ernst, M. (1998). Extension of haff’s cooling law in granular flows. *Europhysics Letters*, 43(5):497.
- Campbell, C. S. (2002). Granular shear flows at the elastic limit. *Journal of fluid mechanics*, 465:261–291.
- Capecelatro, J., Desjardins, O., and Fox, R. O. (2014). Numerical study of collisional particle dynamics in cluster-induced turbulence. *Journal of Fluid Mechanics*, 747:R2.
- Capecelatro, J., Desjardins, O., and Fox, R. O. (2015). On fluid-particle dynamics in fully developed cluster-induced turbulence. *Journal of Fluid Mechanics*, 780:578–635.
- Capecelatro, J., Desjardins, O., and Fox, R. O. (2016). Strongly coupled fluid-particle flows in vertical channels. ii. turbulence modeling. *Physics of Fluids*, 28:033307.
- Carnahan, N. and Starling, K. (1969). Equation of state for nonattractive rigid spheres. *Journal of Chemical Physics*, 51(2):635–636.
- Castellanos, A., Valverde, J. M., Pérez, A. T., Ramos, A., and Watson, P. K. (1999). Flow regimes in fine cohesive powders. *Physical Review Letters*, 82(6):1156.

- Cates, M., Wittmer, J., Bouchaud, J., and Claudin, P. (1998a). Jamming and static stress transmission in granular materials. *Chaos*, 9(3):511–522.
- Cates, M., Wittmer, J., Bouchaud, J., and Claudin, P. (1998b). Jamming, force chains, and fragile matter. *Physical Review Letters*, 81(9):1841–1844.
- Chew, J. W., Parker, D. M., Cocco, R. A., and Hrenya, C. M. (2011). Cluster characteristics of continuous size distributions and binary mixtures of group b particles in dilute riser flow. *Chemical Engineering Journal*, 178:348–358.
- Chialvo, S., Sun, J., and Sundaresan, S. (2012). Bridging the rheology of granular flows in three regimes. *Physical Review E*, 85(2):021305.
- Chun, J., Koch, D. L., Rani, S. L., Ahluwalia, A., and Collins, L. R. (2005). Clustering of aerosol particles in isotropic turbulence. *Journal of Fluid Mechanics*, 536:219–251.
- Cleary, P. W. and Sawley, M. L. (2002). DEM modelling of industrial granular flows: 3D case studies and the effect of particle shape on hopper discharge. *Applied Mathematical Modelling*, 26(2):89–111.
- Cocco, R., Shaffer, F., Hays, R., Karri, S. R., and Knowlton, T. (2010). Particle clusters in and above fluidized beds. *Powder Technology*, 203:3–11.
- Colwell, J., Batiste, S., Horányi, M., Robertson, S., and Sture, S. (2007). Lunar surface: Dust dynamics and regolith mechanics. *Reviews of Geophysics*, 45(2):RG2006.
- Cundall, P. and Strack, O. (1979a). A discrete numerical model for granular assemblies. *Geotechnique*, 29(1):47–65.
- Cundall, P. A. and Strack, O. D. (1979b). A discrete numerical model for granular assemblies. *Geotechnique*, 29(1):47–65.
- Dahneke, B. (1975). Further measurements of the bouncing of small latex spheres. *Journal of Colloid and Interface Science*, 51(1):58–65.

- Daley, D. and Vere-Jones, D. (1988). *An introduction to the theory of point processes*. Springer-Verlag.
- DeCicco, A. and Hartzell, C. (2016). System-level design considerations for asteroid despin via neutral beam emitting spacecraft. In *IEEE Aerospace Conference Proceedings (Big Sky, MT)*.
- Derjaguin, B., Muller, V., and Toporov, Y. (1975). Effect of contact deformations on the adhesion of particles. *Journal of Colloid and Interface Science*, 53(2):314–326.
- Di Renzo, A. and Di Maio, F. P. (2004). Comparison of contact-force models for the simulation of collisions in dem-based granular flow codes. *Chemical Engineering Science*, 59(3):525–541.
- Eaton, J. and Fessler, J. (1994). Preferential concentration of particles by turbulence. *International Journal of Multiphase Flow*, 20:169–209.
- Ernst, M., Dorfman, J., Hoegy, W., and van Leeuwen, J. (1969). Hard-sphere dynamics and binary-collision operators. *Physica*, 45(1):127–146.
- Esipov, S. and Pöschel, T. (1997). The granular phase diagram. *Journal of Statistical Physics*, 86(5/6):1385–1395.
- Ferraris, C., Obla, K., and Hill, R. (2001). The influence of mineral admixtures on the rheology of cement paste and concrete. *Cement and Concrete Research*, 31(2):245–255.
- Fox, R. (2014). On multiphase turbulence models for collisional fluid-particle flows. *Journal of Fluid Mechanics*, 742:368–424.
- Fox, R. O. (2016). Private communication.
- Fullmer, W. D. and Hrenya, C. M. (2016). Quantitative assessment of fine-grid kinetic-theory-based predictions of mean-slip in unbounded fluidization. *AIChE Journal*, 62(1):11–17.
- Galvin, J. E. and Benyahia, S. (2014). The effect of cohesive forces on the fluidization of aeratable powders. *AIChE Journal*, 60(2):473–484.

- Garzo, V., Dufty, J. W., and Hrenya, C. M. (2007a). Enskog theory for polydisperse granular mixtures. i. navier-stokes order transport. *Physical Review E*, 76(3):031303.
- Garzo, V., Fullmer, W. E., Hrenya, C. M., and Yin, X. (2016). Transport coefficients of solid particles immersed in a viscous gas. *Physical Review E*, 93:012905.
- Garzo, V., Hrenya, C. M., and Dufty, J. W. (2007b). Enskog theory for polydisperse granular mixtures. ii. sonine polynomial approximation. *Physical Review E*, 76(3):031304.
- Garzo, V., Tenneti, S., Subramaniam, S., and Hrenya, C. (2012). Enskog kinetic theory for monodisperse gas-solid flows. *Journal of Fluid Mechanics*, 712:129–168.
- Gaume, J., Chambon, G., and Naaim, M. (2011). Quasistatic to inertial transition in granular materials and the role of fluctuations. *Physical Review E*, 84:051304.
- Geldart, D. (1973). Types of gas fluidization. *Powder technology*, 7(5):285–292.
- Gidaspow, D., Jung, J., and Singh, R. K. (2004). Hydrodynamics of fluidization using kinetic theory: an emerging paradigm 2002 flour-daniel lecture. *Powder Technology*, 148:123–141.
- Goldhirsch, I. and Zanetti, G. (1993). Clustering instability in dissipative gases. *Physical Review Letters*, 70(11):1619–1622.
- Goldshtein, A. and Shapiro, M. (1995). Mechanics of collisional motion of granular materials. part 1. general hydrodynamic equations. *Journal of Fluid Mechanics*, 282:75–114.
- Gollin, D., Berzi, D., and Bowman, E. (2017). Extended kinetic theory applied to inclined granular flows: role of boundaries. *Granular Matter*, 19(3):1564–1583.
- Gonzalez, R. G. and Garzo, V. (2016). Instabilities in granular gas-solid flows. *arXiv:1611.03269*.
- Gonzalez, S., Thornton, A., and Luding, S. (2014). Free cooling phase-diagram of hard-spheres with short-and long-range interactions. *The European Physical Journal Special Topics*, 223(11):2205–2225.

- Gourdel, c., Simonin, O., and Brunier, E. (1998). Modelling and simulation of gas-solid turbulent flows with a binary mixture of particles. *Third International Conference on Multiphase Flows*, 315.
- Gourdel, c., Simonin, O., and Brunier, E. (1999). Two-maxwellian equilibrium distribution function for the modelling of a binary mixture of particles. *6th International Conference on Circulating Fluidized Beds*, 315.
- Grierson, D., Flater, E., and Carpick, R. (2005). Accounting for the jkr-dmt transition in adhesion and friction measurements with atomic force microscopy. *Journal of adhesion science and technology*, 19(3-5):291–311.
- Gu, Y., Chialvo, S., and Sundaresan, S. (2014). Rheology of cohesive granular materials across multiple dense-flow regimes. *Physical Review E*, 90(3):032206.
- Gu, Y., Ozel, A., and Sundaresan, S. (2015). A modified cohesion model for CFD–DEM simulations of fluidization. *Powder Technology*, 296:17–28.
- Gu, Y., Ozel, A., and Sundaresan, S. (2016). Numerical studies of the effects of fines on fluidization. *AIChE Journal*.
- Gustavsson, K. and Mehlig, B. (2014a). Clustering of particles falling in a turbulent flow. *Physical Review Letters*, 112:214501.
- Gustavsson, K. and Mehlig, B. (2014b). Relative velocities of inertial particles in turbulent aerosols. *Journal of Turbulence*, 15(1):34–69.
- Gustavsson, K. and Mehlig, B. (2016). Statistical models for spatial patterns of heavy particles in turbulence. *Advances in Physics*, 65(1):1–57.
- Haecker, C., Garboczi, E., J.W., B., Bohn, R., Sun, Z., Shah, S., and Voigt, T. (2005). Modeling the linear elastic properties of portland cement paste. *Cement and Concrete Research*, 35:1948–1960.
- Haff, P. (1983). Grain flow as a fluid-mechanical phenomenon. *Journal of Fluid Mechanics*, 134:401–430.

- Hatzes, A., Bridges, F., Lin, D., and Sachtjen, S. (1991). Coagulation of particles in saturn's rings: Measurement of the cohesive force of water frost. *Icarus*, 89:113–121.
- Hill, R. J., Koch, D., and Ladd, A. (2001a). The first effects of fluid inertia on flows in ordered and random arrays of spheres. *Journal of Fluid Mechanics*, 448:213–241.
- Hill, R. J., Koch, D., and Ladd, A. (2001b). Moderate-reynolds-number flows in ordered and random arrays of spheres. *Journal of Fluid Mechanics*, 448:243–278.
- Irani, E., Chaudhuri, P., and Heussinger, C. (2014). Impact of attractive interactions on the rheology of dense athermal particles. *Physical Review Letters*, 112:188303.
- Irani, E., Chaudhuri, P., and Heussinger, C. (2016). Athermal rheology of weakly attractive soft particles. *Physical Review E*, 94:052608.
- Israelachvili, J. N. (2011). *Intermolecular and surface forces: revised third edition*. Academic press.
- Iveson, S., Litster, J., Hapgood, K., and Ennis, B. (2001). Nucleation, growth and breakage phenomena in agitated wet granulation processes: a review. *Powder Technology*, 117(1-2):3–39.
- Jenkins, J. and Mancini, F. (1987). Balance laws and constitutive relations for plane flows of a dense, binary mixture of smooth, nearly elastic, circular disks. *Journal of Applied Mechanics*, 1(54):27–34.
- Jenkins, J. and Mancini, F. (1989). Kinetic theory for binary mixtures of smooth, nearly elastic spheres. *Physics of Fluids, A*, 1(12):2050–2057.
- Johnson, K. and Greenwood, J. (1997). An adhesion map for the contact of elastic spheres. *Journal of colloid and interface science*, 192(2):326–333.
- Johnson, K., Kendall, K., and Roberts, A. (1971). Surface energy and the contact of elastic solids. *Proceedings of the Royal Society London A*, 324:301–313.

- Jop, P., Forterre, Y., and Pouliquen, O. (2006). A constitutive law for dense granular flows. *Nature*, 441(7094):727–730.
- Kamrin, K. and Koval, G. (2012). Nonlocal constitutive relation for steady granular flow. *Physical Review Letters*, 108(17):178301.
- Kim, H. and Arastoopour, H. (2002). Extension of kinetic theory to cohesive particle flow. *Powder Technology*, 122(1):83–94.
- Kim, S. and Karrila, S. (1991). *Microhydrodynamics: principles and selected applications*. Butterworth-Heinemann.
- Kobayashi, T., Tanaka, T., Shimada, N., and Kawaguchi, T. (2013). Dem-cfd analysis of fluidization behavior of geldart group a particles using a dynamic adhesion force model. *Powder Technology*, 248:143–152.
- Koch, D. L. (1990). Kinetic theory for a monodisperse gas-solid suspension. *Physics of Fluids A*, 2(10):1711–1723.
- Koch, D. L. and Sangani, A. S. (1999). Particle pressure and marginal stability limits for a homogeneous monodisperse gas-fluidized bed: kinetic theory and numerical simulations. *Journal of Fluid Mechanics*, 400:229–263.
- Kolakaluri, R., Murphy, E., Subramaniam, S., Brown, R., and Fox, R. (2015). Filtration model for polydisperse aerosols in gas-solid flow using granule-resolved direct numerical simulation. *AIChE Journal*, 61(11):3594–3606.
- Kothe, S., Blum, J., Weidling, R., and GÃ¼ttler, C. (2013). Free collisions in a microgravity many-particle experiment. iii. the collision behavior of sub-millimeter-sized dust aggregates. *Icarus*, 225:75–85.
- Kulchitsky, A., Johnson, J., Reeves, D., and Wilkinson, A. (2014). Discrete element method simulation of a boulder extraction from an asteroid. In *Proceedings of the 14th ASCE Biennial International Conference on Engineering, Science, Construction, and Operations in Challenging Environments (St. Louis, Missouri, USA,)*, pages 485–494.

- Kumar, A. (2010). *Microscale Dynamics in Suspensions of Non-spherical Particles*. PhD thesis, University of Illinois Urbana-Champaign.
- Kumar, A. and Higdon, J. (2010). Origins of the anomalous stress behavior in charged colloidal suspensions under shear. *Physical Review E*, 82:051401.
- Kuwabara, G. and Kono, K. (1987). Restitution coefficient in a collision between two spheres. *Japanese journal of applied physics*, 26(8R):1230.
- Lanotte, A., Bec, J., Biferale, L., Cencini, M., and Toschi, F. (2011). About scaling properties of relative velocity between heavy particles in turbulence. *Journal of Physics Conference series*, 318:052010.
- Launder, B. (1990). Phenomenological modelling: present.. and future? in j.l. lumley (ed.). *Whither Turbulence? Turbulence at a Crossroads*, pages 439–485.
- Lees, A. and Edwards, S. (1972). The computer study of transport processes under extreme conditions. *Journal of Physics C: Solid State Physics*, 5(15):1921.
- Leyvraz (2003). Scaling theory and exactly solved models in the kinetics of irreversible aggregation. *Physics Reports*, 383:92–212.
- Li, J., Cheng, C., Zhang, Z., Yuan, J., Nemet, A., and Fett, F. (1999). The emms model - its application, development and updated concepts. *Chemical Engineering Science*, 54(22):5409–5425.
- Liard, M., Martys, N., George, W., Lootens, D., and Hebraud, P. (2014). Scaling laws for the flow of generalized newtonian suspensions. *Journal of Rheology*, 58:1993–2015.
- Liu, A. J. and Nagel, S. R. (2010). The jamming transition and the marginally jammed solid. *Annual Reveiw of Condensed Matter Physics*, 1:347–369.
- Liu, L. (2011). Kinetic theory of aggregation in granular flow. *AICHE Journal*, 57(12):3331–3343.

- Liu, P., Kellogg, K., LaMarche, C., and Hrenya, C. (2017). Dynamics of singlet-doublet collisions of cohesive particles. *Chemical Engineering Journal*, 324:380–391.
- Liu, P., LaMarche, C. Q., Kellogg, K. M., and Hrenya, C. M. (2016). Fine-particle deflu-idization: Interaction between cohesion, Young’s modulus and static bed height. *Chemical Engineering Science*, 145:266–278.
- Lois, G., Blawdziewicz, J., and O’Hern, C. S. (2008). Jamming transition and new perco-lation universality classes in particulate systems with attraction. *Physical Review Letters*, 100:028001.
- Lomboy, G., Sundararajan, S., and Wang, K. (2013). Micro- and macroscale coefficients of friction of cementitious materials. *Cement and Concrete Research*, 54:21–28.
- Lomboy, G., Sundararajan, S., Wang, K., and Subramaniam, S. (2011). A test method for determining adhesion forces and hamaker constants of cementitious materials using atomic force microscopy. *Cement and Concrete Research*, 41(11):1157–1166.
- Lomboy, G. R., Wang, K., and Quanji, Z. (2012). Properties of cementitious materials in their dry state and their influences on viscosity of the cementitious pastes. *Powder Technology*, 229:104–111.
- Luding, S. (1998). Collisions & contacts between two particles. In *Physics of dry granular media*, pages 285–304. Springer.
- Luding, S. (2008). Cohesive, frictional powders: contact models for tension. *Granular matter*, 10(4):235–246.
- Luding, S. (2016). Granular matter: So much for the jamming point. *Nature Physics*, 12:531–532.
- Luding, S. and Alonso-Marroquin, F. (2011). The critical-state yield stress (termination locus) of adhesive powders from a single numerical experiment. *Granular Matter*, 13:109–119.

- Luding, S., Clément, E., Blumen, A., Rajchenbach, J., and Duran, J. (1994). Anomalous energy dissipation in molecular-dynamics simulations of grains: The detachment effect. *Physical Review E*, 50(5):4113.
- Luding, S., Huthmann, M., McNamara, S., and Zippelius, A. (1998). Homogeneous cooling of rough, dissipative particles: Theory and simulation. *Physical Review E*, 58(3):3416–3425.
- Majmudar, T., Sperl, M., Luding, S., and Behringer, R. (2007). Jamming transition in granular systems. *Physical Review Letters*, 98:058001.
- Makse, H. A., Johnson, D. L., and Schwartz, L. M. (2000). Packing of compressible granular materials. *Physical review letters*, 84(18):4160.
- Marchisio, D. L. and Fox, R. O. (2013). *Computational Models for Polydisperse Particulate and Multiphase Systems*. Cambridge University Press.
- Markutsya, S., Fox, R., and Subramaniam, S. (2014). Characterization of sheared colloidal aggregation using langevin dynamics simulation. *Physical Review E*, 89:062312.
- Marmur, B. L. and Heindel, T. J. (2016). Effect of particle size, density, and concentration on granular mixing in a double screw pyrolyzer. *Powder Technology*, 302:222–235.
- Martys, N. and Ferraris, C. (2002). Simulation of scc flow. In *First North American Conference on the Design and Use of Self-Consolidating Concrete. Proceedings. Chicago, IL,*
- Martys, N., Khalil, M., George, W., and Lootens, D. (2012). Stress propagation in a concentrated colloidal suspension under shear. *European Physical Journal E*, 35(3):1–7.
- Matsunaga, T., Kim, J., Hardcastle, S., and Rohatgi, P. (2002). Crystallinity and selected properties of fly ash particles. *Materials Science and Engineering*, A325:333–343.
- Maugis, D. (1992). Adhesion of spheres: the jkr-dmt transition using a dugdale model. *Journal of colloid and interface science*, 150(1):243–269.
- Maxey, M. (1987). The gravitational settling of aerosol particles in homogeneous turbulence and random flow fields. *Journal of Fluid Mechanics*, 174:441–465.

- Mckay, W. and Mckay, J. (1971). *Building Construction Vol. Ii (Fourth Edition)*. Orient Longman Private Limited.
- McMillan, J., Shaffer, F., Gopalan, B., Chew, J. W., Hrenya, C., Hays, R., Karri, S. R., and Cocco, R. (2013). Particle cluster dynamics during fluidization. *Chemical Engineering Science*, 100:39–51.
- McNamara, S. and Young, W. (1992). Inelastic collapse and clumping in a one-dimensional granular medium. *Physics of Fluids A*, 4(3):496–504.
- Mehrabadi, M. (2016). *Analysis of gas-solid flow using particle-resolved direct numerical simulation: flow physics and modeling*. PhD thesis, Iowa State University.
- Mehrabadi, M., Murphy, E., and Subramaniam, S. (2016a). Development of a gas-solid drag law for clustered particles using particle-resolved direct numerical simulation. *Chemical Engineering Science*, 152:199–212.
- Mehrabadi, M., Tenneti, S., and Subramaniam, S. (2016b). Importance of the fluid-particle drag model in predicting segregation in bidisperse gas-solid flow. *International Journal of Multiphase Flow*, 86:99–114.
- MiDi, G. (2004). On dense granular flows. *The European Physical Journal E*, 14(4):341–365.
- Miller, A. and Gidaspow, D. (1992). Dense, vertical gas-solid flow in a pipe. *AIChE Journal*, 38(11):1801–1815.
- Mills, P., Rognon, P., and Chevier, F. (2008). Rheology and structure of granular materials near the jamming transition. *EPL (Europhysics Letters)*, 81:64005.
- Miyamoto, H., Kargel, J., Fink, W., and Furfaro, R. (2008). Granular processes on itokawa, a small near-earth asteroid: Implications for resource utilization. *Space Exploration Technologies, Proceedings of SPIE*, 6960:69600I.
- Monchaux, R., Bourgoïn, M., and Cartellier, A. (2010). Preferential concentration of heavy particles: a voronoi analysis. *Physics of Fluids*, 22(10):103304.

- Moreno-Atanasio, R., Xu, B., and Ghadiri, M. (2007). Computer simulation of the effect of contact stiffness and adhesion on the fluidization behaviour of powders. *Chemical engineering science*, 62(1):184–194.
- Morrow, C., Lovell, M., and Ning, X. (2003). A jkr–dmt transition solution for adhesive rough surface contact. *Journal of Physics D: Applied Physics*, 36(5):534.
- Mounfield, C. and Edwards, S. (1994). A model for the packing of irregularly shaped grains. *Physica A*, 210:301–316.
- Müller, M.-K. and Luding, S. (2011). Homogeneous cooling with repulsive and attractive long-range potentials. *Mathematical Modelling of Natural Phenomena*, 6(4):118–150.
- Murphy, E., Mehrabadi, M., Tenneti, S., and Subramaniam, S. (2015). Modeling two-point particle dynamics of homogeneous gas-solid flows to describe clustering and stability. In *68th annual meeting of the American physical society division of fluid dynamics, At Boston, MA*.
- Murphy, E. and Subramaniam, S. (2014). A model for solid-solid drag in bidisperse gas-solid flows. In *67th Annual Meeting of the APS Division of Fluid Dynamics*, volume 59.
- Murphy, E. and Subramaniam, S. (2015). Freely cooling granular gases with short-ranged attractive potentials. *Physics of Fluids (1994-present)*, 27(4):043301.
- Murphy, E. and Subramaniam, S. (2017). Binary collision outcomes for inelastic soft-sphere models with cohesion. *Powder Technology*, 305:462–476.
- Nachenius, R., van de Wardt, T., Ronsse, F., and Prins, W. (2015). Effect of particle size, density, and concentration on granular mixing in a double screw pyrolyzer. *Fuel Processing Technology*, 130:87–95.
- Narayanan, K. and Ramamurthy, K. (2000). Structure and properties of aerated concrete: a review. *Cement and Concrete Composites*, 22(5):321–329.
- Nase, S. T., Vargas, W. L., Abatan, A. A., and McCarthy, J. (2001). Discrete characterization tools for cohesive granular material. *Powder Technology*, 116(2):214–223.

- Nauman, E. B. (2001). *Chemical Reactor Design, Optimization, and Scaleup*. McGraw-Hill.
- Nienow, A., Edwards, M., and Harnby, N. (1992). *Mixing in the Process Industries: Mixing of Cohesive Powders*. Elsevier, Oxford, 2nd edition.
- of Chemistry, T. R. S. (2008). The concrete conundrum. *Chemistry World*.
- Oliver, W. C. and Pharr, G. M. (1992). An improved technique for determining hardness and elastic modulus using load and displacement sensing indentation experiments. *Journal of materials research*, 7(06):1564–1583.
- Ortiz de Zarate, J. and Sengers, J. (2006). *Hydrodynamic Fluctuations in Fluids and Fluid Mixtures*. Elsevier.
- Oseen, C. (1927). Neuere methoden und ergebnisse in der hydrodynamik. *Akademische Verlagsgesellschaft*.
- Otsuki, M., Hayakawa, H., and Luding, S. (2010). Behavior of pressure and viscosity at high densities for two-dimensional hard and soft granular materials. *Progress of Theoretical Physics Supplement*, 184:110–133.
- Pasha, M., Dogbe, S., Hare, C., Hassanpour, A., and Ghadiri, M. (2014). A linear model of elasto-plastic and adhesive contact deformation. *Granular Matter*, 16(1):151–162.
- Pathak, S., Jabeen, Z., Dibyendu, D., and Rajesh, R. (2014). Energy decay in three-dimensional freely cooling granular gas. *Physical Review Letters*, 112:038001.
- Paul, E. L., Atiemo-Obeng, V. A., and Kresta, S. M. (2004). *Handbook of industrial mixing: science and practice*. John Wiley ”&” Sons.
- Perni, S. and Prokopovich, P. (2015). Multi-asperity elliptical jkr model for adhesion of a surface with non-axially symmetric asperities. *Tribology International*, 88:107–114.
- Persson, B. N. and Scaraggi, M. (2014). Theory of adhesion: Role of surface roughness. *The Journal of chemical physics*, 141(12):124701.

- Pettersen, O. (2007). Sandstone compaction, grain packing and critical state theory. *Petroleum Geoscience*, 13:63–67.
- Plimpton, S. (1995). Fast parallel algorithms for short-range molecular dynamics. *Journal of Computational Physics*, 117:1–19.
- Pope, S. B. (2000). *Turbulent Flows*. Cambridge University Press.
- Prokopovich, P. and Starov, V. (2011). Adhesion models: From single to multiple asperity contacts. *Advances in colloid and interface science*, 168(1):210–222.
- Rahman, M., Wiklund, J., Kotze, R., and Hakansson, U. (2017). Yield stress of cement grouts. *Tunnelling and Underground Space Technology*, 61:50–60.
- Rani, S. L., Dhariwal, R., and Koch, D. L. (2014). A stochastic model for the relative motion of high stokes number particles in isotropic turbulence. *Journal of Fluid Mechanics*, 756:870–902.
- Reeks, M. (1980). Eulerian direct interaction applied to the statistical motion of particles in a turbulent flow. *Journal of Fluid Mechanics*, 97:569–590.
- Rognon, P. G., Roux, J.-N., Naaim, M., and Chevoir, F. (2008). Dense flows of cohesive granular materials. *Journal of Fluid Mechanics*, 596:21–47.
- Rong, L., Dong, K., and Yu, A. (2014). Lattice-boltzmann simulation of fluid flow through packed beds of spheres: effect of particle size distribution. *Chemical Engineering Science*, 116:508–523.
- Rotne, J. and Prager, S. (1969). Variational treatment of hydrodynamic interaction in polymers. *Journal of Chemical Physics*, 50:4831–4837.
- Roussel, N., Lemaitre, A., Flatt, R., and Coussot, P. (2010). Steady state flow of cement suspensions: A micromechanical state of the art. *Cement and Concrete Research*, 40(1):77–84.

- Roussel, N., Ovarlez, G., Garrault, S., and Brumaud, C. (2012). The origins of thixotropy of fresh cement pastes. *Cement and Concrete Research*, 42(1):148–157.
- Rumpf, H. (1958). Grundlagen und methoden des granulierens. *Chemie Ingenieur Technik*, 30(3):144–158.
- Rycroft, C., Grest, G., Landry, J., and Bazant, M. (2006). Analysis of granular flow in a pebble-bed nuclear reactor. *Physical Review E*, 74:021306.
- Saha, S. and Alam, M. (2016). Normal stress differences, their origin and constitutive relations for a sheared granular fluid. *Journal of Fluid Mechanics*, 795:549–580.
- Saitoh, K. and Mizuno, H. (2016). Enstrophy cascades in two-dimensional dense granular flows. *Physical Review E*, 94:022908.
- Saitoh, K., Takada, S., and Hayakawa, H. (2015). Hydrodynamic instabilities in shear flows of dry cohesive granular particles. *Soft matter*, 11(32):6371–6385.
- Schäfer, J., Dippel, S., and Wolf, D. (1996). Force schemes in simulation of granular material. *J. Phys. I France*, 6:5–20.
- Schlick, C. P., Isner, A. B., Freireich, B. J., Fan, Y., Umbanhowar, P. B., Ottino, J. M., and Lueptow, R. M. (2016). A continuum approach for predicting segregation in flowing polydisperse granular materials. *Journal of Fluid Mechanics*, 797:95–109.
- Shah, S. and Wang, K. (2004). Development of green cement for sustainable concrete using cement kiln dust and fly ash. In *Proceedings of the International Workshop on Sustainable Development and Concrete Technology*.
- Shannon, C. (1948). A mathematical theory of communication. *Bell System Technical Journal*, 27(3):379–423.
- Silbert, L. E., Ertaş, D., Grest, G. S., Halsey, T. C., Levine, D., and Plimpton, S. J. (2001). Granular flow down an inclined plane: Bagnold scaling and rheology. *Physical Review E*, 64(5):051302.

- Silbert, L. E., Grest, G. S., Brewster, R., and Levine, A. J. (2007). Rheology and contact lifetimes in dense granular flows. *Physical review letters*, 99(6):068002.
- Singh, A., Magnanimo, V., Saitoh, K., and Luding, S. (2014). Effect of cohesion on shear banding in quasistatic granular materials. *Physical Review E*, 90(2):022202.
- Singh, A., Magnanimo, V., Saitoh, K., and Luding, S. (2015). The role of gravity or pressure and contact stiffness in granular rheology. *New journal of physics*, 17(4):043028.
- Sjostrom, S. and Krutka, H. (2009). Evaluation of solid sorbents as a retrofit technology for co2 capture. *Fuel*, 89(6):1298–1306.
- Song, C., Wang, P., and Makse, H. A. (2008). A phase diagram for jammed matter. *Nature*, 453(7195):629–632.
- Stevens, A. and Hrenya, C. (2005). Comparison of soft-sphere models to measurements of collision properties during normal impacts. *Powder Technology*, 154(2):99–109.
- Stoyan, D., Kendall, W., and Mecke, J. (1995). *Stochastic geometry and its applications*. John Wiley and Sons, New York, 2nd edition.
- Stutzman, P. (2004). Scanning electron microscopy imaging of hydraulic cement microstructure. *Cement and Concrete Composites*, 26:957–966.
- Subramaniam, S. (2000). Statistical representation of a spray as a point process. *Physics of Fluids*, 12(10):2413–2431.
- Subramaniam, S. (2001). Statistical modeling of sprays using the droplet distribution function. *Physics of Fluids*, 13(3):624–642.
- Subramaniam, S. (2012). Stability limits for gas-solid suspensions with finite fluid inertia using particle-resolved direct numerical simulations. *NSF Annual Report 1134500*.
- Subramaniam, S. (2014). Stability limits for gas-solid suspensions with finite fluid inertia using particle-resolved direct numerical simulations. *NSF Annual Report 1134500*.

- Sun, J., Battaglia, F., and Subramaniam, S. (2006). Dynamics and structures of segregation in a dense, vibrating granular bed. *Physical Review E*, 74(6):061307.
- Sun, J. and Sundaresan, S. (2011). A constitutive model with microstructure evolution for flow of rate-independent granular materials. *Journal of Fluid Mechanics*, 682:590–616.
- Sundaram, S. and Collins, L. (1997). Collision statistics in an isotropic, particle-laden turbulent suspension i. direct numerical simulations. *Journal of Fluid Mechanics*, 335:75–109.
- Syamlal, M. (1987). The particle-particle drag term in a multiphase model of fluidization. *Technical Report DOE/MC/21353-2373, NTIS/DE87006500, National Technical Information Service.*
- Syamlal, M. and O’Brien, T. (1987). A generalized drag correlation for multiparticle systems. *Technical Report, Morgantown Energy Technology Center DOE Report.*
- Syamlal, M., Rogers, W., and O’Brien, T. (1993). Mfix documentation: Theory guide. *Morgantown Energy Technology Center Morgantown, WV, USA*, page 54.
- Tabor, D. (1977). Surface forces and surface interactions. *Journal of colloid and interface science*, 58(1):2–13.
- Takada, S., Saitoh, K., and Hayakawa, H. (2014). Simulation of cohesive fine powders under a plane shear. *Physical Review E*, 90(6):062207.
- Takada, S., Saitoh, K., and Hayakawa, H. (2015a). Kinetic theory for dilute cohesive granular gases with a square well potential. *arXiv preprint arXiv:1506.04578*.
- Takada, S., Saitoh, K., and Hisao, H. (2015b). Simulation of cohesive fine powders under a plane shear. *Physical Review E*, 90:062207.
- Tenneti, S., Garg, G., and Subramaniam, S. (2011). Drag law for monodisperse gas-solid systems using particle-resolved direct numerical simulation of flow past fixed assemblies of spheres. *International Journal of Multiphase Flows*, 37(9):1072–1092.

- Tenneti, S., Mehrabadi, M., and Subramaniam, S. (2016). Stochastic lagrangian model for hydrodynamic acceleration of inertial particles in gas-solid suspensions. *Journal of Fluid Mechanics*, 788:695–729.
- Tenneti, S. and Subramaniam, S. (2014). Particle-resolved direct numerical simulation for gas-solid flow model development. *Annual Review of Fluid Mechanics*, 46:199–230.
- Thornton, C., Cummins, S. J., and Cleary, P. W. (2013). An investigation of the comparative behaviour of alternative contact force models during inelastic collisions. *Powder Technology*, 233:30–46.
- Thornton, C. and Ning, Z. (1998). A theoretical model for the stick/bounce behaviour of adhesive, elastic-plastic spheres. *Powder technology*, 99(2):154–162.
- Tien, C. and Ramarao, B. (2007). *Granular Filtration of Aerosols and Hydrosols*. Elsevier, Oxford, 2nd edition.
- Tomas, J. (2000). Particle adhesion fundamentals and bulk powder consolidation. *KONA Powder and Particle Journal*, 18(0):157–169.
- Torquato, S. (1995). Mean nearest-neighbor distance in random packings of hard d-dimensional spheres. *Physical Review Letters*, 74(12):2156–2159.
- Trizac, E. and Hansen, J. (1995). Dynamic scaling behavior of ballistic coalescence. *Physical Review Letters*, 74(21):4114–4117.
- Trizac, E. and Hansen, J. (1996). Dynamics and growth of particles undergoing ballistic coalescence. *Journal of Statistical Physics*, 86(5-6):1345–1370.
- Tsuji, Y., Kawaguchi, T., and Tanaka, T. (1993). Discrete particle simulation of two-dimensional fluidized bed. *Powder technology*, 77(1):79–87.
- Uhlmann, M. and Doychev, T. (2014). Sedimentation of a dilute suspension of rigid spheres at intermediate galileo numbers: the effect of clustering upon the particle motion. *Journal of Fluid Mechanics*, 752:310–348.

- UNEP, U. N. E. P. (2012). Greening cement production has a big role to play in reducing greenhouse gas emissions. *UNEP Report 2012, Environmental Science Alert Thematic Focus: Resource Efficiency, Harmful Substances and Hazardous Waste, and Climate Change*.
- van der Hoef, M., Beestra, R., and Kuipers, J. (2005). Lattice-boltzmann simulations of low-reynolds-number flow past mono- and bidisperse arrays of spheres: results for the permeability and drag force. *Journal of Fluid Mechanics*, 528:233–254.
- van Noije, T., Ernst, M., and Brito, R. (1998a). Ring kinetic theory for an idealized granular gas. *Physica A*, 251:266–283.
- van Noije, T., Ernst, M., and Brito, R. (1998b). Spatial correlations in compressible granular flows. *Physical Review E*, 57(5):R4893.
- van Noije, T., Ernst, M., Brito, R., and Orza, J. (1997). Mesoscopic theory of granular fluids. *Physical Review Letters*, 79(3):411–414.
- Vidyapati and Subramaniam, S. (2013). Granular flow in silo discharge: Discrete element method simulations and model assessment. *Industrial "E" Engineering Chemistry Research*, 52(36):13171–13182.
- Vidyapati, V., Langroudi, M. K., Sun, J., Sundaresan, S., Tardos, G., and Subramaniam, S. (2012). Experimental and computational studies of dense granular flow: Transition from quasi-static to intermediate regime in a couette shear device. *Powder Technology*, 220:7–14.
- von Karman, T. and Howarth, L. (1938). On the statistical theory of isotropic turbulence. *Proceedings of the Royal Society of London. Series A, Mathematical and Physical Sciences*, 164(917):192–215.
- Walton, O. R. (1984). Application of molecular dynamics to macroscopic particles. *International Journal of Engineering Science*, 22(8):1097–1107.
- Walton, O. R. (2004). Potential discrete element simulation applications ranging from airborne fines to pellet beds. *SAE 2004 Transactions J. Aerospace*.

- Wang, K., Subramaniam, S., and Sundararajan, S. (2013). Final report: Understanding rheology of cement-based materials through integrated experiments and computations at multiple scales. *Final Report NSF CBET Grant No. 0927660*.
- Waters, J., Lee, S., and Guduru, P. (2009). Mechanics of axisymmetric wavy surface adhesion: Jkr–dmt transition solution. *International Journal of Solids and Structures*, 46(5):1033–1042.
- Weller, H., Tabor, G., Jasak, H., and Fureby, C. (1998). A tensorial approach to computational continuum mechanics using object-oriented techniques. *Computers in Physics*, 12(6):620–631.
- Wilson, R., Dini, D., and van Wachem, B. (2016). A numerical study exploring the effect of particle properties on the fluidization of adhesive particles. *AIChE Journal*, 62(5):1467–1477.
- Wylie, J. J. and Koch, D. L. (2000). Particle clustering due to hydrodynamic interactions. *Physics of Fluids*, 12(5):964–970.
- Xing, Z., Kenty, B., Li, Z., and Lee, S. (2009). Scale-up analysis for a cho cell culture process in large-scale bioreactors. *Biotechnology and Bioengineering*, 103(4):733–746.
- Xu, Y. and Subramaniam, S. (2007). Consistent modeling of interphase turbulent kinetic energy transfer in particle-laden turbulent flows. *Physics of Fluids*, 19:085101.
- Yao, H., Ciavarella, M., and Gao, H. (2007). Adhesion maps of spheres corrected for strength limit. *Journal of colloid and interface science*, 315(2):786–790.
- Yin, X., Zenk, J. R., Mitrano, P. P., and Hrenya, C. M. (2013). Impact of collisional versus viscous dissipation on flow instabilities in gas-solid systems. *Journal of Fluid Mechanics*, 727:R2.
- Zaichik, L. and Alipchenkov, V. (2003). Pair dispersion and preferential concentration of particles in isotropic turbulence. *Physics of Fluids*, 15:1776–1787.
- Zaichik, L. I. and Alipchenkov, V. M. (2009). Statistical models for predicting pair dispersion and particle clustering in isotropic turbulence and their applications. *New Journal of Physics*, 11:103018.

Zamankhan, P. (2005). Kinetic theory of multicomponent dense mixtures of slightly inelastic spherical particles. *Physical Review E*, 52(5):4877–4891.

Zhang, Q. and Kamrin, K. (2017). Microscopic description of the granular fluidity field in nonlocal flow modeling. *Physical Review Letters*, 118:058001.

CHAPTER 5. SIMPLE SHEAR OF A SLURRY WITH COHESIVE MICRO-PARTICLES

This section contains a draft of a manuscript that is in preparation to be submitted for publication.

5.1 Background

Concrete is a strong and versatile building material that shapes much of the cityscapes and infrastructure of the modern world. Its strength is evidenced by its use in the construction of many record setting building projects, such as the tallest structure in the world, the Burj Khalifa in Dubai, and large spanning bridges such as the Tatara bridge in Japan (of Chemistry, 2008). The strength and versatility of concrete has led to it being the most used man-made material on Earth (of Chemistry, 2008). However, despite the ubiquity of concrete, little about the rheology of concrete or its most important constituent, cement, is understood.

The cement in concrete comes in many flavors with varying composition and water content (Ferraris et al., 2001), which can be altered in order to optimize some balance between workability of a concrete and its eventual strength. In traditional Portland cement based concretes, the strongest concrete requires just enough water to complete hydration of the Portland cement particles (Aitcin, 2000). However, such traditional concretes are in general not workable, and cannot be easily cast. Voids from trapped air are also difficult to remove and may compromise the eventual strength (Narayanan and Ramamurthy, 2000). The traditional concretes increased the water content to make concretes more flowable at the expense of strength. To alleviate this problem modern concretes make use of plasticizers, which disperse cementitious particles in the cement paste, and make the concrete more flowable in general (Ferraris et al.,

2001). Such concretes are known as self compacting concrete (SCC). However, many of the rheological properties of these SCCs, much like traditional concretes, have a large degree of variability dependent on the environment and processing conditions. A first-principle approach to optimization of the rheology of concrete and cement for a particular application is desirable but remains elusive.

Adding to this problem of rheological optimization, many more cementitious materials are now being considered in addition to Portland cement. Traditional production of Portland cement particles from the heating of limestone with coal accounts for 7–8% of all anthropogenic CO₂ emissions (UNEP, 2012). Other materials such as fly ash (FA), a byproduct of coal combustion, have often been considered as suitable alternatives to the more CO₂ intensive Portland cement. These concretes are known as green concretes (Shah and Wang, 2004). The changes in the composition of cement pastes and slurries has an effect on the observed rheology and strengths of the resultant concretes (Wang et al., 2013). The origin of the differences in macroscopic rheology and strength between green and traditional concretes are also not yet fully understood. Ultimately, the differences in rheology must arise from the microscopic differences in particle and particle surface properties, such as size, shape, friction, electrical double layer, and van der Waals forces, which have not been quantified.

In addition, to the difficulty of predicting the rheology in large parameter or design space for cements, the rheology of cement pastes also has a number of strange macroscopic behaviors. Cement is often considered a fluid with a yield stress, where it can support a finite amount of stress without flowing (Rahman et al., 2017). These slurries also exhibit thixotropy or hysteresis in the relationship between shear strain rate and shear stress (Roussel et al., 2012). This means that constitutive relations are in some sense time-dependent. The design and optimization of cements for a particular application ultimately depends on the integration of knowledge of the sensitive dependence of cement rheology on microscopic particle properties and macroscale flow phenomenology (Roussel et al., 2010; Bentz et al., 2012).

There are several methods one might use to interrogate the rheology of cement pastes that are currently being used. The most prevalent field method for concrete is the slump test, where a cone is filled with the concrete mixture (Mckay and Mckay, 1971). After the cone is removed

the deformation or spread of the concrete under its own weight is used as an indicator for concrete rheology. For cements the most common empirical lab technique is a rheometer, such as a vane rheometer. However, little information beyond the relationship between macroscopic measurements of stress and strain rate are obtained, due to difficulty in obtaining optical access.

From a computational standpoint, there are several potential methods that may be used in the study of cement paste rheology or as a simulation method. These generally lie on a continuum of methods where there is a trade-off between information and computational cost. The least expensive models seek to represent the cement paste as a collection of discrete objects, whose interactions are intended to simulate the interstitial fluid. Despite the low computational cost, interaction terms in these models are difficult to measure, though they may be tuned to produce the correct phenomenology. A more costly method is to model the cement paste as a single fluid, this may be done through traditional Eulerian methods or particle methods such as smoothed particle hydrodynamics (Liard et al., 2014) or dissipative particle dynamics (Martys and Ferraris, 2002; Martys et al., 2012). However, these methods must be tuned by either more resolved simulations or empirical models to produce the correct rheology, and hence, are not predictive.

First principle models that require few empirical inputs do have the capability of being predictive, not needing to be tuned to macroscopic measurements. This is because first principle models produce predictions about the relationship between stresses and strain rates that the models were not necessarily designed to predict. One of the more costly first-principle methods is to model particle interactions through the discrete element method and perform a model free fluid calculation of the Navier-Stokes equation. Together these two methods are known as a particle-resolved direct numerical simulation (PR-DNS) (Tenneti and Subramaniam, 2014). However, cement pastes at the scale of the particle are at particle Reynolds numbers much less than unity, i.e. in Stokes flow. Significant simplifications may be made in this regime since the non-linear convection term in the Navier-Stokes equations becomes unimportant. In this flow regime, the interactions between particles mediated by the fluid can be calculated, without explicitly solving the fluid flow. Such simulations are known as Stokesian Dynamics (Brady and Bossis, 1988). However, it should be noted that these simulations are still quite

computationally expensive, since every particle directly interacts with every other particle. In flows with relatively large solid volume fractions, the interactions between distant particles can be well represented by an averaged interaction term. The dominant interparticle interactions in these flows are with nearby particle pairs through the so-called lubrication force. Such simulations are known as fast lubrication dynamics (FLD) (Kumar and Higdon, 2010; Kumar, 2010). When FLD is coupled with ordinary DEM interparticle interactions, a computationally efficient first-principle method is obtained that scales well with the number of particles in the domain.

First principle methods though appealing, require empirical inputs from microscale experiments to parameterize the DEM interactions. Note that the FLD interactions take well-known fluid properties as inputs. DEM interaction parameters can include resistance to deformation through the Young's modulus, interparticle friction, attraction from the van der Waals force, and electrical double layer interactions. The last three interactions have been previously quantified using Atomic Force Microscopy (AFM) measurements on different material combinations in an aqueous environment (Lomboy et al., 2011, 2012, 2013). After FLD-DEM simulations are performed using these inputs, a comparison can be made with macroscale rheometer experiments. These simulations yield particle scale interactions and trajectory information that is not easily accessible from lab-scale vane rheometer experiments.

There are also some difficulties in trying to model complicated slurries such as cement pastes using first-principle methods. Ground Portland (PC) cement particles are highly non-spherical, which are difficult and expensive to model exactly. Both PC and FA particle populations are highly polydisperse, with particles from as small as a micron to as large as a millimeter (Bentz et al., 1999). If a simulation were to include all particle sizes, one would run into the problem of having ≈ 1 billion micron-sized particles taking up the same volume as a single one millimeter particle. From a measurement standpoint, PC particles are also multi-component (Stutzman, 2004), making measurements of representative interparticle surface interactions difficult (Lomboy et al., 2011). Despite these difficulties many things can still be learned by simulating simpler model systems. Namely, the question of which interactions are most essential to predicting cement rheology can be answered.

The aim of this manuscript is to answer whether first principle studies may be used to predict the macroscale rheological behavior of cement pastes. However, this may be seen as just the first step in the goal of accurately predicting complex flows of cements and concretes. Steric interactions present in SCC can be modeled to further the capabilities in predicting the rheology of modern cements. Larger parameter space studies may be carried out to further elucidate the connection between different microscale forces and structure and macroscale stress response. Moreover, coarse-grained rheological models can be cast in the form of constitutive equations or interaction models for particle methods. This information on the connection of microscale properties to macroscale rheology will be both useful for and expedite the design of new concretes and concrete pumping technologies.

5.2 Methods

The methods section is ordered in the following manner. First, the appropriate particle and system parameters and associated non-dimensional quantities for slurries of cementitious particles are discussed. Next, a time-scale analysis is presented to aid in the understanding of cement paste rheology. Lastly, the methodology for carrying out fast lubrication dynamics (FLD) and discrete element method (DEM) simulations is discussed.

5.2.1 Parameters

In the first-principle based approach taken in this manuscript, slurries of cementitious particles, such as Portland cement (PC) and fly ash (FA) often used in 'green' cements, are modeled as particulate suspensions. Suspensions require modeling for fluid and interparticle interactions. The physical slurries exhibit a number of features that are challenging to model, such as particle size distributions ranging over many orders magnitude, e.g. 1-1000 microns (Bentz et al., 1999), highly non-spherical/angular particles (Lomboy et al., 2013), multicomponent particles (Lomboy et al., 2011), and reacting surfaces. Simplifying assumptions must be made in order to simulate shear flows of such suspensions at a reasonable computational cost. Including such simplifying assumptions also gives the added benefit of aiding in identifying what features of the fluid and interparticle interaction are essential for interrogating the rheological behavior

of cement pastes. Firstly, it will be assumed that particle and fluid properties do not vary in time, which is a good assumption for particles in fresh pastes with less than approximately 45 minutes of water exposure (Lomboy et al., 2011). In this time interval an initial surface hydration reaction saturates and rheological properties remain relatively stable. It will also be assumed that local rheological models will be sufficient to represent the particulate flow, so that homogeneous shear simulations can be used to extract suspension stresses in terms of shear rates. By local we mean that other factors, such as granular temperature and local particle arrangements, are slaved to the mean flow kinematics, i.e. they relax infinitely fast and are only related in space through the local strain rate tensor. To simplify the computational modeling component monodispersed single component spherical particles will be used. As a result, representative or characteristic particle properties will be chosen for simulation of different cementitious materials.

There are several parameters that specify the microscopic interactions, i.e., contact force models, between particles that may be measured by different microscopy techniques. For example, the size of particles and representative contact geometries may be obtained from scanning electron microscopy (SEM) and atomic force microscopy (AFM) (Lomboy et al., 2011, 2013). The size of particles will be characterized by a representative diameter D , while the contact geometry will be characterized by a representative radius of a contact asperities R_{eff} (Wang et al., 2013). The forces experienced by particles due to cohesive van der Waals forces (Lomboy et al., 2011) and sliding against one another (Lomboy et al., 2013) can be measured using atomic force microscopy. Unfortunately, due to the complicated surface chemistry of cement pastes, interparticle forces that lead to repulsion such as those from the electrical double layer (EDL) are difficult to isolate. These forces combined with the the cohesive van der Waals force are commonly known as the Derjaguin, Landau, Verwey, Overbeek (DLVO) model (Israelachvili, 2011). Because of the difficulty in isolating the effect of the EDL this work the we characterize these forces by an effective Hamaker constant A , which is always cohesive (Lomboy et al., 2011). The forces resisting the sliding between particle surfaces will be characterized by a friction coefficient μ_f . The specific particles under consideration in this manuscript are Portland cement and fly ash. Other parameters such as material density ρ_s ,

Table 5.1 Typical system parameters for lab-scale shear simulations of cementitious materials (Wang et al., 2013).

Parameter	Portland Cement	Fly Ash
Hamaker Constant (A)	$0.15 \times 10^{-20} \text{ J}$	$0.04 \times 10^{-20} \text{ J}$
Coefficient of Friction (μ_f)	0.2	0.07
Characteristic Particle Diameter (D)	$2 \times 10^{-5} \text{ m}$	$2 \times 10^{-5} \text{ m}$
Characteristic Asperity Radius at contact (R_{eff})	$1.0 \times 10^{-6} \text{ m}$	$0.5 \times 10^{-6} \text{ m}$
Material density (ρ_s)	$3.15 \times 10^3 \text{ kg/m}^3$	$2.66 \times 10^3 \text{ kg/m}^3$
Young's modulus (E)	$20 - 120 \times 10^9 \text{ Pa}$	$98 \times 10^9 \text{ Pa}$
Fluid density (ρ_f)	$1.0 \times 10^3 \text{ kg/m}^3$	$1.0 \times 10^3 \text{ kg/m}^3$
Fluid Viscosity (μ)	$8.509 \times 10^{-4} \text{ Pa} \cdot \text{s}$	$8.509 \times 10^{-4} \text{ Pa} \cdot \text{s}$
Temperature (T)	300 K	300 K
Shear rate ($\dot{\gamma}$)	10 – 100 s^{-1}	10 – 100 s^{-1}

Table 5.2 Important non-dimensional groups for sheared cementitious slurries and their typical values.

Parameter	Definition	Portland Cement	Fly Ash
Re	$\frac{\rho_f \dot{\gamma} D^2}{\mu}$	$(5 \times 10^{-3} - 5 \times 10^{-2})$	$(5 \times 10^{-3} - 5 \times 10^{-2})$
ϕ_s	$\frac{n\pi D^3}{6}$	0.367; 0.414; 0.476	0.406; 0.455; 0.518
ρ_s/ρ_f		3.15	2.66
Pe	$\frac{\pi\mu\dot{\gamma}D^3}{k_B T}$	$(5.2 \times 10^4 - 5.2 \times 10^5)$	$(5.2 \times 10^4 - 5.2 \times 10^5)$
$\Phi_{vdW}/k_B T$	$\frac{AR_{eff}}{6d_0 k_B T}$	3.61×10^2	4.82×10^1

fluid density ρ_f , fluid viscosity μ , temperature T , and shear rate $\dot{\gamma}$ are also needed to complete the physical picture of the slurry. Typical values for these particle parameters obtained from microscopy techniques are given in Table 5.1.

Note that the Young's modulus of PC and FA were taken from Haecker et al. (2005) and Matsunaga et al. (2002), respectively. These different physical parameters can be expressed as several non-dimensional parameters that may be used to better understand the structure of the equations that we need to solve. A list of the non-dimensional quantities, their definitions, and order of magnitude are given in Table 5.2.

The most important parameter here is the Reynolds number Re , which is the ratio of

characteristic inertial to viscous forces. Here the Reynolds number is much less than unity, indicating that the flow is in the Stokes flow regime. Particle laden flows in this regime may be simulated via the Stokesian dynamics framework (Brady and Bossis, 1988). Two similarly related measures are the solid volume fraction ϕ_s and ratio of the solid to fluid density ρ_s/ρ_f , which indicates the relative importance of inertia in the solid phase. The ratio of particle and fluid density is of order unity, so that the effect of particle inertia is also relatively unimportant. Lastly, there are two thermally dependent parameters, that indicate the relative importance of Brownian motion to other phenomena. The first is a ratio of fluid to the thermal motion time-scales known as the Peclet number, Pe . Large Peclet numbers, i.e. much larger than unity, indicate that thermal motion is relatively unimportant, when compared to motion from hydrodynamics. The last term $\Phi_{vdW}/k_B T$ assesses the long-term thermodynamic stability of the slurry, and is a ratio of the minimum in the van der Waals potential well to the random thermal kinetic energy. Values much greater than unity indicate that the slurry is unstable and will aggregate over time. Since both of these numbers are quite large, the system will be approximated as athermal, i.e. Brownian motion will be neglected.

Given this assortment of non-dimensional terms indicating both the flow regime and relative importance of thermal motion, it is predicted that the dynamics will be controlled by the interplay between hydrodynamic forces and cohesion. Yet, little is understood about how these two forces might compete in a generic scenario. In order to assess this, a time-scale analysis must be carried out.

5.2.2 Time-scale for clustering

The time-scale analysis that is carried out in this section looks to answer the question of how quickly a sheared system might aggregate. If we expect aggregation events to occur on the time-scale of particle rearrangements, it would be plausible that the formation of a large particle network or gel should be expected on the time-scale that it takes to achieve a shear strain of 1. In order to study this time-scale, a simple model system equation for two particles is set-up. This model describes a balance between so-called lubrication forces arising from fluid being squeezed out as particles approach and cohesive forces become dominant. Particle inertia

is disregarded due to density ratios of order unity. As a result, such a set of particles may not reconstitute, since all energy will be dissipated during cohesion induced collision process. Note that additional lubrication terms exist but we retain only the dominant term here

$$\frac{3\pi\mu D^2}{2x} \frac{dx}{dt} + \frac{AR_{eff}}{6x^2} = 0 \quad (5.1)$$

Here the separation is given in terms of the relative separation vector $\mathbf{r}^{(jk)}$ between particles j and k as $x = |\mathbf{r}^{(jk)}| - D + d_0$. The term d_0 is the atomic separation distance, which is generally taken to be between 0.167nm (Israelachvili, 2011) and 4nm (Liu et al., 2016). This separable first-order ordinary differential equation can be solved via integration to yield the time to traverse from an initial separation of x_0 to $x = d_0$. The ratio of this time-scale to the shear rate time-scale is given as

$$\hat{t} = \frac{t_{approach}}{t_{separate}} \approx \frac{9\pi\mu D^2 \dot{\gamma} x_0^2}{2AR_{eff}} = \frac{3}{4} Pe \frac{k_B T}{\Phi_{vdW}} \frac{D}{d_0} \hat{x}_0^2 \quad (5.2)$$

In the non-dimensional form the initial separation has been rendered dimensionless as $\hat{x}_0 = x/D$. This term can be estimated using equilibrium estimates for the surface to surface distance between three-dimensional hard-spheres, which is $\hat{x}_0 = \frac{1 - \phi_s}{24\phi_s}$ (Torquato, 1995). The order of magnitude for this is $\mathcal{O}(10^{-2})$ for the volume fractions considered. The dimensionless form shows us that the first three terms are also in the range of $\mathcal{O}(10^6) - \mathcal{O}(10^9)$. Leaving us with the non-dimensional time-scale of $\hat{t} = \mathcal{O}(10^2) - \mathcal{O}(10^5)$. This means that rearrangements due to shear occur much faster than particles can pull one another together in equilibrium. However, some particles are squeezed together as shearing occurs, and will ultimately come to stick if a small enough non-dimensional separation is achieved. These aggregated particles will then pick up more particles until the system has percolated. This indicates that thixotropic behavior is highly dependent on volume fraction, as the time to percolation will depend on initial the distribution of nearest neighbor distances.

5.2.3 Simulation method

The simulations herein have been carried out using the software package LAMMPS (Plimpton, 1995). The direct interactions between particles due to contact mechanics and cohesion are simulated using DEM, while the interactions mediated by the fluid are simulated using an accelerated version of Stokesian Dynamics (Brady and Bossis, 1988), known as fast lubrication dynamics (Kumar and Higdon, 2010; Kumar, 2010). The normal forces arising from DEM are given by

$$\mathbf{F}_n^{(ij)} = \begin{cases} (R_{\text{eff}}|\delta|)^p \left(-b_n \mathbf{v}_n^{(ij)} - k_n \delta \hat{\mathbf{r}}^{(ij)} \right) + \mathbf{F}_{c,vdW} & : \delta \leq 0 \\ \frac{-AR_{\text{eff}}}{6(\delta + d_0)^2} \hat{\mathbf{r}}^{(ij)} & : 0 < \delta \leq 100d_0 \end{cases}, \quad (5.3)$$

This contact force depends on both the surface to surface distance between particles $\delta = x - d_0$ and the normal relative velocity, $\mathbf{v}_n^{(ij)} = \mathbf{v}^{(ij)} \cdot \hat{\mathbf{r}}^{(ij)} \hat{\mathbf{r}}^{(ij)}$. At contact, the force has two terms that arise due to deformation of the particles. The first is a damping force, which is parameterized by the damping parameter b_n . The other is a repulsive and energy conserving spring force, parameterized by k_n . Together these terms, along with the particle masses, determine the restitution coefficient for non-cohesive particles (Brilliantov and Pöschel, 2004). Note that the exponent p differentiates between the linear spring dash-pot model (Cundall and Strack, 1979a) with $p = 0$ and the Kono-Kuwabara (KK) model (Kuwabara and Kono, 1987) with $p = 1/2$. Only the KK model is considered in this work, with an additional attractive force. This attractive force in contact is the same as that for when particles are separated, saturating at $\delta = 0$, $\mathbf{F}_{c,vdW} = -\frac{AR_{\text{eff}}}{6d_0}$.

Tangential forces take a form similar to the normal forces

$$F_t^{(ij)} = \begin{cases} (R_{\text{eff}}|\delta|)^p \left(-b_t \mathbf{v}_t^{(ij)} - k_t \mathbf{u}^{(ij)} \right) & : \delta < 0, |F_t| \leq |\mu_f F_n| \\ -\mu_f |F_n| \hat{\mathbf{u}}^{(ij)} & : \delta < 0, |F_t| \geq |\mu_f F_n| \\ 0 & : \delta > 0 \end{cases}. \quad (5.4)$$

Here the damping and spring terms are controlled by the tangential velocity at the point of contact between two spheres $\mathbf{v}_t^{(ij)}$ and the displacement of the point of contact $\mathbf{u}^{(ij)}$. A spring

constant k_t and damping parameter b_t are again used. Note that the damping for both the tangential and normal directions in this work have been set to zero, since lubrication forces already constitute a substantial source of energy dissipation. The typical value of k_t/k_n used in this work is $2/7$. This tangential force saturates when a particular tangential force is obtained, and the particle slips experiencing dynamic friction, i.e. $|\mathbf{F}_n| = \mu_f \mathbf{F}_n$.

The low Reynolds number fluid dynamics will be simulated using FLD. The ordinary Stokesian dynamics treats the forces felt between particles in two ways (Brady and Bossis, 1988). At large distances, forces and velocities are related by a mobility tensor as $\mathbf{U}^{(i)} = \mathbf{M} \cdot \mathbf{F}^{(i)}$. Examples of this tensor exist for both point particles (Oseen, 1927) and spherical particles (Rotne and Prager, 1969). Both rely on expansions in spherical harmonics of the velocity field due to the presence of force sources from two particles. However, such expansions converge very slowly for particle separations $\delta < D$. As a result, the so-called lubrication theory is used for spheres that are closer than this distance. This theory solves the flow field between two spherical surfaces and produces a force in terms of velocities, which are related by a resistance tensor \mathbf{R}_{lub} via $\mathbf{F}^{(i)} = \mathbf{R}_{lub} \cdot \mathbf{U}^{(i)}$. Both the resistance and mobility tensors depend only on particle separations. The Stokesian dynamics framework is relatively expensive due to the need to calculate and invert the long-ranged mobility matrix, which is an $\mathcal{O}(N^3)$ operation.

Fast lubrication dynamics expedites calculations in two ways. Here the mobility tensor is not calculated directly. Instead the mobility matrix is modeled, as an isotropic resistance matrix \mathbf{R}_0 . This resistance matrix has been chosen such that it matches the short-time translational and rotational self-diffusivity as well as the stress of a randomly forced suspension of particles. In a sense this term models the average drag on a particle due to the presence of other particles in the fluid. It has been shown that this method is capable of reproducing the average eigenvalues for the mobility matrix in Stokesian dynamics (Kumar, 2010). This method was made more computationally efficient firstly by relieving us of having to invert the long-range mobility matrix. Secondly, the only two particle interactions that need to be calculated are the near-field hydrodynamic interactions or lubrication resistance matrix, which is sparsely populated. The entire matrix takes the following form

$$\begin{bmatrix} \mathbf{F} \\ \mathbf{T} \\ \mathbf{S} \end{bmatrix} = \left(\begin{bmatrix} R_0^{FU} & 0 & 0 \\ 0 & R_0^{T\Omega} & 0 \\ 0 & 0 & R_0^{SE} \end{bmatrix} + \begin{bmatrix} \mathbf{R}_{lub}^{FU} & \mathbf{R}_{lub}^{F\Omega} & \mathbf{R}_{lub}^{FE} \\ \mathbf{R}_{lub}^{TU} & \mathbf{R}_{lub}^{T\Omega} & \mathbf{R}_{lub}^{TE} \\ \mathbf{R}_{lub}^{SU} & \mathbf{R}_{lub}^{S\Omega} & \mathbf{R}_{lub}^{SE} \end{bmatrix} \right) \cdot \begin{bmatrix} \mathbf{U} - \mathbf{U}^\infty \\ \boldsymbol{\Omega} \\ \mathbf{E}^\infty \end{bmatrix} \quad (5.5)$$

The fits for the values of the scalar terms in the isotropic resistance matrices can be found in Kumar (2010), while the terms in the lubrication resistance matrices can be found in (Ball and Melrose, 1997; Kim and Karrila, 1991). Note that in these simulations an inner cut-off distance of $\delta = d_0$ has been used, where the force saturates, since the continuum hypothesis should not be valid at atomic length-scales. An outer cut-off, below which particles do not feel one another, is also used. That value is taken to be $\delta = 1.5D$ in the above simulations. Beyond this separation, terms of order $\log \delta$ diverge.

The time-steps chosen in these simulations are set in the same way as in (Murphy and Subramaniam, 2017). There the limiting time-step is due to the stiffness of the particles. Note also that in this problem the temporal evolution of the cohesive force is stiffer than the leading order lubrication force in Eq. 5.1. Triclinic boundaries are used for shearing the assemblies (Plimpton, 1995) at a variety of solid volume fractions $0.35 < \phi_s < 0.55$ and shear rates $10 \text{ s}^{-1} < \dot{\gamma} < 100 \text{ s}^{-1}$, see Table 5.2.

5.3 Results

The results have been organized as follows. First, we present the stress measurements obtained from coupled DEM-FLD simulations with fits obtained from experimental data (Wang et al., 2013). Differences in results are discussed. Next a study on the effect of rough walls is discussed, as well as a few details on the observed microstructure.

5.3.1 Homogeneous Shearing

As discussed in Section 5.2.3, the two cementitious materials that we are most interested in are the often used Portland cement and fly ash. Fly ash, a by-product from combustion, is typically spherical in shape, whereas Portland cement particles are a ground material that is angular in appearance. In addition to the geometry of these particles, the particle types both

have friction coefficients and effective Hamaker constants that differ by orders of magnitude. Portland cement is both more frictional and cohesive. As a result, one expects a sheared Portland cement paste to experience more stress than a fly ash paste, with volume fraction and shear rate held constant.

The Portland cement case is shown in Figure 5.1. The choice of axes was chosen for ease of comparison between experiments and simulations. The ordinate axis is the stress normalized by the equivalent shear stress at a given shear rate in the suspending liquid, namely water. The abscissa axis is the van der Waals energy scaled by the square of the shear rate, which is useful for scaling in dry systems (Murphy and Subramaniam, 2015; Mehrabadi et al., 2016a; Murphy and Subramaniam, 2017). It is given as $Ha = \Phi_{vdW} / (m_{eff} D^2 \dot{\gamma}^2)$. The lines are experimental fits from vane rheometer experiments (Wang et al., 2013). Experiments were performed by ramping up the shear rates from $\dot{\gamma} = 0 \text{ s}^{-1}$ to $\dot{\gamma} = 100 \text{ s}^{-1}$ over a time period of 60 seconds. A subsequent ramp down of the shear rates was then carried out over the same time period. One should note that there was considerable hysteresis or thixotropy between the ramp up and ramp down shear strain rate versus shear stress. We note that thixotropy, though interesting, is not the focus of this study.

The experimental fit is that of a Bingham fluid, which has a finite yield stress. Most importantly, this Bingham model trend is matched qualitatively by the coupled DEM-FLD simulations. However, the stresses observed in the DEM-FLD differ by about an order of magnitude from vane rheometer measurements. Both show a significant increase in the stress due to both the presence of particles in the flow field, which inhibit deformation through lubrication, long-ranged hydrodynamics, and particle contacts. We note that the best agreement is found in the lowest volume fraction of $\phi_s = 0.367$. We expect that the large quantitative discrepancies are ultimately due to the idealized representation of the particles, which will be discussed further.

The stresses observed for a fly ash slurry in both DEM-FLD simulations and vane rheometer experiments is shown in Figure 5.2. Here Bingham fluid type behavior is again observed in the DEM-FLD simulations, in agreement with the experimental fits. Qualitatively, there are still large discrepancies between simulations and experiments. However, here less than order

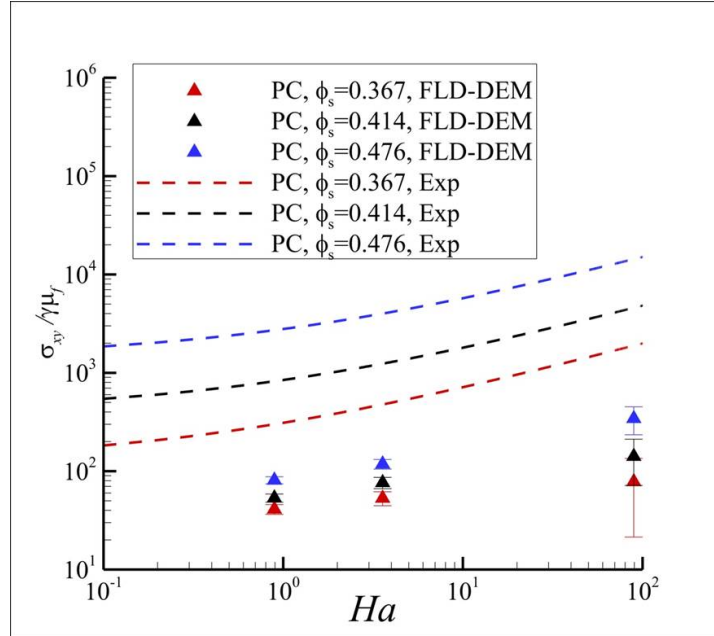


Figure 5.1 The stress comparison between experiment and FLD-DEM are shown for a Portland cement slurry at 3 different volume fractions and shear rates.

of magnitude difference is observed between the macroscale experiments and simulations. The quantitative difference between the stresses at the lowest volume fraction of $\phi_s = 0.406$ is least severe. Lastly, we note that the fly ash particles experience considerably less stress than the Portland cement cases.

Now we can compare the differences in predictions between the two materials, which have different strengths of both friction and cohesion. Figure 5.3 makes an effort to account for the effects of cohesion, while differences in friction and volume fraction are not accounted for in the scalings. Unfortunately, the experiments made an effort to keep mass fraction or water to binder ratio of the two materials consistent, which lead to different volume fractions due to differing densities between PC and FA. Nonetheless, when the differing particle systems are compared here, the qualitative differences between FA and PC are predicted well by the DEM-FLD. For example, if we compare the blue triangles (PC) with the blue squares (FA), PC consistently yields higher values for stress. This indicates that the inclusion of friction and cohesion largely predict the qualitative trends observed in experiment. However, we note that in addition to the large quantitative discrepancies, we do not see as near of a strong dependence on volume

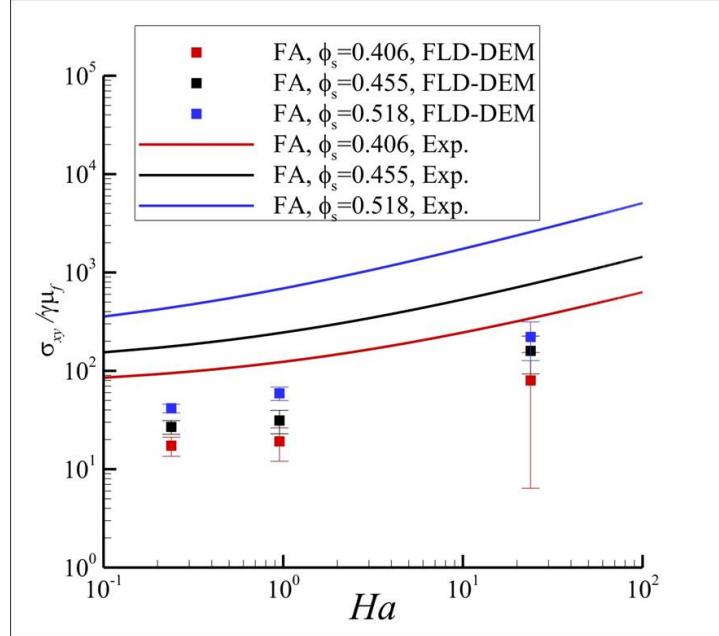


Figure 5.2 The stress comparison between experiment and FLD-DEM are shown for a fly ash slurry at 3 different volume fractions and shear rates.

fraction (see Figs. 5.1 and 5.2) in simulations as is seen in experiments. The sensitivity to friction in DEM-FLD appears to be much larger, e.g. at $Ha \approx 1$ compare data points for PC $\phi_s = 0.476$ with FA $\phi_s = 0.455$ and for PC $\phi_s = 0.414$ with FA $\phi_s = 0.406$.

5.3.2 Rough Wall Shearing

One reason for the larger discrepancy in PC than in FA could be that the highly non-spherical particles frustrate the movement of particles past one another in shear. Setting any uncertainty in friction and cohesion measurements aside, two differences between model particles used in DEM-FLD and particles used in experiments could also lead to differences in observed shear stress. Both PC and FA have large polydispersity, ranging from micron to near millimeter sizes (Bentz et al., 1999). If the large particles are still much smaller than the rheometer, this large degree of polydispersity would likely decrease the amount of shear stress observed. Small particles are able to move within the interstices between larger particles with ease, reducing the apparent stress. Rough walls or boundaries in general are another potential source of increased stress, since it constrains the movements of particles, as compared to infinite

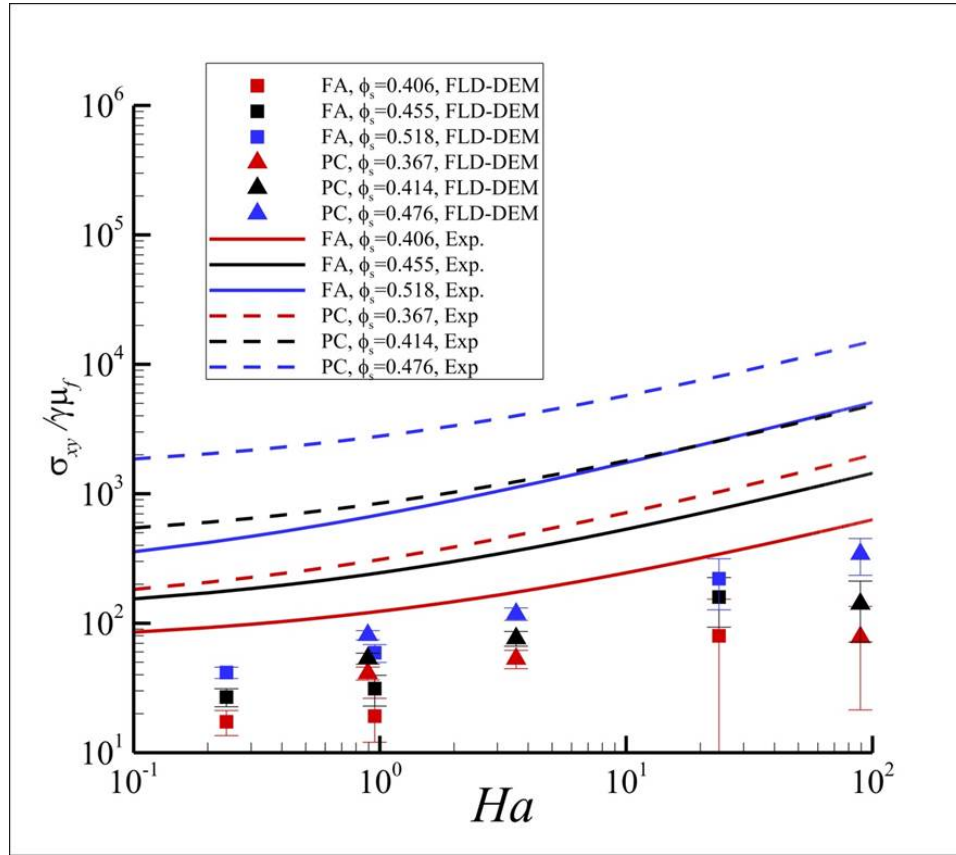


Figure 5.3 The stress comparison between experiment and FLD-DEM are shown for both Portland cement and fly ash at different volume fractions and shear rates.

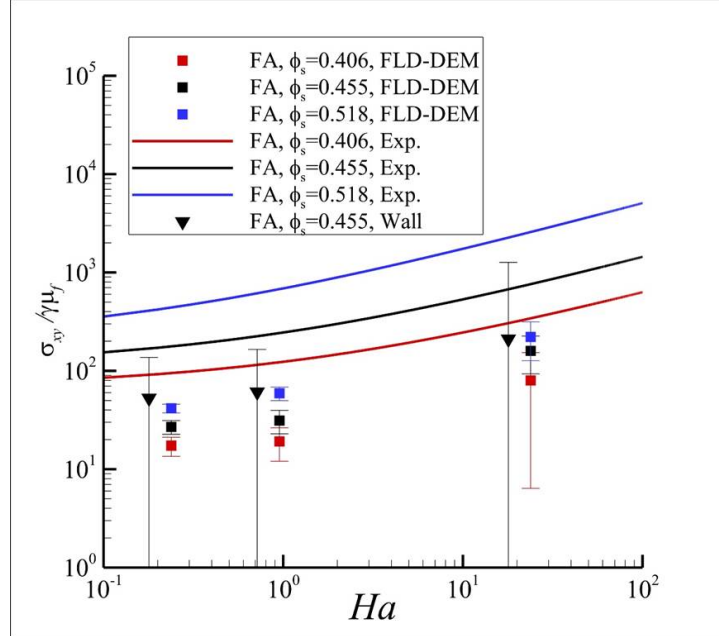


Figure 5.4 The stress comparison between experiment and FLD-DEM, with and without walls, are shown for fly ash at varying volume fractions and shear rates.

or periodic domains.

To check whether the stress is substantially affected by sources of particle frustration, we carry out DEM-FLD simulations with rough walls made out of particles, see Fig. 5.4. These wall particles are the same size as the FA particles with a gap between the two walls of $H = 15D$. We note that the rheometer used has a gap of 17 mm, which is of the same order of magnitude large than a millimeter sized particle. A simulation is performed at the intermediate volume fraction of $\phi_s = 0.455$. The inclusion of walls improves the prediction by increasing the observed stress by a factor of 2. The new values of the stress differ from the experimental observations by a factor of 3, which is a substantial improvement over the periodic simulations.

It is clear that the sources of particle frustration, namely non-sphericity, polydispersity, and walls, do affect the stress observed in a quantitative manner. This is also supported by the large differences observed in experiments between PC and FA suspensions at similar volume fractions. The highly non-spherical cement particles lead to stresses, that are not easily explained by differences in cohesion strength or friction alone. Lastly, we note that for the same strain, walled domains lead to substantially larger stress fluctuations, which is indicated

by the large error bars. These are likely due to force chains that bridge a connection to both walls.

5.4 Conclusions

Coupled FLD-DEM simulations have been used to simulate the rheology of traditional cement pastes such as Portland cement and green cements composed of fly ash. These simulations use a first of its kind first-principle based approach, where the coefficients for particle interactions have been obtained from atomic force microscopy. Results are then compared with macroscale vane rheometer experiments. Predictions are in qualitative agreement with experiments in regards to dependence on varying volume fraction, shear strain rate, cohesion strength, and friction. Quantitative agreement is improved with the inclusion of walls to within a factor of three. It is suggested that the predictions may be quantitatively improved if factors affecting the frustration of particle movements were included, such as polydispersity and non-sphericity. However, we note that for qualitative agreement inclusion of these effects are not necessary. This demonstrates the ability of a first-principle approach to connect the dependence of macroscale rheology on microscale interactions, which may be used in cement and concrete design.

Acknowledgment

We gratefully acknowledge the support provided for this work from NSF CMMI grant no. 0927660.

5.5 Bibliography

- Aarons, L. and Sundaresan, S. (2006). Shear flow of assemblies of cohesive and non-cohesive granular materials. *Powder Technology*, 169(1):10–21.
- Abbasfard, H., Evans, G., and Moreno-Atanasio, R. (2016). Effect of van der Waals force cut-off distance on adhesive collision parameters in DEM simulation. *Powder Technology*, 299:9–18.

- Afferrante, L., Ciavarella, M., and Demelio, G. (2015). Adhesive contact of the weierstrass profile. In *Proc. R. Soc. A*, volume 471, page 20150248. The Royal Society.
- Aitcin, P. (2000). Cements of yesterday and today - concrete of tomorrow. *Cement and Concrete Research*, 31(9):1349–1359.
- Alam, M., Trujillo, L., and Herrmann, H. (2006). Hydrodynamic theory for reverse brazil nut segregation and the non-monotonic ascension dynamics. *Journal of Statistical Physics*, 124:587–623.
- Bagnold, R. A. (1954). Experiments on a gravity-free dispersion of large solid spheres in a newtonian fluid under shear. In *Proceedings of the Royal Society of London A: Mathematical, Physical and Engineering Sciences*, volume 225, pages 49–63. The Royal Society.
- Ball, R. and Melrose, J. (1997). A simulation technique for many spheres in quasi-static motion under frame-invariant pair drag and brownian forces. *Physica A*, 247:444–472.
- Baranyai, A. and Evans, D. (1989). Direct entropy calculation from computer-simulation of liquids. *Physical Review A*, 40(7):3817–3822.
- Batrak, O., Patino, G., Simonin, O., Flour, I., Le Guevel, T., and Perez, E. (2005). Unlike particles size collision model in 3d unsteady polydispersed simulation of circulating fluidized bed. *8th Annual Conference on Fluidized Bed Technology*, 315.
- Bec, J., Biferale, L., Cencini, M., Lanotte, A., and Toschi, F. (2010). Intermittency in the velocity distribution of heavy particles in turbulence. *Journal of Fluid Mechanics*, 646:527–536.
- Beetstra, R., van der Hoef, M., and Kuipers, J. (2007). Drag force of intermediate reynolds number flows past mono- and bidisperse arrays of spheres. *AIChE Journal*, 53:489.
- Bentz, D., Ferraris, C., Galler, M., Hansen, A., and Guynn, J. (2012). Influence of particle size distributions on yield stress and viscosity of cement-fly ash pastes. *Cement and Concrete Research*, 42(2):404–409.

- Bentz, D. P., Garboczi, E. J., Haecker, C. J., and Jensen, O. M. (1999). Effects of cement particle size distribution on performance properties of portland cement-based materials. *Cement and Concrete Research*, 29:1663–1671.
- Berger, N., Azéma, E., Douce, J.-F., and Radjai, F. (2016). Scaling behaviour of cohesive granular flows. *EPL (Europhysics Letters)*, 112(6):64004.
- Berzi, D. and Jenkins, J. T. (2015a). Inertial shear bands in granular materials. *Physics of Fluids*, 27:033303.
- Berzi, D. and Jenkins, J. T. (2015b). Steady shearing flows of deformable, inelastic spheres. *Soft matter*, 11(24):4799–4808.
- Binnig, G., Quate, C. F., and Gerber, C. (1986). Atomic force microscope. *Physical review letters*, 56(9):930.
- Blum, J., Wurm, G., Kempf, S., Poppe, T., Klahr, H., Kozasa, T., Rott, M., Henning, T., Dorschner, J., Schrapler, R., Keller, H., Markiewicz, W., Mann, I., Gustafson, B., Giovane, F., Neuhaus, D., Fechtig, H., Grun, E., Feuerbacher, B., Kochan, H., Ratke, L., El Goresy, A., Morfill, G., Weidenschilling, S., Schwehm, G., Metzler, K., and Ip, W. (2000). Growth and form of planetary seedlings: Results from a microgravity aggregation experiment. *Physical Review Letters*, 85(12):2426–2429.
- Bradley, R. S. (1932). Lxxix. the cohesive force between solid surfaces and the surface energy of solids. *The London, Edinburgh, and Dublin Philosophical Magazine and Journal of Science*, 13(86):853–862.
- Brady, J. F. and Bossis, G. (1988). Stokesian dynamics. *Annual Reviews of Fluid Mechanics*, 20:111–157.
- Bragg, A. D. and Collins, L. R. (2014a). New insights from comparing statistical theories for inertial particles in turbulence: I. spatial distribution of particles. *New Journal of Physics*, 16:055013.

- Bragg, A. D. and Collins, L. R. (2014b). New insights from comparing statistical theories for inertial particles in turbulence: II. relative velocities. *New Journal of Physics*, 16:055014.
- Bragg, A. D., Ireland, P. J., and Collins, L. R. (2015). On the relationship between the non-local clustering mechanism and preferential concentration. *Journal of Fluid Mechanics*, 780:327–343.
- Brewster, R., Grest, G. S., Landry, J. W., and Levine, A. J. (2005). Plug flow and the breakdown of bagnold scaling in cohesive granular flows. *Physical Review E*, 72(6):061301.
- Bridges, F. G., Supulver, K. D., Lin, D., Knight, R., and Zafra, M. (1996). Energy loss and sticking mechanisms in particle aggregation in planetesimal formation. *Icarus*, 123(2):422–435.
- Brilliantov, N. V., Albers, N., Spahn, F., and Pöschel, T. (2007). Collision dynamics of granular particles with adhesion. *Physical Review E*, 76(5):051302.
- Brilliantov, N. V. and Pöschel, T. (2004). Collision of adhesive viscoelastic particles. *HINRICHSEN:GRANULAR MEDIA O-BK*, pages 189–209.
- Brilliantov, N. V. and Pöschel, T. (2004). *Kinetic Theory of Granular Gases*. Oxford University Press, New York.
- Brilliantov, N. V., Spahn, F., Hertzsch, J.-M., and Pöschel, T. (1996). Model for collisions in granular gases. *Physical review E*, 53(5):5382.
- Brito, R. and Ernst, M. (1998). Extension of haff’s cooling law in granular flows. *Europhysics Letters*, 43(5):497.
- Campbell, C. S. (2002). Granular shear flows at the elastic limit. *Journal of fluid mechanics*, 465:261–291.
- Capecelatro, J., Desjardins, O., and Fox, R. O. (2014). Numerical study of collisional particle dynamics in cluster-induced turbulence. *Journal of Fluid Mechanics*, 747:R2.

- Capecelatro, J., Desjardins, O., and Fox, R. O. (2015). On fluid-particle dynamics in fully developed cluster-induced turbulence. *Journal of Fluid Mechanics*, 780:578–635.
- Capecelatro, J., Desjardins, O., and Fox, R. O. (2016). Strongly coupled fluid-particle flows in vertical channels. ii. turbulence modeling. *Physics of Fluids*, 28:033307.
- Carnahan, N. and Starling, K. (1969). Equation of state for nonattractive rigid spheres. *Journal of Chemical Physics*, 51(2):635–636.
- Castellanos, A., Valverde, J. M., Pérez, A. T., Ramos, A., and Watson, P. K. (1999). Flow regimes in fine cohesive powders. *Physical Review Letters*, 82(6):1156.
- Cates, M., Wittmer, J., Bouchaud, J., and Claudin, P. (1998a). Jamming and static stress transmission in granular materials. *Chaos*, 9(3):511–522.
- Cates, M., Wittmer, J., Bouchaud, J., and Claudin, P. (1998b). Jamming, force chains, and fragile matter. *Physical Review Letters*, 81(9):1841–1844.
- Chew, J. W., Parker, D. M., Cocco, R. A., and Hrenya, C. M. (2011). Cluster characteristics of continuous size distributions and binary mixtures of group b particles in dilute riser flow. *Chemical Engineering Journal*, 178:348–358.
- Chialvo, S., Sun, J., and Sundaresan, S. (2012). Bridging the rheology of granular flows in three regimes. *Physical Review E*, 85(2):021305.
- Chun, J., Koch, D. L., Rani, S. L., Ahluwalia, A., and Collins, L. R. (2005). Clustering of aerosol particles in isotropic turbulence. *Journal of Fluid Mechanics*, 536:219–251.
- Cleary, P. W. and Sawley, M. L. (2002). DEM modelling of industrial granular flows: 3D case studies and the effect of particle shape on hopper discharge. *Applied Mathematical Modelling*, 26(2):89–111.
- Cocco, R., Shaffer, F., Hays, R., Karri, S. R., and Knowlton, T. (2010). Particle clusters in and above fluidized beds. *Powder Technology*, 203:3–11.

- Colwell, J., Batiste, S., Horányi, M., Robertson, S., and Sture, S. (2007). Lunar surface: Dust dynamics and regolith mechanics. *Reviews of Geophysics*, 45(2):RG2006.
- Cundall, P. and Strack, O. (1979a). A discrete numerical model for granular assemblies. *Geotechnique*, 29(1):47–65.
- Cundall, P. A. and Strack, O. D. (1979b). A discrete numerical model for granular assemblies. *Geotechnique*, 29(1):47–65.
- Dahneke, B. (1975). Further measurements of the bouncing of small latex spheres. *Journal of Colloid and Interface Science*, 51(1):58–65.
- Daley, D. and Vere-Jones, D. (1988). *An introduction to the theory of point processes*. Springer-Verlag.
- DeCicco, A. and Hartzell, C. (2016). System-level design considerations for asteroid despin via neutral beam emitting spacecraft. In *IEEE Aerospace Conference Proceedings (Big Sky, MT)*.
- Derjaguin, B., Muller, V., and Toporov, Y. (1975). Effect of contact deformations on the adhesion of particles. *Journal of Colloid and Interface Science*, 53(2):314–326.
- Di Renzo, A. and Di Maio, F. P. (2004). Comparison of contact-force models for the simulation of collisions in dem-based granular flow codes. *Chemical Engineering Science*, 59(3):525–541.
- Eaton, J. and Fessler, J. (1994). Preferential concentration of particles by turbulence. *International Journal of Multiphase Flow*, 20:169–209.
- Ernst, M., Dorfman, J., Hoegy, W., and van Leeuwen, J. (1969). Hard-sphere dynamics and binary-collision operators. *Physica*, 45(1):127–146.
- Esipov, S. and Pöschel, T. (1997). The granular phase diagram. *Journal of Statistical Physics*, 86(5/6):1385–1395.
- Ferraris, C., Obla, K., and Hill, R. (2001). The influence of mineral admixtures on the rheology of cement paste and concrete. *Cement and Concrete Research*, 31(2):245–255.

- Fox, R. (2014). On multiphase turbulence models for collisional fluid-particle flows. *Journal of Fluid Mechanics*, 742:368–424.
- Fox, R. O. (2016). Private communication.
- Fullmer, W. D. and Hrenya, C. M. (2016). Quantitative assessment of fine-grid kinetic-theory-based predictions of mean-slip in unbounded fluidization. *AIChE Journal*, 62(1):11–17.
- Galvin, J. E. and Benyahia, S. (2014). The effect of cohesive forces on the fluidization of aeratable powders. *AIChE Journal*, 60(2):473–484.
- Garzo, V., Dufty, J. W., and Hrenya, C. M. (2007a). Enskog theory for polydisperse granular mixtures. i. navier-stokes order transport. *Physical Review E*, 76(3):031303.
- Garzo, V., Fullmer, W. E., Hrenya, C. M., and Yin, X. (2016). Transport coefficients of solid particles immersed in a viscous gas. *Physical Review E*, 93:012905.
- Garzo, V., Hrenya, C. M., and Dufty, J. W. (2007b). Enskog theory for polydisperse granular mixtures. ii. sonine polynomial approximation. *Physical Review E*, 76(3):031304.
- Garzo, V., Tenneti, S., Subramaniam, S., and Hrenya, C. (2012). Enskog kinetic theory for monodisperse gas-solid flows. *Journal of Fluid Mechanics*, 712:129–168.
- Gaume, J., Chambon, G., and Naaim, M. (2011). Quasistatic to inertial transition in granular materials and the role of fluctuations. *Physical Review E*, 84:051304.
- Geldart, D. (1973). Types of gas fluidization. *Powder technology*, 7(5):285–292.
- Gidaspow, D., Jung, J., and Singh, R. K. (2004). Hydrodynamics of fluidization using kinetic theory: an emerging paradigm 2002 flour-daniel lecture. *Powder Technology*, 148:123–141.
- Goldhirsch, I. and Zanetti, G. (1993). Clustering instability in dissipative gases. *Physical Review Letters*, 70(11):1619–1622.
- Goldshtein, A. and Shapiro, M. (1995). Mechanics of collisional motion of granular materials. part 1. general hydrodynamic equations. *Journal of Fluid Mechanics*, 282:75–114.

- Gollin, D., Berzi, D., and Bowman, E. (2017). Extended kinetic theory applied to inclined granular flows: role of boundaries. *Granular Matter*, 19(3):1564–1583.
- Gonzalez, R. G. and Garzo, V. (2016). Instabilities in granular gas-solid flows. *arXiv:1611.03269*.
- Gonzalez, S., Thornton, A., and Luding, S. (2014). Free cooling phase-diagram of hard-spheres with short-and long-range interactions. *The European Physical Journal Special Topics*, 223(11):2205–2225.
- Gourdel, c., Simonin, O., and Brunier, E. (1998). Modelling and simulation of gas-solid turbulent flows with a binary mixture of particles. *Third International Conference on Multiphase Flows*, 315.
- Gourdel, c., Simonin, O., and Brunier, E. (1999). Two-maxwellian equilibrium distribution function for the modelling of a binary mixture of particles. *6th International Conference on Circulating Fluidized Beds*, 315.
- Grierson, D., Flater, E., and Carpick, R. (2005). Accounting for the jkr–dmt transition in adhesion and friction measurements with atomic force microscopy. *Journal of adhesion science and technology*, 19(3-5):291–311.
- Gu, Y., Chialvo, S., and Sundaresan, S. (2014). Rheology of cohesive granular materials across multiple dense-flow regimes. *Physical Review E*, 90(3):032206.
- Gu, Y., Ozel, A., and Sundaresan, S. (2015). A modified cohesion model for CFD–DEM simulations of fluidization. *Powder Technology*, 296:17–28.
- Gu, Y., Ozel, A., and Sundaresan, S. (2016). Numerical studies of the effects of fines on fluidization. *AIChE Journal*.
- Gustavsson, K. and Mehlig, B. (2014a). Clustering of particles falling in a turbulent flow. *Physical Review Letters*, 112:214501.
- Gustavsson, K. and Mehlig, B. (2014b). Relative velocities of inertial particles in turbulent aerosols. *Journal of Turbulence*, 15(1):34–69.

- Gustavsson, K. and Mehlig, B. (2016). Statistical models for spatial patterns of heavy particles in turbulence. *Advances in Physics*, 65(1):1–57.
- Haecker, C., Garboczi, E., J.W., B., Bohn, R., Sun, Z., Shah, S., and Voigt, T. (2005). Modeling the linear elastic properties of portland cement paste. *Cement and Concrete Research*, 35:1948–1960.
- Haff, P. (1983). Grain flow as a fluid-mechanical phenomenon. *Journal of Fluid Mechanics*, 134:401–430.
- Hatzes, A., Bridges, F., Lin, D., and Sachtjen, S. (1991). Coagulation of particles in saturn’s rings: Measurement of the cohesive force of water frost. *Icarus*, 89:113–121.
- Hill, R. J., Koch, D., and Ladd, A. (2001a). The first effects of fluid inertia on flows in ordered and random arrays of spheres. *Journal of Fluid Mechanics*, 448:213–241.
- Hill, R. J., Koch, D., and Ladd, A. (2001b). Moderate-reynolds-number flows in ordered and random arrays of spheres. *Journal of Fluid Mechanics*, 448:243–278.
- Irani, E., Chaudhuri, P., and Heussinger, C. (2014). Impact of attractive interactions on the rheology of dense athermal particles. *Physical Review Letters*, 112:188303.
- Irani, E., Chaudhuri, P., and Heussinger, C. (2016). Athermal rheology of weakly attractive soft particles. *Physical Review E*, 94:052608.
- Israelachvili, J. N. (2011). *Intermolecular and surface forces: revised third edition*. Academic press.
- Iveson, S., Litster, J., Hapgood, K., and Ennis, B. (2001). Nucleation, growth and breakage phenomena in agitated wet granulation processes: a review. *Powder Technology*, 117(1-2):3–39.
- Jenkins, J. and Mancini, F. (1987). Balance laws and constitutive relations for plane flows of a dense, binary mixture of smooth, nearly elastic, circular disks. *Journal of Applied Mechanics*, 1(54):27–34.

- Jenkins, J. and Mancini, F. (1989). Kinetic theory for binary mixtures of smooth, nearly elastic spheres. *Physics of Fluids, A*, 1(12):2050–2057.
- Johnson, K. and Greenwood, J. (1997). An adhesion map for the contact of elastic spheres. *Journal of colloid and interface science*, 192(2):326–333.
- Johnson, K., Kendall, K., and Roberts, A. (1971). Surface energy and the contact of elastic solids. *Proceedings of the Royal Society London A*, 324:301–313.
- Jop, P., Forterre, Y., and Pouliquen, O. (2006). A constitutive law for dense granular flows. *Nature*, 441(7094):727–730.
- Kamrin, K. and Koval, G. (2012). Nonlocal constitutive relation for steady granular flow. *Physical Review Letters*, 108(17):178301.
- Kim, H. and Arastoopour, H. (2002). Extension of kinetic theory to cohesive particle flow. *Powder Technology*, 122(1):83–94.
- Kim, S. and Karrila, S. (1991). *Microhydrodynamics: principles and selected applications*. Butterworth-Heinemann.
- Kobayashi, T., Tanaka, T., Shimada, N., and Kawaguchi, T. (2013). Dem-cfd analysis of fluidization behavior of geldart group a particles using a dynamic adhesion force model. *Powder Technology*, 248:143–152.
- Koch, D. L. (1990). Kinetic theory for a monodisperse gas-solid suspension. *Physics of Fluids A*, 2(10):1711–1723.
- Koch, D. L. and Sangani, A. S. (1999). Particle pressure and marginal stability limits for a homogeneous monodisperse gas-fluidized bed: kinetic theory and numerical simulations. *Journal of Fluid Mechanics*, 400:229–263.
- Kolakaluri, R., Murphy, E., Subramaniam, S., Brown, R., and Fox, R. (2015). Filtration model for polydisperse aerosols in gas-solid flow using granule-resolved direct numerical simulation. *AIChE Journal*, 61(11):3594–3606.

- Kothe, S., Blum, J., Weidling, R., and GÃ¼ttler, C. (2013). Free collisions in a microgravity many-particle experiment. iii. the collision behavior of sub-millimeter-sized dust aggregates. *Icarus*, 225:75–85.
- Kulchitsky, A., Johnson, J., Reeves, D., and Wilkinson, A. (2014). Discrete element method simulation of a boulder extraction from an asteroid. In *Proceedings of the 14th ASCE Biennial International Conference on Engineering, Science, Construction, and Operations in Challenging Environments (St. Louis, Missouri, USA,)*, pages 485–494.
- Kumar, A. (2010). *Microscale Dynamics in Suspensions of Non-spherical Particles*. PhD thesis, University of Illinois Urbana-Champaign.
- Kumar, A. and Higdon, J. (2010). Origins of the anomalous stress behavior in charged colloidal suspensions under shear. *Physical Review E*, 82:051401.
- Kuwabara, G. and Kono, K. (1987). Restitution coefficient in a collision between two spheres. *Japanese journal of applied physics*, 26(8R):1230.
- Lanotte, A., Bec, J., Biferale, L., Cencini, M., and Toschi, F. (2011). About scaling properties of relative velocity between heavy particles in turbulence. *Journal of Physics Conference series*, 318:052010.
- Launder, B. (1990). Phenomenological modelling: present... and future? in j.l. lumley (ed.). *Whither Turbulence? Turbulence at a Crossroads*, pages 439–485.
- Lees, A. and Edwards, S. (1972). The computer study of transport processes under extreme conditions. *Journal of Physics C: Solid State Physics*, 5(15):1921.
- Leyvraz (2003). Scaling theory and exactly solved models in the kinetics of irreversible aggregation. *Physics Reports*, 383:92–212.
- Li, J., Cheng, C., Zhang, Z., Yuan, J., Nemet, A., and Fett, F. (1999). The emms model - its application, development and updated concepts. *Chemical Engineering Science*, 54(22):5409–5425.

- Liard, M., Martys, N., George, W., Lootens, D., and Hebraud, P. (2014). Scaling laws for the flow of generalized newtonian suspensions. *Journal of Rheology*, 58:1993–2015.
- Liu, A. J. and Nagel, S. R. (2010). The jamming transition and the marginally jammed solid. *Annual Reveiw of Condensed Matter Physics*, 1:347–369.
- Liu, L. (2011). Kinetic theory of aggregation in granular flow. *AICHE Journal*, 57(12):3331–3343.
- Liu, P., Kellogg, K., LaMarche, C., and Hrenya, C. (2017). Dynamics of singlet-doublet collisions of cohesive particles. *Chemical Engineering Journal*, 324:380–391.
- Liu, P., LaMarche, C. Q., Kellogg, K. M., and Hrenya, C. M. (2016). Fine-particle deflu-idization: Interaction between cohesion, Young’s modulus and static bed height. *Chemical Engineering Science*, 145:266–278.
- Lois, G., Blawdziewicz, J., and O’Hern, C. S. (2008). Jamming transition and new perco-lation universality classes in particulate systems with attraction. *Physical Review Letters*, 100:028001.
- Lomboy, G., Sundararajan, S., and Wang, K. (2013). Micro- and macroscale coefficients of friction of cementitious materials. *Cement and Concrete Research*, 54:21–28.
- Lomboy, G., Sundararajan, S., Wang, K., and Subramaniam, S. (2011). A test method for determining adhesion forces and hamaker constants of cementitious materials using atomic force microscopy. *Cement and Concrete Research*, 41(11):1157–1166.
- Lomboy, G. R., Wang, K., and Quanji, Z. (2012). Properties of cementitious materials in their dry state and their influences on viscosity of the cementitious pastes. *Powder Technology*, 229:104–111.
- Luding, S. (1998). Collisions & contacts between two particles. In *Physics of dry granular media*, pages 285–304. Springer.
- Luding, S. (2008). Cohesive, frictional powders: contact models for tension. *Granular matter*, 10(4):235–246.

- Luding, S. (2016). Granular matter: So much for the jamming point. *Nature Physics*, 12:531–532.
- Luding, S. and Alonso-Marroquin, F. (2011). The critical-state yield stress (termination locus) of adhesive powders from a single numerical experiment. *Granular Matter*, 13:109–119.
- Luding, S., Clément, E., Blumen, A., Rajchenbach, J., and Duran, J. (1994). Anomalous energy dissipation in molecular-dynamics simulations of grains: The detachment effect. *Physical Review E*, 50(5):4113.
- Luding, S., Huthmann, M., McNamara, S., and Zippelius, A. (1998). Homogeneous cooling of rough, dissipative particles: Theory and simulation. *Physical Review E*, 58(3):3416–3425.
- Majmudar, T., Sperl, M., Luding, S., and Behringer, R. (2007). Jamming transition in granular systems. *Physical Review Letters*, 98:058001.
- Makse, H. A., Johnson, D. L., and Schwartz, L. M. (2000). Packing of compressible granular materials. *Physical review letters*, 84(18):4160.
- Marchisio, D. L. and Fox, R. O. (2013). *Computational Models for Polydisperse Particulate and Multiphase Systems*. Cambridge University Press.
- Markutsya, S., Fox, R., and Subramaniam, S. (2014). Characterization of sheared colloidal aggregation using langevin dynamics simulation. *Physical Review E*, 89:062312.
- Marmur, B. L. and Heindel, T. J. (2016). Effect of particle size, density, and concentration on granular mixing in a double screw pyrolyzer. *Powder Technology*, 302:222–235.
- Martys, N. and Ferraris, C. (2002). Simulation of scc flow. In *First North American Conference on the Design and Use of Self-Consolidating Concrete. Proceedings. Chicago, IL,*.
- Martys, N., Khalil, M., George, W., and Lootens, D. (2012). Stress propagation in a concentrated colloidal suspension under shear. *European Physical Journal E*, 35(3):1–7.
- Matsunaga, T., Kim, J., Hardcastle, S., and Rohatgi, P. (2002). Crystallinity and selected properties of fly ash particles. *Materials Science and Engineering*, A325:333–343.

- Maugis, D. (1992). Adhesion of spheres: the jkr-dmt transition using a dugdale model. *Journal of colloid and interface science*, 150(1):243–269.
- Maxey, M. (1987). The gravitational settling of aerosol particles in homogeneous turbulence and random flow fields. *Journal of Fluid Mechanics*, 174:441–465.
- Mckay, W. and Mckay, J. (1971). *Building Construction Vol. Ii (Fourth Edition)*. Orient Longman Private Limited.
- McMillan, J., Shaffer, F., Gopalan, B., Chew, J. W., Hrenya, C., Hays, R., Karri, S. R., and Cocco, R. (2013). Particle cluster dynamics during fluidization. *Chemical Engineering Science*, 100:39–51.
- McNamara, S. and Young, W. (1992). Inelastic collapse and clumping in a one-dimensional granular medium. *Physics of Fluids A*, 4(3):496–504.
- Mehrabadi, M. (2016). *Analysis of gas-solid flow using particle-resolved direct numerical simulation: flow physics and modeling*. PhD thesis, Iowa State University.
- Mehrabadi, M., Murphy, E., and Subramaniam, S. (2016a). Development of a gas-solid drag law for clustered particles using particle-resolved direct numerical simulation. *Chemical Engineering Science*, 152:199–212.
- Mehrabadi, M., Tenneti, S., and Subramaniam, S. (2016b). Importance of the fluid-particle drag model in predicting segregation in bidisperse gas-solid flow. *International Journal of Multiphase Flow*, 86:99–114.
- MiDi, G. (2004). On dense granular flows. *The European Physical Journal E*, 14(4):341–365.
- Miller, A. and Gidaspow, D. (1992). Dense, vertical gas-solid flow in a pipe. *AIChE Journal*, 38(11):1801–1815.
- Mills, P., Rognon, P., and Chevier, F. (2008). Rheology and structure of granular materials near the jamming transition. *EPL (Europhysics Letters)*, 81:64005.

- Miyamoto, H., Kargel, J., Fink, W., and Furfaro, R. (2008). Granular processes on itokawa, a small near-earth asteroid: Implications for resource utilization. *Space Exploration Technologies, Proceedings of SPIE*, 6960:69600I.
- Monchaux, R., Bourgoïn, M., and Cartellier, A. (2010). Preferential concentration of heavy particles: a voronoi analysis. *Physics of Fluids*, 22(10):103304.
- Moreno-Atanasio, R., Xu, B., and Ghadiri, M. (2007). Computer simulation of the effect of contact stiffness and adhesion on the fluidization behaviour of powders. *Chemical engineering science*, 62(1):184–194.
- Morrow, C., Lovell, M., and Ning, X. (2003). A jkr–dmt transition solution for adhesive rough surface contact. *Journal of Physics D: Applied Physics*, 36(5):534.
- Mounfield, C. and Edwards, S. (1994). A model for the packing of irregularly shaped grains. *Physica A*, 210:301–316.
- Müller, M.-K. and Luding, S. (2011). Homogeneous cooling with repulsive and attractive long-range potentials. *Mathematical Modelling of Natural Phenomena*, 6(4):118–150.
- Murphy, E., Mehrabadi, M., Tenneti, S., and Subramaniam, S. (2015). Modeling two-point particle dynamics of homogeneous gas-solid flows to describe clustering and stability. In *68th annual meeting of the American physical society division of fluid dynamics, At Boston, MA*.
- Murphy, E. and Subramaniam, S. (2014). A model for solid-solid drag in bidisperse gas-solid flows. In *67th Annual Meeting of the APS Division of Fluid Dynamics*, volume 59.
- Murphy, E. and Subramaniam, S. (2015). Freely cooling granular gases with short-ranged attractive potentials. *Physics of Fluids (1994-present)*, 27(4):043301.
- Murphy, E. and Subramaniam, S. (2017). Binary collision outcomes for inelastic soft-sphere models with cohesion. *Powder Technology*, 305:462–476.
- Nachenius, R., van de Wardt, T., Ronsse, F., and Prins, W. (2015). Effect of particle size, density, and concentration on granular mixing in a double screw pyrolyzer. *Fuel Processing Technology*, 130:87–95.

- Narayanan, K. and Ramamurthy, K. (2000). Structure and properties of aerated concrete: a review. *Cement and Concrete Composites*, 22(5):321–329.
- Nase, S. T., Vargas, W. L., Abatan, A. A., and McCarthy, J. (2001). Discrete characterization tools for cohesive granular material. *Powder Technology*, 116(2):214–223.
- Nauman, E. B. (2001). *Chemical Reactor Design, Optimization, and Scaleup*. McGraw-Hill.
- Nienow, A., Edwards, M., and Harnby, N. (1992). *Mixing in the Process Industries: Mixing of Cohesive Powders*. Elsevier, Oxford, 2nd edition.
- of Chemistry, T. R. S. (2008). The concrete conundrum. *Chemistry World*.
- Oliver, W. C. and Pharr, G. M. (1992). An improved technique for determining hardness and elastic modulus using load and displacement sensing indentation experiments. *Journal of materials research*, 7(06):1564–1583.
- Ortiz de Zarate, J. and Sengers, J. (2006). *Hydrodynamic Fluctuations in Fluids and Fluid Mixtures*. Elsevier.
- Oseen, C. (1927). Neuere methoden und ergebnisse in der hydrodynamik. *Akademische Verlagsgesellschaft*.
- Otsuki, M., Hayakawa, H., and Luding, S. (2010). Behavior of pressure and viscosity at high densities for two-dimensional hard and soft granular materials. *Progress of Theoretical Physics Supplement*, 184:110–133.
- Pasha, M., Dogbe, S., Hare, C., Hassanpour, A., and Ghadiri, M. (2014). A linear model of elasto-plastic and adhesive contact deformation. *Granular Matter*, 16(1):151–162.
- Pathak, S., Jabeen, Z., Dibyendu, D., and Rajesh, R. (2014). Energy decay in three-dimensional freely cooling granular gas. *Physical Review Letters*, 112:038001.
- Paul, E. L., Atiemo-Obeng, V. A., and Kresta, S. M. (2004). *Handbook of industrial mixing: science and practice*. John Wiley ”&” Sons.

- Perni, S. and Prokopovich, P. (2015). Multi-asperity elliptical jkr model for adhesion of a surface with non-axially symmetric asperities. *Tribology International*, 88:107–114.
- Persson, B. N. and Scaraggi, M. (2014). Theory of adhesion: Role of surface roughness. *The Journal of chemical physics*, 141(12):124701.
- Pettersen, O. (2007). Sandstone compaction, grain packing and critical state theory. *Petroleum Geoscience*, 13:63–67.
- Plimpton, S. (1995). Fast parallel algorithms for short-range molecular dynamics. *Journal of Computational Physics*, 117:1–19.
- Pope, S. B. (2000). *Turbulent Flows*. Cambridge University Press.
- Prokopovich, P. and Starov, V. (2011). Adhesion models: From single to multiple asperity contacts. *Advances in colloid and interface science*, 168(1):210–222.
- Rahman, M., Wiklund, J., Kotze, R., and Hakansson, U. (2017). Yield stress of cement grouts. *Tunnelling and Underground Space Technology*, 61:50–60.
- Rani, S. L., Dhariwal, R., and Koch, D. L. (2014). A stochastic model for the relative motion of high stokes number particles in isotropic turbulence. *Journal of Fluid Mechanics*, 756:870–902.
- Reeks, M. (1980). Eulerian direct interaction applied to the statistical motion of particles in a turbulent flow. *Journal of Fluid Mechanics*, 97:569–590.
- Rognon, P. G., Roux, J.-N., Naaim, M., and Chevoir, F. (2008). Dense flows of cohesive granular materials. *Journal of Fluid Mechanics*, 596:21–47.
- Rong, L., Dong, K., and Yu, A. (2014). Lattice-boltzmann simulation of fluid flow through packed beds of spheres: effect of particle size distribution. *Chemical Engineering Science*, 116:508–523.
- Rotne, J. and Prager, S. (1969). Variational treatment of hydrodynamic interaction in polymers. *Journal of Chemical Physics*, 50:4831–4837.

- Roussel, N., Lemaitre, A., Flatt, R., and Coussot, P. (2010). Steady state flow of cement suspensions: A micromechanical state of the art. *Cement and Concrete Research*, 40(1):77–84.
- Roussel, N., Ovarlez, G., Garrault, S., and Brumaud, C. (2012). The origins of thixotropy of fresh cement pastes. *Cement and Concrete Research*, 42(1):148–157.
- Rumpf, H. (1958). Grundlagen und methoden des granulierens. *Chemie Ingenieur Technik*, 30(3):144–158.
- Rycroft, C., Grest, G., Landry, J., and Bazant, M. (2006). Analysis of granular flow in a pebble-bed nuclear reactor. *Physical Review E*, 74:021306.
- Saha, S. and Alam, M. (2016). Normal stress differences, their origin and constitutive relations for a sheared granular fluid. *Journal of Fluid Mechanics*, 795:549–580.
- Saitoh, K. and Mizuno, H. (2016). Enstrophy cascades in two-dimensional dense granular flows. *Physical Review E*, 94:022908.
- Saitoh, K., Takada, S., and Hayakawa, H. (2015). Hydrodynamic instabilities in shear flows of dry cohesive granular particles. *Soft matter*, 11(32):6371–6385.
- Schäfer, J., Dippel, S., and Wolf, D. (1996). Force schemes in simulation of granular material. *J. Phys. I France*, 6:5–20.
- Schlick, C. P., Isner, A. B., Freireich, B. J., Fan, Y., Umbanhowar, P. B., Ottino, J. M., and Lueptow, R. M. (2016). A continuum approach for predicting segregation in flowing polydisperse granular materials. *Journal of Fluid Mechanics*, 797:95–109.
- Shah, S. and Wang, K. (2004). Development of green cement for sustainable concrete using cement kiln dust and fly ash. In *Proceedings of the International Workshop on Sustainable Development and Concrete Technology*.
- Shannon, C. (1948). A mathematical theory of communication. *Bell System Technical Journal*, 27(3):379–423.

- Silbert, L. E., Ertaş, D., Grest, G. S., Halsey, T. C., Levine, D., and Plimpton, S. J. (2001). Granular flow down an inclined plane: Bagnold scaling and rheology. *Physical Review E*, 64(5):051302.
- Silbert, L. E., Grest, G. S., Brewster, R., and Levine, A. J. (2007). Rheology and contact lifetimes in dense granular flows. *Physical review letters*, 99(6):068002.
- Singh, A., Magnanimo, V., Saitoh, K., and Luding, S. (2014). Effect of cohesion on shear banding in quasistatic granular materials. *Physical Review E*, 90(2):022202.
- Singh, A., Magnanimo, V., Saitoh, K., and Luding, S. (2015). The role of gravity or pressure and contact stiffness in granular rheology. *New journal of physics*, 17(4):043028.
- Sjostrom, S. and Krutka, H. (2009). Evaluation of solid sorbents as a retrofit technology for co2 capture. *Fuel*, 89(6):1298–1306.
- Song, C., Wang, P., and Makse, H. A. (2008). A phase diagram for jammed matter. *Nature*, 453(7195):629–632.
- Stevens, A. and Hrenya, C. (2005). Comparison of soft-sphere models to measurements of collision properties during normal impacts. *Powder Technology*, 154(2):99–109.
- Stoyan, D., Kendall, W., and Mecke, J. (1995). *Stochastic geometry and its applications*. John Wiley and Sons, New York, 2nd edition.
- Stutzman, P. (2004). Scanning electron microscopy imaging of hydraulic cement microstructure. *Cement and Concrete Composites*, 26:957–966.
- Subramaniam, S. (2000). Statistical representation of a spray as a point process. *Physics of Fluids*, 12(10):2413–2431.
- Subramaniam, S. (2001). Statistical modeling of sprays using the droplet distribution function. *Physics of Fluids*, 13(3):624–642.
- Subramaniam, S. (2012). Stability limits for gas-solid suspensions with finite fluid inertia using particle-resolved direct numerical simulations. *NSF Annual Report 1134500*.

- Subramaniam, S. (2014). Stability limits for gas-solid suspensions with finite fluid inertia using particle-resolved direct numerical simulations. *NSF Annual Report 1134500*.
- Sun, J., Battaglia, F., and Subramaniam, S. (2006). Dynamics and structures of segregation in a dense, vibrating granular bed. *Physical Review E*, 74(6):061307.
- Sun, J. and Sundaresan, S. (2011). A constitutive model with microstructure evolution for flow of rate-independent granular materials. *Journal of Fluid Mechanics*, 682:590–616.
- Sundaram, S. and Collins, L. (1997). Collision statistics in an isotropic, particle-laden turbulent suspension i. direct numerical simulations. *Journal of Fluid Mechanics*, 335:75–109.
- Syamlal, M. (1987). The particle-particle drag term in a multiphase model of fluidization. *Technical Report DOE/MC/21353-2373, NTIS/DE87006500, National Technical Information Service*.
- Syamlal, M. and O'Brien, T. (1987). A generalized drag correlation for multiparticle systems. *Technical Report, Morgantown Energy Technology Center DOE Report*.
- Syamlal, M., Rogers, W., and O'Brien, T. (1993). Mfix documentation: Theory guide. *Morgantown Energy Technology Center Morgantown, WV, USA*, page 54.
- Tabor, D. (1977). Surface forces and surface interactions. *Journal of colloid and interface science*, 58(1):2–13.
- Takada, S., Saitoh, K., and Hayakawa, H. (2014). Simulation of cohesive fine powders under a plane shear. *Physical Review E*, 90(6):062207.
- Takada, S., Saitoh, K., and Hayakawa, H. (2015a). Kinetic theory for dilute cohesive granular gases with a square well potential. *arXiv preprint arXiv:1506.04578*.
- Takada, S., Saitoh, K., and Hisao, H. (2015b). Simulation of cohesive fine powders under a plane shear. *Physical Review E*, 90:062207.

- Tenneti, S., Garg, G., and Subramaniam, S. (2011). Drag law for monodisperse gas-solid systems using particle-resolved direct numerical simulation of flow past fixed assemblies of spheres. *International Journal of Multiphase Flows*, 37(9):1072–1092.
- Tenneti, S., Mehrabadi, M., and Subramaniam, S. (2016). Stochastic lagrangian model for hydrodynamic acceleration of inertial particles in gas-solid suspensions. *Journal of Fluid Mechanics*, 788:695–729.
- Tenneti, S. and Subramaniam, S. (2014). Particle-resolved direct numerical simulation for gas-solid flow model development. *Annual Review of Fluid Mechanics*, 46:199–230.
- Thornton, C., Cummins, S. J., and Cleary, P. W. (2013). An investigation of the comparative behaviour of alternative contact force models during inelastic collisions. *Powder Technology*, 233:30–46.
- Thornton, C. and Ning, Z. (1998). A theoretical model for the stick/bounce behaviour of adhesive, elastic-plastic spheres. *Powder technology*, 99(2):154–162.
- Tien, C. and Ramarao, B. (2007). *Granular Filtration of Aerosols and Hydrosols*. Elsevier, Oxford, 2nd edition.
- Tomas, J. (2000). Particle adhesion fundamentals and bulk powder consolidation. *KONA Powder and Particle Journal*, 18(0):157–169.
- Torquato, S. (1995). Mean nearest-neighbor distance in random packings of hard d-dimensional spheres. *Physical Review Letters*, 74(12):2156–2159.
- Trizac, E. and Hansen, J. (1995). Dynamic scaling behavior of ballistic coalescence. *Physical Review Letters*, 74(21):4114–4117.
- Trizac, E. and Hansen, J. (1996). Dynamics and growth of particles undergoing ballistic coalescence. *Journal of Statistical Physics*, 86(5-6):1345–1370.
- Tsuji, Y., Kawaguchi, T., and Tanaka, T. (1993). Discrete particle simulation of two-dimensional fluidized bed. *Powder technology*, 77(1):79–87.

- Uhlmann, M. and Doychev, T. (2014). Sedimentation of a dilute suspension of rigid spheres at intermediate galileo numbers: the effect of clustering upon the particle motion. *Journal of Fluid Mechanics*, 752:310–348.
- UNEP, U. N. E. P. (2012). Greening cement production has a big role to play in reducing greenhouse gas emissions. *UNEP Report 2012, Environmental Science Alert Thematic Focus: Resource Efficiency, Harmful Substances and Hazardous Waste, and Climate Change*.
- van der Hoef, M., Beestra, R., and Kuipers, J. (2005). Lattice-boltzmann simulations of low-reynolds-number flow past mono- and bidisperse arrays of spheres: results for the permeability and drag force. *Journal of Fluid Mechanics*, 528:233–254.
- van Noije, T., Ernst, M., and Brito, R. (1998a). Ring kinetic theory for an idealized granular gas. *Physica A*, 251:266–283.
- van Noije, T., Ernst, M., and Brito, R. (1998b). Spatial correlations in compressible granular flows. *Physical Review E*, 57(5):R4893.
- van Noije, T., Ernst, M., Brito, R., and Orza, J. (1997). Mesoscopic theory of granular fluids. *Physical Review Letters*, 79(3):411–414.
- Vidyapati and Subramaniam, S. (2013). Granular flow in silo discharge: Discrete element method simulations and model assessment. *Industrial "E" Engineering Chemistry Research*, 52(36):13171–13182.
- Vidyapati, V., Langroudi, M. K., Sun, J., Sundaresan, S., Tardos, G., and Subramaniam, S. (2012). Experimental and computational studies of dense granular flow: Transition from quasi-static to intermediate regime in a couette shear device. *Powder Technology*, 220:7–14.
- von Karman, T. and Howarth, L. (1938). On the statistical theory of isotropic turbulence. *Proceedings of the Royal Society of London. Series A, Mathematical and Physical Sciences*, 164(917):192–215.
- Walton, O. R. (1984). Application of molecular dynamics to macroscopic particles. *International Journal of Engineering Science*, 22(8):1097–1107.

- Walton, O. R. (2004). Potential discrete element simulation applications ranging from airborne fines to pellet beds. *SAE 2004 Transactions J. Aerospace*.
- Wang, K., Subramaniam, S., and Sundararajan, S. (2013). Final report: Understanding rheology of cement-based materials through integrated experiments and computations at multiple scales. *Final Report NSF CBET Grant No. 0927660*.
- Waters, J., Lee, S., and Guduru, P. (2009). Mechanics of axisymmetric wavy surface adhesion: Jkr-dmt transition solution. *International Journal of Solids and Structures*, 46(5):1033–1042.
- Weller, H., Tabor, G., Jasak, H., and Fureby, C. (1998). A tensorial approach to computational continuum mechanics using object-oriented techniques. *Computers in Physics*, 12(6):620–631.
- Wilson, R., Dini, D., and van Wachem, B. (2016). A numerical study exploring the effect of particle properties on the fluidization of adhesive particles. *AIChE Journal*, 62(5):1467–1477.
- Wylie, J. J. and Koch, D. L. (2000). Particle clustering due to hydrodynamic interactions. *Physics of Fluids*, 12(5):964–970.
- Xing, Z., Kenty, B., Li, Z., and Lee, S. (2009). Scale-up analysis for a cho cell culture process in large-scale bioreactors. *Biotechnology and Bioengineering*, 103(4):733–746.
- Xu, Y. and Subramaniam, S. (2007). Consistent modeling of interphase turbulent kinetic energy transfer in particle-laden turbulent flows. *Physics of Fluids*, 19:085101.
- Yao, H., Ciavarella, M., and Gao, H. (2007). Adhesion maps of spheres corrected for strength limit. *Journal of colloid and interface science*, 315(2):786–790.
- Yin, X., Zenk, J. R., Mitrano, P. P., and Hrenya, C. M. (2013). Impact of collisional versus viscous dissipation on flow instabilities in gas-solid systems. *Journal of Fluid Mechanics*, 727:R2.
- Zaichik, L. and Alipchenkov, V. (2003). Pair dispersion and preferential concentration of particles in isotropic turbulence. *Physics of Fluids*, 15:1776–1787.

- Zaichik, L. I. and Alipchenkov, V. M. (2009). Statistical models for predicting pair dispersion and particle clustering in isotropic turbulence and their applications. *New Journal of Physics*, 11:103018.
- Zamankhan, P. (2005). Kinetic theory of multicomponent dense mixtures of slightly inelastic spherical particles. *Physical Review E*, 52(5):4877–4891.
- Zhang, Q. and Kamrin, K. (2017). Microscopic description of the granular fluidity field in nonlocal flow modeling. *Physical Review Letters*, 118:058001.

CHAPTER 6. DEVELOPMENT OF A SOLID-SOLID DRAG LAW AT ARBITRARY MACH NUMBER

This section contains a manuscript that is in preparation to be submitted for publication.

6.1 Background

Fluidized (FB) and circulating fluidized beds (CFB) are indispensable tools for many chemical industries, e.g. petro-chemical, pharmaceutical, bio-energy, carbon capture, etc. Such technologies aim to suspend a solid granular phase in a carrier flow. In suspending the solid phase, the efficiency of reactions between the particulate and gas phases, heat transfer between particles and fluid, and also catalysis at particulate surfaces are all aided. Still, many problems arise in the scale-up of FBs and CFBs. The efficiency of these reactors are affected by two phenomena in particular. Clustering of the particulate phase often occurs, which increases the mixing time-scale and delays processing times (Nauman, 2001; Paul et al., 2004; Xing et al., 2009). Also segregation of particles of different size, shape, and species may also occur (Mehrabadi et al., 2016b). In this work, we will focus on studying the latter of these two problems.

FB's and CFB's can be massive in scale, with even experimental scale studies using devices several meters in height (Gidaspow et al., 2004), while commonly used particles such as fluid cracking catalysts are in the 100 micron size range (Miller and Gidaspow, 1992). As a result, solving device scale problems requires coarse-graining of both the particulate and fluid phases. The commonly used Euler-Euler coarse-grained description is the so-called two-fluid description, where separate phases are treated as two interpenetrating continua. The averaged terms that often couple descriptions of the fluid and particle momentum are so-called 'drag laws', which is a mechanism of interphase momentum transfer. These drag laws, in general,

have a dependence mainly on Reynolds number Re and solids volume fraction ϕ_s , and also on the sub-scale configuration of particles and potentially on the ratio of densities ρ_s/ρ_f . These dependencies on particle properties that are encapsulated by these non-dimensional parameters, and may by themselves may lead to segregation of particle phases. Additionally, the interphase momentum transfer between 2 different solid phases alone have also shown to lead to segregation, with many mechanisms having previous been studied. For example, in very dense flows the Brazil nut and reverse Brazil nut effect, where large particles segregate from smaller particles, are two transport phenomena unique to granular materials (Alam et al., 2006). In rapidly flowing granular materials, gradients in number density and temperature can lead to segregation of particle species (Garzo et al., 2007a,b). However, even in the absence of gradients, counter flowing particle phases experience a source of friction, the 'solid-solid drag force', which affects the transport and segregation of fluidized granular flows. It is this specific interaction that we will explore in this paper within the two-fluid context.

While the two-fluid framework is useful in the design of devices, modeling of the interphase coupling terms must be done at finer scales using more physically resolved simulations. The most physically precise modeling studies are often carried out using Particle-Resolved Direct Numerical Simulation (PR-DNS), which solves the Navier-Stokes equations using no-slip/no-penetration boundary conditions at particle interfaces (Tenneti and Subramaniam, 2014). This approach provides detailed information about the forces experienced both in the fluid and at solid interfaces. This high-fidelity information is invaluable as it is these forces that eventually lead to segregation.

A number of drag laws have been proposed using PR-DNS for a single monodispersed particle phase (Hill et al., 2001a,b; van der Hoef et al., 2005; Tenneti et al., 2011). State-of-the-art polydispersed drag laws are typically extended from a monodispersed drag law using an appropriate weighting (Syamlal and O'Brien, 1987; Beetstra et al., 2007; Rong et al., 2014; Mehrabadi et al., 2016b). It should be noted that there is little doubt that the the effects of imposed shear and particle non-sphericity in monodispersed systems should be included, however, studies of this type for monodispersed cases are still in their infancy.

In PR-DNS studies where particles are allowed to move and collide, the collisional forces

between unlike particles may be used to provide data for the construction of solid-solid drag laws, and are the general method for proposing averaged phase coupling terms. Fortunately, in FBs and CFBs, large density ratios and relatively low solid volume fraction ($< 40\%$) are the norm, and hence, collision velocities are largely unaffected by the fluid between neighboring particles. The kinetic theory of granular flows, uncoupled from the fluid phase, is a promising route to obtaining transport closures in this domain. Though we also note that fluid effects can, in principle, also be incorporated (Garzo et al., 2012). Before discussing methods further, however, we must first establish the domain of applicability in more detail. One characteristic of particle flows in FBs and CFBs is the low level of fluctuations or variance in the particle speed, characterized by the granular temperature T . The ratio of the mean to fluctuations of the particle speed characterize a Mach number $Ma = \langle |v| \rangle / \sqrt{T}$, which can become large in FBs. Indeed, these large Mach numbers are also seen when analysing freely evolving bidisperse PR-DNS simulations of particles of different sizes (Mehrabadi et al., 2016b), see fig. 6.1. As a result, we should judge competing kinetic descriptions on their ability to meet the criterion that any Mach number be able to be simulated.

The most basic of these models is the Syamlal model (Syamlal, 1987), which uses δ -functions as the velocity probability density function (PDF) and contains no dependence on the granular temperature. Such a description is at infinite Mach number. Hydrodynamic descriptions, where one has applied the Chapman-Enskog theory, represent the other extreme, i.e. and infinitesimal Mach number with a diffusion velocity much smaller than the characteristic thermal speed. These theories provide descriptions of transport due to counter flow and gradients in number density and temperature (Jenkins and Mancini, 1987, 1989; Garzo et al., 2007a,b). However, their domain of applicability is a severe limitation and they are not considered appropriate if the Mach number becomes appreciable. Other descriptions that lend themselves to describing a broad range of Mach numbers do exist. The quadrature method of moments, for example, can be used to produce solutions to the Boltzmann equation for arbitrary distributions (Marchisio and Fox, 2013). However, the generality of this simulation methodology does not provide us with easily parameterized drag laws that can be provided to existing computational fluid dynamics codes. Others have sought to provide descriptions for presumed velocity PDFs

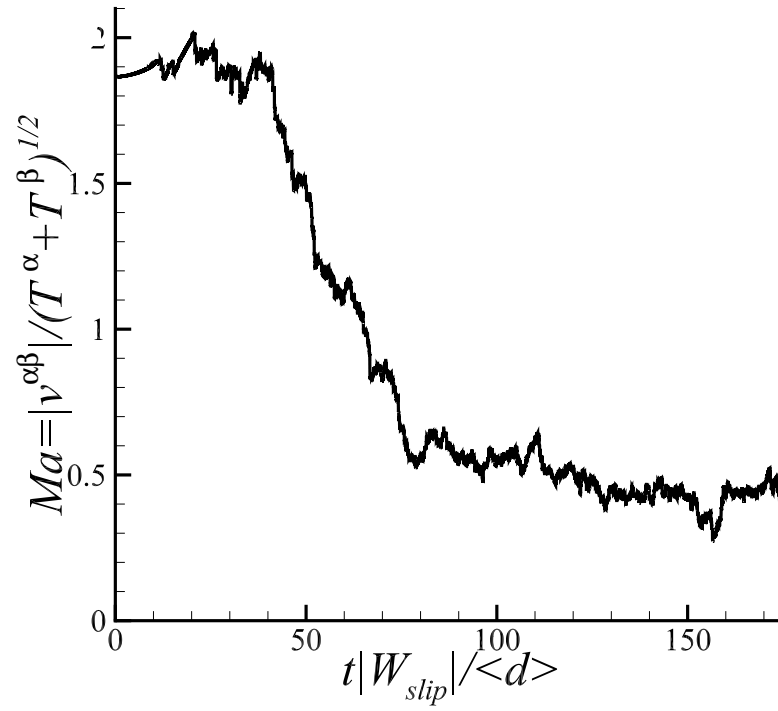


Figure 6.1 The evolution of the Mach number in gas-solid flow for a DNS case (Mehrabadi et al., 2016b) with two phases of different sized spheres $a_\alpha/a_\beta = 1/3$, Reynolds number $Re = 50$, solid phase volume fraction $\phi_s = 0.3$, $\rho_s/\rho_f = 1000$, and ratio of volume fractions of $\phi_{s,\alpha}/\phi_{s,\beta} = 3$. The Mach number assumes values as large as 1.6 and levels off between 0.3 and 0.4. These Mach numbers are too large to be accurately described by a diffusion velocity.

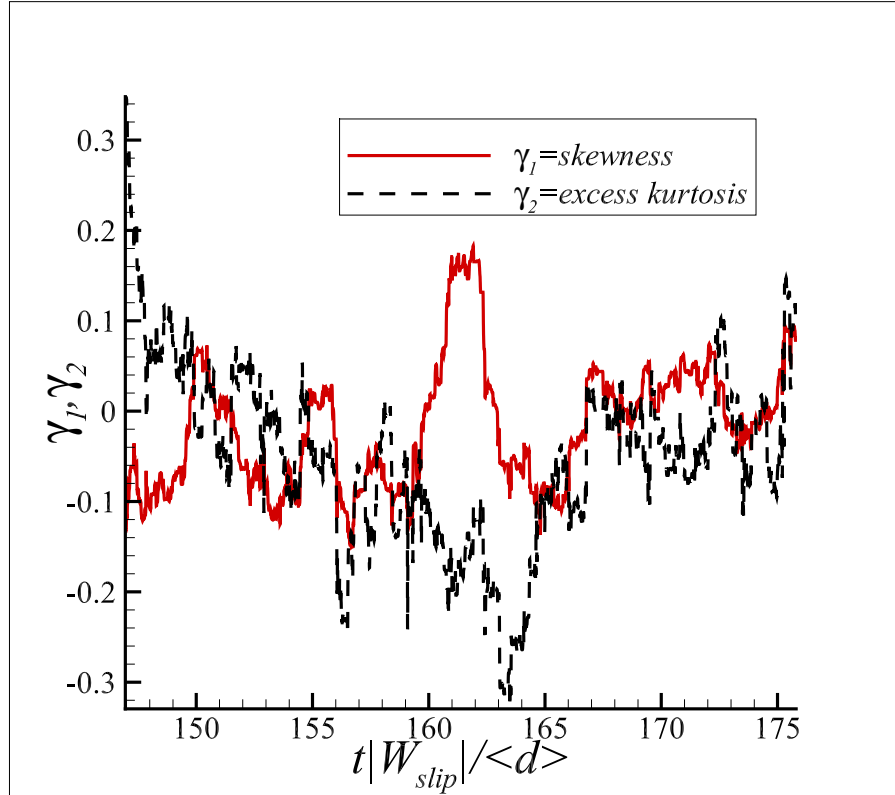


Figure 6.2 Time evolution for the skewness and excess kurtosis for a DNS case (Mehrabadi et al., 2016b) with two phases of different sized spheres $a_\alpha/a_\beta = 1/3$, Reynolds number $Re = 50$, solid phase volume fraction $\phi_s = 0.3$, solid to fluid phase density of $\rho_s/\rho_f = 1000$, and ratio of volume fractions of $\phi_{s,\alpha}/\phi_{s,\beta} = 3$. These moments of the smaller phase closely mirror that of a equidistributed Maxwellian distribution. There are too few samples in the large particle phase to produce accurate time-resolved statistics.

(Zamankhan, 2005), most frequently using Maxwellians (Gourdel et al., 1998, 1999; Batrak et al., 2005). These approaches produce evolution equations for the mean velocities and temperatures of the particle phases that are coupled, but cannot be guaranteed to be accurate, in general. However, we should note that the velocity PDFs obtained from PR-DNS are nearly Maxwellian. In Figure 6.2, the excess kurtosis and skewness have been plot for one of the particle phases using PR-DNS data (Mehrabadi et al., 2016b) for particles of different sizes but the same density.

The approach adopted in this work is a presumed distribution approach, which makes use of two independent Maxwellians as their velocity PDFs. The moments of the distribution evolve in

time through their coupled dynamics. The novelty of our approach is in its rigor in integrating the collision integral that appears in the Boltzmann equation. This rigor is necessary when faced with highly anisotropic PDFs of the relative velocity between unlike particle phases, as is the case with large Mach numbers. In that case, the limits of integration on at least one angle in the velocity space must be appropriately cast in terms of the remaining angles in the velocity space and physical separation space. This careful approach will allow us to be accurate, in terms of the approach, up to large Mach numbers. We intend to assess this approach using data from both discrete element simulations (DEM) and PR-DNS.

6.2 Analytic Methods

The Pseudo-Liouville (PL) operator formalism (Ernst et al., 1969; van Noije et al., 1998a) is the analytic method that will be used to derive the interphasic (solid-solid) momentum and energy transfer equations for a homogeneous bidisperse system with mean interphasic slip. The mean slip ensures that the PDF for relative velocities between unlike particles is anisotropic. The anisotropy makes the integrations become much more involved than in isotropic cases (Luding et al., 1998; Müller and Luding, 2011; Murphy and Subramaniam, 2015). With the additional complexity in mind, we have separated this section into the following pieces. Section 6.2.1 covers the macroscopic equations of motion that we will seek to derive, while Section 6.2.2 will cover the derivation of the PL operators. In the following Sections 6.2.4 and 6.2.5, we discuss the integration that results in the macroscopic transport equations.

6.2.1 Macroscopic Equations

The macroscopic equations that we seek to derive are the mean slip between phases $\langle v_i^{(\alpha\beta)} \rangle$, α and β , the energies $\langle E^{(\alpha)} \rangle$ and $\langle E^{(\beta)} \rangle$ in the α and β phases respectively. An equation for the center of mass can also be derived, but will not be necessary. These three equations will be coupled through their dependence on the moments of the PDF. Unfortunately, the PL operators do not allow us to easily deal with number weighting arising from integration, and so we will first find the evolution of the number weighted sum $\langle W_i^{(\alpha\beta)} \rangle$ and and difference $\langle w_i^{(\alpha\beta)} \rangle$ of

mean velocities. We first introduce these equations weighted by N_α , the number of particles in the α phase,

$$\frac{d\langle w_i^{(\alpha\beta)} \rangle}{dt} = N_\beta \frac{d\langle u_i^{(\beta)} \rangle}{dt} - N_\alpha \frac{d\langle u_i^{(\alpha)} \rangle}{dt} \quad (6.1)$$

$$\frac{d\langle W_i^{(\alpha\beta)} \rangle}{dt} = N_\beta \frac{d\langle u_i^{(\beta)} \rangle}{dt} + N_\alpha \frac{d\langle u_i^{(\alpha)} \rangle}{dt}. \quad (6.2)$$

The mean slip $\langle v_i^{(\alpha\beta)} \rangle$ can be found through simple algebraic manipulation

$$\frac{d\langle v_i^{(\alpha\beta)} \rangle}{dt} = \frac{1}{2N_\alpha N_\beta} \left((N_\alpha + N_\beta) \frac{d\langle w_i^{(\alpha\beta)} \rangle}{dt} + (N_\alpha - N_\beta) \frac{d\langle W_i^{(\alpha\beta)} \rangle}{dt} \right). \quad (6.3)$$

The energy equations then appear as

$$\frac{d\langle E^{(\alpha)} \rangle}{dt} = \frac{3N_\alpha m_\alpha}{2} \left(\frac{dT^{(\alpha)}}{dt} + \frac{2\langle u_i^{(\alpha)} \rangle}{3} \frac{d\langle u_i^{(\alpha)} \rangle}{dt} \right) \quad (6.4)$$

$$\frac{d\langle E^{(\beta)} \rangle}{dt} = \frac{3N_\beta m_\beta}{2} \left(\frac{dT^{(\beta)}}{dt} + \frac{2\langle u_i^{(\beta)} \rangle}{3} \frac{d\langle u_i^{(\beta)} \rangle}{dt} \right). \quad (6.5)$$

Here m and T are the mass of a particle and temperature of a phase, respectively. The first term in the parentheses represents the change in the granular temperature, i.e. the average of the trace of the velocity covariance matrix, due to interactions between the two-phases. The second term represents the power going into the center of mass motion of the respective phase. In the absence of any other forces besides the solid-solid drag, the forces are equal and opposite in direction to one another. This means that $N_\alpha m_\alpha \frac{d\langle u_i^{(\alpha)} \rangle}{dt} = -N_\beta m_\beta \frac{d\langle u_i^{(\beta)} \rangle}{dt}$.

6.2.2 The Pseudo-Liouville Operators

We now focus on how constructing PL operators from collision laws will allow us to precisely calculate the macroscopic laws discussed in Section 6.2.1. The general collision law between particles 1 and 2 for constant coefficient of restitution particles is

$$u_i'^{(1)} = u_i^{(1)} - \frac{m_2(1 + \varepsilon_{12})}{m_1 + m_2} \left(u_j^{(21)} \hat{r}_j^{(12)} \right) \hat{r}_i^{(12)} \quad (6.6)$$

$$u_i'^{(2)} = u_i^{(2)} - \frac{m_1(1 + \varepsilon_{12})}{m_1 + m_2} \left(u_j^{(12)} \hat{r}_j^{(12)} \right) \hat{r}_i^{(12)}. \quad (6.7)$$

We have used $r_i^{(12)}$ as the separation vector. Here we have used the notation convention where a single superscript denotes a quantity calculated in the laboratory frame. Two superscripts means that the quantity is a relative quantity calculated from the moving frame of the particle with the first superscript, e.g. $u_i^{(12)} = u_i^{(2)} - u_i^{(1)}$. A caret denotes a unit vector. Granular collisions are often modeled using this model due to its simplicity. The collision law exhibits loss in energy due to collisions, characterized by a coefficient of restitution ε , and yet still conserves linear momentum. This collision law will aid us in the construction of the appropriate PL operators for obtaining the macroscopic equations.

The generic PL operator for monodispersed particles takes the form (Ernst et al., 1969)

$$i\mathcal{L}^+ = \sum_{j=1}^N u_i^{(j)} \frac{\partial}{\partial r_i^{(j)}} + \sum_{j=1}^{N-1} \sum_{k=j+1}^N \left| u_i^{(jk)} \hat{r}_i^{(jk)} \right| \Theta \left(-u_i^{(jk)} \hat{r}_i^{(jk)} \right) \delta \left(\left| r_i^{(jk)} \right| - 2a \right) \left(b^{+(jk)} - 1 \right). \quad (6.8)$$

Note that the summation limits differ slightly if collisions are between unlike particles. In that case, every particle in the α phase may collide with any particle in the β phase. The first term on the right hand side (RHS) represents advection and will not be considered since the system that we are considering is statistically homogeneous. The second term represents the change in some velocity dependent quantity due to collisions. It has been constructed to have particular characteristic qualities. Firstly, the $\left| u_i^{(jk)} \hat{r}_i^{(jk)} \right|$ is the normal relative velocity between the two particles, which will help to calculate the collision rate. The next two terms are sifting terms that determine which particles are colliding. The delta function selects only particles in contact i.e. separated by 2 particle radii a , and the Heaviside function selects only approaching particles. Lastly, the term $(b^{+(jk)} - 1)$ is largely symbolic. It determines the change in some velocity dependent quantity after a collision. For example, if we select this quantity to operate on the energy of a particle, it can also be expressed as $(b^{+(jk)} - 1) E^{(\alpha j)} =$

$\Delta E^{(\alpha j)} = m_\alpha \Delta \left(u_i^{(\alpha j)^2} \right) / 2$. That is to say, it gives the net change in energy for particle j in the α phase. We must use the collision laws to determine what these operators look like.

We first focus on the difference and sum of particle velocities. In principle we must form these for all possible interactions, i.e. collisions between pairs of $\alpha\alpha$, $\beta\beta$, and $\alpha\beta$ particles. This would leave us with 6 operators to form, however, we can argue that only two will be important. The relative velocity PDF for $\alpha\alpha$ interactions is isotropic, so there can be no net change in momentum. In other words, there is no net drag between particles in the same phase. We need only determine $\Delta w_i^{(\alpha j, \beta k)}$ and $\Delta W_i^{(\alpha j, \beta k)}$. Note that the number weighting will appear during integration. These operators can be shown through algebra to be

$$\Delta w_i^{(\alpha j, \beta k)} = - (1 + \varepsilon_{\alpha\beta}) u_l^{(\alpha j, \beta k)} \hat{r}_l^{(\alpha j, \beta k)} \hat{r}_i^{(\alpha j, \beta k)} \quad (6.9)$$

$$\Delta W_i^{(\alpha j, \beta k)} = - \frac{m_\alpha - m_\beta}{m_\alpha + m_\beta} (1 + \varepsilon_{\alpha\beta}) u_l^{(\alpha j, \beta k)} \hat{r}_l^{(\alpha j, \beta k)} \hat{r}_i^{(\alpha j, \beta k)}. \quad (6.10)$$

Interestingly, these only differ by a ratio of particle masses, and hence, only one integration will be needed to obtain the equation for the evolution of the slip. The energy equations have slightly more terms, because intraphase interactions will eventually lead to the emergence of other terms. We will need to alter our notation here slightly for the energy terms. Here two superscripts separated by a colon, indicates the type of interaction. For example, the energy in phase α can be broken up into

$$\Delta E^{(\alpha j)} = \Delta E^{(\alpha j: \alpha k)} + E^{(\alpha j: \beta k)}. \quad (6.11)$$

For brevity, we only give the α phase version of these operators here, as the β phase can easily be found by substituting superscripts. The energy operators are

$$\Delta E^{(\alpha j: \alpha k)} = - \frac{m_\alpha}{4} (1 - \varepsilon_{\alpha\alpha})^2 \left(u_i^{(\alpha j, \alpha k)} \hat{r}_i^{(\alpha j, \alpha k)} \right)^2 \quad (6.12)$$

$$\Delta E^{(\alpha j: \beta k)} = - \frac{m_\alpha m_\beta (1 + \varepsilon_{\alpha\beta})}{2(m_\alpha + m_\beta)} \left(\frac{m_\beta (1 + \varepsilon_{\alpha\beta})}{m_\alpha + m_\beta} \left(u_l^{(\alpha j, \beta k)} \hat{r}_l^{(\alpha j, \beta k)} \right)^2 - \left(2 u_i^{(\alpha j)} \hat{r}_i^{(\alpha j, \beta k)} u_l^{(\alpha j, \beta k)} \hat{r}_l^{(\alpha j, \beta k)} \right) \right). \quad (6.13)$$

Fortunately, the results of the operator for intraphase particles $\Delta E^{(\alpha j:\alpha k)}$ is well known, and yields Haff's law (Haff, 1983) when the entire formalism is carried out. The second equation can also be broken down further, into the the first piece that looks a great deal like the intraphase term and a term that depends on the raw particle velocity. We will carry out the integration for both these terms differently. To close the set of macroscopic equations, we will have to find a way to reduce the number of integrals and then evaluate the remaining ones explicitly.

6.2.3 The Kinetic Integrals

Formally, we must define how to carry out these integrals such that they properly define the evolution of some average quantity. This has been done previously for the monodisperse case (van Noije et al., 1998a). This may be straightforwardly extended to a bidisperse case by extending the number of variables. The kinetic integrals for some macroscopic quantity A take the form

$$\left\langle \frac{dA}{dt} \right\rangle = \int d\Gamma \rho(\Gamma; 0) \frac{dA(\Gamma(t))}{dt} = \int d\Gamma \rho(\Gamma; 0) i\mathcal{L}^+ A(\Gamma). \quad (6.14)$$

Here we only require the initial time ensemble distribution $\rho(\Gamma; 0)$. The phase space over which we are integrating and the integral are then

$$\Gamma = \{r_i^{(\alpha 1)}, r_i^{(\alpha 2)}, \dots, r_i^{(\alpha N_\alpha)}; u_i^{(\alpha 1)}, u_i^{(\alpha 2)}, \dots, u_i^{(\alpha N_\alpha)}; r_i^{(\beta 1)}, r_i^{(\beta 2)}, \dots, r_i^{(\beta N_\beta)}; u_i^{(\beta 1)}, u_i^{(\beta 2)}, \dots, u_i^{(\beta N_\beta)}\} \quad (6.15)$$

$$\int d\Gamma = \int \prod_{\mu \in \alpha j \cup \beta k} \left(dr_i^{(\mu)} dv_j^{(\mu)} \right) \prod_{\kappa < \mu} \Theta(|r_i^{\mu\kappa} - a_\mu - a_\kappa|). \quad (6.16)$$

This integral integrates over all positions and velocities of all the particles in the α and β phases in the phase space. The Heaviside function also restricts the integral to only regions that are dynamically defined, i.e. particles cannot overlap. In this work we will restrict ourselves to a Maxwellian particle distribution (as discussed in the introduction), though this method will work in general for any ensemble distribution. For completeness, we give that distribution as

$$\rho(\Gamma; 0) = \frac{1}{V^{N_\alpha + N_\beta}} \left(\frac{1}{2\pi T^{(\alpha)}} \right)^{\frac{3N_\alpha}{2}} \left(\frac{1}{2\pi T^{(\beta)}} \right)^{\frac{3N_\beta}{2}} \times \exp \left(\frac{-\sum_{\alpha j=1}^{N_\alpha} \left(u_i^{(\alpha j)} - \langle u_i^{(\alpha)} \rangle \right)^2}{2T^{(\alpha)}} + \frac{-\sum_{\beta k=1}^{N_\beta} \left(u_i^{(\beta k)} - \langle u_i^{(\beta)} \rangle \right)^2}{2T^{(\beta)}} \right). \quad (6.17)$$

Now that the integrals and operators have been satisfactorily defined, we can begin to manipulate the equations and begin integrating. The procedure for reducing this high dimensional integral to a 6-dimensional integral is well documented, (Müller and Luding, 2011; Luding et al., 1998). Note that the operators are unaffected by this dimensional reduction. Here we give the result for the term $\frac{d\langle w_i^{(\alpha\beta)} \rangle}{dt}$

$$\frac{d\langle w_i^{(\alpha\beta)} \rangle}{dt} = N_\alpha n_\beta \left(\frac{1}{2\pi (T^{(\alpha)} + T^{(\beta)})} \right)^{\frac{3}{2}} \int dr_i^{(\alpha\beta)} du_i^{(\alpha\beta)} \exp \left(\frac{\left(u_i^{(\alpha\beta)} - \langle v_i^{(\alpha\beta)} \rangle \right)^2}{2(T^{(\alpha)} + T^{(\beta)})} \right) \times g \left(r_i^{(\alpha\beta)} \right) \Theta \left(-u_i^{(\alpha\beta)} \hat{r}_i^{(\alpha\beta)} \right) \delta \left(\left| r_i^{(\alpha\beta)} \right| - a_\alpha + a_\beta \right) \left| u_i^{(\alpha\beta)} \hat{r}_i^{(\alpha\beta)} \right| \Delta w_i^{(\alpha\beta)}. \quad (6.18)$$

Here the term $g \left(r_i^{(\alpha\beta)} \right)$ arises as the density of pairs in contact, we will also make the additional assumption here that the mean counter flow of unlike particles does not significantly alter the pair contact density from equilibrium values. The integration procedure is identical for nearly all of the operators we have discussed, with exception to the second term in Eq. 6.13. This term is somewhat different, because it does not depend exclusively on quantities in the relative frame. There we must carry out some explicit integration to get it into the form we require. The integral in $u_i^{(\alpha)}$ takes the form

$$\frac{N_\alpha m_\alpha n_\beta m_\beta}{m_\alpha + m_\beta} (1 + \varepsilon_{\alpha\beta}) \left(\frac{1}{2\pi T^{(\alpha)}} \right)^{\frac{3}{2}} \left(\frac{1}{2\pi T^{(\beta)}} \right)^{\frac{3}{2}} \int dr_i^{(\alpha\beta)} du_i^{(\alpha)} du_i^{(\alpha\beta)} \times \exp \left(-\frac{\left(u_i^{(\alpha)} - \langle u_i^{(\alpha)} \rangle \right)^2}{2T^{(\alpha)}} - \frac{\left(u_i^{(\alpha\beta)} + u_i^{(\alpha)} - \langle u_i^{(\beta)} \rangle \right)^2}{2T^{(\beta)}} \right) g \left(r_i^{(\alpha\beta)} \right) \Theta \left(-u_i^{(\alpha\beta)} \hat{r}_i^{(\alpha\beta)} \right) \times \delta \left(\left| r_i^{(\alpha\beta)} \right| - a_\alpha + a_\beta \right) \left| u_i^{(\alpha\beta)} \hat{r}_i^{(\alpha\beta)} \right| \left(u_i^{(\alpha\beta)} \hat{r}_i^{(\alpha\beta)} \right) u_i^{(\alpha)} \hat{r}_i^{(\alpha\beta)}. \quad (6.19)$$

Integrating over $u_i^{(\alpha)}$ we obtain

$$\begin{aligned}
& \left(\frac{1}{2\pi T^{(\alpha)}} \right)^{\frac{3}{2}} \left(\frac{1}{2\pi T^{(\beta)}} \right)^{\frac{3}{2}} \int_{-\infty}^{\infty} du_i^{(\alpha)} u_i^{(\alpha)} r_l^{(\alpha\beta)} \exp \left(-\frac{\left(u_i^{(\alpha)} - \langle u_i^{(\alpha)} \rangle \right)^2}{2T^{(\alpha)}} - \frac{\left(u_i^{(\alpha\beta)} + u_i^{(\alpha)} - \langle u_i^{(\beta)} \rangle \right)^2}{2T^{(\beta)}} \right) \\
&= \frac{1}{2\sqrt{2}\pi^{\frac{3}{2}} (T^{(\alpha)} + T^{(\beta)})^{\frac{3}{2}}} \exp \left(\frac{\left(u_i^{(\alpha\beta)} - \langle v_i^{(\alpha\beta)} \rangle \right)^2}{2(T^{(\alpha)} + T^{(\beta)})} \right) \\
&\times \left(\langle u_i^{(\alpha)} \rangle \hat{r}_l^{(\alpha\beta)} + \frac{\langle v_l^{(\alpha\beta)} \rangle \hat{r}_l^{(\alpha\beta)} T^{(\alpha)}}{T^{(\alpha)} + T^{(\beta)}} - \frac{u_l^{(\alpha\beta)} \hat{r}_l^{(\alpha\beta)} T^{(\alpha)}}{T^{(\alpha)} + T^{(\beta)}} \right).
\end{aligned} \tag{6.20}$$

All three of these terms in the last set of parentheses represent different processes. The first term on the last line $\langle u_i^{(\alpha)} \rangle \hat{r}_l^{(\alpha\beta)}$ we have already seen in the macroscopic equation Eq. 6.4 and is the kinetic energy in the center of mass. This piece does not affect the evolution of the granular temperature. The second term that depends explicitly on $\langle v_l^{(\alpha\beta)} \rangle$ represents the heating term, which comes from the friction felt as the two phases flow against one another. The resultant integral for these first two terms is of the same form as that seen in for the slip between particulate phases. Note that the amount of energy supplied to the α and β phases is different. The last term is the partitioning term that determines how much of the energy loss in the collisions between unlike particles comes from the α phase. This resultant integral takes the same form as the first term in Eq. 6.13. Fortunately, this shows that there are actually only two new sets of integrals that need to be performed to obtain both the energy and slip equations. We will now break up the energy equation equation in the following way

$$\frac{d\langle E^{(\alpha)} \rangle}{dt} = \frac{d\langle E_{CM}^{(\alpha)} \rangle}{dt} + \frac{d\langle E_{Haff}^{(\alpha)} \rangle}{dt} + \frac{d\langle E_{Inter}^{(\alpha)} \rangle}{dt} + \frac{d\langle E_{partition}^{(\alpha)} \rangle}{dt} + \frac{d\langle E_{Heat}^{(\alpha)} \rangle}{dt} \tag{6.21}$$

Now that we have broken down the energy equation into recognizable macroscopic effects, we can move forward to evaluating the last set of integrals. The integrals will have to be evaluated in spherical coordinates. The problem that we are solving is not isotropic but still axisymmetric. This axisymmetry allows us to simplify the integrals in spherical

coordinates. The change of variables produces the differential relationship $dr_i^{(\alpha\beta)} du_i^{(\alpha\beta)} = u_r^2 r^2 |\sin(\theta)| |\sin(\theta_u)| du_r dr d\theta_u d\theta d\phi_u d\phi$. The velocity components are $\{u_r, \theta_u, \phi_u\}$. The change of variables for both the velocity and spatial components follows

$$u_1^{(\alpha\beta)} = u_r \sin \theta_u \cos \phi_u \quad (6.22)$$

$$u_2^{(\alpha\beta)} = u_r \sin \theta_u \sin \phi_u \quad (6.23)$$

$$u_3^{(\alpha\beta)} = u_r \cos \theta_u. \quad (6.24)$$

The simplest geometry of the mean counter-flow that we can give, in terms of equation simplicity, is with the mean slip between the two phases being aligned with the $\hat{r}_3^{(\alpha\beta)}$ -direction. Note that solving the equations in this geometry is not limiting, as the eventual vector equation can be rotated using rotation matrices. In this case the final two sets of integrals that appear in multiple terms are

$$\begin{aligned} \frac{d\langle w_i^{(\alpha\beta)} \rangle}{dt} = & -N_\alpha n_\beta (1 + \varepsilon_{\alpha\beta}) \left(\frac{1}{2\pi (T^{(\alpha)} + T^{(\beta)})} \right)^{\frac{3}{2}} \int dr du_r d\theta d\theta_u d\phi d\phi_u \\ & \times r^2 u_r^2 |\sin \theta| |\sin \theta_u| \exp \left(\frac{-u_r^2 - \langle v_3^{(\alpha\beta)} \rangle^2 + 2u_r \langle v_3^{(\alpha\beta)} \rangle \cos \theta_u}{2 (T^{(\alpha)} + T^{(\beta)})} \right) \\ & \times g(r) \Theta \left(-u_i^{(\alpha\beta)} \hat{r}_i^{(\alpha\beta)} \right) \delta (|r| - a_\alpha + a_\beta) |u_r (\sin \theta \sin \theta_u \cos (\phi - \phi_u) + \cos \theta \cos \theta_u)| \\ & (u_r (\sin \theta \sin \theta_u \cos (\phi - \phi_u) + \cos \theta \cos \theta_u)) \cos \theta \hat{r}_3^{(\alpha\beta)} \end{aligned} \quad (6.25)$$

$$\begin{aligned} \frac{d\langle E_{Inter}^{(\alpha)} \rangle}{dt} = & -\frac{N_\alpha n_\beta m_\alpha m_\beta^2 (1 + \varepsilon_{\alpha\beta})^2}{2 (m_\alpha + m_\beta)^2} \left(\frac{1}{2\pi (T^{(\alpha)} + T^{(\beta)})} \right)^{\frac{3}{2}} \int dr du_r d\theta d\theta_u d\phi d\phi_u \\ & \times r^2 u_r^2 |\sin \theta| |\sin \theta_u| \exp \left(\frac{-u_r^2 - \langle v_3^{(\alpha\beta)} \rangle^2 + 2u_r \langle v_3^{(\alpha\beta)} \rangle \cos \theta_u}{2 (T^{(\alpha)} + T^{(\beta)})} \right) \\ & \times g(r) \Theta \left(-u_i^{(\alpha\beta)} \hat{r}_i^{(\alpha\beta)} \right) \delta (|r| - a_\alpha + a_\beta) |u_r (\sin \theta \sin \theta_u \cos (\phi - \phi_u) + \cos \theta \cos \theta_u)| \\ & (u_r (\sin \theta \sin \theta_u \cos (\phi - \phi_u) + \cos \theta \cos \theta_u))^2. \end{aligned} \quad (6.26)$$

6.2.4 Momentum Transfer

The slip equation is obtained by using the relationships between the operators in Eqs. 6.9 and 6.10 with Eq. 6.3. Before writing we have also made a few additional alterations to the equation. Namely, we have integrated out the radial component of the separation vector and completed the square within the exponential to simplify the trigonometric terms. Additionally, the velocity magnitudes u_r have been collected. Note that u_r is strictly non-negative. The momentum equation is then

$$\begin{aligned}
\frac{d\langle v_i^{(\alpha\beta)} \rangle}{dt} &= - (a_\alpha + a_\beta)^2 g_c^{\alpha\beta} (1 + \varepsilon_{\alpha\beta}) \frac{n_\alpha m_\alpha + n_\beta m_\beta}{m_\alpha + m_\beta} \left(\frac{1}{2\pi (T^{(\alpha)} + T^{(\beta)})} \right)^{\frac{3}{2}} \int du_r d\theta d\theta_u d\phi d\phi_u \\
&\times u_r^4 |\sin \theta| |\sin \theta_u| \exp \left(\frac{- \left(u_r - \langle v_3^{(\alpha\beta)} \rangle \cos \theta_u \right)^2}{2 (T^{(\alpha)} + T^{(\beta)})} \right) \exp \left(\frac{- \left(\langle v_3^{(\alpha\beta)} \rangle \sin \theta_u \right)^2}{2 (T^{(\alpha)} + T^{(\beta)})} \right) \\
&\times \Theta \left(-u_i^{(\alpha\beta)} \hat{r}_i^{(\alpha\beta)} \right) |(\sin \theta \sin \theta_u \cos (\phi - \phi_u) + \cos \theta \cos \theta_u)| \\
&(\sin \theta \sin \theta_u \cos (\phi - \phi_u) + \cos \theta \cos \theta_u) \cos \theta \hat{r}_3^{(\alpha\beta)} \\
&= - (a_\alpha + a_\beta)^2 g_c^{\alpha\beta} (1 + \varepsilon_{\alpha\beta}) \frac{n_\alpha m_\alpha + n_\beta m_\beta}{m_\alpha + m_\beta} I \left(\langle v_3^{(\alpha\beta)} \rangle, T^{(\alpha)} + T^{(\beta)} \right).
\end{aligned} \tag{6.27}$$

Here $g_c^{\alpha\beta}$ is the radial distribution function (RDF) at contact for the mixture, with no directional effects. We also introduce the generic integral $I_1 \left(\langle v_3^{(\alpha\beta)} \rangle, T^{(\alpha)} + T^{(\beta)} \right)$, which also appears in terms in the energy equation. In this form, we can easily integrate out the magnitude importance as we only have to find an integral of the form $\int_0^\infty dx x^4 \exp(-(x - y)/2\sigma)$. The resultant integral equation, containing only trigonometric terms, is

$$\begin{aligned}
I_1 = & \left(\frac{1}{2\pi (T^{(\alpha)} + T^{(\beta)})} \right)^{\frac{1}{2}} \int d\theta d\theta_u d\phi_u \\
& \times \Theta \left(-u_i^{(\alpha\beta)} \hat{r}_i^{(\alpha\beta)} \right) |\sin \theta| |\sin \theta_u| |(\sin \theta \sin \theta_u \cos(\phi_u) + \cos \theta \cos \theta_u)| \\
& (\sin \theta \sin \theta_u \cos(\phi_u) + \cos \theta \cos \theta_u) \cos \theta \hat{r}_3^{(\alpha\beta)} \\
& \times \left[\exp \left(\frac{-\langle v_3^{(\alpha\beta)} \rangle^2}{2(T^{(\alpha)} + T^{(\beta)})} \right) \left(5(T^{(\alpha)} + T^{(\beta)}) + (\langle v_3^{(\alpha\beta)} \rangle \cos \theta_u)^3 \right) \right. \\
& + \sqrt{\frac{\pi}{2}} \exp \left(\frac{-\left(\langle v_3^{(\alpha\beta)} \rangle \sin \theta_u \right)^2}{2(T^{(\alpha)} + T^{(\beta)})} \right) \left(1 + \operatorname{erf} \left(\frac{\langle v_3^{(\alpha\beta)} \rangle \cos \theta_u}{\sqrt{2(T^{(\alpha)} + T^{(\beta)})}} \right) \right) \\
& \left. \times \left(3(T^{(\alpha)} + T^{(\beta)})^{\frac{3}{2}} + 6(T^{(\alpha)} + T^{(\beta)})^{\frac{1}{2}} (\langle v_3^{(\alpha\beta)} \rangle \cos \theta_u)^2 + \frac{(\langle v_3^{(\alpha\beta)} \rangle \cos \theta_u)^4}{(T^{(\alpha)} + T^{(\beta)})^{\frac{1}{2}}} \right) \right].
\end{aligned} \tag{6.28}$$

Note that we have also integrated out the angle ϕ , due to azimuthal symmetry and contributes only a factor of 2π to the equation. In order to simplify notation, we will refer to the last 3 lines, which depend only on θ_u , as $K_1(\theta_u)$. This equation has become exceptionally complex in appearance. However, there is another degree of complexity hidden in the limits of the remaining integrals imposed by the Heaviside function and the absolute values. We must break up the domain in phase space that we integrate over such that 3 criteria are satisfied.

1. The signs of $\sin \theta_u$ **and** $\sin \theta$ must be the same over the entire sub-domain.
2. The particles must always be approaching, that is $\sin \theta \sin \theta_u \cos(\phi_u) + \cos \theta \cos \theta_u \leq 0$.

The first two pieces are trivially satisfied, if we restrict ourselves to values of θ and θ_u in $(0, \pi)$. The last piece may be trivially satisfied in isotropic cases, and is much simpler to address in two dimensions. When polar or azimuthal symmetry is not present, evaluation becomes more complex. A graphical interpretation of the integration is given in Fig. 6.3.

We will set the limits of integration such that they satisfy the inequality. The slip equation is

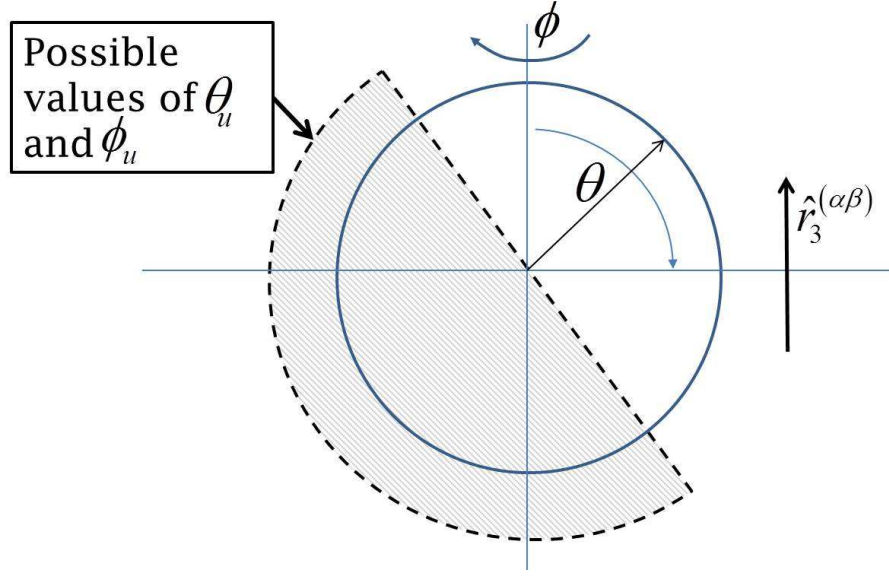


Figure 6.3 A graphical illustration of the domain in phase space over which integration will occur. For a given angle θ only some combinations of θ_u and ϕ_u allow collisions to occur. This leads to complicated expressions in the limits of integration. Note that the physical sphere that we are integrating over has a radius of $a_\alpha + a_\beta$, which is where contact takes place.

$$I_1 = -2 \left(\frac{1}{2\pi (T^{(\alpha)} + T^{(\beta)})} \right)^{\frac{1}{2}} \int_0^\pi \int_0^\pi \int_{\arccos(-\cot \theta \cot \theta_u)}^\pi d\phi_u d\theta d\theta_u \sin \theta \sin \theta_u \cos \theta K_1(\theta_u) \\ \times (\sin \theta \sin \theta_u \cos(\phi_u) + \cos \theta \cos \theta_u)^2 \hat{r}_3^{(\alpha\beta)}. \quad (6.29)$$

Here we have taken advantage of azimuthal symmetry to simplify the upper limit in ϕ_u , which introduces a factor of 2. The factor of -1 arose from the terms inside of the absolute value, which are negative everywhere inside the integral limits. From here we must more straightforwardly evaluate the integrals to obtain the final form of the slip evolution equation. The integration work beyond this point is left for future work.

6.2.5 Energy Balance

To complete the energy equation we must carry out the additional integration from Eq. 6.26. After applying the same tricks used to obtain Eq. 6.27, the equation for the rate of

interphase energy loss is

$$\begin{aligned}
\frac{d\langle E_{inter}^{(\alpha)} \rangle}{dt} &= - (a_\alpha + a_\beta)^2 g_c^{\alpha\beta} \frac{N_\alpha m_\alpha n_\beta m_\beta^2 (1 + \varepsilon_{\alpha\beta})^2}{2 (m_\alpha + m_\beta)^2} \left(\frac{1}{2\pi (T^{(\alpha)} + T^{(\beta)})} \right)^{\frac{3}{2}} \int du_r d\theta d\theta_u d\phi d\phi_u \\
&\times u_r^5 |\sin \theta| |\sin \theta_u| \exp \left(\frac{- (u_r - \langle v_3^{(\alpha\beta)} \rangle \cos \theta_u)^2}{2 (T^{(\alpha)} + T^{(\beta)})} \right) \exp \left(\frac{- (\langle v_3^{(\alpha\beta)} \rangle \sin \theta_u)^2}{2 (T^{(\alpha)} + T^{(\beta)})} \right) \\
&\times \Theta \left(-u_i^{(\alpha\beta)} \hat{r}_i^{(\alpha\beta)} \right) |(\sin \theta \sin \theta_u \cos (\phi - \phi_u) + \cos \theta \cos \theta_u)| \\
&\times (\sin \theta \sin \theta_u \cos (\phi - \phi_u) + \cos \theta \cos \theta_u)^2 \\
&= - (a_\alpha + a_\beta)^2 g_c^{\alpha\beta} \frac{N_\alpha m_\alpha n_\beta m_\beta^2 (1 + \varepsilon_{\alpha\beta})^2}{2 (m_\alpha + m_\beta)^2} I_2 \left(\langle v_3^{(\alpha\beta)} \rangle, T^{(\alpha)} + T^{(\beta)} \right).
\end{aligned} \tag{6.30}$$

Here again, we opt for the simplified and more general integral to treat without it's pre-multipliers, $I_2 \left(\langle v_3^{(\alpha\beta)} \rangle, T^{(\alpha)} + T^{(\beta)} \right)$. Integration over the radial component of the velocity and the physical azimuthal angle ϕ then yields a more complex equation

$$\begin{aligned}
I_2 &= \left(\frac{1}{2\pi (T^{(\alpha)} + T^{(\beta)})} \right)^{\frac{1}{2}} \int d\theta d\theta_u d\phi_u \\
&\times |\sin \theta| |\sin \theta_u| \Theta \left(-u_i^{(\alpha\beta)} \hat{r}_i^{(\alpha\beta)} \right) |(\sin \theta \sin \theta_u \cos \phi_u + \cos \theta \cos \theta_u)| \\
&\times (\sin \theta \sin \theta_u \cos \phi_u + \cos \theta \cos \theta_u)^2 \\
&\times \left[\exp \left(\frac{- \langle v_3^{(\alpha\beta)} \rangle^2}{2 (T^{(\alpha)} + T^{(\beta)})} \right) \left(8 (T^{(\alpha)} + T^{(\beta)})^2 + 9 (T^{(\alpha)} + T^{(\beta)}) \left(\langle v_3^{(\alpha\beta)} \rangle \cos \theta_u \right)^2 \right. \right. \\
&+ \left. \left(\langle v_3^{(\alpha\beta)} \rangle \cos \theta_u \right)^4 \right) + \sqrt{\frac{\pi}{2}} \exp \left(\frac{- (\langle v_3^{(\alpha\beta)} \rangle \sin \theta_u)^2}{2 (T^{(\alpha)} + T^{(\beta)})} \right) \\
&\times \left(1 + \operatorname{erf} \left(\frac{\langle v_3^{(\alpha\beta)} \rangle \cos \theta_u}{\sqrt{2 (T^{(\alpha)} + T^{(\beta)})}} \right) \right) \left(15 (T^{(\alpha)} + T^{(\beta)})^{\frac{3}{2}} \langle v_3^{(\alpha\beta)} \rangle \cos \theta_u \right. \\
&+ \left. \left. 10 (T^{(\alpha)} + T^{(\beta)})^{\frac{1}{2}} \left(\langle v_3^{(\alpha\beta)} \rangle \cos \theta_u \right)^3 + \frac{\left(\langle v_3^{(\alpha\beta)} \rangle \cos \theta_u \right)^5}{(T^{(\alpha)} + T^{(\beta)})^{\frac{1}{2}}} \right) \right].
\end{aligned} \tag{6.31}$$

We again take the last four lines of the expression in 6.31, which depend only on θ_u , and refer to it as $K_2(\theta_u)$. Now the limits of integration can be given explicitly using the same tricks as before.

$$I_2 = -2 \left(\frac{1}{2\pi (T^{(\alpha)} + T^{(\beta)})} \right)^{\frac{1}{2}} \int_0^\pi \int_0^\pi \int_{\arccos(-\cot\theta \cot\theta_u)}^\pi d\theta d\theta_u d\phi_u \sin\theta \sin\theta_u K_2(\theta_u) \quad (6.32)$$

$$\times (\sin\theta \sin\theta_u \cos(\phi_u) + \cos\theta \cos\theta_u)^3.$$

The additional integration will be left for future work. We reiterate that after the integrals in Eqs. 6.29 and 6.32 are fully evaluated, every term in the evolution equations for the 0th-2nd moments will be known.

6.3 Future Work

There are a few next steps that remain to be carried out on this project. First, the two remaining integrals must be fully evaluated to obtain the necessary terms in the energy and slip equations. Secondly, the terms in the evolution equations will be compared with existing works, appropriate for different Mach numbers (Syamlal, 1987; Jenkins and Mancini, 1987, 1989; Marchisio and Fox, 2013; Gourdel et al., 1998, 1999; Batrak et al., 2005). The aim of this exercise will also be to emphasize the differences between the current work and existing approaches and also understand where different descriptions produce similar and dissimilar answers.

The next step will be to compare predictions with simulation data. At least three cases will be considered using DEM. Firstly, the accuracy of the interphase exchange and cooling terms will be assessed by producing granular gases consisting of two different particle sizes. Next the accuracy of the drag terms will be assessed by setting up a granular gas with a mean slip between phases. The temperature and slip in this case like the bidispersed granular gas will be transient. Lastly, a steady mismatch in an applied body force will be applied to each phase, which will allow us to study the obtained steady states in detail. The last and most important step will be a comparison with PR-DNS, which is much more expensive compared to DEM. There a mean slip between the center of mass of the two particle phases and the fluid phase

will be maintained. The evolution of the slip will then be compared with the predictions of the drag law developed herein coupled to a recent polydispersed drag model (Mehrabadi et al., 2016b).

6.4 Bibliography

- Aarons, L. and Sundaresan, S. (2006). Shear flow of assemblies of cohesive and non-cohesive granular materials. *Powder Technology*, 169(1):10–21.
- Abbasfard, H., Evans, G., and Moreno-Atanasio, R. (2016). Effect of van der Waals force cut-off distance on adhesive collision parameters in DEM simulation. *Powder Technology*, 299:9–18.
- Afferrante, L., Ciavarella, M., and Demelio, G. (2015). Adhesive contact of the weierstrass profile. In *Proc. R. Soc. A*, volume 471, page 20150248. The Royal Society.
- Aitcin, P. (2000). Cements of yesterday and today - concrete of tomorrow. *Cement and Concrete Research*, 31(9):1349–1359.
- Alam, M., Trujillo, L., and Herrmann, H. (2006). Hydrodynamic theory for reverse brazil nut segregation and the non-monotonic ascension dynamics. *Journal of Statistical Physics*, 124:587–623.
- Bagnold, R. A. (1954). Experiments on a gravity-free dispersion of large solid spheres in a newtonian fluid under shear. In *Proceedings of the Royal Society of London A: Mathematical, Physical and Engineering Sciences*, volume 225, pages 49–63. The Royal Society.
- Ball, R. and Melrose, J. (1997). A simulation technique for many spheres in quasi-static motion under frame-invariant pair drag and brownian forces. *Physica A*, 247:444–472.
- Baranyai, A. and Evans, D. (1989). Direct entropy calculation from computer-simulation of liquids. *Physical Review A*, 40(7):3817–3822.

- Batrak, O., Patino, G., Simonin, O., Flour, I., Le Guevel, T., and Perez, E. (2005). Unlike particles size collision model in 3d unsteady polydispersed simulation of circulating fluidized bed. *8th Annual Conference on Fluidized Bed Technology*, 315.
- Bec, J., Biferale, L., Cencini, M., Lanotte, A., and Toschi, F. (2010). Intermittency in the velocity distribution of heavy particles in turbulence. *Journal of Fluid Mechanics*, 646:527–536.
- Beetstra, R., van der Hoef, M., and Kuipers, J. (2007). Drag force of intermediate reynolds number flows past mono- and bidisperse arrays of spheres. *AIChE Journal*, 53:489.
- Bentz, D., Ferraris, C., Galler, M., Hansen, A., and Guynn, J. (2012). Influence of particle size distributions on yield stress and viscosity of cement-fly ash pastes. *Cement and Concrete Research*, 42(2):404–409.
- Bentz, D. P., Garboczi, E. J., Haecker, C. J., and Jensen, O. M. (1999). Effects of cement particle size distribution on performance properties of portland cement-based materials. *Cement and Concrete Research*, 29:1663–1671.
- Berger, N., Azéma, E., Douce, J.-F., and Radjai, F. (2016). Scaling behaviour of cohesive granular flows. *EPL (Europhysics Letters)*, 112(6):64004.
- Berzi, D. and Jenkins, J. T. (2015a). Inertial shear bands in granular materials. *Physics of Fluids*, 27:033303.
- Berzi, D. and Jenkins, J. T. (2015b). Steady shearing flows of deformable, inelastic spheres. *Soft matter*, 11(24):4799–4808.
- Binnig, G., Quate, C. F., and Gerber, C. (1986). Atomic force microscope. *Physical review letters*, 56(9):930.
- Blum, J., Wurm, G., Kempf, S., Poppe, T., Klahr, H., Kozasa, T., Rott, M., Henning, T., Dorschner, J., Schrapler, R., Keller, H., Markiewicz, W., Mann, I., Gustafson, B., Giovane, F., Neuhaus, D., Fechtig, H., Grun, E., Feuerbacher, B., Kochan, H., Ratke, L., El Goresy, A.,

- Morfill, G., Weidenschilling, S., Schwehm, G., Metzler, K., and Ip, W. (2000). Growth and form of planetary seedlings: Results from a microgravity aggregation experiment. *Physical Review Letters*, 85(12):2426–2429.
- Bradley, R. S. (1932). Lxxix. the cohesive force between solid surfaces and the surface energy of solids. *The London, Edinburgh, and Dublin Philosophical Magazine and Journal of Science*, 13(86):853–862.
- Brady, J. F. and Bossis, G. (1988). Stokesian dynamics. *Annual Reviews of Fluid Mechanics*, 20:111–157.
- Bragg, A. D. and Collins, L. R. (2014a). New insights from comparing statistical theories for inertial particles in turbulence: I. spatial distribution of particles. *New Journal of Physics*, 16:055013.
- Bragg, A. D. and Collins, L. R. (2014b). New insights from comparing statistical theories for inertial particles in turbulence: II. relative velocities. *New Journal of Physics*, 16:055014.
- Bragg, A. D., Ireland, P. J., and Collins, L. R. (2015). On the relationship between the non-local clustering mechanism and preferential concentration. *Journal of Fluid Mechanics*, 780:327–343.
- Brewster, R., Grest, G. S., Landry, J. W., and Levine, A. J. (2005). Plug flow and the breakdown of bagnold scaling in cohesive granular flows. *Physical Review E*, 72(6):061301.
- Bridges, F. G., Supulver, K. D., Lin, D., Knight, R., and Zafra, M. (1996). Energy loss and sticking mechanisms in particle aggregation in planetesimal formation. *Icarus*, 123(2):422–435.
- Brilliantov, N. V., Albers, N., Spahn, F., and Pöschel, T. (2007). Collision dynamics of granular particles with adhesion. *Physical Review E*, 76(5):051302.
- Brilliantov, N. V. and Pöschel, T. (2004). Collision of adhesive viscoelastic particles. *HINRICHSEN:GRANULAR MEDIA O-BK*, pages 189–209.

- Brilliantov, N. V. and Pöschel, T. (2004). *Kinetic Theory of Granular Gases*. Oxford University Press, New York.
- Brilliantov, N. V., Spahn, F., Hertzsch, J.-M., and Pöschel, T. (1996). Model for collisions in granular gases. *Physical review E*, 53(5):5382.
- Brito, R. and Ernst, M. (1998). Extension of haff's cooling law in granular flows. *Europhysics Letters*, 43(5):497.
- Campbell, C. S. (2002). Granular shear flows at the elastic limit. *Journal of fluid mechanics*, 465:261–291.
- Capecelatro, J., Desjardins, O., and Fox, R. O. (2014). Numerical study of collisional particle dynamics in cluster-induced turbulence. *Journal of Fluid Mechanics*, 747:R2.
- Capecelatro, J., Desjardins, O., and Fox, R. O. (2015). On fluid-particle dynamics in fully developed cluster-induced turbulence. *Journal of Fluid Mechanics*, 780:578–635.
- Capecelatro, J., Desjardins, O., and Fox, R. O. (2016). Strongly coupled fluid-particle flows in vertical channels. ii. turbulence modeling. *Physics of Fluids*, 28:033307.
- Carnahan, N. and Starling, K. (1969). Equation of state for nonattractive rigid spheres. *Journal of Chemical Physics*, 51(2):635–636.
- Castellanos, A., Valverde, J. M., Pérez, A. T., Ramos, A., and Watson, P. K. (1999). Flow regimes in fine cohesive powders. *Physical Review Letters*, 82(6):1156.
- Cates, M., Wittmer, J., Bouchaud, J., and Claudin, P. (1998a). Jamming and static stress transmission in granular materials. *Chaos*, 9(3):511–522.
- Cates, M., Wittmer, J., Bouchaud, J., and Claudin, P. (1998b). Jamming, force chains, and fragile matter. *Physical Review Letters*, 81(9):1841–1844.
- Chew, J. W., Parker, D. M., Cocco, R. A., and Hrenya, C. M. (2011). Cluster characteristics of continuous size distributions and binary mixtures of group b particles in dilute riser flow. *Chemical Engineering Journal*, 178:348–358.

- Chialvo, S., Sun, J., and Sundaresan, S. (2012). Bridging the rheology of granular flows in three regimes. *Physical Review E*, 85(2):021305.
- Chun, J., Koch, D. L., Rani, S. L., Ahluwalia, A., and Collins, L. R. (2005). Clustering of aerosol particles in isotropic turbulence. *Journal of Fluid Mechanics*, 536:219–251.
- Cleary, P. W. and Sawley, M. L. (2002). DEM modelling of industrial granular flows: 3D case studies and the effect of particle shape on hopper discharge. *Applied Mathematical Modelling*, 26(2):89–111.
- Cocco, R., Shaffer, F., Hays, R., Karri, S. R., and Knowlton, T. (2010). Particle clusters in and above fluidized beds. *Powder Technology*, 203:3–11.
- Colwell, J., Batiste, S., Horányi, M., Robertson, S., and Sture, S. (2007). Lunar surface: Dust dynamics and regolith mechanics. *Reviews of Geophysics*, 45(2):RG2006.
- Cundall, P. and Strack, O. (1979a). A discrete numerical model for granular assemblies. *Geotechnique*, 29(1):47–65.
- Cundall, P. A. and Strack, O. D. (1979b). A discrete numerical model for granular assemblies. *Geotechnique*, 29(1):47–65.
- Dahneke, B. (1975). Further measurements of the bouncing of small latex spheres. *Journal of Colloid and Interface Science*, 51(1):58–65.
- Daley, D. and Vere-Jones, D. (1988). *An introduction to the theory of point processes*. Springer-Verlag.
- DeCicco, A. and Hartzell, C. (2016). System-level design considerations for asteroid despin via neutral beam emitting spacecraft. In *IEEE Aerospace Conference Proceedings (Big Sky, MT)*.
- Derjaguin, B., Muller, V., and Toporov, Y. (1975). Effect of contact deformations on the adhesion of particles. *Journal of Colloid and Interface Science*, 53(2):314–326.

- Di Renzo, A. and Di Maio, F. P. (2004). Comparison of contact-force models for the simulation of collisions in dem-based granular flow codes. *Chemical Engineering Science*, 59(3):525–541.
- Eaton, J. and Fessler, J. (1994). Preferential concentration of particles by turbulence. *International Journal of Multiphase Flow*, 20:169–209.
- Ernst, M., Dorfman, J., Hoegy, W., and van Leeuwen, J. (1969). Hard-sphere dynamics and binary-collision operators. *Physica*, 45(1):127–146.
- Esipov, S. and Pöschel, T. (1997). The granular phase diagram. *Journal of Statistical Physics*, 86(5/6):1385–1395.
- Ferraris, C., Obla, K., and Hill, R. (2001). The influence of mineral admixtures on the rheology of cement paste and concrete. *Cement and Concrete Research*, 31(2):245–255.
- Fox, R. (2014). On multiphase turbulence models for collisional fluid-particle flows. *Journal of Fluid Mechanics*, 742:368–424.
- Fox, R. O. (2016). Private communication.
- Fullmer, W. D. and Hrenya, C. M. (2016). Quantitative assessment of fine-grid kinetic-theory-based predictions of mean-slip in unbounded fluidization. *AIChE Journal*, 62(1):11–17.
- Galvin, J. E. and Benyahia, S. (2014). The effect of cohesive forces on the fluidization of aeratable powders. *AIChE Journal*, 60(2):473–484.
- Garzo, V., Dufty, J. W., and Hrenya, C. M. (2007a). Enskog theory for polydisperse granular mixtures. i. navier-stokes order transport. *Physical Review E*, 76(3):031303.
- Garzo, V., Fullmer, W. E., Hrenya, C. M., and Yin, X. (2016). Transport coefficients of solid particles immersed in a viscous gas. *Physical Review E*, 93:012905.
- Garzo, V., Hrenya, C. M., and Dufty, J. W. (2007b). Enskog theory for polydisperse granular mixtures. ii. sonine polynomial approximation. *Physical Review E*, 76(3):031304.
- Garzo, V., Tenneti, S., Subramaniam, S., and Hrenya, C. (2012). Enskog kinetic theory for monodisperse gas-solid flows. *Journal of Fluid Mechanics*, 712:129–168.

- Gaume, J., Chambon, G., and Naaim, M. (2011). Quasistatic to inertial transition in granular materials and the role of fluctuations. *Physical Review E*, 84:051304.
- Geldart, D. (1973). Types of gas fluidization. *Powder technology*, 7(5):285–292.
- Gidaspow, D., Jung, J., and Singh, R. K. (2004). Hydrodynamics of fluidization using kinetic theory: an emerging paradigm 2002 flour-daniel lecture. *Powder Technology*, 148:123–141.
- Goldhirsch, I. and Zanetti, G. (1993). Clustering instability in dissipative gases. *Physical Review Letters*, 70(11):1619–1622.
- Goldshtein, A. and Shapiro, M. (1995). Mechanics of collisional motion of granular materials. part 1. general hydrodynamic equations. *Journal of Fluid Mechanics*, 282:75–114.
- Gollin, D., Berzi, D., and Bowman, E. (2017). Extended kinetic theory applied to inclined granular flows: role of boundaries. *Granular Matter*, 19(3):1564–1583.
- Gonzalez, R. G. and Garzo, V. (2016). Instabilities in granular gas-solid flows. *arXiv:1611.03269*.
- Gonzalez, S., Thornton, A., and Luding, S. (2014). Free cooling phase-diagram of hard-spheres with short-and long-range interactions. *The European Physical Journal Special Topics*, 223(11):2205–2225.
- Gourdel, c., Simonin, O., and Brunier, E. (1998). Modelling and simulation of gas-solid turbulent flows with a binary mixture of particles. *Third International Conference on Multiphase Flows*, 315.
- Gourdel, c., Simonin, O., and Brunier, E. (1999). Two-maxwellian equilibrium distribution function for the modelling of a binary mixture of particles. *6th International Conference on Circulating Fluidized Beds*, 315.
- Grierson, D., Flater, E., and Carpick, R. (2005). Accounting for the jkr–dmt transition in adhesion and friction measurements with atomic force microscopy. *Journal of adhesion science and technology*, 19(3-5):291–311.

- Gu, Y., Chialvo, S., and Sundaresan, S. (2014). Rheology of cohesive granular materials across multiple dense-flow regimes. *Physical Review E*, 90(3):032206.
- Gu, Y., Ozel, A., and Sundaresan, S. (2015). A modified cohesion model for CFD–DEM simulations of fluidization. *Powder Technology*, 296:17–28.
- Gu, Y., Ozel, A., and Sundaresan, S. (2016). Numerical studies of the effects of fines on fluidization. *AIChE Journal*.
- Gustavsson, K. and Mehlig, B. (2014a). Clustering of particles falling in a turbulent flow. *Physical Review Letters*, 112:214501.
- Gustavsson, K. and Mehlig, B. (2014b). Relative velocities of inertial particles in turbulent aerosols. *Journal of Turbulence*, 15(1):34–69.
- Gustavsson, K. and Mehlig, B. (2016). Statistical models for spatial patterns of heavy particles in turbulence. *Advances in Physics*, 65(1):1–57.
- Haecker, C., Garboczi, E., J.W., B., Bohn, R., Sun, Z., Shah, S., and Voigt, T. (2005). Modeling the linear elastic properties of portland cement paste. *Cement and Concrete Research*, 35:1948–1960.
- Haff, P. (1983). Grain flow as a fluid-mechanical phenomenon. *Journal of Fluid Mechanics*, 134:401–430.
- Hatzes, A., Bridges, F., Lin, D., and Sachtjen, S. (1991). Coagulation of particles in saturn’s rings: Measurement of the cohesive force of water frost. *Icarus*, 89:113–121.
- Hill, R. J., Koch, D., and Ladd, A. (2001a). The first effects of fluid inertia on flows in ordered and random arrays of spheres. *Journal of Fluid Mechanics*, 448:213–241.
- Hill, R. J., Koch, D., and Ladd, A. (2001b). Moderate-reynolds-number flows in ordered and random arrays of spheres. *Journal of Fluid Mechanics*, 448:243–278.
- Irani, E., Chaudhuri, P., and Heussinger, C. (2014). Impact of attractive interactions on the rheology of dense athermal particles. *Physical Review Letters*, 112:188303.

- Irani, E., Chaudhuri, P., and Heussinger, C. (2016). Athermal rheology of weakly attractive soft particles. *Physical Review E*, 94:052608.
- Israelachvili, J. N. (2011). *Intermolecular and surface forces: revised third edition*. Academic press.
- Iveson, S., Litster, J., Hapgood, K., and Ennis, B. (2001). Nucleation, growth and breakage phenomena in agitated wet granulation processes: a review. *Powder Technology*, 117(1-2):3–39.
- Jenkins, J. and Mancini, F. (1987). Balance laws and constitutive relations for plane flows of a dense, binary mixture of smooth, nearly elastic, circular disks. *Journal of Applied Mechanics*, 1(54):27–34.
- Jenkins, J. and Mancini, F. (1989). Kinetic theory for binary mixtures of smooth, nearly elastic spheres. *Physics of Fluids, A*, 1(12):2050–2057.
- Johnson, K. and Greenwood, J. (1997). An adhesion map for the contact of elastic spheres. *Journal of colloid and interface science*, 192(2):326–333.
- Johnson, K., Kendall, K., and Roberts, A. (1971). Surface energy and the contact of elastic solids. *Proceedings of the Royal Society London A*, 324:301–313.
- Jop, P., Forterre, Y., and Pouliquen, O. (2006). A constitutive law for dense granular flows. *Nature*, 441(7094):727–730.
- Kamrin, K. and Koval, G. (2012). Nonlocal constitutive relation for steady granular flow. *Physical Review Letters*, 108(17):178301.
- Kim, H. and Arastoopour, H. (2002). Extension of kinetic theory to cohesive particle flow. *Powder Technology*, 122(1):83–94.
- Kim, S. and Karrila, S. (1991). *Microhydrodynamics: principles and selected applications*. Butterworth-Heinemann.

- Kobayashi, T., Tanaka, T., Shimada, N., and Kawaguchi, T. (2013). Dem-cfd analysis of fluidization behavior of geldart group a particles using a dynamic adhesion force model. *Powder Technology*, 248:143–152.
- Koch, D. L. (1990). Kinetic theory for a monodisperse gas-solid suspension. *Physics of Fluids A*, 2(10):1711–1723.
- Koch, D. L. and Sangani, A. S. (1999). Particle pressure and marginal stability limits for a homogeneous monodisperse gas-fluidized bed: kinetic theory and numerical simulations. *Journal of Fluid Mechanics*, 400:229–263.
- Kolakaluri, R., Murphy, E., Subramaniam, S., Brown, R., and Fox, R. (2015). Filtration model for polydisperse aerosols in gas-solid flow using granule-resolved direct numerical simulation. *AIChE Journal*, 61(11):3594–3606.
- Kothe, S., Blum, J., Weidling, R., and GÄttler, C. (2013). Free collisions in a microgravity many-particle experiment. iii. the collision behavior of sub-millimeter-sized dust aggregates. *Icarus*, 225:75–85.
- Kulchitsky, A., Johnson, J., Reeves, D., and Wilkinson, A. (2014). Discrete element method simulation of a boulder extraction from an asteroid. In *Proceedings of the 14th ASCE Biennial International Conference on Engineering, Science, Construction, and Operations in Challenging Environments (St. Louis, Missouri, USA,)*, pages 485–494.
- Kumar, A. (2010). *Microscale Dynamics in Suspensions of Non-spherical Particles*. PhD thesis, University of Illinois Urbana-Champaign.
- Kumar, A. and Higdon, J. (2010). Origins of the anomalous stress behavior in charged colloidal suspensions under shear. *Physical Review E*, 82:051401.
- Kuwabara, G. and Kono, K. (1987). Restitution coefficient in a collision between two spheres. *Japanese journal of applied physics*, 26(8R):1230.

- Lanotte, A., Bec, J., Biferale, L., Cencini, M., and Toschi, F. (2011). About scaling properties of relative velocity between heavy particles in turbulence. *Journal of Physics Conference series*, 318:052010.
- Launder, B. (1990). Phenomenological modelling: present... and future? in j.l. lumley (ed.). *Whither Turbulence? Turbulence at a Crossroads*, pages 439–485.
- Lees, A. and Edwards, S. (1972). The computer study of transport processes under extreme conditions. *Journal of Physics C: Solid State Physics*, 5(15):1921.
- Leyvraz (2003). Scaling theory and exactly solved models in the kinetics of irreversible aggregation. *Physics Reports*, 383:92–212.
- Li, J., Cheng, C., Zhang, Z., Yuan, J., Nemet, A., and Fett, F. (1999). The emms model - its application, development and updated concepts. *Chemical Engineering Science*, 54(22):5409–5425.
- Liard, M., Martys, N., George, W., Lootens, D., and Hebraud, P. (2014). Scaling laws for the flow of generalized newtonian suspensions. *Journal of Rheology*, 58:1993–2015.
- Liu, A. J. and Nagel, S. R. (2010). The jamming transition and the marginally jammed solid. *Annual Review of Condensed Matter Physics*, 1:347–369.
- Liu, L. (2011). Kinetic theory of aggregation in granular flow. *AIChE Journal*, 57(12):3331–3343.
- Liu, P., Kellogg, K., LaMarche, C., and Hrenya, C. (2017). Dynamics of singlet-doublet collisions of cohesive particles. *Chemical Engineering Journal*, 324:380–391.
- Liu, P., LaMarche, C. Q., Kellogg, K. M., and Hrenya, C. M. (2016). Fine-particle deflu-idization: Interaction between cohesion, Young’s modulus and static bed height. *Chemical Engineering Science*, 145:266–278.
- Lois, G., Blawdziewicz, J., and O’Hern, C. S. (2008). Jamming transition and new perco-lation universality classes in particulate systems with attraction. *Physical Review Letters*, 100:028001.

- Lomboy, G., Sundararajan, S., and Wang, K. (2013). Micro- and macroscale coefficients of friction of cementitious materials. *Cement and Concrete Research*, 54:21–28.
- Lomboy, G., Sundararajan, S., Wang, K., and Subramaniam, S. (2011). A test method for determining adhesion forces and hamaker constants of cementitious materials using atomic force microscopy. *Cement and Concrete Research*, 41(11):1157–1166.
- Lomboy, G. R., Wang, K., and Quanji, Z. (2012). Properties of cementitious materials in their dry state and their influences on viscosity of the cementitious pastes. *Powder Technology*, 229:104–111.
- Luding, S. (1998). Collisions & contacts between two particles. In *Physics of dry granular media*, pages 285–304. Springer.
- Luding, S. (2008). Cohesive, frictional powders: contact models for tension. *Granular matter*, 10(4):235–246.
- Luding, S. (2016). Granular matter: So much for the jamming point. *Nature Physics*, 12:531–532.
- Luding, S. and Alonso-Marroquin, F. (2011). The critical-state yield stress (termination locus) of adhesive powders from a single numerical experiment. *Granular Matter*, 13:109–119.
- Luding, S., Clément, E., Blumen, A., Rajchenbach, J., and Duran, J. (1994). Anomalous energy dissipation in molecular-dynamics simulations of grains: The detachment effect. *Physical Review E*, 50(5):4113.
- Luding, S., Huthmann, M., McNamara, S., and Zippelius, A. (1998). Homogeneous cooling of rough, dissipative particles: Theory and simulation. *Physical Review E*, 58(3):3416–3425.
- Majmudar, T., Sperl, M., Luding, S., and Behringer, R. (2007). Jamming transition in granular systems. *Physical Review Letters*, 98:058001.
- Makse, H. A., Johnson, D. L., and Schwartz, L. M. (2000). Packing of compressible granular materials. *Physical review letters*, 84(18):4160.

- Marchisio, D. L. and Fox, R. O. (2013). *Computational Models for Polydisperse Particulate and Multiphase Systems*. Cambridge University Press.
- Markutsya, S., Fox, R., and Subramaniam, S. (2014). Characterization of sheared colloidal aggregation using langevin dynamics simulation. *Physical Review E*, 89:062312.
- Marmur, B. L. and Heindel, T. J. (2016). Effect of particle size, density, and concentration on granular mixing in a double screw pyrolyzer. *Powder Technology*, 302:222–235.
- Martys, N. and Ferraris, C. (2002). Simulation of scc flow. In *First North American Conference on the Design and Use of Self-Consolidating Concrete. Proceedings. Chicago, IL,*.
- Martys, N., Khalil, M., George, W., and Lootens, D. (2012). Stress propagation in a concentrated colloidal suspension under shear. *European Physical Journal E*, 35(3):1–7.
- Matsunaga, T., Kim, J., Hardcastle, S., and Rohatgi, P. (2002). Crystallinity and selected properties of fly ash particles. *Materials Science and Engineering*, A325:333–343.
- Maugis, D. (1992). Adhesion of spheres: the jkr-dmt transition using a dugdale model. *Journal of colloid and interface science*, 150(1):243–269.
- Maxey, M. (1987). The gravitational settling of aerosol particles in homogeneous turbulence and random flow fields. *Journal of Fluid Mechanics*, 174:441–465.
- Mckay, W. and Mckay, J. (1971). *Building Construction Vol. Ii (Fourth Edition)*. Orient Longman Private Limited.
- McMillan, J., Shaffer, F., Gopalan, B., Chew, J. W., Hrenya, C., Hays, R., Karri, S. R., and Cocco, R. (2013). Particle cluster dynamics during fluidization. *Chemical Engineering Science*, 100:39–51.
- McNamara, S. and Young, W. (1992). Inelastic collapse and clumping in a one-dimensional granular medium. *Physics of Fluids A*, 4(3):496–504.
- Mehrabadi, M. (2016). *Analysis of gas-solid flow using particle-resolved direct numerical simulation: flow physics and modeling*. PhD thesis, Iowa State University.

- Mehrabadi, M., Murphy, E., and Subramaniam, S. (2016a). Development of a gas-solid drag law for clustered particles using particle-resolved direct numerical simulation. *Chemical Engineering Science*, 152:199–212.
- Mehrabadi, M., Tenneti, S., and Subramaniam, S. (2016b). Importance of the fluid-particle drag model in predicting segregation in bidisperse gas-solid flow. *International Journal of Multiphase Flow*, 86:99–114.
- MiDi, G. (2004). On dense granular flows. *The European Physical Journal E*, 14(4):341–365.
- Miller, A. and Gidaspow, D. (1992). Dense, vertical gas-solid flow in a pipe. *AIChE Journal*, 38(11):1801–1815.
- Mills, P., Rognon, P., and Chevier, F. (2008). Rheology and structure of granular materials near the jamming transition. *EPL (Europhysics Letters)*, 81:64005.
- Miyamoto, H., Kargel, J., Fink, W., and Furfaro, R. (2008). Granular processes on itokawa, a small near-earth asteroid: Implications for resource utilization. *Space Exploration Technologies, Proceedings of SPIE*, 6960:69600I.
- Monchaux, R., Bourgoïn, M., and Cartellier, A. (2010). Preferential concentration of heavy particles: a voronoi analysis. *Physics of Fluids*, 22(10):103304.
- Moreno-Atanasio, R., Xu, B., and Ghadiri, M. (2007). Computer simulation of the effect of contact stiffness and adhesion on the fluidization behaviour of powders. *Chemical engineering science*, 62(1):184–194.
- Morrow, C., Lovell, M., and Ning, X. (2003). A jkr-dmt transition solution for adhesive rough surface contact. *Journal of Physics D: Applied Physics*, 36(5):534.
- Mounfield, C. and Edwards, S. (1994). A model for the packing of irregularly shaped grains. *Physica A*, 210:301–316.
- Müller, M.-K. and Luding, S. (2011). Homogeneous cooling with repulsive and attractive long-range potentials. *Mathematical Modelling of Natural Phenomena*, 6(4):118–150.

- Murphy, E., Mehrabadi, M., Tenneti, S., and Subramaniam, S. (2015). Modeling two-point particle dynamics of homogeneous gas-solid flows to describe clustering and stability. In *68th annual meeting of the American physical society division of fluid dynamics, At Boston, MA*.
- Murphy, E. and Subramaniam, S. (2014). A model for solid-solid drag in bidisperse gas-solid flows. In *67th Annual Meeting of the APS Division of Fluid Dynamics*, volume 59.
- Murphy, E. and Subramaniam, S. (2015). Freely cooling granular gases with short-ranged attractive potentials. *Physics of Fluids (1994-present)*, 27(4):043301.
- Murphy, E. and Subramaniam, S. (2017). Binary collision outcomes for inelastic soft-sphere models with cohesion. *Powder Technology*, 305:462–476.
- Nachenius, R., van de Wardt, T., Ronsse, F., and Prins, W. (2015). Effect of particle size, density, and concentration on granular mixing in a double screw pyrolyzer. *Fuel Processing Technology*, 130:87–95.
- Narayanan, K. and Ramamurthy, K. (2000). Structure and properties of aerated concrete: a review. *Cement and Concrete Composites*, 22(5):321–329.
- Nase, S. T., Vargas, W. L., Abatan, A. A., and McCarthy, J. (2001). Discrete characterization tools for cohesive granular material. *Powder Technology*, 116(2):214–223.
- Nauman, E. B. (2001). *Chemical Reactor Design, Optimization, and Scaleup*. McGraw-Hill.
- Nienow, A., Edwards, M., and Harnby, N. (1992). *Mixing in the Process Industries: Mixing of Cohesive Powders*. Elsevier, Oxford, 2nd edition.
- of Chemistry, T. R. S. (2008). The concrete conundrum. *Chemistry World*.
- Oliver, W. C. and Pharr, G. M. (1992). An improved technique for determining hardness and elastic modulus using load and displacement sensing indentation experiments. *Journal of materials research*, 7(06):1564–1583.
- Ortiz de Zarate, J. and Sengers, J. (2006). *Hydrodynamic Fluctuations in Fluids and Fluid Mixtures*. Elsevier.

- Oseen, C. (1927). Neuere methoden und ergebnisse in der hydrodynamik. *Akademische Verlagsgesellschaft*.
- Otsuki, M., Hayakawa, H., and Luding, S. (2010). Behavior of pressure and viscosity at high densities for two-dimensional hard and soft granular materials. *Progress of Theoretical Physics Supplement*, 184:110–133.
- Pasha, M., Dogbe, S., Hare, C., Hassanpour, A., and Ghadiri, M. (2014). A linear model of elasto-plastic and adhesive contact deformation. *Granular Matter*, 16(1):151–162.
- Pathak, S., Jabeen, Z., Dibyendu, D., and Rajesh, R. (2014). Energy decay in three-dimensional freely cooling granular gas. *Physical Review Letters*, 112:038001.
- Paul, E. L., Atiemo-Obeng, V. A., and Kresta, S. M. (2004). *Handbook of industrial mixing: science and practice*. John Wiley ”&” Sons.
- Perni, S. and Prokopovich, P. (2015). Multi-asperity elliptical jkr model for adhesion of a surface with non-axially symmetric asperities. *Tribology International*, 88:107–114.
- Persson, B. N. and Scaraggi, M. (2014). Theory of adhesion: Role of surface roughness. *The Journal of chemical physics*, 141(12):124701.
- Petterson, O. (2007). Sandstone compaction, grain packing and critical state theory. *Petroleum Geoscience*, 13:63–67.
- Plimpton, S. (1995). Fast parallel algorithms for short-range molecular dynamics. *Journal of Computational Physics*, 117:1–19.
- Pope, S. B. (2000). *Turbulent Flows*. Cambridge University Press.
- Prokopovich, P. and Starov, V. (2011). Adhesion models: From single to multiple asperity contacts. *Advances in colloid and interface science*, 168(1):210–222.
- Rahman, M., Wiklund, J., Kotze, R., and Hakansson, U. (2017). Yield stress of cement grouts. *Tunnelling and Underground Space Technology*, 61:50–60.

- Rani, S. L., Dhariwal, R., and Koch, D. L. (2014). A stochastic model for the relative motion of high stokes number particles in isotropic turbulence. *Journal of Fluid Mechanics*, 756:870–902.
- Reeks, M. (1980). Eulerian direct interaction applied to the statistical motion of particles in a turbulent flow. *Journal of Fluid Mechanics*, 97:569–590.
- Rognon, P. G., Roux, J.-N., Naaim, M., and Chevoir, F. (2008). Dense flows of cohesive granular materials. *Journal of Fluid Mechanics*, 596:21–47.
- Rong, L., Dong, K., and Yu, A. (2014). Lattice-boltzmann simulation of fluid flow through packed beds of spheres: effect of particle size distribution. *Chemical Engineering Science*, 116:508–523.
- Rotne, J. and Prager, S. (1969). Variational treatment of hydrodynamic interaction in polymers. *Journal of Chemical Physics*, 50:4831–4837.
- Roussel, N., Lemaitre, A., Flatt, R., and Coussot, P. (2010). Steady state flow of cement suspensions: A micromechanical state of the art. *Cement and Concrete Research*, 40(1):77–84.
- Roussel, N., Ovarlez, G., Garrault, S., and Brumaud, C. (2012). The origins of thixotropy of fresh cement pastes. *Cement and Concrete Research*, 42(1):148–157.
- Rumpf, H. (1958). Grundlagen und methoden des granulierens. *Chemie Ingenieur Technik*, 30(3):144–158.
- Rycroft, C., Grest, G., Landry, J., and Bazant, M. (2006). Analysis of granular flow in a pebble-bed nuclear reactor. *Physical Review E*, 74:021306.
- Saha, S. and Alam, M. (2016). Normal stress differences, their origin and constitutive relations for a sheared granular fluid. *Journal of Fluid Mechanics*, 795:549–580.
- Saitoh, K. and Mizuno, H. (2016). Enstrophy cascades in two-dimensional dense granular flows. *Physical Review E*, 94:022908.

- Saitoh, K., Takada, S., and Hayakawa, H. (2015). Hydrodynamic instabilities in shear flows of dry cohesive granular particles. *Soft matter*, 11(32):6371–6385.
- Schäfer, J., Dippel, S., and Wolf, D. (1996). Force schemes in simulation of granular material. *J. Phys. I France*, 6:5–20.
- Schlick, C. P., Isner, A. B., Freireich, B. J., Fan, Y., Umbanhowar, P. B., Ottino, J. M., and Lueptow, R. M. (2016). A continuum approach for predicting segregation in flowing polydisperse granular materials. *Journal of Fluid Mechanics*, 797:95–109.
- Shah, S. and Wang, K. (2004). Development of green cement for sustainable concrete using cement kiln dust and fly ash. In *Proceedings of the International Workshop on Sustainable Development and Concrete Technology*.
- Shannon, C. (1948). A mathematical theory of communication. *Bell System Technical Journal*, 27(3):379–423.
- Silbert, L. E., Ertas, D., Grest, G. S., Halsey, T. C., Levine, D., and Plimpton, S. J. (2001). Granular flow down an inclined plane: Bagnold scaling and rheology. *Physical Review E*, 64(5):051302.
- Silbert, L. E., Grest, G. S., Brewster, R., and Levine, A. J. (2007). Rheology and contact lifetimes in dense granular flows. *Physical review letters*, 99(6):068002.
- Singh, A., Magnanimo, V., Saitoh, K., and Luding, S. (2014). Effect of cohesion on shear banding in quasistatic granular materials. *Physical Review E*, 90(2):022202.
- Singh, A., Magnanimo, V., Saitoh, K., and Luding, S. (2015). The role of gravity or pressure and contact stiffness in granular rheology. *New journal of physics*, 17(4):043028.
- Sjostrom, S. and Krutka, H. (2009). Evaluation of solid sorbents as a retrofit technology for co2 capture. *Fuel*, 89(6):1298–1306.
- Song, C., Wang, P., and Makse, H. A. (2008). A phase diagram for jammed matter. *Nature*, 453(7195):629–632.

- Stevens, A. and Hrenya, C. (2005). Comparison of soft-sphere models to measurements of collision properties during normal impacts. *Powder Technology*, 154(2):99–109.
- Stoyan, D., Kendall, W., and Mecke, J. (1995). *Stochastic geometry and its applications*. John Wiley and Sons, New York, 2nd edition.
- Stutzman, P. (2004). Scanning electron microscopy imaging of hydraulic cement microstructure. *Cement and Concrete Composites*, 26:957–966.
- Subramaniam, S. (2000). Statistical representation of a spray as a point process. *Physics of Fluids*, 12(10):2413–2431.
- Subramaniam, S. (2001). Statistical modeling of sprays using the droplet distribution function. *Physics of Fluids*, 13(3):624–642.
- Subramaniam, S. (2012). Stability limits for gas-solid suspensions with finite fluid inertia using particle-resolved direct numerical simulations. *NSF Annual Report 1134500*.
- Subramaniam, S. (2014). Stability limits for gas-solid suspensions with finite fluid inertia using particle-resolved direct numerical simulations. *NSF Annual Report 1134500*.
- Sun, J., Battaglia, F., and Subramaniam, S. (2006). Dynamics and structures of segregation in a dense, vibrating granular bed. *Physical Review E*, 74(6):061307.
- Sun, J. and Sundaresan, S. (2011). A constitutive model with microstructure evolution for flow of rate-independent granular materials. *Journal of Fluid Mechanics*, 682:590–616.
- Sundaram, S. and Collins, L. (1997). Collision statistics in an isotropic, particle-laden turbulent suspension i. direct numerical simulations. *Journal of Fluid Mechanics*, 335:75–109.
- Syamlal, M. (1987). The particle-particle drag term in a multiphase model of fluidization. *Technical Report DOE/MC/21353-2373, NTIS/DE87006500, National Technical Information Service*.
- Syamlal, M. and O’Brien, T. (1987). A generalized drag correlation for multiparticle systems. *Technical Report, Morgantown Energy Technology Center DOE Report*.

- Syamlal, M., Rogers, W., and O'Brien, T. (1993). Mfix documentation: Theory guide. *Morgantown Energy Technology Center Morgantown, WV, USA*, page 54.
- Tabor, D. (1977). Surface forces and surface interactions. *Journal of colloid and interface science*, 58(1):2–13.
- Takada, S., Saitoh, K., and Hayakawa, H. (2014). Simulation of cohesive fine powders under a plane shear. *Physical Review E*, 90(6):062207.
- Takada, S., Saitoh, K., and Hayakawa, H. (2015a). Kinetic theory for dilute cohesive granular gases with a square well potential. *arXiv preprint arXiv:1506.04578*.
- Takada, S., Saitoh, K., and Hisao, H. (2015b). Simulation of cohesive fine powders under a plane shear. *Physical Review E*, 90:062207.
- Tenneti, S., Garg, G., and Subramaniam, S. (2011). Drag law for monodisperse gas-solid systems using particle-resolved direct numerical simulation of flow past fixed assemblies of spheres. *International Journal of Multiphase Flows*, 37(9):1072–1092.
- Tenneti, S., Mehrabadi, M., and Subramaniam, S. (2016). Stochastic lagrangian model for hydrodynamic acceleration of inertial particles in gas-solid suspensions. *Journal of Fluid Mechanics*, 788:695–729.
- Tenneti, S. and Subramaniam, S. (2014). Particle-resolved direct numerical simulation for gas-solid flow model development. *Annual Review of Fluid Mechanics*, 46:199–230.
- Thornton, C., Cummins, S. J., and Cleary, P. W. (2013). An investigation of the comparative behaviour of alternative contact force models during inelastic collisions. *Powder Technology*, 233:30–46.
- Thornton, C. and Ning, Z. (1998). A theoretical model for the stick/bounce behaviour of adhesive, elastic-plastic spheres. *Powder technology*, 99(2):154–162.
- Tien, C. and Ramarao, B. (2007). *Granular Filtration of Aerosols and Hydrosols*. Elsevier, Oxford, 2nd edition.

- Tomas, J. (2000). Particle adhesion fundamentals and bulk powder consolidation. *KONA Powder and Particle Journal*, 18(0):157–169.
- Torquato, S. (1995). Mean nearest-neighbor distance in random packings of hard d-dimensional spheres. *Physical Review Letters*, 74(12):2156–2159.
- Trizac, E. and Hansen, J. (1995). Dynamic scaling behavior of ballistic coalescence. *Physical Review Letters*, 74(21):4114–4117.
- Trizac, E. and Hansen, J. (1996). Dynamics and growth of particles undergoing ballistic coalescence. *Journal of Statistical Physics*, 86(5-6):1345–1370.
- Tsuji, Y., Kawaguchi, T., and Tanaka, T. (1993). Discrete particle simulation of two-dimensional fluidized bed. *Powder technology*, 77(1):79–87.
- Uhlmann, M. and Doychev, T. (2014). Sedimentation of a dilute suspension of rigid spheres at intermediate galileo numbers: the effect of clustering upon the particle motion. *Journal of Fluid Mechanics*, 752:310–348.
- UNEP, U. N. E. P. (2012). Greening cement production has a big role to play in reducing greenhouse gas emissions. *UNEP Report 2012, Environmental Science Alert Thematic Focus: Resource Efficiency, Harmful Substances and Hazardous Waste, and Climate Change*.
- van der Hoef, M., Beestra, R., and Kuipers, J. (2005). Lattice-boltzmann simulations of low-reynolds-number flow past mono- and bidisperse arrays of spheres: results for the permeability and drag force. *Journal of Fluid Mechanics*, 528:233–254.
- van Noije, T., Ernst, M., and Brito, R. (1998a). Ring kinetic theory for an idealized granular gas. *Physica A*, 251:266–283.
- van Noije, T., Ernst, M., and Brito, R. (1998b). Spatial correlations in compressible granular flows. *Physical Review E*, 57(5):R4893.
- van Noije, T., Ernst, M., Brito, R., and Orza, J. (1997). Mesoscopic theory of granular fluids. *Physical Review Letters*, 79(3):411–414.

- Vidyapati and Subramaniam, S. (2013). Granular flow in silo discharge: Discrete element method simulations and model assessment. *Industrial "E" Engineering Chemistry Research*, 52(36):13171–13182.
- Vidyapati, V., Langroudi, M. K., Sun, J., Sundaresan, S., Tardos, G., and Subramaniam, S. (2012). Experimental and computational studies of dense granular flow: Transition from quasi-static to intermediate regime in a couette shear device. *Powder Technology*, 220:7–14.
- von Karman, T. and Howarth, L. (1938). On the statistical theory of isotropic turbulence. *Proceedings of the Royal Society of London. Series A, Mathematical and Physical Sciences*, 164(917):192–215.
- Walton, O. R. (1984). Application of molecular dynamics to macroscopic particles. *International Journal of Engineering Science*, 22(8):1097–1107.
- Walton, O. R. (2004). Potential discrete element simulation applications ranging from airborne fines to pellet beds. *SAE 2004 Transactions J. Aerospace*.
- Wang, K., Subramaniam, S., and Sundararajan, S. (2013). Final report: Understanding rheology of cement-based materials through integrated experiments and computations at multiple scales. *Final Report NSF CBET Grant No. 0927660*.
- Waters, J., Lee, S., and Guduru, P. (2009). Mechanics of axisymmetric wavy surface adhesion: Jkr–dmt transition solution. *International Journal of Solids and Structures*, 46(5):1033–1042.
- Weller, H., Tabor, G., Jasak, H., and Fureby, C. (1998). A tensorial approach to computational continuum mechanics using object-oriented techniques. *Computers in Physics*, 12(6):620–631.
- Wilson, R., Dini, D., and van Wachem, B. (2016). A numerical study exploring the effect of particle properties on the fluidization of adhesive particles. *AIChE Journal*, 62(5):1467–1477.
- Wylie, J. J. and Koch, D. L. (2000). Particle clustering due to hydrodynamic interactions. *Physics of Fluids*, 12(5):964–970.
- Xing, Z., Kenty, B., Li, Z., and Lee, S. (2009). Scale-up analysis for a cho cell culture process in large-scale bioreactors. *Biotechnology and Bioengineering*, 103(4):733–746.

- Xu, Y. and Subramaniam, S. (2007). Consistent modeling of interphase turbulent kinetic energy transfer in particle-laden turbulent flows. *Physics of Fluids*, 19:085101.
- Yao, H., Ciavarella, M., and Gao, H. (2007). Adhesion maps of spheres corrected for strength limit. *Journal of colloid and interface science*, 315(2):786–790.
- Yin, X., Zenk, J. R., Mitrano, P. P., and Hrenya, C. M. (2013). Impact of collisional versus viscous dissipation on flow instabilities in gas-solid systems. *Journal of Fluid Mechanics*, 727:R2.
- Zaichik, L. and Alipchenkov, V. (2003). Pair dispersion and preferential concentration of particles in isotropic turbulence. *Physics of Fluids*, 15:1776–1787.
- Zaichik, L. I. and Alipchenkov, V. M. (2009). Statistical models for predicting pair dispersion and particle clustering in isotropic turbulence and their applications. *New Journal of Physics*, 11:103018.
- Zamankhan, P. (2005). Kinetic theory of multicomponent dense mixtures of slightly inelastic spherical particles. *Physical Review E*, 52(5):4877–4891.
- Zhang, Q. and Kamrin, K. (2017). Microscopic description of the granular fluidity field in nonlocal flow modeling. *Physical Review Letters*, 118:058001.

CHAPTER 7. CLUSTERING IN GAS-SOLID FLOWS

This section contains the background development for the theory and modeling of the statistics of clustering in two-way coupled flows containing gas and inertial particles. The section will serve as the background for the future publication of several manuscripts in preparation.

7.1 Background

An issue at the heart of scale-up of gas-solid reactors is the increase in the mixing time scale with increasing reactor size (Nauman, 2001; Paul et al., 2004; Xing et al., 2009). This problem of increasing mixing time affects many industries from the traditional petro-chemicals, bio-energy, and bio-pharmaceuticals. The phenomena of clustering of particles not only inhibits mixing by retaining correlations in the relative positions of particles, but also inhibits evenly distributed gas-solid phase contact throughout the reactor. The phenomena is also not well-understood or predictable. This causes problems for designers/engineers who would like to inhibit clustering or even harness it. The goal of this work will be to develop a statistical theory leading to a better understanding of clustering in gas-solid flows.

Statistical descriptions of gas-solid flows in realistic environments are affected by inhomogeneity in the form of walls. Though they strongly affect the flow patterns, these "wall effects" pose difficulty to modeling as they are geometry and scale dependent. Instead, the coupling between the gas and particle phases and how their natural fluctuations lead to clustering is the focus of this work. To explore this, we look at unbounded domains, which produce *statistically homogeneous* systems. Evidence from several sources support that clustering does occur in systems absent of wall effects. For example, Yin et al. (2013) looked at pseudo 2D homogeneously cooling systems of initially agitated granules immersed in a gas-phase using a

lattice-Boltzmann solver. These particles were found to cluster due to inelasticity in collisions and to form vortices due to both the viscosity of the gas and inelasticity. Capecelatro et al. (2014) studied clustering of particles in a massive ($L/d_p > 3500$) mesoscopic simulation of a gas-solid sedimenting flow. Particles were observed to form large clusters, which drove turbulence in the gas-phase. This turbulence then also entrained much of the solid-phase, producing the so-called cluster induced turbulence (CIT). Smaller-scale particle-resolved direct numerical simulations (PR-DNS) have also revealed the emergence of clustering in gas-solid flows (Uhlmann and Doychev, 2014; Murphy et al., 2015). In addition, stability analysis of single-point hydrodynamic theories in the Stokes flow regime have given some credence to clustering of gas-solid flows (Koch, 1990; Koch and Sangani, 1999; Wylie and Koch, 2000). In this work we focus on producing models to describe clustering using data from PR-DNS.

There are several mechanisms that are argued to lead to clustering in flows of realistic particles that have nothing to do with the statistically heterogeneous wall effects. The most straightforward mechanism is the existence of attractive forces due to a variety of sources, e.g. liquid bridging, van der Waals forces, and electrostatics. However, in the absence of such attractive forces, dissipation from particle collisions has also been shown to lead to the formation of coherent particle vortices and particle clusters (Goldhirsch and Zanetti, 1993; van Noije et al., 1998a, 1997). On the hydrodynamic side, the preferential concentration of particles (Maxey, 1987; Eaton and Fessler, 1994), where particles are centrifuged out of regions of high vorticity into regions of high strain, has been the dominant mechanism of discussion in the literature. The modeling effort undertaken in this work makes an effort to distinguish between these sources of instability producing distinct terms to model collisional and hydrodynamic forcing. However, these mechanisms will not be the theoretical focus of the work.

Among the theories commonly produced for describing instability and clustering in non-dilute gas-solid flows with large solid to fluid density ratios $\rho_s/\rho_f \gg 1$, the most popular are single-point hydrodynamic theories. One of the earliest attempts (Koch, 1990) to form a hydrodynamic theory focused on particles in a fluid in the Stokes flow regime. This theory argued that instabilities occur due to a non-linear dependence of the interphase drag on the coarse-grained particle phase volume fraction. However, theories in Stokes flow necessarily

ignore momentum transport in the fluid phase and in some sense are only one way coupled. More recent hydrodynamic theories (Garzo et al., 2012; Fullmer and Hrenya, 2016; Garzo et al., 2016; Gonzalez and Garzo, 2016) attempt to account for the absence of fluid phase momentum by extracting and incorporating fluctuations that arise due to the fluid-solid phase coupling at steady-state from PR-DNS.

Other coarse-grained theories also exist that seek to directly account for the effects of clustering. One of the more popular, the energy minimization multi-scale (EMMS) approach (Li et al., 1999), augments the interphase momentum transfer closure due to clusters appearing in the flow. More recent mesoscopic theories seek to differentiate between the scales at which clusters occur and those at which slower varying flow patterns emerge (Fox, 2014; Capecelatro et al., 2016). However, all single point theories lack a few necessary features to properly predict clustering in homogeneous settings (van Noije et al., 1997; Ortiz de Zarate and Sengers, 2006). At the most basic level, single point theories are by definition statistically homogeneous and lack an adequate description of the sub-grid/coarse-grained fluctuations that lead to instability. Additional problems arise for a single-point description when considering the effect of interstitial fluid on molecular chaos in closures of the Boltzmann equation and spatio-temporal correlation in fluid-particle forces (Gustavsson and Mehlig, 2014b). To address some of these issues, a higher-level multi-point description is necessary.

The study of clustering of inertial particles in homogeneous isotropic turbulence is more developed. The flow field statistics arising from isotropic turbulence are well-studied. In addition, these flows are only one-way coupled, i.e. the momentum of the fluid is unaffected by the momentum of the particles. The microscopic drag forces, which depend only on the local slip between the fluid and particle centers, that a point particle will sample as it traverses the flow field can be studied in detail. Note, however, that this approach is not general. For example, the velocity of the fluid seen by a particle that defines the microscopic drag force is a poorly defined quantity in a PR-DNS simulation, where momentum transfer occurs through surface boundary conditions rather than through drag laws. What remains general from the approach are the coupled hierarchy of moment equations Reeks (1980) that can be formed that describe the dispersion of particles in terms of relative separation and relative velocities (Chun

et al., 2005; Zaichik and Alipchenkov, 2003, 2009; Bragg and Collins, 2014a,b; Rani et al., 2014). This hierarchy may be closed at any number of levels, though typically at the zeroth or first moment through means of a diffusion approximation for higher-order interactions with the carrier flow. Approaches do differ in the quantities that are used to make up the state vector and hence the number and type of closures.

Models which close the hierarchy of moment equations in the area of clustering inertial particles in isotropic turbulence must account for a number of peculiar phenomena, which should be general to clustering in gas-solid flows and are difficult to model using diffusion closures. Perhaps most importantly relative velocities are not observed to be Gaussian (Sundaram and Collins, 1997), which is not possible using traditional diffusion models such as the Smoluchowski (inertia-less) or Ornstein-Uhlenbeck (inertial) models. Additionally, even the particle-pair relative acceleration statistics are non-Gaussian (Bec et al., 2010; Lanotte et al., 2011) and display finite correlation times (Gustavsson and Mehlig, 2016), both indicative of intermittency. At the very least, a model that produces clustering by definition must also produce a higher concentration of pairs in close proximity. The motions that bring particles into close proximity are quite complex, with particles often being categorized as 'flyers' or caustics and 'lingerers' (Sundaram and Collins, 1997; Gustavsson and Mehlig, 2014b; Rani et al., 2014; Bragg et al., 2015). Flyers are characterized as pairs of particles, which come to cluster that are initially well separated. We note that some of these characteristic behaviors have been accounted for by using an inertial particle description with spatially dependent diffusion (Rani et al., 2014).

The theory that we develop herein follows the spirit of the efforts in the isotropic turbulence community. Namely, exact equations for modeling, the moment hierarchy equations for the solid-phase, are sought in Sections 7.2.1-7.2.5, which may be closed via simulation from PR-DNS. This approach is in lieu of characterization on the behavior of two-way coupled gas-solid flows. The physical meaning of many terms and their connection to the theory of non-particle laden isotropic turbulence is discussed. Lastly, some initial details on modeling via Fokker-Planck equations are discussed, as well as efforts to model certain terms appearing in the exact hierarchy. The moment equations produced by the Fokker-Planck equations closely mimic those obtained from the exact equations. Eventually, closure at the second-order moments

and a state-dependent, i.e. velocity and spatially dependent, diffusion is advocated. Lastly, simulation using stochastic differential equations is discussed, since closure of the transport terms that couple the moment hierarchy is not necessary.

In analyzing the exact and stochastic moment equations, several features and capabilities stand-out. Firstly, from the exact equations two possible mechanisms of clustering are identified. Clustering can be the result of some mean force felt by particles at a given separation or due to a spatially varying source and sink of fluctuations, similar to the unstable heat modes identified in the mesoscopic fluctuating hydrodynamics treatment of granular fluids (van Noije et al., 1998b). The spatially varying source and sink of fluctuations is consistent with observations that vorticity formation often precedes the formation of clusters. We note that inertial Fokker-Planck equations with separation dependent diffusion and friction are capable of modeling this behavior as well as non-Gaussian Lagrangian velocity statistics due to transport and to some extent the coexistence of flyers and lingerers at close separations.

The exact statistical equations developed herein can be used to assess the more precise dynamics of clustering, as opposed to the "state of clustering," which have been used in two-way coupled studies (Yin et al., 2013). In other words, the dynamical equations tell us that particles *will* cluster as opposed to the more complicated and nuanced notion of whether particles *are* clustered. Because the exact equation hierarchy is also simulation agnostic, the accuracy of different numerical methods can also be compared in a more detailed manner than looking at global single point quantities. Finally, these exact equations enable us to directly assess the accuracy of single-point hydrodynamic theories. Using two-point Karman-Howarth (Pope, 2000) type descriptions, which can be obtained from any one-point Eulerian description, one may directly compare rates of change for statistical quantities produced from both the exact two-point description and single point models. Although beyond the scope of this work, the two-point exact equations allow us to assess the capabilities and accuracy of single-point hydrodynamic descriptions to describe realizations of a particulate flow, as is often current practice in multiphase flow simulations.

7.2 Theory

The theory presented in this section focuses on producing transport equations for statistical quantities, i.e. moments of the particle phase distribution, in gas-solid flows. These equations comprise an infinite set of exact equations governing the transport of solid particles that are coupled to one another through convection terms. A realistic treatment of the equation set requires truncation and subsequent modeling of unclosed terms. Data from sources such as PR-DNS can then be used to model unclosed terms in the equations through both deterministic and stochastic means.

7.2.1 Statistics

In addressing the stability of homogeneous gas-solid and even granular flows, there exist a few standard statistics that assess the amount of clustering and correlated motion inherent to such flows. In granular materials for example, a common measure of clustering is the pair correlation or radial distribution function, $g(r_i)$. This function determines the relative likelihood that a particle will have a neighbor at some separation distance r_i . This quantity is then compared to equivalent assemblies in thermodynamic equilibrium to assess the degree of excess correlation in particle positions. While this is a useful quantity for measuring the 'state' of clustering at some time, it provides a rather incomplete description of the dynamics that lead to clustering. To complete this dynamic picture requires additional statistics about the flow of particles.

One of the statistical quantities commonly used to describe the flow of particles is $\langle u_i(x_i) u_j(x_i + r_i) \rangle$. This is the spatial autocorrelation of the velocity field, which when normalized by $\langle u'_i(x_i) u'_j(x_i) \rangle$ becomes a correlation coefficient. In turbulence, this function is equal to unity at $r_i = 0$ and tends towards 0 as $r_i \rightarrow \infty$. However, in the particle problem, this term is calculated for pairs only and hence is 0 at $r_i = 0$. If the term remains 0 for all particles beyond $r_i = D$, there is no correlation between the velocities of a particle and its neighbors. This term is used considerably in both the granular community (van Noije et al., 1997, 1998a,b) and to a larger extent homogeneous turbulence communities (Pope, 2000). Note that for an isotropic incompressible

case, this tensor function depends on a single scalar function (Pope, 2000). Lastly, this tensor function is useful when studying the behavior of systems described by continuum or Eulerian dynamical equations. However, for Lagrangian descriptions is more natural to express equations in the closely related structure function form, which are in general related to the spatial autocorrelation as

$$\frac{1}{2} (\langle u_i(x_i) u_j(x_i + r_i) \rangle + \langle u_i(x_i + r_i) u_j(x_i) \rangle) = \frac{1}{2} \left(2 \langle v_i v_j(r_i) \rangle - \frac{1}{2} \langle w_i w_j(r_i) \rangle \right). \quad (7.1)$$

Here the center of mass velocity and relative velocity vectors (or structure functions) for identical monodispersed particles are given by $v_i = \frac{1}{2} (u_i(x_i) + u_i(x_i + r_i))$ and $w_i = u_i(x_i + r_i) - u_i(x_i)$. The left hand side of the expression above is the symmeterized version and will be equal to $\langle u_i(x_i) u_j(x_i + r_i) \rangle$ if the tensor is symmetric, as in the case of isotropic flows. Note also that we have used the fact that in statistically homogeneous problems no quantity should depend on the position x_i . All quantities depend only on the separation vector r_i .

In the specific case of an isotropic gas-solid flow, Eq. 7.1 can be expressed more compactly.

$$\frac{\langle u_i(x_i) u_j(x_i + r_i) \rangle}{T} = \delta_{ij} - \frac{1}{2T} \left(\frac{\langle w_{\perp} w_{\perp}(r_i) \rangle}{2} \delta_{ij} + \left(\langle w_{\parallel} w_{\parallel}(r_i) \rangle - \frac{\langle w_{\perp} w_{\perp}(r_i) \rangle}{2} \right) \hat{r}_i \hat{r}_j \right). \quad (7.2)$$

Here the subscripts \parallel and \perp indicate longitudinal (or direction of normal relative separation) and transverse components (perpendicular to the normal relative separation) of the relative velocity. It is noteworthy to mention that the evolution of $g(r_i)$ depends only on the structure factors given from the relative velocity at a given separation $\langle w_i | r_i \rangle$ directly, and so we will find Eqs. 7.1 and 7.2 to be a useful relationships when comparing different descriptions of clustering. In addition, the quantity w_i is Galilean invariant, while the center of mass velocity is not. More will be discussed on these moments and their dynamical relationships to one another in the context of the moment transport equation in Section 7.2.4.

7.2.2 The PDF transport equation

In a statistically homogeneous flow of N-particles, the lowest level of description that allows structure formation is a two-particle description. All quantities at the 1-particle level of

description do not depend on space. Therefore, we begin our analytic treatment by considering the equation for the evolution of the two-particle PDF $\rho^{(2)}(x_i^{(1)}, x_i^{(2)}, u_i^{(1)}, u_i^{(2)}; t)$, which does not directly account for angular particle motion. Here the superscript on coordinates in the parameter space discriminates (temporarily) between particle 1 and 2. The transport equation takes the form

$$\frac{\partial \rho^{(2)}}{\partial t} + \frac{\partial u_i^{(1)} \rho^{(2)}}{\partial x_i^{(1)}} + \frac{\partial \langle A_i^{(1)} | x_i^{(1)}, x_i^{(2)}, u_i^{(1)}, u_i^{(2)}; t \rangle \rho^{(2)}}{\partial u_i^{(1)}} + \frac{\partial u_i^{(2)} \rho^{(2)}}{\partial x_i^{(2)}} + \frac{\partial \langle A_i^{(2)} | x_i^{(1)}, x_i^{(2)}, u_i^{(1)}, u_i^{(2)}; t \rangle \rho^{(2)}}{\partial u_i^{(2)}} = 0. \quad (7.3)$$

This equation is in essence a statement of conservation of probability. The additional acceleration terms here, e.g. $\langle A_i^{(1)} | x_i^{(1)}, x_i^{(2)}, u_i^{(1)}, u_i^{(2)}; t \rangle$, are the average accelerations felt by a particle due to both collisions with neighboring particles and interactions with the surrounding fluid that leads to stresses at the particle surface. As such, it is an average over all additional degrees of freedom inherent to the problem, i.e. the other $N-2$ particles, all coordinates within the fluid phase, and particle angular motion. This averaging can be thought of in an abstract way as an integral over these additional phase-space coordinates $\Gamma - \Gamma^{(2)}$,

$$\langle A | \Gamma^{(2)}; t \rangle = \langle A_i^{(1)} | x_i^{(1)}, x_i^{(2)}, u_i^{(1)}, u_i^{(2)}; t \rangle = \frac{\int d(\Gamma - \Gamma^{(2)}) A(\Gamma) \rho(\Gamma; t)}{\rho^2(\Gamma^{(2)}; t)}. \quad (7.4)$$

This acceleration may be split up in several ways, depending on the nature of the collisions. The easiest way to separate these is in terms of interparticle/collisional and hydrodynamic, i.e. interactions with the gas phases, pieces as $\langle A_i^{(1)} | x_i^{(1)}, x_i^{(2)}, u_i^{(1)}, u_i^{(2)}; t \rangle = \langle A_i^{(1), hydro} | x_i^{(1)}, x_i^{(2)}, u_i^{(1)}, u_i^{(2)}; t \rangle + \langle A_i^{(1), coll} | x_i^{(1)}, x_i^{(2)}, u_i^{(1)}, u_i^{(2)}; t \rangle$. This collisional piece can further be broken down. For example, if interparticle interactions are binary in nature, e.g. hard and soft-sphere interactions, the BBGKY hierarchy may be used to split the term into two pieces. The first is the deterministic interaction between the two particles in the joint pdf $A_i^{(1), coll, det} = A_i^{(12)} = F_i^{(12)}/m_1$. The second is an averaged piece, which is an integral over interactions with a third particle. In dilute and hard-sphere systems, this results in the so-called collision integrals. These 3 particle interactions, though exact, are difficult to treat. Instead this term will be treated as a mean force - the average force felt by a particle due to

the presence of a other particles than the pair under consideration. From this point onward, we will absorb the 3-particle interactions and hydrodynamic interactions into a single averaged acceleration term.

The next step is to get Eq. 7.3 in a more natural form for describing clustering. Making a change in variables from the laboratory to the center of mass and relative frame produces

$$\frac{\partial \rho^{(2)}}{\partial t} + \frac{\partial (v_i \rho^{(2)})}{\partial y_i} + \frac{\partial (A_i^C \rho^{(2)})}{\partial v_i} + \frac{\partial (w_i \rho^{(2)})}{\partial r_i} + \frac{\partial (A_i^r \rho^{(2)})}{\partial w_i} + \frac{\partial (A_i^{r,(12)} \rho^{(2)})}{\partial w_i} = 0. \quad (7.5)$$

Here the center of mass coordinate is $y_i = (x_i^{(1)} + x_i^{(2)})/2$. The notation for the acceleration terms has also been simplified beyond this point making the conditional average on the particle neighborhood implicit. They are comprised of a center of mass A_i^C and a relative component A_i^r . Note, however, that the deterministic piece $A_i^{r,(12)}$ only affects the relative degrees of freedom, and is now given by $A_i^{r,(12)} = A_i^{(21)} - A_i^{(12)}$. This form is useful for several reasons. Firstly, the relative frame provides a natural setting in which to study the clustering of particles. Secondly, we know that no quantities will depend on the center of mass of a particle, so that upon averaging the 2nd term will vanish. Thirdly, in this case two particle collisions may be treated naturally. As previously noted, collisions after a given two particles collide must, however, be accounted for in the averaged center of mass and relative separation acceleration terms. We now provide the rules for averaging this equation such that the proper moment transport equations will be produced.

7.2.3 Averaging

The averaged equations derived here are Eulerian, in the sense that they will be conditioned on given a separation. The first average that we wish to produce is the pair density, which takes the form

$$n^{(2)}(r_i; t) = \int dy_i dv_i dr_i dw_i \rho^{(2)}(y_i, v_i, r_i, w_i; t). \quad (7.6)$$

We note that this pair density can be related to the pair correlation function by $n^{(2)} = N(N-1)g(r_i)/V$, where N and V are the number of particles and volume, respectively. The

trick now is to condition all quantities on this separation using the pair density. For example, the average relative velocity at separation r_i is defined by

$$\langle w_i | r_i; t \rangle = \frac{\int dy_i dv_i dr_i dw_i \rho^{(2)}(y_i, v_i, r_i, w_i; t)}{n^{(2)}(r_i; t)}. \quad (7.7)$$

All additional terms in the moment equations use the same method of averaging. Note that beyond this point, we will drop the notation for conditional on separation $|r_i$ for simplicity. All quantities will be separation dependent unless otherwise noted. This method of averaging can now be used to produce the sought after moment transport equations.

7.2.4 Moment Transport

We begin by seeking the moment transport equation of the zero-th order. This equation will be the so-called pair-density conservation equation. For generality, we proceed without considering the more specific isotropic cases in our equations. The pair-density equation is

$$\frac{\partial n^{(2)}}{\partial t} + \frac{\partial (n^{(2)} \langle w_i \rangle)}{\partial r_i} = 0. \quad (7.8)$$

Perhaps unsurprisingly the equation for the conservation of pairs looks exactly like the equation for the conservation number density in the single particle description. Indeed most of the equations that we see here will bear many similarities to the equations encountered in hydrodynamics and statistical theories of turbulence. We note that this equation is explicitly coupled in the second term to higher-order statistics, namely the mean pair-relative velocity, which is 0 in incompressible turbulence. Hence, the mean relative velocity is directly responsible for clustering in gas-solid flows. The features of this equation have been explored in detail for the case of clustering in one-way coupled isotropic turbulence.

We can now proceed to presenting the two first order equations that can be obtained. These equations are for the center of mass and relative velocities

$$\frac{\partial \langle w_i \rangle}{\partial t} + \frac{1}{n^{(2)}} \frac{\partial (n^{(2)} \langle w_i w_j \rangle)}{\partial r_j} = \langle A_i^r \rangle + \langle A_i^{r(12)} \rangle \quad (7.9)$$

$$\frac{\partial \langle v_i \rangle}{\partial t} + \frac{1}{n^{(2)}} \frac{\partial (n^{(2)} \langle v_i w_j \rangle)}{\partial r_j} = \langle A_i^C \rangle. \quad (7.10)$$

From these equations we learn some additional information about how particles might come to cluster. We first focus on the Eq. 7.9 since it is directly coupled to the pair density equation. First, the mean velocity at a given separation can change do to two mechanisms. The more naive mechanism states that the particles can be pushed together due to some mean attractive force. The second mechanism is due to transport from a second-order velocity term. For this mechanism, it is the evolution of the second-order velocity tensor that is responsible clustering. This equation has also been closed and modeled using diffusion/stochastic differential equations (SDE) in the context of clustering in 1-way coupled isotropic turbulence (Rani et al., 2014). The SDEs were able to reproduce several characteristics of such flows, such as the structure of the mean relative velocity field.

The velocity of the pair center of mass evolution in Eq. 7.10 takes a similar form. The main difference is that the center of mass velocity is still transported in separation space by the relative velocity. While this equation does not couple directly to the relative coordinate, it is likely that it will need to be used for the purposes of modeling closures for terms containing the averaged acceleration A_i^r . Additionally, it is required to complete Eq. 7.1.

The highest order equations that we will consider are the 2nd moments, which are tensors. Again these equations take familiar forms.

$$\frac{\partial \langle w_i w_j \rangle}{\partial t} + \frac{1}{n^{(2)}} \frac{\partial (n^{(2)} \langle w_i w_j w_k \rangle)}{\partial r_k} = \left\langle \left(A_i^r + A_i^{r(12)} \right) w_j \right\rangle + \left\langle w_i \left(A_j^r + A_j^{r(12)} \right) \right\rangle \quad (7.11)$$

$$\frac{\partial \langle v_i v_j \rangle}{\partial t} + \frac{1}{n^{(2)}} \frac{\partial (n^{(2)} \langle v_i v_j w_k \rangle)}{\partial r_k} = \langle A_i^C v_j \rangle + \langle v_i A_j^C \rangle \quad (7.12)$$

$$\frac{\partial \langle v_i w_j \rangle}{\partial t} + \frac{1}{n^{(2)}} \frac{\partial (n^{(2)} \langle v_i w_j w_k \rangle)}{\partial r_k} = \langle A_i^C w_j \rangle + \left\langle v_i \left(A_j^r + A_j^{r(12)} \right) \right\rangle. \quad (7.13)$$

Equation 7.11 again consists of 3 distinct parts. The first arises from the transport tied to the third order equation. This term will be discussed in greater detail when we consider

the central moments, i.e. covariance. The right hand side contains the acceleration-velocity mixed moments. It will be shown that these provide a source or sink to fluctuations. The simple way to understand these are as follows, if a relative velocity is aligned with the direction the pair is being forced, the second-order velocity moment will grow. If the directions of the acceleration and velocity are opposite than the second-order velocity moment will decay, which will be discussed further in Section 7.3. All three second-order moment equations take the same form, and it is apparent that if we stop at this level of description, all structure will arise from the modeling of the transport and acceleration-velocity mixed moment terms. However, we can shed more clarity here by separating central and raw moments. This means that we will use the relationship between the variance and first two raw moments $\langle w'_i w'_j \rangle = \langle w_i w_j \rangle - \langle w_i \rangle \langle w_j \rangle$. For brevity, we only show here the moments that contain only the relative velocity. These moment equations appear as

$$\frac{\partial n^{(2)}}{\partial t} + \frac{\partial (n^{(2)} \langle w_i \rangle)}{\partial r_i} = 0 \quad (7.14)$$

$$\frac{\partial \langle w_i \rangle}{\partial t} + \frac{1}{n^{(2)}} \frac{\partial (n^{(2)} \langle w_i \rangle \langle w_j \rangle)}{\partial r_j} + \frac{1}{n^{(2)}} \frac{\partial (n^{(2)} \langle w'_i w'_j \rangle)}{\partial r_j} = \langle (A_i^r + A_i^{r(12)}) \rangle \quad (7.15)$$

$$\begin{aligned} & \frac{\partial \langle w'_i w'_j \rangle}{\partial t} + \frac{(\langle w'_i w'_j \rangle - \langle w_i \rangle \langle w_j \rangle)}{n^{(2)}} \frac{\partial (n^{(2)} \langle w_k \rangle)}{\partial r_k} + \langle w_k \rangle \frac{\partial \langle w'_i w'_j \rangle}{\partial r_k} + \frac{1}{n^{(2)}} \frac{\partial (n^{(2)} \langle w'_i w'_j w'_k \rangle)}{\partial r_k} \\ & + \langle w'_i w'_k \rangle \frac{\partial \langle w_j \rangle}{\partial r_k} + \langle w'_j w'_k \rangle \frac{\partial \langle w_i \rangle}{\partial r_k} = \langle (A_i^{r'} + A_i^{r'(12)}) w'_j \rangle + \langle w'_i (A_j^{r'} + A_j^{r'(12)}) \rangle. \end{aligned} \quad (7.16)$$

In this presentation of the equations, both how these equations are coupled and where the unclosed terms are become clear. The unclosed terms come in two flavors. The first is from the yet to be prescribed acceleration statistics, i.e. mean acceleration and the velocity-acceleration covariance. These can be modeled in many ways, most straightforwardly from fitting PR-DNS data. However, for generality, one should model the un-closed terms in terms of the velocity and pair density statistics that we already know. The second type of terms contain the so-called triple correlation $\langle w'_i w'_j w'_k \rangle$, which is generally not considered an important ingredient to turbulence modeling (Launder, 1990; Pope, 2000). These terms are the only transport terms that remain unclosed and coupled to the evolution of higher-order moments.

We now address individual terms in these equations. If one were to apply the chain rule to Eq. 7.14, it would become apparent from the non-vanishing divergence of the relative velocity that the flow field is non-solenoidal. In other words, this phase space is *compressible*, which should introduce terms that are absent from the Reynolds Stress Transport (RST) theory of incompressible turbulence, which is comparable in form, and the related Karman Howarth description of homogeneous isotropic incompressible turbulence. In the relative velocity evolution in Eq. 7.15, we have important additional terms as well - in total there are now 2 distinct transport terms. The first term accounts for the transport due to mean convection and has a clear interpretation. The second term has two familiar interpretations, it is the divergence of the stress in terms of a microscopic kinetic theory and the divergence of the Reynolds stress in turbulence. This term shows the direct effect that the velocity covariance has on the momentum equation, and how stresses may arise from the covariance or temperature-like statistics to influence clustering.

Equation 7.16 for the 2nd-order central moments again has many similarities to the RST of isotropic turbulence. The correspondence between this work and RST becomes clear when we write out the meaning of these terms in a symbolic manner as follows

$$\begin{aligned} \frac{\partial \langle w'_i w'_j \rangle}{\partial t} + \text{Deformational Heating} + \text{Convection} + \text{Triple Correlation} \\ + \text{Production} = \text{Acceleration Source/Sink.} \end{aligned} \quad (7.17)$$

Note that all of the terms are displayed in the order that they appear in Eq. 7.16. The convection, production, and triple correlation terms all appear in the theory for incompressible turbulence. The deformational heating term, however, does not appear there. This term is in reality two terms contained in parentheses. The first term depends on the Reynolds stress and is the power supplied to the fluctuations from compression by the mean velocity field. The second term is opposite in sign and is a sink of fluctuating energy. Because these two terms are multiplied by the divergence of the velocity field, they do not occur in theories of incompressible turbulence.

The remaining matter to discuss are the acceleration statistics. The important thing to

notice is that the mean acceleration and velocity-acceleration covariance show up independent of one another. This is important from the stand-point of modeling, as they can now be modeled independent of one another if a stochastic model is chosen. While the exact form in Eqs. 7.14-7.16 generic, there are a few simplifications that can be gleaned if we are facing an isotropic problem, as is the case in the Homogeneously Cooling Gas-Solid Flow (HCGSF).

7.2.5 Isotropic case

In the case of an isotropic flow, as is the case in the HCGSF, modeling is greatly simplified. This flow is quite similar to those studied in clustering in both isotropic turbulence. The main difference here is that the particles are inertial and supply energy to the fluid in a non-trivial manner. Kinetic energy is eventually dissipated both by both viscosity in the gas and collisions in the particle phase. The spherical symmetry inherent to 3D isotropic flows simplify the equations contained in Section 7.2.4 considerably. Here we present the equations in raw moment form and in spherical coordinates $\{r, \theta, \phi\}$

$$\frac{\partial n^{(2)}}{\partial t} + \frac{1}{r^{(2)}} \frac{\partial (r^2 n^{(2)} \langle w_i \rangle)}{\partial r} = 0 \quad (7.18)$$

$$\frac{\partial \langle w_r \rangle}{\partial t} + \frac{1}{n^{(2)} r^2} \frac{\partial (r^2 n^{(2)} \langle w_r w_r \rangle)}{\partial r} - \frac{\langle w_\phi w_\phi \rangle + \langle w_\theta w_\theta \rangle}{r} = \left\langle \left(A_r^r + A_r^{r(12)} \right) \right\rangle \quad (7.19)$$

$$\frac{\partial \langle w_r w_r \rangle}{\partial t} + \frac{1}{r^2 n^{(2)}} \frac{\partial (r^2 n^{(2)} \langle w_r w_r w_r \rangle)}{\partial r} - \frac{2 \langle w_r w_\phi w_\phi \rangle + 2 \langle w_r w_\theta w_\theta \rangle}{r} = 2 \left\langle w_r \left(A_r^r + A_r^{r(12)} \right) \right\rangle. \quad (7.20)$$

These are the equations that affect clustering directly. It is important to note the appearance of terms like such as $\langle w_\phi w_\phi \rangle$ which are additional transport terms that couple the relative motion to the transport of transverse velocities. We have used several features of our statistical flow here. An isotropic flow in the laboratory frame, means that our separation statistics will be spherically symmetric, i.e. $\langle w_\theta \rangle = \langle w_\phi \rangle = 0$. We also recognized that the radial velocity is independent of the direction in the azimuthal and polar directions so that $\langle w_r w_\theta \rangle = \langle w_r w_\phi \rangle = 0$. And lastly the magnitude of the radial velocity is independent of the direction, so that $\langle w_r w_r w_\theta \rangle = \langle w_r w_r w_\phi \rangle = 0$. The transport of relative velocities is tied only through direct

appearance of transverse velocity components. Note that similar equations can be made in the center of mass velocity statistics.

In the granular gas community the variance of the angular quantities or transverse velocity components also matter, as these correspond to the strength of vortices. More specifically terms like $\langle w_\phi w_\phi \rangle$ characterize the variance in the rotational speeds of the two particles separated by some distance r . Here we produce the 2nd order equation for w_θ , which are the first order of angular equations in our set that admit structure formation in separation space

$$\frac{\partial \langle w_\theta w_\theta \rangle}{\partial t} + \frac{1}{r^2 n^{(2)}} \frac{\partial (r^2 n^{(2)} \langle w_r w_\theta w_\theta \rangle)}{\partial r} + \frac{2 \langle w_r w_\theta w_\theta \rangle}{r} = 2 \langle A_\theta^r w_\theta \rangle. \quad (7.21)$$

The same equation structure is admitted for the ϕ direction. One of the most striking observations here is that the coupling terms that appear in the Eq. 7.20 appear in these equations as well, and serve as a transport of fluctuations between the longitudinal and transverse modes. We note that the deterministic acceleration for smooth spheres generally only has a radial component. Here we note that the mixed moments quantities of the form $\langle w_\theta w_\phi \rangle$, $\langle w_\theta w_\phi w_\phi \rangle$, and $\langle w_\phi w_\phi w_\phi \rangle$ are also zero due to independence of the angular directions and magnitudes and homogeneity. Simplified equations can be obtained by noting that $w_\parallel = w_r$ and $w_\perp^2 = w_\phi^2 + w_\theta^2$.

The structure in these equations is important. Many authors have noted that the appearance of coherent vortices, indicated by structure in w_\perp^2 precedes the formation of clusters in homogeneous cooling systems, including the HCGSF (van Noije et al., 1998a, 1997; Yin et al., 2013). We note that this equation implies that vorticity formation is due to a separation dependent source and sink to fluctuations that couples to the lower order through transport terms. So if clustering occurs due not to unstable mean accelerations, but rather due to unstable separation dependent heating mechanisms, i.e. acceleration-velocity covariances such as $\langle A_r^t w_r' \rangle$, then vorticity formation *must* precede clustering. The clustering must occur on a much longer time-scale due to structure formation in higher-order statistics.

7.3 Modeling

We intend to model these equations in a general context, using the raw moment equation set. For now, we focus only on the separation components, though the center of mass components would no doubt be important in the general context. We can see this because in general the accelerations in Euler Lagrange simulations are modeled in terms of the **mean-slip** $\langle W_i^{fluid} \rangle$ between the gas and solid phases. This can be found from the definition of the pair center of mass $\langle v_i \rangle = \langle u_i^{(2)} + u_i^{(1)} \rangle / 2 = \int dy_i du_i^{(1)} du_i^{(2)} (u_i^{(2)} + u_i^{(1)}) \rho^{(2)} / 2n^{(2)}$. The center of mass velocity for the entire particle system can be worked out from this definition. We find that the velocity of the center of mass of the entire system is given by $\langle V_i \rangle = \int_{\mathcal{V}} dr_i n^{(2)}(r_i) \langle v_i | r_i \rangle / N(N-1)$, where the full notation has been used to avoid confusion. In other words, the pair center of mass velocity averaged over all pairs is equal to the center of mass velocity of the system. The mean slip between the solids and fluid is then $\langle W_i^{fluid} \rangle = \langle V_i \rangle - \langle V_i^{fluid} \rangle$. Note that the local slip between a particle and fluid is meaningless in PR-DNS, so the details of the slip for a statistically stationary gas-phase are fully contained within the particle phase equations.

The intended method for modeling here will be to use stochastic differential equations. These SDEs have a complementary description that yields the same weak solution as an SDE known as Fokker-Planck equations (FPE). On one hand, the simulation of SDEs is straightforward. On the other, the moment equations obtained from the corresponding FPE allows us to straightforwardly identify sources and sinks that we can model from PR-DNS. The appropriate generic form of the SDEs using the Ito calculus and its corresponding FPEs are given as

$$d\mathbf{R}_T = \mathbf{W}_T dt \quad (7.22)$$

$$d\mathbf{W}_T = \mu(\mathbf{R}_T, \mathbf{W}_T) dt + \mathbf{A}_T^{r(12)}(\mathbf{R}_T, \mathbf{W}_T) dt + \Sigma(\mathbf{R}_T, \mathbf{W}_T) d\mathbf{B}_T \quad (7.23)$$

$$\frac{\partial f}{\partial t} + \frac{\partial(w_k f)}{\partial r_k} + \frac{\partial}{\partial w_k} \left(\left(\mu_k + A_k^{r(12)} \right) f - \frac{1}{2} \frac{\partial(\sigma_{km} \sigma_{lm} f)}{\partial w_l} \right). \quad (7.24)$$

Here $d\mathbf{B}_T$ is a matrix of Brownian motion increments, also known as a Wiener process. The relative velocity equation has both a deterministic piece (drift) and a stochastic white noise forcing. Additionally, we find that the deterministic two-particle interaction here does not need

to be modeled in the FPE or SDE. The moments of the FPE will take forms similar to those produced by the exact equations. There are also a number of features of this generic SDE that will allow for some degree of modeling freedom. Firstly, these coupled SDEs model transport terms exactly, reducing the number of terms that require explicit modeling. Second, the SDE for the velocity has a diffusion Σ and drift μ that depend on the path of the particle pair through separation space, i.e. the integral of the relative velocity, and not just relative velocities. Hence, this equation does not obey detailed balance and will allow for clustering without resorting to fictitious effective potentials. Particles in this model are also allowed to retain memory of where they have come from, which is important in inertial flows (Gustavsson and Mehlig, 2016). The memory effect combined with the arbitrary spatial and velocity dependence in the drift and diffusion terms also allows for additional desirable properties of the acceleration for inertial particles in turbulent-like conditions. Namely, the acceleration statistics for a given particle will not be drawn from the same Gaussian distribution due to the spatial dependence of the diffusion term. In fact, these equations can be given even more freedom if the diffusion terms are changed from white/memoryless noise as the result of some other stochastic process, and can also produce sample distribution different from a Gaussian. However, we will not explore more complicated models in this work.

In order to model these problems we need to identify sources and sinks in the 2nd order moment equations. These terms will correspond to the sources and sinks in the exact equations, given by $S_{ij}(r_i) = \langle A_i^r w_j^+ | r_i \rangle + \langle w_i' A_j^{r+} | r_i \rangle$ and $\Gamma_{ij}(r_i) = \langle A_i^r w_i^- | r_i \rangle + \langle w_i' A_j^{r+} | r_i \rangle$, respectively. These terms can be found from the DNS via

$$\langle A_i^r w_j^+ | r_i \rangle = \frac{1}{n^{(2)}(r_i, t)} \int dy_i dv_i dw_i A_i^r w_j^+ \Theta(A_i^r w_j^+) \rho^{(2)}(y_i, r_i, v_i, w_i; t) \quad (7.25)$$

$$\langle A_i^r w_j^- | r_i \rangle = \frac{1}{n^{(2)}(r_i, t)} \int dy_i dv_i dw_i A_i^r w_j^- \Theta(-A_i^r w_j^-) \rho^{(2)}(y_i, r_i, v_i, w_i; t). \quad (7.26)$$

Here the Heaviside function $\Theta(\cdot)$ serves to sift through the population of pairs to determine positive and negative values for the product of the fluctuations. Figure 7.1 gives graphical depiction for how this Heaviside function works on the sample space to select the positive and negative products of fluctuations in the acceleration and velocity. This figure was taken for

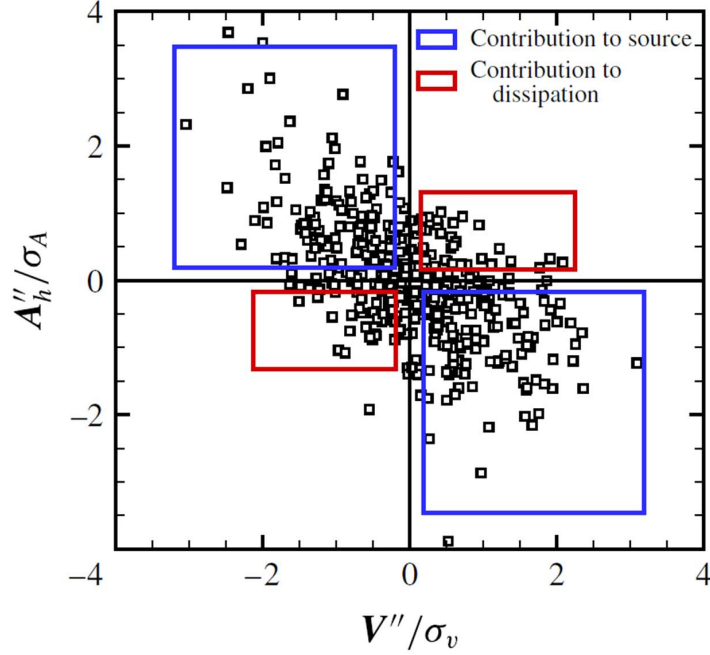


Figure 7.1 A scatter plot is given for fluctuations in acceleration and velocity. These plot helped to model SDEs governing the evolution of single point velocity using the Ornstein-Uhlenbeck process. Figure reprinted from Tenneti et al. (2016).

the single point velocity statistics for a mean pressure gradient driven flow at constant mean slip (Tenneti et al., 2016). Note that we do not include the deterministic accelerations in the budgets for the source and sink terms, since they need not be modeled.

7.3.1 Ornstein-Uhlenbeck

Of the possible models to consider, a position dependent Ornstein-Uhlenbeck (OU) model is perhaps the most simplistic. Here we will make all dependence of the drift and diffusion on the relative velocity $\langle w_i | r_i \rangle$ explicit. Additionally, this assumes a mean slip that does not vary in time and disregards any dependence on the center of mass velocity of the particular pair. The SDE appears as

$$d\mathbf{R}_T = \mathbf{W}_T dt \quad (7.27)$$

$$d\mathbf{W}_T = -\mu(\mathbf{R}_T) \langle \mathbf{W}_T \rangle dt - \gamma \mathbf{W}'_T dt + \mathbf{A}_T^{r(12)} dt + \Sigma(\mathbf{R}_T) d\mathbf{B}_T. \quad (7.28)$$

Here we have unique drifts $\mu \langle \mathbf{W}_T \rangle$ and $\gamma \mathbf{W}'_T$ for the mean and fluctuations in relative velocity, respectively. The mean acts as a relative mean drag law, while the fluctuating component can be identified clearly as a sink in the moment equations. After substituting this SDE into the generic FPE (Eq. 7.24) and integrating, we find the following moment equations

$$\frac{\partial n^{(2)}}{\partial t} + \frac{\partial (n^{(2)} \langle w_i \rangle)}{\partial r_i} = 0 \quad (7.29)$$

$$\frac{\partial \langle w_i \rangle}{\partial t} + \frac{1}{n^{(2)}} \frac{\partial (n^{(2)} \langle w_i w_j \rangle)}{\partial r_j} = -\mu_{ij} \langle w_j \rangle + A_i^{r(12)} \quad (7.30)$$

$$\begin{aligned} \frac{\partial \langle w'_i w'_j \rangle}{\partial t} + \text{Transport Terms} = & -\langle \gamma_{ik} w'_k w'_j \rangle - \langle w'_i \gamma_{jk} w'_k \rangle + \frac{1}{2} (\sigma_{ik} \sigma_{kj} + \sigma_{jk} \sigma_{ki}) \\ & + \langle A_i^{r(12)} w'_j \rangle + \langle w'_i A_j^{r(12)} \rangle. \end{aligned} \quad (7.31)$$

This simple model gives a clear indication as to how to go about modeling the sources and sinks. Moreover, by separating the dissipation into a piece dependent on the mean and one on the fluctuating relative velocity we can model the mean force and sink separately. Namely we find that the sources and sinks in the OU model are given by

$$S_{ij}(r_i) = \frac{1}{2} (\sigma_{ik} \sigma_{kj} + \sigma_{jk} \sigma_{ki}) \quad (7.32)$$

$$\Gamma_{ij}(r_i) = \langle \gamma_{ik} w'_k w'_j \rangle + \langle w'_i \gamma_{jk} w'_k \rangle. \quad (7.33)$$

While this model works quite well for describing the evolution of single particle velocities (Garzo et al., 2012; Tenneti et al., 2016), this model is over-determined in the compressible case. In essence, while the sources and sinks can be fit to whatever spatial field is extracted, we cannot control what transport arises from this model. There are too few parameters to guarantee that this model will work in general. Fortunately, if multiplicative or velocity dependent diffusion is allowed we do obtain enough free parameters to model this problem.

7.3.2 Multiplicative Noise

In resorting to multiplicative or state-dependent noise, the assumption is made that the source of fluctuations depends on the current relative velocity between two particles. This

assumption is physically reasonable. Moreover, the source should only be a function of the fluctuation in the relative velocity, since it could be argued that the additive noise in an OU-process already implicitly models the dependence on $\langle w_i \rangle$. The Ito SDE for this process is given by

$$d\mathbf{R}_T = \mathbf{W}_T dt \quad (7.34)$$

$$d\mathbf{W}_T = -\mu(\mathbf{R}_T) \langle \mathbf{W}_T \rangle dt - \gamma \mathbf{W}'_T dt + \mathbf{A}_T^{r(12)} dt + \Sigma(\mathbf{R}_T) d\mathbf{B}_{1,T} + \Omega(\mathbf{R}_T) \mathbf{W}'_T d\mathbf{B}_{2,T}. \quad (7.35)$$

Here the processes $d\mathbf{B}_{1,T}$ and $d\mathbf{B}_{2,T}$ are two independent Brownian motion increments. Taking this additional term, the altered moment equations from integrating the FPE become

$$\frac{\partial n^{(2)}}{\partial t} + \frac{\partial (n^{(2)} \langle w_i \rangle)}{\partial r_i} = 0 \quad (7.36)$$

$$\frac{\partial \langle w_i \rangle}{\partial t} + \frac{1}{n^{(2)}} \frac{\partial (n^{(2)} \langle w_i w_j \rangle)}{\partial r_j} = -\mu_{ij} \langle w_j \rangle + \langle A_i^r \rangle \quad (7.37)$$

$$\begin{aligned} \frac{\partial \langle w'_i w'_j \rangle}{\partial t} + \text{Transport Terms} &= -\langle \gamma_{ik} w'_k w'_j \rangle - \langle w'_i \gamma_{jk} w'_k \rangle + \frac{1}{2} (\sigma_{ik} \sigma_{kj} + \sigma_{jk} \sigma_{ki}) \\ &+ \frac{1}{2} (\langle \omega_{imn} w'_n \omega_{jmn} w'_n \rangle + \langle \omega_{jmn} w'_n \omega_{imn} w'_n \rangle) \\ &+ \langle A_i^{r(12)} w'_j \rangle + \langle w'_i A_j^{r(12)} \rangle. \end{aligned} \quad (7.38)$$

Here the noise has been given in its most general tensorial form, where the noise coefficient ω_{imn} is a 3rd order tensor. The sources and sinks here are given by

$$S_{ij}(r_i) = \frac{1}{2} (\sigma_{ik} \sigma_{kj} + \sigma_{jk} \sigma_{ki} + \langle \omega_{imn} w'_n \omega_{jmn} w'_n \rangle + \langle \omega_{jmn} w'_n \omega_{imn} w'_n \rangle) \quad (7.39)$$

$$\Gamma_{ij}(r_i) = \langle \gamma_{ik} w'_k w'_j \rangle + \langle w'_i \gamma_{jk} w'_k \rangle. \quad (7.40)$$

This model is under-determined. To demonstrate this we will disregard the transport terms and take γ and ω to be scalars and treat an isotropic irrotational case. For a known steady-state velocity covariance $\langle w'_i w'_i \rangle$, we find the relationship $\sigma_{ik} \sigma_{ki} = (2\gamma - \omega^2) \langle w'_i w'_i \rangle$. Here, the value of γ is also known from measuring either S_{ij} or Γ_{ij} , which are equal by definitions. This equality is satisfied so long as the relationship between the two noise strengths is satisfied at

every point. There are an infinite many ways to satisfy the noise strength criterion. Note also that this equality also guarantees stability, since σ_{ik} is positive definite. In practice, some optimization will need to be done to assure that both the velocity covariance and transport terms are matched by the stochastic model.

7.4 Future Work

The works that make use of the theory developed in this Chapter are contained in Chapters 8 and ???. There two problems will be discussed, the homogeneously cooling gas-solid flow and the homogeneous pressure-driven flow with mean slip. Both of these flows have been observed to cluster.

7.5 Bibliography

- Aarons, L. and Sundaresan, S. (2006). Shear flow of assemblies of cohesive and non-cohesive granular materials. *Powder Technology*, 169(1):10–21.
- Abbasfard, H., Evans, G., and Moreno-Atanasio, R. (2016). Effect of van der Waals force cut-off distance on adhesive collision parameters in DEM simulation. *Powder Technology*, 299:9–18.
- Afferrante, L., Ciavarella, M., and Demelio, G. (2015). Adhesive contact of the weierstrass profile. In *Proc. R. Soc. A*, volume 471, page 20150248. The Royal Society.
- Aitcin, P. (2000). Cements of yesterday and today - concrete of tomorrow. *Cement and Concrete Research*, 31(9):1349–1359.
- Alam, M., Trujillo, L., and Herrmann, H. (2006). Hydrodynamic theory for reverse brazil nut segregation and the non-monotonic ascension dynamics. *Journal of Statistical Physics*, 124:587–623.
- Bagnold, R. A. (1954). Experiments on a gravity-free dispersion of large solid spheres in a newtonian fluid under shear. In *Proceedings of the Royal Society of London A: Mathematical, Physical and Engineering Sciences*, volume 225, pages 49–63. The Royal Society.

- Ball, R. and Melrose, J. (1997). A simulation technique for many spheres in quasi-static motion under frame-invariant pair drag and brownian forces. *Physica A*, 247:444–472.
- Baranyai, A. and Evans, D. (1989). Direct entropy calculation from computer-simulation of liquids. *Physical Review A*, 40(7):3817–3822.
- Batrak, O., Patino, G., Simonin, O., Flour, I., Le Guevel, T., and Perez, E. (2005). Unlike particles size collision model in 3d unsteady polydispersed simulation of circulating fluidized bed. *8th Annual Conference on Fluidized Bed Technology*, 315.
- Bec, J., Biferale, L., Cencini, M., Lanotte, A., and Toschi, F. (2010). Intermittency in the velocity distribution of heavy particles in turbulence. *Journal of Fluid Mechanics*, 646:527–536.
- Beetstra, R., van der Hoef, M., and Kuipers, J. (2007). Drag force of intermediate reynolds number flows past mono- and bidisperse arrays of spheres. *AIChE Journal*, 53:489.
- Bentz, D., Ferraris, C., Galler, M., Hansen, A., and Guynn, J. (2012). Influence of particle size distributions on yield stress and viscosity of cement-fly ash pastes. *Cement and Concrete Research*, 42(2):404–409.
- Bentz, D. P., Garboczi, E. J., Haecker, C. J., and Jensen, O. M. (1999). Effects of cement particle size distribution on performance properties of portland cement-based materials. *Cement and Concrete Research*, 29:1663–1671.
- Berger, N., Azéma, E., Douce, J.-F., and Radjai, F. (2016). Scaling behaviour of cohesive granular flows. *EPL (Europhysics Letters)*, 112(6):64004.
- Berzi, D. and Jenkins, J. T. (2015a). Inertial shear bands in granular materials. *Physics of Fluids*, 27:033303.
- Berzi, D. and Jenkins, J. T. (2015b). Steady shearing flows of deformable, inelastic spheres. *Soft matter*, 11(24):4799–4808.
- Binnig, G., Quate, C. F., and Gerber, C. (1986). Atomic force microscope. *Physical review letters*, 56(9):930.

- Blum, J., Wurm, G., Kempf, S., Poppe, T., Klahr, H., Kozasa, T., Rott, M., Henning, T., Dorschner, J., Schrapler, R., Keller, H., Markiewicz, W., Mann, I., Gustafson, B., Giovane, F., Neuhaus, D., Fechtig, H., Grun, E., Feuerbacher, B., Kochan, H., Ratke, L., El Goresy, A., Morfill, G., Weidenschilling, S., Schwehm, G., Metzler, K., and Ip, W. (2000). Growth and form of planetary seedlings: Results from a microgravity aggregation experiment. *Physical Review Letters*, 85(12):2426–2429.
- Bradley, R. S. (1932). Lxxix. the cohesive force between solid surfaces and the surface energy of solids. *The London, Edinburgh, and Dublin Philosophical Magazine and Journal of Science*, 13(86):853–862.
- Brady, J. F. and Bossis, G. (1988). Stokesian dynamics. *Annual Reviews of Fluid Mechanics*, 20:111–157.
- Bragg, A. D. and Collins, L. R. (2014a). New insights from comparing statistical theories for inertial particles in turbulence: I. spatial distribution of particles. *New Journal of Physics*, 16:055013.
- Bragg, A. D. and Collins, L. R. (2014b). New insights from comparing statistical theories for inertial particles in turbulence: II. relative velocities. *New Journal of Physics*, 16:055014.
- Bragg, A. D., Ireland, P. J., and Collins, L. R. (2015). On the relationship between the non-local clustering mechanism and preferential concentration. *Journal of Fluid Mechanics*, 780:327–343.
- Brewster, R., Grest, G. S., Landry, J. W., and Levine, A. J. (2005). Plug flow and the breakdown of bagnold scaling in cohesive granular flows. *Physical Review E*, 72(6):061301.
- Bridges, F. G., Supulver, K. D., Lin, D., Knight, R., and Zafra, M. (1996). Energy loss and sticking mechanisms in particle aggregation in planetesimal formation. *Icarus*, 123(2):422–435.
- Brilliantov, N. V., Albers, N., Spahn, F., and Pöschel, T. (2007). Collision dynamics of granular particles with adhesion. *Physical Review E*, 76(5):051302.

- Brilliantov, N. V. and Pöschel, T. (2004). Collision of adhesive viscoelastic particles. *HINRICHSEN:GRANULAR MEDIA O-BK*, pages 189–209.
- Brilliantov, N. V. and Pöschel, T. (2004). *Kinetic Theory of Granular Gases*. Oxford University Press, New York.
- Brilliantov, N. V., Spahn, F., Hertzsch, J.-M., and Pöschel, T. (1996). Model for collisions in granular gases. *Physical review E*, 53(5):5382.
- Brito, R. and Ernst, M. (1998). Extension of haff’s cooling law in granular flows. *Europhysics Letters*, 43(5):497.
- Campbell, C. S. (2002). Granular shear flows at the elastic limit. *Journal of fluid mechanics*, 465:261–291.
- Capecelatro, J., Desjardins, O., and Fox, R. O. (2014). Numerical study of collisional particle dynamics in cluster-induced turbulence. *Journal of Fluid Mechanics*, 747:R2.
- Capecelatro, J., Desjardins, O., and Fox, R. O. (2015). On fluid-particle dynamics in fully developed cluster-induced turbulence. *Journal of Fluid Mechanics*, 780:578–635.
- Capecelatro, J., Desjardins, O., and Fox, R. O. (2016). Strongly coupled fluid-particle flows in vertical channels. ii. turbulence modeling. *Physics of Fluids*, 28:033307.
- Carnahan, N. and Starling, K. (1969). Equation of state for nonattractive rigid spheres. *Journal of Chemical Physics*, 51(2):635–636.
- Castellanos, A., Valverde, J. M., Pérez, A. T., Ramos, A., and Watson, P. K. (1999). Flow regimes in fine cohesive powders. *Physical Review Letters*, 82(6):1156.
- Cates, M., Wittmer, J., Bouchaud, J., and Claudin, P. (1998a). Jamming and static stress transmission in granular materials. *Chaos*, 9(3):511–522.
- Cates, M., Wittmer, J., Bouchaud, J., and Claudin, P. (1998b). Jamming, force chains, and fragile matter. *Physical Review Letters*, 81(9):1841–1844.

- Chew, J. W., Parker, D. M., Cocco, R. A., and Hrenya, C. M. (2011). Cluster characteristics of continuous size distributions and binary mixtures of group b particles in dilute riser flow. *Chemical Engineering Journal*, 178:348–358.
- Chialvo, S., Sun, J., and Sundaresan, S. (2012). Bridging the rheology of granular flows in three regimes. *Physical Review E*, 85(2):021305.
- Chun, J., Koch, D. L., Rani, S. L., Ahluwalia, A., and Collins, L. R. (2005). Clustering of aerosol particles in isotropic turbulence. *Journal of Fluid Mechanics*, 536:219–251.
- Cleary, P. W. and Sawley, M. L. (2002). DEM modelling of industrial granular flows: 3D case studies and the effect of particle shape on hopper discharge. *Applied Mathematical Modelling*, 26(2):89–111.
- Cocco, R., Shaffer, F., Hays, R., Karri, S. R., and Knowlton, T. (2010). Particle clusters in and above fluidized beds. *Powder Technology*, 203:3–11.
- Colwell, J., Batiste, S., Horányi, M., Robertson, S., and Sture, S. (2007). Lunar surface: Dust dynamics and regolith mechanics. *Reviews of Geophysics*, 45(2):RG2006.
- Cundall, P. and Strack, O. (1979a). A discrete numerical model for granular assemblies. *Geotechnique*, 29(1):47–65.
- Cundall, P. A. and Strack, O. D. (1979b). A discrete numerical model for granular assemblies. *Geotechnique*, 29(1):47–65.
- Dahneke, B. (1975). Further measurements of the bouncing of small latex spheres. *Journal of Colloid and Interface Science*, 51(1):58–65.
- Daley, D. and Vere-Jones, D. (1988). *An introduction to the theory of point processes*. Springer-Verlag.
- DeCicco, A. and Hartzell, C. (2016). System-level design considerations for asteroid despin via neutral beam emitting spacecraft. In *IEEE Aerospace Conference Proceedings (Big Sky, MT)*.

- Derjaguin, B., Muller, V., and Toporov, Y. (1975). Effect of contact deformations on the adhesion of particles. *Journal of Colloid and Interface Science*, 53(2):314–326.
- Di Renzo, A. and Di Maio, F. P. (2004). Comparison of contact-force models for the simulation of collisions in dem-based granular flow codes. *Chemical Engineering Science*, 59(3):525–541.
- Eaton, J. and Fessler, J. (1994). Preferential concentration of particles by turbulence. *International Journal of Multiphase Flow*, 20:169–209.
- Ernst, M., Dorfman, J., Hoegy, W., and van Leeuwen, J. (1969). Hard-sphere dynamics and binary-collision operators. *Physica*, 45(1):127–146.
- Esipov, S. and Pöschel, T. (1997). The granular phase diagram. *Journal of Statistical Physics*, 86(5/6):1385–1395.
- Ferraris, C., Obla, K., and Hill, R. (2001). The influence of mineral admixtures on the rheology of cement paste and concrete. *Cement and Concrete Research*, 31(2):245–255.
- Fox, R. (2014). On multiphase turbulence models for collisional fluid-particle flows. *Journal of Fluid Mechanics*, 742:368–424.
- Fox, R. O. (2016). Private communication.
- Fullmer, W. D. and Hrenya, C. M. (2016). Quantitative assessment of fine-grid kinetic-theory-based predictions of mean-slip in unbounded fluidization. *AIChE Journal*, 62(1):11–17.
- Galvin, J. E. and Benyahia, S. (2014). The effect of cohesive forces on the fluidization of aeratable powders. *AIChE Journal*, 60(2):473–484.
- Garzo, V., Dufty, J. W., and Hrenya, C. M. (2007a). Enskog theory for polydisperse granular mixtures. i. navier-stokes order transport. *Physical Review E*, 76(3):031303.
- Garzo, V., Fullmer, W. E., Hrenya, C. M., and Yin, X. (2016). Transport coefficients of solid particles immersed in a viscous gas. *Physical Review E*, 93:012905.
- Garzo, V., Hrenya, C. M., and Dufty, J. W. (2007b). Enskog theory for polydisperse granular mixtures. ii. sonine polynomial approximation. *Physical Review E*, 76(3):031304.

- Garzo, V., Tenneti, S., Subramaniam, S., and Hrenya, C. (2012). Enskog kinetic theory for monodisperse gas-solid flows. *Journal of Fluid Mechanics*, 712:129–168.
- Gaume, J., Chambon, G., and Naaim, M. (2011). Quasistatic to inertial transition in granular materials and the role of fluctuations. *Physical Review E*, 84:051304.
- Geldart, D. (1973). Types of gas fluidization. *Powder technology*, 7(5):285–292.
- Gidaspow, D., Jung, J., and Singh, R. K. (2004). Hydrodynamics of fluidization using kinetic theory: an emerging paradigm 2002 flour-daniel lecture. *Powder Technology*, 148:123–141.
- Goldhirsch, I. and Zanetti, G. (1993). Clustering instability in dissipative gases. *Physical Review Letters*, 70(11):1619–1622.
- Goldshtein, A. and Shapiro, M. (1995). Mechanics of collisional motion of granular materials. part 1. general hydrodynamic equations. *Journal of Fluid Mechanics*, 282:75–114.
- Gollin, D., Berzi, D., and Bowman, E. (2017). Extended kinetic theory applied to inclined granular flows: role of boundaries. *Granular Matter*, 19(3):1564–1583.
- Gonzalez, R. G. and Garzo, V. (2016). Instabilities in granular gas-solid flows. *arXiv:1611.03269*.
- Gonzalez, S., Thornton, A., and Luding, S. (2014). Free cooling phase-diagram of hard-spheres with short-and long-range interactions. *The European Physical Journal Special Topics*, 223(11):2205–2225.
- Gourdel, c., Simonin, O., and Brunier, E. (1998). Modelling and simulation of gas-solid turbulent flows with a binary mixture of particles. *Third International Conference on Multiphase Flows*, 315.
- Gourdel, c., Simonin, O., and Brunier, E. (1999). Two-maxwellian equilibrium distribution function for the modelling of a binary mixture of particles. *6th International Conference on Circulating Fluidized Beds*, 315.

- Grierson, D., Flater, E., and Carpick, R. (2005). Accounting for the jkr–dmt transition in adhesion and friction measurements with atomic force microscopy. *Journal of adhesion science and technology*, 19(3-5):291–311.
- Gu, Y., Chialvo, S., and Sundaresan, S. (2014). Rheology of cohesive granular materials across multiple dense-flow regimes. *Physical Review E*, 90(3):032206.
- Gu, Y., Ozel, A., and Sundaresan, S. (2015). A modified cohesion model for CFD–DEM simulations of fluidization. *Powder Technology*, 296:17–28.
- Gu, Y., Ozel, A., and Sundaresan, S. (2016). Numerical studies of the effects of fines on fluidization. *AIChE Journal*.
- Gustavsson, K. and Mehlig, B. (2014a). Clustering of particles falling in a turbulent flow. *Physical Review Letters*, 112:214501.
- Gustavsson, K. and Mehlig, B. (2014b). Relative velocities of inertial particles in turbulent aerosols. *Journal of Turbulence*, 15(1):34–69.
- Gustavsson, K. and Mehlig, B. (2016). Statistical models for spatial patterns of heavy particles in turbulence. *Advances in Physics*, 65(1):1–57.
- Haecker, C., Garboczi, E., J.W., B., Bohn, R., Sun, Z., Shah, S., and Voigt, T. (2005). Modeling the linear elastic properties of portland cement paste. *Cement and Concrete Research*, 35:1948–1960.
- Haff, P. (1983). Grain flow as a fluid-mechanical phenomenon. *Journal of Fluid Mechanics*, 134:401–430.
- Hatzes, A., Bridges, F., Lin, D., and Sachtjen, S. (1991). Coagulation of particles in saturn’s rings: Measurement of the cohesive force of water frost. *Icarus*, 89:113–121.
- Hill, R. J., Koch, D., and Ladd, A. (2001a). The first effects of fluid inertia on flows in ordered and random arrays of spheres. *Journal of Fluid Mechanics*, 448:213–241.

- Hill, R. J., Koch, D., and Ladd, A. (2001b). Moderate-reynolds-number flows in ordered and random arrays of spheres. *Journal of Fluid Mechanics*, 448:243–278.
- Irani, E., Chaudhuri, P., and Heussinger, C. (2014). Impact of attractive interactions on the rheology of dense athermal particles. *Physical Review Letters*, 112:188303.
- Irani, E., Chaudhuri, P., and Heussinger, C. (2016). Athermal rheology of weakly attractive soft particles. *Physical Review E*, 94:052608.
- Israelachvili, J. N. (2011). *Intermolecular and surface forces: revised third edition*. Academic press.
- Iveson, S., Litster, J., Hapgood, K., and Ennis, B. (2001). Nucleation, growth and breakage phenomena in agitated wet granulation processes: a review. *Powder Technology*, 117(1-2):3–39.
- Jenkins, J. and Mancini, F. (1987). Balance laws and constitutive relations for plane flows of a dense, binary mixture of smooth, nearly elastic, circular disks. *Journal of Applied Mechanics*, 1(54):27–34.
- Jenkins, J. and Mancini, F. (1989). Kinetic theory for binary mixtures of smooth, nearly elastic spheres. *Physics of Fluids, A*, 1(12):2050–2057.
- Johnson, K. and Greenwood, J. (1997). An adhesion map for the contact of elastic spheres. *Journal of colloid and interface science*, 192(2):326–333.
- Johnson, K., Kendall, K., and Roberts, A. (1971). Surface energy and the contact of elastic solids. *Proceedings of the Royal Society London A*, 324:301–313.
- Jop, P., Forterre, Y., and Pouliquen, O. (2006). A constitutive law for dense granular flows. *Nature*, 441(7094):727–730.
- Kamrin, K. and Koval, G. (2012). Nonlocal constitutive relation for steady granular flow. *Physical Review Letters*, 108(17):178301.

- Kim, H. and Arastoopour, H. (2002). Extension of kinetic theory to cohesive particle flow. *Powder Technology*, 122(1):83–94.
- Kim, S. and Karrila, S. (1991). *Microhydrodynamics: principles and selected applications*. Butterworth-Heinemann.
- Kobayashi, T., Tanaka, T., Shimada, N., and Kawaguchi, T. (2013). Dem–cfD analysis of fluidization behavior of Geldart group A particles using a dynamic adhesion force model. *Powder Technology*, 248:143–152.
- Koch, D. L. (1990). Kinetic theory for a monodisperse gas-solid suspension. *Physics of Fluids A*, 2(10):1711–1723.
- Koch, D. L. and Sangani, A. S. (1999). Particle pressure and marginal stability limits for a homogeneous monodisperse gas-fluidized bed: kinetic theory and numerical simulations. *Journal of Fluid Mechanics*, 400:229–263.
- Kolakaluri, R., Murphy, E., Subramaniam, S., Brown, R., and Fox, R. (2015). Filtration model for polydisperse aerosols in gas-solid flow using granule-resolved direct numerical simulation. *AIChE Journal*, 61(11):3594–3606.
- Kothe, S., Blum, J., Weidling, R., and GÄ¼ttler, C. (2013). Free collisions in a microgravity many-particle experiment. iii. the collision behavior of sub-millimeter-sized dust aggregates. *Icarus*, 225:75–85.
- Kulchitsky, A., Johnson, J., Reeves, D., and Wilkinson, A. (2014). Discrete element method simulation of a boulder extraction from an asteroid. In *Proceedings of the 14th ASCE Biennial International Conference on Engineering, Science, Construction, and Operations in Challenging Environments (St. Louis, Missouri, USA,)*, pages 485–494.
- Kumar, A. (2010). *Microscale Dynamics in Suspensions of Non-spherical Particles*. PhD thesis, University of Illinois Urbana-Champaign.
- Kumar, A. and Higdon, J. (2010). Origins of the anomalous stress behavior in charged colloidal suspensions under shear. *Physical Review E*, 82:051401.

- Kuwabara, G. and Kono, K. (1987). Restitution coefficient in a collision between two spheres. *Japanese journal of applied physics*, 26(8R):1230.
- Lanotte, A., Bec, J., Biferale, L., Cencini, M., and Toschi, F. (2011). About scaling properties of relative velocity between heavy particles in turbulence. *Journal of Physics Conference series*, 318:052010.
- Launder, B. (1990). Phenomenological modelling: present... and future? in j.l. lumley (ed.). *Whither Turbulence? Turbulence at a Crossroads*, pages 439–485.
- Lees, A. and Edwards, S. (1972). The computer study of transport processes under extreme conditions. *Journal of Physics C: Solid State Physics*, 5(15):1921.
- Leyvraz (2003). Scaling theory and exactly solved models in the kinetics of irreversible aggregation. *Physics Reports*, 383:92–212.
- Li, J., Cheng, C., Zhang, Z., Yuan, J., Nemet, A., and Fett, F. (1999). The emms model - its application, development and updated concepts. *Chemical Engineering Science*, 54(22):5409–5425.
- Liard, M., Martys, N., George, W., Lootens, D., and Hebraud, P. (2014). Scaling laws for the flow of generalized newtonian suspensions. *Journal of Rheology*, 58:1993–2015.
- Liu, A. J. and Nagel, S. R. (2010). The jamming transition and the marginally jammed solid. *Annual Review of Condensed Matter Physics*, 1:347–369.
- Liu, L. (2011). Kinetic theory of aggregation in granular flow. *AIChE Journal*, 57(12):3331–3343.
- Liu, P., Kellogg, K., LaMarche, C., and Hrenya, C. (2017). Dynamics of singlet-doublet collisions of cohesive particles. *Chemical Engineering Journal*, 324:380–391.
- Liu, P., LaMarche, C. Q., Kellogg, K. M., and Hrenya, C. M. (2016). Fine-particle deflu-idization: Interaction between cohesion, Young’s modulus and static bed height. *Chemical Engineering Science*, 145:266–278.

- Lois, G., Blawdziewicz, J., and O'Hern, C. S. (2008). Jamming transition and new percolation universality classes in particulate systems with attraction. *Physical Review Letters*, 100:028001.
- Lomboy, G., Sundararajan, S., and Wang, K. (2013). Micro- and macroscale coefficients of friction of cementitious materials. *Cement and Concrete Research*, 54:21–28.
- Lomboy, G., Sundararajan, S., Wang, K., and Subramaniam, S. (2011). A test method for determining adhesion forces and hamaker constants of cementitious materials using atomic force microscopy. *Cement and Concrete Research*, 41(11):1157–1166.
- Lomboy, G. R., Wang, K., and Quanji, Z. (2012). Properties of cementitious materials in their dry state and their influences on viscosity of the cementitious pastes. *Powder Technology*, 229:104–111.
- Luding, S. (1998). Collisions & contacts between two particles. In *Physics of dry granular media*, pages 285–304. Springer.
- Luding, S. (2008). Cohesive, frictional powders: contact models for tension. *Granular matter*, 10(4):235–246.
- Luding, S. (2016). Granular matter: So much for the jamming point. *Nature Physics*, 12:531–532.
- Luding, S. and Alonso-Marroquin, F. (2011). The critical-state yield stress (termination locus) of adhesive powders from a single numerical experiment. *Granular Matter*, 13:109–119.
- Luding, S., Clément, E., Blumen, A., Rajchenbach, J., and Duran, J. (1994). Anomalous energy dissipation in molecular-dynamics simulations of grains: The detachment effect. *Physical Review E*, 50(5):4113.
- Luding, S., Huthmann, M., McNamara, S., and Zippelius, A. (1998). Homogeneous cooling of rough, dissipative particles: Theory and simulation. *Physical Review E*, 58(3):3416–3425.
- Majmudar, T., Sperl, M., Luding, S., and Behringer, R. (2007). Jamming transition in granular systems. *Physical Review Letters*, 98:058001.

- Makse, H. A., Johnson, D. L., and Schwartz, L. M. (2000). Packing of compressible granular materials. *Physical review letters*, 84(18):4160.
- Marchisio, D. L. and Fox, R. O. (2013). *Computational Models for Polydisperse Particulate and Multiphase Systems*. Cambridge University Press.
- Markutsya, S., Fox, R., and Subramaniam, S. (2014). Characterization of sheared colloidal aggregation using langevin dynamics simulation. *Physical Review E*, 89:062312.
- Marmur, B. L. and Heindel, T. J. (2016). Effect of particle size, density, and concentration on granular mixing in a double screw pyrolyzer. *Powder Technology*, 302:222–235.
- Martys, N. and Ferraris, C. (2002). Simulation of scc flow. In *First North American Conference on the Design and Use of Self-Consolidating Concrete. Proceedings. Chicago, IL.*
- Martys, N., Khalil, M., George, W., and Lootens, D. (2012). Stress propagation in a concentrated colloidal suspension under shear. *European Physical Journal E*, 35(3):1–7.
- Matsunaga, T., Kim, J., Hardcastle, S., and Rohatgi, P. (2002). Crystallinity and selected properties of fly ash particles. *Materials Science and Engineering*, A325:333–343.
- Maugis, D. (1992). Adhesion of spheres: the jkr-dmt transition using a dugdale model. *Journal of colloid and interface science*, 150(1):243–269.
- Maxey, M. (1987). The gravitational settling of aerosol particles in homogeneous turbulence and random flow fields. *Journal of Fluid Mechanics*, 174:441–465.
- Mckay, W. and Mckay, J. (1971). *Building Construction Vol. Ii (Fourth Edition)*. Orient Longman Private Limited.
- McMillan, J., Shaffer, F., Gopalan, B., Chew, J. W., Hrenya, C., Hays, R., Karri, S. R., and Cocco, R. (2013). Particle cluster dynamics during fluidization. *Chemical Engineering Science*, 100:39–51.
- McNamara, S. and Young, W. (1992). Inelastic collapse and clumping in a one-dimensional granular medium. *Physics of Fluids A*, 4(3):496–504.

- Mehrabadi, M. (2016). *Analysis of gas-solid flow using particle-resolved direct numerical simulation: flow physics and modeling*. PhD thesis, Iowa State University.
- Mehrabadi, M., Murphy, E., and Subramaniam, S. (2016a). Development of a gas-solid drag law for clustered particles using particle-resolved direct numerical simulation. *Chemical Engineering Science*, 152:199–212.
- Mehrabadi, M., Tenneti, S., and Subramaniam, S. (2016b). Importance of the fluid-particle drag model in predicting segregation in bidisperse gas-solid flow. *International Journal of Multiphase Flow*, 86:99–114.
- MiDi, G. (2004). On dense granular flows. *The European Physical Journal E*, 14(4):341–365.
- Miller, A. and Gidaspow, D. (1992). Dense, vertical gas-solid flow in a pipe. *AIChE Journal*, 38(11):1801–1815.
- Mills, P., Rognon, P., and Chevier, F. (2008). Rheology and structure of granular materials near the jamming transition. *EPL (Europhysics Letters)*, 81:64005.
- Miyamoto, H., Kargel, J., Fink, W., and Furfaro, R. (2008). Granular processes on itokawa, a small near-earth asteroid: Implications for resource utilization. *Space Exploration Technologies, Proceedings of SPIE*, 6960:69600I.
- Monchaux, R., Bourgoïn, M., and Cartellier, A. (2010). Preferential concentration of heavy particles: a voronoi analysis. *Physics of Fluids*, 22(10):103304.
- Moreno-Atanasio, R., Xu, B., and Ghadiri, M. (2007). Computer simulation of the effect of contact stiffness and adhesion on the fluidization behaviour of powders. *Chemical engineering science*, 62(1):184–194.
- Morrow, C., Lovell, M., and Ning, X. (2003). A jkr–dmt transition solution for adhesive rough surface contact. *Journal of Physics D: Applied Physics*, 36(5):534.
- Mounfield, C. and Edwards, S. (1994). A model for the packing of irregularly shaped grains. *Physica A*, 210:301–316.

- Müller, M.-K. and Luding, S. (2011). Homogeneous cooling with repulsive and attractive long-range potentials. *Mathematical Modelling of Natural Phenomena*, 6(4):118–150.
- Murphy, E., Mehrabadi, M., Tenneti, S., and Subramaniam, S. (2015). Modeling two-point particle dynamics of homogeneous gas-solid flows to describe clustering and stability. In *68th annual meeting of the American physical society division of fluid dynamics, At Boston, MA*.
- Murphy, E. and Subramaniam, S. (2014). A model for solid-solid drag in bidisperse gas-solid flows. In *67th Annual Meeting of the APS Division of Fluid Dynamics*, volume 59.
- Murphy, E. and Subramaniam, S. (2015). Freely cooling granular gases with short-ranged attractive potentials. *Physics of Fluids (1994-present)*, 27(4):043301.
- Murphy, E. and Subramaniam, S. (2017). Binary collision outcomes for inelastic soft-sphere models with cohesion. *Powder Technology*, 305:462–476.
- Nachenius, R., van de Wardt, T., Ronsse, F., and Prins, W. (2015). Effect of particle size, density, and concentration on granular mixing in a double screw pyrolyzer. *Fuel Processing Technology*, 130:87–95.
- Narayanan, K. and Ramamurthy, K. (2000). Structure and properties of aerated concrete: a review. *Cement and Concrete Composites*, 22(5):321–329.
- Nase, S. T., Vargas, W. L., Abatan, A. A., and McCarthy, J. (2001). Discrete characterization tools for cohesive granular material. *Powder Technology*, 116(2):214–223.
- Nauman, E. B. (2001). *Chemical Reactor Design, Optimization, and Scaleup*. McGraw-Hill.
- Nienow, A., Edwards, M., and Harnby, N. (1992). *Mixing in the Process Industries: Mixing of Cohesive Powders*. Elsevier, Oxford, 2nd edition.
- of Chemistry, T. R. S. (2008). The concrete conundrum. *Chemistry World*.
- Oliver, W. C. and Pharr, G. M. (1992). An improved technique for determining hardness and elastic modulus using load and displacement sensing indentation experiments. *Journal of materials research*, 7(06):1564–1583.

- Ortiz de Zarate, J. and Sengers, J. (2006). *Hydrodynamic Fluctuations in Fluids and Fluid Mixtures*. Elsevier.
- Oseen, C. (1927). Neuere methoden und ergebnisse in der hydrodynamik. *Akademische Verlagsgesellschaft*.
- Otsuki, M., Hayakawa, H., and Luding, S. (2010). Behavior of pressure and viscosity at high densities for two-dimensional hard and soft granular materials. *Progress of Theoretical Physics Supplement*, 184:110–133.
- Pasha, M., Dogbe, S., Hare, C., Hassanpour, A., and Ghadiri, M. (2014). A linear model of elasto-plastic and adhesive contact deformation. *Granular Matter*, 16(1):151–162.
- Pathak, S., Jabeen, Z., Dibyendu, D., and Rajesh, R. (2014). Energy decay in three-dimensional freely cooling granular gas. *Physical Review Letters*, 112:038001.
- Paul, E. L., Atiemo-Obeng, V. A., and Kresta, S. M. (2004). *Handbook of industrial mixing: science and practice*. John Wiley ”&” Sons.
- Perni, S. and Prokopovich, P. (2015). Multi-asperity elliptical jkr model for adhesion of a surface with non-axially symmetric asperities. *Tribology International*, 88:107–114.
- Persson, B. N. and Scaraggi, M. (2014). Theory of adhesion: Role of surface roughness. *The Journal of chemical physics*, 141(12):124701.
- Petterson, O. (2007). Sandstone compaction, grain packing and critical state theory. *Petroleum Geoscience*, 13:63–67.
- Plimpton, S. (1995). Fast parallel algorithms for short-range molecular dynamics. *Journal of Computational Physics*, 117:1–19.
- Pope, S. B. (2000). *Turbulent Flows*. Cambridge University Press.
- Prokopovich, P. and Starov, V. (2011). Adhesion models: From single to multiple asperity contacts. *Advances in colloid and interface science*, 168(1):210–222.

- Rahman, M., Wiklund, J., Kotze, R., and Hakansson, U. (2017). Yield stress of cement grouts. *Tunnelling and Underground Space Technology*, 61:50–60.
- Rani, S. L., Dhariwal, R., and Koch, D. L. (2014). A stochastic model for the relative motion of high stokes number particles in isotropic turbulence. *Journal of Fluid Mechanics*, 756:870–902.
- Reeks, M. (1980). Eulerian direct interaction applied to the statistical motion of particles in a turbulent flow. *Journal of Fluid Mechanics*, 97:569–590.
- Rognon, P. G., Roux, J.-N., Naaim, M., and Chevoir, F. (2008). Dense flows of cohesive granular materials. *Journal of Fluid Mechanics*, 596:21–47.
- Rong, L., Dong, K., and Yu, A. (2014). Lattice-boltzmann simulation of fluid flow through packed beds of spheres: effect of particle size distribution. *Chemical Engineering Science*, 116:508–523.
- Rotne, J. and Prager, S. (1969). Variational treatment of hydrodynamic interaction in polymers. *Journal of Chemical Physics*, 50:4831–4837.
- Roussel, N., Lemaitre, A., Flatt, R., and Coussot, P. (2010). Steady state flow of cement suspensions: A micromechanical state of the art. *Cement and Concrete Research*, 40(1):77–84.
- Roussel, N., Ovarlez, G., Garrault, S., and Brumaud, C. (2012). The origins of thixotropy of fresh cement pastes. *Cement and Concrete Research*, 42(1):148–157.
- Rumpf, H. (1958). Grundlagen und methoden des granulierens. *Chemie Ingenieur Technik*, 30(3):144–158.
- Rycroft, C., Grest, G., Landry, J., and Bazant, M. (2006). Analysis of granular flow in a pebble-bed nuclear reactor. *Physical Review E*, 74:021306.
- Saha, S. and Alam, M. (2016). Normal stress differences, their origin and constitutive relations for a sheared granular fluid. *Journal of Fluid Mechanics*, 795:549–580.

- Saitoh, K. and Mizuno, H. (2016). Enstrophy cascades in two-dimensional dense granular flows. *Physical Review E*, 94:022908.
- Saitoh, K., Takada, S., and Hayakawa, H. (2015). Hydrodynamic instabilities in shear flows of dry cohesive granular particles. *Soft matter*, 11(32):6371–6385.
- Schäfer, J., Dippel, S., and Wolf, D. (1996). Force schemes in simulation of granular material. *J. Phys. I France*, 6:5–20.
- Schlick, C. P., Isner, A. B., Freireich, B. J., Fan, Y., Umbanhowar, P. B., Ottino, J. M., and Lueptow, R. M. (2016). A continuum approach for predicting segregation in flowing polydisperse granular materials. *Journal of Fluid Mechanics*, 797:95–109.
- Shah, S. and Wang, K. (2004). Development of green cement for sustainable concrete using cement kiln dust and fly ash. In *Proceedings of the International Workshop on Sustainable Development and Concrete Technology*.
- Shannon, C. (1948). A mathematical theory of communication. *Bell System Technical Journal*, 27(3):379–423.
- Silbert, L. E., Ertas, D., Grest, G. S., Halsey, T. C., Levine, D., and Plimpton, S. J. (2001). Granular flow down an inclined plane: Bagnold scaling and rheology. *Physical Review E*, 64(5):051302.
- Silbert, L. E., Grest, G. S., Brewster, R., and Levine, A. J. (2007). Rheology and contact lifetimes in dense granular flows. *Physical review letters*, 99(6):068002.
- Singh, A., Magnanimo, V., Saitoh, K., and Luding, S. (2014). Effect of cohesion on shear banding in quasistatic granular materials. *Physical Review E*, 90(2):022202.
- Singh, A., Magnanimo, V., Saitoh, K., and Luding, S. (2015). The role of gravity or pressure and contact stiffness in granular rheology. *New journal of physics*, 17(4):043028.
- Sjostrom, S. and Krutka, H. (2009). Evaluation of solid sorbents as a retrofit technology for co2 capture. *Fuel*, 89(6):1298–1306.

- Song, C., Wang, P., and Makse, H. A. (2008). A phase diagram for jammed matter. *Nature*, 453(7195):629–632.
- Stevens, A. and Hrenya, C. (2005). Comparison of soft-sphere models to measurements of collision properties during normal impacts. *Powder Technology*, 154(2):99–109.
- Stoyan, D., Kendall, W., and Mecke, J. (1995). *Stochastic geometry and its applications*. John Wiley and Sons, New York, 2nd edition.
- Stutzman, P. (2004). Scanning electron microscopy imaging of hydraulic cement microstructure. *Cement and Concrete Composites*, 26:957–966.
- Subramaniam, S. (2000). Statistical representation of a spray as a point process. *Physics of Fluids*, 12(10):2413–2431.
- Subramaniam, S. (2001). Statistical modeling of sprays using the droplet distribution function. *Physics of Fluids*, 13(3):624–642.
- Subramaniam, S. (2012). Stability limits for gas-solid suspensions with finite fluid inertia using particle-resolved direct numerical simulations. *NSF Annual Report 1134500*.
- Subramaniam, S. (2014). Stability limits for gas-solid suspensions with finite fluid inertia using particle-resolved direct numerical simulations. *NSF Annual Report 1134500*.
- Sun, J., Battaglia, F., and Subramaniam, S. (2006). Dynamics and structures of segregation in a dense, vibrating granular bed. *Physical Review E*, 74(6):061307.
- Sun, J. and Sundaresan, S. (2011). A constitutive model with microstructure evolution for flow of rate-independent granular materials. *Journal of Fluid Mechanics*, 682:590–616.
- Sundaram, S. and Collins, L. (1997). Collision statistics in an isotropic, particle-laden turbulent suspension i. direct numerical simulations. *Journal of Fluid Mechanics*, 335:75–109.
- Syamlal, M. (1987). The particle-particle drag term in a multiphase model of fluidization. *Technical Report DOE/MC/21353-2373, NTIS/DE87006500, National Technical Information Service*.

- Syamlal, M. and O'Brien, T. (1987). A generalized drag correlation for multiparticle systems. *Technical Report, Morgantown Energy Technology Center DOE Report.*
- Syamlal, M., Rogers, W., and O'Brien, T. (1993). Mfix documentation: Theory guide. *Morgantown Energy Technology Center Morgantown, WV, USA*, page 54.
- Tabor, D. (1977). Surface forces and surface interactions. *Journal of colloid and interface science*, 58(1):2–13.
- Takada, S., Saitoh, K., and Hayakawa, H. (2014). Simulation of cohesive fine powders under a plane shear. *Physical Review E*, 90(6):062207.
- Takada, S., Saitoh, K., and Hayakawa, H. (2015a). Kinetic theory for dilute cohesive granular gases with a square well potential. *arXiv preprint arXiv:1506.04578*.
- Takada, S., Saitoh, K., and Hisao, H. (2015b). Simulation of cohesive fine powders under a plane shear. *Physical Review E*, 90:062207.
- Tenneti, S., Garg, G., and Subramaniam, S. (2011). Drag law for monodisperse gas-solid systems using particle-resolved direct numerical simulation of flow past fixed assemblies of spheres. *International Journal of Multiphase Flows*, 37(9):1072–1092.
- Tenneti, S., Mehrabadi, M., and Subramaniam, S. (2016). Stochastic lagrangian model for hydrodynamic acceleration of inertial particles in gas-solid suspensions. *Journal of Fluid Mechanics*, 788:695–729.
- Tenneti, S. and Subramaniam, S. (2014). Particle-resolved direct numerical simulation for gas-solid flow model development. *Annual Review of Fluid Mechanics*, 46:199–230.
- Thornton, C., Cummins, S. J., and Cleary, P. W. (2013). An investigation of the comparative behaviour of alternative contact force models during inelastic collisions. *Powder Technology*, 233:30–46.
- Thornton, C. and Ning, Z. (1998). A theoretical model for the stick/bounce behaviour of adhesive, elastic-plastic spheres. *Powder technology*, 99(2):154–162.

- Tien, C. and Ramarao, B. (2007). *Granular Filtration of Aerosols and Hydrosols*. Elsevier, Oxford, 2nd edition.
- Tomas, J. (2000). Particle adhesion fundamentals and bulk powder consolidation. *KONA Powder and Particle Journal*, 18(0):157–169.
- Torquato, S. (1995). Mean nearest-neighbor distance in random packings of hard d-dimensional spheres. *Physical Review Letters*, 74(12):2156–2159.
- Trizac, E. and Hansen, J. (1995). Dynamic scaling behavior of ballistic coalescence. *Physical Review Letters*, 74(21):4114–4117.
- Trizac, E. and Hansen, J. (1996). Dynamics and growth of particles undergoing ballistic coalescence. *Journal of Statistical Physics*, 86(5-6):1345–1370.
- Tsuji, Y., Kawaguchi, T., and Tanaka, T. (1993). Discrete particle simulation of two-dimensional fluidized bed. *Powder technology*, 77(1):79–87.
- Uhlmann, M. and Doychev, T. (2014). Sedimentation of a dilute suspension of rigid spheres at intermediate galileo numbers: the effect of clustering upon the particle motion. *Journal of Fluid Mechanics*, 752:310–348.
- UNEP, U. N. E. P. (2012). Greening cement production has a big role to play in reducing greenhouse gas emissions. *UNEP Report 2012, Environmental Science Alert Thematic Focus: Resource Efficiency, Harmful Substances and Hazardous Waste, and Climate Change*.
- van der Hoef, M., Beestra, R., and Kuipers, J. (2005). Lattice-boltzmann simulations of low-reynolds-number flow past mono- and bidisperse arrays of spheres: results for the permeability and drag force. *Journal of Fluid Mechanics*, 528:233–254.
- van Noije, T., Ernst, M., and Brito, R. (1998a). Ring kinetic theory for an idealized granular gas. *Physica A*, 251:266–283.
- van Noije, T., Ernst, M., and Brito, R. (1998b). Spatial correlations in compressible granular flows. *Physical Review E*, 57(5):R4893.

- van Noije, T., Ernst, M., Brito, R., and Orza, J. (1997). Mesoscopic theory of granular fluids. *Physical Review Letters*, 79(3):411–414.
- Vidyapati and Subramaniam, S. (2013). Granular flow in silo discharge: Discrete element method simulations and model assessment. *Industrial "E" Engineering Chemistry Research*, 52(36):13171–13182.
- Vidyapati, V., Langroudi, M. K., Sun, J., Sundaresan, S., Tardos, G., and Subramaniam, S. (2012). Experimental and computational studies of dense granular flow: Transition from quasi-static to intermediate regime in a couette shear device. *Powder Technology*, 220:7–14.
- von Karman, T. and Howarth, L. (1938). On the statistical theory of isotropic turbulence. *Proceedings of the Royal Society of London. Series A, Mathematical and Physical Sciences*, 164(917):192–215.
- Walton, O. R. (1984). Application of molecular dynamics to macroscopic particles. *International Journal of Engineering Science*, 22(8):1097–1107.
- Walton, O. R. (2004). Potential discrete element simulation applications ranging from airborne fines to pellet beds. *SAE 2004 Transactions J. Aerospace*.
- Wang, K., Subramaniam, S., and Sundararajan, S. (2013). Final report: Understanding rheology of cement-based materials through integrated experiments and computations at multiple scales. *Final Report NSF CBET Grant No. 0927660*.
- Waters, J., Lee, S., and Guduru, P. (2009). Mechanics of axisymmetric wavy surface adhesion: Jkr–dmt transition solution. *International Journal of Solids and Structures*, 46(5):1033–1042.
- Weller, H., Tabor, G., Jasak, H., and Fureby, C. (1998). A tensorial approach to computational continuum mechanics using object-oriented techniques. *Computers in Physics*, 12(6):620–631.
- Wilson, R., Dini, D., and van Wachem, B. (2016). A numerical study exploring the effect of particle properties on the fluidization of adhesive particles. *AIChE Journal*, 62(5):1467–1477.
- Wylie, J. J. and Koch, D. L. (2000). Particle clustering due to hydrodynamic interactions. *Physics of Fluids*, 12(5):964–970.

- Xing, Z., Kenty, B., Li, Z., and Lee, S. (2009). Scale-up analysis for a CHO cell culture process in large-scale bioreactors. *Biotechnology and Bioengineering*, 103(4):733–746.
- Xu, Y. and Subramaniam, S. (2007). Consistent modeling of interphase turbulent kinetic energy transfer in particle-laden turbulent flows. *Physics of Fluids*, 19:085101.
- Yao, H., Ciavarella, M., and Gao, H. (2007). Adhesion maps of spheres corrected for strength limit. *Journal of colloid and interface science*, 315(2):786–790.
- Yin, X., Zenk, J. R., Mitrano, P. P., and Hrenya, C. M. (2013). Impact of collisional versus viscous dissipation on flow instabilities in gas-solid systems. *Journal of Fluid Mechanics*, 727:R2.
- Zaichik, L. and Alipchenkov, V. (2003). Pair dispersion and preferential concentration of particles in isotropic turbulence. *Physics of Fluids*, 15:1776–1787.
- Zaichik, L. I. and Alipchenkov, V. M. (2009). Statistical models for predicting pair dispersion and particle clustering in isotropic turbulence and their applications. *New Journal of Physics*, 11:103018.
- Zamankhan, P. (2005). Kinetic theory of multicomponent dense mixtures of slightly inelastic spherical particles. *Physical Review E*, 52(5):4877–4891.
- Zhang, Q. and Kamrin, K. (2017). Microscopic description of the granular fluidity field in nonlocal flow modeling. *Physical Review Letters*, 118:058001.

CHAPTER 8. THE HOMOGENEOUSLY COOLING GAS-SOLID FLOW

This chapter is in preparation as a manuscript to be submitted for publication.

8.1 Introduction

This chapter utilizes the theory developed in Chapter 7 to investigate clustering in a canonical problem, the homogeneously cooling gas-solid flow as simulated by particle-resolved direct numerical simulation. This problem is isotropic and begins as a system with randomly distributed particles with Maxwellian velocities in a quiescent fluid. The problem is much simpler in form than unbounded fluidization (Fullmer and Hrenya, 2016) or cluster induced turbulence (Capecelatro et al., 2015), but still contains rich physics that lead particles to cluster and spontaneously form vortices.

The problem was previously studied by (Yin et al., 2013), who made several observations that could not be fully explained by looking at the "state" of clustering. Some observations are that vorticity formation precedes clustering and that the presence of fluid inhibits the time it takes to cluster. The two-point transport equations used here are able to identify mechanisms that explain observed phenomena and provides a view of clustering as a dynamic process rather than a state or event. Comparison is then made with a sedimenting case, where particle wakes are shown to have an effect of causing plane-wave structures to appear in the two-point density. Fruitful new directions are also discussed.

8.2 Methods

This section is split up into 2 subsections. First the numerical set-up of the problem will be discussed. Then analytical methods for studying the homogeneous and isotropic gas-solid

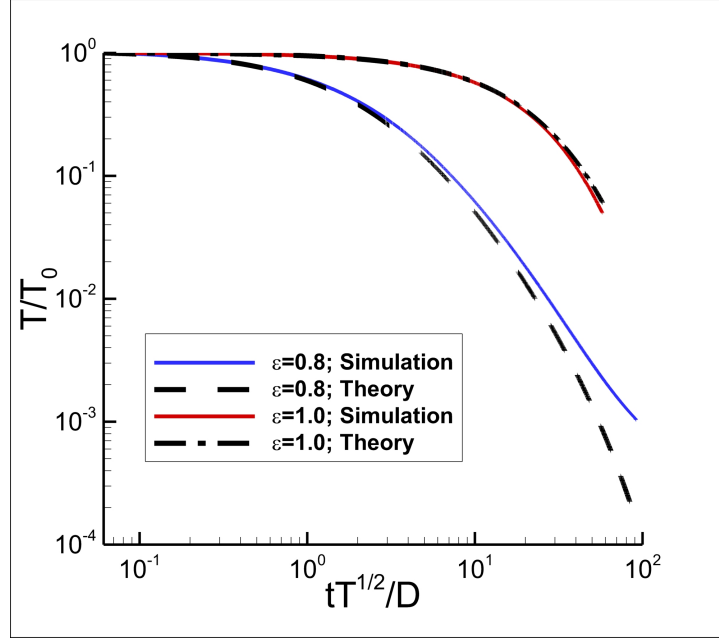


Figure 8.1 The temperature evolution is compared between two HCGSF cases, one inelastic and one elastic. The inelastic cools noticeably faster than the elastic case, which cools only through interaction with the fluid. Eventually, large discrepancies grow between the analytic prediction and DNS for the inelastic case, presumably due to structure formation.

flow will be introduced

8.2.1 Computational Set-up

The problem of interest is known as the homogeneously cooling gas-solid flow (HCGSF). We have simulated this problem using the particle-resolved direct numerical simulation (PR-DNS) code PReIBM (Tenneti et al., 2011), which has been validated for a suite of test cases. Particles are prepared with random positions and Maxwellian velocities in a quiescent fluid and allowed to evolve through both soft-sphere collisions (Cundall and Strack, 1979b) and interactions with the viscous fluid. As in the case of granular gases and previous study of the HCGSF, we expect the granular temperature, which is related to the trace of the velocity covariance matrix $T = \langle u'_i u'_i \rangle / 3$, begins to decay, see Fig. 8.1. How this decay rate depends on both system and particle parameters will be discussed further in 8.2.2.

The parameters of this study were chosen to mimic those in Yin et al. (2013) so that some

Table 8.1 Parameters for the preliminary studies on the HCGSF using the PR-DNS code PReIBM.

	Case 1	Case2
Realizations	5	5
thermal Reynolds number (Re_T)	3	3
solid volume fraction (ϕ_s)	0.2	0.2
density ratio (ρ_s/ρ_f)	1000	1000
Coefficient of Restitution (ε)	1	0.8
Diameter in grid units ($D/\Delta x$)	10	10
box length (L/D)	30	30

comparison could be made. There is a notable difference between the study undertaken and the previous authors. In order to expedite PR-DNS simulations Yin et al. (2013) used quasi-2D domains, with a thickness of 4 particle diameters, D , compared to a length of $30D$. The scaling observed in instabilities in ordinary granular as well as fluid flows are known to have a sensitive dependence on dimensionality of the problem, with velocity correlation lengths in granular gases being much larger for two dimensions compared to three dimensions (van Noije et al., 1998a). As a result, our domains have been chosen as cubic domains with the length of the box being $L = 30D$. Additionally, 5 realizations have been used for each case to better converge statistics. The remaining parameters of the study can be found in ???. The thermal Reynolds number is given as $Re_T = \sqrt{T}D/\nu$ and ν is the kinematic viscosity of the fluid.

While the canonical system under consideration here has no net source of energy to the fluctuations, it remains of practical interest to consider what physical system might be responsible for producing velocity fluctuations as characterized by Re_T . The ratio of steady-state velocity fluctuations in the particle phase to mean slip has been previously characterized by Tenneti et al. (2016) as a function of mean slip Reynolds number Re and ϕ_s . A value of $Re_T = 3$ at $\phi_s = 0.2$ is found to correlate to a mean slip Reynolds number of $Re = 159$. Combining with a drag law (Tenneti et al., 2011) provides everything needed to calculate the particle size and mean slip $\langle W_i \rangle$ for a sedimenting gas-solid flow with $\langle W_i \rangle = 2.9m/s$ and $D = 1.25mm$.

8.2.2 Analytical Methods

In homogeneously cooling particulate systems, that are by definition in absence of mean flow in the particulate and fluid phases, the evolution of granular temperature here is described by a single ODE (Yin et al., 2013). The ODE for this systems uses the combined mean-field theories of Garzo et al. (2012) and Koch (1990); Koch and Sangani (1999), which can be found in (Yin et al., 2013). The ODE and it's solution takes the form

$$\frac{\partial T}{\partial t} = -AT^{3/2} - BT \quad (8.1)$$

$$\frac{T}{T_0} = \frac{B^2 \exp(-Bt)}{(B + A\sqrt{T_0}(1 - \exp(-Bt/2)))^2}. \quad (8.2)$$

There T_0 is the initial granular temperature, A is the combined affect of viscous and collisional dissipation and B is the effect of the fluid not dependent on Re_T . The solution is plot alongside PR-DNS results in 8.1. The granular temperature for the elastic case appears to be well predicted by the mean-field theory, whereas departure is observed for the case of $\varepsilon = 0.8$. This is surprising given that the mean field description of the hydrodynamics is strictly valid only in the limit of Stokes flow. This departure is often attributed to the formation of structure within the flow, which alters the production and dissipation of energy in some way. However, we note that for a homogeneous system structure cannot appear on the single point level and must be described by evolution of two-point or higher statistics, as in the case of homogeneous isotropic turbulence (Pope, 2000).

In order to rigorously explore the origin of structure formation in the HCGSF and its affect on the evolution of the granular temperature, we introduce the equations of motion describing the evolution of the isotropic and separation dependent two-point structure functions. Up to the 2nd order this introduces a system of 4 PDEs, which are coupled to one another through mean transport terms

$$\frac{\partial n^{(2)}}{\partial t} + \frac{1}{r^2} \frac{\partial r^2 n^{(2)} \langle w_{\parallel} \rangle}{\partial r} = 0 \quad (8.3)$$

$$\frac{\partial \langle w_{\parallel} \rangle}{\partial t} + \frac{1}{r^2 n^{(2)}} \frac{\partial r^2 n^{(2)} \langle w_{\parallel} \rangle^2}{\partial r} = - \frac{1}{r^2 n^{(2)}} \frac{\partial r^2 n^{(2)} \langle w'_{\parallel} w'_{\parallel} \rangle}{\partial r} + \frac{\langle w_{\perp}^2 \rangle}{r} + \langle A_{\parallel} \rangle \quad (8.4)$$

$$\frac{\partial \langle w_{\parallel}^2 \rangle}{\partial t} + \frac{1}{r^2 n^{(2)}} \frac{\partial r^2 n^{(2)} \langle w_{\parallel}^3 \rangle}{\partial r} - \frac{2 \langle w_{\parallel} w_{\perp}^2 \rangle}{r} = 2 \langle A_{\parallel} w_{\parallel} \rangle \quad (8.5)$$

$$\frac{\partial \langle w_{\perp}^2 \rangle}{\partial t} + \frac{1}{r^2 n^{(2)}} \frac{\partial r^2 n^{(2)} \langle w_{\parallel} w_{\perp}^2 \rangle}{\partial r} + \frac{2 \langle w_{\parallel} w_{\perp}^2 \rangle}{r} = 2 \langle A_{\perp} w_{\perp} \rangle. \quad (8.6)$$

The first equation describes the evolution of the pair density, which is related to the radial distribution function by (Rani et al., 2014) $n^{(2)} = 2g(r)V/(N(N-1))$, where V volume of the domain and N is the number of particles. This equation is clearly connected to the first-order moment equation for $\langle w_{\parallel} \rangle$ by the transport term. The first-order moment $\langle w_{\parallel} \rangle$ is the expected normal relative velocity between a pair particles separated by a distance r . This is also known as the longitudinal velocity in turbulence. Note that these are Eulerian averages in separation space. This equation takes a familiar form, with a mean transport term on the LHS and a divergence of a Reynolds stress like term on the RHS, which resembles an ideal gas law in form. The second term on the RHS is connected to the transverse velocity modes, which characterizes vorticity (van Noije et al., 1997, 1998b,a). The two 2nd order equations describe the evolution of the structure functions in the longitudinal and transverse modes respectively, and do not contain self-correlations. Thus they are related to the ordinary Karman-Howarth equations for isotropic turbulence (von Karman and Howarth, 1938). They are related to the normalized auto-correlation functions in turbulence by $g = \langle w_{\perp}^2 \rangle / 4T$ and $f = \langle w_{\parallel}^2 \rangle / 2T$ (Pope, 2000). We note that the relationship $g = f + \frac{r}{2} \frac{\partial f}{\partial r}$ implied by incompressibility is not valid here because the particle phase is compressible. Note also that Eqs. 8.5 and 8.6 are directly coupled through a 3rd order moment.

Lastly, the acceleration terms in Eqs. 8.4-8.6 arise from three sources of origin: 1) direct collisions, 2) indirect collisions, and 3) hydrodynamic interactions. Direct interactions are closed at this two-particle description, and model the collisions that occur between the two-particles considered in the averaging procedure. Indirect collisions are events where the relative velocity of two particles is altered via interaction with a third particle. In modern kinetic theory of hard

spheres these are known as ring collisions (Ernst et al., 1969; van Noije et al., 1998a). Finally, the hydrodynamic interactions that two particles experience also give rise to indirect relative accelerations. The effect mean relative acceleration is obvious, if it is negative it will tend to bring particles together. In direct interactions with inelasticity it will also cause particles to lose momentum from a collision. However, the Acceleration-velocity term is more mysterious. In single-point statistics it can be shown that this term describes the dissipation and source of energy in the granular phase (Tenneti et al., 2016). In the HCGSF this 2-point term provides a net sink to energy in relative velocities that may depend on separation. This dependence on separation provides a source of correlations that develop in the HCGSF, which in time couple strongly to the relative velocity and pair density through transport terms. This structure is an important feature of these equations. For example, it is often noted that the emergence of vorticity in these systems precedes the appearance of clusters (Yin et al., 2013). If the structure arises out of the 2nd order moments, vorticity must appear before clustering. Clustering can only occur after 2nd order moments have developed sufficiently enough to drive clustering via the transport terms.

8.3 Results and Discussion

This section is organized as follows. First we explore the spatio-temporal evolution of the two-point moments. Next different terms are investigated in the evolution equations outlined in Section 8.2.2 to help explain clustering and vortex instabilities as dynamical processes. The effect of collisional versus hydrodynamic forces are also compared.

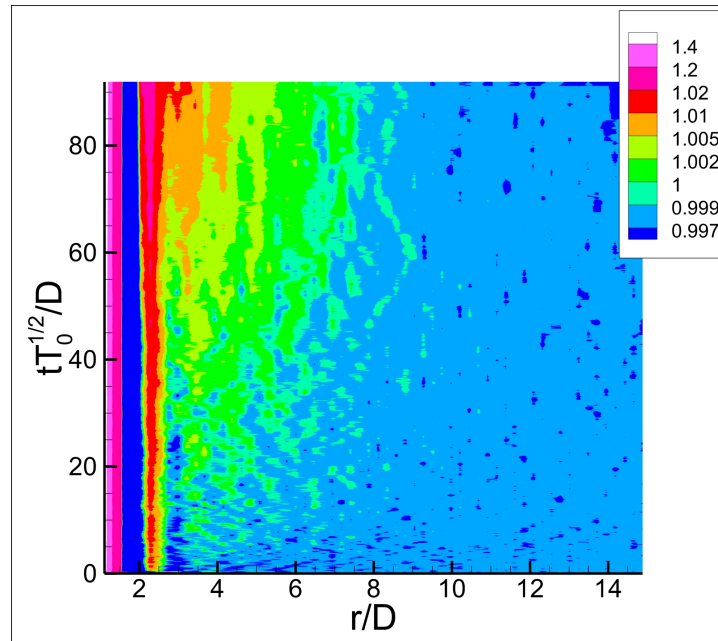
8.3.1 Moments

The radial distribution function is the first quantity of interest, since it offers the most clear evidence of clustering. Recall that $g(r)$ quantifies the likelihood of a particle having a neighbor located at some distance r relative to a completely random distribution of particles. Figures 8.2(a) and 8.2(b) display $g(r)$ for cases with and without cohesion. Both show some generic features, including a significant peak at contact, a depletion zone between the first and second coordination shells, and another peak near $r = 2D$. The inelastic case shows

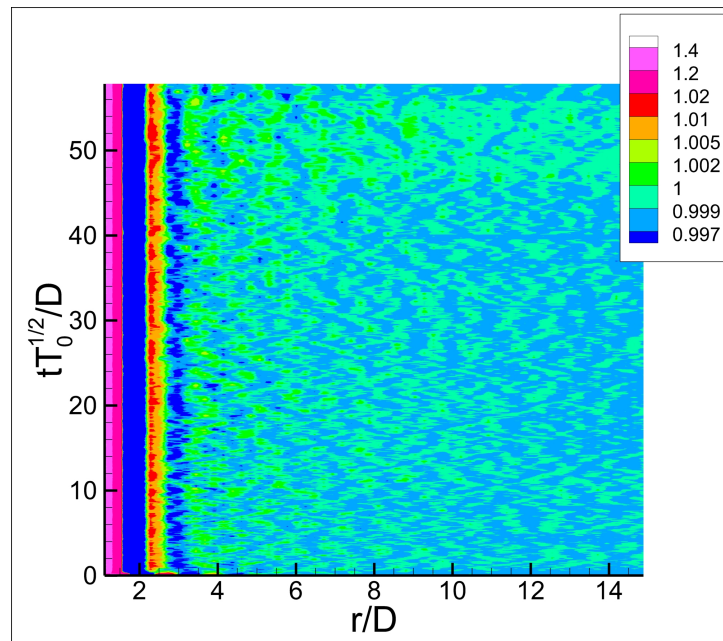
clear evidence of clustering, whereas the elastic case is not observed to cluster, inline with the previous study (Yin et al., 2013). Though the differences in the magnitude appear only slight, by the end of the simulation, excess particles are observed compared to the initial condition at distances of up to $r = 8D$. We also note that the development of correlations begins very early in the inelastic case, at times $t\sqrt{T_0}/D$ well before significant divergence is observed in the temperature predictions. This demonstrates that clustering is a dynamic process.

Regardless of the mechanism behind clustering, if clustering occurs the mean relative velocity between particles $\langle w_{\parallel} \rangle$ must be negative on average for neighbor particles at some distance. Figures 8.3(a) and 8.3(b) display $\langle w_{\parallel} \rangle / \sqrt{2T}$, with the inelastic case showing the development of significant structure. As with $g(r)$, the development of negative relative velocities begins as early as $t\sqrt{T}/D = 20$, and increases in magnitude and length-scale as time progresses. This further emphasizes the importance of clustering being considered as a dynamical process rather than a state of being. By the end of the simulation, we see that negative relative velocities extend to the nearly the edge of the box, with the strongest clustering occurring just outside of the second coordination shell.

Finally, we wish to look at the normalized structure functions in the longitudinal and transverse directions, see figs. 8.4(a), 8.4(b) and 8.5(a), 8.5(b), respectively. Interestingly, all four plots show the development of structure in time. Structure in the inelastic case fields shows up almost immediately. By the end of the simulation velocity fluctuations in both the normal and transverse relative directions are 30% and 40% of what they should be if no correlations were present. Particles separated by long distances are much less affected. We note that $\langle w_{\perp}^2 \rangle$ characterizes the level of correlated rotations of particle about one another, i.e. vorticity. Consistent with observations in both granular gases (van Noije et al., 1998a) and the HCGSF (Yin et al., 2013), vortices appear to gain much more significant signatures before the emergence of clustering. Structure in the elastic case remains much shorter ranged and less significant, but nonetheless appears consistent with previous findings. It is clear from the study of raw moments themselves that inelasticity is essential for the development of strong correlations in the HCGSF, and are much stronger than the influence of hydrodynamics.

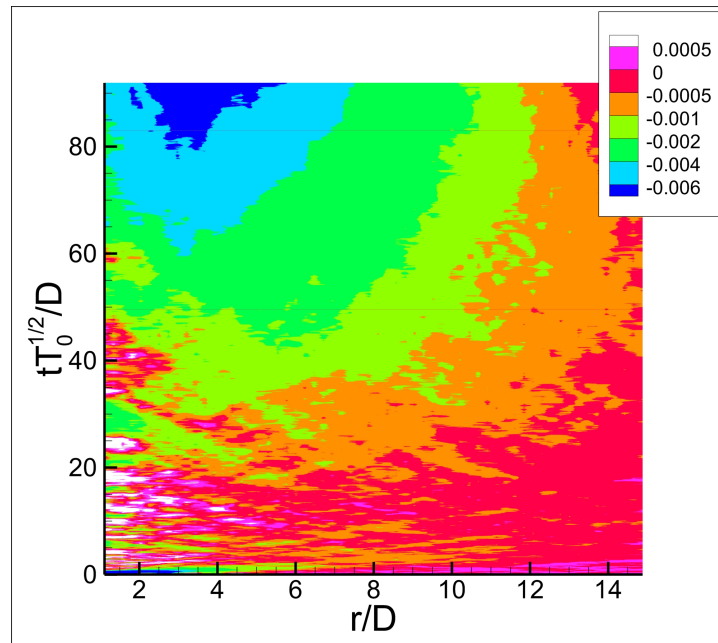


(a)

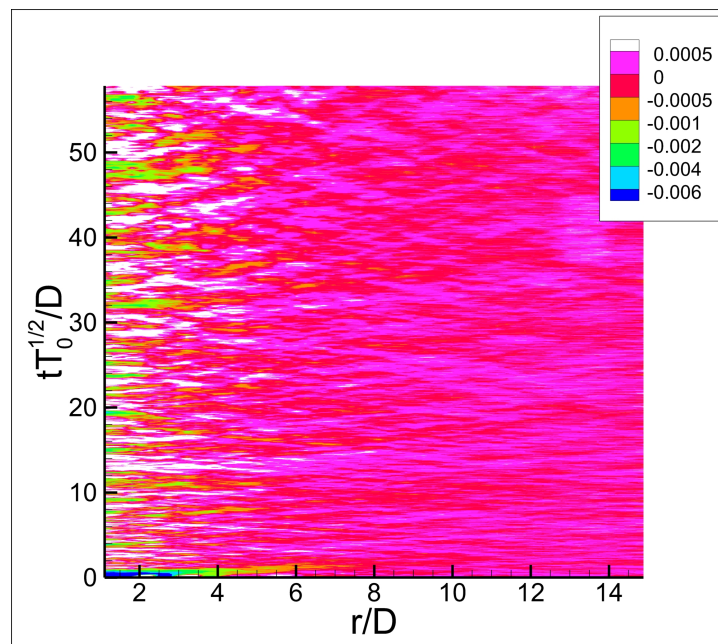


(b)

Figure 8.2 The evolution of the radial distribution function $g(r)$ is plot for (a) $\varepsilon = 0.8$ and (b) $\varepsilon = 1$. In the case of inelastic particles, there is clear evidence that clustering is occurring in the domain.

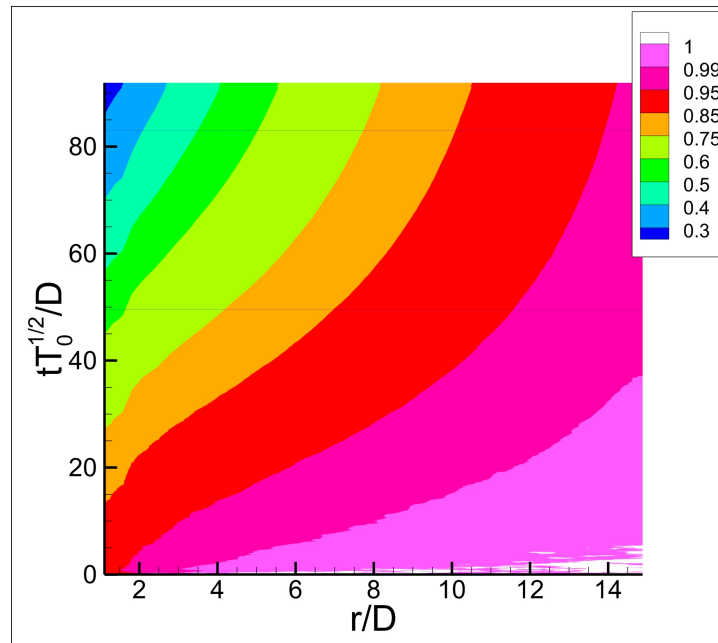


(a)

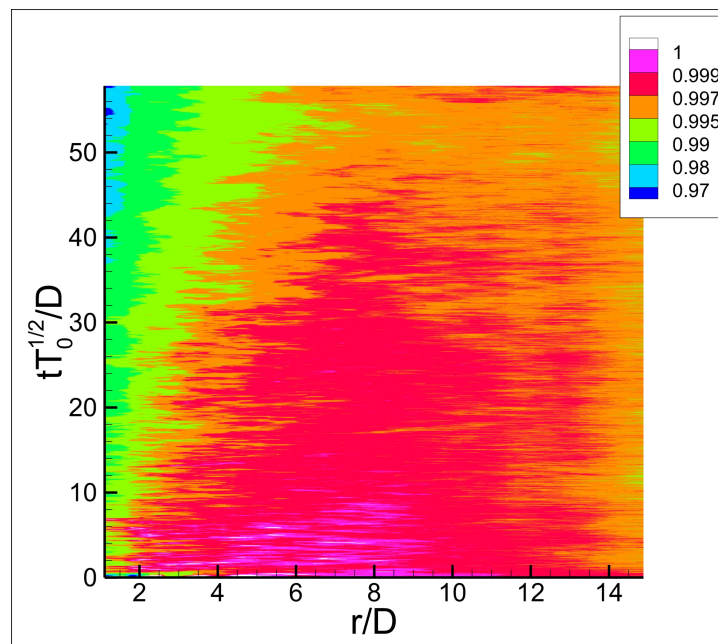


(b)

Figure 8.3 The evolution of the normalized normal relative velocity $\langle w_{\parallel} \rangle / \sqrt{2T}$ is plot for (a) $\varepsilon = 0.8$ and (b) $\varepsilon = 1$. The elastic case is the only case to show the emergence of significant structure.

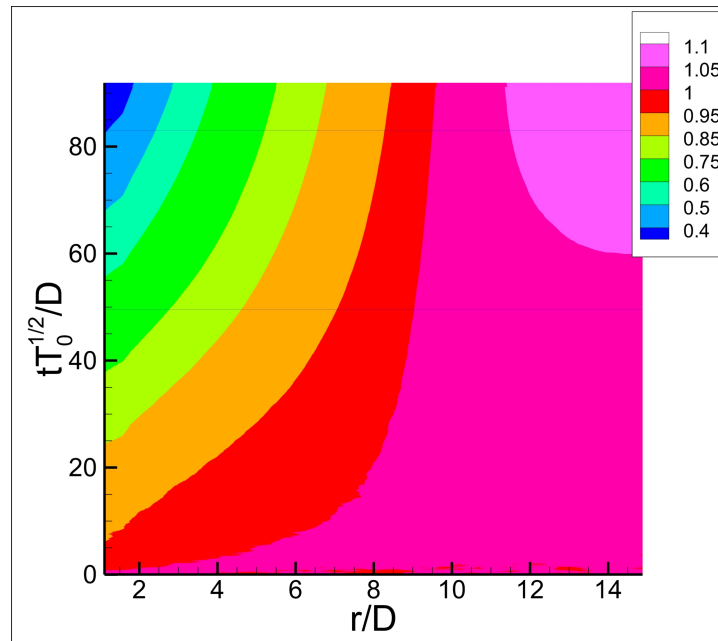


(a)

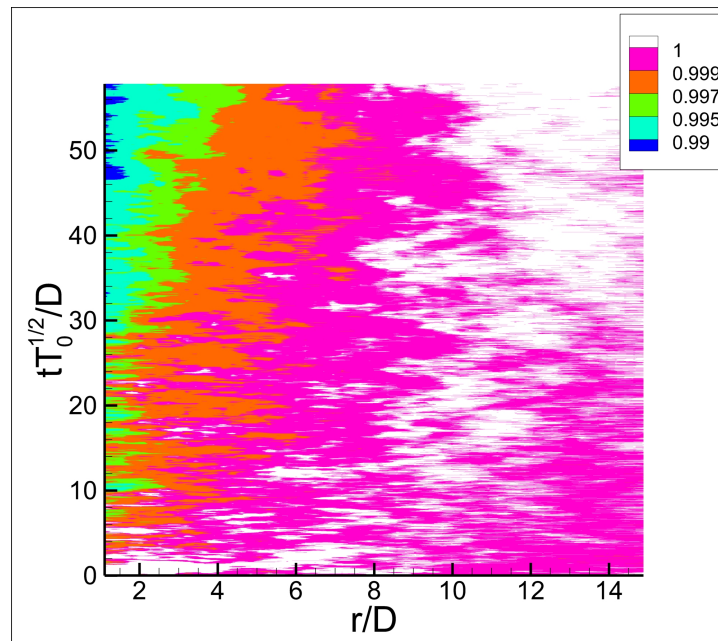


(b)

Figure 8.4 The evolution of the normalized second-order longitudinal structure function $\langle w_{\parallel}^2 \rangle / 2T$ is plot for (a) $\varepsilon = 0.8$ and (b) $\varepsilon = 1$. Both cases show some structure formation with the inelastic case being far more significant.



(a)



(b)

Figure 8.5 The evolution of the normalized second-order longitudinal structure function $\langle w_{\perp}^2 \rangle / 4T$ is plot for (a) $\varepsilon = 0.8$ and (b) $\varepsilon = 1$. Both cases show some structure formation with the inelastic case being far more significant.

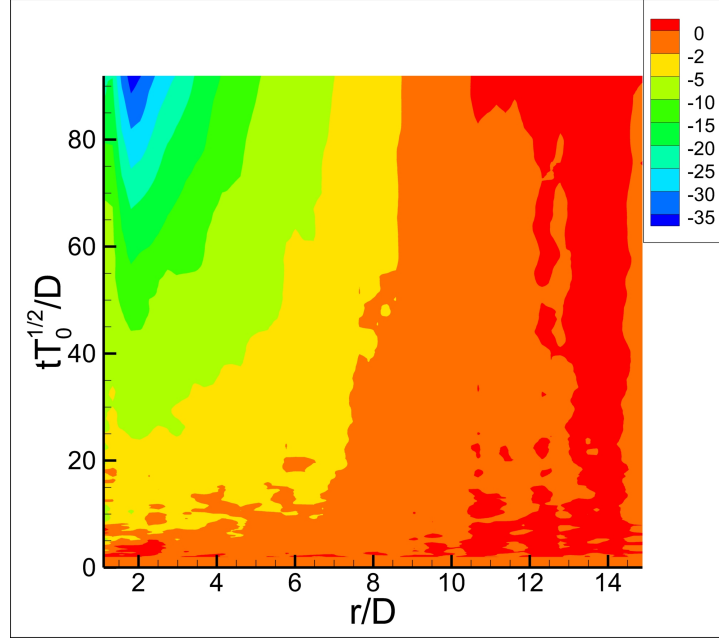


Figure 8.6 The evolution of the net change in the number density of pairs at a given separation as calculated from $\int_0^t \frac{1}{r^2} \frac{\partial r^2 n^{(2)} \langle w_{\parallel} \rangle}{\partial r} d\tau$.

8.3.2 Evolution Equations

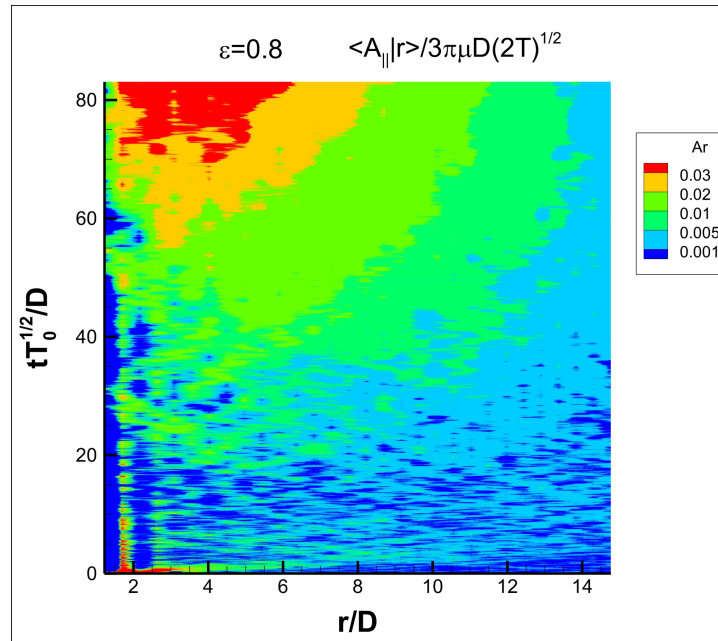
Now we examine the terms that arise in the moment transport equations to observe their affect on clustering. In extracting these terms we encounter two difficulties. Finite difference approximation of averages with some degree of uncertainty can produce noisy signals. Also collisions in this system are rare events, with usually only 1 or no particles colliding in at any given time-step, producing noisy signals. We can alleviate this by time integrating these signals. For example, fig. 8.6 displays the integral of the transport term in the 0th order equation $\int_0^t \frac{1}{r^2} \frac{\partial r^2 n^{(2)} \langle w_{\parallel} \rangle}{\partial r} d\tau$, which represents the net-change in the pair number density at the some separation. Note the sign change on taking the terms to the RHS. This signal shows significant structure and evidence of clustering despite the computational challenges.

The first two terms that we would like to observe is the competition between the relative acceleration and pressure-like term, which explicitly couples the relative momentum equation to the 2nd order equation. Figure 8.7(a) displays the relative acceleration normalized by Stokes drag $\langle A_{\parallel} \rangle m_r / 3\pi\rho_f\nu D\sqrt{2T}$ due to hydrodynamics between two particles for the inelastic case.

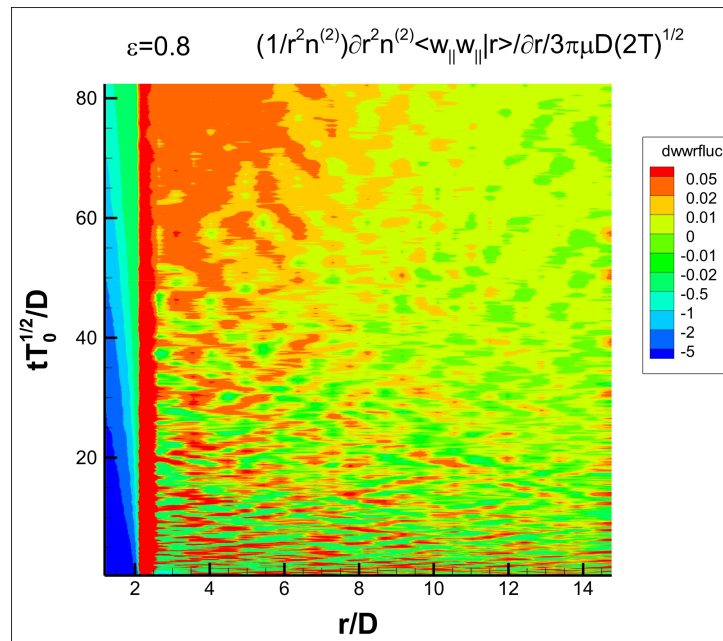
Surprisingly, the relative acceleration is positive and has a spatial signature similar to the relative velocity. There is no affect of particle wakes observed. This is due to a mean relative drag that develops as clustering particles display fluid. This average repulsive signature also explains an observation made in the previous study (Yin et al., 2013), that the presence of a viscous fluid tends to delay the onset of clustering. The collective pressure gradient-like term $\frac{1}{r^2 n^{(2)}} \frac{\partial r^2 n^{(2)} \langle w'_{\parallel} w'_{\parallel} \rangle}{\partial r} - \frac{\langle w_{\perp}^2 \rangle}{r}$ is shown in fig. 8.7(b) and is normalized by Stokes drag. When taken to the RHS of eq. 8.4 this term becomes negative and shows a tendency to lead to clustering. This is the first clear link showing that it is the evolution of second moments that directly leads to clustering in the HCGSF, and confirms that the moment hierarchy is responsible for the smaller time-scale in the evolution of vorticity compared to clustering. Similar findings arise in the mesoscopic study of granular flows (van Noije et al., 1998b), where the second order structure evolves due to it's tie to the 2nd moment equation through an equation of state.

Finally, we wish to show how structure in the second moments arise. The two unclosed terms in the central moment version of Eqs. 8.5 and 8.6 are the triple correlations, e.g., $\langle w_{\parallel}^3 \rangle$, and the Acceleration-velocity covariance $\langle A'_{\parallel} w'_{\parallel} \rangle$. If the third order moments are insignificant to the development of clustering, we can be satisfied on the decision to truncate at the 2nd moments. First, we show the integral of the entire transport terms involving raw third order moments in Eq. 8.6, see fig. 8.8. The net transport due to the third order moment transport terms is positive, meaning that these transport terms hinder the formation of structure in the structure functions, and thus clustering itself. The same story is told for the transverse modes, not pictured. This means that the development of structure in the structure functions is due to the acceleration-velocity moments.

The acceleration-velocity moments represent a net sink of fluctuation energy in the relative velocities of particles. The dependence of this sink on separation will tell us how energy in the granular phase is dissipated at different scales. Figure 8.9(a) shows the sink of energy due to hydrodynamic interactions normalized by what is expected from Stokes drag for $\varepsilon = 0.8$. At large separations of $r/D > 8$ the function does not appear to depend on the separation, but remains negative. This is due to the fact that energy decays at all distances. So it is the



(a)



(b)

Figure 8.7 (a) The relative acceleration between particles due to hydrodynamics for the inelastic case is shown and is found to have a repulsive character. (b) The normalized pressure like term is shown and has the tendency to lead to clustering particles.

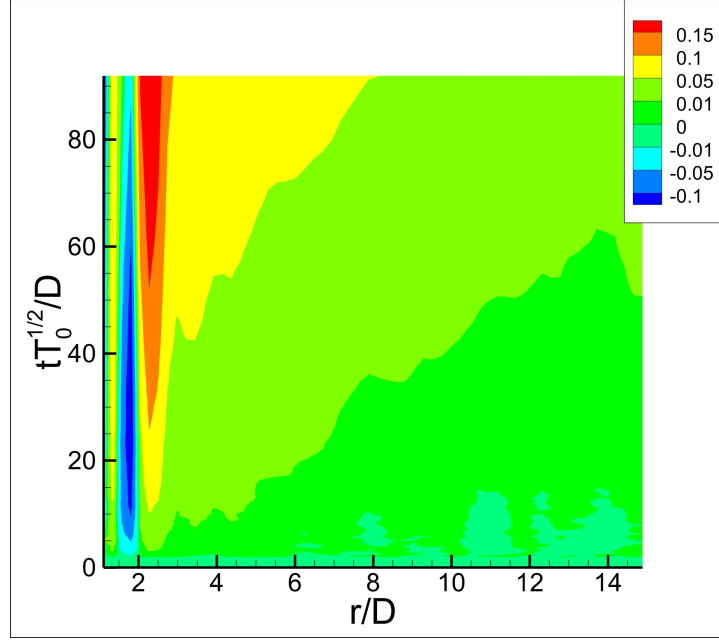
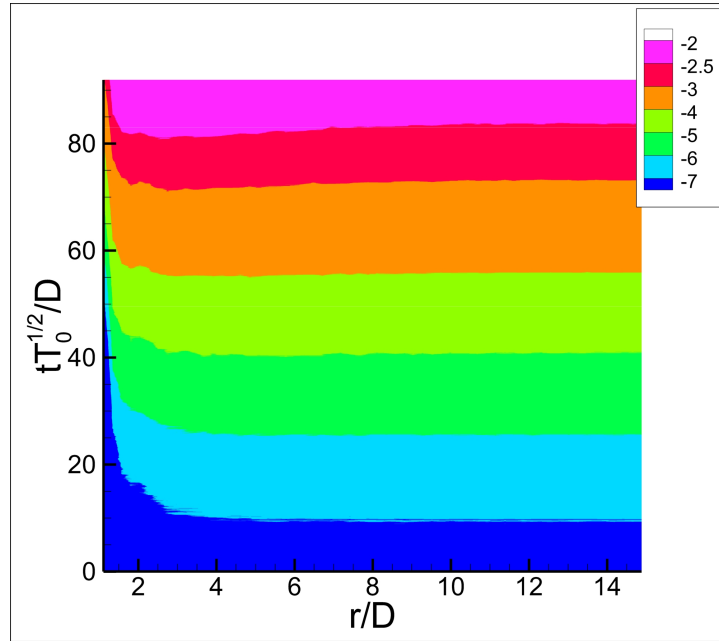


Figure 8.8 The evolution of the net change in the normalized longitudinal structure function

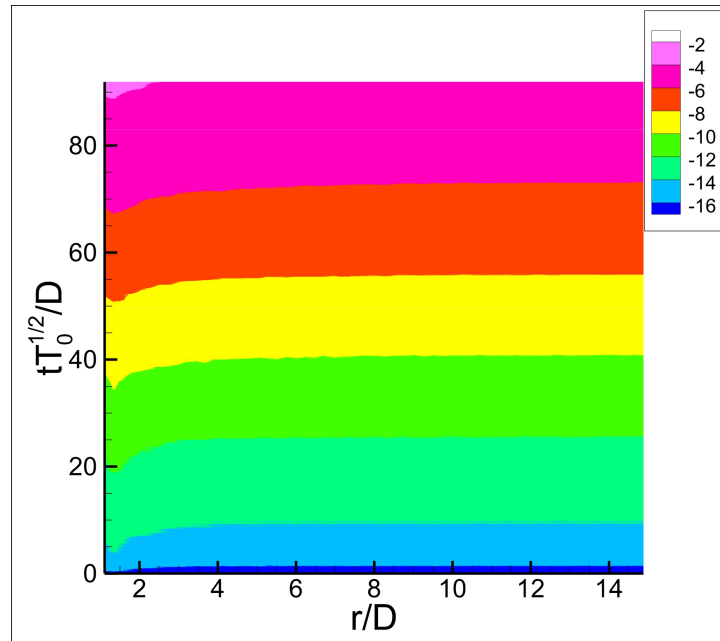
due to transport given by
$$-\frac{1}{2T} \int_0^t \frac{1}{r^2 n^{(2)}} \frac{\partial r^2 n^{(2)} \langle w_{\parallel}^3 \rangle}{\partial r} - \frac{2 \langle w_{\parallel} w_{\perp}^2 \rangle}{r} d\tau.$$

spatially varying structure that leads to correlations in the structure functions. Energy loss due to hydrodynamics is much stronger at close separations, and is consistent with observation of the lower energy at closer separations and also expectations due to lubrication effects. The transverse sink is shown in fig. 8.9(b). Note that it is roughly twice as large as the longitudinal component because it is counting both transverse modes. This has the opposite structure of what is expected. Particles that are close together experience less of a sink, which would tend to inhibit the vorticity structure in the transverse structure function. This is likely due to the two particles in close proximity entraining local fluid in their local eddy. As a result, the slip between fluid and particles is lower for close pairs, and the spatial signature is the result of the coupled dynamics with the fluid field variables, which have been averaged out. As a result, the vortical structures that appear in the HCGSF must be due to the sink of energy due to energy dissipation in indirect particle collisions.

For completeness, we look at the same acceleration-velocity plots for the elastic case, see figs. 8.10(a) and 8.10(b). The exact same spatial structure is observed in these sinks, though



(a)



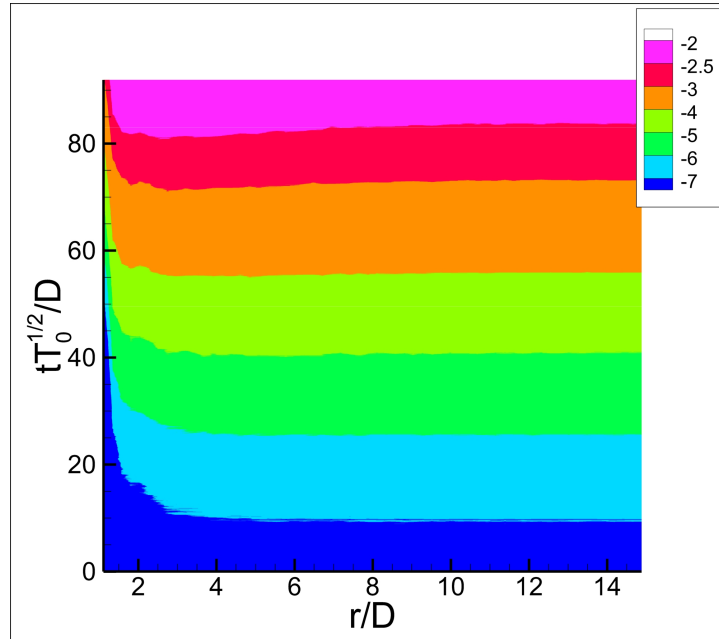
(b)

Figure 8.9 (a) The sink of energy from the longitudinal structure function due to hydrodynamic interactions $2\langle A_{\parallel}w_{\parallel} \rangle m_r/3\pi D\rho_f\nu 2T$. (b) The sink of energy from the transverse structure function due to hydrodynamic interactions $2\langle A_{\perp}w_{\perp} \rangle m_r/3\pi D\rho_f\nu 2T$. Both are for the case of $\varepsilon = 0.8$.

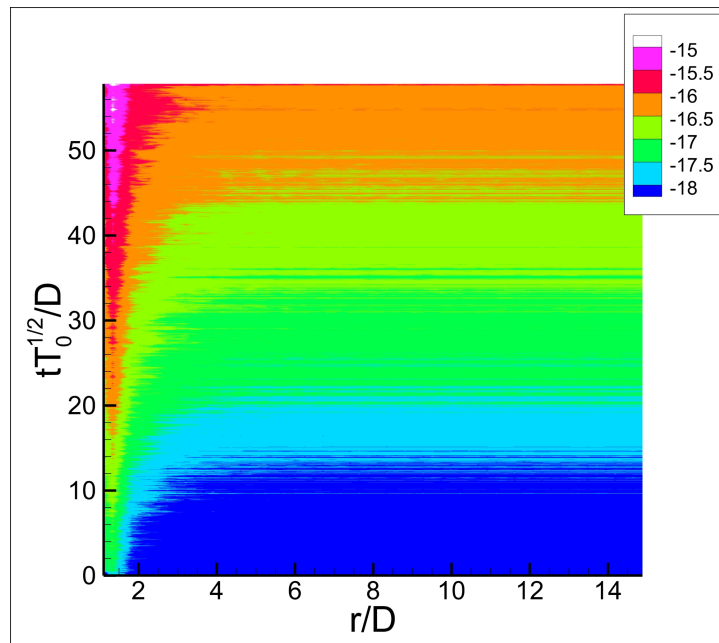
the sinks are overall much stronger, likely due to the high temperature of the elastic case. One question remains: if the acceleration-velocity moments in the longitudinal modes appear to promote structure formation, why are the correlations so weak in the elastic case? The collisional piece of the acceleration-velocity statistics has been inferred (rather than measured) from the balance implied in Eq. 8.5 and is shown in fig. 8.11. Here we see the exact opposite signature. The collisions provide a source of energy, which is stronger at closer separations. If particles slow due to interaction with the hydrodynamics, collisions with particles with faster particles will serve to redistribute energy in separation space. We may think of this as akin to thermal conductivity. It is of interest how the balance of sink due to hydrodynamics and redistribution due to collisions might change if for example the viscosity of the fluid, i.e. Reynolds numbers were to change. Such changes would increase the hydrodynamic sink, while presumably lowering the ability of particles to redistribute energy through less energetic collisions. So while clustering was not observed in this study, it is not out of the question for all possible combinations of elastic particles and fluid in the HCGSF.

An interesting proposition would be to provide a model for the acceleration-velocity covariance due to collisions and hydrodynamic interactions. The hydrodynamic terms appear especially stable in their functional form, while the collisional piece could be modeled by the two behaviors we have seen, energy loss due to indirect collisions and redistribution of energy in separation space due to gradients in the structure functions. If the transport due to triple correlations are ignored, a closed system of equations are the result, and the system model could then be solved and studied.

While we have shown in this paper how particle cluster in an isotropic case, real systems such as sedimenting or fluidized flows are necessarily anisotropic due to mean particle slip. There the effect of wakes appearing in the the relative acceleration and acceleration-velocity statistics might fundamentally change the nature of clustering in fluid particle systems. This mean slip also provides a source of energy to the particulate phase, whose dependence on scale may be non-trivial. In fig. 8.12, we show the mean relative acceleration due to hydrodynamics in the flow direction from a pressure driven DNS at $Re = 30$. It is clear that the relative acceleration is tending to drive particle together, with positive separations having negative



(a)



(b)

Figure 8.10 (a) The sink of energy from the longitudinal structure function due to hydrodynamic interactions $2\langle A_{\parallel}w_{\parallel}\rangle m_r/3\pi D\rho_f\nu 2T$. (b) The sink of energy from the transverse structure function due to hydrodynamic interactions $2\langle A_{\perp}w_{\perp}\rangle m_r/3\pi D\rho_f\nu 2T$. Both are for the case of $\varepsilon = 1$.

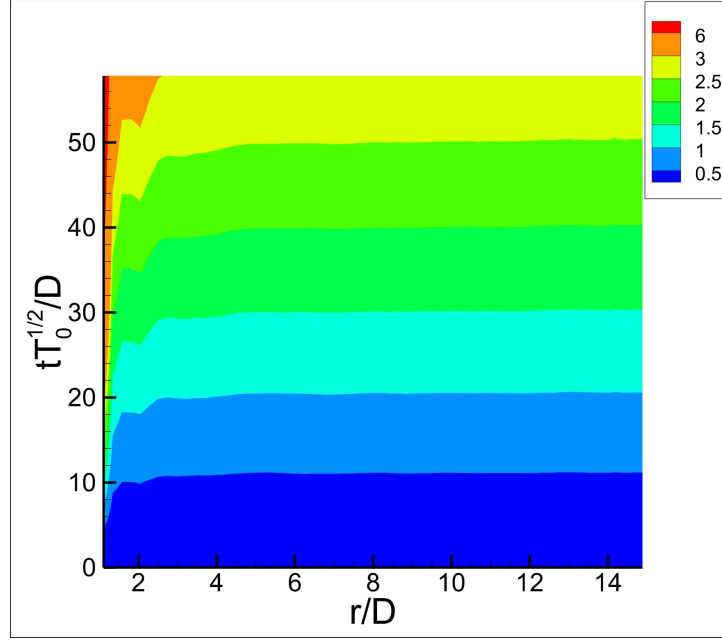


Figure 8.11 The time integrated longitudinal acceleration-velocity statistics due to collisions

$$-\frac{1}{2T} \int_0^t 2 \langle A_{\parallel, coll} w_{\parallel} \rangle d\tau.$$

accelerations. Indeed, plane-wave type instabilities are observed in these cases ??, which shows that the spatial signature of these flows is still intimately tied to the dynamics imposed by the mean fluid flow.

8.4 Conclusions

In this work we have presented a first-principles study of the homogeneously cooling gas-solid flow simulated via PR-DNS. The approach relies on a hierarchy of exact moment equations governing the transport of the radial distribution function in separation space. This framework allows for study of the dynamic process of clustering, and the growth correlations. By quantifying the terms appearing in the transport equations, we are able to identify mechanisms responsible for the development of correlations, which are identified as vortices and clustering.

The mechanisms causing clustering and spontaneous formation of vorticity are found to have the same origin, the scale dependence of the sink term in the evolution equation for structure function. These particles that are near to one another dissipate energy more quickly than

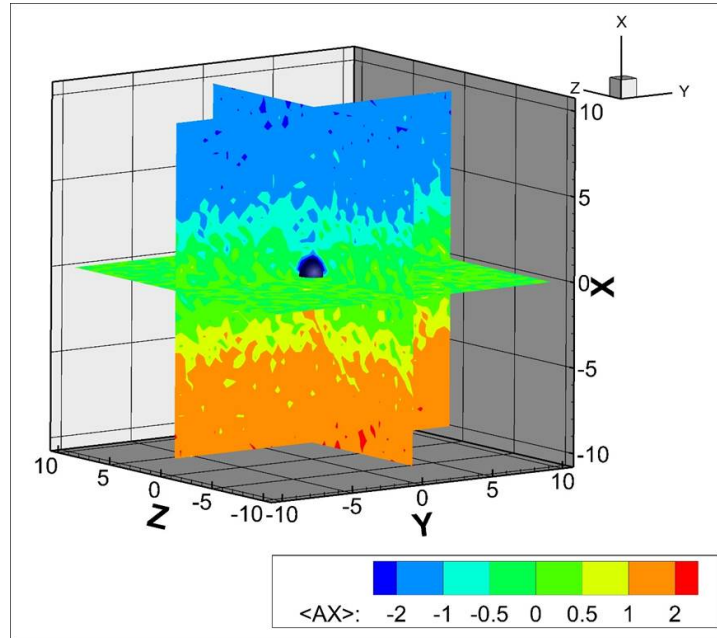


Figure 8.12 The mean acceleration in the flow direction $\langle A_x \rangle$ for a pressure driven gas-solid flow.

particles separated by larger distances. The developing correlations in the longitudinal structure function then couple to the lower order moment equations through transport terms and affect the clustering of particles. Hence the structure of the moment equations are able to clearly explain the reason vorticity formation precedes the emergence of clusters. The observation that fluid impedes the clustering of granules is also explained by the appearance of a mean relative drag that arises due to particles displacing fluid during clustering. Finally, a mechanism similar to thermal conductivity is observed in elastic particles, where energy redistributes in separation space to destroy correlations from the fluid flow.

The framework utilized in this study is applicable to other homogeneous systems as well, such as in sedimenting cases or unbounded fluidization. The physics responsible for clustering are found to be much different in those cases, with anisotropy leading to important interactions between particles and wake interactions. The framework may also be used to rigorously compare the predictions and accuracy of PR-DNS and other coarse-grained Lagrangian-Eulerian simulations, and can provide essential data for mesoscopic Eulerian-Eulerian simulations.

CHAPTER 9. SUMMARY AND FUTURE WORK

9.1 Summary

This thesis has sought to study a number of problems in multiphase flows, seeking to incorporate the effects of structure in modeling. The problems roughly fall under rheological studies of cohesive particle systems, the kinetic theory of polydispersed solid-solid drag, and finally clustering in homogeneous gas-solid flows.

In Chapters 2 - 5 focus is given to the study of cohesive particles. These studies are ordered by increasing complexity in the interactions that are included. Chapter 2 focuses on the accuracy of simulations of collisions between cohesive inelastic particles. Rigorous limits on numerical time steps as well as stiffness of particles are developed. It is shown that if too soft of particles are used, rheological behavior in simply sheared systems of moderately dense systems is not well predicted. This study has shown the large cost incurred from including cohesion in granular systems, since computational cost is inversely proportional to the stiffness.

In Chapter 3 the effect of cohesion on the canonical homogeneously cooling granular gas is studied via kinetic theory and discrete element method (DEM) simulations. Generally, cohesion is shown to increase the cooling rate in granular gases. The kinetic theory predictions are shown to be accurate, when the majority of collisions are between monomers and is shown to be more accurate than theories developed for long-ranged potentials. Developing structure in the structure functions is then investigated, and it is shown how instabilities due to cohesion qualitatively differ from those due to inelasticity alone.

Chapter 4 focuses on the study of a regime transition in the rheology of moderately dense cohesive assemblies under simple shear. The simply sheared systems remain dispersed at high shear rates, while they tend to cluster and percolate the domain under a critical shear rate.

This critical shear rate in smooth particle systems is shown to depend only on the inelasticity of particles and an energetic scaling parameter Ha , which is the ratio between the the potential at contact to the kinetic energy. When friction is included, the transition remains energetic, which is at odds with many state-of-the-art models. The connection between friction and contact anisotropy is also shown to be responsible for anomalous behavior of the shear stress and shear stress ratio as friction is increased.

The cohesive studies conclude with Chapter 5, where the rheology of portland cement and fly ash slurries are simulated via fast lubrication dynamics and DEM. Particle interaction parameters such as particle friction and Hamaker constants are taken from atomic force microscopy measurements. Good qualitative agreement in the shear stress is observed when compared with vane-rheometer experiments. Quantitative comparison with experiments is improved when confinement effects are included.

A theory for the friction felt between two counter-flowing particular phases is developed using the pseudo-Liouville kinetic theory in Chapter 6. Operators are developed for use it the theory for polydispersed particles. Proper care is taken so that anisotropy of the pair-relative velocity at contact is properly integrated. Additionally, four unique terms are identified in the temperature evolution equation, cooling due to intraphase collisions, cooling due to interphase collisions, exchange due to interphase collisions, and heating from the solid-solid drag. Equations are reduced to the point where two integrals are left to be evaluated.

The last two chapters 7 and 8 focus on properly describing clustering in the homogeneous gas-solid flows. An exact framework governing the evolution of two-point statistics is introduced, and used to study clustering in the isotropic homogeneously cooling gas-solid flow. Terms in the transport equations for 2-point statistics are quantified using DNS. Mechanisms for the development of correlations are identified and explain phenomenology observed in prior studies. A stochastic method for modeling the these 2-point problems is also introduced.

9.2 Future Work

The focus of the future work will be on two different problems, which are the subject of previous chapters. Those problems are listed below:

1. Development of a solid-solid drag law for polydisperse granular gases at arbitrary Mach number.
2. Modeling of clustering in homogeneous pressure-driven or sedimenting gas-solid flows.

For the future work pertaining to the solid-solid drag law, the reader is pointed to Section 6.3, which contains a thorough discussion of the relevant next steps in that problem. This section will focus on the next steps on the clustering of sedimenting gas-solid flow. Preliminary results will be presented, which give context for the next steps. Note that a more formal introduction to the problem was given in Section 7.1.

9.3 The homogeneously sedimenting gas-solid flow

The homogeneously sedimenting gas-solid flow has not received much attention from the PR-DNS community. Though other various two-way coupled Euler-Lagrange methods have treated the system (Capece de Almeida et al., 2014; Fullmer and Hrenya, 2016). These methods both find that clustering occurs, and give some treatment for modeling how such clustering can occur. We treat this system using our exact equations, and hope to formalize what mechanisms might lead to clustering in these systems. Again, PReIBM is used to examine these cases. This system has two density ratios of $\rho_s/\rho_f = 1000$ and $\rho_s/\rho_f = 100$, a volume fraction of $\phi_s = 0.2$, with cubic domains of size $L/D = 20$, and resolution of $D/\Delta x = 20$. This system is driven with a pressure gradient to achieve a Reynolds number of $Re = 30$.

Initially, the system has no granular temperature, but slowly heats up through interaction with velocity fluctuations in the fluid. Particles are also elastic. The domain is initially homogeneous and is observed to cluster for the first time using PReIBM, see Figs. 9.1 and 9.2. Note that particles are colored by their axial velocity. It appears as though particles are separating into regions of particles, which are moving in opposite directions. The red particles that are moving in direction of the pressure gradient with lower mean slip are arranged in denser plane wave like structures, whereas the blue particles moving against the pressure gradient having higher slip are more dilute. This is in agreement with two pieces of intuition 1) higher volume

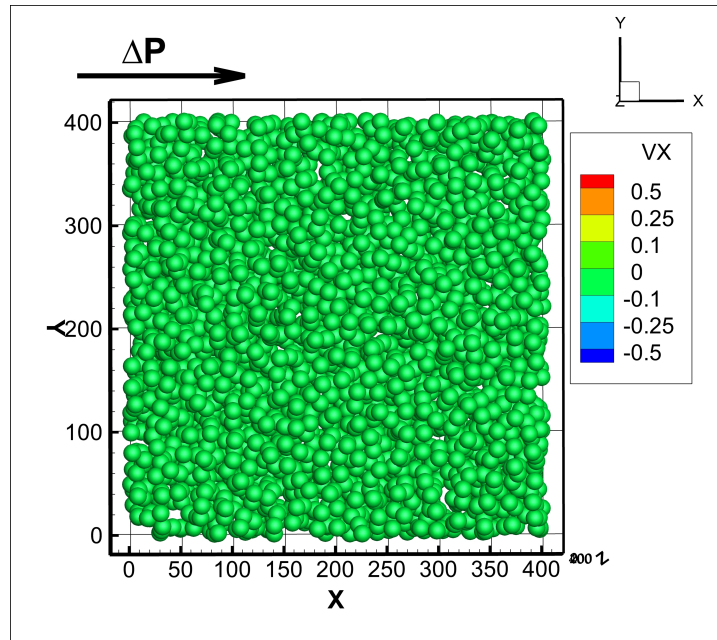


Figure 9.1 The initial distribution of particles in a pressure driven gas-solid flow is shown. Particles are initially homogeneously distributed with no axial velocity.

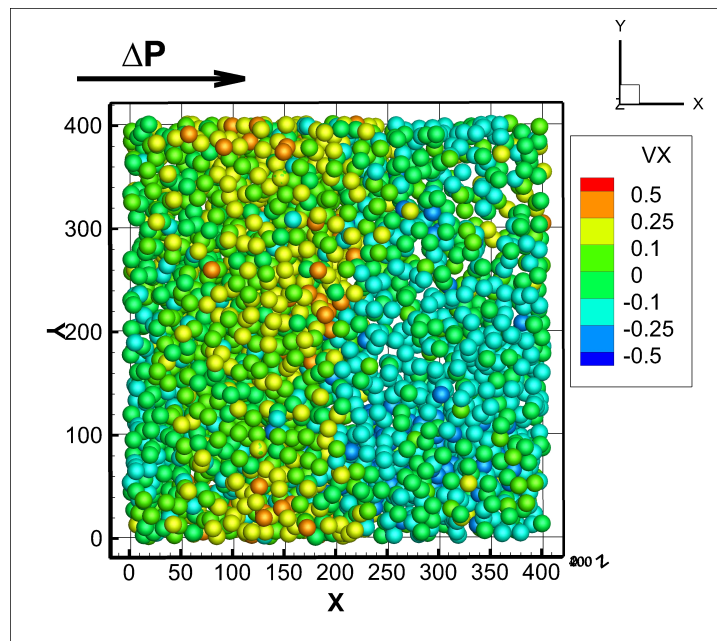


Figure 9.2 The final configuration of particles in a pressure driven gas-solid flow has less uniformity. Particles are colored by their axial velocity and normalized by their granular temperature, i.e. v_x/T_g . Positively traveling particles are in denser regions than particles moving in the negative direction.

fractions exhibit higher drag and 2) higher volume fractions increase the Reynolds numbers, further increasing the drag force.

Unfortunately, it is difficult to obtain converged statistics for transient anisotropic problems, where spherical averaging cannot be carried out. As a result, averaging has been carried out after the global drag reaches an initially steady behavior. Note that each simulation herein has been performed on a 16-core node on the Cyence supercomputer at Iowa State using over 11,000 cpu hrs. As a result, statistics here are time averaged and should not be taken as quantitative.

We report here only a few of the statistics from Section 7, without any transport terms. These interesting statistics are the pair correlation function $g(r)$, and the streamwise components of the mean relative velocity $\langle w_1 \rangle$, relative velocity fluctuations $\langle w'_1 w'_1 \rangle$, relative acceleration $\langle A_1 \rangle$, and finally the source and sink of the acceleration-velocity covariance $\langle A_1^r w_1'^{+,-} \rangle$. The pair correlation function in Fig. 9.3 is in agreement with the observations of the formation of plane-wave like structures, with a band of higher pair densities at the location of the central particle perpendicular to the mean flow. The mean velocity tells the same story with particles on average moving towards the central band, see Fig 9.4.

The velocity fluctuations in the direction of mean flow are plot in Fig. 9.5. A similar picture is given to that of the HCGSF, with larger fluctuations found in pairs separated far away from one another and lower fluctuations between pairs close to one another. However, this structure does not indicate that the scale dependent heating mechanism is responsible for clustering alone. In Fig. 9.6, the mean acceleration in the stream-wise direction shows considerable structure. The values indicate that there is a mean force pushing particles towards the central band. Note, that the magnitude of the mean acceleration has not yet been compared to the transport term. Lastly, the heating mechanism is explored. Figures 9.7 and 9.8 show the source and sink of the stream-wise velocity fluctuations. Both display some structure as the distance is increased. The source of fluctuations appears much stronger than the sink for particles that are separated by a greater distance. However, the magnitude of the sink is about the same magnitude as the source for both closely separated particles and particles in the wake of the central particle. This should lead to a similar unstable scale dependent heating mechanism to the one present in the HCGSF.

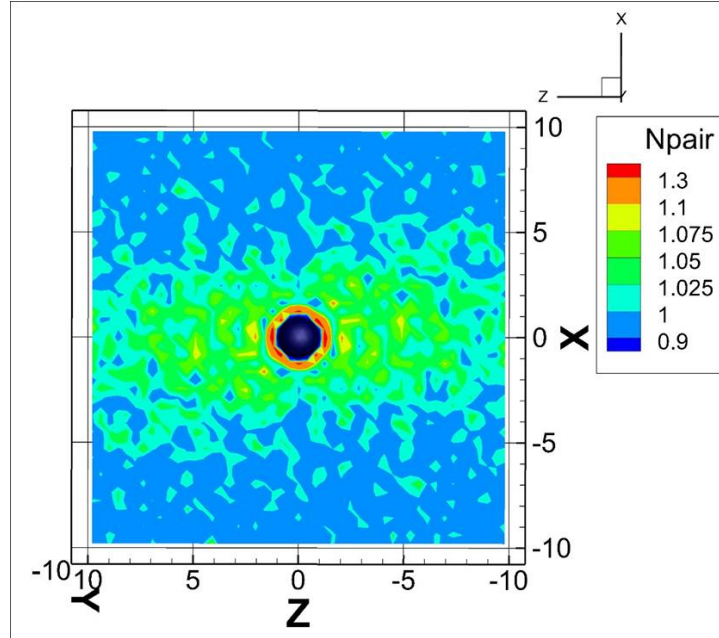


Figure 9.3 The three dimensional pair correlation function $g\left(r_i^{(jk)}\right)$ is shown. Here X is the stream-wise direction. We see strong evidence for clustering in this direction in a plane wave-like structure.

Ultimately, PR-DNS simulations are too slow and expensive to be able to simulate sedimenting flows in large domains over long time-scales required to reach a steady state in the clustering problem. In order to collect the statistics necessary for stochastic modeling of the clustering dynamics, a less computationally expensive method is required at this time. Future work will focus on obtaining data for modeling from less expensive Euler-Lagrange methods, e.g., Capecelatro et al. (2014), as a proof of concept for the stochastic modeling framework. After such data is obtained, stochastic modeling and simulations will be carried out as outlined in Section 7.3.

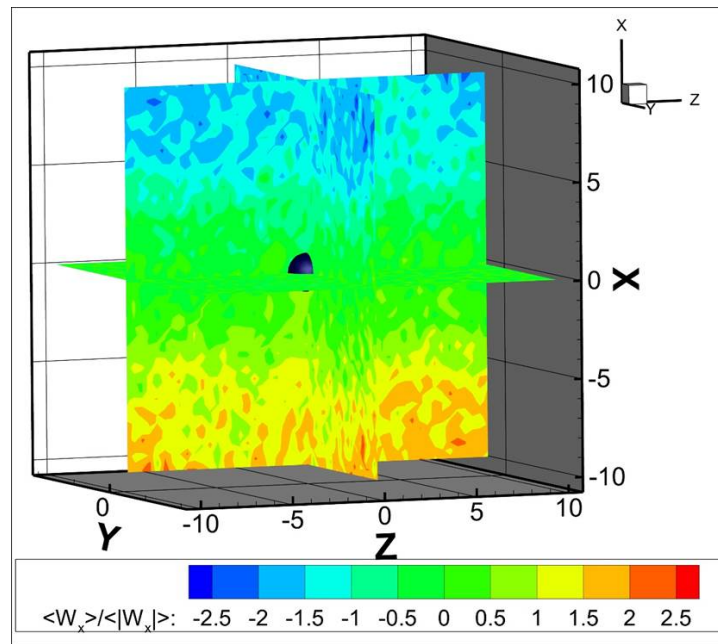


Figure 9.4 The mean relative velocity normalized by its spatial average in the stream-wise direction $\langle w_x | r_i^{(jk)} \rangle / \langle |w_x| \rangle$ is given. We see that particles that are positively separated have negative relative velocities on average, and vice-versa for particles with negative separations in the stream-wise direction. This indicates particles are moving towards one another on average.

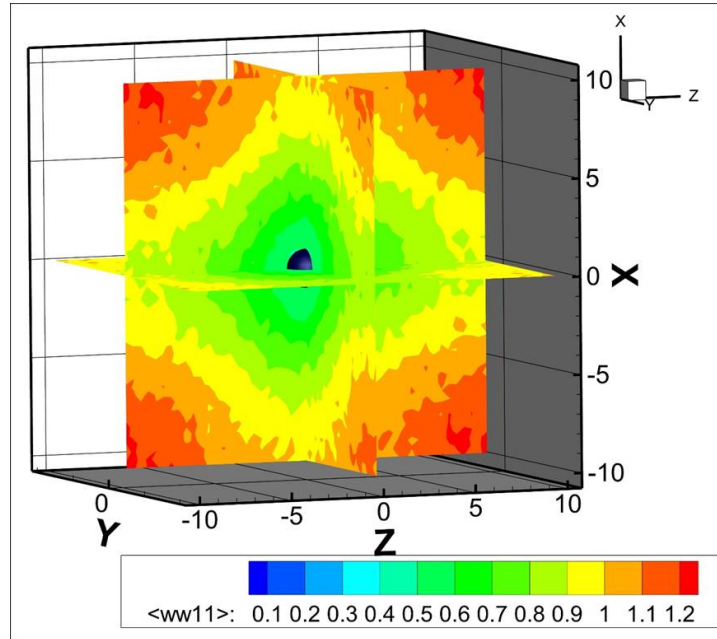


Figure 9.5 The fluctuating relative velocity normalized by its spatial average in the stream-wise direction $\langle w'_x w'_x | r_i^{(jk)} \rangle / T_g$ is given. Similar structure to that of the HCGSF is seen. The velocities of particles closer to one another are less random.

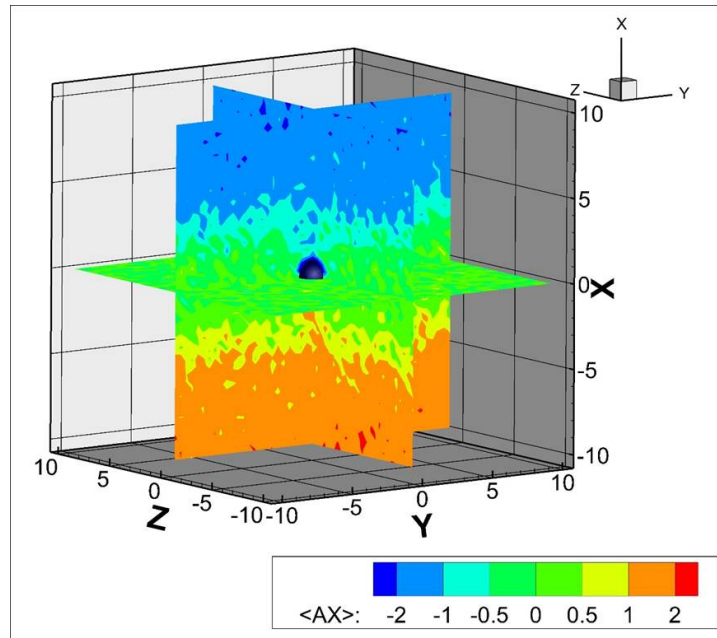


Figure 9.6 The scaled mean relative acceleration normalized by its spatial average in the stream-wise direction $\langle A_x | r_i^{(jk)} \rangle / \langle A_x \rangle$ is given. It shows significantly more structure than that of the HCGSF, and like the mean relative velocity shows evidence for clustering.

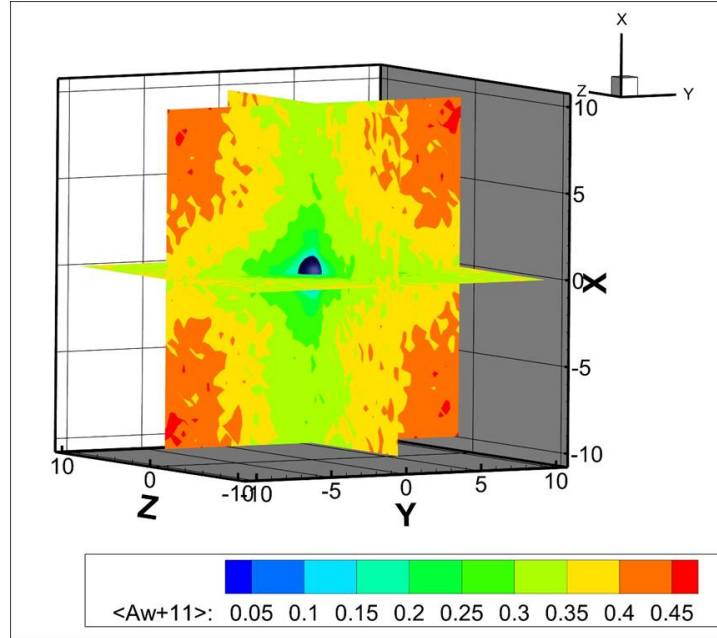


Figure 9.7 The scaled source component of the acceleration-velocity covariance in the stream-wise direction $\langle A'_x w'_x | r_i^{(jk)+} \rangle / \langle A'_x w'_x \rangle$ is given. Significant structure shows that the source of fluctuations is stronger for particles that are well separated. Some wake structure is also seen.

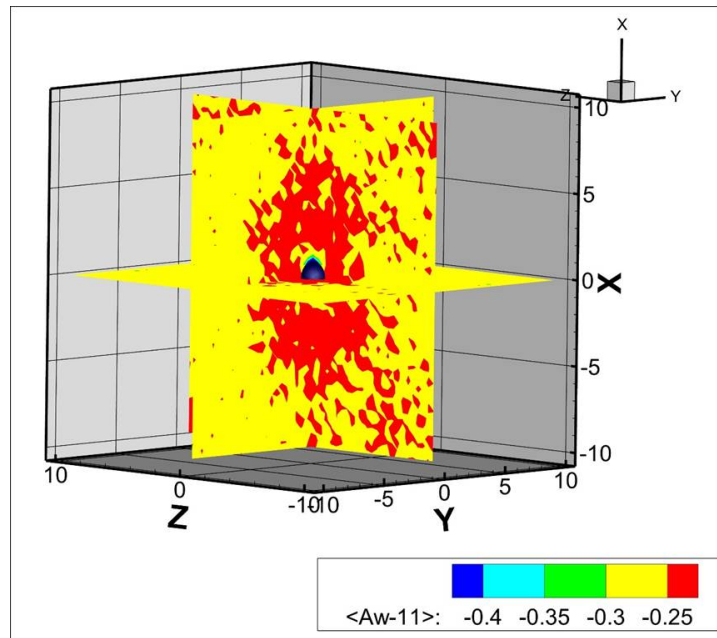


Figure 9.8 The scaled sink component of the acceleration-velocity covariance in the stream-wise direction $\langle A'_x w'_x | r_i^{(jk)-} \rangle / \langle A'_x w'_x \rangle$ is given. Some structure is seen in this statistic, with the strongest sink being between particles that are well separated.

BIBLIOGRAPHY

- Aarons, L. and Sundaresan, S. (2006). Shear flow of assemblies of cohesive and non-cohesive granular materials. *Powder Technology*, 169(1):10–21.
- Abbasfard, H., Evans, G., and Moreno-Atanasio, R. (2016). Effect of van der Waals force cut-off distance on adhesive collision parameters in DEM simulation. *Powder Technology*, 299:9–18.
- Afferrante, L., Ciavarella, M., and Demelio, G. (2015). Adhesive contact of the weierstrass profile. In *Proc. R. Soc. A*, volume 471, page 20150248. The Royal Society.
- Aitcin, P. (2000). Cements of yesterday and today - concrete of tomorrow. *Cement and Concrete Research*, 31(9):1349–1359.
- Alam, M., Trujillo, L., and Herrmann, H. (2006). Hydrodynamic theory for reverse brazil nut segregation and the non-monotonic ascension dynamics. *Journal of Statistical Physics*, 124:587–623.
- Bagnold, R. A. (1954). Experiments on a gravity-free dispersion of large solid spheres in a newtonian fluid under shear. In *Proceedings of the Royal Society of London A: Mathematical, Physical and Engineering Sciences*, volume 225, pages 49–63. The Royal Society.
- Ball, R. and Melrose, J. (1997). A simulation technique for many spheres in quasi-static motion under frame-invariant pair drag and brownian forces. *Physica A*, 247:444–472.
- Baranyai, A. and Evans, D. (1989). Direct entropy calculation from computer-simulation of liquids. *Physical Review A*, 40(7):3817–3822.

- Batrak, O., Patino, G., Simonin, O., Flour, I., Le Guevel, T., and Perez, E. (2005). Unlike particles size collision model in 3d unsteady polydispersed simulation of circulating fluidized bed. *8th Annual Conference on Fluidized Bed Technology*, 315.
- Bec, J., Biferale, L., Cencini, M., Lanotte, A., and Toschi, F. (2010). Intermittency in the velocity distribution of heavy particles in turbulence. *Journal of Fluid Mechanics*, 646:527–536.
- Beetstra, R., van der Hoef, M., and Kuipers, J. (2007). Drag force of intermediate reynolds number flows past mono- and bidisperse arrays of spheres. *AIChE Journal*, 53:489.
- Bentz, D., Ferraris, C., Galler, M., Hansen, A., and Guynn, J. (2012). Influence of particle size distributions on yield stress and viscosity of cement-fly ash pastes. *Cement and Concrete Research*, 42(2):404–409.
- Bentz, D. P., Garboczi, E. J., Haecker, C. J., and Jensen, O. M. (1999). Effects of cement particle size distribution on performance properties of portland cement-based materials. *Cement and Concrete Research*, 29:1663–1671.
- Berger, N., Azéma, E., Douce, J.-F., and Radjai, F. (2016). Scaling behaviour of cohesive granular flows. *EPL (Europhysics Letters)*, 112(6):64004.
- Berzi, D. and Jenkins, J. T. (2015a). Inertial shear bands in granular materials. *Physics of Fluids*, 27:033303.
- Berzi, D. and Jenkins, J. T. (2015b). Steady shearing flows of deformable, inelastic spheres. *Soft matter*, 11(24):4799–4808.
- Binnig, G., Quate, C. F., and Gerber, C. (1986). Atomic force microscope. *Physical review letters*, 56(9):930.
- Blum, J., Wurm, G., Kempf, S., Poppe, T., Klahr, H., Kozasa, T., Rott, M., Henning, T., Dorschner, J., Schrapler, R., Keller, H., Markiewicz, W., Mann, I., Gustafson, B., Giovane, F., Neuhaus, D., Fechtig, H., Grun, E., Feuerbacher, B., Kochan, H., Ratke, L., El Goresy, A.,

- Morfill, G., Weidenschilling, S., Schwehm, G., Metzler, K., and Ip, W. (2000). Growth and form of planetary seedlings: Results from a microgravity aggregation experiment. *Physical Review Letters*, 85(12):2426–2429.
- Bradley, R. S. (1932). Lxxix. the cohesive force between solid surfaces and the surface energy of solids. *The London, Edinburgh, and Dublin Philosophical Magazine and Journal of Science*, 13(86):853–862.
- Brady, J. F. and Bossis, G. (1988). Stokesian dynamics. *Annual Reviews of Fluid Mechanics*, 20:111–157.
- Bragg, A. D. and Collins, L. R. (2014a). New insights from comparing statistical theories for inertial particles in turbulence: I. spatial distribution of particles. *New Journal of Physics*, 16:055013.
- Bragg, A. D. and Collins, L. R. (2014b). New insights from comparing statistical theories for inertial particles in turbulence: II. relative velocities. *New Journal of Physics*, 16:055014.
- Bragg, A. D., Ireland, P. J., and Collins, L. R. (2015). On the relationship between the non-local clustering mechanism and preferential concentration. *Journal of Fluid Mechanics*, 780:327–343.
- Brewster, R., Grest, G. S., Landry, J. W., and Levine, A. J. (2005). Plug flow and the breakdown of bagnold scaling in cohesive granular flows. *Physical Review E*, 72(6):061301.
- Bridges, F. G., Supulver, K. D., Lin, D., Knight, R., and Zafra, M. (1996). Energy loss and sticking mechanisms in particle aggregation in planetesimal formation. *Icarus*, 123(2):422–435.
- Brilliantov, N. V., Albers, N., Spahn, F., and Pöschel, T. (2007). Collision dynamics of granular particles with adhesion. *Physical Review E*, 76(5):051302.
- Brilliantov, N. V. and Pöschel, T. (2004). Collision of adhesive viscoelastic particles. *HINRICHSEN:GRANULAR MEDIA O-BK*, pages 189–209.

- Brilliantov, N. V. and Pöschel, T. (2004). *Kinetic Theory of Granular Gases*. Oxford University Press, New York.
- Brilliantov, N. V., Spahn, F., Hertzsch, J.-M., and Pöschel, T. (1996). Model for collisions in granular gases. *Physical review E*, 53(5):5382.
- Brito, R. and Ernst, M. (1998). Extension of haff's cooling law in granular flows. *Europhysics Letters*, 43(5):497.
- Campbell, C. S. (2002). Granular shear flows at the elastic limit. *Journal of fluid mechanics*, 465:261–291.
- Capecelatro, J., Desjardins, O., and Fox, R. O. (2014). Numerical study of collisional particle dynamics in cluster-induced turbulence. *Journal of Fluid Mechanics*, 747:R2.
- Capecelatro, J., Desjardins, O., and Fox, R. O. (2015). On fluid-particle dynamics in fully developed cluster-induced turbulence. *Journal of Fluid Mechanics*, 780:578–635.
- Capecelatro, J., Desjardins, O., and Fox, R. O. (2016). Strongly coupled fluid-particle flows in vertical channels. ii. turbulence modeling. *Physics of Fluids*, 28:033307.
- Carnahan, N. and Starling, K. (1969). Equation of state for nonattractive rigid spheres. *Journal of Chemical Physics*, 51(2):635–636.
- Castellanos, A., Valverde, J. M., Pérez, A. T., Ramos, A., and Watson, P. K. (1999). Flow regimes in fine cohesive powders. *Physical Review Letters*, 82(6):1156.
- Cates, M., Wittmer, J., Bouchaud, J., and Claudin, P. (1998a). Jamming and static stress transmission in granular materials. *Chaos*, 9(3):511–522.
- Cates, M., Wittmer, J., Bouchaud, J., and Claudin, P. (1998b). Jamming, force chains, and fragile matter. *Physical Review Letters*, 81(9):1841–1844.
- Chew, J. W., Parker, D. M., Cocco, R. A., and Hrenya, C. M. (2011). Cluster characteristics of continuous size distributions and binary mixtures of group b particles in dilute riser flow. *Chemical Engineering Journal*, 178:348–358.

- Chialvo, S., Sun, J., and Sundaresan, S. (2012). Bridging the rheology of granular flows in three regimes. *Physical Review E*, 85(2):021305.
- Chun, J., Koch, D. L., Rani, S. L., Ahluwalia, A., and Collins, L. R. (2005). Clustering of aerosol particles in isotropic turbulence. *Journal of Fluid Mechanics*, 536:219–251.
- Cleary, P. W. and Sawley, M. L. (2002). DEM modelling of industrial granular flows: 3D case studies and the effect of particle shape on hopper discharge. *Applied Mathematical Modelling*, 26(2):89–111.
- Cocco, R., Shaffer, F., Hays, R., Karri, S. R., and Knowlton, T. (2010). Particle clusters in and above fluidized beds. *Powder Technology*, 203:3–11.
- Colwell, J., Batiste, S., Horányi, M., Robertson, S., and Sture, S. (2007). Lunar surface: Dust dynamics and regolith mechanics. *Reviews of Geophysics*, 45(2):RG2006.
- Cundall, P. and Strack, O. (1979a). A discrete numerical model for granular assemblies. *Geotechnique*, 29(1):47–65.
- Cundall, P. A. and Strack, O. D. (1979b). A discrete numerical model for granular assemblies. *Geotechnique*, 29(1):47–65.
- Dahneke, B. (1975). Further measurements of the bouncing of small latex spheres. *Journal of Colloid and Interface Science*, 51(1):58–65.
- Daley, D. and Vere-Jones, D. (1988). *An introduction to the theory of point processes*. Springer-Verlag.
- DeCicco, A. and Hartzell, C. (2016). System-level design considerations for asteroid despin via neutral beam emitting spacecraft. In *IEEE Aerospace Conference Proceedings (Big Sky, MT)*.
- Derjaguin, B., Muller, V., and Toporov, Y. (1975). Effect of contact deformations on the adhesion of particles. *Journal of Colloid and Interface Science*, 53(2):314–326.

- Di Renzo, A. and Di Maio, F. P. (2004). Comparison of contact-force models for the simulation of collisions in dem-based granular flow codes. *Chemical Engineering Science*, 59(3):525–541.
- Eaton, J. and Fessler, J. (1994). Preferential concentration of particles by turbulence. *International Journal of Multiphase Flow*, 20:169–209.
- Ernst, M., Dorfman, J., Hoegy, W., and van Leeuwen, J. (1969). Hard-sphere dynamics and binary-collision operators. *Physica*, 45(1):127–146.
- Esipov, S. and Pöschel, T. (1997). The granular phase diagram. *Journal of Statistical Physics*, 86(5/6):1385–1395.
- Ferraris, C., Obla, K., and Hill, R. (2001). The influence of mineral admixtures on the rheology of cement paste and concrete. *Cement and Concrete Research*, 31(2):245–255.
- Fox, R. (2014). On multiphase turbulence models for collisional fluid-particle flows. *Journal of Fluid Mechanics*, 742:368–424.
- Fox, R. O. (2016). Private communication.
- Fullmer, W. D. and Hrenya, C. M. (2016). Quantitative assessment of fine-grid kinetic-theory-based predictions of mean-slip in unbounded fluidization. *AIChE Journal*, 62(1):11–17.
- Galvin, J. E. and Benyahia, S. (2014). The effect of cohesive forces on the fluidization of aeratable powders. *AIChE Journal*, 60(2):473–484.
- Garzo, V., Dufty, J. W., and Hrenya, C. M. (2007a). Enskog theory for polydisperse granular mixtures. i. navier-stokes order transport. *Physical Review E*, 76(3):031303.
- Garzo, V., Fullmer, W. E., Hrenya, C. M., and Yin, X. (2016). Transport coefficients of solid particles immersed in a viscous gas. *Physical Review E*, 93:012905.
- Garzo, V., Hrenya, C. M., and Dufty, J. W. (2007b). Enskog theory for polydisperse granular mixtures. ii. sonine polynomial approximation. *Physical Review E*, 76(3):031304.
- Garzo, V., Tenneti, S., Subramaniam, S., and Hrenya, C. (2012). Enskog kinetic theory for monodisperse gas-solid flows. *Journal of Fluid Mechanics*, 712:129–168.

- Gaume, J., Chambon, G., and Naaim, M. (2011). Quasistatic to inertial transition in granular materials and the role of fluctuations. *Physical Review E*, 84:051304.
- Geldart, D. (1973). Types of gas fluidization. *Powder technology*, 7(5):285–292.
- Gidaspow, D., Jung, J., and Singh, R. K. (2004). Hydrodynamics of fluidization using kinetic theory: an emerging paradigm 2002 flour-daniel lecture. *Powder Technology*, 148:123–141.
- Goldhirsch, I. and Zanetti, G. (1993). Clustering instability in dissipative gases. *Physical Review Letters*, 70(11):1619–1622.
- Goldshtein, A. and Shapiro, M. (1995). Mechanics of collisional motion of granular materials. part 1. general hydrodynamic equations. *Journal of Fluid Mechanics*, 282:75–114.
- Gollin, D., Berzi, D., and Bowman, E. (2017). Extended kinetic theory applied to inclined granular flows: role of boundaries. *Granular Matter*, 19(3):1564–1583.
- Gonzalez, R. G. and Garzo, V. (2016). Instabilities in granular gas-solid flows. *arXiv:1611.03269*.
- Gonzalez, S., Thornton, A., and Luding, S. (2014). Free cooling phase-diagram of hard-spheres with short-and long-range interactions. *The European Physical Journal Special Topics*, 223(11):2205–2225.
- Gourdel, c., Simonin, O., and Brunier, E. (1998). Modelling and simulation of gas-solid turbulent flows with a binary mixture of particles. *Third International Conference on Multiphase Flows*, 315.
- Gourdel, c., Simonin, O., and Brunier, E. (1999). Two-maxwellian equilibrium distribution function for the modelling of a binary mixture of particles. *6th International Conference on Circulating Fluidized Beds*, 315.
- Grierson, D., Flater, E., and Carpick, R. (2005). Accounting for the jkr–dmt transition in adhesion and friction measurements with atomic force microscopy. *Journal of adhesion science and technology*, 19(3-5):291–311.

- Gu, Y., Chialvo, S., and Sundaresan, S. (2014). Rheology of cohesive granular materials across multiple dense-flow regimes. *Physical Review E*, 90(3):032206.
- Gu, Y., Ozel, A., and Sundaresan, S. (2015). A modified cohesion model for CFD–DEM simulations of fluidization. *Powder Technology*, 296:17–28.
- Gu, Y., Ozel, A., and Sundaresan, S. (2016). Numerical studies of the effects of fines on fluidization. *AIChE Journal*.
- Gustavsson, K. and Mehlig, B. (2014a). Clustering of particles falling in a turbulent flow. *Physical Review Letters*, 112:214501.
- Gustavsson, K. and Mehlig, B. (2014b). Relative velocities of inertial particles in turbulent aerosols. *Journal of Turbulence*, 15(1):34–69.
- Gustavsson, K. and Mehlig, B. (2016). Statistical models for spatial patterns of heavy particles in turbulence. *Advances in Physics*, 65(1):1–57.
- Haecker, C., Garboczi, E., J.W., B., Bohn, R., Sun, Z., Shah, S., and Voigt, T. (2005). Modeling the linear elastic properties of portland cement paste. *Cement and Concrete Research*, 35:1948–1960.
- Haff, P. (1983). Grain flow as a fluid-mechanical phenomenon. *Journal of Fluid Mechanics*, 134:401–430.
- Hatzes, A., Bridges, F., Lin, D., and Sachtjen, S. (1991). Coagulation of particles in saturn’s rings: Measurement of the cohesive force of water frost. *Icarus*, 89:113–121.
- Hill, R. J., Koch, D., and Ladd, A. (2001a). The first effects of fluid inertia on flows in ordered and random arrays of spheres. *Journal of Fluid Mechanics*, 448:213–241.
- Hill, R. J., Koch, D., and Ladd, A. (2001b). Moderate-reynolds-number flows in ordered and random arrays of spheres. *Journal of Fluid Mechanics*, 448:243–278.
- Irani, E., Chaudhuri, P., and Heussinger, C. (2014). Impact of attractive interactions on the rheology of dense athermal particles. *Physical Review Letters*, 112:188303.

- Irani, E., Chaudhuri, P., and Heussinger, C. (2016). Athermal rheology of weakly attractive soft particles. *Physical Review E*, 94:052608.
- Israelachvili, J. N. (2011). *Intermolecular and surface forces: revised third edition*. Academic press.
- Iveson, S., Litster, J., Hapgood, K., and Ennis, B. (2001). Nucleation, growth and breakage phenomena in agitated wet granulation processes: a review. *Powder Technology*, 117(1-2):3–39.
- Jenkins, J. and Mancini, F. (1987). Balance laws and constitutive relations for plane flows of a dense, binary mixture of smooth, nearly elastic, circular disks. *Journal of Applied Mechanics*, 1(54):27–34.
- Jenkins, J. and Mancini, F. (1989). Kinetic theory for binary mixtures of smooth, nearly elastic spheres. *Physics of Fluids, A*, 1(12):2050–2057.
- Johnson, K. and Greenwood, J. (1997). An adhesion map for the contact of elastic spheres. *Journal of colloid and interface science*, 192(2):326–333.
- Johnson, K., Kendall, K., and Roberts, A. (1971). Surface energy and the contact of elastic solids. *Proceedings of the Royal Society London A*, 324:301–313.
- Jop, P., Forterre, Y., and Pouliquen, O. (2006). A constitutive law for dense granular flows. *Nature*, 441(7094):727–730.
- Kamrin, K. and Koval, G. (2012). Nonlocal constitutive relation for steady granular flow. *Physical Review Letters*, 108(17):178301.
- Kim, H. and Arastoopour, H. (2002). Extension of kinetic theory to cohesive particle flow. *Powder Technology*, 122(1):83–94.
- Kim, S. and Karrila, S. (1991). *Microhydrodynamics: principles and selected applications*. Butterworth-Heinemann.

- Kobayashi, T., Tanaka, T., Shimada, N., and Kawaguchi, T. (2013). Dem-cfd analysis of fluidization behavior of geldart group a particles using a dynamic adhesion force model. *Powder Technology*, 248:143–152.
- Koch, D. L. (1990). Kinetic theory for a monodisperse gas-solid suspension. *Physics of Fluids A*, 2(10):1711–1723.
- Koch, D. L. and Sangani, A. S. (1999). Particle pressure and marginal stability limits for a homogeneous monodisperse gas-fluidized bed: kinetic theory and numerical simulations. *Journal of Fluid Mechanics*, 400:229–263.
- Kolakaluri, R., Murphy, E., Subramaniam, S., Brown, R., and Fox, R. (2015). Filtration model for polydisperse aerosols in gas-solid flow using granule-resolved direct numerical simulation. *AIChE Journal*, 61(11):3594–3606.
- Kothe, S., Blum, J., Weidling, R., and GÄttler, C. (2013). Free collisions in a microgravity many-particle experiment. iii. the collision behavior of sub-millimeter-sized dust aggregates. *Icarus*, 225:75–85.
- Kulchitsky, A., Johnson, J., Reeves, D., and Wilkinson, A. (2014). Discrete element method simulation of a boulder extraction from an asteroid. In *Proceedings of the 14th ASCE Biennial International Conference on Engineering, Science, Construction, and Operations in Challenging Environments (St. Louis, Missouri, USA,)*, pages 485–494.
- Kumar, A. (2010). *Microscale Dynamics in Suspensions of Non-spherical Particles*. PhD thesis, University of Illinois Urbana-Champaign.
- Kumar, A. and Higdon, J. (2010). Origins of the anomalous stress behavior in charged colloidal suspensions under shear. *Physical Review E*, 82:051401.
- Kuwabara, G. and Kono, K. (1987). Restitution coefficient in a collision between two spheres. *Japanese journal of applied physics*, 26(8R):1230.

- Lanotte, A., Bec, J., Biferale, L., Cencini, M., and Toschi, F. (2011). About scaling properties of relative velocity between heavy particles in turbulence. *Journal of Physics Conference series*, 318:052010.
- Launder, B. (1990). Phenomenological modelling: present... and future? in j.l. lumley (ed.). *Whither Turbulence? Turbulence at a Crossroads*, pages 439–485.
- Lees, A. and Edwards, S. (1972). The computer study of transport processes under extreme conditions. *Journal of Physics C: Solid State Physics*, 5(15):1921.
- Leyvraz (2003). Scaling theory and exactly solved models in the kinetics of irreversible aggregation. *Physics Reports*, 383:92–212.
- Li, J., Cheng, C., Zhang, Z., Yuan, J., Nemet, A., and Fett, F. (1999). The emms model - its application, development and updated concepts. *Chemical Engineering Science*, 54(22):5409–5425.
- Liard, M., Martys, N., George, W., Lootens, D., and Hebraud, P. (2014). Scaling laws for the flow of generalized newtonian suspensions. *Journal of Rheology*, 58:1993–2015.
- Liu, A. J. and Nagel, S. R. (2010). The jamming transition and the marginally jammed solid. *Annual Review of Condensed Matter Physics*, 1:347–369.
- Liu, L. (2011). Kinetic theory of aggregation in granular flow. *AIChE Journal*, 57(12):3331–3343.
- Liu, P., Kellogg, K., LaMarche, C., and Hrenya, C. (2017). Dynamics of singlet-doublet collisions of cohesive particles. *Chemical Engineering Journal*, 324:380–391.
- Liu, P., LaMarche, C. Q., Kellogg, K. M., and Hrenya, C. M. (2016). Fine-particle deflu-idization: Interaction between cohesion, Young’s modulus and static bed height. *Chemical Engineering Science*, 145:266–278.
- Lois, G., Blawdziewicz, J., and O’Hern, C. S. (2008). Jamming transition and new perco-lation universality classes in particulate systems with attraction. *Physical Review Letters*, 100:028001.

- Lomboy, G., Sundararajan, S., and Wang, K. (2013). Micro- and macroscale coefficients of friction of cementitious materials. *Cement and Concrete Research*, 54:21–28.
- Lomboy, G., Sundararajan, S., Wang, K., and Subramaniam, S. (2011). A test method for determining adhesion forces and hamaker constants of cementitious materials using atomic force microscopy. *Cement and Concrete Research*, 41(11):1157–1166.
- Lomboy, G. R., Wang, K., and Quanji, Z. (2012). Properties of cementitious materials in their dry state and their influences on viscosity of the cementitious pastes. *Powder Technology*, 229:104–111.
- Luding, S. (1998). Collisions & contacts between two particles. In *Physics of dry granular media*, pages 285–304. Springer.
- Luding, S. (2008). Cohesive, frictional powders: contact models for tension. *Granular matter*, 10(4):235–246.
- Luding, S. (2016). Granular matter: So much for the jamming point. *Nature Physics*, 12:531–532.
- Luding, S. and Alonso-Marroquin, F. (2011). The critical-state yield stress (termination locus) of adhesive powders from a single numerical experiment. *Granular Matter*, 13:109–119.
- Luding, S., Clément, E., Blumen, A., Rajchenbach, J., and Duran, J. (1994). Anomalous energy dissipation in molecular-dynamics simulations of grains: The detachment effect. *Physical Review E*, 50(5):4113.
- Luding, S., Huthmann, M., McNamara, S., and Zippelius, A. (1998). Homogeneous cooling of rough, dissipative particles: Theory and simulation. *Physical Review E*, 58(3):3416–3425.
- Majmudar, T., Sperl, M., Luding, S., and Behringer, R. (2007). Jamming transition in granular systems. *Physical Review Letters*, 98:058001.
- Makse, H. A., Johnson, D. L., and Schwartz, L. M. (2000). Packing of compressible granular materials. *Physical review letters*, 84(18):4160.

- Marchisio, D. L. and Fox, R. O. (2013). *Computational Models for Polydisperse Particulate and Multiphase Systems*. Cambridge University Press.
- Markutsya, S., Fox, R., and Subramaniam, S. (2014). Characterization of sheared colloidal aggregation using langevin dynamics simulation. *Physical Review E*, 89:062312.
- Marmur, B. L. and Heindel, T. J. (2016). Effect of particle size, density, and concentration on granular mixing in a double screw pyrolyzer. *Powder Technology*, 302:222–235.
- Martys, N. and Ferraris, C. (2002). Simulation of scc flow. In *First North American Conference on the Design and Use of Self-Consolidating Concrete. Proceedings. Chicago, IL,*.
- Martys, N., Khalil, M., George, W., and Lootens, D. (2012). Stress propagation in a concentrated colloidal suspension under shear. *European Physical Journal E*, 35(3):1–7.
- Matsunaga, T., Kim, J., Hardcastle, S., and Rohatgi, P. (2002). Crystallinity and selected properties of fly ash particles. *Materials Science and Engineering*, A325:333–343.
- Maugis, D. (1992). Adhesion of spheres: the jkr-dmt transition using a dugdale model. *Journal of colloid and interface science*, 150(1):243–269.
- Maxey, M. (1987). The gravitational settling of aerosol particles in homogeneous turbulence and random flow fields. *Journal of Fluid Mechanics*, 174:441–465.
- Mckay, W. and Mckay, J. (1971). *Building Construction Vol. Ii (Fourth Edition)*. Orient Longman Private Limited.
- McMillan, J., Shaffer, F., Gopalan, B., Chew, J. W., Hrenya, C., Hays, R., Karri, S. R., and Cocco, R. (2013). Particle cluster dynamics during fluidization. *Chemical Engineering Science*, 100:39–51.
- McNamara, S. and Young, W. (1992). Inelastic collapse and clumping in a one-dimensional granular medium. *Physics of Fluids A*, 4(3):496–504.
- Mehrabadi, M. (2016). *Analysis of gas-solid flow using particle-resolved direct numerical simulation: flow physics and modeling*. PhD thesis, Iowa State University.

- Mehrabadi, M., Murphy, E., and Subramaniam, S. (2016a). Development of a gas-solid drag law for clustered particles using particle-resolved direct numerical simulation. *Chemical Engineering Science*, 152:199–212.
- Mehrabadi, M., Tenneti, S., and Subramaniam, S. (2016b). Importance of the fluid-particle drag model in predicting segregation in bidisperse gas-solid flow. *International Journal of Multiphase Flow*, 86:99–114.
- MiDi, G. (2004). On dense granular flows. *The European Physical Journal E*, 14(4):341–365.
- Miller, A. and Gidaspow, D. (1992). Dense, vertical gas-solid flow in a pipe. *AIChE Journal*, 38(11):1801–1815.
- Mills, P., Rognon, P., and Chevier, F. (2008). Rheology and structure of granular materials near the jamming transition. *EPL (Europhysics Letters)*, 81:64005.
- Miyamoto, H., Kargel, J., Fink, W., and Furfaro, R. (2008). Granular processes on itokawa, a small near-earth asteroid: Implications for resource utilization. *Space Exploration Technologies, Proceedings of SPIE*, 6960:69600I.
- Monchaux, R., Bourgoïn, M., and Cartellier, A. (2010). Preferential concentration of heavy particles: a voronoi analysis. *Physics of Fluids*, 22(10):103304.
- Moreno-Atanasio, R., Xu, B., and Ghadiri, M. (2007). Computer simulation of the effect of contact stiffness and adhesion on the fluidization behaviour of powders. *Chemical engineering science*, 62(1):184–194.
- Morrow, C., Lovell, M., and Ning, X. (2003). A jkr-dmt transition solution for adhesive rough surface contact. *Journal of Physics D: Applied Physics*, 36(5):534.
- Mounfield, C. and Edwards, S. (1994). A model for the packing of irregularly shaped grains. *Physica A*, 210:301–316.
- Müller, M.-K. and Luding, S. (2011). Homogeneous cooling with repulsive and attractive long-range potentials. *Mathematical Modelling of Natural Phenomena*, 6(4):118–150.

- Murphy, E., Mehrabadi, M., Tenneti, S., and Subramaniam, S. (2015). Modeling two-point particle dynamics of homogeneous gas-solid flows to describe clustering and stability. In *68th annual meeting of the American physical society division of fluid dynamics, At Boston, MA*.
- Murphy, E. and Subramaniam, S. (2014). A model for solid-solid drag in bidisperse gas-solid flows. In *67th Annual Meeting of the APS Division of Fluid Dynamics*, volume 59.
- Murphy, E. and Subramaniam, S. (2015). Freely cooling granular gases with short-ranged attractive potentials. *Physics of Fluids (1994-present)*, 27(4):043301.
- Murphy, E. and Subramaniam, S. (2017). Binary collision outcomes for inelastic soft-sphere models with cohesion. *Powder Technology*, 305:462–476.
- Nachenius, R., van de Wardt, T., Ronsse, F., and Prins, W. (2015). Effect of particle size, density, and concentration on granular mixing in a double screw pyrolyzer. *Fuel Processing Technology*, 130:87–95.
- Narayanan, K. and Ramamurthy, K. (2000). Structure and properties of aerated concrete: a review. *Cement and Concrete Composites*, 22(5):321–329.
- Nase, S. T., Vargas, W. L., Abatan, A. A., and McCarthy, J. (2001). Discrete characterization tools for cohesive granular material. *Powder Technology*, 116(2):214–223.
- Nauman, E. B. (2001). *Chemical Reactor Design, Optimization, and Scaleup*. McGraw-Hill.
- Nienow, A., Edwards, M., and Harnby, N. (1992). *Mixing in the Process Industries: Mixing of Cohesive Powders*. Elsevier, Oxford, 2nd edition.
- of Chemistry, T. R. S. (2008). The concrete conundrum. *Chemistry World*.
- Oliver, W. C. and Pharr, G. M. (1992). An improved technique for determining hardness and elastic modulus using load and displacement sensing indentation experiments. *Journal of materials research*, 7(06):1564–1583.
- Ortiz de Zarate, J. and Sengers, J. (2006). *Hydrodynamic Fluctuations in Fluids and Fluid Mixtures*. Elsevier.

- Oseen, C. (1927). Neuere methoden und ergebnisse in der hydrodynamik. *Akademische Verlagsgesellschaft*.
- Otsuki, M., Hayakawa, H., and Luding, S. (2010). Behavior of pressure and viscosity at high densities for two-dimensional hard and soft granular materials. *Progress of Theoretical Physics Supplement*, 184:110–133.
- Pasha, M., Dogbe, S., Hare, C., Hassanpour, A., and Ghadiri, M. (2014). A linear model of elasto-plastic and adhesive contact deformation. *Granular Matter*, 16(1):151–162.
- Pathak, S., Jabeen, Z., Dibyendu, D., and Rajesh, R. (2014). Energy decay in three-dimensional freely cooling granular gas. *Physical Review Letters*, 112:038001.
- Paul, E. L., Atiemo-Obeng, V. A., and Kresta, S. M. (2004). *Handbook of industrial mixing: science and practice*. John Wiley ”&” Sons.
- Perni, S. and Prokopovich, P. (2015). Multi-asperity elliptical jkr model for adhesion of a surface with non-axially symmetric asperities. *Tribology International*, 88:107–114.
- Persson, B. N. and Scaraggi, M. (2014). Theory of adhesion: Role of surface roughness. *The Journal of chemical physics*, 141(12):124701.
- Petterson, O. (2007). Sandstone compaction, grain packing and critical state theory. *Petroleum Geoscience*, 13:63–67.
- Plimpton, S. (1995). Fast parallel algorithms for short-range molecular dynamics. *Journal of Computational Physics*, 117:1–19.
- Pope, S. B. (2000). *Turbulent Flows*. Cambridge University Press.
- Prokopovich, P. and Starov, V. (2011). Adhesion models: From single to multiple asperity contacts. *Advances in colloid and interface science*, 168(1):210–222.
- Rahman, M., Wiklund, J., Kotze, R., and Hakansson, U. (2017). Yield stress of cement grouts. *Tunnelling and Underground Space Technology*, 61:50–60.

- Rani, S. L., Dhariwal, R., and Koch, D. L. (2014). A stochastic model for the relative motion of high stokes number particles in isotropic turbulence. *Journal of Fluid Mechanics*, 756:870–902.
- Reeks, M. (1980). Eulerian direct interaction applied to the statistical motion of particles in a turbulent flow. *Journal of Fluid Mechanics*, 97:569–590.
- Rognon, P. G., Roux, J.-N., Naaim, M., and Chevoir, F. (2008). Dense flows of cohesive granular materials. *Journal of Fluid Mechanics*, 596:21–47.
- Rong, L., Dong, K., and Yu, A. (2014). Lattice-boltzmann simulation of fluid flow through packed beds of spheres: effect of particle size distribution. *Chemical Engineering Science*, 116:508–523.
- Rotne, J. and Prager, S. (1969). Variational treatment of hydrodynamic interaction in polymers. *Journal of Chemical Physics*, 50:4831–4837.
- Roussel, N., Lemaitre, A., Flatt, R., and Coussot, P. (2010). Steady state flow of cement suspensions: A micromechanical state of the art. *Cement and Concrete Research*, 40(1):77–84.
- Roussel, N., Ovarlez, G., Garrault, S., and Brumaud, C. (2012). The origins of thixotropy of fresh cement pastes. *Cement and Concrete Research*, 42(1):148–157.
- Rumpf, H. (1958). Grundlagen und methoden des granulierens. *Chemie Ingenieur Technik*, 30(3):144–158.
- Rycroft, C., Grest, G., Landry, J., and Bazant, M. (2006). Analysis of granular flow in a pebble-bed nuclear reactor. *Physical Review E*, 74:021306.
- Saha, S. and Alam, M. (2016). Normal stress differences, their origin and constitutive relations for a sheared granular fluid. *Journal of Fluid Mechanics*, 795:549–580.
- Saitoh, K. and Mizuno, H. (2016). Enstrophy cascades in two-dimensional dense granular flows. *Physical Review E*, 94:022908.

- Saitoh, K., Takada, S., and Hayakawa, H. (2015). Hydrodynamic instabilities in shear flows of dry cohesive granular particles. *Soft matter*, 11(32):6371–6385.
- Schäfer, J., Dippel, S., and Wolf, D. (1996). Force schemes in simulation of granular material. *J. Phys. I France*, 6:5–20.
- Schlick, C. P., Isner, A. B., Freireich, B. J., Fan, Y., Umbanhowar, P. B., Ottino, J. M., and Lueptow, R. M. (2016). A continuum approach for predicting segregation in flowing polydisperse granular materials. *Journal of Fluid Mechanics*, 797:95–109.
- Shah, S. and Wang, K. (2004). Development of green cement for sustainable concrete using cement kiln dust and fly ash. In *Proceedings of the International Workshop on Sustainable Development and Concrete Technology*.
- Shannon, C. (1948). A mathematical theory of communication. *Bell System Technical Journal*, 27(3):379–423.
- Silbert, L. E., Ertas, D., Grest, G. S., Halsey, T. C., Levine, D., and Plimpton, S. J. (2001). Granular flow down an inclined plane: Bagnold scaling and rheology. *Physical Review E*, 64(5):051302.
- Silbert, L. E., Grest, G. S., Brewster, R., and Levine, A. J. (2007). Rheology and contact lifetimes in dense granular flows. *Physical review letters*, 99(6):068002.
- Singh, A., Magnanimo, V., Saitoh, K., and Luding, S. (2014). Effect of cohesion on shear banding in quasistatic granular materials. *Physical Review E*, 90(2):022202.
- Singh, A., Magnanimo, V., Saitoh, K., and Luding, S. (2015). The role of gravity or pressure and contact stiffness in granular rheology. *New journal of physics*, 17(4):043028.
- Sjostrom, S. and Krutka, H. (2009). Evaluation of solid sorbents as a retrofit technology for co2 capture. *Fuel*, 89(6):1298–1306.
- Song, C., Wang, P., and Makse, H. A. (2008). A phase diagram for jammed matter. *Nature*, 453(7195):629–632.

- Stevens, A. and Hrenya, C. (2005). Comparison of soft-sphere models to measurements of collision properties during normal impacts. *Powder Technology*, 154(2):99–109.
- Stoyan, D., Kendall, W., and Mecke, J. (1995). *Stochastic geometry and its applications*. John Wiley and Sons, New York, 2nd edition.
- Stutzman, P. (2004). Scanning electron microscopy imaging of hydraulic cement microstructure. *Cement and Concrete Composites*, 26:957–966.
- Subramaniam, S. (2000). Statistical representation of a spray as a point process. *Physics of Fluids*, 12(10):2413–2431.
- Subramaniam, S. (2001). Statistical modeling of sprays using the droplet distribution function. *Physics of Fluids*, 13(3):624–642.
- Subramaniam, S. (2012). Stability limits for gas-solid suspensions with finite fluid inertia using particle-resolved direct numerical simulations. *NSF Annual Report 1134500*.
- Subramaniam, S. (2014). Stability limits for gas-solid suspensions with finite fluid inertia using particle-resolved direct numerical simulations. *NSF Annual Report 1134500*.
- Sun, J., Battaglia, F., and Subramaniam, S. (2006). Dynamics and structures of segregation in a dense, vibrating granular bed. *Physical Review E*, 74(6):061307.
- Sun, J. and Sundaresan, S. (2011). A constitutive model with microstructure evolution for flow of rate-independent granular materials. *Journal of Fluid Mechanics*, 682:590–616.
- Sundaram, S. and Collins, L. (1997). Collision statistics in an isotropic, particle-laden turbulent suspension i. direct numerical simulations. *Journal of Fluid Mechanics*, 335:75–109.
- Syamlal, M. (1987). The particle-particle drag term in a multiphase model of fluidization. *Technical Report DOE/MC/21353-2373, NTIS/DE87006500, National Technical Information Service*.
- Syamlal, M. and O’Brien, T. (1987). A generalized drag correlation for multiparticle systems. *Technical Report, Morgantown Energy Technology Center DOE Report*.

- Syamlal, M., Rogers, W., and O'Brien, T. (1993). Mfix documentation: Theory guide. *Morgantown Energy Technology Center Morgantown, WV, USA*, page 54.
- Tabor, D. (1977). Surface forces and surface interactions. *Journal of colloid and interface science*, 58(1):2–13.
- Takada, S., Saitoh, K., and Hayakawa, H. (2014). Simulation of cohesive fine powders under a plane shear. *Physical Review E*, 90(6):062207.
- Takada, S., Saitoh, K., and Hayakawa, H. (2015a). Kinetic theory for dilute cohesive granular gases with a square well potential. *arXiv preprint arXiv:1506.04578*.
- Takada, S., Saitoh, K., and Hisao, H. (2015b). Simulation of cohesive fine powders under a plane shear. *Physical Review E*, 90:062207.
- Tenneti, S., Garg, G., and Subramaniam, S. (2011). Drag law for monodisperse gas-solid systems using particle-resolved direct numerical simulation of flow past fixed assemblies of spheres. *International Journal of Multiphase Flows*, 37(9):1072–1092.
- Tenneti, S., Mehrabadi, M., and Subramaniam, S. (2016). Stochastic lagrangian model for hydrodynamic acceleration of inertial particles in gas-solid suspensions. *Journal of Fluid Mechanics*, 788:695–729.
- Tenneti, S. and Subramaniam, S. (2014). Particle-resolved direct numerical simulation for gas-solid flow model development. *Annual Review of Fluid Mechanics*, 46:199–230.
- Thornton, C., Cummins, S. J., and Cleary, P. W. (2013). An investigation of the comparative behaviour of alternative contact force models during inelastic collisions. *Powder Technology*, 233:30–46.
- Thornton, C. and Ning, Z. (1998). A theoretical model for the stick/bounce behaviour of adhesive, elastic-plastic spheres. *Powder technology*, 99(2):154–162.
- Tien, C. and Ramarao, B. (2007). *Granular Filtration of Aerosols and Hydrosols*. Elsevier, Oxford, 2nd edition.

- Tomas, J. (2000). Particle adhesion fundamentals and bulk powder consolidation. *KONA Powder and Particle Journal*, 18(0):157–169.
- Torquato, S. (1995). Mean nearest-neighbor distance in random packings of hard d-dimensional spheres. *Physical Review Letters*, 74(12):2156–2159.
- Trizac, E. and Hansen, J. (1995). Dynamic scaling behavior of ballistic coalescence. *Physical Review Letters*, 74(21):4114–4117.
- Trizac, E. and Hansen, J. (1996). Dynamics and growth of particles undergoing ballistic coalescence. *Journal of Statistical Physics*, 86(5-6):1345–1370.
- Tsuji, Y., Kawaguchi, T., and Tanaka, T. (1993). Discrete particle simulation of two-dimensional fluidized bed. *Powder technology*, 77(1):79–87.
- Uhlmann, M. and Doychev, T. (2014). Sedimentation of a dilute suspension of rigid spheres at intermediate galileo numbers: the effect of clustering upon the particle motion. *Journal of Fluid Mechanics*, 752:310–348.
- UNEP, U. N. E. P. (2012). Greening cement production has a big role to play in reducing greenhouse gas emissions. *UNEP Report 2012, Environmental Science Alert Thematic Focus: Resource Efficiency, Harmful Substances and Hazardous Waste, and Climate Change*.
- van der Hoef, M., Beestra, R., and Kuipers, J. (2005). Lattice-boltzmann simulations of low-reynolds-number flow past mono- and bidisperse arrays of spheres: results for the permeability and drag force. *Journal of Fluid Mechanics*, 528:233–254.
- van Noije, T., Ernst, M., and Brito, R. (1998a). Ring kinetic theory for an idealized granular gas. *Physica A*, 251:266–283.
- van Noije, T., Ernst, M., and Brito, R. (1998b). Spatial correlations in compressible granular flows. *Physical Review E*, 57(5):R4893.
- van Noije, T., Ernst, M., Brito, R., and Orza, J. (1997). Mesoscopic theory of granular fluids. *Physical Review Letters*, 79(3):411–414.

- Vidyapati and Subramaniam, S. (2013). Granular flow in silo discharge: Discrete element method simulations and model assessment. *Industrial "E" Engineering Chemistry Research*, 52(36):13171–13182.
- Vidyapati, V., Langroudi, M. K., Sun, J., Sundaresan, S., Tardos, G., and Subramaniam, S. (2012). Experimental and computational studies of dense granular flow: Transition from quasi-static to intermediate regime in a couette shear device. *Powder Technology*, 220:7–14.
- von Karman, T. and Howarth, L. (1938). On the statistical theory of isotropic turbulence. *Proceedings of the Royal Society of London. Series A, Mathematical and Physical Sciences*, 164(917):192–215.
- Walton, O. R. (1984). Application of molecular dynamics to macroscopic particles. *International Journal of Engineering Science*, 22(8):1097–1107.
- Walton, O. R. (2004). Potential discrete element simulation applications ranging from airborne fines to pellet beds. *SAE 2004 Transactions J. Aerospace*.
- Wang, K., Subramaniam, S., and Sundararajan, S. (2013). Final report: Understanding rheology of cement-based materials through integrated experiments and computations at multiple scales. *Final Report NSF CBET Grant No. 0927660*.
- Waters, J., Lee, S., and Guduru, P. (2009). Mechanics of axisymmetric wavy surface adhesion: Jkr–dmt transition solution. *International Journal of Solids and Structures*, 46(5):1033–1042.
- Weller, H., Tabor, G., Jasak, H., and Fureby, C. (1998). A tensorial approach to computational continuum mechanics using object-oriented techniques. *Computers in Physics*, 12(6):620–631.
- Wilson, R., Dini, D., and van Wachem, B. (2016). A numerical study exploring the effect of particle properties on the fluidization of adhesive particles. *AIChE Journal*, 62(5):1467–1477.
- Wylie, J. J. and Koch, D. L. (2000). Particle clustering due to hydrodynamic interactions. *Physics of Fluids*, 12(5):964–970.
- Xing, Z., Kenty, B., Li, Z., and Lee, S. (2009). Scale-up analysis for a cho cell culture process in large-scale bioreactors. *Biotechnology and Bioengineering*, 103(4):733–746.

- Xu, Y. and Subramaniam, S. (2007). Consistent modeling of interphase turbulent kinetic energy transfer in particle-laden turbulent flows. *Physics of Fluids*, 19:085101.
- Yao, H., Ciavarella, M., and Gao, H. (2007). Adhesion maps of spheres corrected for strength limit. *Journal of colloid and interface science*, 315(2):786–790.
- Yin, X., Zenk, J. R., Mitrano, P. P., and Hrenya, C. M. (2013). Impact of collisional versus viscous dissipation on flow instabilities in gas-solid systems. *Journal of Fluid Mechanics*, 727:R2.
- Zaichik, L. and Alipchenkov, V. (2003). Pair dispersion and preferential concentration of particles in isotropic turbulence. *Physics of Fluids*, 15:1776–1787.
- Zaichik, L. I. and Alipchenkov, V. M. (2009). Statistical models for predicting pair dispersion and particle clustering in isotropic turbulence and their applications. *New Journal of Physics*, 11:103018.
- Zamankhan, P. (2005). Kinetic theory of multicomponent dense mixtures of slightly inelastic spherical particles. *Physical Review E*, 52(5):4877–4891.
- Zhang, Q. and Kamrin, K. (2017). Microscopic description of the granular fluidity field in nonlocal flow modeling. *Physical Review Letters*, 118:058001.

APPENDIX A. THE APPROACH TIME SCALE

We define the approach portion of the dynamics as being at times when the separation distance is between a maximum cut-off, where particles do not strongly interact, i.e. $x/d_0 < 100$, and mechanical contact, $x = 0$. The dynamics in this region are conservative and obey Hamiltonian mechanics given by Eq. 2.3. By solving this ODE, we can recover the time required for a pair of separated particles to approach one another through the potential well to contact. This time-scale may then be used to form constraints on numerical time steps ensuring convergence and energy conservation. Fortunately, time-independent Hamiltonian equations are separable, and hence, soluble by direct integration. Three different solutions are possible arising from different Hamiltonians, two of which are non-invertible.

$$\begin{aligned}
 \tilde{t} &= \frac{1}{\mathcal{H}^*} \left(\sqrt{\tilde{x} (Ha_0 - \mathcal{H}^* \tilde{x})} - \frac{Ha_0}{\sqrt{\mathcal{H}^*}} \arctan \sqrt{\frac{\mathcal{H}^* \tilde{x}}{Ha_0 - \mathcal{H}^* \tilde{x}}} \right) + C^- & \forall \mathcal{H}^* < 0 \\
 \tilde{x} &= \left(\tilde{x}_0^{3/2} - \frac{3}{2} \sqrt{Ha_0 \tilde{t}} \right)^{2/3} & \forall \mathcal{H}^* = 0 \\
 \tilde{t} &= \frac{1}{\mathcal{H}^*} \left(\frac{Ha_0}{\sqrt{\mathcal{H}^*}} \ln \left[\mathcal{H}^* \left(\sqrt{\tilde{x}} + \sqrt{\tilde{x} + \frac{Ha_0}{\mathcal{H}^*}} \right) \right] - \sqrt{\tilde{x} (\mathcal{H}^* \tilde{x} + Ha_0)} \right) + C^+ & \forall \mathcal{H}^* > 0,
 \end{aligned} \tag{A.1}$$

where C^- and C^+ are constants of integration obtained by including the initial condition \tilde{x}_0 and initial time $\tilde{t}_0 = 0$. Note that here we give $\tilde{x}_0 = x_0/d_0$ as an initial particle separation and the time is now non-dimensionalized as $\tilde{t} = tv_f/d_0$. The full solutions in Eq. A.1 can be compared to the numerical fit for all Ha_0 by Eq. 2.6.

APPENDIX B. CONVERGENCE CRITERIA TO RESOLVE PARTICLE CROSSING OF THE POTENTIAL WELL

In Section 2.2.4, details regarding a characteristic time-scale for crossing the potential well were discussed. Ultimately, we want to know how well the potential well needs to be resolved, in order to satisfactorily obey the energy conservation constraints. If the potential well is not sufficiently resolved, the initial conditions for relative velocity in the contact portion of the dynamics, see Eq. 2.5, will not be correct. This ultimately corrupts the predicted sticking behavior of the system.

To address the appropriate time-step question, we have performed a suite of simulations of binary systems using velocity-Verlet integration in LAMMPS. All systems were prepared with initial separations just outside of the potential well cut-off of $x = 100d_0$. We then compared the change in kinetic energy between the initial condition and just before particle contact, see fig. B.1, which we know from conservation of energy. The parameters v_f , l_{ref}/d_0 , A , and $\tilde{t}_{a,fit}/\Delta\tilde{t}_a$ were all varied in this study by two orders of magnitude, $O(10^3 - 10^6)$, four orders of magnitude, and $\approx 40 - 260$ time steps respectively.

We plot the error in energy conservation in fig. B.1. In addition to the chosen time step, the error seems to depend on Ha_0 , due to inaccuracies in the first-order fit in Eq. 2.6. For stronger cohesion (larger Ha_0) we find that more time-steps are needed to produce the same error. If we restrict ourselves to systems where $Ha_0 < 1000$, we find that $\tilde{t}_{a,fit}/\Delta\tilde{t}_a = 100$ is sufficient to keep the error in energy conservation to within 1% of the analytic solution. We also note that values of very large Ha_0 are not of much concern. Such systems are typically in a bound state, i.e. stuck in the potential well, even without the presence of dissipation.

In Fig. B.2, we plot the full error in the coefficient of restitution incurred by the LSD model for the limiting time-step chosen. This is for the case of coefficient of restitution of

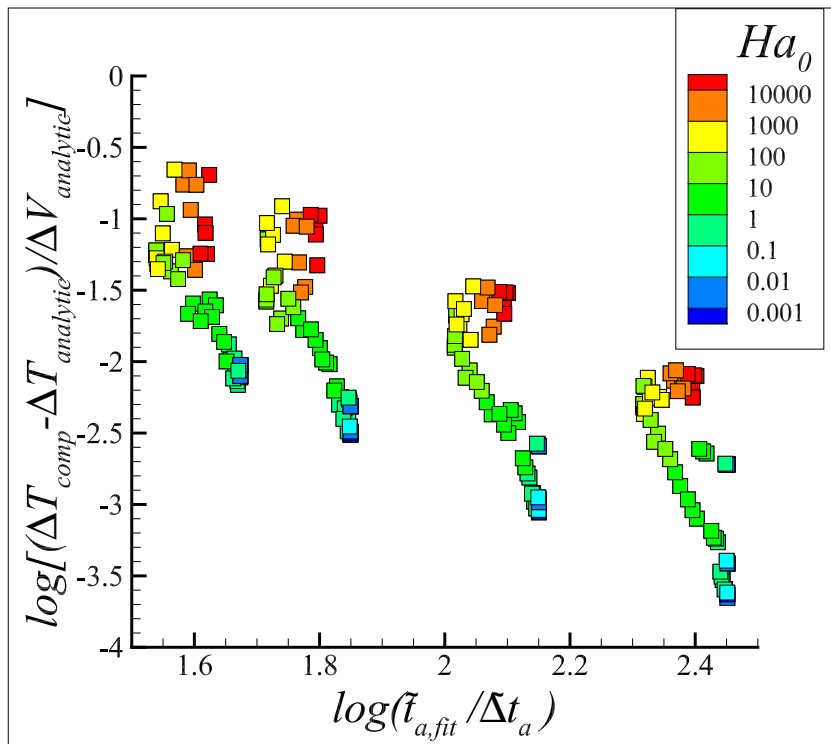


Figure B.1 Error in energy conservation for the binary particle system for different time steps is shown. Symbols are colored by the non-dimensional well-strength Ha_0 .

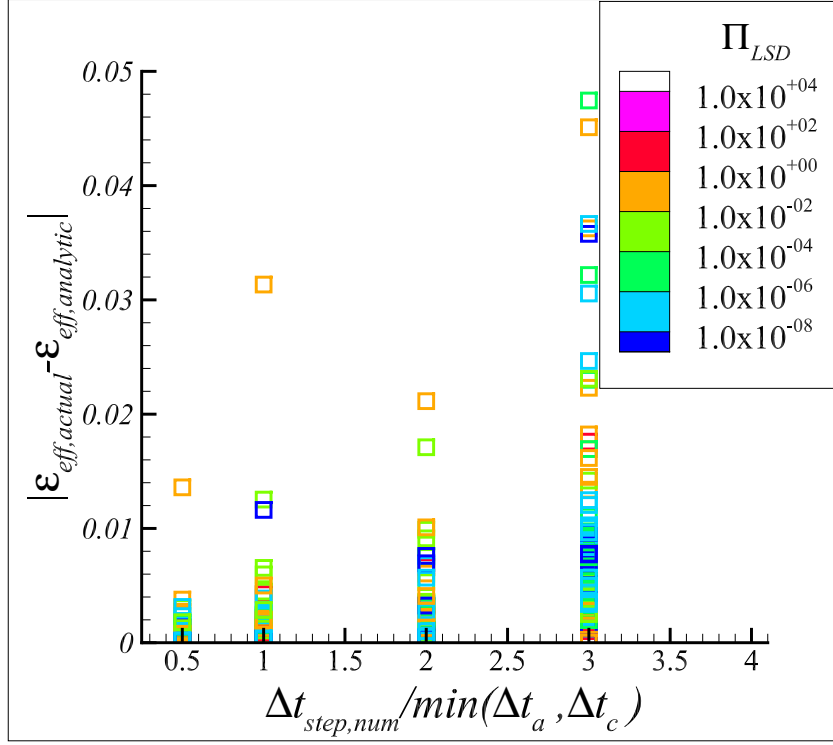


Figure B.2 This is the error in the full collision dynamics for the LSD system. If the limiting time-step is used, the total error in the effective coefficient of restitution is as high as 3% when the correct minimum time step is used.

$\varepsilon_{LSD} = 0.9$, while the samples are the same as chosen in the study of energy conservation within the potential well. The numerical solutions are compared to the ε_{eff} obtained from the solutions of the cohesive particle system in stage two in Eqs. C.1 and C.3 and the expression for ε_{eff} in Eq. 2.7. Symbols are colored by their value of the non-dimensional group Π_{LSD} . We find that error is as large as 3%, and is generally highest for particles with values of Π_{LSD} near the critical value where contact sticking occurs.

APPENDIX C. SOLUTION OF CONTACT DYNAMICS

Much as in the case of the non-cohesive KK and LSD models, we are interested in understanding the behavior of the coefficient of restitution when cohesion is added. The approach we take here is exactly the same as taken to understand non-cohesive systems: find the solution to the ODE for position and velocity, invert the position solution to find t_c , and find ε_c from the velocity solution. In this section we solve only the linear model; the KK type model is explored numerically in Section 2.3.2.

The linear version of Eq. 2.5 is easily solved via Laplace transforms. The full solution is best expressed in terms of the non-dimensional quantities given in Table C,

$$\delta^* = Bo^* \left(\sqrt{1 + \tan^2 \theta} \exp(-\tau^* t^*) \cos(\omega^* t^* + \theta) - 1 \right). \quad (\text{C.1})$$

In order to make a comparison to the non-cohesive case, we also give here the solution to the LSD model,

$$\delta^* = -\frac{1}{\omega^*} \exp(-\tau^* t^*) \sin(\omega^* t^*). \quad (\text{C.2})$$

We first see that Eq. C.1 is much more complex than Eq. C.2. However, there are a few similarities. The time scale for the decaying envelope, given by the exponential term, is identical for both cases. We note that in taking the non-cohesive limit, i.e. that $Bo^* \rightarrow 0$,

Table C.1 Parameters in solution of contact dynamics

Parameter	Symbol	Definition
Dissipation time scale	τ^*	$\frac{b^* k^*}{2}$
Undamped natural frequency	ω_0^*	$\sqrt{k^*}$
Damped natural frequency	ω^*	$\sqrt{k^* - \frac{b^{*2} k^{*2}}{4}} = \sqrt{\omega_0^{*2} - \tau^{*2}}$
Cohesion induced phase shift	θ	$\arctan\left(\frac{1}{\omega^* Bo^*} - \frac{\tau^*}{\omega^*}\right)$

the phase shift $\theta \rightarrow \pi/2$, producing a negative sine term. Expanding the $\sqrt{1 + \tan^2 \theta}$ term and multiplying by Bo^* also reveals that only the $1/\omega^*$ term survives. There is one important characteristic of the solution given by Eq. C.1 that is absent in Eq. C.2. Due to the presence both damping and the -1 term, it is possible for Eq. C.1 to have only one zero. The contact time can be infinite; particles can stick to one another from contact dynamics alone. Moreover, even when a finite contact time is given, we cannot invert C.1 to obtain the contact time. In Section 2.3.2, we explore the ε_c numerically using Eq. C.1 and the velocity solution given by

$$v^* = -Bo^* \sqrt{1 + \tan^2 \theta} \exp(-\tau^* t^*) (\tau^* \cos(\omega^* t^* + \theta) + \omega^* \sin(\omega^* t^* + \theta)). \quad (\text{C.3})$$

APPENDIX D. THE GEOMETRIC INTERPRETATION OF COLLISION LAWS

It is useful to consider the limiting behavior of the collision rule, and how the post-collisional trajectory of the two-particle system with a short-ranged attractive potential differs from the completely inelastic case. For example, taking $\epsilon = 1$, one recovers elastic hard-sphere behavior. If we employ the geometric interpretation of these collision laws plotted in the inertial frame of particle j (see figs. D.1(a)- D.1(c)), we find that ϵ serves to alter the angle of separation, the angle between the collision plane $\hat{r}_{\perp}^{(jk)}$ and post-collisional relative velocity vector $v_i^{(jk)}$. For $\epsilon = 1$ this angle is equal to the angle of the approach. Lower values of ϵ attenuate this angle. For the limiting completely inelastic case, $\epsilon = 0$, this angle is parallel to the collision plane $\hat{r}_{\perp}^{(jk)}$. All energy in the relative velocity corresponding to the normal $(\hat{v}_{\parallel}^{(jk)})$ degree of freedom is dissipated. It is important to note that a completely inelastic collision does not imply that particles remain in post-collisional contact. This can only occur for the inelastic model if the tangential components of relative velocity, $\hat{v}_{\perp}^{(jk)}$, are identically zero.

The effective coefficient of restitution discussed in section 3.2.1 has similar behavior as discussed above. Where particles do not stick, the attenuation of the angle of separation occurs identically to the process above. However, for sub-critical impact velocities, $(v_{\parallel}^{(jk)}) \in (v_{crit}, 0)$ particles stick to one another, creating dimers (see fig. D.1(d)). The effect of adding short-ranged attraction causes particles to not only lose more energy, but also to aggregate.

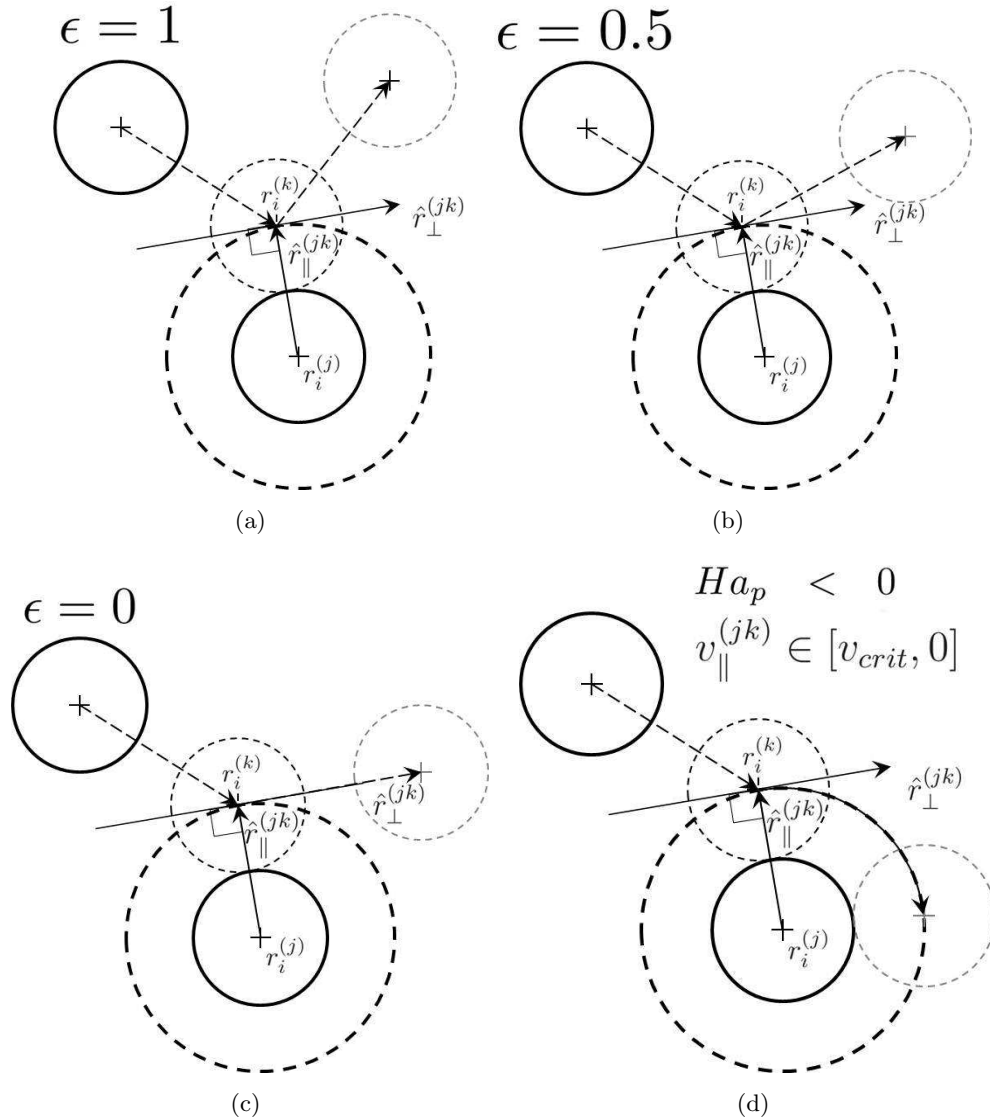


Figure D.1 (a)-(c) The geometric interpretation of inelastic hard sphere collisions is shown for varying values of ϵ , from elastic, $\epsilon = 1$ to completely inelastic $\epsilon = 0$. The main difference comes from the changing angle of separation of post-collided particles. Note that for all cases, the system is plotted in particle j 's frame of reference. (d) The collision outcome for a particle pair with sub-critical velocity impact velocity. Post-collision, a rotating particle doublet is formed.

APPENDIX E. CONSTRUCTING THE EFFECTIVE COEFFICIENT OF RESTITUTION

This section considers, in detail, how collision laws may be constructed for inelastic hard-sphere systems with an additional short-ranged attractive potential. The details that follow focus on the interaction contained in eqn. 3.2, but in principle may be straightforwardly extended to arbitrary short-ranged attractive potentials. Before forming the collision laws, we must establish some facts that are helpful in our construction. Firstly, the van der Waals potential is not singular at contact but instead reaches a minimum at the inter-atomic separation d_0 , i.e. the approximate diameter of the electron cloud of an atomic nucleus, typically ~ 0.2 nm for most materials (Israelachvili, 2011). Note that the interatomic length-scale d_0 is not physically meaningful for macroscopic particles, where such information has essentially been sacrificed due to coarse graining. Particles at this separation are in mechanical contact, and d_0 simply serves as a parameter to set the attractive force between two particles contact. This is the reason for setting the effective separation to $x = d_0$ at contact, i.e. $\left| r_{\parallel}^{(jk)} \right| = 2a$.

This model is applicable for particle diameters much larger than the length-scale d_0 . As a side note, because our particles are hard, i.e. rigid, we do not consider any increase in the attractive force at contact due to contact deformation, consistent with the DMT theory (Derjaguin et al., 1975). We stress here that the analysis that follows is not restricted to the van der Waals interaction and is applicable to any generic short-ranged attractive potential.

The short-ranged attractive nature of these wells assures that particles effectively do not feel one another at even relatively close separations. For example, two particles separated by $100d_0$ have 99% of the potential energy of two particles at infinite separation, $(\Phi_c - \Phi(100d_0)) / (\Phi_c - \Phi(\infty)) = 0.99$. Due to this fact, we are justified in using the approximation $\Phi(l_{well}) \cong \Phi(\infty)$. There is essentially no difference between a collision with two spheres initially separated by very large

distances or initially separated by $O(10\text{nm})$.

The outcome of a collision between two particles with short-ranged attractive potentials can now be determined. Collisions between cohesive spheres consists of three stages: (1) the approach where particles accelerate towards contact, (2) reflection and loss of energy due to the coefficient of restitution, (3) slowing as particles separate. Equations E.1-E.3 describe the collision process between two identical particles. The relationship between initial and final velocities are completely determined by a conserved Hamiltonian in stages one and three and by the coefficient of restitution in the second stage:

$$\frac{m}{4}v_{\parallel,2}^{(jk)2} + \Phi_c = \frac{m}{4}v_{\parallel,1}^{(jk)2} + \Phi(l_{well}) \quad (\text{E.1})$$

$$v_{\parallel,3}^{(jk)} = -\epsilon v_{\parallel,2}^{(jk)} \quad (\text{E.2})$$

$$\frac{m}{4}v_{\parallel,4}^{(jk)2} + \Phi(l_{well}) = \frac{m}{4}v_{\parallel,3}^{(jk)2} + \Phi_c. \quad (\text{E.3})$$

APPENDIX F. THE PSEUDO-LIOUVILLE OPERATOR APPROACH FOR SYSTEMS WITHOUT SHORT-RANGED ATTRACTION

The backbone of the analytic approach for hard-sphere gases in this paper is the pseudo-Liouville operator (Ernst et al., 1969; van Noije et al., 1998a). For inelastic hard-spheres the pseudo-Liouville operator takes the form

$$i\mathcal{L}^+ = \sum_{j=1}^N v_i^{(j)} \frac{\partial}{\partial r_i^{(j)}} + \sum_{j=1}^{N-1} \sum_{k=j+1}^N \left| v_i^{(jk)} \hat{r}_i^{(jk)} \right| \Theta \left(-v_i^{(jk)} \hat{r}_i^{(jk)} \right) \delta \left(\left| r_i^{(jk)} \right| - 2a \right) \left(b^{+(jk)} - 1 \right). \quad (\text{F.1})$$

The first term on the RHS is the streaming piece, which has no effect on the change in energy for statistically homogeneous problems. The second term, known as the collision operator, consists of two sifting terms: a Heaviside function Θ which works to select only pairs approaching one another and a Dirac delta function δ that selects pairs in contact to operate on, respectively. The last piece, $(b^{+(jk)} - 1)$ is a difference operator that replaces pre-collisional quantities with post collisional quantities. One uses collision rules to derive the form of these difference operators. For example, using the collision rules in eqn. 3.1 for monodisperse particles, the difference operator for the change in kinetic energy from a binary collision between particles j and k takes the form

$$\left(b^{+(jk)} - 1 \right) E_{kin}^{(jk)} = \left(\frac{m}{2} v_i'^{(j)2} + \frac{m}{2} v_i'^{(k)2} \right) - \left(\frac{m}{2} v_i^{(j)2} + \frac{m}{2} v_i^{(k)2} \right) = -\frac{m}{4} (1 - \epsilon^2) \left(v_i^{(jk)} \hat{r}_i^{(jk)} \right)^2. \quad (\text{F.2})$$

Here the $(')$ superscript distinguishes a post-collisional value from a pre-collisional value. The main use of the pseudo-Liouville operator is to evolve functions of phase space variables, such as $E_{kin}(\Gamma)$, in time. By taking the ensemble average of the interaction portion of the pseudo-Liouville operator we can obtain the cooling behavior,

$$\left\langle \frac{\partial E_{kin}}{\partial t} \right\rangle (t) = \int d\Gamma \rho(\Gamma; 0) \frac{E_{kin}(\Gamma(t))}{dt} = \int d\Gamma \rho(\Gamma; 0) i\mathcal{L}^+ E_{kin}(\Gamma) = \langle i\mathcal{L}^+ E_{kin}(\Gamma) \rangle (t). \quad (\text{F.3})$$

The initial joint probability distribution $\rho(\Gamma; 0)$ for all particles is chosen to be i.i.d. Maxwellian in velocity space and uniform in position space. Note that the set of phase space variables are abbreviated as $\Gamma = \{r_i^{(1)}, r_i^{(2)}, \dots, r_i^{(N)}; v_i^{(1)}, v_i^{(2)}, \dots, v_i^{(N)}\}$, and the differential $d\Gamma$ is given as $d\Gamma = \prod_j^N dv_i^{(j)} dr_i^{(j)} \prod_{k < j} \Theta(|r_i^{(jk)}| - 2a)$. We point the readers to previous works Müller and Luding (2011); Luding et al. (1998) for the well-documented intermediate treatment, where the $6N$ dimensional integral is reduced to a 12 dimensional integral containing only the two-particle distribution. A few key assumptions must be made in order to perform this reduction, namely:

1. Molecular chaos or the mean-field approximation, i.e. pre-collisional velocities are uncorrelated.
2. The joint velocity distribution remains close to that of an equilibrium hard-sphere gas, which is implied by combining eqn. F.3, our initial distribution, and our previous assumption.
3. The collision velocities remain isotropic, implied by the same reasons as above.
4. Excluded volume effects are the only spatial correlations present in the system, and appear in the radial distribution function at contact, $g_c = g(|r^{(12)}| = 2a)$. We approximate the pair contact density using the model of Carnahan and Starling Carnahan and Starling (1969) ($g_c = (1 - \nu/2) / (1 - \nu)^3$) with volume fraction ν .
5. The number of particles is sufficiently large that $(N - 1)/V \approx n$, where N, n , and V are the number of particles, number density, and volume of the system, respectively.

The resultant integral equation for the two-particle system is then found to be

$$\begin{aligned} \left\langle \frac{\partial E_{kin,p}(t)}{\partial t} \right\rangle &= -\frac{Nm}{8V^2} \left(\frac{1}{2\pi T_g} \right)^3 \int dr_i^{(1)} dr_i^{(2)} dv_i^{(1)} dv_i^{(2)} g(|r_i^{(12)}|) (1 - \epsilon^2) |v_i^{(12)} \hat{r}_i^{(12)}| \\ &\times \exp\left(-\frac{v_i^{(1)2} + v_i^{(2)2}}{2T}\right) \Theta(-v_i^{(12)} \hat{r}_i^{(12)}) \delta(|r_i^{(12)}| - 2a) \left(-v_i^{(12)} \hat{r}_i^{(12)}\right)^2, \end{aligned} \quad (\text{F.4})$$

where T_g is the granular temperature that is related to the average kinetic energy of a particle and the system via $\langle E_{kin,p} \rangle = \langle E_{kin} \rangle / N = 3mT_g/2$. A change of variables is performed ($r_i^{(12)} = r_i^{(1)} - r_i^{(2)}$, $R_i^{(1)} = r_i^{(1)}$, $v_i = (v_i^{(1)} - v_i^{(2)})/\sqrt{2}$, and $V_i = (v_i^{(1)} + v_i^{(2)})/\sqrt{2}$) in order

to simplify the final integro-differential equation. By integrating eqn. F.4 over all components except for the normal component of $v_{\parallel} = v_i \hat{r}_i^{(12)}$ one obtains the following one-dimensional integral in terms of instantaneous collision frequency, $\omega = 16\pi^{1/2} a^2 n_g c T_g^{1/2} (t)$:

$$\left\langle \frac{\partial E_{kin,p}(t)}{\partial t} \right\rangle = \frac{-\omega m}{4\sqrt{2}T_g} \int_{-\infty}^0 dv_{\parallel} (1 - \epsilon^2) \exp\left(-\frac{v_{\parallel}^2}{2T_g}\right) |\sqrt{2}v_{\parallel}| v_{\parallel}^2. \quad (\text{F.5})$$

The problem has been reduced from a many-body problem to an ensemble of isolated particles interacting with a mean-field distribution. Hence, we expect that if correlations in two-point statistics remain small, this theory should provide a good model for the trajectory of the macroscopic system. Note that this is equivalent to saying that the molecular chaos approximation is adequate.

The ODE obtained by evaluating F.5 is

$$\left\langle \frac{\partial E_{kin,p}(t)}{\partial t} \right\rangle = -\frac{m}{2} \omega (1 - \epsilon^2) T_g, \quad (\text{F.6})$$

with solution

$$\frac{T_g}{T_{g,0}} = \frac{1}{(1 + t/\tau_{\text{Haff}})^2}, \quad (\text{F.7})$$

where the time scale τ_{Haff} is given by

$$\tau_{\text{Haff}} = (\omega(t=0) (1 - \epsilon^2) / 6)^{-1}. \quad (\text{F.8})$$

The temperature evolution is commonly referred to as Haff's Law.

APPENDIX G. THE EXTENDED PSEUDO-LIOUVILLE OPERATOR FOR SYSTEMS WITH SHORT-RANGE ATTRACTION

In section 3.2.1, we observed that the nature of the hard-sphere inelastic system is qualitatively changed by the introduction of short-ranged attractive wells. Particles become sticky forming aggregates from low energy collisions. This causes problems when trying to straightforwardly apply the pseudo-Liouville operator (Ernst et al., 1969; van Noije et al., 1998a), which was originally developed for colliding and separating particles. Instead, the operator must be altered to account for the fact that particles can stick and form aggregates. Here we develop a Smoluchowski-type aggregation theory or birth-death process in the pseudo-Liouville operator framework, which will have the ability to account for annihilation of monomers and birth of dimers from collisions. Such a theory could be extended to larger size aggregates. However, the only aggregation kernel that we can compute explicitly using the collision laws is the source to the dimer phase from the monomer phase.

The first task in extending the pseudo-Liouville operator to the attractive problem is to split the operator into three pieces:

$$i\mathcal{L}^+ = \sum_{j=1}^N v_i^{(j)} \frac{\partial}{\partial r_i^{(j)}} + i\mathcal{L}^{+,r} + i\mathcal{L}^{+,s}, \quad (\text{G.1})$$

where the three terms on the right hand side of equation G.1 are (i) the free-streaming operator, (ii) a piece handling restituting collisions $i\mathcal{L}^{+,r}$, and (iii) one handling sticking collisions $i\mathcal{L}^{+,s}$, respectively.

The restituting operator is straightforwardly constructed as

$$i\mathcal{L}^{+,r} = \sum_{j=1}^{N-1} \sum_{k=j+1}^N \left| v_i^{(jk,1p)} \hat{r}_i^{(jk,1p)} \right| \Theta \left(v_{crit} - v_i^{(jk,1p)} \hat{r}_i^{(jk,1p)} \right) \delta \left(\left| r_i^{(jk,1p)} \right| - 2a \right) \left(b^{+,r(jk,1p)} - 1 \right). \quad (\text{G.2})$$

The only part in eqn. G.2 that is altered is the argument for the Heaviside function, which controls the limits of integration. We alter notation here to distinguish between particle phases. For example, a superscript $(1p)$ indicates the monomer phase, $(2p)$ the dimer phase, etc. The restituting operator maintains many of the same features of the pseudo-Liouville operator for hard-spheres. Both particle number and linear momentum are conserved. The source and sink term operating on the energy also takes a familiar form given in eqn. F.2 with ϵ being replaced by ϵ_{eff} .

The second operator for sticking collisions takes a slightly different form:

$$\begin{aligned} i\mathcal{L}^{+,s} = & \sum_{j=1}^{N-1} \sum_{k=j+1}^N \left| v_i^{(jk,1p)} \hat{r}_i^{(jk,1p)} \right| \Theta \left(v_i^{(jk,1p)} \hat{r}_i^{(jk,1p)} - v_{\text{crit}} \right) \Theta \left(-v_i^{(jk,1p)} \hat{r}_i^{(jk,1p)} \right) \\ & \times \delta \left(\left| r_i^{(jk,1p)} \right| - 2a \right) \left(b^{+,s(j,2p)} - b^{s(jk,1p)} \right). \end{aligned} \quad (\text{G.3})$$

We first notice that the limits of integration have again been changed so that only sticking collisions are operated upon. Next we notice that the source and sink operators have changed here. The sink is denoted by $b^{s(jk,1p)}$, which accounts for the annihilation of quantities from the monomer phase. The source, given by $b^{+,s(j,2p)}$, serves as a source of some quantity to the dimer phase. The operator is non-zero only when operating on the denoted phase, e.g. the source term with a $2p$ superscript operating on the number of particles in the monomer phase is zero $b^{+,s(j,2p)} N^{(jk,1p)} = 0$.

All that remains is to define these source and sink operators for the quantities of interest in this study, namely phasic number and energy. The number equations for the monomer and dimer phases are:

$$\begin{aligned} \left(b^{+,s(j,2p)} - b^{s(jk,1p)} \right) N^{(jk,1p)} &= -2 \\ \left(b^{+,s(j,2p)} - b^{s(jk,1p)} \right) N^{(j,2p)} &= 1. \end{aligned} \quad (\text{G.4})$$

The number equation tells us that in a sticking collision 2 monomers are annihilated to form a single dimer. Note that this is valid for monodisperse monomers in a statistically isotropic environment. Extension to account for both polydispersity and anisotropy is straight-forward but not as clean.

The energy equations for the monomer and dimer phases include the energies in the translational and rotational degrees of freedom for the dimer phase:

$$\begin{aligned} \left(b^{+,s(j,2p)} - b^{s(jk,1p)}\right) E_{kin}^{(jk,1p)} &= -\frac{3m^{(1p)}}{4} \left(v_i^{(jk,1p)} \hat{r}_i^{(jk,1p)}\right)^2 \\ &\quad - 3m^{(1p)} \left(w_i^{(jk,1p)} \hat{R}_i^{(jk,1p)}\right)^2 \end{aligned} \quad (\text{G.5})$$

$$\left(b^{+,s(j,2p)} - b^{s(jk,1p)}\right) E_{kin,trans}^{(j,2p)} = 3m^{(1p)} \left(w_i^{(jk,1p)} \hat{R}_i^{(jk,1p)}\right)^2 \quad (\text{G.6})$$

$$\left(b^{+,s(j,2p)} - b^{s(jk,1p)}\right) E_{kin,rot}^{(j,2p)} = \frac{m^{(1p)}}{2} \left(v_i^{(jk,1p)} \hat{r}_i^{(jk,1p)}\right)^2, \quad (\text{G.7})$$

where the vectors given by $w_i^{(jk,1p)}$ and $R_i^{(jk,1p)}$ refer to the center of mass velocity and position of the collision partners. Next, all energy in the 6 degrees of freedom of the binary system are annihilated (eqn. G.5). The energy in the center of mass degrees of freedom are straightforwardly transformed into the energy in the translational degrees of freedom for the dimer (eqn. G.6). The degrees of freedom in the tangential components of the relative velocity are transformed into rotational energy for the dimer (eqn. G.7). Lastly, the energy in the normal relative velocity degree of freedom is completely dissipated due to the enhanced dissipation from the attractive potential.

Despite having this nice extension, we cannot make adequate use of it without knowledge of how larger aggregates form and break-up. Indeed, this could only be meaningfully obtained through either experimental or, most likely, numerical means. So we will restrict ourselves to the case where aggregation is ignored, i.e. there is no coupling to an N -particle phase. We account for energy dissipation only. In that case the source and sink operators takes the form:

$$\left(b^{+,s(jk,1p)} - b^{s(jk,1p)}\right) E_{kin}^{(1p,jk)} = \left(b^{+(jk)} - 1\right) E_{kin}^{(jk)} = -\frac{m}{4} \left(v_i^{(jk)} \hat{r}_i^{(jk)}\right)^2. \quad (\text{G.8})$$

APPENDIX H. TEMPERATURE SCALING IN HOMOGENEOUS SHEAR OF COHESIVE GRANULAR PARTICLES

To understand the stress scaling in Fig. 4.3.1 a little better we look at the temperature response given in Fig. H. The trends for the temperature well in the quasistatic and inertial regimes here can easily be explained by an energy balance. For small $Ha_{\dot{\gamma}}$, $T/\dot{\gamma}^2$ is constant, meaning that $T \propto \dot{\gamma}^2$, which one can find from simple dimensional analysis. However, for large $Ha_{\dot{\gamma}}$, $T/\dot{\gamma}^2 \propto Ha_{\dot{\gamma}}^{1/2}$ which translates to $T \propto \dot{\gamma}$. Note also that the transition between these two scalings does not appear to be smooth.

The energy balance at steady state for these systems can be seen as a competition between energy input from macroscopic deformations and dissipation by the viscous dash-pot interaction. The energy input in to the temperature equation is equal to viscous heating, i.e., $\dot{E}_{in} = \sigma_{xy}\dot{\gamma}$, while the dissipation of energy is proportional to the energy dissipated by particles and number of interactions. In the collisional or inertial regime the rate of dissipation of granular temperature \dot{E}_{diss} is proportional to $(1 - \varepsilon^2)T^{3/2}$. The extra $T^{3/2}$ arises from the collisional frequency, which determines how often particles are in contact within a given time period. The shear stress σ_{xy} is proportional to $\dot{\gamma}^2$, and viscous heating \dot{E}_{in} is then proportional to $\dot{\gamma}^3$. The end result yields the result that $T \propto \dot{\gamma}^2$. The dependence of $T/\dot{\gamma}^2$ on the coefficient of restitution in the inertial regime is also explained by these arguments.

For quasistatic flows, particles are always interacting or in contact and the stress does not depend on the shear rate. In that case, one finds that the dissipation is directly proportional to the temperature $\dot{E}_{diss} \propto bT$. The energy input also becomes $\dot{E}_{in} \propto \dot{\gamma}$, since stress does not depend on the shear rate. Hence, one finds that $T \propto \dot{\gamma}$ for quasistatic cases. This makes sense from the standpoint of physical intuition as well; in a well connected assemblage of spheres, fluctuating or non-affine velocities depend only on rearrangements that are caused

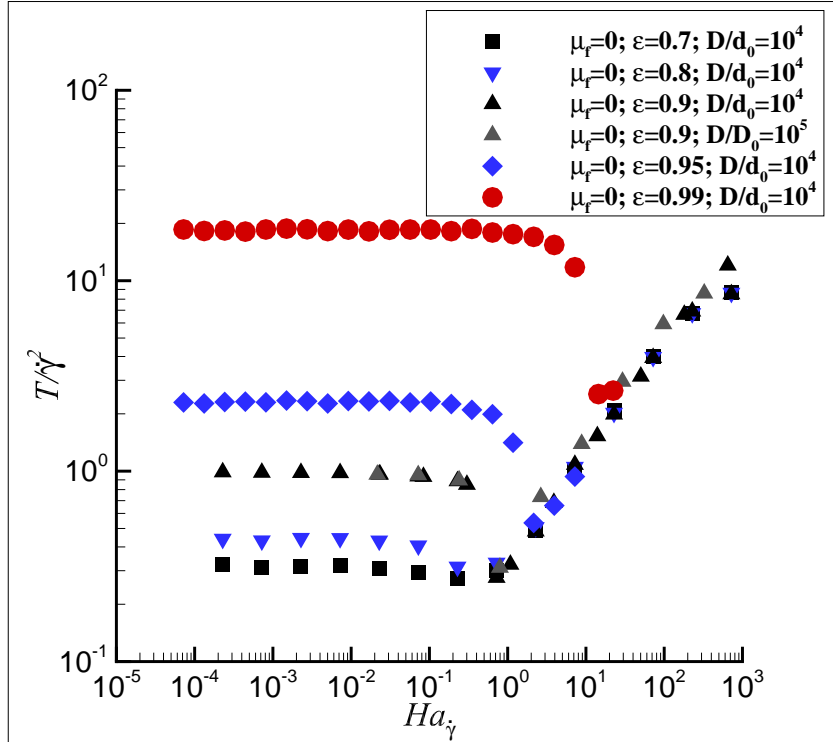


Figure H.1 The scaling of temperature by the squared shear rate for frictionless particles in simple shear.

by the imposed deformation. Dissipation happens on a much faster time-scale than particles rearrangements caused by shear. This view is backed up by a unique scaled temperature among differing ϵ in the quasistatic regime. In a sense, each case with differing ϵ are kinematically identical if particles are completely clustered.

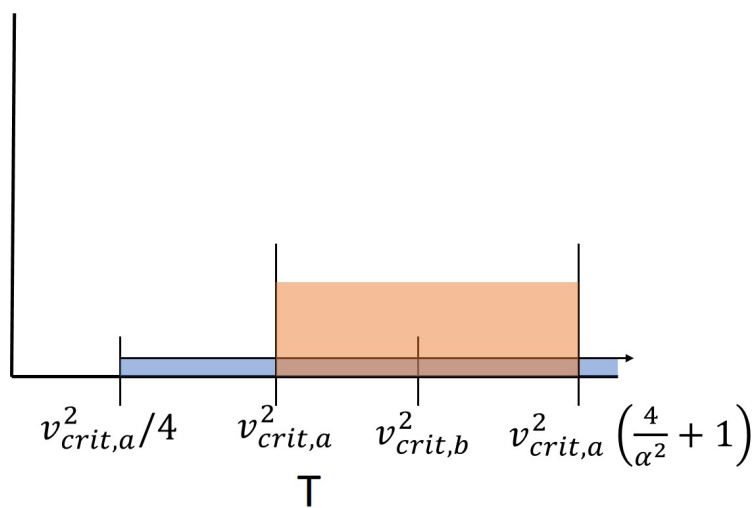
Finally, in between these two scaling regimes we see a dramatic drop in the scaled temperature, which is likely caused by the sticking of particles and an essential loss of modes that large fluctuating velocities can occupy (Murphy and Subramaniam, 2015). This large drop in $T/\dot{\gamma}$ is ultimately responsible for the collapse of the stress transition at $Ha_T = 1$ for smooth particle systems. We note that frictional cases exhibit the same temperature scaling in the inertial and quasistatic regimes, but as with the scaled shear stress they do not transition at the same Ha_T .

APPENDIX I. SCALING OF THE CLUSTER LENGTH-SCALE IN HOMOGENEOUS SHEAR OF MODERATELY DENSE COHESIVE SYSTEMS

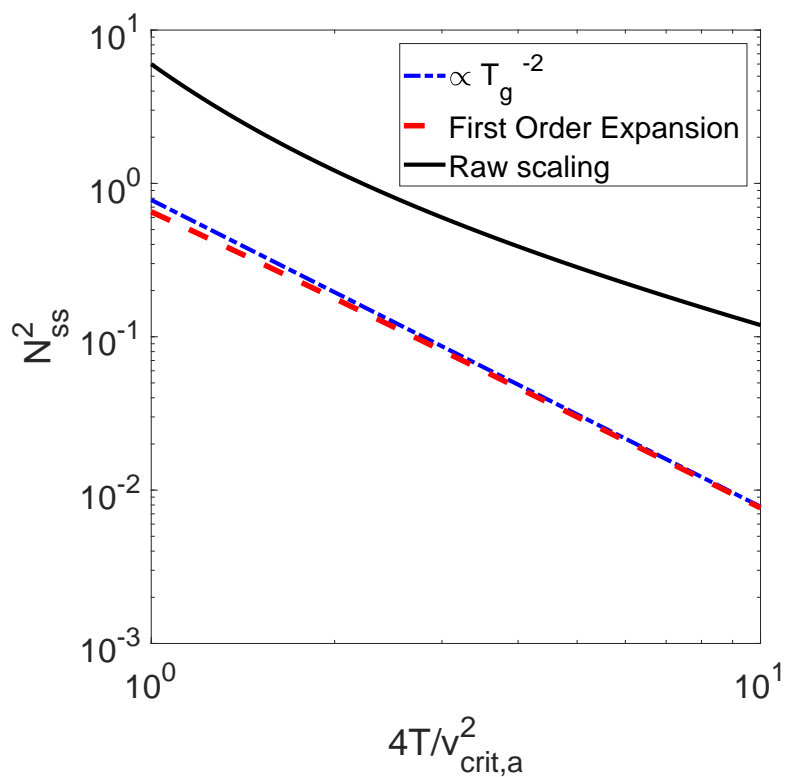
Here we explore how the cluster length-scale should grow and eventually cause a regime transition in the rheological scaling. The length-scale $\langle \xi_i \rangle$ introduced in Chapter 4 is normalized by the number of clusters, where the normalization is such that a monomer is also considered a single particle cluster. Incidentally, when only dimers and monomers are present, as is the case for $Ha_{\dot{\gamma}} \ll Ha_{\dot{\gamma},crit}$, the average coordination number $\langle Z \rangle$ will scale exactly the same with $Ha_{\dot{\gamma}}$ as $\langle \xi_i \rangle$. This is because the length-scale for a dimer is a constant and the problem becomes simple counting. In this regime, where $\langle \xi_i \rangle \propto \langle Z \rangle$, we can predict how the cluster length scale might scale with shear rate through the use of population balance equations. The source of dimers due to monomer collisions has been derived in Murphy and Subramaniam (2015). A similar integration can be made to estimate the sink of dimers due to collisions that result in break-up. Here we assume that the critical velocity that leads to break-up is slightly larger than the critical velocity under which monomers stick and we assume that this critical velocity is constant. Here $v_{crit,b} = \alpha v_{crit,a}$, where $\alpha > 1$. It is also assumed that the sink of dimers must be proportional to the number of dimers present, such that the rate of loss vanishes when dimers are not present. Sources and sinks to larger aggregates are ignored. The resulting rate equation for the number of dimers $N^{(2)}$ is given by

$$\frac{dN^{(2)}}{dt} = C_1 \sqrt{T_g} \left(1 - \exp \left(-\frac{v_{crit,a}^2}{4T_g} \right) \right) - C_2 N^{(2)} \sqrt{T_g} \exp \left(-\frac{v_{crit,b}^2}{4T_g} \right). \quad (\text{I.1})$$

Hereafter we drop the constants C_1 and C_2 , since they do not affect the scaling. To find the leading order scaling these terms are expanded in Taylor series. Terms in the power series



(a)



(b)

Figure I.1 (a) The regions where the first order expansions of eq. I.1 are the leading order terms. (b) The scalings of the steady state dimer population are compared showing that the population scales as $v_{crit,a}^4/T_g^2$ in the area near the stress transition.

in the temperature range of interest must be less than unity to ensure that higher order terms are of decreasing importance. Due to the exponential term, neither term can be expanded in T_g around $T_g = 0$. The rate of dimer break-up term grows with the temperature, while the rate of monomer aggregation grows with the inverse temperature. We will expand each term in those respective variables, with the aggregation rate being expanded around $1/T_g = 0$ and the break-up rate around $T_g = v_{crit,a}^2$. See fig. I.1(a) for a depiction of the areas, where the first order linear terms are the leading order terms in the expansion. The steady state number of dimers is then given to first order as

$$N_{SS}^{(2)} \propto \frac{\frac{v_{crit,a}^2}{4T_g}}{\left(1 - \frac{\alpha^2}{4} + \frac{\alpha^2 T_g}{4v_{crit,a}^2}\right) \exp\left(-\frac{\alpha^2}{4}\right)}. \quad (\text{I.2})$$

The scaling of the steady-state dimer population is plot in fig. I.1(b). There the raw scaling using eq. I.1, expansion to first-order in eq. I.2, and the power law $v_{crit,a}^4/T_g^2$ term, without the additive constants in the denominator, are compared for the case of $\alpha = 1.5$. We see that the slope is quite accurate, going as T^{-2} . A power-law curve fit of the raw scaling also produces an exponent of 2.03. Comparison of this scaling law is shown in 4.3.2.

APPENDIX J. MEASURES FOR DETECTING CLUSTERS IN A DISPERSED SOLID PHASE

The majority of the following appendix appeared in a final report for the NSF grant CBET 1134500 (Subramaniam, 2014).

In order to study the clustering of systems, we must be able to detect the existence of clusters in a domain. In a statistical sense, this means that we must be able to distinguish between cases where particles appear next to each other purely due to chance (so-called natural variation) and cases where bona fide correlations exist. The measure of choice in Chapter 7 is the radial distribution function (rdf). In this appendix, we consider two additional measures of clustering and compare and contrast their uses. The first is the excess two-body entropy, which helps map structure in the rdf to a scalar measure (Baranyai and Evans, 1989). The second is the configurational entropy of a point process, which compares the entropy in the distribution of the number of particles in a random sub-domain to that of a Poisson process.

J.0.1 Natural fluctuations in a sub-sample and the roll of domain size

Previously, the stability behavior of gas-solid flows driven by a pressure gradient in small simulation boxes (Subramaniam, 2012), e.g., $L/D = 10$, have been probed and no instabilities were found to arise. Using objective measures, such as the rdf $g(r)$ of the solid-phase, we found no evidence of structure formation. Clearly, there are many mechanisms controlling the stability of gas-solid flows that depend intimately on the simulation set-up and have yet to be satisfactorily understood. Note, however, that larger simulation boxes have demonstrated structure formation as found in Chapters 8 and 9.

In order for a statistically homogeneous system to become unstable, natural fluctuations that arise purely by chance in a realization must be able to evolve to produce an instability.

Smaller simulation boxes prevent and subdue such instabilities in two ways. The first reason is simply due to the allowable fluctuations in the initial number of particles and their spatial distribution. If we consider particles distributed as a Poisson point process, the number of particles present in a simulation domain has the distribution

$$P(N_p = k) = \frac{(\langle n \rangle V)^k \exp^{-\langle n \rangle V}}{k!}. \quad (\text{J.1})$$

Here, $\langle n \rangle$ is the expected number density of the process and V is the volume of the simulation domain. The variance in the number of particles present in a simulation is simply, $\text{var}(N_p) = \langle n \rangle V$. Fluctuations of this type are connected to the grand canonical ensemble. However, it is important to note that the number of particles in a simulation domain is **fixed**. If we consider that our simulation box has a given number of particles N_p , but is a realization of a Poisson point process, then a subdomain V_s has the following distribution of particles:

$$P(N_s(V_s) = k | N_V(V) = N_p) = \frac{N_p!}{k! (N_p - k)!} \left(\frac{V_s}{V}\right)^k \left(1 - \frac{V_s}{V}\right)^{N_p - k}. \quad (\text{J.2})$$

All subscripts s denote a measurement on a sub-domain, while N_V is the number of particles in the entire domain. This set-up corresponds to the canonical or microcanonical ensemble. We recognize that this is a binomial distribution with variance, $\text{var}(N_s) = nV_s(1 - V_s/V)$. From this expression for the variance, we immediately see that fluctuations in number scale as $(1 - V^{-1})$, meaning that local fluctuations in the number of particles in a sub-domain grow as the total system domain increases. Clearly, if large fluctuations are needed to produce an instability we need a large domain to produce them through natural variation/fluctuations.

Small boxes also subdue instabilities by constraining the dynamics of the system to sub-domains of phase space. If the dynamics in the accessible regions of phase space prevent correlations from developing, such as those present in the pair correlation function, instabilities may not arise in these simulations.

J.0.2 Cluster Characterization

Instabilities in homogeneous systems are characterized by the emergence of structure. These structures manifest in a number of ways, e.g. vortex structure, clusters, etc. A major challenge in the study of these instabilities is finding an objective and effective way to characterize structure. Two-point correlations, such as structure functions, have often been used to demonstrate the emergence of clustering and vortex structure (van Noije et al., 1997, 1998a; Murphy and Subramaniam, 2015).

While two point statistics readily show the emergence of structure, it is difficult to objectively measure the distance between two states of particle configurations. We would like to construct a measure of the particle configuration $\mu(\{\mathbf{X}^{(j)}\})$ that will tell us how far different one distribution of particles is from another.

When considering a measure for clustering, we concern ourselves with measures that satisfy the following four criteria.

1. The clustering metric should discriminate between uniform and clustered states over a range of characteristic cluster length scales and for different interactions, e.g. cohesion, inelastic, hydrodynamic, etc.
2. The clustering metric should depend on few numerical parameters, e.g. multiple independent simulations, sampling volume, etc.
3. The metric should be fast to compute. Competing measurements like the pdf of Voronoi cell volumes can be $O(N_p^2 \ln N_p)$ to $O(N_p \ln N_p)$ (Monchaux et al., 2010).
4. A transport equation for the metric should be able to be formed, so that it can be used in the averaged equations of computational fluid dynamics.

A standard measure often used is Shannon's information entropy (Shannon, 1948) given by the equation

$$S(\{\mathbf{X}^{(j)}\}) = - \int \prod_{j=1}^{N_p} d\mathbf{X}^{(j)} f(\{\mathbf{X}^{(j)}\}) \ln f(\{\mathbf{X}^{(j)}\}). \quad (\text{J.3})$$

The information entropy is really a measure of uncertainty in the system. The measure is maximal for the uniform distribution. The useful characteristic of the entropy is that it produces zero for a single delta function $f(\mathbf{X}) = \delta(\mathbf{X})$, which is a deterministic outcome. The entropy measure expresses the distance between a distribution and determinism; it measures randomness. Any distribution with more structure than randomly distributed particles will produce lower entropy than that of the random reference state. There are two types of entropy that we are interested in: the so-called excess entropy which can be calculated from $g(r)$ and the entropy in the distribution of particles in a sub-volume.

J.0.3 The Excess Two-Body Entropy

The excess two-body entropy in a distribution of particles can be calculated according to Baranyai and Evans (1989) and is ensemble invariant

$$S_{excess}^{(2)} = -2\pi n \left(\int r^2 g(r) \ln g(r) dr + \int r^2 (g(r) - 1) dr \right). \quad (\text{J.4})$$

Here r is the separation distance between particles. We should note that in the entire expression for excess entropy, corrections from additional 3-body and higher correlations must be included. To leading order, the two-body should be sufficient to show the emergence of structure. We note that this expression is a correction to the ideal gas state, which has uniform density n . If $g(r) = 1$ at all distances, as in the case of the ideal gas, the excess entropy is 0. We should also note that any deviation from the uniform state produces a negative correction. This is equivalent to saying that the entropy in a system has decreased, and hence, the particle configuration is more ordered. For a hard-core system we can calculate the entropy straightforwardly up to the hard-core distance, since the first term disappears. Integrating up to the hard-core distance one obtains $S_{excess}^{(2)} = -2\pi n R_{HC}^3/3$, where R_{HC} . Corrections at further distances can be obtained for Matérn point processes and are typically not significant for extremely dilute non-clustered systems.

J.0.4 The Configurational Entropy of a Point Process

Another way of looking at spatial structure in the particle field in granular and multiphase flows is to model the particles as a stochastic point process (Daley and Vere-Jones, 1988; Subramaniam, 2000, 2001). The complete description of the particle field in granular and multiphase flows using a stochastic point process representation is given by (Subramaniam, 2000):

$$\left\{ p_k, \mathbf{X}^{(k)}, k = 1, \dots, N(t) \right\}. \quad (\text{J.5})$$

Here N is a random variable denoting the total number of particles and $\mathbf{X}^{(k)}$ is a random vector denoting the position of the k -th particle. The probability that the total number of particles N takes the value k is p_k . The configurational entropy of this point process is $\sum_k p_k \ln p_k$. Note that this definition of the configurational entropy does not account for the spatial distribution of the particles. It can be easily extended to capture the dependence of configurational entropy on spatial length scales by considering a similarly defined quantity on sub-volumes.

A similar and complementary method for defining entropy arises when considering a sub-volume taken from a simulation. If we consider the one-particle density function, constructed from a measurement volume V_m , for a grand canonical ensemble, that is with a variable number of particles, we obtain the expression

$$f(x_i, v_i, t; V_m) = \sum_k P(k; V_m) f^{(k)}(x_i, v_i, t; V_m). \quad (\text{J.6})$$

The probability mass function $P(k; V_m)$ denotes the probability that there are k particles in a realization of the point process in sub-volume V_m . We want to find the entropy of this probability mass function, constructed from a simulation.

There are two simple situations for which we can obtain analytic results. These solutions serve as reference systems that can tell us what is happening in our simulation. The first is the well-studied Poisson point process, given in J.1. For an expected number density $\langle n \rangle$ and measurement volume V_m the probability mass function takes the form in Eq. J.1. The Poisson distribution has an entropy of

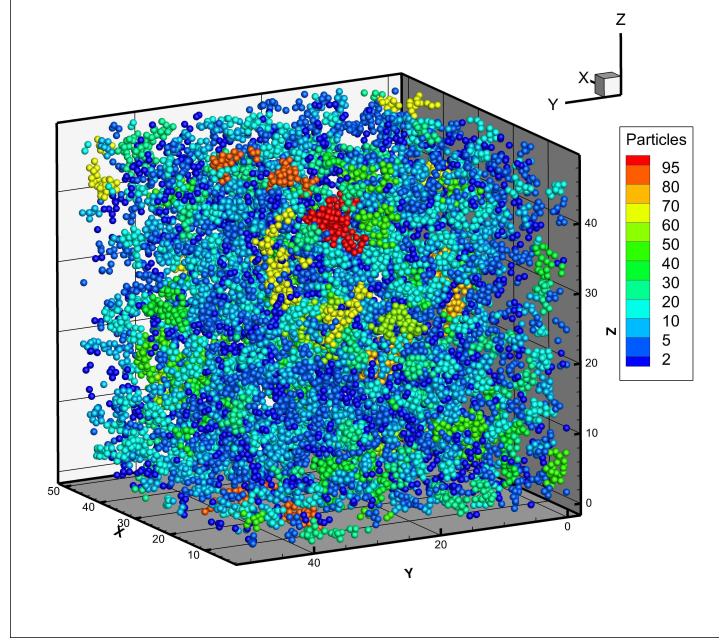


Figure J.1 A snapshot of the homogeneously cooling granular gas at some later time. Particles have begun to collect into clusters due to energy loss coupled with cohesion.

$$S_N(V_m) = \sum_{k=0}^{\infty} \frac{(\langle n \rangle V_m)^k \exp^{-\langle n \rangle V_m}}{k!} (\langle n \rangle V_m - k \ln \langle n \rangle V_m + \ln k!). \quad (\text{J.7})$$

A more accurate description would be to condition our sub-domain, i.e. measurement volume, to be a Poisson process, inside of a domain where the number of particles is conserved, since that is a practical constraint in computations. Given that the large system has a number of particles N_p , we want to find the probability that the small sub-system has k particles. This was done in (Subramaniam, 2014), yielding Eq. J.2. The entropy for this distribution is given as

$$S_N(V_m) = \sum_{k=0}^{N_p} \frac{N_p!}{k!(N_p - k)!} \left(\frac{V_m}{V}\right)^k \left(1 - \frac{V_m}{V}\right)^{(N_p - k)} \times \left(\ln \left(\frac{N_p!}{k!(N_p - k)!} \right) + k \ln \left(\frac{V_m}{V} \right) + N_p - k \ln \left(1 - \frac{V_m}{V} \right) \right). \quad (\text{J.8})$$

J.0.5 Results and Comparison for Clustering Measures

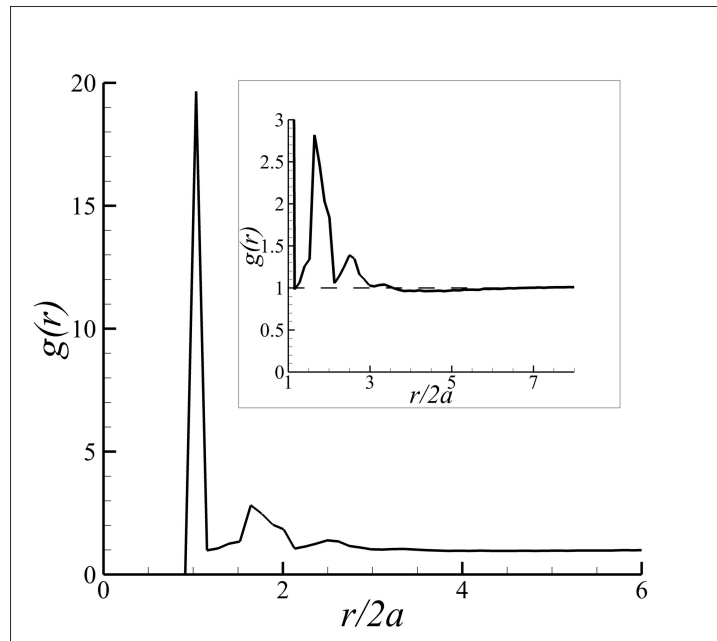
The following results were all constructed for different cases of the homogeneous cooling granular gas (HCG). The two main cases we focus on are the cohesive model and the model with a vanishing coefficient of restitution, $\varepsilon = 0$ (Murphy and Subramaniam, 2015). An example of a configuration for the cohesive HCG is shown in Fig. J.1. The statistics gathered from the cohesive case are presented in Fig. J.2(a); see Fig. J.2(b) for the pair statistics, including structure functions, at the end of the $\varepsilon = 0$ case.

We note that both metrics depend on the correct construction of a distribution function. Unlike moments, which converge rapidly, reconstruction of a distribution function requires many additional samples. Accurate measures require an accurate construction of the entire distribution function.

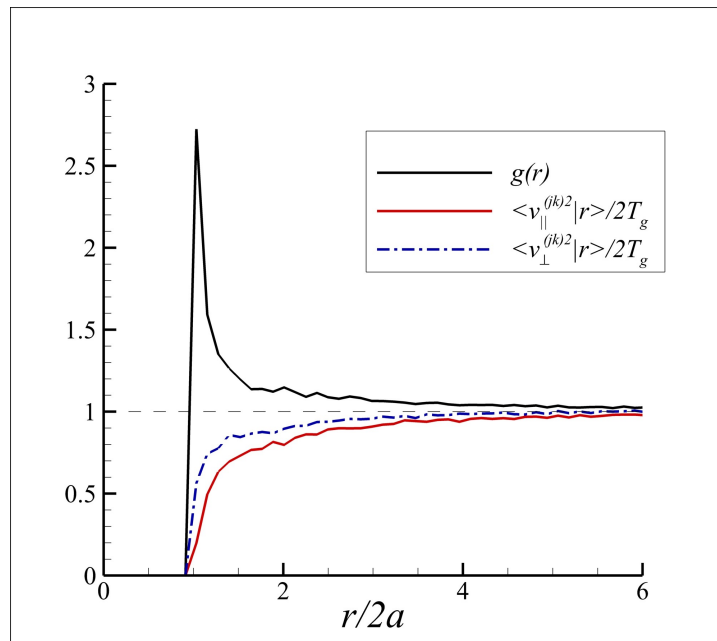
J.0.6 Excess Entropy Results

In order to compute the entropy according to Eq. J.4, we need first to construct a second-order density. Fortunately, there are $N_p^2 - N_p$ samples for a two-point quantity in any realization. Unfortunately, for certain pathological cases, accurate reconstruction of the two-point density becomes difficult. For example, in the cohesive HCG, after a collision particles may not have sufficient kinetic energy to exit the attractive potential energy well. In this case, particles experience a successive series of re-collisions, losing energy every time the pair comes into contact. As all energy is dissipated, particles approach closer and closer to the bottom of the potential well. As time progresses there is a very large population of particle pairs in a very small region of separation space. The density of these pair in contact is so large that is very hard to accurately reconstruct, leading to inaccuracy for the cohesive case.

In Fig. J.3(a), we look at the $S_{excess}^{(2)}$ as a function of spatial separation, we see that below the hard-core separation distance the entropy correction begins to decrease and then experiences a sharp drop concomitant with the first contact peak in $g(r)$. The excess entropy continues to drop, until a plateau is reached, beyond which no additional structure is seen in the radial distribution function. One of the advantages of this $S_{excess}^{(2)}$ metric is that it appears to retain



(a)



(b)

Figure J.2 The evolution of the rdf $g(r)$ is plot for (a) the case where particles are cohesive (b) $\varepsilon = 0$. Note that the 2nd order structure functions are shown alongside the rdf for the non-cohesive case.

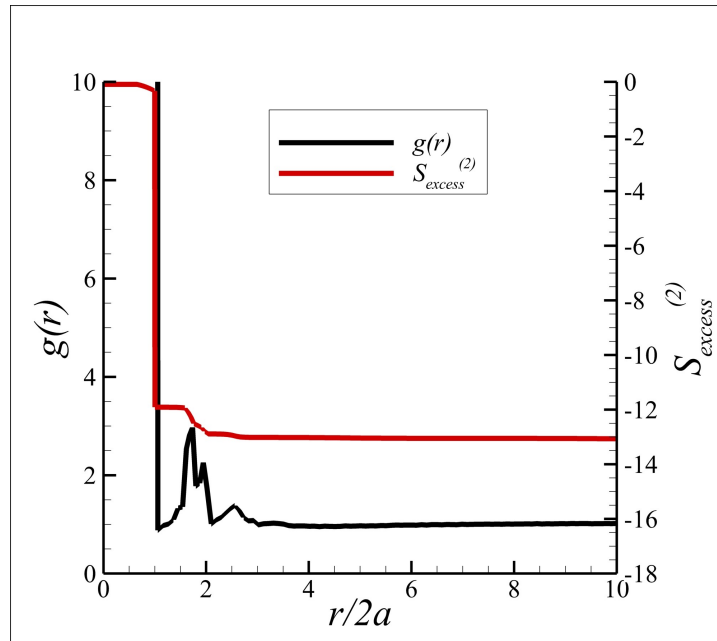
spatial information, about the length-scale of correlations within the system.

The value for $S_{excess}^{(2)}$ for a particle configuration clearly depends very strongly on having converged values at all separations in $g(r)$, especially in the peaks, see Fig. J.3(a). Comparing the time evolution of for the completely inelastic and cohesive cases, further exacerbates this point, see Fig. J.3(b). We find that the cohesive case, which continues to aggregate into sticky collections of particles, produces an order of magnitude larger value of $S_{excess}^{(2)}$ compared to the completely inelastic system. As a last note, the cohesive system, when compared to structure likely to exist in many gas-solid flows, is pathological, and provides an extreme test on the utility of the $S_{excess}^{(2)}$ measure. Such narrow and large peaks may only be produced by particles in static particle contacts, which are unlikely to occur in the more dilute spatial clusters occurring in gas-solid flows.

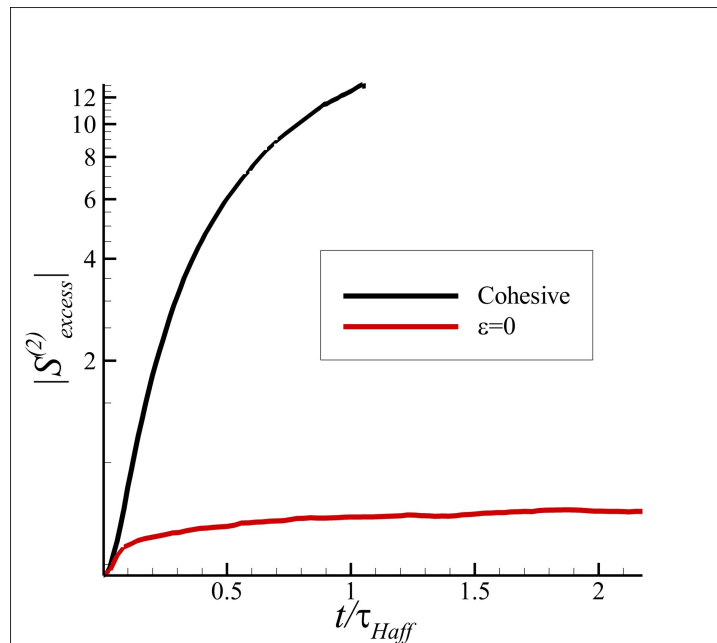
J.0.7 Configurational Entropy of a Point Process Results

Using the sub-domain approach, we calculated a test volume dependent entropy $S_N(V_m)$ for the distribution of $P(k; V_m)$, see Eq. J.8. The cases we study are again the cohesive and inelastic HCG systems. First, however, we are interested in defining the reference state of the system, given from the Poisson point process conditional on constant N_p in the simulation box. We wanted to observe the trend of the random case. For the binomial distribution we know that the distribution becomes a delta function for a probability of occurrence being $p = 1$ or $p = 0$, where for example $p = V_s/V$. We also know that the entropy vanishes for a delta function; there is no uncertainty. For values in between we know that if we make the change of variables $q = 1 - p$ and $l = N_p - k$, we obtain the same binomial distribution for q . Hence, the entropy is also symmetric about $V_m/V = 1/2$, which is the scale at which the maximum entropy value must be located. Shown in Fig. J.4(a), is the entropy obtained for a Poisson point process, alongside the result from the HCG initial condition with 2500 cubic test volumes at each V_m . We have performed these calculations with up to 12500 test volumes, and the results appear to be converged. However, as a future task, we intend to perform MIS to assure that our entropy estimates are also accurate.

Next we looked at the evolution of the measure for both the cohesive and inelastic HCG.



(a)



(b)

Figure J.3 (a) The radial distribution function is compared to the indefinite integral form of $S_{excess}^{(2)}$ for the cohesive HCG gas. Both evidence of structure at different distances. (b) The $S_{excess}^{(2)}$ metric is compared for the cohesive HCG case and the completely inelastic case. It is clear that the cohesive case is forming far more structure due to a large number of particles in contact.

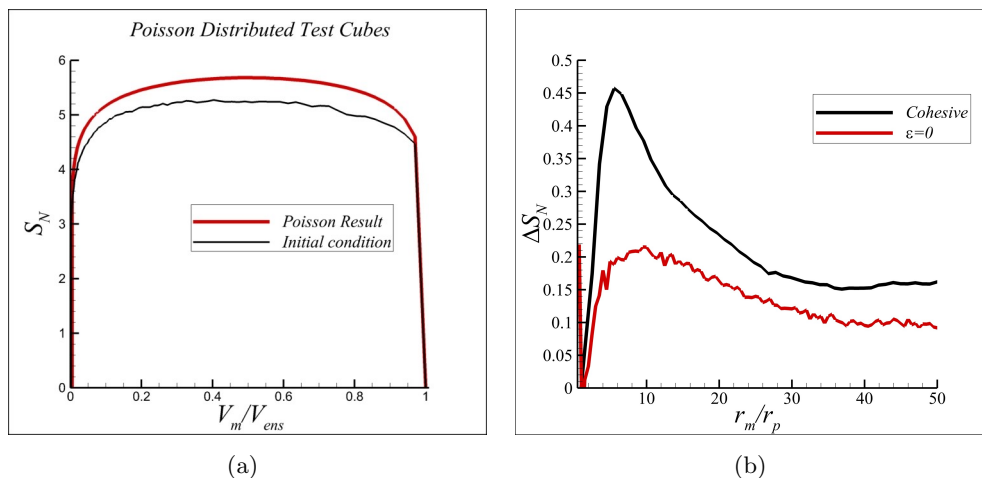


Figure J.4 (a) The convergence of S_N to the expected results is shown. Slow convergence is expected due to the need to converge the entire distribution. (b) The normalized ΔS_N is shown for both the cohesive and completely inelastic case. Here, we use the radius r_m of a measurement volume which is a ball rather than V_m . The normalization is by the particle radius r_p . More order is observed in the cohesive clustering case.

For both systems, we see that the entropy grows, again more substantially for the cohesive case. When comparing the final state of the entropy S_N for the cohesive and completely inelastic cases, we would like to define it in relation to some reference state, for the time being that will be the entropy of the initial condition, $S_{N,i}$. In Fig. J.4(b), we plot the scaled entropy, defined as $\Delta S_N = (S_N - S_{N,i})/S_{N,i}$, for both the cohesive and completely inelastic cases. We find a similar trend in this plot, where the cohesive case appears to have more structure than the inelastic case.

J.0.8 Evaluation

It is useful now to evaluate the performance of these two metrics against the first three criteria we had set earlier, see Fig. J.5. Both of these methods are able to distinguish between structured and uniform states. The $S_{excess}^{(2)}$ measure is much more sensitive than the ΔS_N measure to short-range order. However, we experience difficulty when trying to accurately calculate the excess two-body entropy, when large peaks in $g(r)$ are present, which with a constant bin width approach requires many samples to reduce the noise to signal ratio. ΔS_N

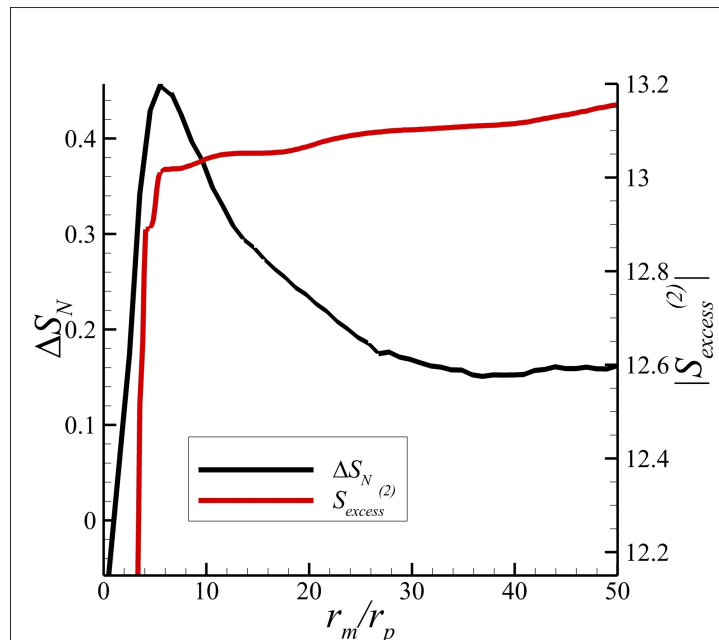


Figure J.5 A comparison of the two entropic measures at different length scales. Both show similar sensitivity to structure at different scales.

is somewhat more noise resistant due to having an unlimited number of test volumes at its disposal, but takes longer to converge. We note also that moments such as the variance may also show evidence for structure, which takes far fewer samples to converge.

The sub-domain method is by far the cheaper method to employ. Computational complexity goes as $O(N)$, which outperforms even the construction of a Voronoi diagram. As a last note, we have shown in Fig. J.5 both measures for the final state of the cohesive HCG problem. The length scale of a cluster, i.e. density correlations, appears in $g(r)$. At distances slightly farther than the hard-core distance in r , deviations are expected from unity due to either excluded volume effects or dynamic correlations. As r is increased, we expect that the magnitude of these correlations will decrease, until at some length-scale $g(r)$ stays at unity for increasing separation. This length-scale indicates the length-scale of a cluster. Most interesting is that both methods show a rapid change in behavior at the length scale of structure in $g(r)$, indicated by a peak in $S_{excess}^{(2)}$ and an abrupt change in the slope of ΔS_N . We hope that the use of either of these methods will provide us with excellent measures of particle structure on which we may condition the mean drag (Mehrabadi et al., 2016a).